EXPERIMENTAL PROPERTIES OF BONDED SOILS

by

Luiz Antônio Bressani

October 1990

A thesis submitted to the University of London
(Imperial College of Science, Technology and Medicine)
in partial fulfillment of the requirements for the degree of
Doctor of Philosophy in the Faculty of Engineering
and for the Diploma of Membership of the Imperial College

ABSTRACT

The properties of weakly bonded soil have been studied experimentally, mainly by an extension of recent work on artificial bonded sand. Higher stresses were used to fully examine yield of this soil when at denser states.

Triaxial equipment applying confining pressures of 3.5 MPa and a belt for measuring radial strain on triaxial soil samples were developed.

The influence of saturation procedures on test results was investigated. A new loading arrangement has been used and comparative studies carried out to evaluate its influence. The new arrangement improves the stress distribution in the sample and the quality of the conventional strain measurements taken platen to platen. It also reduces premature failure of the sample due to non-uniform stresses.

Two natural materials with some degree of cementation were also tested: the Corinth marl (a soft carbonaceous rock from Greece) and the Chemususu Dam soil (a red lateritic soil from Kenya). Both materials have similar characteristics to the artificial soil when tested in triaxial compression.

The bonded soils have shown a characteristic variation of stiffness with confining pressure. As the pressure is increased the secant initial stiffness increases initially but, at some treshold value of confining stress, show stabilization or even a drop on its absolute value, depending on the initial void ratio and the strength of the bonding.

The bonded soils have a curved yield locus which is coincident with the failure envelope at low stresses. The failure envelope in the low stress region is dependent of the stress path, being lower for conventional drained compression tests.

ACKNOWLEDGEMENTS

The author received help from a number of people without whom I would have done much less, worked much more and less successfully.

Dr P.R. Vaughan provided the most useful introduction for the thesis. Our initial discussions directed the whole work, and his ever present willingness to sort out my doubts were reassuring. His encouragement gave me the confidence to follow my own ideas (and I naturally lost some time due to that).

Duve encouraged me to study for the Master Degree, convinced me that I could learn English against all my fears and supported me all the way through the thesis. Her typing, cross-checking of the text and references, and the sharp eye for inconsistencies made the final preparations almost effortless (to me, I mean). To Duve, my wife, my love. Thank you, we did it.

My parents, although on the other side of the ocean, kept in constant contact, supporting me in many ways.

The preparation of a thesis has many hurdles and writing it seemed a high one. Mike Crilly and Jamie Standing coached me in a very professional way. Their encouragement and hard work in correcting my English taught me a great deal about style and clarity of writing (I exempt them for this page). They certainly made Prof. Vaughan's task much easier. Andrew Riddley and Deneys Schreiner also read and criticized parts of the thesis. Many thanks for them all.

Dr. C.R. Clayton lent me the pair of local axial strain transducers used here. They were important to verify some ideas and results. My friend and colleague A.V. Bica gave me much advice on the use of Hall sensors.

Dr. R. Jardine shared his enthusiasm and gave me strong encouragement with my work on external measurements of axial strain.

Prof. J. Burland provided the initial contacts with Prof. A. Anagnostopoulos (NTUA) with whom the cooperative research described in Chapter 8 was established.

Dr. D. Potts and Dr. D. Toll provided the computational support for data acquisition and test calculations. Dr. Potts' help was crucial during my two weeks crash course (after the hard disk crashed). Thanks a lot David.

Lou Spall and Steve Ackerley provided the ideal conditions for the experimental work. Lou's patience and constant willingness to make yet another modification on the top cap kept me trying. I learnt a great deal about intrumentation with Steve. We worked closely in many occasions and it always proved fruitful.

The author has been sponsored by CAPES (a Brazilian government agency) and Universidade Federal do Rio Grande do Sul. The author also received an ORS grant (UK).

CONTENTS

1. INTRODUCTION

1.1 THESIS BACKGROUND

The study described here developed as a continuation of the work on artificial residual soils, initiated by Maccarini (1987), under the supervision of Prof. P.R. Vaughan. They developed an artificial soil which could simulate a natural one to overcome the problems associated with sampling and testing of residual soils (sampling disturbance, variability of samples and unknown stress history). The main advantage of this idea is that it allows the production and testing of a number of samples of great similarity. The success of the technique allowed many interesting conclusions to be reached on the stress-strain behaviour of bonded materials as discussed by Vaughan, Maccarini and Mokhtar (1988) and Vaughan (1988).

The emphasis of this work has been the influence of the bonding on the mechanical behaviour of different materials at confining stresses up to 3.5 MPa. Almost all of the triaxial tests were carried out under fully saturated conditions, with no soil suction present, making the interpretation of the test results in terms of effective stress straightforward. Although the influence of suction was not studied it has been measured for the Kenyan residual soil and is thought to interfere with the field behaviour of the Corinth Marl.

1.2 SCOPE OF THE WORK

A total of eighty five triaxial soil samples were tested comprising a soft rock, a residual soil and various artificial soil mixtures. The presentation of their results has been separated into chapters on subject and on materials.

It is well known that there is a large difference between the stiffness determined in-situ

and that calculated from laboratory tests. This is particularly so for residual soils. A series of tests were carried out to identify the causes of such differences and the results and conclusions obtained are described in Chapter 3. A modification of the top-cap and load cell arrangement was adopted following these studies and used throughout the thesis.

The work associated with the artificial soil had as a starting point the study of the influence of creep. Chapter 4 describes the results gained to observe this influence as well as the effect of the method of saturation (back-pressure or vacuum dry) and stress uniformity in the sample. The tests described there had no local axial strain measurements such as were used in later tests.

A series of tests were performed on the artificial soil taking into consideration the conclusions of Chapter 4, i.e., all samples were saturated with dry vacuum method and the new loading arrangement was used. Chapters 5 and 6 describe the results of this new series for the artificial soil at two different void ratios. The strength, yield curves and stiffnesses are examined.

A high pressure cell, a controller for pressures of up to 3.5 MPa and a radial belt for measuring the radial strain of triaxial samples which were developed during the work are also described in Chapter 6.

In Chapter 7 additional tests on other compositions of the artificial soil are presented and compared in terms of strength, yield curves and stiffnesses.

The test results of a soft rock from the Corinth Canal are presented in Chapter 8 including some tests carried out in Greece following an agreed programme between Imperial College and Prof. A. Anagnostopoulos, from the National Technical University of Athens.

The results of permeability tests together with the compressibility and shear strength from triaxial tests on a residual soil from Kenya are presented in Chapter 9.

Finally, Chapter 10 contains the discussion of results and a summary of the main conclusions of the thesis.

2. LITERATURE REVIEW

The behaviour of bonded materials has been studied at Imperial College for some time, under the supervision of Prof. P.R. Vaughan. Most of the conclusions that have been obtained are described on papers presented in two international conferences on tropical soils and international journals (Vaughan, 1985, 1988; Vaughan et al., 1988; Leroueil & Vaughan, 1990).

This chapter will cover the subject of bonded materials in general, leaving specific subjects for the chapters where the topics are analysed in more detail, particularly in the case of the artificial bonded soil and the Corinth Marl.

The presence of cementation or bonding in rocks has been recognized for a long time. The possession of tensile strength, and of an unconfined strength higher than usual in soils are, perhaps, its most evident indications. For one particular type of rock, e.g. sandstone, the cementation between grains and the grain size and packing pattern influences markedly the rock strength and stiffness (Brady & Brown, 1985).

Bonded soils, on the other hand, have for the most part been treated as special cases because they do not fit the classical model of behaviour developed for sands and sedimentary clays. In such models the soil void ratio and previous stress history alone are considered to control their behaviour. However, it will be shown that bonded soils can surpass these predictions.

A review of the literature shows that bonding or cementation is more common than is usually anticipated presenting itself in a large range of materials, i.e., soft clays, sands, residual soils and soft rocks. The recognition of the similarities in behaviour between these materials was made in a comprehensive paper by Leroueil & Vaughan (1990). In it the authors described the combined effect of grain arrangement and bonding as structure. This structure can be destroyed by remoulding the soil, which typically affects the strength and the behaviour during one-dimensional consolidation. An example of such a remoulding effect for two clays is

shown in Fig. 2.1. It was also observed that the clays had a yield curve associated with their structure which is centred more or less around the stress path for one-dimensional consolidation (or K_0 line).

The influence of the bonding is made very clear when the void ratio is high. This was the case for a weak volcanic mudstone from Japan (Ohtsuki et al., 1984). Its initial void ratio was 1.40 and the "apparent" pre-consolidation pressure was 5 MPa. Triaxial test results obtained in this mudstone are presented in Fig. 2.2(a) and (b) and the yield points are shown in (c). The yield curve obtained indicates a degree of anisotropy.

A number of soft rocks also show yield when loaded above certain stress levels. The loading of a silo in chalk (Burland & Baylis, 1989) showed a marked yield in the plot of applied pressure at the surface versus deformation (Fig. 2.3).

Another large group of materials which present structure is residual soils. They are widespread in areas of high rainfall and high average annual temperatures, often being present in layers of varying thickness in tropical and sub-tropical areas. These soils are the product of in-situ weathering which tends to reduce their density while still retaining some of the original structure of the parent rock. More advanced weathering may recement this soil in laterites. Their general behaviour is similar in many cases presenting a strong influence of the bonding. No relation seems to exist between the virtual pre-consolidation pressure[1] and stress history or void ratio. Both soils will be examined here under the loose term of residual soils.

Vargas (1953) already recognized the influence of structure in residual soils and suggested that the one-dimensional test on the intact sample compared with the remoulded soil would give the results of Fig. 2.4.

This sketch fits well to the data obtained by Wesley (1974) on a residual soil from Java (Fig. 2.5). The undisturbed soil is initially stiffer than the remoulded one and it can maintain much larger pressures than the remoulded soil for the same void ratios.

[1]The use of the word apparent, or "virtual" as proposed by Vargas (1953), refers to the effect of bonding while the usual definition refers to the maximum vertical pressure which acted upon the soil in the past.

Residual soils show yield surfaces associated with their structure. Yield surfaces from three residual soils are presented in Fig. 2.6. They were obtained from a number of tests and represent a range of materials: a volcanic agglomerate from the Canary Islands (Uriel & Serrano, 1973); a residual soil from gneiss, Brazil (Sandroni, 1981) and a residual soil from basalt, Mauritius (Maccarini, 1987). The yield curves defined for each are centred on the isotropic line, indicating an isotropic structure.

Leroueil & Vaughan (1990) used most of these examples to show that the bonded materials have many similarities. In particular they show the close comparison that can be made between a triaxial test on a soft clay (Saint-Vallier clay) and one on a soft carbonate rock (oolitic limestone, Bath stone, e=0.23 to 0.37, σ_c=23 MPa, Elliott & Brown, 1985) (see Fig. 2.7). All tests were drained compression following isotropic consolidation. At low confining pressures the failure is abrupt and the peak strength is due to structure and coincides with yield. The materials are brittle and dilatant but the dilatancy occurs only after the peak strength had been reached. For high confining pressures the material is stiff until the yield is reached. This yield is well below the stress level which the samples can withstand without failure. The maximum stress requires a large axial deformation associated with large volumetric compression of the sample.

Another aspect emphasized by Leroueil & Vaughan (1990) relates to the behaviour of structured materials when loaded in one-dimensional compression (K_0). The stress-paths resulting from such tests in four structured materials are reproduced in Fig. 2.8. The set again includes a soft clay, and two rocks in addition to the artificial soil developed by Maccarini (1987) and used in this thesis. The stress-paths show an initial steep phase which approaches the failure envelopes defined for each material. The yield then occurs, the compressibility increases and the stress path changes direction.

In a study of chalk samples from various sites in England, Ledra (1990) performed one-dimensional tests on samples with different initial void ratios. The stress paths of tests in three samples are shown in Fig. 2.9(a) and the respective compression curves in Fig. 2.9(b).

The general format of the stress-paths is again similar to that obtained in other bonded materials. The curves tend to approach a unique stress-ratio at high stresses [Fig. 2.9(a)] and the yield point is associated with the start of larger compressions. The data also indicates clearly that the yield stress increases with increasing density and that the void ratio - effective stress curves tend to a unique line. This dependence of the yield stress on the initial void ratio was well established in chalk with results obtained by Jones and his co-workers (Fig. 2.10, Jones & Preston, 1987).

Goldsmith (1989) presented another example of the yield in K_0 compression tests and its influence on the structure. Testing sandstones (in K_0 tests) he measured the vertical permeability of the sample at different stress levels. His results showed once more the same stress path trends. The permeability measurements indicated a considerable change once the yield stress had been reached (Fig. 2.11).

Using these observations about the yield stress Leroueil & Vaughan (1990) proposed that the yield curve may be divided into three zones (see Fig. 2.12). The yield can be caused by shearing when the failure envelope and the yield coincide at low confining stresses (test 1, Fig. 2.7); a compression yield will be caused when the value of average stress s' equalizes the structure admissible level, i.e., the stress level that the soil can only sustain because of bonding, as happens with a triaxial test at high confining pressure (test 3, Fig. 2.7); the swelling of expansive minerals when effective stress is reduced may cause enough volumetric strain to cause yield of a bonded structure. The latter has been shown to occur in the heavily over-consolidated London Clay when allowed to swell to isotropic pressures below 275 kPa (Webb, 1966; Leroueil & Vaughan, 1990).

The complete yield curve represented in Fig. 2.12 may not be present in all soils and the orientation and shape of it may change. The swelling yield may not be present in some materials if their swelling is not large enough to break the bonds. The yield curve may have different shapes and a prismatic example was found on Labrador Clay by Sangrey (1972) (see Fig. 2.13).

The destruction of the bonded structure requires considerable straining and is not achieved immediately after the main yield. The progressive loss of tensile strength on samples loaded to different strains was studied by Maccarini (1987) for the artificial soil (Fig. 2.14). Around 5% volumetric strain was necessary to destroy the available tensile strength of that soil.

A natural cause of loss of structure, as defined by Leroueil & Vaughan (1990), is weathering. Chemical weathering can reduce the material strength and increase its compressibility. Typical examples are given by Chandler (1969) and Kimmance (1988). The latter author carried out a comprehensive testing programme of the weathered granites from which the white kaolin known as China Clay is produced. The strength envelopes obtained from direct shear tests on materials with different degrees of weathering are shown in Fig. 2.15. He obtained a good correlation between the strength parameters and mineralogical indices that indicated the degree of rock weathering.

The existence of bonding can be verified by the use of tensile tests. They have been made in a number of the materials described here and the value of tensile strength is usually relatively small. The artificial soil had tensile strengths of 2.8 kPa (e=1.6) and 5 kPa (e=1.2) when tested saturated in diametrical compression (Maccarini, 1987). Drained tensile tests done on the Labrador Clay showed values of 7 kPa (Sangrey, 1972). Bishop and Garga (1969) measured values of 26-33 kPa in drained extension tests on London Clay and these values agree with the strength envelope obtained from compression tests (Fig. 2.16) on similar samples. In the same figure they also show the effect of remoulding in the behaviour of the clay in compression tests.

Small values of tensile strength can produce small cohesion intercepts (c') on the failure envelopes of the materials. This has a great influence on the stability of slopes as can be seen in Fig. 2.17 (Vaughan, 1988). This is supported by field evidence of steep slopes (sometimes vertical) cut in tropical soil that could be described as a clay (Wallace, 1973 among others).

In order to classify the residual soils according to their compression potential, Vaughan

(1988) introduced the definition of relative void ratio, e_R , as

$$e_R = \frac{e - e_{OPT}}{e_L - e_{OPT}}$$

where the soil natural void ratio (e) is compared with the void ratio at the plastic limit using the maximum soil density obtained from a standard compaction test (e_{OPT}), as a datum. Examples are given in his paper showing that for high relative void ratios the soil compressibility is high, whereas if the value is negative (natural void ratio is smaller than at its plastic limit), the compressibility is quite small (Fig. 2.18).

The general soil behaviour can be studied with results of one-dimensional tests in natural and remoulded samples (Fig. 2.19(a), Vaughan, 1988). The one-dimensional compression line of the remoulded soil will generally be parallel to the critical state line. Zones 1, 2 and 3 are defined as void ratio - stress combinations at which soils will show different behaviours during further loading. In zone 1 the soils show a stiff behaviour and no tendency to liquify. If the soil is, however, in zone 3, the post-yield behaviour will be very compressible and large pore-pressures can be generated during undrained loading. Zone 2 represents an intermediate behaviour. An example of the use of such a plot is given in Fig. 2.19(b) for the artificial residual soil. Unconfined drained shear strengths are marked on the curves. The large variation of compressibility only happens in zone 3. The yield stress is also dependent of the void ratio of the sample.

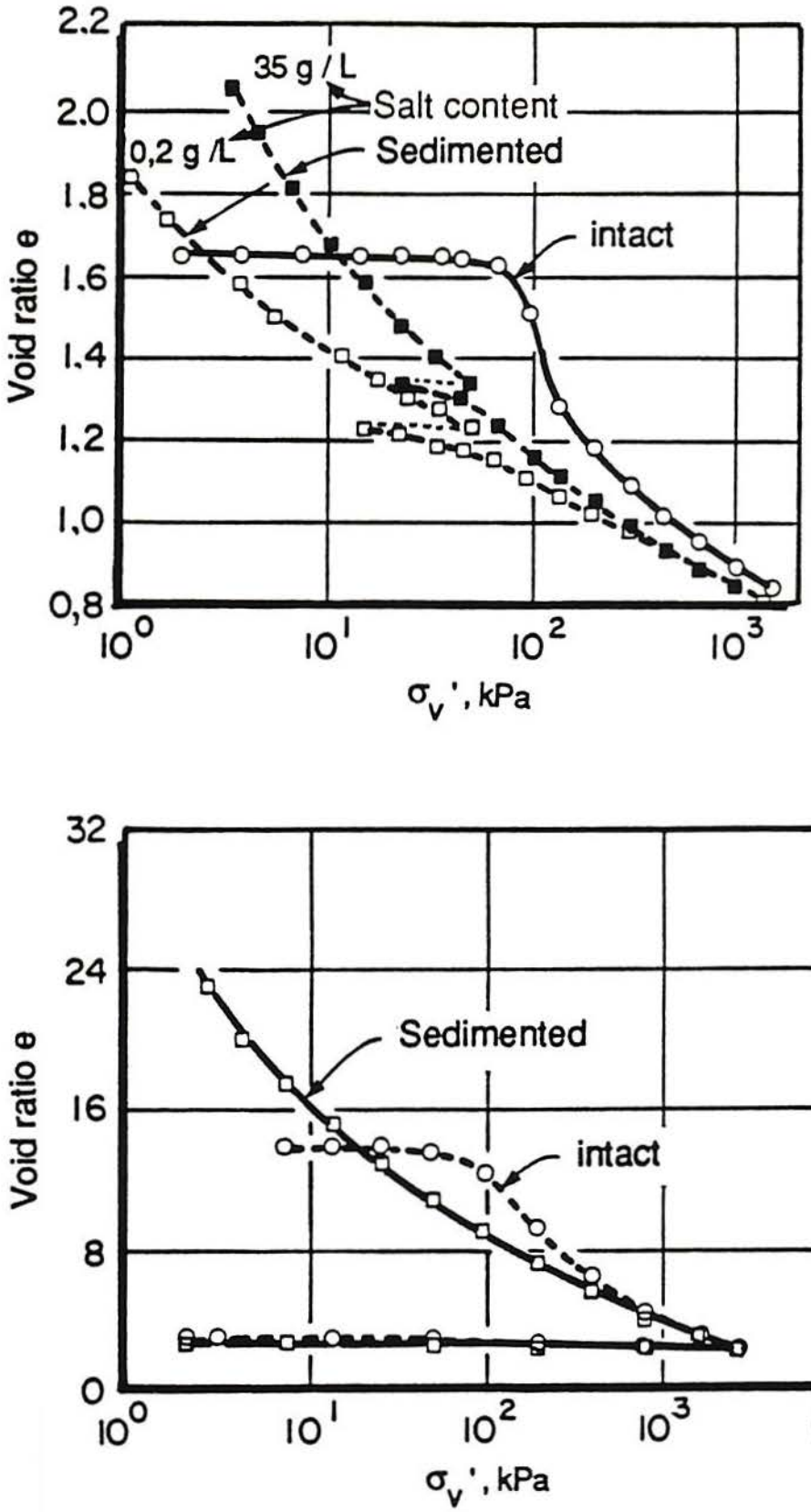

Figure 2.1 – One-dimensional behaviour of two natural clays after remoulding (after Leroueil & Vaughan, 1990)

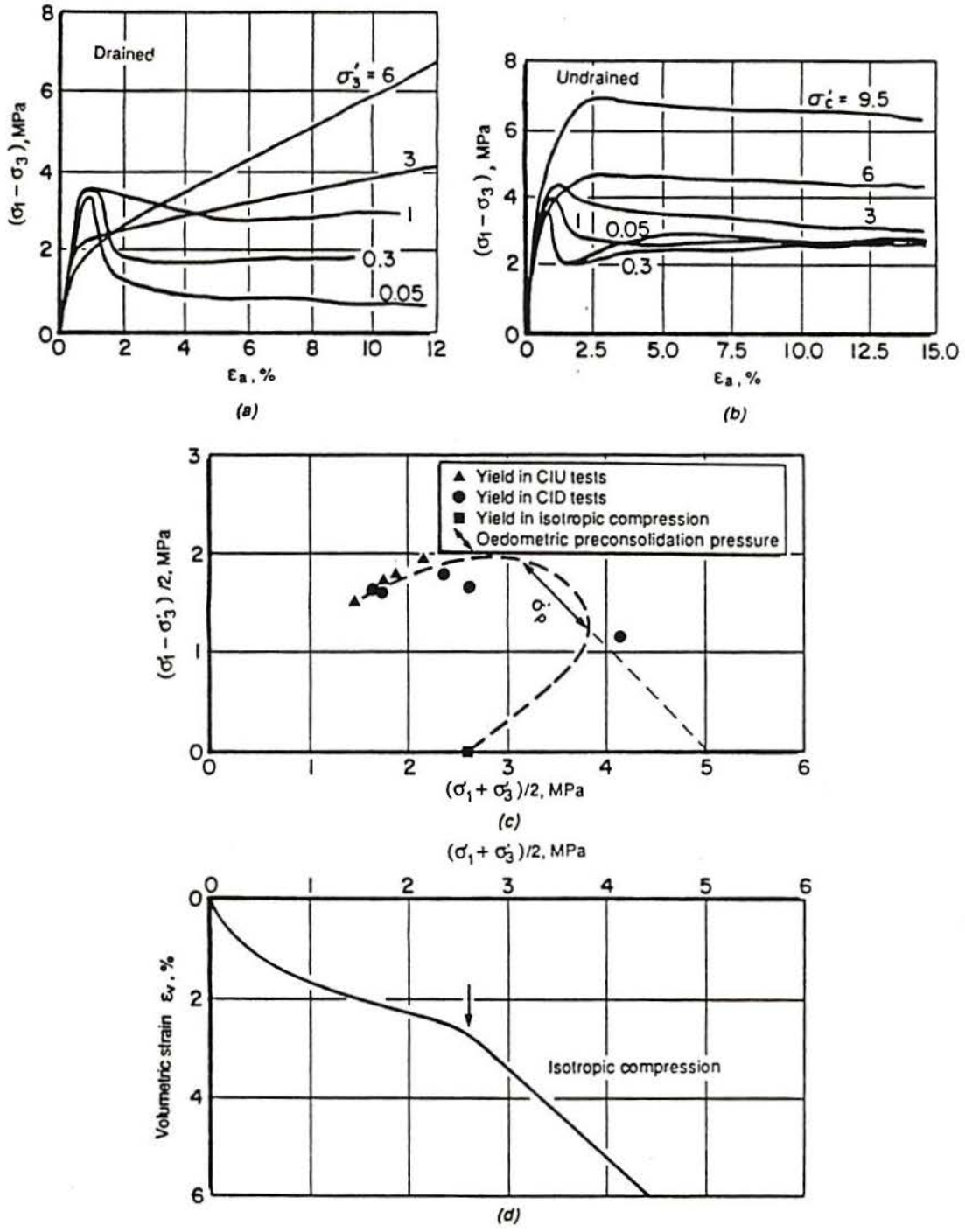

Figure 2.2 – Triaxial test results and yield of a silty mudstone from Japan (Ohtsuki et al., 1981)

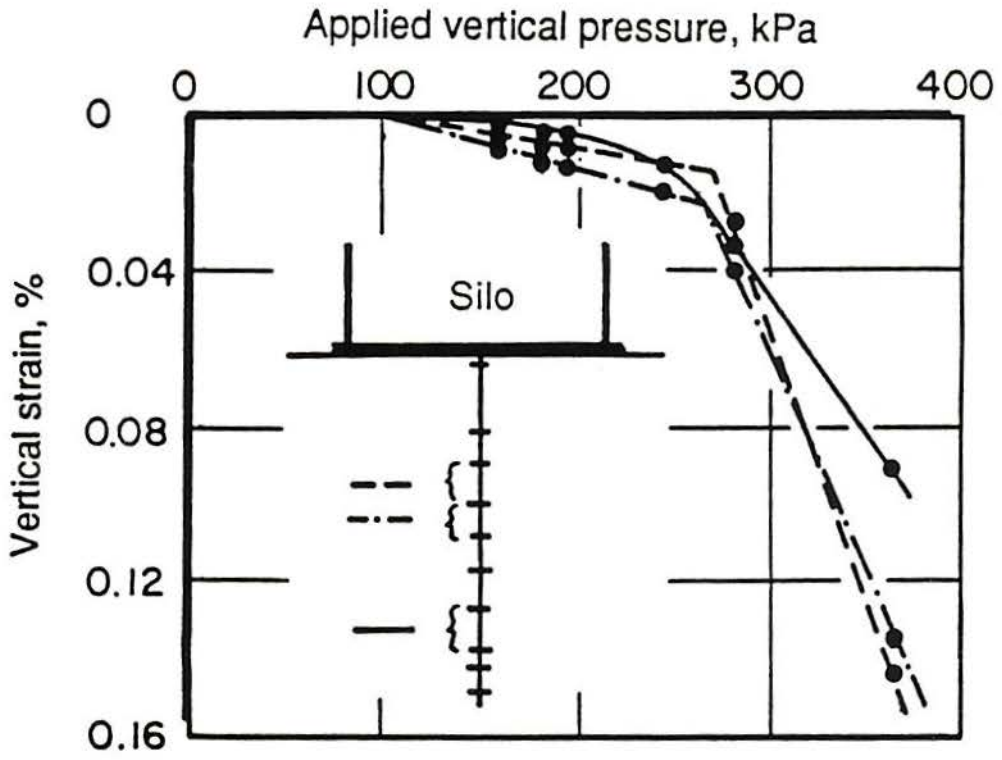

Figure 2.3 – Stress-strain behaviour of chalk under a silo foundation (after Burland & Baylis, 1989)

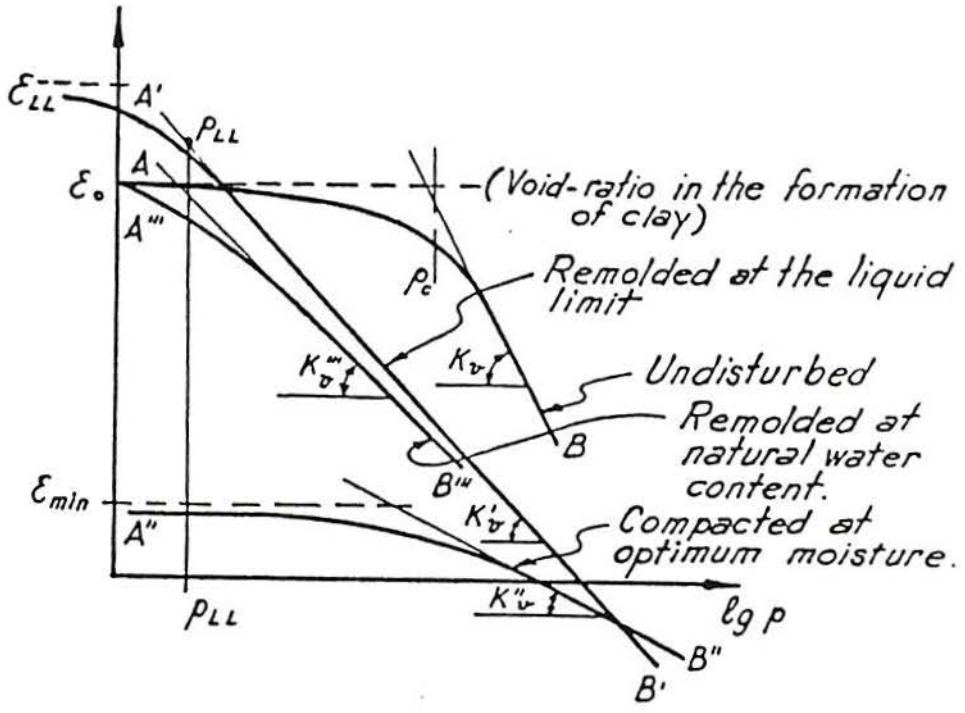

Figure 2.4 – One-dimensional test results on residual soils (after Vargas, 1953)

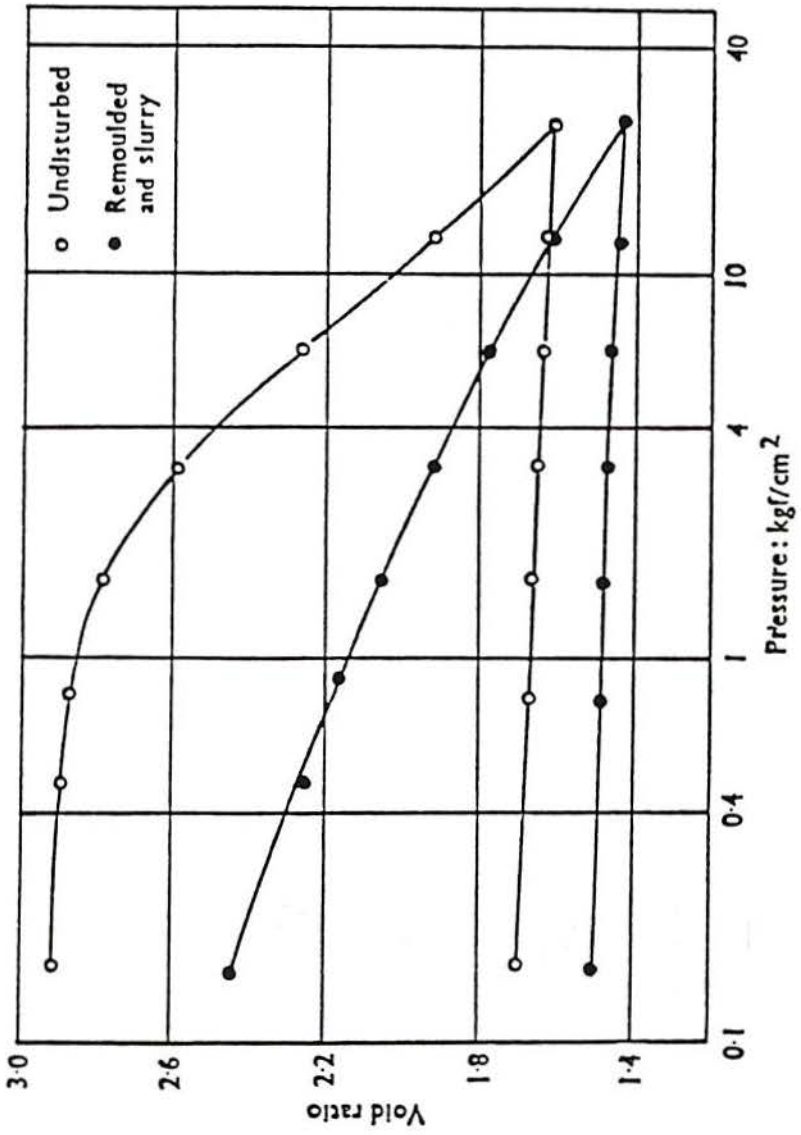

Figure 2.5 – One-dimensional compression tests on a residual soil from Java (after Wesley, 1974)

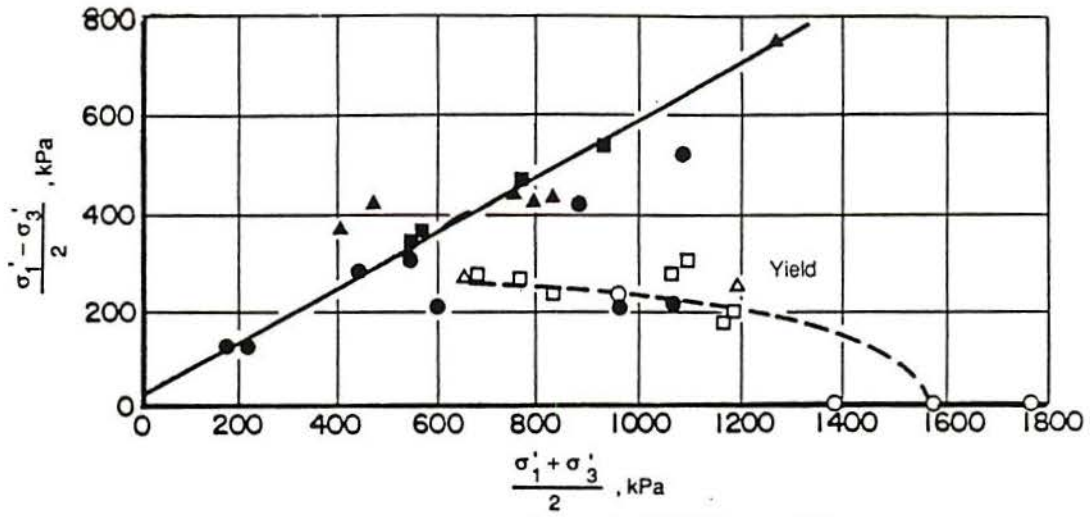

a) Volcanic agglomerate (Uriel & Serrano, 1973)

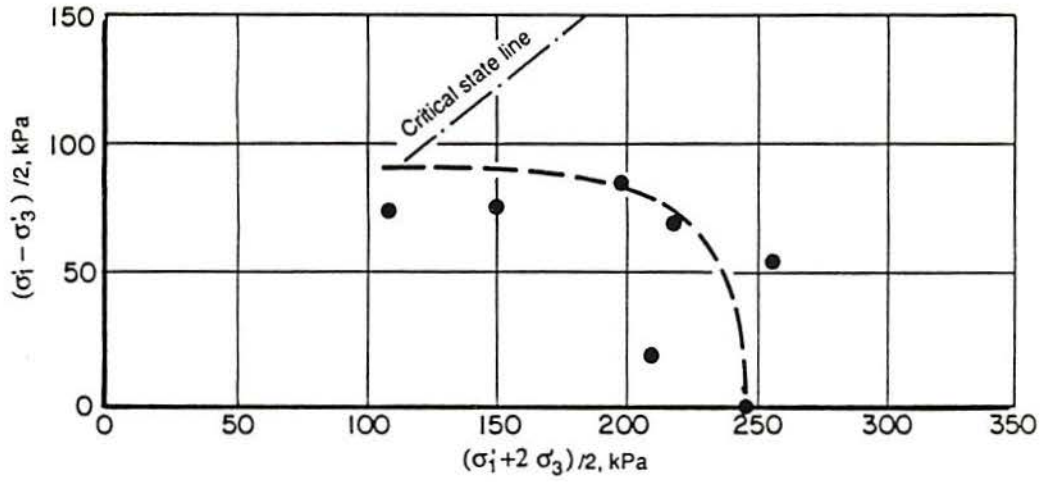

b) Residual soil from gneiss (Sandroni, 1981)

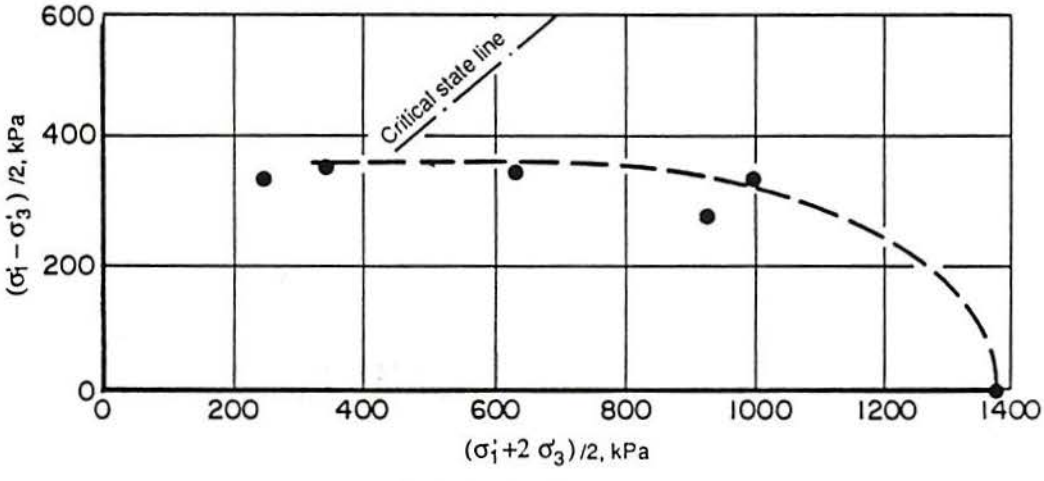

c) Residual soil from basalt (Maccarini, 1987)

Figure 2.6 – Yield curves from three structured materials (after Leroueil & Vaughan, 1990)

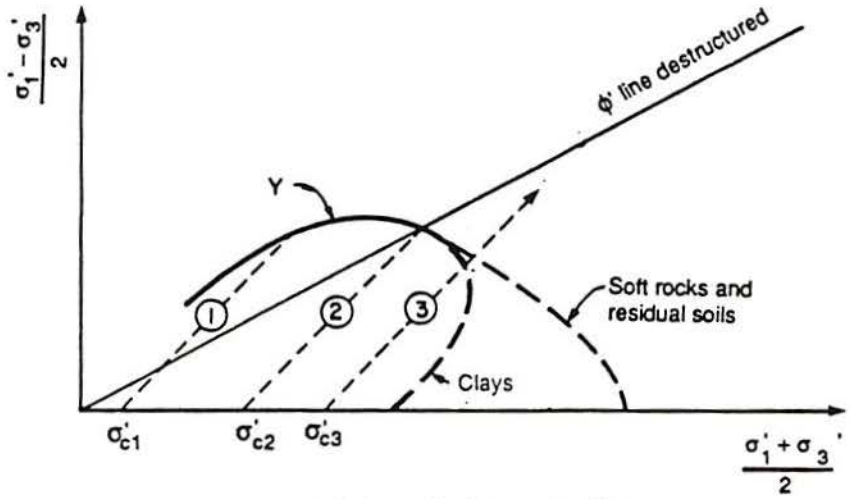

a) Schematical stress paths

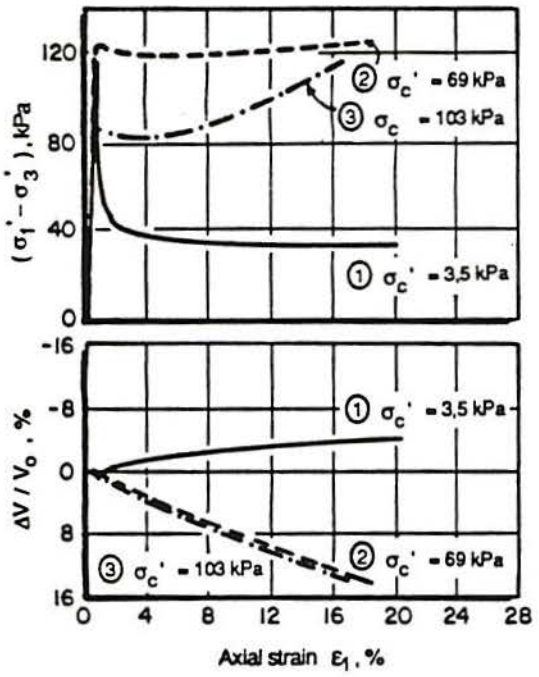

b) Stress-strain curves for Saint-Vallier clay (from Lefebvre, 1970)

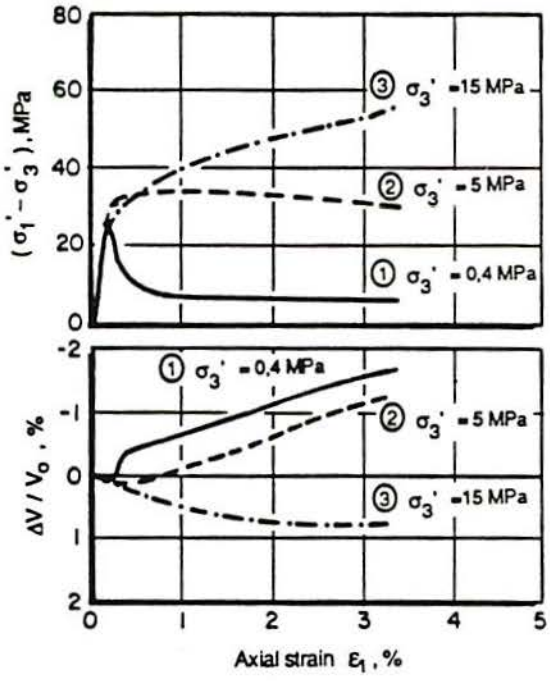

c) Stress-strain curves for a soft, high porosity, oolitic limestone
(from Elliott & Brown, 1985)

Figure 2.7 - Results of triaxial drained tests on two structured materials (after Leroueil & Vaughan, 1990)

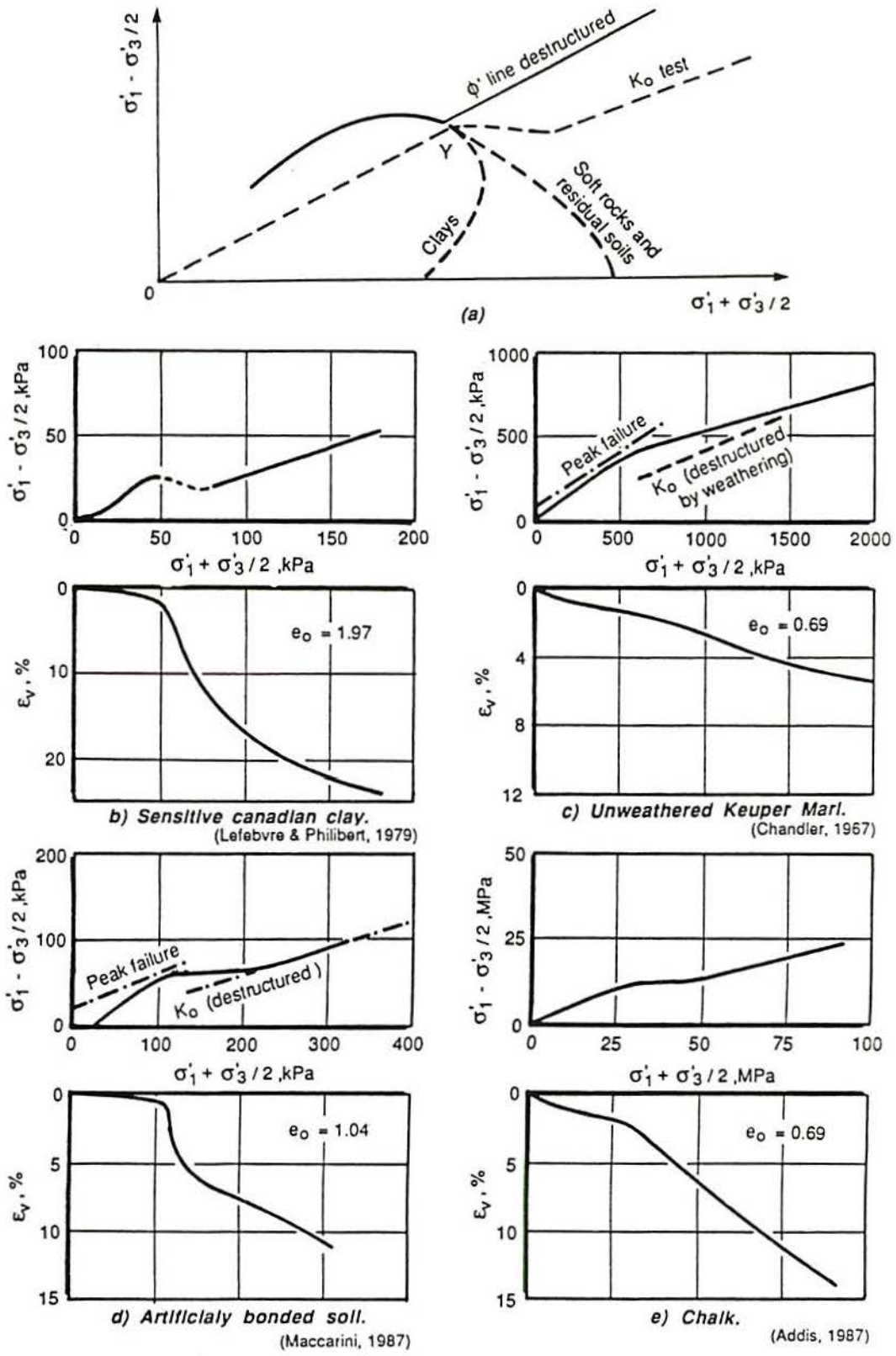

Figure 2.8 – Results of one-dimensional tests on structured materials (after Leroueil and Vaughan, 1990)

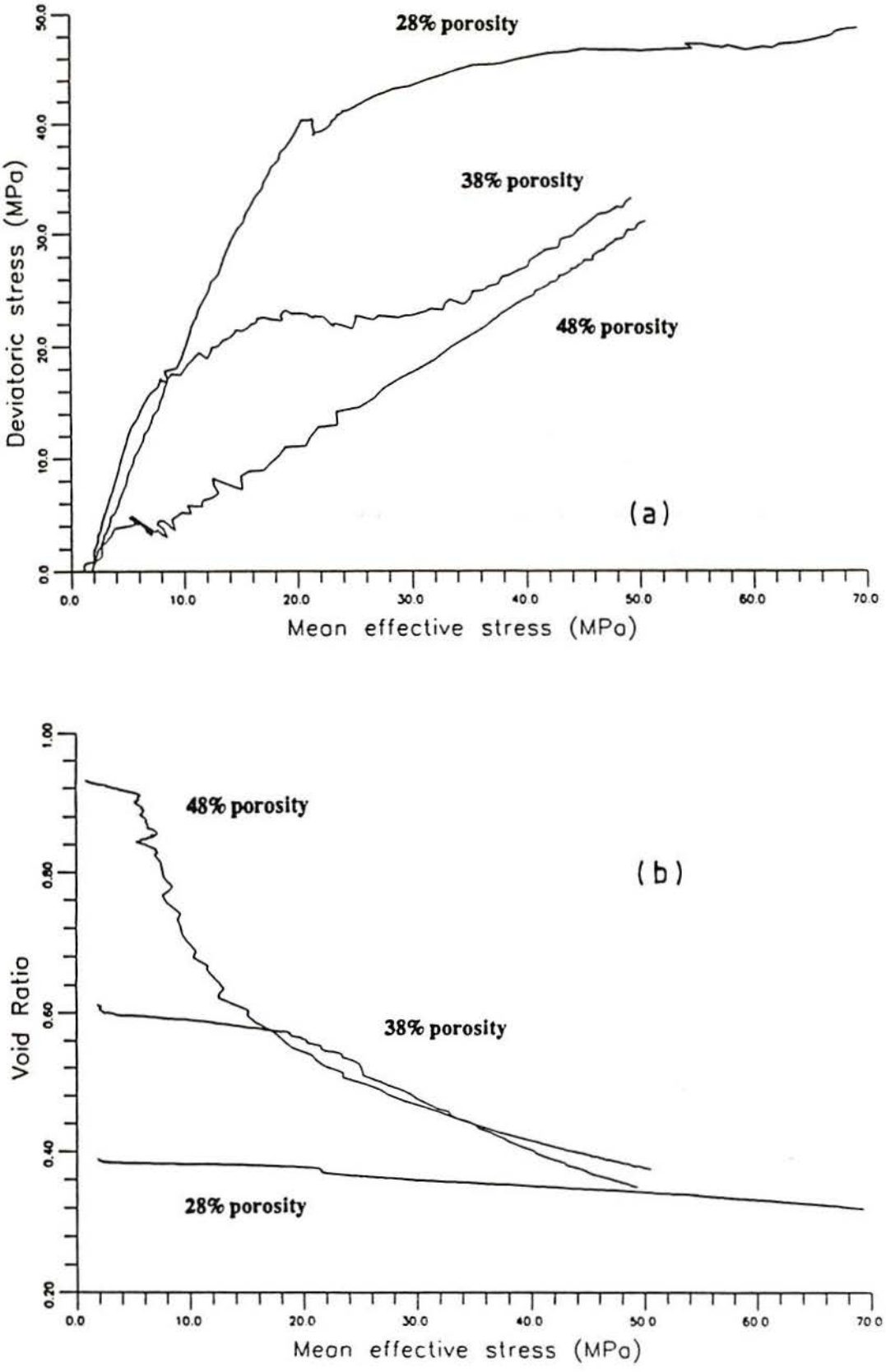

Figure 2.9 – One-dimensional compression tests on chalk (after Ledra, 1990)

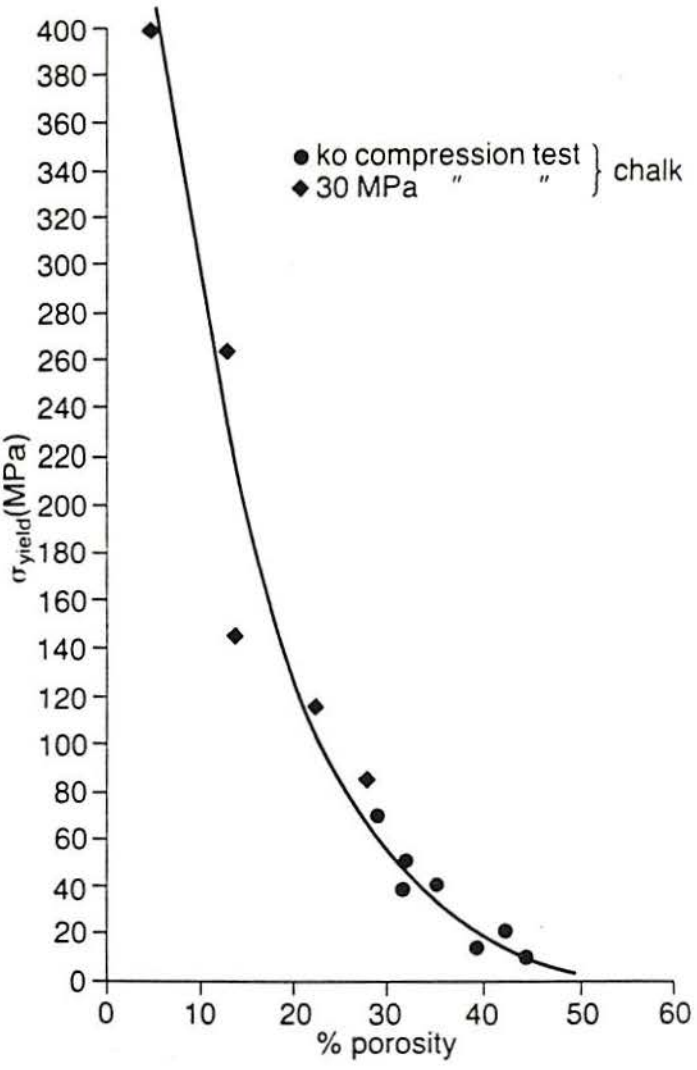

Figure 2.10 – Variation of yield stress with porosity in chalk (after Jones & Preston, 1987)

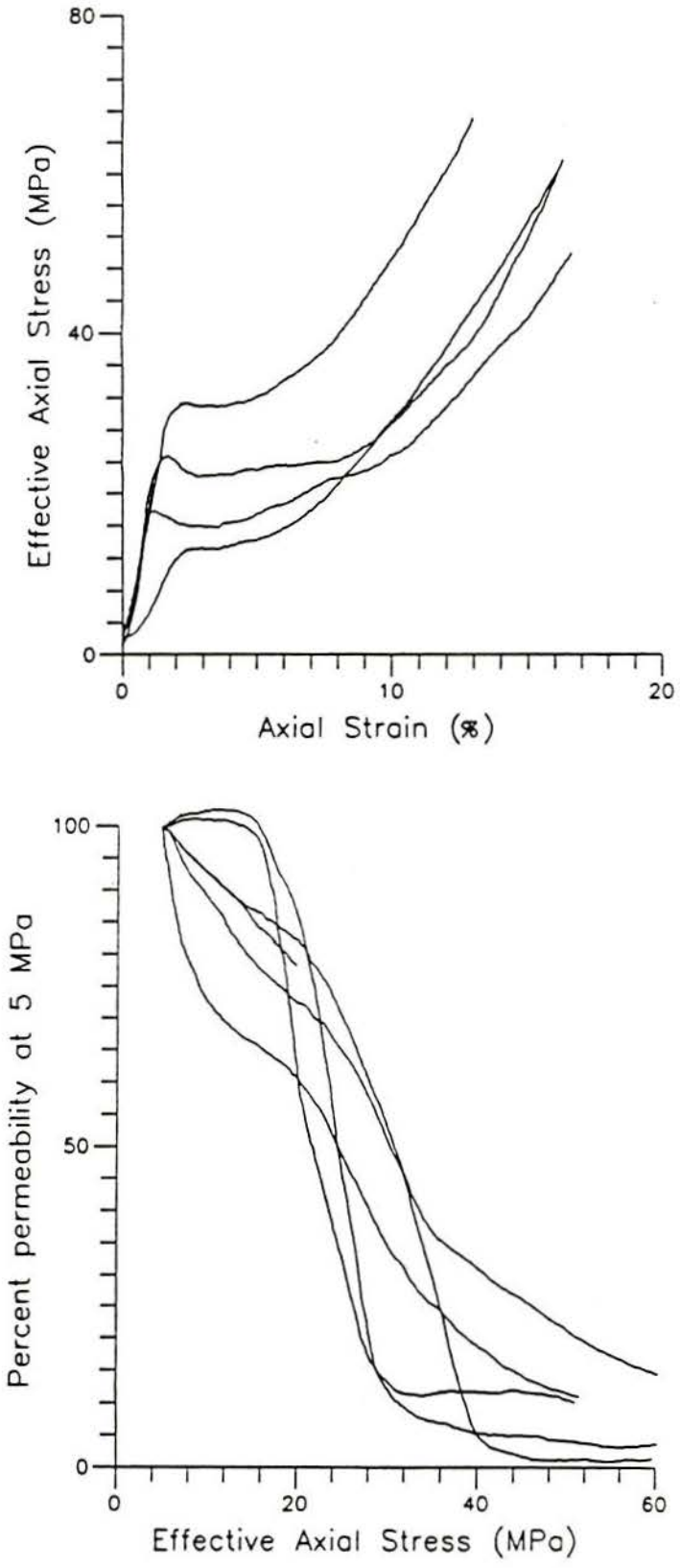

Figure 2.11 – One-dimensional tests on sandstones and associated permeability variation (after Goldsmith, 1989)

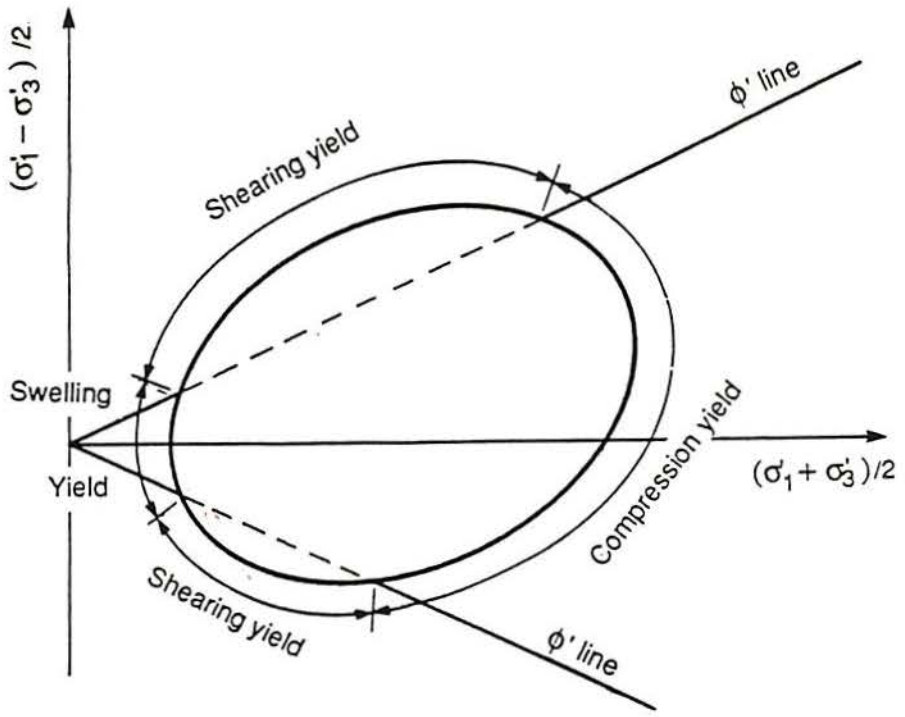

Figure 2.12 – Schematic zones of yield of structured soils (after Leroueil & Vaughan, 1990)

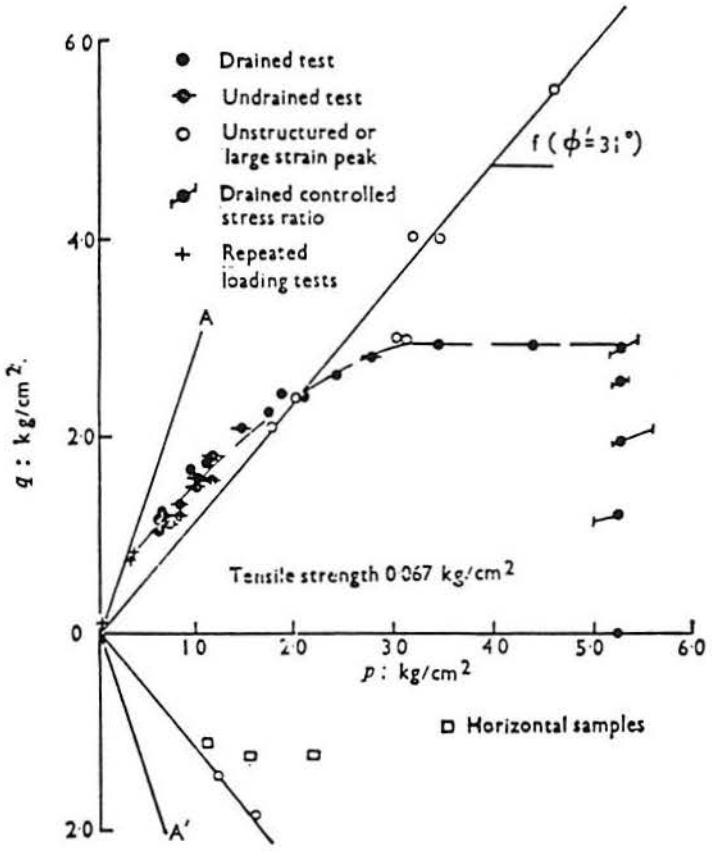

Figure 2.13 – Yield curve for Labrador clay (after Sangrey, 1972)

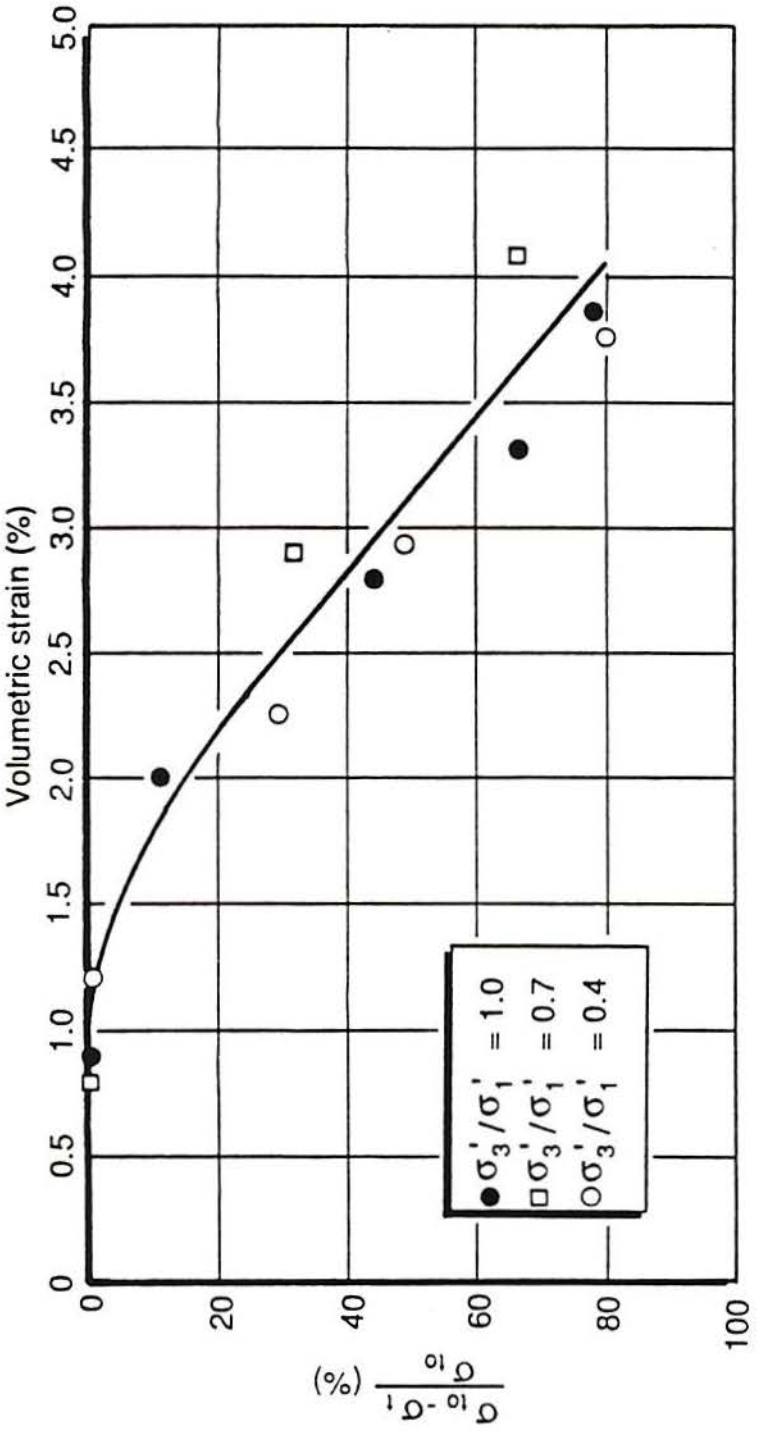

Figure 2.14 - Loss of tensile strength with volumetric strain in the artificial soil (after Maccarini, 1987)

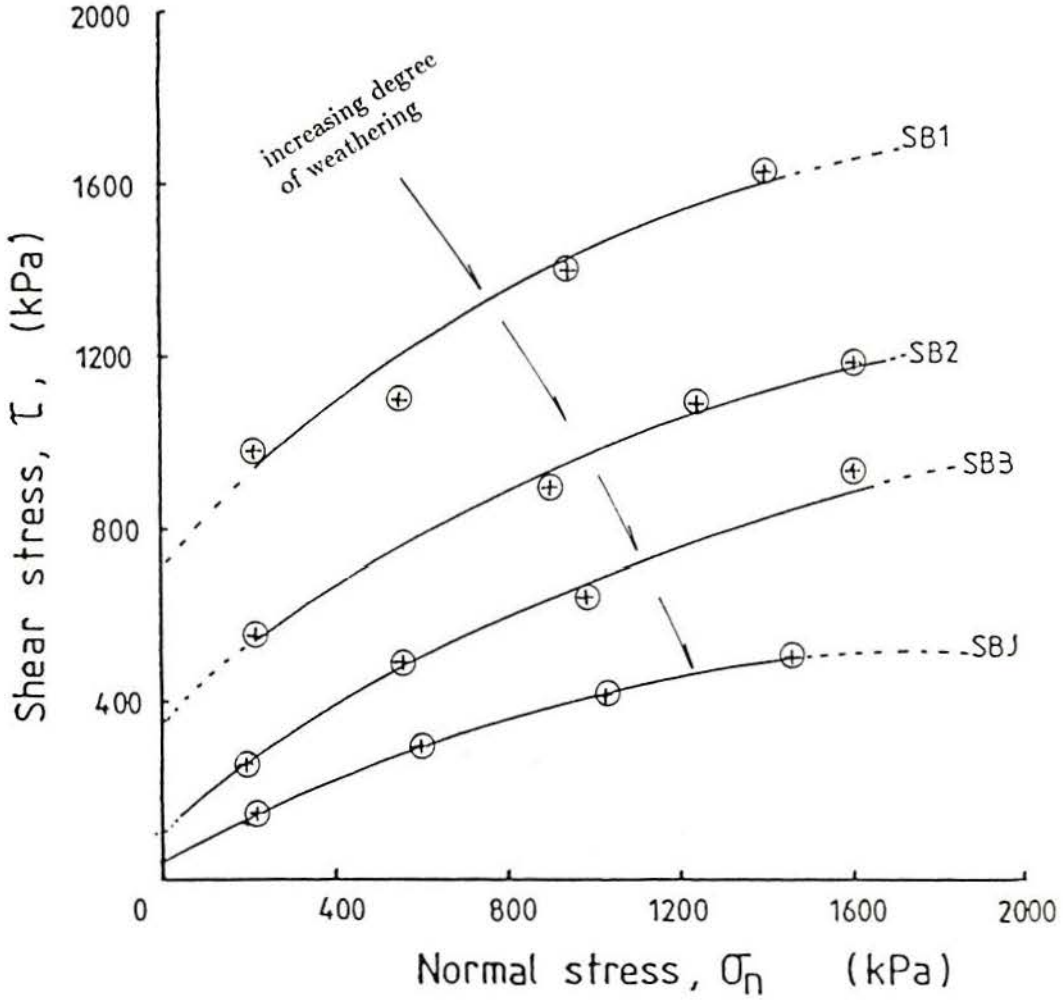

Figure 2.15 – Shear strength envelopes for different degrees of weathering of granites (after Kimmance, 1988)

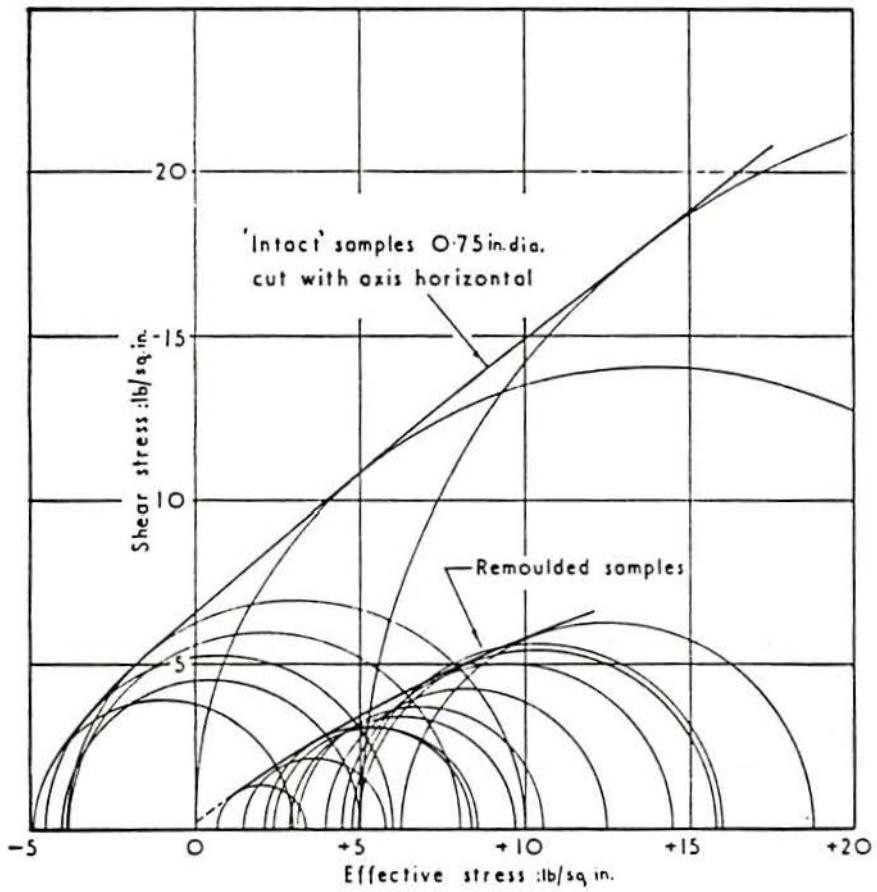

Figure 2.16 – Triaxial test results on London Clay (after Bishop & Garga, 1969)

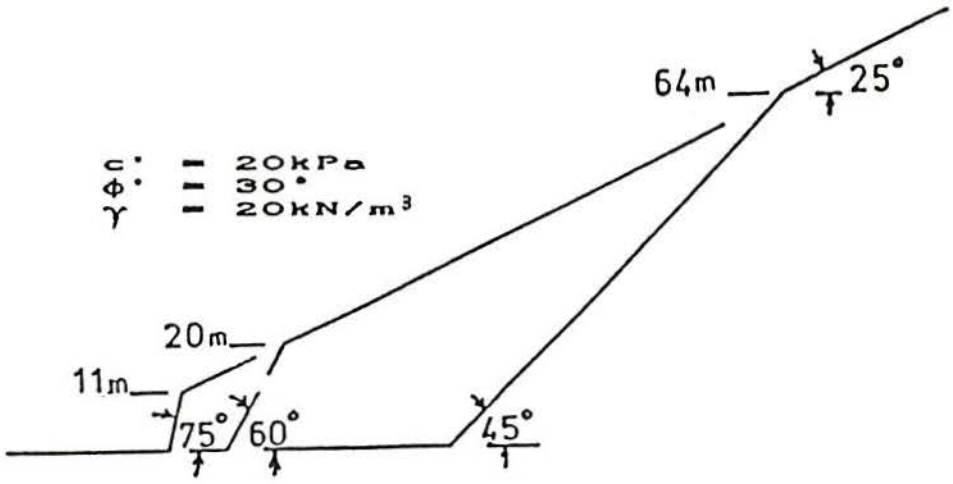

Figure 2.17 – Influence of cohesion on the drained stability of slopes (after Vaughan, 1988)

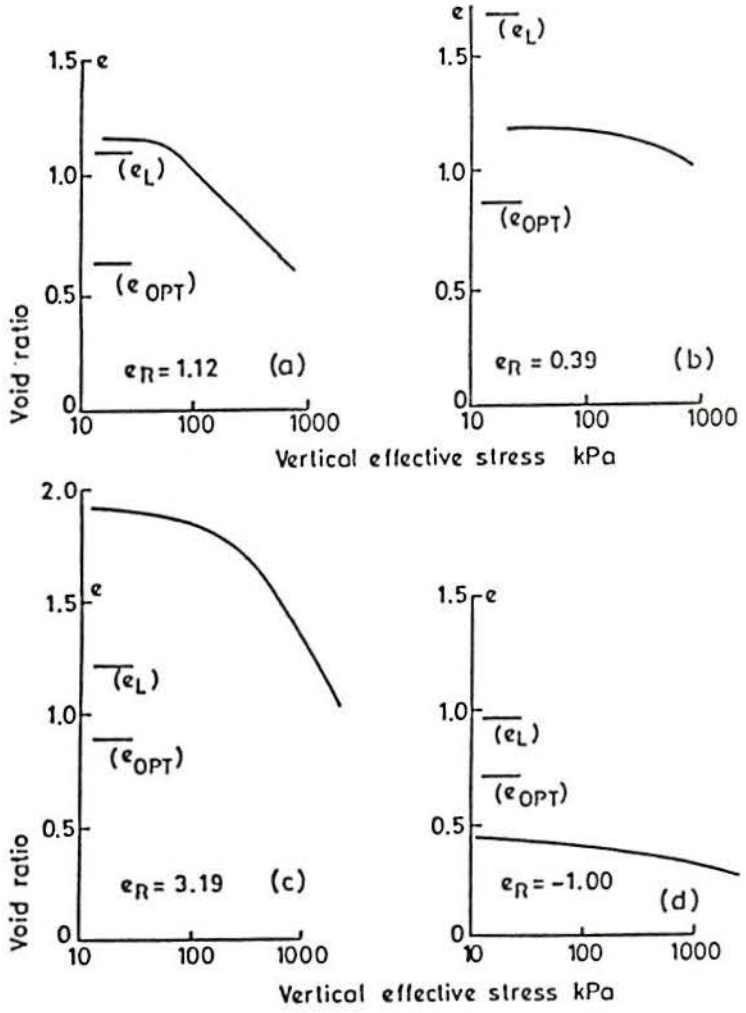

Figure 2.18 – The use of relative void ratio in some tropical soils from Brazil (after Vaughan, 1988)

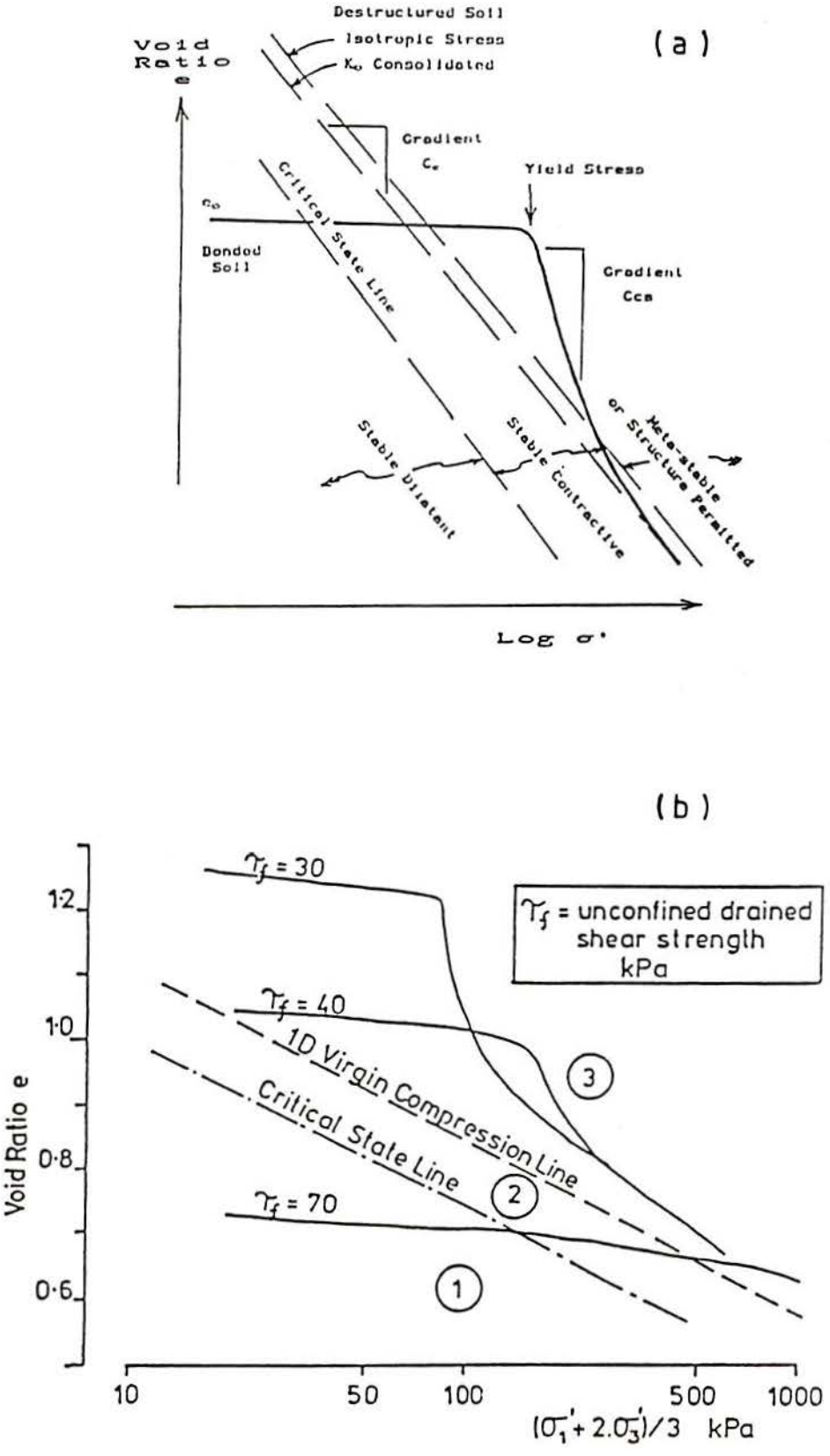

Figure 2.19 – One-dimensional compression of structured soils (*a*) hypothetical behaviour: (*b*) results of artificial soil (after Vaughan, 1988)

3. MEASUREMENT OF SMALL AXIAL STRAINS IN THE TRIAXIAL TEST

3.1 INTRODUCTION

In the past ten years some work has been carried out in measuring accurately small axial strains (say, less than 0.5%) in the triaxial test. Most of this work has been done at Imperial College. The experimental evidence seems to indicate that large errors occur when the classical determination of axial strain is made. This procedure uses the displacement of loading ram measured externally. The author has tried to determine what are the causes of such errors. Different experimental arrangements were used and different soils were tested. The results and conclusions are presented here. Some of the tests will be discussed only in terms of their stress-strain curves; later on they will be referred to in relation to other tests using the same material. This chapter condenses the work of several months and overlaps information given in other chapters which follow a chronological order. A paper was submitted in 1989 to the Geotechnical Testing Journal, ASTM, based on this subject.

Three materials were used in the tests: the artificial soil described in this thesis, remoulded reconsolidated London Clay and a soft rock (marl) from the Corinth Canal region, Greece.

All of the tests were performed on samples 38 mm diameter by 76 mm height and all were triaxial compression tests starting from isotropic conditions.

Three kinds of local transducers were used: the electrolytic device described by Burland and Symes (1982); a similar mechanical arrangement but with a strain gauged sensitive pendulum (Ackerley et al., 1987); and the device based on the Hall effect (Clayton and Katrush, 1986).

3.2 SUMMARY OF PREVIOUS WORK

The use of transducers fixed directly to the sample to measure deformations has for some time been a common technique in rocks and structural materials (e.g. steel and concrete). In soils, however, this technique has been applied only for the last 15 years. Brown and Smith (1974) described the use of local instrumentation on samples of asphalt.

Daramola (1978) used two small linear variable displacement transducers (LVDT) measuring between the pedestal and different positions on sand samples. He used these measurements to calculate strains over different lengths of the sample [Fig. 3.1(b)]. The results show large differences between the strains determined using the local transducers at the middle portion and the strains determined from external measurements [Fig. 3.1(a)]. Comparing the external and the central strains he noticed that the errors were smaller on denser samples although there was significant scatter between tests. Higher isotropic consolidation stresses did not produce any appreciable reduction in the average errors. Initial errors at about 0.1% of strain could be as high as 90% (i.e. the external measurement being 0.19%) and "probably not less than 30%".

There was, however, a substantial reduction in the average errors for anisotropically consolidated tests. In some cases, the average error at 0.1% strain "was almost negligible" (Daramola, 1978, pp 144-145). The axial strains in the middle of the sample were used as the reference to calculate errors.

Costa Filho (1980) carried out a series of tests on undisturbed London Clay, using three similar local transducers. The positions of the pins are shown in Fig. 3.2(b) and his results in Fig. 3.2(a).

In a paper published later (Costa Filho, 1985) he made a comprehensive review of the available literature and a summary of his own results. The main conclusion was that significant errors were involved in computing small strains by conventional techniques. He observed that in London Clay and sands the overall strains [ϵ_a in Fig. 3.2(b)] are affected by

the large displacements at the top of the sample while little or no bedding errors were observed at the bottom. However, generally, bedding was the main factor contributing to error (the same opinion has been expressed by Daramola and Vaughan, 1982).

A summary of previous results and additional tests on soft rocks (Upper Chalk) and reconstituted clay from the North Sea was presented by Jardine, Symes and Burland (1984). They extended the range of small strains down to 0.001%, using local transducers developed at Imperial College (Burland and Symes, 1982). A consistent set of axial contours were determined in special tests (Fig. 3.3). The axial strains obtained from the external measurements were sometimes an order of magnitude larger than the local ones, causing large differences in the calculated stiffness.

These studies have proved the great importance of using local strain transducers in order to obtain reliable soil parameters, especially stiffness. This work explained much of the apparent disparity between field behaviour and laboratory tests (Costa Filho and Vaughan, 1980; Jardine and Potts, 1988).

3.3 THE USE OF EXTERNAL MEASUREMENTS OF STRAIN

Although the results presented above seem to prove beyond doubt the difference between local and external measurements, the local measurements are only now being used in general commercial testing rather than just in research institutions. Most test results reported in the literature were obtained using the conventional external measurements of strain. In residual soil there is little precise data. Not surprisingly, large differences are reported between the in-situ and laboratory stiffness values (Lacerda, 1985 ; Sandroni, 1985).

Fig. 3.4 is an attempt to summarize the components which comprise the total external displacement from which the external sample strain is calculated in conventional triaxial equipment. The reference points for the displacement transducer readings are also shown. The

transducer is normally fixed directly onto a rigid beam connected to the loading ram and measures displacements relative to the pedestal.

3.3.1 Equipment deflection

This is the most obvious source of extraneous displacements. Although undesirable, it is relatively simple to take into account through careful calibration. The equipment deflection includes all displacements developed between the two reference points of the external measurements when a very stiff dummy sample (brass) is loaded. Therefore, it includes the deformation of load cell, top cap and porous stones at a specified effective confining stress.

The accuracy with which this can be done may be illustrated by some of the author's data. In the first attempt filter paper discs were incorporated as usual. Two confining pressures were employed and the calibration was carried out. Fig. 3.5 shows the results of the calibrations under different confining pressures (deviator stress, q, in the vertical axis as usual). The results show quite clearly that it is very difficult to use such measurements as a correction due to hysteresis and the large effect of the applied effective stress.

As the artificial soil is quite permeable ($k=10^{-6}m/s$) and does not tend to clog the porous stones, the filter papers are not necessary. So, new calibrations were carried out without them. The results obtained were very much improved. A comparison between the apparent strains measured when using filter paper and when calibrating without is shown in Fig. 3.6 (confining pressure of 60 kPa). Various calibrations were done with different confining stresses and the results were similar. Without filter paper the hysteresis was considerably reduced and the calibrations obtained were very much closer. The calibration curves had similar shapes with smooth curvature at small loads. The system as a whole has a tendency to become stiffer as the confining pressure increases due to the decreasing compressibility of the porous stones.

3.3.2 Other sources of spurious deformation

The removal of the filter paper considerably reduced the spurious deformation. However, the results obtained from soil tests were still poor. Two factors caused this: one is the true bedding that exists at the interface of the porous stone and soil; the other is described as follows.

The difficulties involved in obtaining perfectly parallel and horizontal ends on soil samples are well known. Even when ideal initial conditions are approached during the initial set-up, isotropic consolidation can cause distortion due to non-homogeneity within the sample. The assumption of a perfect right cylindrical sample becomes inaccurate. For this reason, when loading starts the sample may develop a stress concentration at the corner in contact with the flat load cell (Fig. 3.7, case 1). The magnitude of this concentration will be a function of the stiffness and brittleness of the sample as well as of the magnitude of the non-parallelism itself, and it may influence the test results. The calculated stress-strain curve considering the sample deformation as a whole will be concave upwards initially, and localized failure may even occur as the localized stress concentrations are redistributed. It is not surprising that tilting of the sample can occur as was shown by Jardine, Brooks and Smith (1985) in soft rock tests. These initially concave stress-strain curves are familiar to soil engineers and are found even when the equipment deflection is taken into account.

3.3.3 The proposed external measurements

During the experimental investigation of the artificial soil it was discovered that the material has a degree of brittleness and sensitivity to stress concentration (see Chapter 4 and Bressani and Vaughan, 1989). It is important to achieve uniform stress conditions in the test. Attempts were made to improve the end conditions by using materials like plaster of Paris or resins without success.

A simple mechanical arrangement was tried with satisfactory results. It comprises a combination of a loading button (half-sphere) attached to the load cell and a flat top cap on

the sample. The load is then applied at one point and the resulting distribution of stress is very much improved, although some degree of non-axiallity may still persist. The stress-strain curve obtained is also improved (Fig. 3.7, case 2).

The mechanical arrangement used is represented in Fig. 3.8(a). Such geometry causes very little friction due to lateral contact between the loading button and the top cap and it does constrain the tilting of the top cap during the later stages of the tests, while always providing a unique vertical contact point. This unique point of loading is its main characteristic.

An arrangement which is widely used with poor results is a similar loading button acting against a top cap with a spherical seating. The exact alignment of the two pieces is unlikely to occur thus causing some adjusting movements during loading which are attributed to soil deformation.

Although the filter paper was eliminated from the artificial soil tests, in other soils this cannot be done easily. However in such soils (clays especially), it can be positioned out of the influence of the vertical loading. For the tests on clay samples the pore pressure was hydraulically connected to the measuring system through the pedestal with the arrangement shown in Fig. 3.8(b). The porous stone had one of its surfaces made impervious and a strip of filter paper around its border provided the hydraulic bridge to the soil. A polished resin coating (Araldite) was used to waterproof the upper porous stone surface. This introduced some degree of radial drainage but the pore pressure measurements so obtained do not seem to have been affected by the arrangement (see item 3.4.2).

External measurements made during tests in which (*a*) the spherical loading button is used; (*b*) the use of filter paper between the sample and the loading surfaces is avoided, and (*c*) the load cell deflection is taken into account will be referred to here as "proposed external measurements" as opposed to conventional external measurements where only the load cell corrections (if any) are applied and a flat load cell is used.

3.4 COMPARATIVE TEST RESULTS

In order to determine the quality of the strains obtained from the proposed external measurements, a number of tests were performed in which local strain transducers were used. In most of the tests two types of transducer were used at once (four transducers in total) which created a good opportunity to compare their performance.

3.4.1 Artificial soil

Results of a drained triaxial compression test with isotropic consolidation to 160 kPa are plotted in Fig. 3.9. The axial stress-strain curves obtained with the electro-levels and Hall effect local transducers are compared with those obtained using the proposed external strain measurements. There is no significant difference between the strains calculated from the two kinds of local transducers. The proposed external strain curve is surprisingly close up to, say, 0.02%. Using such curves the values of stiffness at deviator stresses of 50 and 100 kPa (30 and 60% of the peak stress for this sample) are 111 and 67 MPa, local strains, and 70 and 38 MPa, proposed external strain. The proposed external measurements underestimate the true values by 63% and 57%.

Although these values are not yet satisfactory they represent a considerable improvement in relation to the conventional external measurements. The results of three other tests in which the strains were calculated from conventional measurements are plotted in the same figure. The same soil was used and the initial isotropic effective stress was 100 kPa. The difference is striking. The stiffnesses calculated at the same deviator stress levels are 10-30% of the values calculated using local strain measurements (12-20 MPa and 16-20 MPa).

The traditional form of strain determination tends to grossly over-estimate the strains at the beginning of loading in sharp contrast with the proposed external measurements. Note that in these conventional tests the load-cell deflection was taken into account in the calculations and no filter paper was used. The main cause of error is the tilting of the top cap.

Other tests were performed with different initial effective confining stresses and different soil strengths. In some tests the results were even more promising (Fig. 3.10) but the general pattern remained the same; agreement between local and proposed external strains up to some level of strain after which they start to diverge.

In order to see if the same behaviour would occur in different soils, and also to check the possible influence of the connections between the local transducers and the sample, further tests were made with London Clay and Corinth Marl.

3.4.2 Remoulded reconsolidated London Clay

Four samples of remoulded London Clay were tested in undrained compression. The material was obtained from a depth of 10 m in a borehole at Imperial College. It was thoroughly remoulded and shaped into cylinders. Each sample was then isotropically consolidated to 330 kPa effective stress. After the consolidation, the samples were taken from the cell, weighed, measured and reassembled with four local transducers attached to them. The method of attachment of the transducers reference points, or pads, varied for each case. In one case the eight pads of the local transducers were pinned to the sample through the membrane using 16 pins (each 8 mm long and 0.8 mm diameter). In other cases the pads were simply glued on to the membrane or only the top pads of one pair of local transducers were pinned. In all of the tests the upper pads were held against the sample with the use of a membrane strip about 5-8 mm wide put over them.

The use of pins proved inconvenient due to the occurrence of leaks in some tests. As the type of connection between the pads and the sample did not show any influence on the results of these London Clay samples their effect will not be discussed further.

The complete stress-strain curves of the tests using the local measurements are given in Fig. 3.11 and their effective stress-paths are shown in Fig. 3.12. The initial suction varied between the individual tests reducing the initial mean stress from the 330 kPa applied during consolidation to values in the range 160 to 210 kPa due to handling during reassembly.

Most of the tests were sheared at a rate of external displacement of 0.15 mm/h (0.2%/h). To check the accuracy of the pore pressure obtained through the new filter paper arrangement the strain rates were varied in some tests (see Table 3.1). These variations in rate did not affect the form of the stress paths (Fig. 3.12), this indicates a high degree of equalization and proper functioning of the modified filter paper arrangement.

The verticality and smoothness of the stress-paths may be a consequence of the stress uniformity induced in the samples by the loading arrangement.

The stress-strain curves of two tests are plotted in Fig. 3.13 to a much enlarged scale. On test (3) the strains determined from both pairs of local devices are in such good agreement that the curve plotted represents both accurately. The strains calculated using the proposed external measurements are also plotted and they show a very satisfactory agreement with the others.

The strain origin of test (2) has been shifted for clarity but the scale is the same. There is an even better agreement between the local and proposed external strains. Unfortunately, in this test the output of one pair of local measurement transducers was not reliable (one transducer was out of range) and so only one pair is represented. Although there is some scatter in the local strains the agreement between the two measurements is well illustrated.

The results of the other tests are not so straightforward to interpret. Test (4) had a small leakage and quite large bulging developed in the top 20 mm of the sample at later stages. Such deformation was not measured by local transducers as their reference points were below that level.

In all of the tests the strains calculated from the different measurements were close to each other. To quantify their differences a plot was prepared of secant stiffness, obtained from each individual strain, against q (Fig. 3.14). Such a plot highlights any difference between the strains, especially at small values of q, and so must be used with caution. The stiffness curves from the local measurements were plotted directly from the computer calculated results with minimum manipulation. The external strain stiffnesses were calculated from the stress-strain

curves by adopting a best fit line to define the origin so introducing some degree of judgement to their values.

The secant stiffnesses are tabulated in Table 3.2 using the stress levels as reference. If the initial loads are ignored, the values obtained from the external and local measurements are remarkably close. They are consistent between tests and have comparable magnitudes and scatter.

3.4.3 Corinth Marl

This soft rock from the Corinth Canal region, Greece, was the subject of a cooperative research programme between the National Technical University of Athens and Imperial College. The main characteristics of the material and the results of the testing programme are presented in Chapter 8.

Stiffness values determined from two consolidated undrained tests carried out at Imperial College using local transducers and the proposed external measurements are plotted against axial strain (log scale) in Fig. 3.15 (tests 2 and 3, initial isotropic effective confining pressure of 525 kPa). There is less than 25% difference between the stiffnesses calculated from the local and the proposed external strains.

Although such differences are not small, the results obtained from the proposed external method are considerably better than those from traditional measurements. The dotted band in Fig. 3.15 represents the limits of results of three consolidated drained tests with conventional measurements on the same material collected from the same location (Anagnostopoulos, 1989). The confining pressures used were 500, 900 and 1200 kPa but the stiffnesses only represent a fraction of the values obtained with the local transducers in tests (2) and (3).

The general trend of the two tests presented here was also found in other tests. Although the material is fine grained and the finishing of the ends seemed quite good, the technique described is pushed to its limits in such stiff material. The deflection correction that has to be made at the load levels used in these tests is large; nevertheless, the improved

results obtained from the proposed external method compared with the conventional one, in such a demanding situation, makes its usefulness quite clear.

3.5 COMMENTS ON THE EXPERIMENTAL PROCEDURES

For tests with the artificial soil some support should be provided for the local transducers or, alternatively, suction should be applied to the sample during its assembly. Failure to do so causes the membrane to sag locally under the weight of the transducer. The resulting membrane convolution remains even under quite large effective confining pressures and the local measurements are not reliable (preliminary tests). This type of problem was also encountered by Maccarini (1987). Most of the tests presented in this thesis had some form of support for the upper pads of the local transducers (normally a strip of membrane, sometimes suction applied before gluing them). The few preliminary tests that do not have this support are indicated.

The correction of the system compliance was based on the loads observed during the test. Difficulties in defining a precise zero load associated with zero deflection led to the choice of a load of 4N as reference. In most tests this represented quite a small load and extrapolation back to zero did not present difficulties.

Although most of the tests were performed in a conventional strain controlled triaxial cell, similar results were also obtained from tests in a stress path cell as described by Bishop and Wesley (1975). However, the top reference point for external measurements was fixed on the load cell ram instead of the top cell plate. The reason for this is that the threads between load cell and top plate can have relative movement under certain conditions (Ninis, 1988).

3.6 CONCLUSIONS

The results presented contradict the modern idea that axial strain determined from external measurements are inherently wrong. In fact, in some respects, the measurements are remarkably precise. A better understanding of the problems referred to in past works such as bedding and differences in the strains measured at the top and bottom thirds of a soil sample (Costa Filho, 1980; Daramola, 1978) has been achieved.

The proposed external measurement technique described involves some small mechanical modifications, calibrations of the loading system compliance (including all pieces involved in a normal test), and careful preparation of the sample end surfaces. Although the technique is reliable for clays, some errors arose with materials that have a rough surface or that were quite stiff (Esec of the order of 1 GPa). The general results, however, are encouraging.

The influence of true bedding in some materials is still important (e.g. artificial soil) but the most significant factor leading to errors is the tilting of the top cap due to its misalignment in relation to the loading ram/load cell. The true bedding referred here is the deformation due to non-uniform contacts between the loading surface (usually the porous stone) and the soil sample. It is more likely to occur in soils in which the surface is rough and in situations where the stress levels are not large enough to smooth the irregularities by compression.

All of the tests were performed in triaxial compression, drained or undrained. The conclusions may well apply to extension tests as well provided that a reliable mechanical contact between loading ram and top cap is found.

Three different types of local transducers were used in the tests, with different operational principles involved: electro-level (Burland and Symes, 1982), pendulum with strain-gages (Ackerley, Hellings and Jardine, 1987) and Hall effect (Clayton and Katrush, 1986). The use of different types of local transducers simultaneously on the same sample allowed a direct comparison of their performance under a variety of situations. Except for cases in which non-uniformity of strains or shear planes were present, all three types of

transducers used in the tests gave very similar measurements of axial displacements in soil samples.

The connections of the local transducers to the sample (pinned through the membrane or just glued to it) did not have any influence on the results of tests on clay samples. On coarse sandy samples in which the initial effective stresses are zero (e.g., artificial soil) some form of support to the transducers should be provided initially. If possible, suction should be applied to the sample before gluing the pads. Failure to do so may lead to incorrect measurements due to membrane convolution.

The main advantage of the procedure described here is to provide a simple, inexpensive and ready-to-use alternative method of determining axial strain which would considerably improve the quality of test results obtained from most of the worlds soil laboratories.

Test	wc	p'_0	Rates		
	(%)	(kPa)	(0.034%/h)	(0.2%/h)	(1%/h)
1	32.2	210	0 - 0.45	0.45 - 3.4	
2	33.3	159	0.65 - 2.2	0 - 0.65 2.2 - end	
3	32.2	175		0 - end	
4	30.7	194		0 - 0.09	0.09 - end

Table 3.1 – London Clay tests — initial water contents, suction measured before shearing and the rates applied to the tests (strain limits of each rate)

Test	q (kPa)	Undrained stiffness — Eu_{sec} (MPa)		
		Local transducer A	Local transducer B	External transducer
1	30	-	60	60
	50	-	36	31
	70	-	25	19
2	30	44	35[a]	67
	50	27	19[a]	31
	70	21	15[a]	23
3	30	50	70	75
	50	38	45	44
	70	26	32	29
4	30	61	59	61
	50	38	37	31
	70	22	22	18

(a) Only one transducer working properly

Table 3.2 — Reconsolidated remoulded London Clay tests - comparison between the stiffnesses derived from different measurements

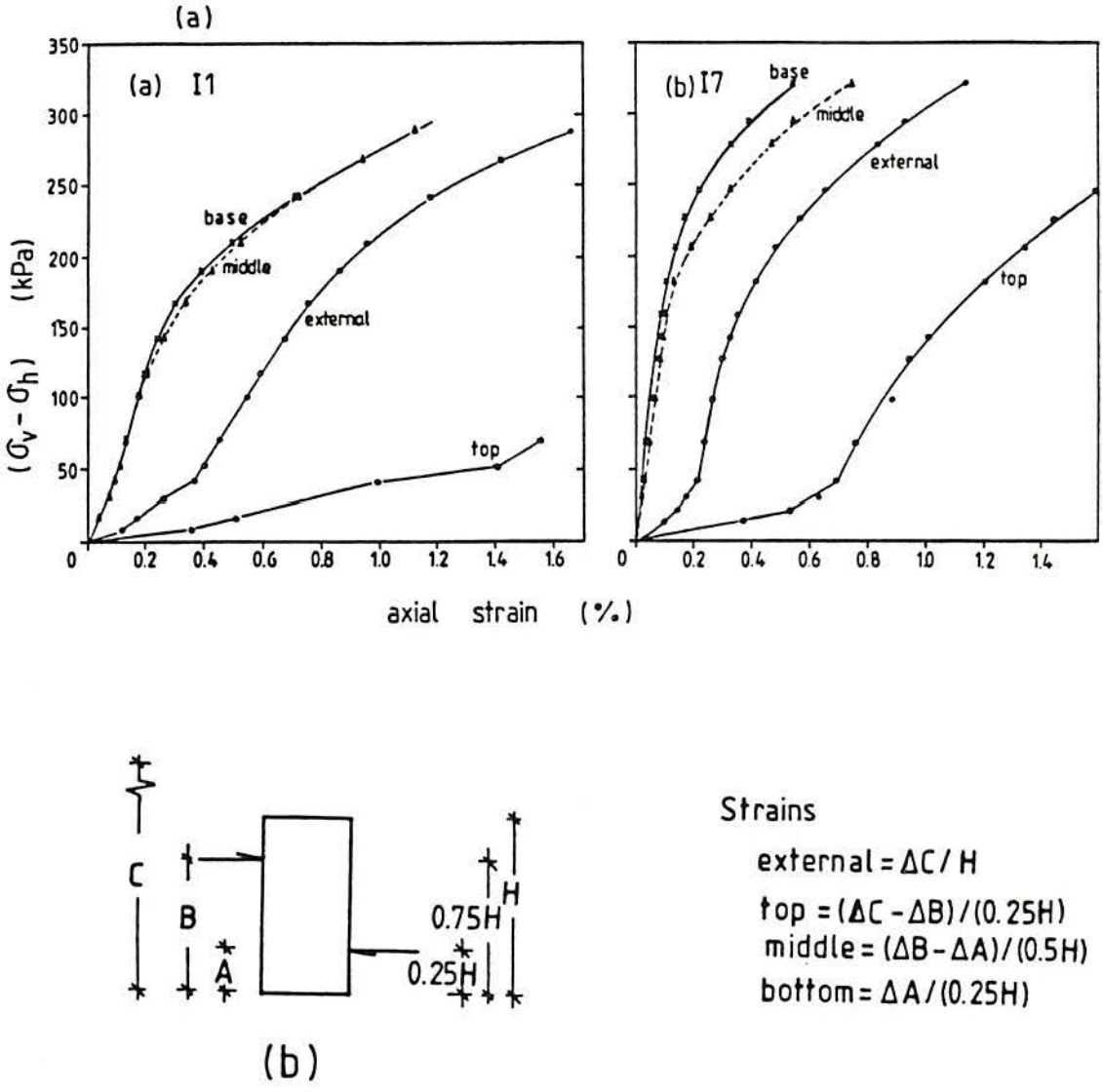

Figure 3.1 – (*a*) Results of triaxial tests on sand obtained by Daramola (1978). Sample I7 was overconsolidated (OCR=7; e=0.66) and sample I1 was normally consolidated (e=0.60), both sheared at σ'_H=100kPa; (*b*) Schematic representation of reference points and lengths used for strain calculations

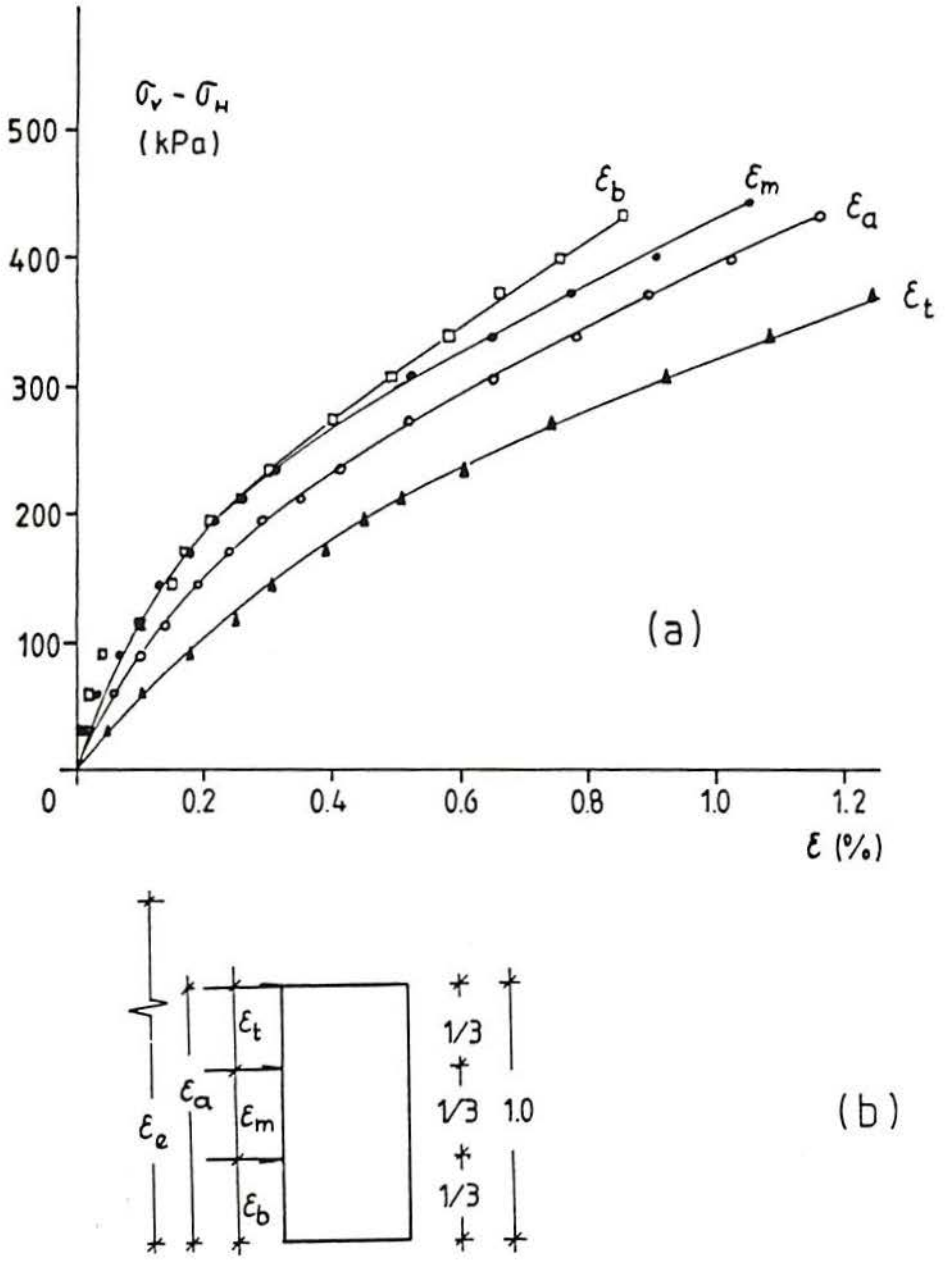

Figure 3.2 – (*a*) Results of triaxial tests on undisturbed London Clay (after Costa Filho, 1980); (*b*) Schematic representation of reference points used (observe that ϵ_a is measured between the top cap and pedestal, and ϵ_e is external to the cell)

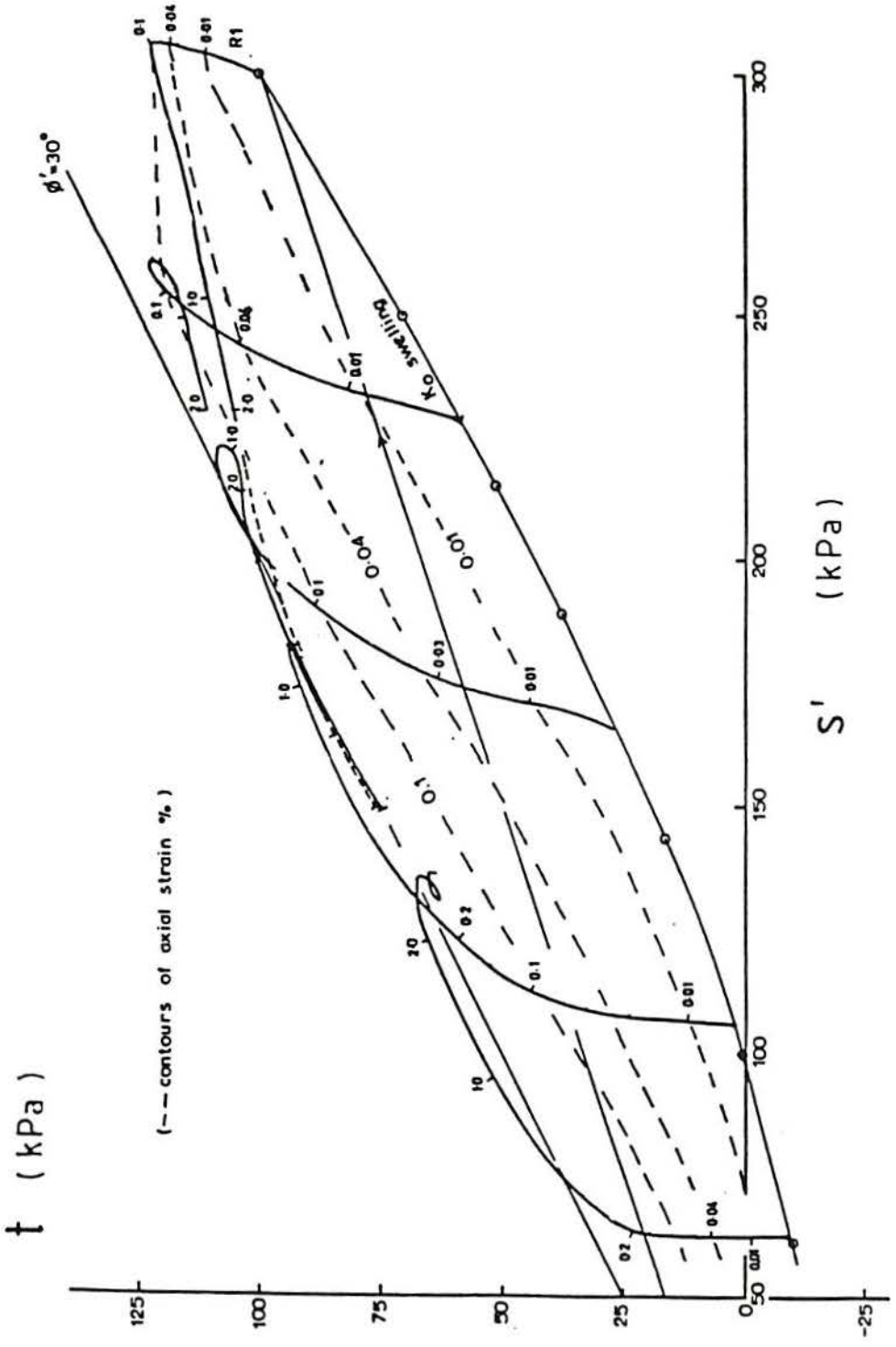

Figure 3.3 – Axial strain contours obtained from local measurements on K_0 reconsolidated clays from the North Sea (after Jardine et al., 1984)

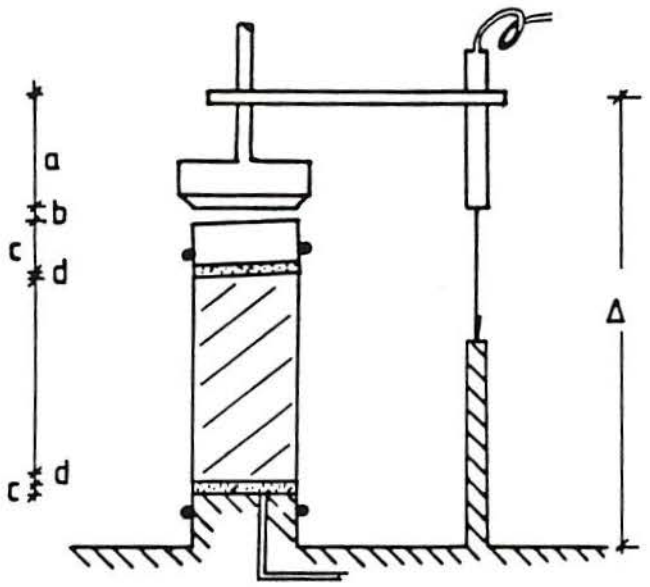

Δ: total relative displacement measured externally
a: deflection of loading equipment
b: tilting of the top cap due to non-parallelism
c: deflection of porous stone, top cap and filter paper
d: bedding

Figure 3.4 - Possible sources of error in the external measurements of axial strain

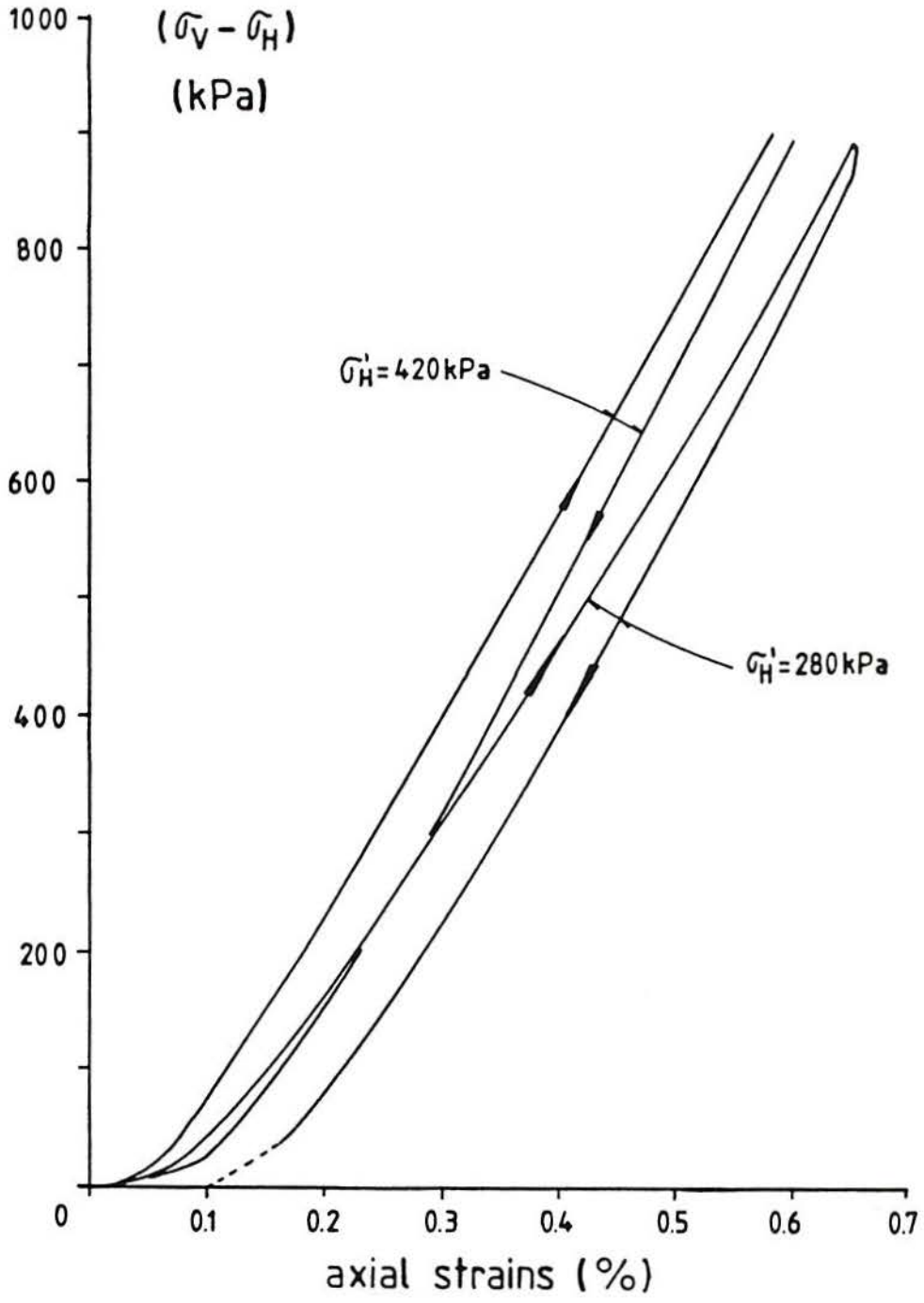

Figure 3.5 – Deviator stress versus apparent strain curves obtained from testing a brass dummy sample with filter paper discs and porous stones

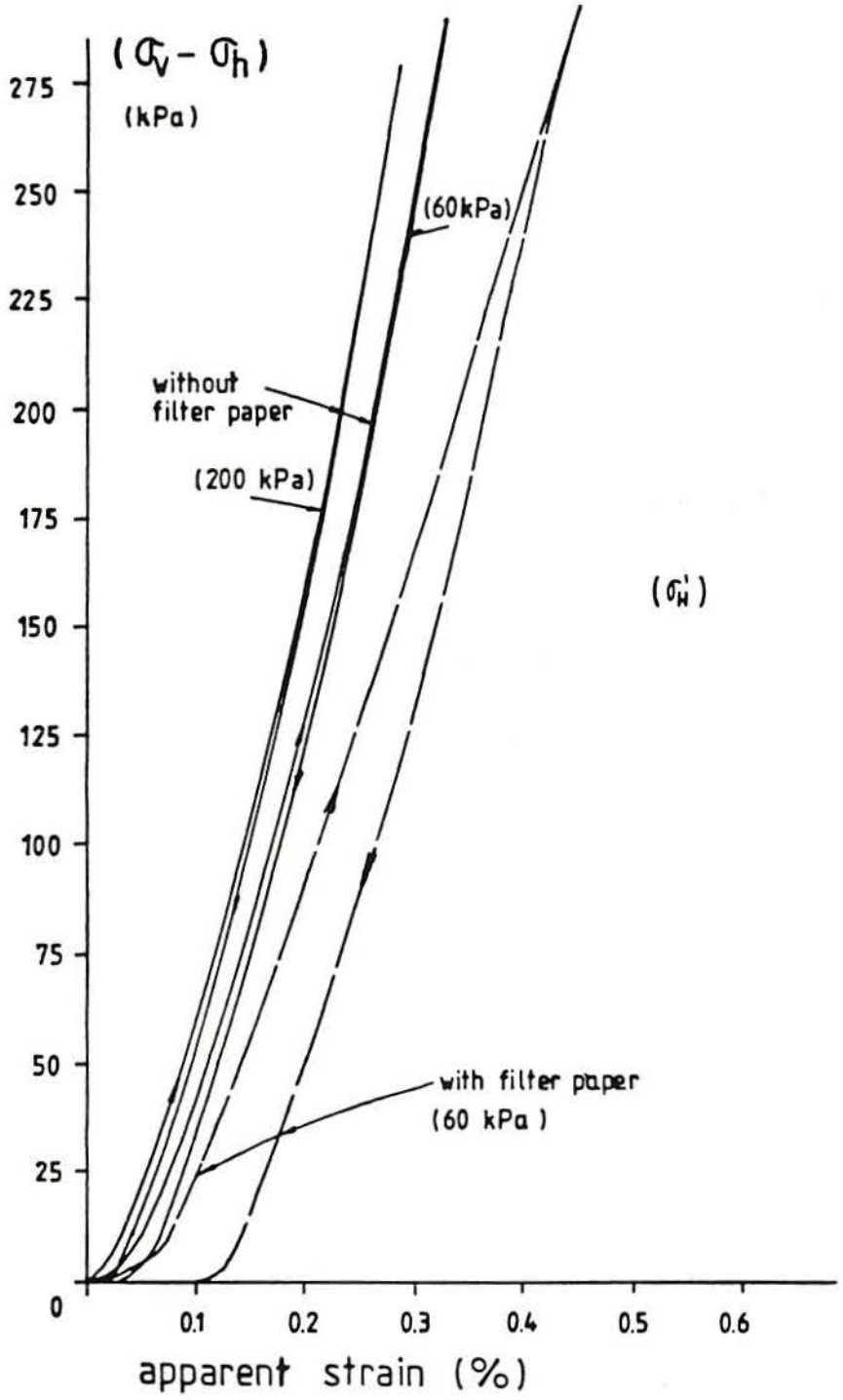

Figure 3.6 – Comparison between the stress versus apparent strain curves obtained with and without filter paper. (For σ_v-σ_H=100 kPa, F=113 N; apparent strain=0.1%, displacement=0.076 mm)

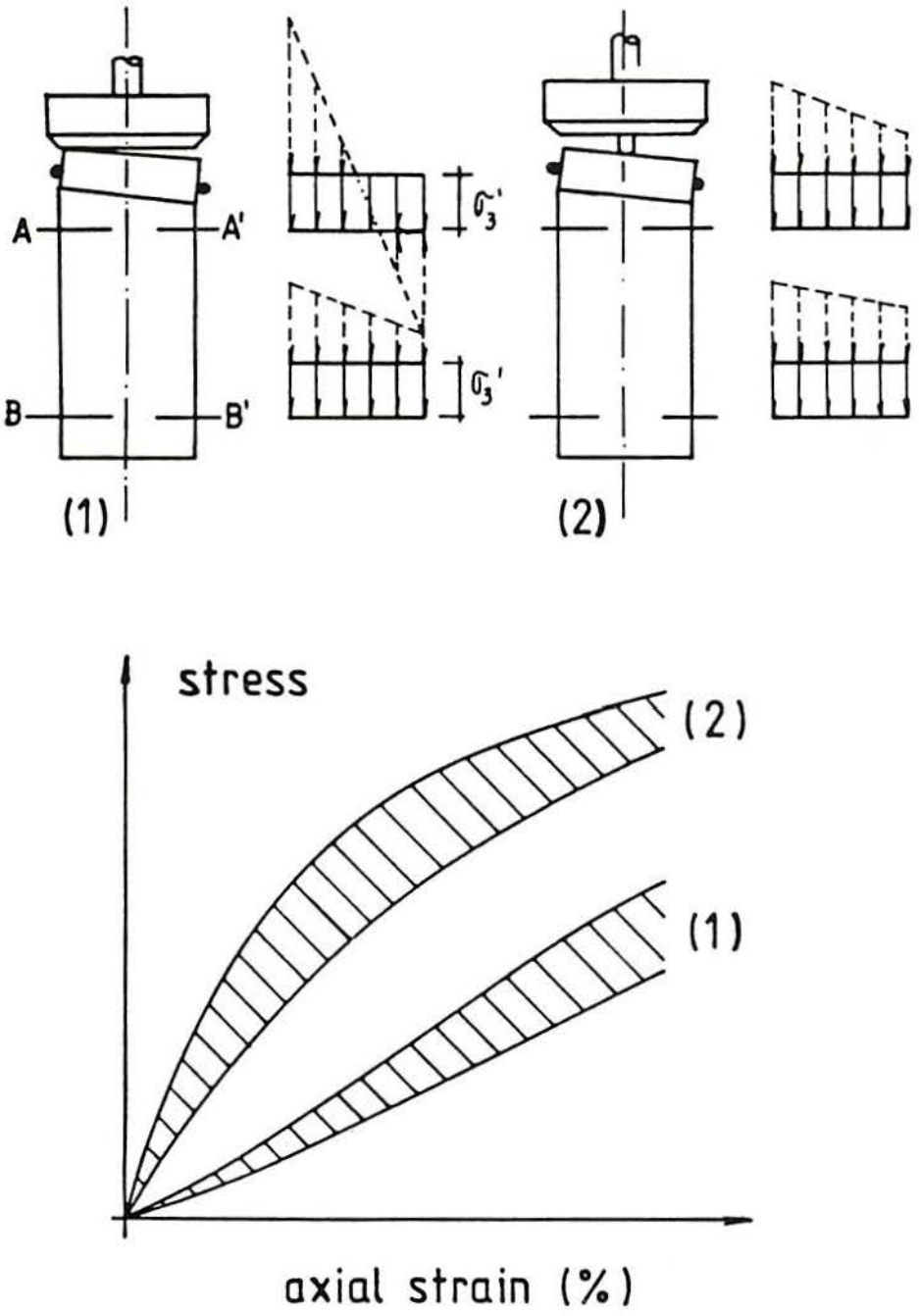

Figure 3.7 – Likely stress distributions in a sample and associated stress versus apparent strain curves resulting from two different loading procedures

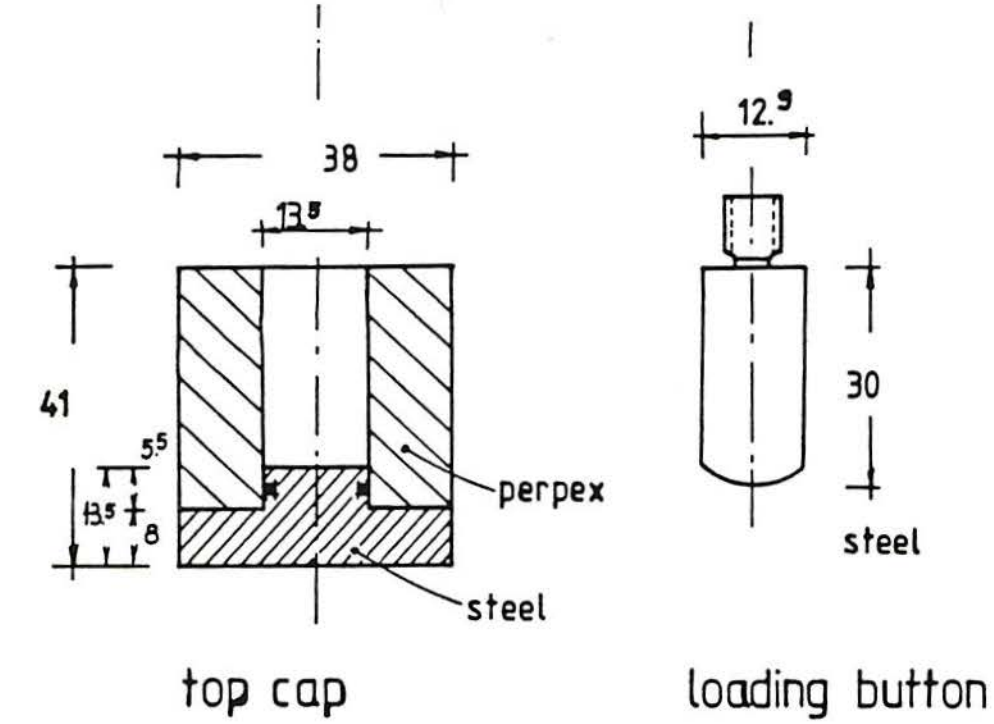

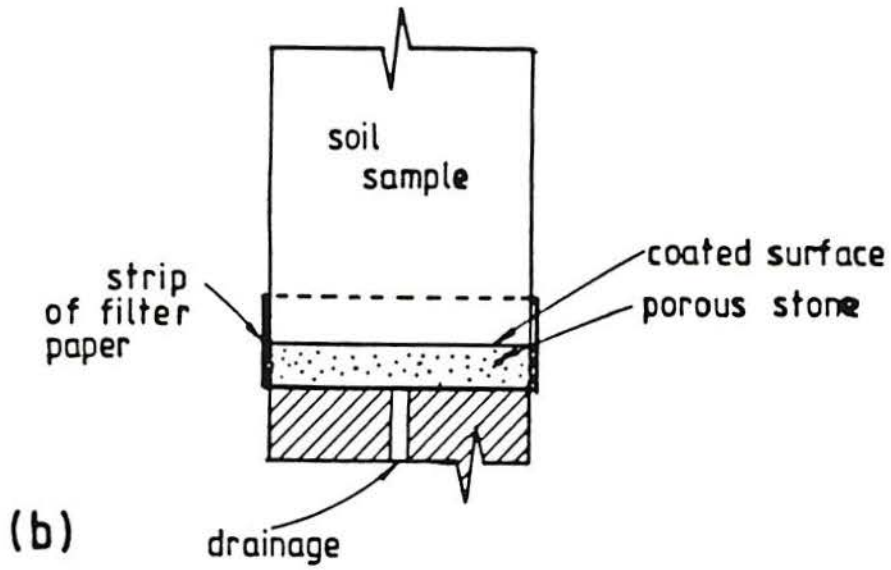

Figure 3.8 - (*a*) Top cap and loading button used in most of the tests; (*b*) Arrangement used to avoid the influence of filter paper on the vertical displacement

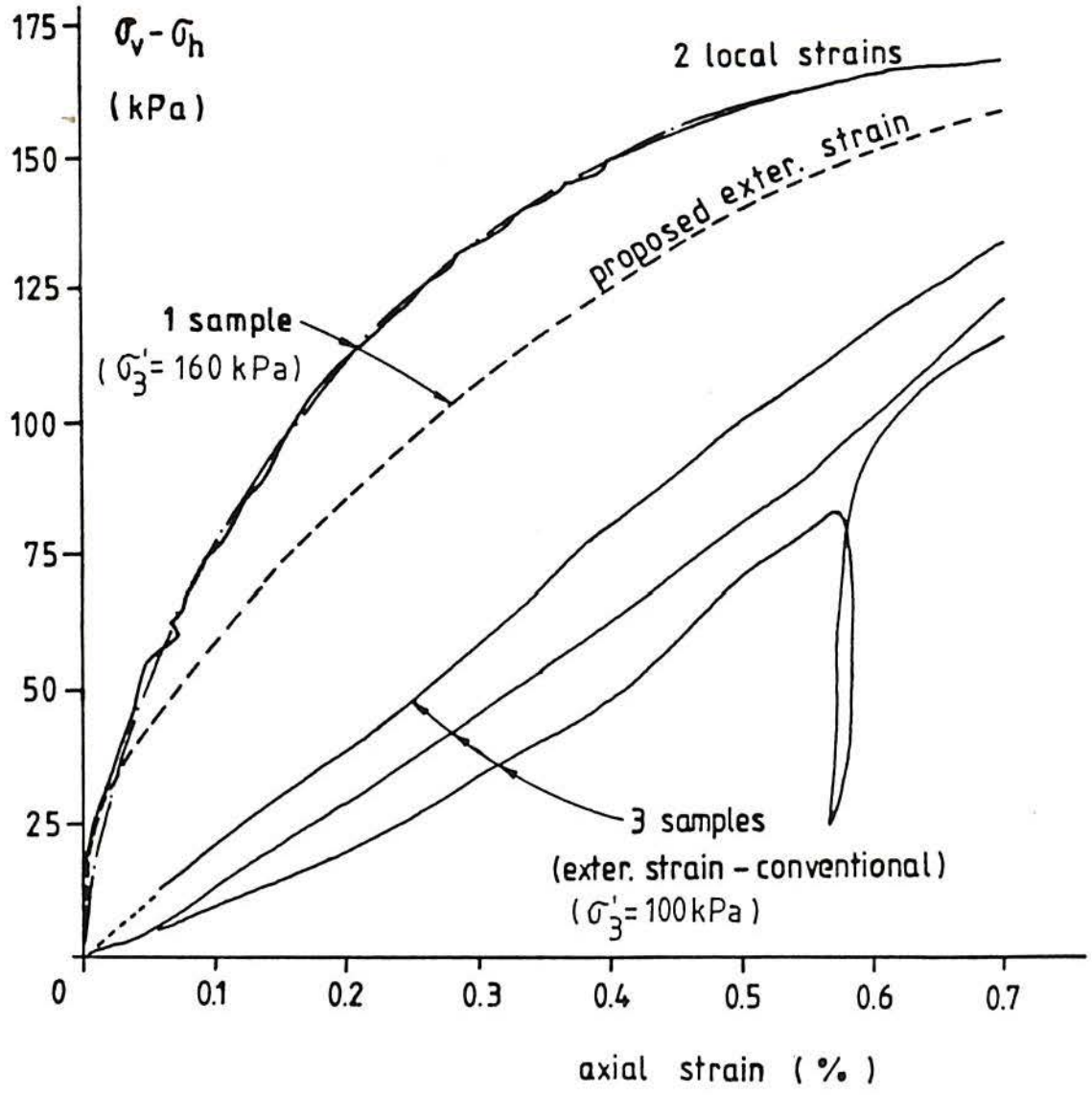

Figure 3.9 – Results of triaxial compression tests on four samples of artificial residual soil (σ'_H=100 kPa and 160 kPa, e_0=1.4)

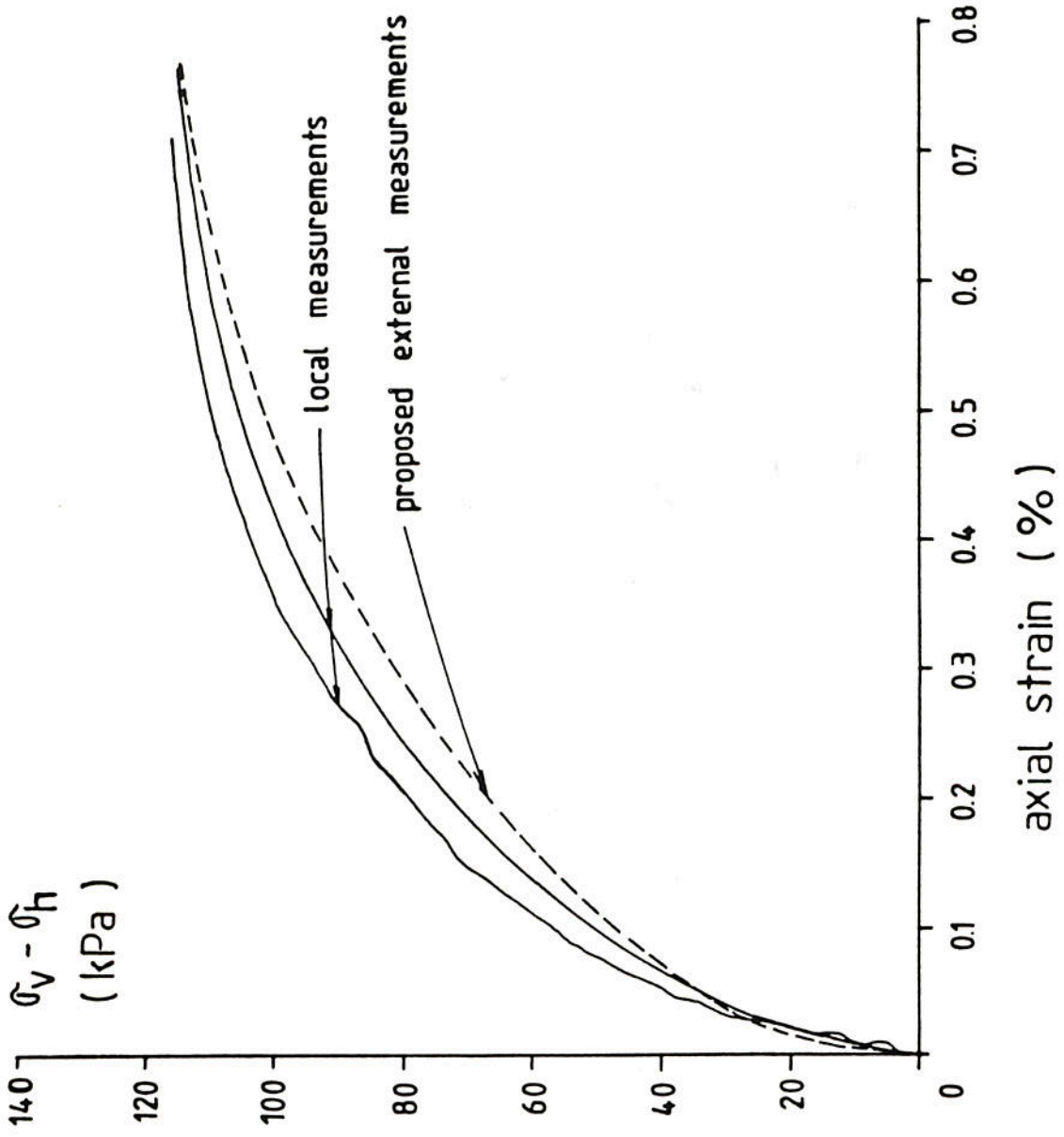

Figure 3.10 – Results of triaxial compression test on artificial residual soil (σ'_H=200 kPa, e_0=1.46)

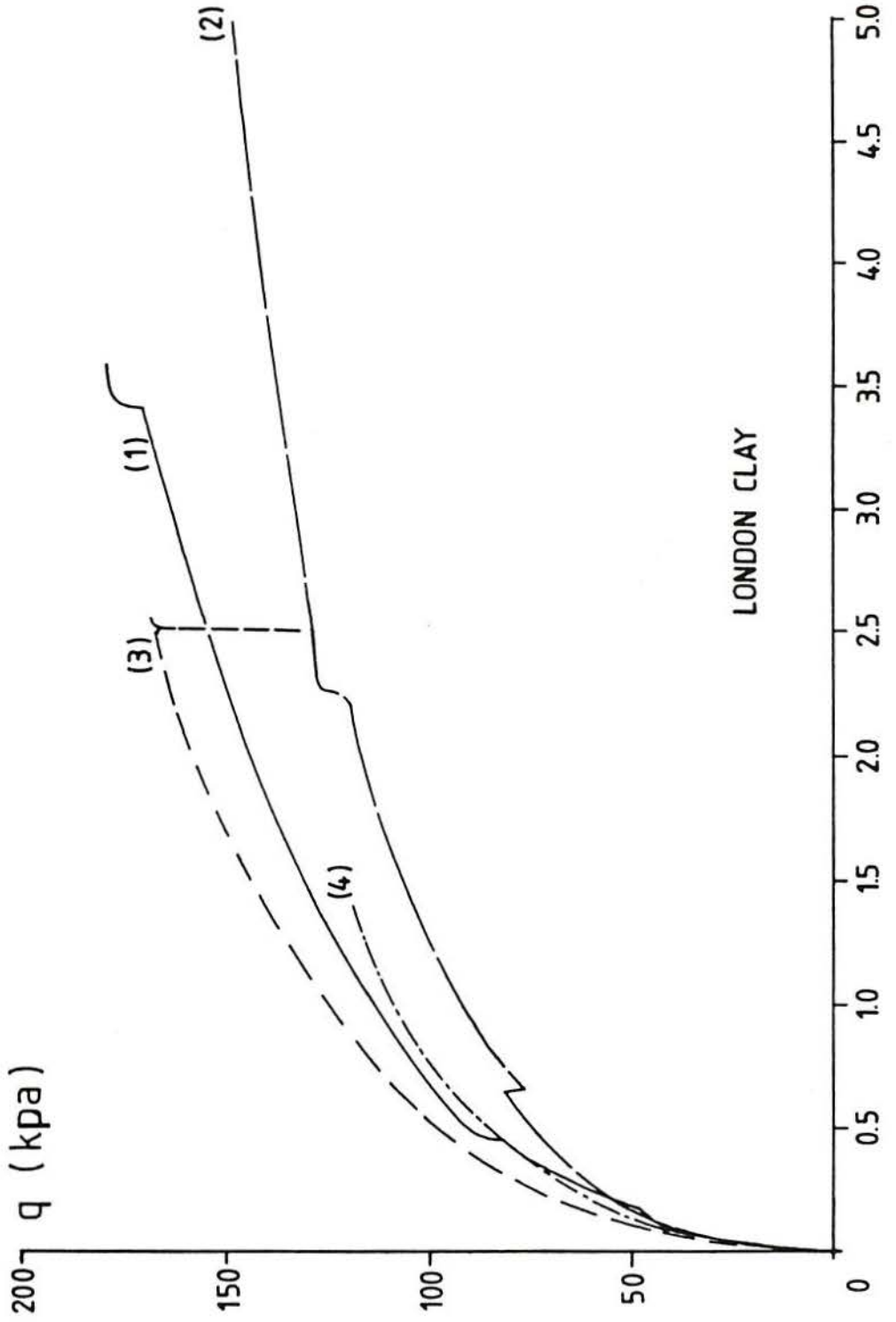

Figure 3.11 – Complete stress-strain curves of London Clay tests (based on local measurements)

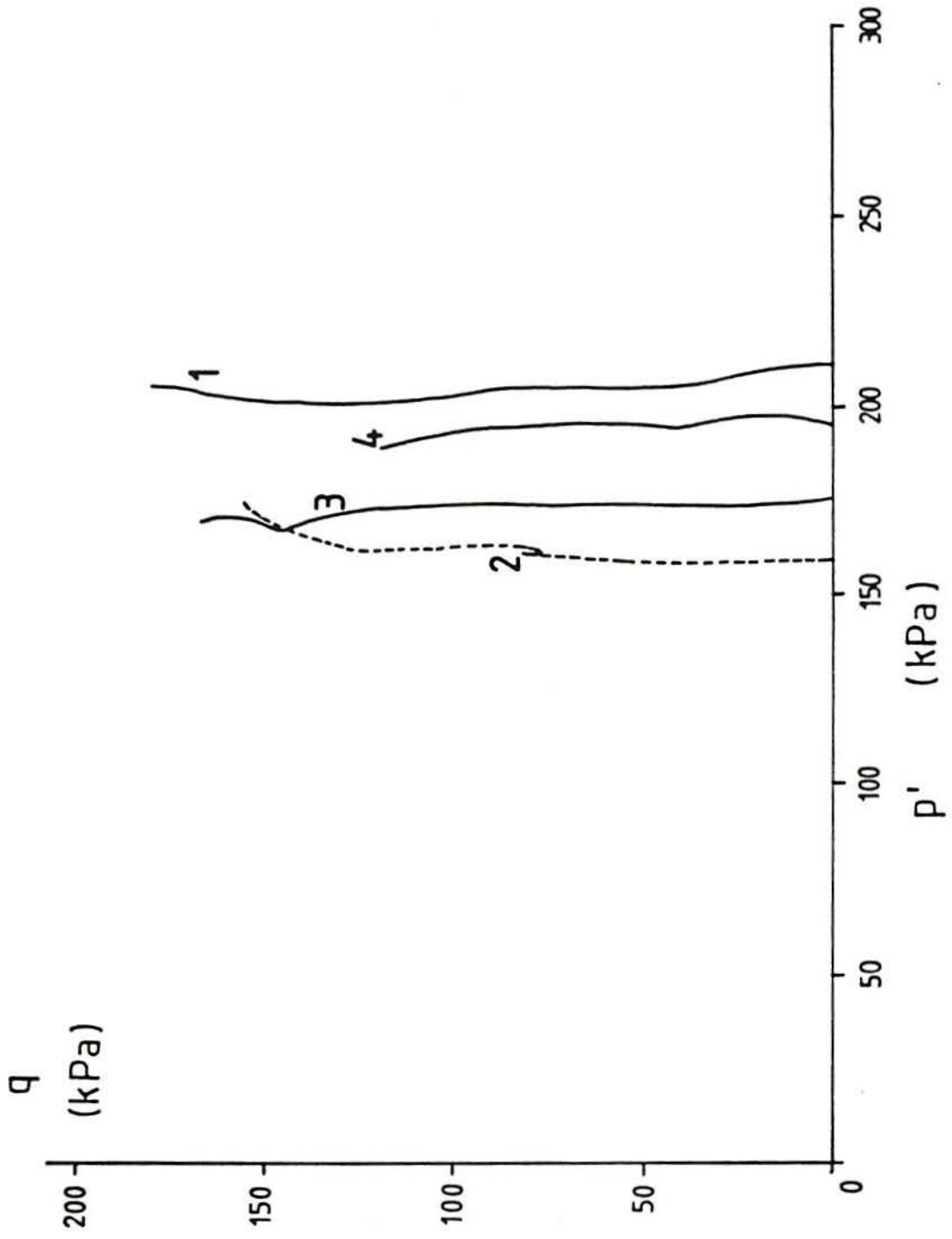

Figure 3.12 - Stress paths of London Clay tests using modified filter paper arrangement ($q=\sigma_v-\sigma_H$; $p'=(\sigma'_v+2\sigma'_H)/3$)

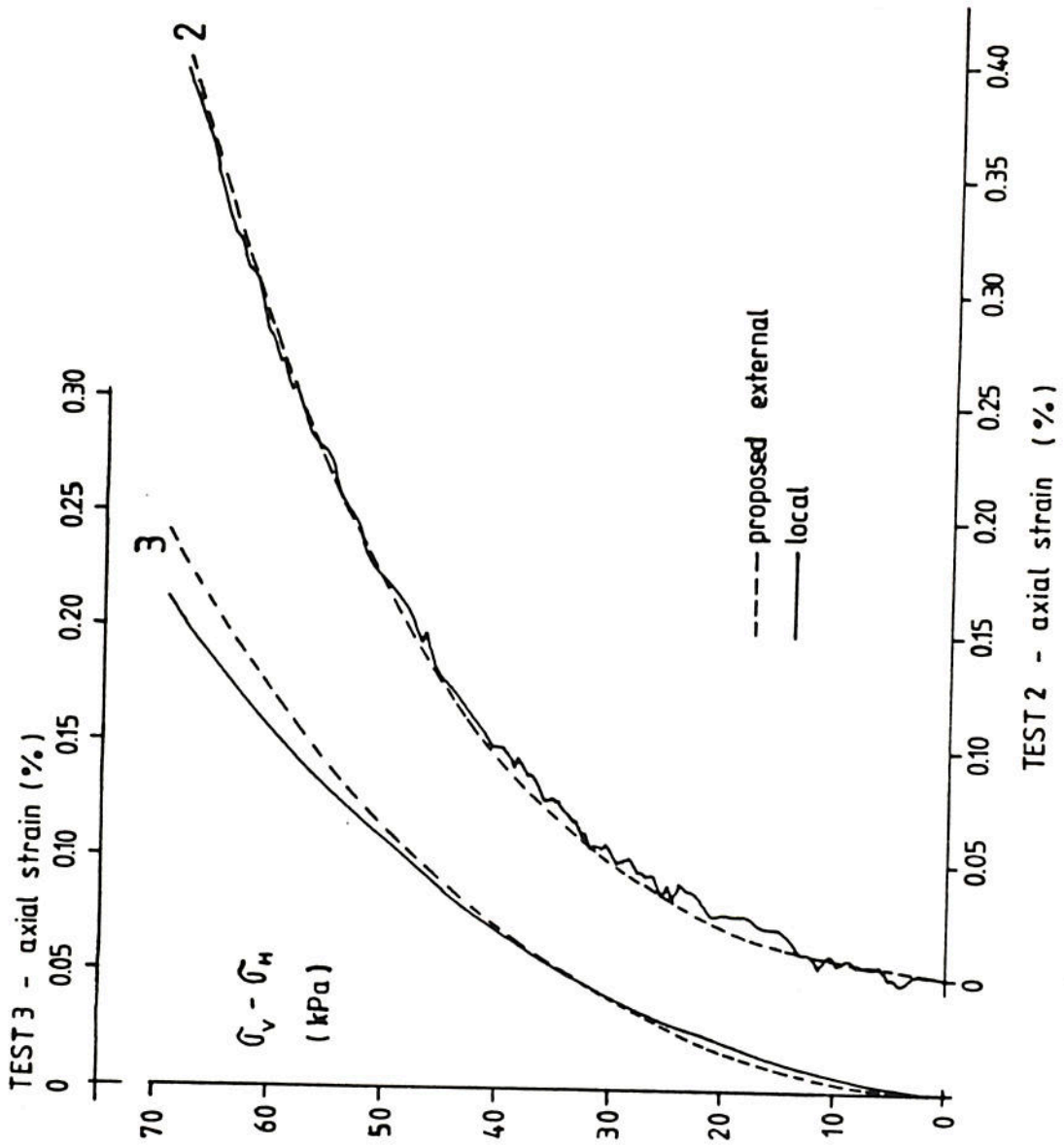

Figure 3.13 – Comparison between local and proposed external strains on London Clay (tests 2 and 3)

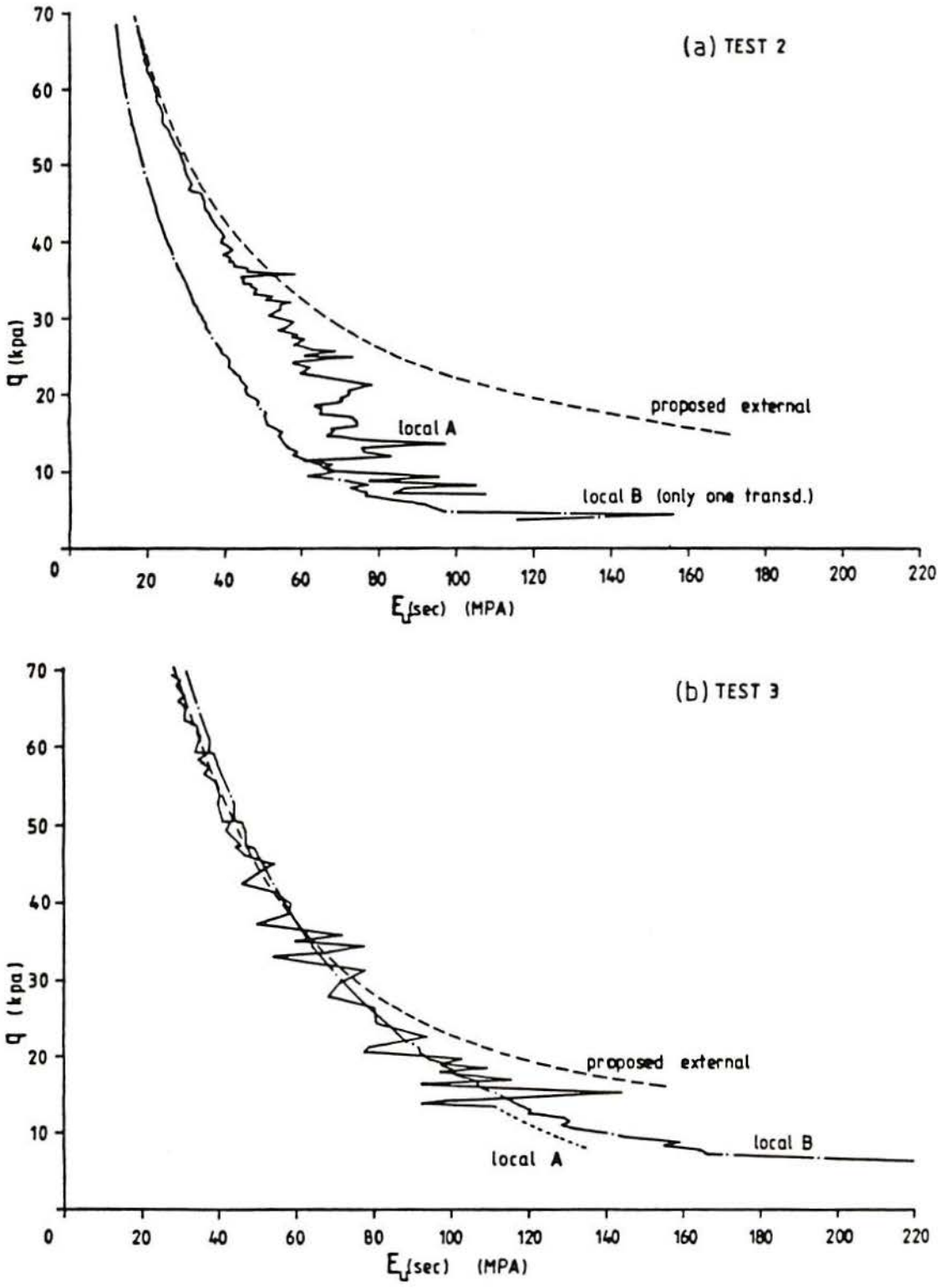

Figure 3.14 - London Clay test results comparing stiffnesses calculated from different strains versus deviator stress; (*a*) test (2); (*b*) test (3); (cont.)

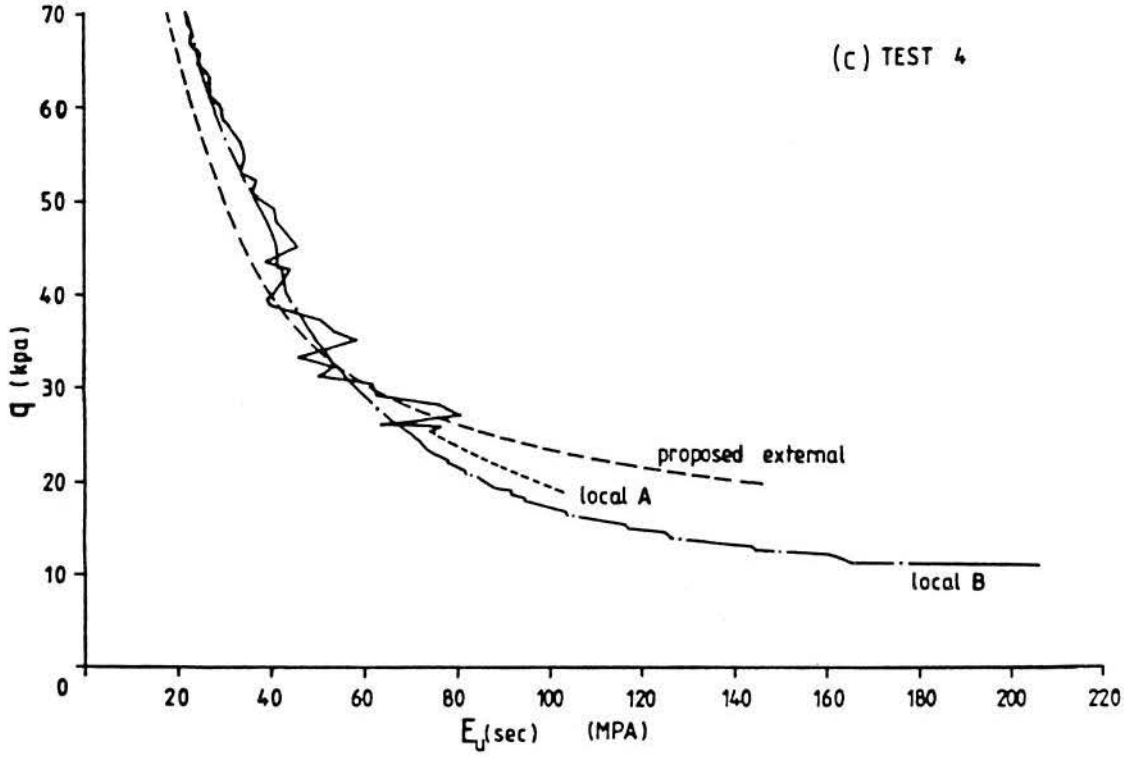

Figure 3.14 – (cont.) (*c*) test (4)

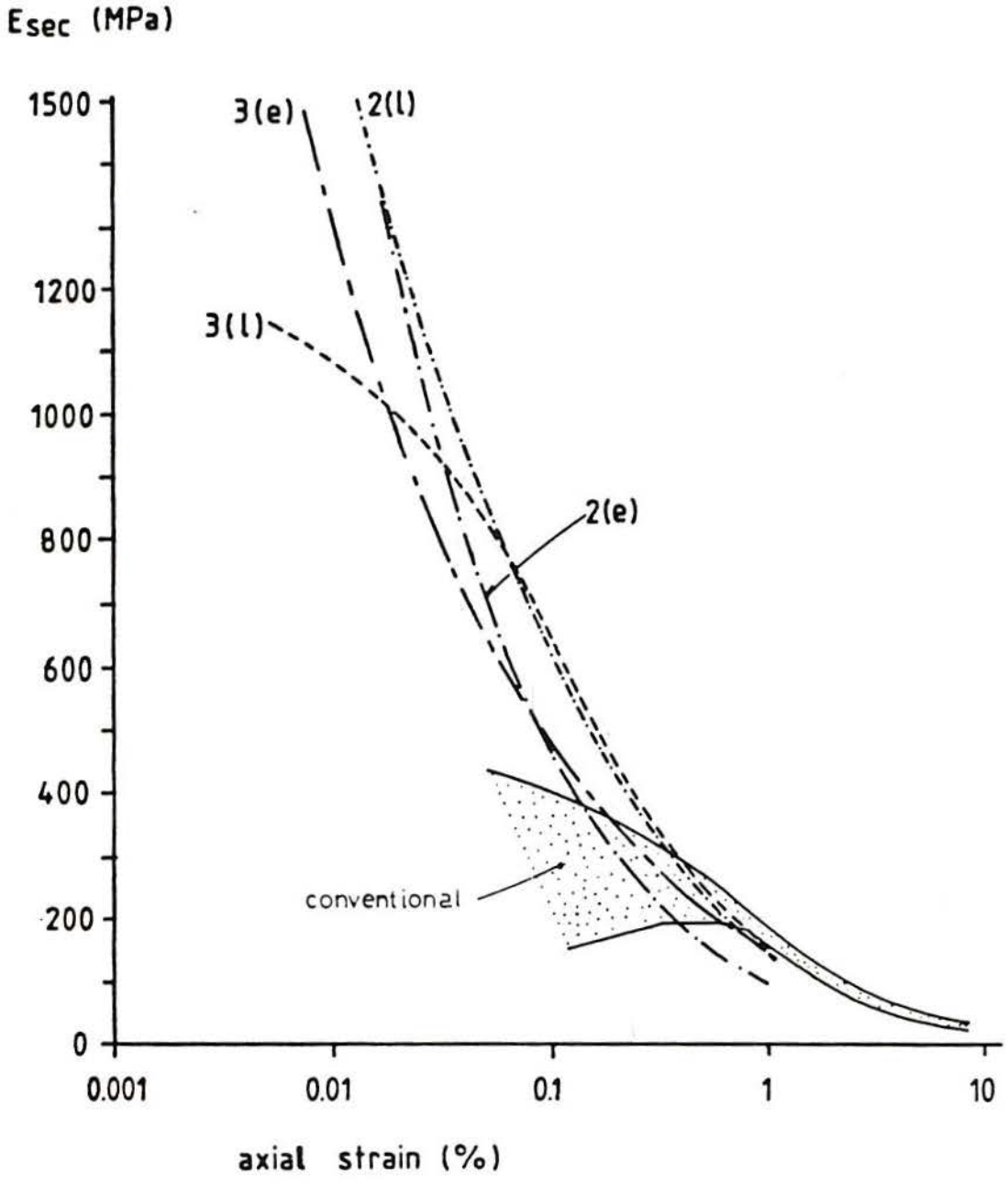

Figure 3.15 - Corinth Marl test results (tests 2 and 3) comparing stiffnesses determined from local (l) and proposed external (e) measurements

4. ARTIFICIAL BONDED SOIL – INITIAL STUDIES

4.1 INTRODUCTION

An artificial soil has been developed to help investigate the influence of bonding strength, void ratio or density and to some extent particle composition. The ability to reproduce these characteristics in any number of identical samples gives the researcher the capability to investigate the influence of factors such as stress path and stress history in addition to the previous factors.

The subject of artificial bonded soil has been divided into two chapters. In this chapter the constituent materials and the procedure for making the artificial soil are described, and the influence of creep and test technique are then investigated. Once these studies were complete and conclusions drawn, the main investigation was carried out as detailed in Chapter 5.

4.2 PREPARATION OF BONDED SAMPLES

4.2.1 Materials

Analysis of the structure of residual soil shows that weathering produces typically a structure composed of quartz and weaker grains bonded together by products of other decomposed minerals. The results of tests on trial mixtures indicated that reasonably realistic behaviour (compared to natural residual soils) could be obtained with a mixture called 133057 (Maccarini, 1987). This form of identification has been retained here for consistency. The code represents the partial percentages in dry weight of three components: 13% of kaolin, 30% of weak sand grains (CFK) and 57% of quartz sand grains. The quartz sand is a uniform medium grained sand (Fig. 4.1) commercially available. The CFK stands for crushed fired kaolin and is obtained by heating a previously dried paste of kaolin in a kiln. The temperature

is maintained at 1000°C for 5 hours. After switching off the power, the new hardened material is left to cool inside the closed kiln overnight. When cool, the hardened kaolin (now transformed into methakaolin – Grim, 1962) is crushed in a mortar or mechanical grinder. Sieving was carried out to obtain the same grading as the quartz sand.

4.2.2 Mixing

The required quantities (by dry weight) of the two sands was put in a bowl together with the dry powdered kaolin. After the dry components were thoroughly mixed, water was added. The amount of water influences to some extent the final void ratio but enough has to be used to assure that the kaolin is completely wet and that a liquid mixture is obtained.

4.2.3 Moulding

The wet mixture was poured into paper moulds to dry so that cylindrical samples close to the final geometry could be obtained (Fig. 4.2). These paper moulds were prepared from sheets of normal filter paper (Whatman No. 1). One rectangular piece was cut to the required length and width [Fig. 4.2(a)]. Three thin strips of paper (5 mm x 80 mm) were glued by their extremities onto that piece as shown in the figure.

A brass tube was used to prepare the moulds. The rectangular piece was wrapped around it with the strips inside. The overlapping side was glued forming a paper tube. The bottom was prepared using a circular piece of paper in which a series of slits had been cut leaving a central area intact [Fig. 4.2(b)]. This central area formed the bottom of the paper mould. Having positioned the tube on the central area, the cuts could be neatly bent over and glued onto the surface of the paper tube. The final mould looked like the sketch of Fig. 4.2(c).

Once the constituents had been thoroughly mixed, the same brass tube was inserted into the paper moulds again. The closed bottom was protected by placing it in a small tin and the wet soil mixture was poured into the mould. The tube was inclined so that the wet mixture slid down the side to avoid air being trapped. Once the brass tube was full it was positioned

vertically and pulled out of the mould. Normally it slid out without problems leaving the mould standing inside the tin. The process was repeated usually for six to eight samples at a time, depending on the volume prepared.

4.2.4 Drying

The wet samples were allowed to dry exposed to air in the laboratory. After 2 to 3 days they were further dried for a day or so beneath a set of infra-red lamps. In drying, the samples reduced in volume. This shrinkage was more significant in the wetter samples. As the material shrunk, the paper mould was dragged with it. The paper strips had the effect of breaking the continuity of the paper skin, providing more uniformly shaped samples.

4.2.5 Firing

The dried samples could be handled without special precautions and the paper could be peeled off easily. Following the initial drying stages, the samples were loaded into the kiln and the temperature adjusted to 500°C. The kiln was left switched on for 5 hours and the samples left inside to cool down overnight. In some special cases, samples were fired at 800°C for 3 hours.

4.2.6 Control of the void ratio

The description given so far is valid for most of the soils discussed in this thesis or by Maccarini (1987). The variation in the relative percentage of the constituents produced different "soils" such as 130087 and 138700 with their own associated characteristics. To be able to vary the void ratio of a particular mixture over a large range, Maccarini used two methods. To densify the soil he vibrated the wet mixture inside the moulds and to reduce the density he added a special "sand" to the wet mixture. Such "sand" was produced from household candle wax to the same grading as the other two sands. The candles were chopped and sieved to obtain the required result. The firing of the samples at 500°C burnt away the

wax leaving an open structure difficult to obtain by any method that involves pouring or sedimentation and drying of the wet mixture.

The mixture of these four components was made as usual. Care had to be taken so that not too much water is used as the wax will tend to float and segregate from the mixture. Careful and thorough mixing is essential.

The burning of the wax produces a fair amount of smoke and so, usually, the wax was partly burnt in an open space before being put in the kiln. This was done using a pan half filled with quartz sand in which the dry samples were semi-buried; the pan was heated outside the building. The samples were occasionally turned over until most of the smoking had stopped. As the temperature at which the wax burns is around 200°C, any influence from this initial firing is likely to be masked by the higher temperature (500°C) used afterwards.

If the same amount of water is used in the preparation, similar samples are obtained. Table 4.1 presents the proportions of the main constituents of the mixtures discussed in this thesis and the typical densities obtained. The density referred to in the table is that of the main materials fired at 500°C for 5 hours. If other temperatures are used, the density changes to some degree. Table 4.2 summarizes the code naming of the different soil series used here. Further details about individual samples and their physical properties (void ratio, tensile strength, density, etc.) will be given in the sections where their results are discussed.

4.3 SUMMARY OF PREVIOUS WORK

Maccarini (1987) carried out a series of tests on samples with different densities and bonding strength. The main results, however, were obtained from the material 133057 fired at 500°C for 5 hours. Three densities were used: that of the natural state and those obtained with vibration or wax addition. All samples were fully saturated, by boiling, before testing.

4.3.1 Intergranular void ratio

The void ratio has long been used in soil mechanics to compare different soils or the same soil under different conditions or with different structure. It is basically a measure of the volume of voids inside the soil structure and it is assumed that this is related to the spatial arrangement of the grains. However, because the fired kaolin (CFK) is porous itself, the normal definition of void ratio would incorporate these internal voids so giving a much higher value than if the grains were solid. Its use may be misleading when comparing this artificial soil with other soils composed of solid particles as two different structures may have the same void ratio.

These reasons led to the proposal of the intergranular void ratio (Maccarini, 1987) where only the space between grains is taken into account. The definition of intergranular void ratio is given by:

$$e_{int} = \frac{V_T - V_S^*}{V_S^*}$$

where:

V_T = total volume of the sample

V_S^* = the sum of the overall grain volumes, including the internal voids, i.e.

= volume of quartz sand + volume of the CFK sand + volume of the bonding links

Although this concept has some advantages, there would be difficulties in determining the internal voids of the grains for natural soils; typical values would have to be determined for the different grain mineralogies present in the soil. It has therefore been decided to use the traditional definition in this thesis. The reader is therefore reminded that the high void ratio of some mixtures is partly caused by the intragranular voids. The same condition may occur in lateritic soils, calcareous sands, marls and other natural materials.

The relationship between the intergranular void ratio and the conventional definition is

discussed in detail in Appendix 1 for all variants of the artificial soil.

4.3.2 Mechanical stability with time

The samples were prepared typically in batches of six, following the procedures given in item 4.2. The variation in densities within a batch of samples could be maintained within $\pm 1\%$ and the variation between batches was $\pm 2\%$ (Maccarini, 1987). Therefore the simultaneous preparation of a large number of samples is preferable. However, the larger the number, the greater will be the time variation between the firing and the testing and this storage time could influence results.

To investigate the effect of time, three samples were tested under isotropic compression. The samples had a similar preparation but one was tested 40 days after being fired and the other two after only one day. The results are presented in Fig. 4.3. As there is no significant difference between the behaviour of the different samples, it has been assumed that the storage time had no influence on the behaviour of the samples.

During typical curing processes, such as for cement or lime reactions, the strength of the material increases with the logarithm of time. The reactions are most active at the beginning and reduce considerably with time. It is unlikely that longer storage times will have any influence on the samples.

4.3.3 Isotropic structure

The form of preparation of the artificial soil (item 4.2) tends to produce a uniform structure. The stresses to which the soil is subjected are derived from (*a*) the suction due to the drying out, and (*b*) the contraction/expansion of the structure when the sample is heated/cooled. These processes are isotropic and so a consequent isotropic behaviour is expected. Fig. 4.4 shows the results obtained from two samples of artificial soil when subjected to isotropic stress. A radial strain belt was used and the axial strain was measured with electro-level local strain sensors. One of the samples had frictionless ends and the other had

the usual porous stones. Maccarini (1987) concluded that (*a*) the soil has an isotropic behaviour after 0.1% of axial strain and (*b*) that the use of frictionless ends was not necessary.

4.3.4 Results from isotropic compression tests

A number of samples were triaxially tested in isotropic compression to evaluate their stiffness and yield characteristics. The tests were divided in two groups. The first involved the use of standard equipment and the measurements of strain were based purely on the volume gauge readings. The tests were carried out by applying incremental loadings. The second group of tests involved the use of more sophisticated equipment. The stress was increased at a constant rate (through the use of a manostat driven by a stepper motor). Local measurement of axial strain was achieved by using electro-level devices.

The measured volume strain was influenced considerably by the effect of membrane penetration. The magnitude of volume strain arising from this penetration was evaluated with the use of the radial strain belt in some tests and a correction was applied to the samples of the first group. For the second set of tests the volume strain was calculated from the local measurements of axial strain assuming isotropic behaviour (volumetric strain equal to three times axial strain).

During the constant rate of stress increase tests two yield points were defined. The first yield was defined as the stress at which initial deviation from near linear behaviour occurs. The second yield was defined by the point of maximum curvature of the stress strain curve. Fig. 4.5 has been redrawn from Fig. 4.3 of Maccarini (1987) and it shows the differences in behaviour between the two type of tests. The plot (*a*) of the figure contains the results of samples with strong bond (fired at 800°C) and plot (*b*) the results of samples fired at 500°C. The arrows on tests of constant rate stress increase (CRSI) mark the two yields so defined.

In the analysis of the results, Maccarini (1987) concluded that:

(*a*) pre-yield compressibility is much lower in the CRSI than in incremental load tests;

(*b*) the major yield which occurs in the incremental tests is much more severe and occurs at a much lower stress than the second yield which occurs in the CRSI tests.

His conclusion was that the substantial differences between the compressibilities of similar samples (same porosity and bond strength) could not be explained by problems arising from test procedure or from the previously described corrections. The most likely factors causing such differences were assumed to be rate effects or creep.

4.4 INITIAL STUDIES

4.4.1 Testing equipment

Two triaxial apparatus were used for the studies described in this thesis. One was a stress-path triaxial cell (Bishop and Wesley, 1975) with the cell and the ram pressures controlled by manostats connected to stepper motors. Electronic signals at a chosen frequency could make the motors turn the manostat either way, so increasing or decreasing the air pressure between the limits of 25 to 800 kPa. This air pressure was transmitted to the water filled triaxial cell by using an air-water interface. The rate of stress increase or decrease could be varied between the limits of 210 kPa/min and 0.2 kPa/min in steps of 0.2 kPa/min and between the limits of 4.2 kPa/min and 0.004 kPa/min in steps of 0.004 kPa/min.

The other triaxial apparatus was a conventional constant strain rate type (Bishop and Henkel, 1962) with loading by mechanical gears and pressures provided by mercury pots. This cell was later adapted for use with pressures of up to 3500 kPa (see Chapter 6).

Both triaxial cells were equipped with an internal load cell and external volume gauge of the Imperial College design. Displacements of the loading ram were measured by strain gauge based displacement transducers. No local instrumentation of the sample was used for this phase.

4.4.2 Saturation and test set-up

The samples were produced by the methods described in item 4.2. They were cut to the final dimensions for testing on a soil lathe, using a piece of taut wire on a steel arch. The surface was usually rough due to the coarse grains present but the overall shape was regular. Samples of 38 mm diameter and between 74 to 76 mm height were typical. The samples typically had less than 1% water content at this stage (equilibrium with the laboratory conditions).

All of the tests were done under fully saturated conditions so that the effect of bonding could be investigated in terms of effective stress. Use of back-pressure for saturation of soil samples is a well established procedure (Lowe and Johnson, 1960). However it is a time consuming process and it does limit the range of effective stress possible as, to be effective, back-pressure of the order of 300-400 kPa is necessary to be employed.

Maccarini (1987) used saturation by boiling in most of his tests. The sample was put into a bowl with distilled water and the water boiled for 20 min. This procedure achieved full saturation and it was unsuccessful only for the most dense samples where it caused spalling of the ends.

Another method of saturation currently used for rocks, is the application of vacuum. The sample is submerged in water in an air-tight container which is subjected to an incremental reduction in pressure. After the pressure has reached a minimum it is maintained for some time (usually overnight). The time period depends on the porosity, initial saturation, permeability and size of the sample. The pressure is then increased again to the atmospheric value.

An attempt using this method was made with one sample of the artificial bonded soil. The result was disastrous: the expansion of the air bubbles inside it, caused by the reduction in pressure, led to the almost complete disintegration of the sample. A similar problem was described by Carter et al. (1988) when working with calcarenite of North Rankin oil field in Australia. Clearly, the method could not be used as proposed. A modification of this

arrangement was tried and has been successfully used on all of the tests: the dry vacuum method.

Dry samples (usually two at a time) were placed inside an empty air-tight cell (Fig. 4.6) which was evacuated gradually to about 90% of full vacuum (700 mm Hg). After 10 to 15 minutes the cell was slowly flooded with de-aired water from the base with the vacuum maintained throughout. The control of the inflow of water was achieved by the reduction in section of the tube at the water supply. The water was previously de-aired by boiling. Failure to do this caused it to cavitate when entering the vacuum cell which resulted in unwanted oscillations in the internal pressure. When the cell was full, the water valve was closed and the samples left under vacuum overnight. The vacuum was then released slowly using the cone-seated valve. The sample saturation obtained was high with typical B values of 0.96 or more.

The saturated sample was then assembled in the triaxial cell with porous stones and filter paper. Normally some air was trapped inside the membrane but with careful handling most of it could be expelled by water circulation between membrane and sample. The cell chamber was assembled and filled with de-aired water from the laboratory system. An effective stress of 10-20 kPa was immediately applied to expel any excess water before proper consolidation measurements were started.

4.4.3 Investigation of rate effects

The results of isotropic compression tests indicated that the influence of rate of stress application could be considerable (item 4.3.4). So the first consideration was to which extent the yield curves were affected by creep.

Various samples were prepared using a mixture without the crushed fired kaolin (CFK) sand. This mixture was easier to prepare and was used on different occasions to investigate factors like sample size, saturation procedure and creep. It will be referred here as soil 130087 (13% of bonding kaolin plus 87% of quartz sand). The basic hypothesis is that the behaviour of any of the artificial soil samples is principally influenced by the bonding and so a sample

sensitivity to a particular factor can be isolated for any particular mixture.

A series of preliminary tests (tests 001 to 009) were carried out varying the method of saturation, sample preparation, sample trimming, etc. These tests indicated that creep had little influence but that other factors could be of importance.

A new batch of samples was then prepared (Table 4.3) to isolate the influence of each factor. Fig. 4.7 shows the results of two triaxial tests carried out on two similar samples. The samples were tested in drained compression after an isotropic consolidation of 60 kPa. The only difference between the two tests is the rate of straining. Sample 11 was sheared at 5%/h while sample 12 was sheared at 0.03%/h. There is very little difference between their stress-strain curves at the beginning. There is some difference in the peak strengths between them and the yield points could be defined at values of t of 150 kPa and 162.5 kPa, so indicating some influence of creep. However, this influence can be considered negligible when compared with the much stronger effects of isotropic cyclic loading and stress non-uniformity which were apparent from tests 15 and 10 (Fig. 4.8). These samples had the same preparation as the others (11 and 12) and a similar void ratio.

The tilt of sample 10 after consolidation was much greater than for any of the other samples. A flat top cap and load cell were being used and thus a stress concentration was induced on the side first touched by the load cell. Although the rate used was 0.03%/h and some creep may have occurred, the difference in the yield stress was considerable when compared with sample 12. The axial strain determined from external measurements is greatly increased due to this tilt. It is interesting that the stress-strain curve shows some disturbance at around 20 kPa. This may be an indication of localized failure.

This result led the author to look for mechanical arrangements in which this stress concentration could be avoided. Test 15 was the first test in which a loading ball was attached to the load cell and loaded against a flat top cap (see Chapter 3 for details). The result obtained is much improved in relation to the other tests, especially in relation to test 10. However, sample 15 was isotropically loaded/unloaded 3 times between 0 and 60 kPa before

shearing and this seems to have affected its yield point (t=121 kPa) by a considerable amount. Note that in this test the loading stress should have been quite uniform due to the ball seat arrangement and so the drop in yield stress is probably only related to the cyclic loading (sample 15 was sheared at 5%/h).

These results indicate that the creep is not a major influence on the yield stress. Stress concentration and cyclic stress application seem to be more important.

4.4.4 Influence of saturation techniques

The results obtained with the mixture 130087 indicate that the creep was unlikely to have caused the big differences in the isotropic yield stress reported by Maccarini (1987). The results of test 15 (Fig. 4.8) indicate that the cyclic application of stress is a major factor. In the case of test 15 this was caused by a membrane puncture (first unload) and subsequent cyclic loading by the author. Similar effects can be caused by a typical procedure for back-pressure saturation. The first application of cell pressure will not be fully countered by the pore fluid and the sample will be loaded. The subsequent increase in back-pressure will unload it. Further, it is unlikely that the subsequent increases in cell pressure and back-pressure are made in such a way that their difference (i.e. the effective stress in the sample) remains constant all the time. Normally the degree of saturation is ascertained by determining a B value. If its value is less than unity there is again a cycle of loading/unloading the size of which is dependent on the difference between applied pressure and pore pressure generated.

A new series of tests was carried out to verify this point. Table 4.4 contains the information about the samples. They are samples of series 100 i.e. with CFK and quartz sand plus the bonding kaolin. To obtain low densities, wax sand was also added.

When comparing the results it is important to keep in mind that some of the samples did not have the mechanical arrangement of ball loading and most did not have local transducers for axial strain determination. So the stiffness should not be used to examine their behaviour.

Two samples (102 and 103) were saturated by back-pressure using small cell and pore pressure increments of 5 kPa until the desired pressures were achieved. Three other samples (104 to 106) were saturated by the dry vacuum method (as described in item 4.4.2). The stress-strain curves are shown in Fig. 4.9.

All samples were sheared from an initial effective stress of 100 kPa in drained compression. Sample 105 was sheared at 5%/h and sample 106 at 0.03%/h up to 45 kPa, unloaded and reloaded at a faster rate (0.17%/h). There is a slight difference in the results and the unload/reload seems to have affected the result of test 106. Sample 104 was also sheared at 0.03%/h and there is not a significant difference with the results from sample 105 which was sheared faster, both showing a t yield value around 95 kPa.

The results of tests 102 and 103 gave some evidence of the effects of back-pressure saturation in reducing the yield stress. Sample 103 was initially sheared at 0.03%/h, unloaded and then reloaded at 0.17%/h (similar to sample 106). Its yield value is around 80 kPa. Sample 102 showed a similar low yield although it was strained at a different set of rates (initially 0.17%, unload and reloaded at 0.03%/h).

Clearer proof of the damaging effects of isotropic stress oscillation came from the results of tests 107 and 109. They were saturated together by dry vacuum but during the filling of the vacuum cell with deaired water the water inlet tube was accidentally left open to the air for about a minute. The entrance of air in the vacuum cell made the pressure inside oscillate quickly in an uncontrollable way. The samples ended up fully saturated and were tested in the same way as samples 102 to 106. Fig. 4.10 shows the test results together with the shadowed area of tests 104 and 105. There is a clear difference. The yield stresses dropped to 54 and 62 kPa. The effect of cyclic isotropic loading is thus made evident by these extreme cases.

The final evidence of the effects from saturation by back-pressure was provided by Maccarini (1988). He confirmed that the samples used in his first tests were saturated by back-pressure; among these were the samples used in the tests with incremental loading presented in Fig. 4.5.

A summary of the results discussed here has been published by Bressani and Vaughan (1989) together with some evidence from literature.

It appears from the differences in test results that damage to the soil structure during saturation is governed by the intensity of the cycling. If the back-pressure procedure is used carefully the damage can be reduced to a minimum. The most beneficial improvement would be to have a system that simultaneously increases the cell and the pore pressures maintaining a constant effective stress in the sample. The rate of increase should be a function of soil permeability and initial saturation. This procedure was successfully carried out for the soil 130087. For the artificial soil, however, the dry vacuum method proved to be more convenient and was used throughout the work.

There is not much in the literature about the effect of the back-pressure technique in relation to strength. Brand (1975) studied its effect on the behaviour of undisturbed samples of soft Bangkok Clay. He found that the soil structure was destroyed even when confining stress and pore pressure were slowly raised simultaneously. To determine B values, increments of cell pressure of 69 kPa were applied. Brand's results show that the undrained behaviour of samples consolidated against zero back-pressure gave the stiffer and stronger responses. Note that all of the samples could be assumed to be virtually saturated prior to shear, based on the calculations of water content and void ratio.

Dias (1987) found that samples of lateritic soils from Brazil which were soaked by percolation (no back-pressure) showed higher strengths than when fully saturated by back-pressure. The percolation achieved degrees of saturation of 85%. Tests performed to determine suction equilibrium in the same soil indicated that small values of suction (less than 20 kPa) can be expected for this condition.

4.4.5 Influence of sample size during preparation

One initial idea was to develop a model test of a pressuremeter or of a plate loading test to study the influence of cementation under controlled conditions.

The first step was to produce large enough samples in which such tests could be carried out. The procedure of sample preparation followed that described earlier for the smaller samples. The wet mixture was poured into a double layer paper mould of 100 mm diameter and 180 mm height.

The first two samples had cracks across their length after firing. The heating and cooling times were varied, so also was the position of the samples during firing. The first samples were laid on their sides (as the kiln was not large enough to stand them upright) and fired as usual (500°C, 5 hours). In order to try to avoid the cracking, the third sample was dried under lamps and then placed in an oven at 80°C with forced air circulation. Then with the sample upright (in a larger kiln), the temperature was raised to 500°C in a larger number of small increments in temperature (Fig. 4.11). The temperature reduction was controlled and more gradual. Even so the sample cracked near the top but to a lesser degree. The points in the figure represent the steps of temperature/time used. The first two samples were left to cool overnight for their final stages. The third, however, had its temperature lowered to 260°C before the kiln was switched off.

The samples were later cut down to triaxial sample sizes (38 mm diameter x 76 mm height). Fig. 4.12 shows the results obtained (t versus ϵ_a) when they were sheared. As before, they were saturated using the dry vacuum method, consolidated to 60 kPa and sheared in drained compression.

Samples 16 and 18 were cut from the first large sample and they have similar failure stresses (although their rate of straining was 0.03%/h and 15%/h respectively). Sample 20 was cut from the third large sample and sheared at 5%/h. It seems that the behaviour of this sample is similar to that of the ones produced in smaller sizes. However, it is still affected by the preparation technique as it failed at lower stresses than samples 11 and 13 described earlier (shaded area in the plot). It would seem that the history of firing in large sample sizes is an important factor to consider when producing larger samples.

Mixture Code	Composition on mixing[a]					γ_d
	Kaolin (%)	CFK (%)	Quartz (%)	Wax (%)[b]	Water (%)	(kN/m^3)
133057	13	30	57	8	45	10.6
	13	30	57	-	41	12.5
130087	13	-	87	-	35	15.5
168400	16	84[c]	-	-	74	10.1

(a) Percentage of the dry weight of the soil
(b) Percentage over the other solid constituents
(c) In this mixture the CFK was obtained from kaolin fired at 500°C (300 series)

Table 4.1 — Composition of artificial soil-mixtures used

Series	Composition (%)				Firing		Density
	Kaolin	CFK	Quartz	Wax	(°C)	(h)	(kN/m^3)
000	13	-	87	-	500	5	15.5
100	13	30	57	8	500	5	10.6
200	13	30	57	-	500	5	12.5
300	16	84	-	-	500	5	10.1
500	13	30	57	8	800	3	10.6
600	13	30	57	-	800	3	12.5

Table 4.2 — Code naming of the artificial soil series

Sample	γd (kN/m^3)	e_0	Saturation (see text)	σ'_3 (kPa)	Local axial instrum.
10	16.03	0.610	Suction	60	No
11	15.98	0.615	Suction	60	No
12	15.89	0.624	Suction	60	No
13	16.19	0.595	Suction	60	No
14	15.95	0.618	Back-press	60	No
15	15.89	0.624	Suction	60	No
16	15.85	0.628	Suction	60	Yes
17	15.87	0.627	Back-press	60	No
18	16.01	0.612	Suction	60	No
19	16.16	0.597	Back-press (not satur.)	100	Yes
20	16.24	0.589	Suction	60	Yes

$G_s = 2.631$

Table 4.3 — Samples of soil 130087 fired at 500°C/5 h

Sample	γd (kN/m^3)	e_0	Saturation	σ'_3 (kPa)	Local axial instrum.
U101	10.97	1.37	Suction	100	No
101	10.87	1.39	Wet suction[a]	-	-
102	10.95	1.37	Back-press	100	No
103	10.90	1.39	Back-press	100	No
104	10.98	1.37	Suction	100	No
105	10.87	1.39	Suction	100	No
106	11.17	1.33	Suction	100	No
107	10.50	1.48	Suction[b]	100	Yes
108	10.49	1.48	Boiling[c]	100	Yes[d]
109	10.51	1.47	Suction[b]	100	Yes

$G_S = 2.65$
(a) Sample destroyed
(b) Accident during saturation
(c) Not fully saturated
(d) Bad measurements

Table 4.4 — Samples of soil 133057 fired at 500°C/5 h

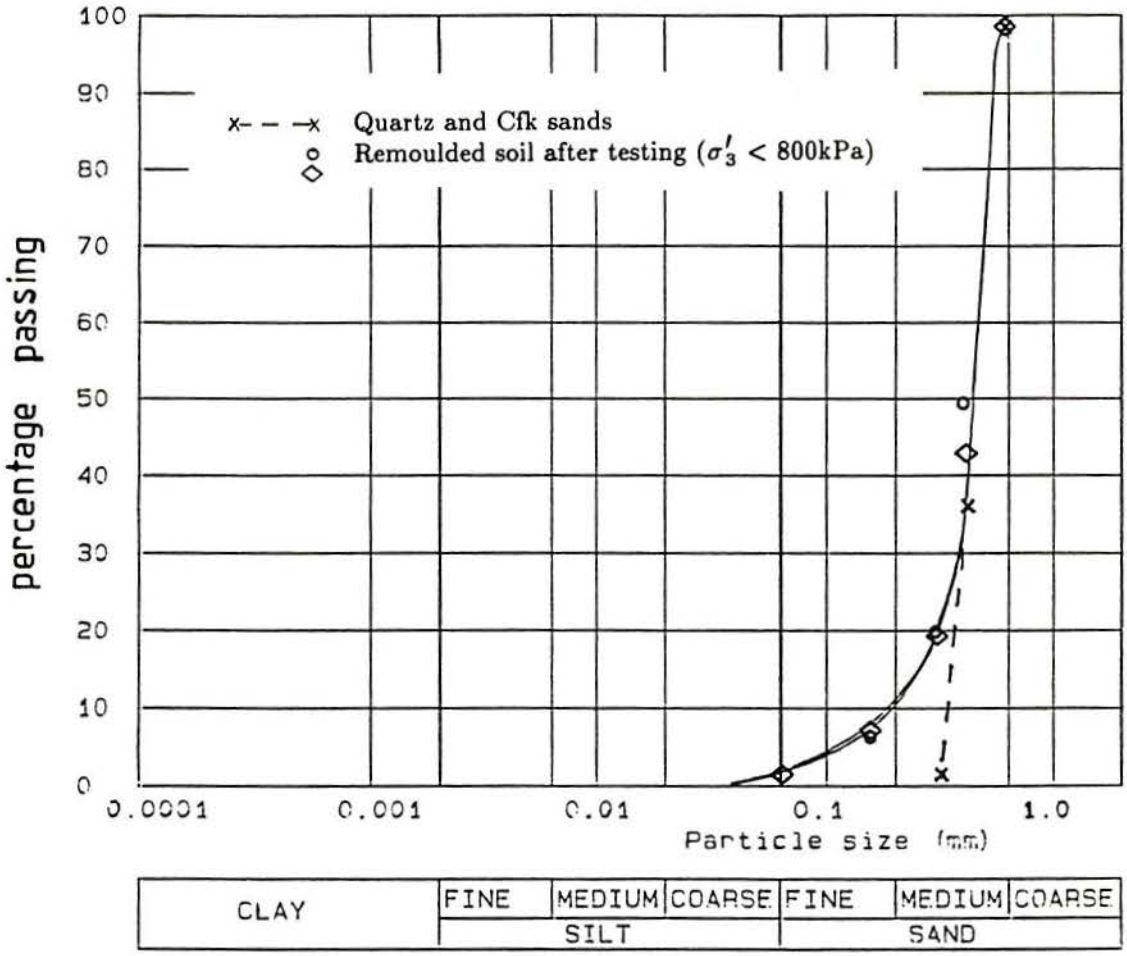

Figure 4.1 – Grading curves of the sands used in the artificial soil

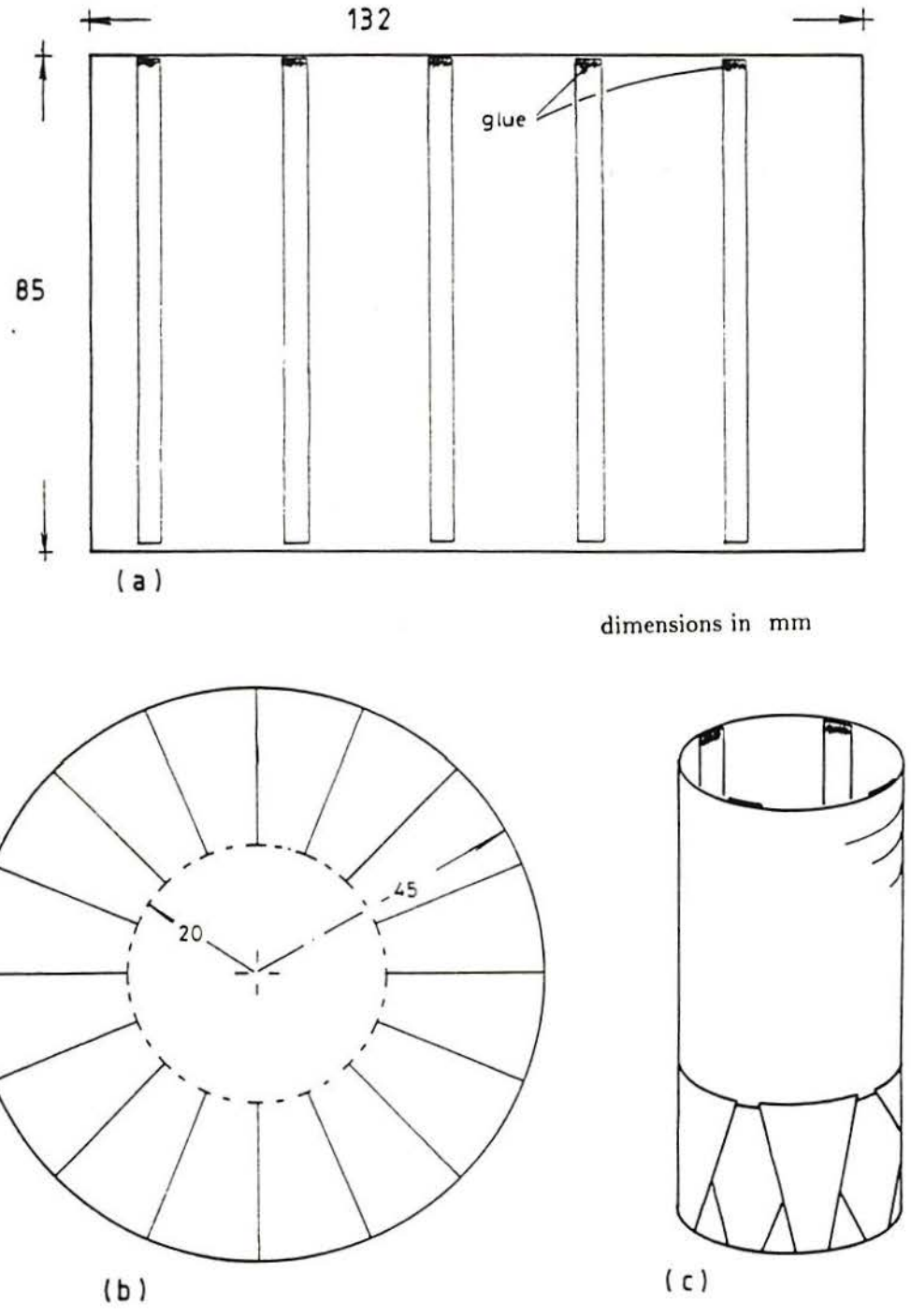

Figure 4.2 – Paper mould into which the wet mixture is poured; (*a*) tube piece; (*b*) bottom and (*c*) complete mould

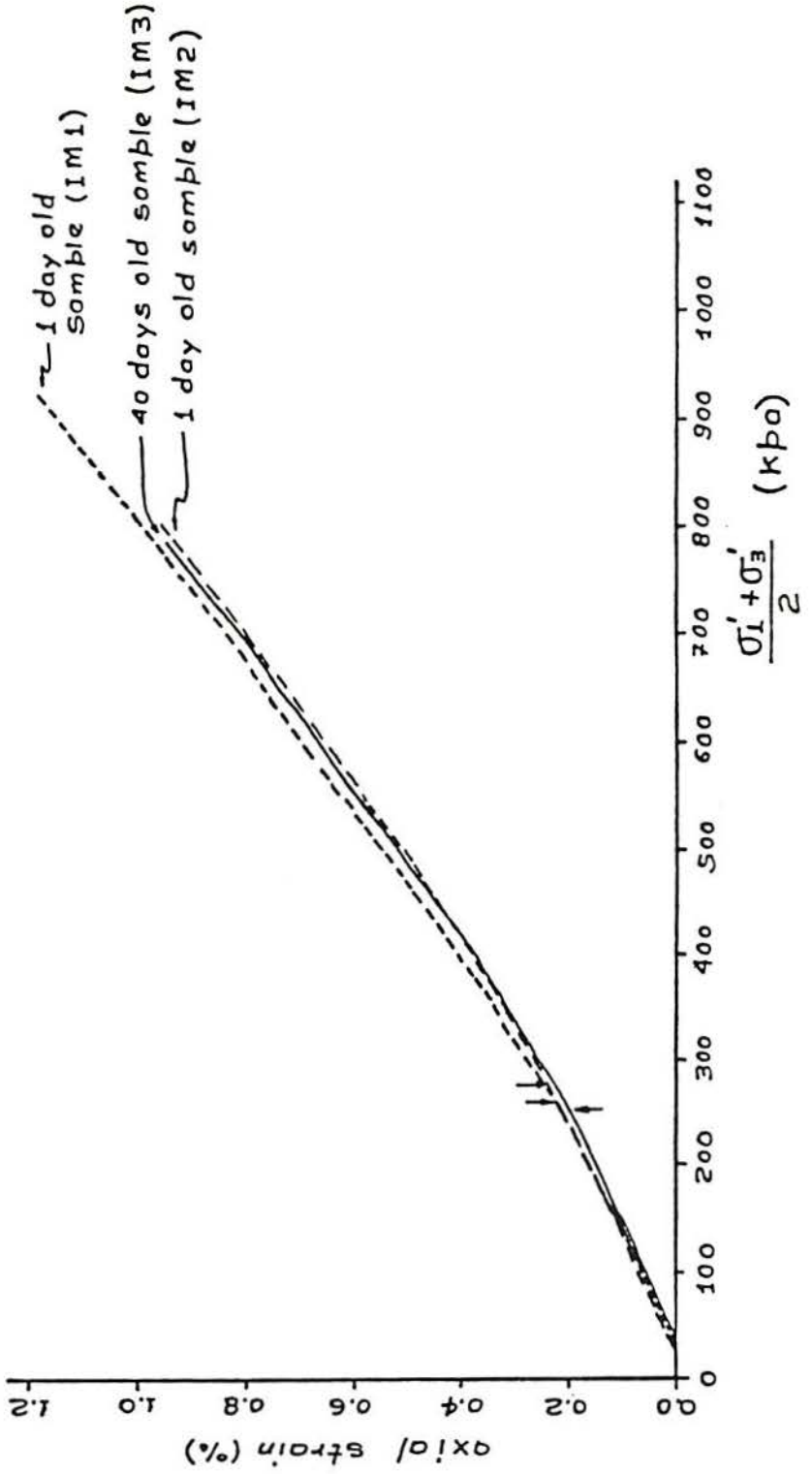

Figure 4.3 – Effect of time storage on the artificial soil behaviour (after Maccarini, 1987)

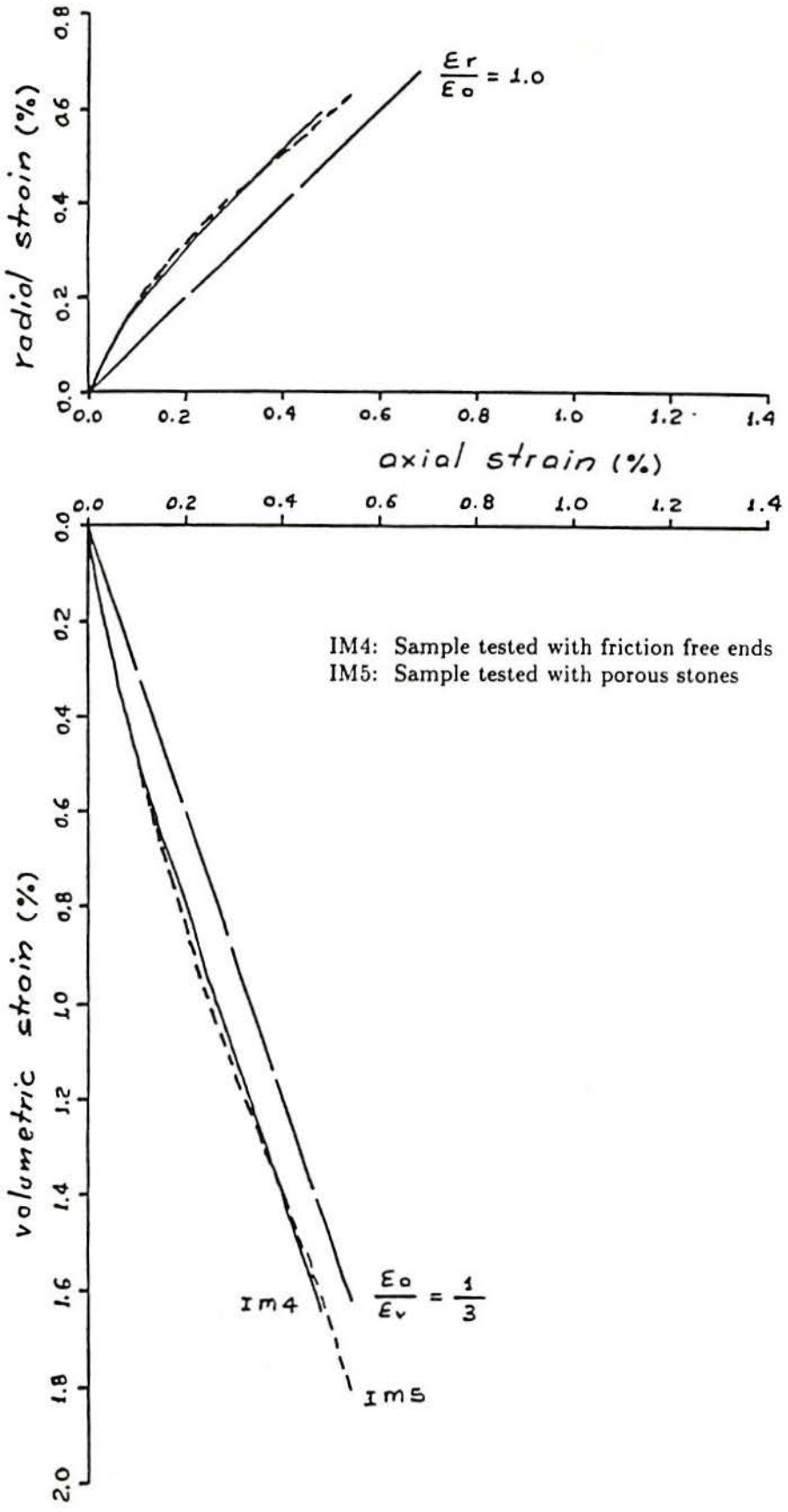

Figure 4.4 – Behaviour of the artificial soil during isotropic compression (after Maccarini, 1987)

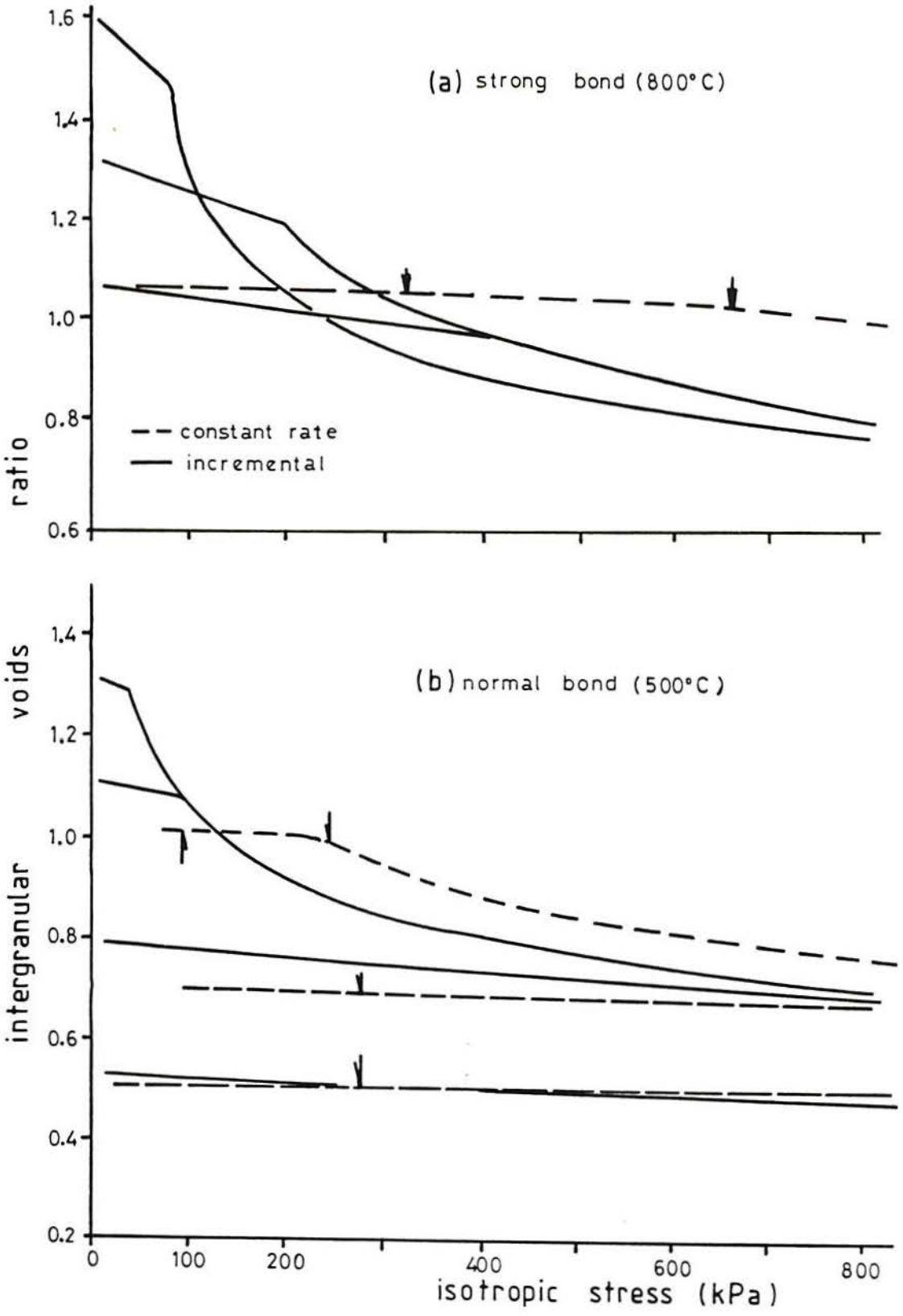

Figure 4.5 – Compressibility and yield of artificial soil under incremental and constant stress increase loadings (redrawn from Maccarini, 1987)

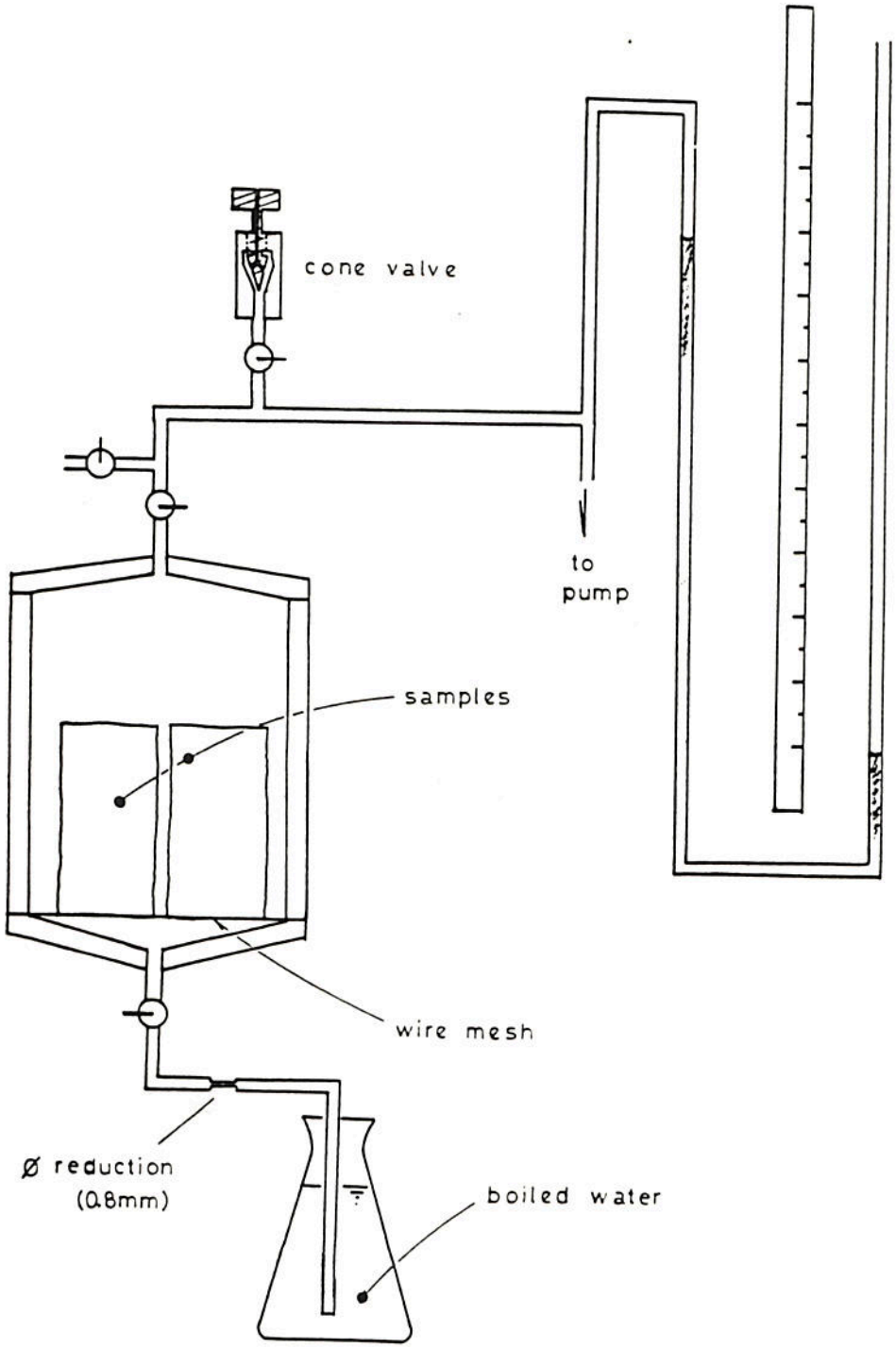

Figure 4.6 - Equipment used to saturate artificial soil samples (not to scale)

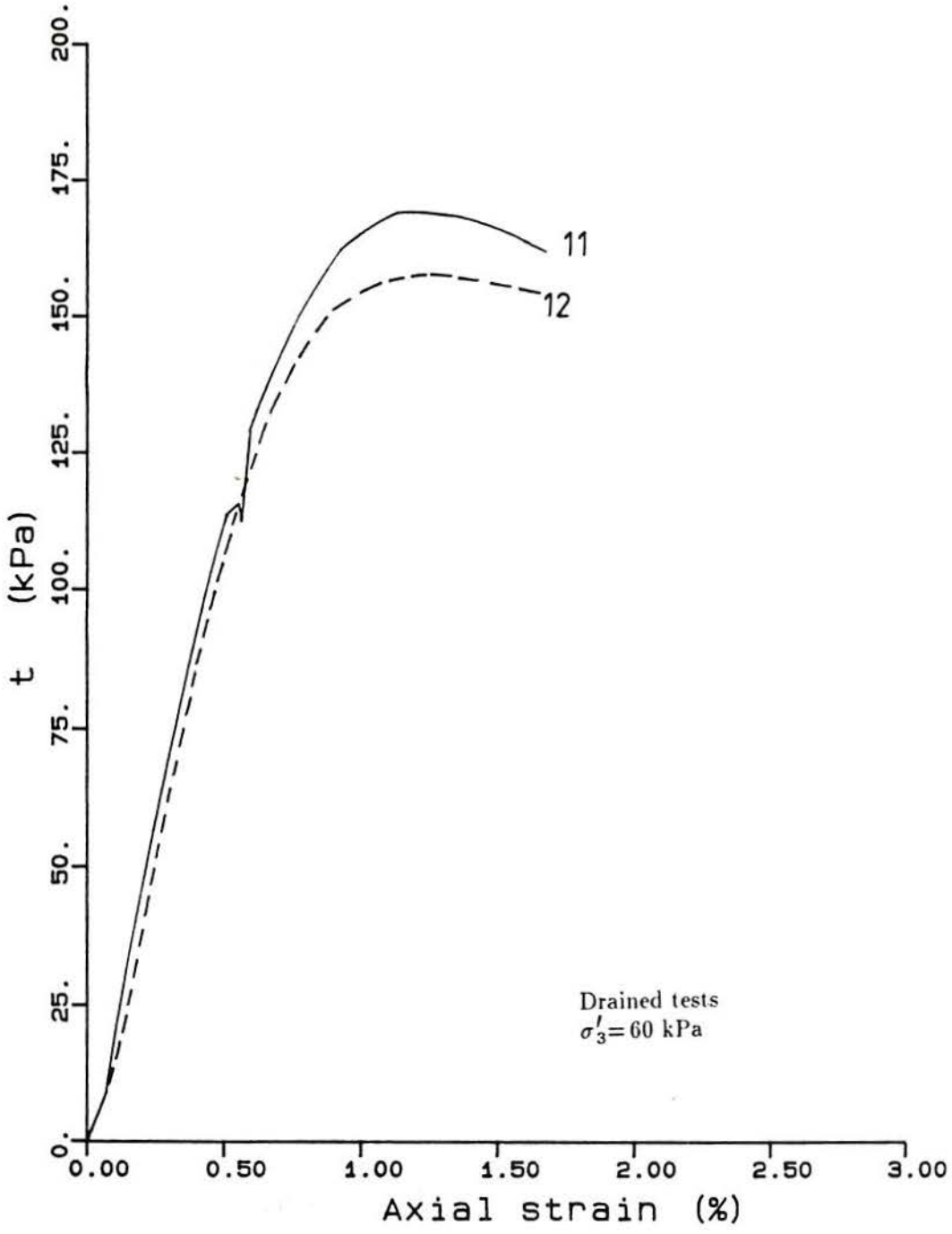

Figure 4.7 - Triaxial drained compression test results of soil 130087 (00 series). Influence of rate of shearing

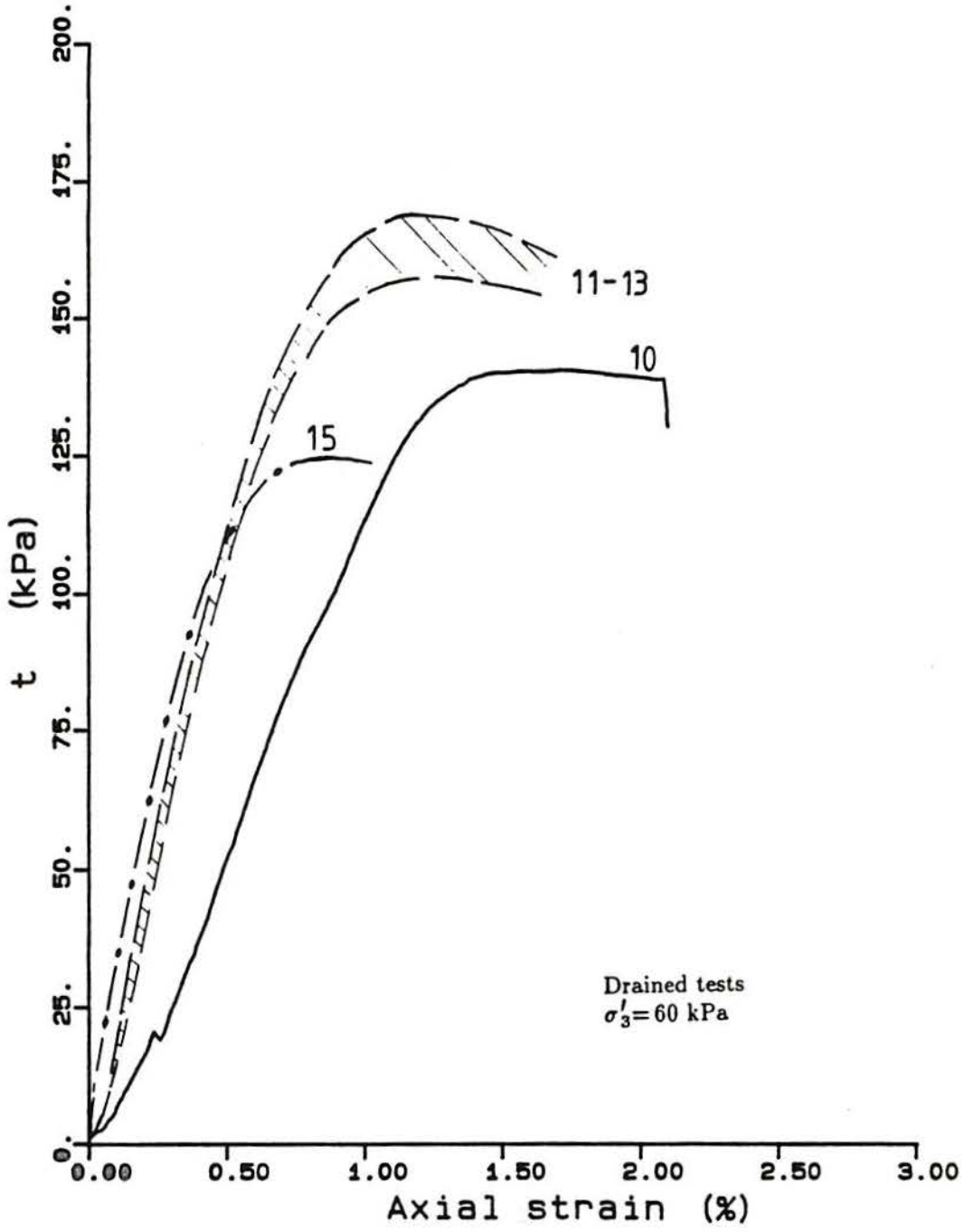

Figure 4.8 – Triaxial drained compression test results of soil 130087 (00 series).
Influence of isotropic cycling and non-uniformity of loading

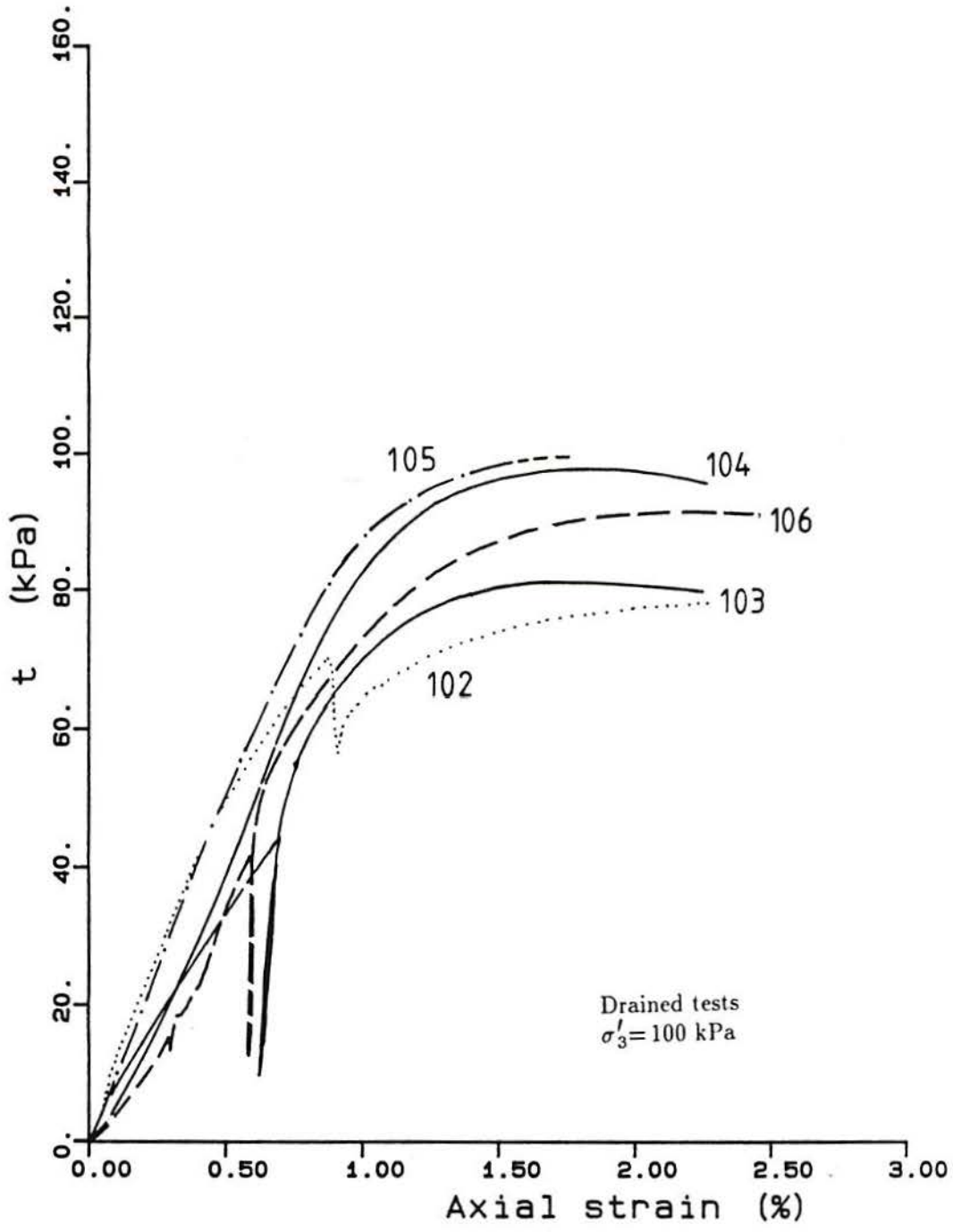

Figure 4.9 – Triaxial drained compression test results of soil 133057 (100 series). Influence of saturation procedures

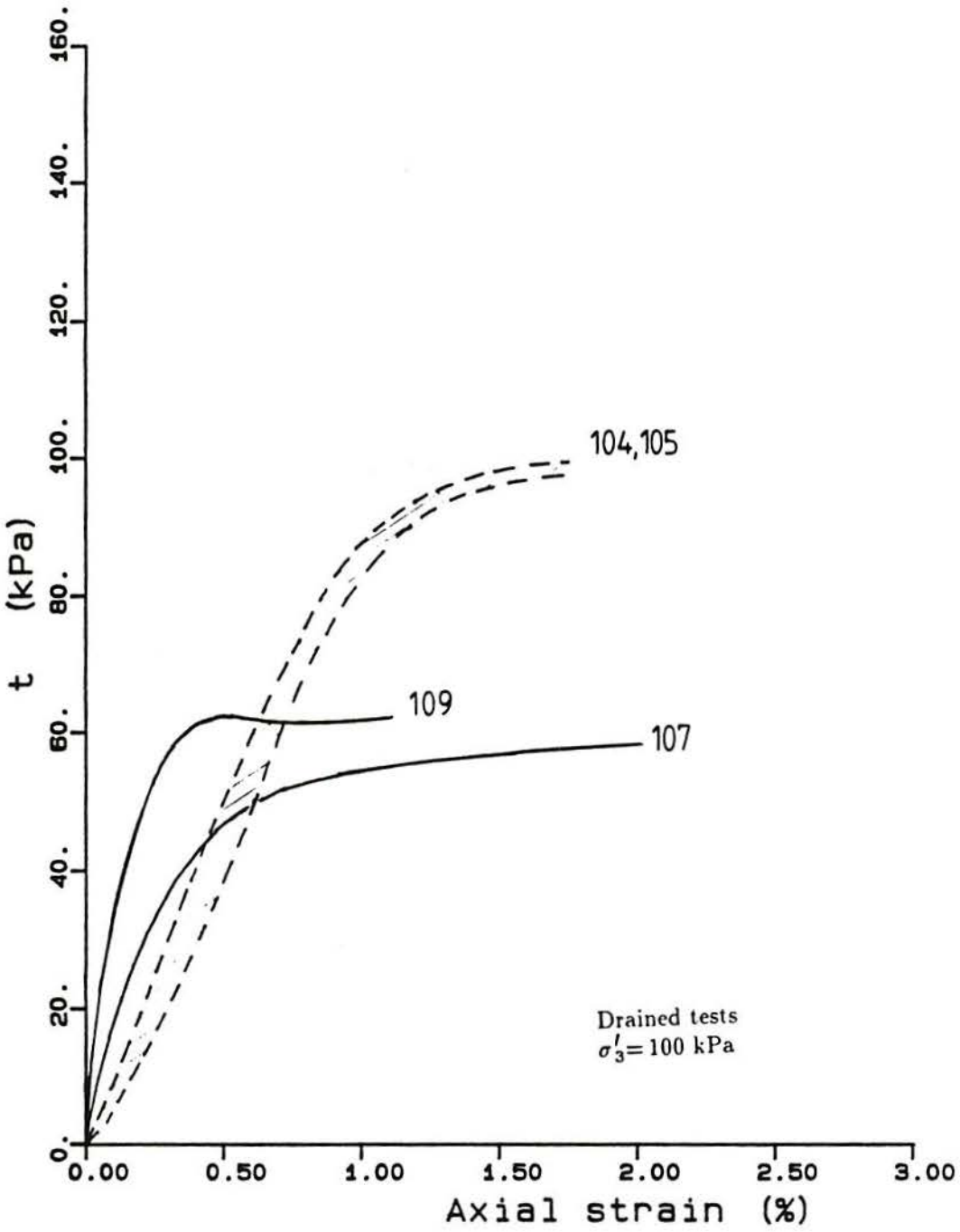

Figure 4.10 – Triaxial drained compression test results of soil 133057 (100 series). Influence of past cyclic loading during saturation

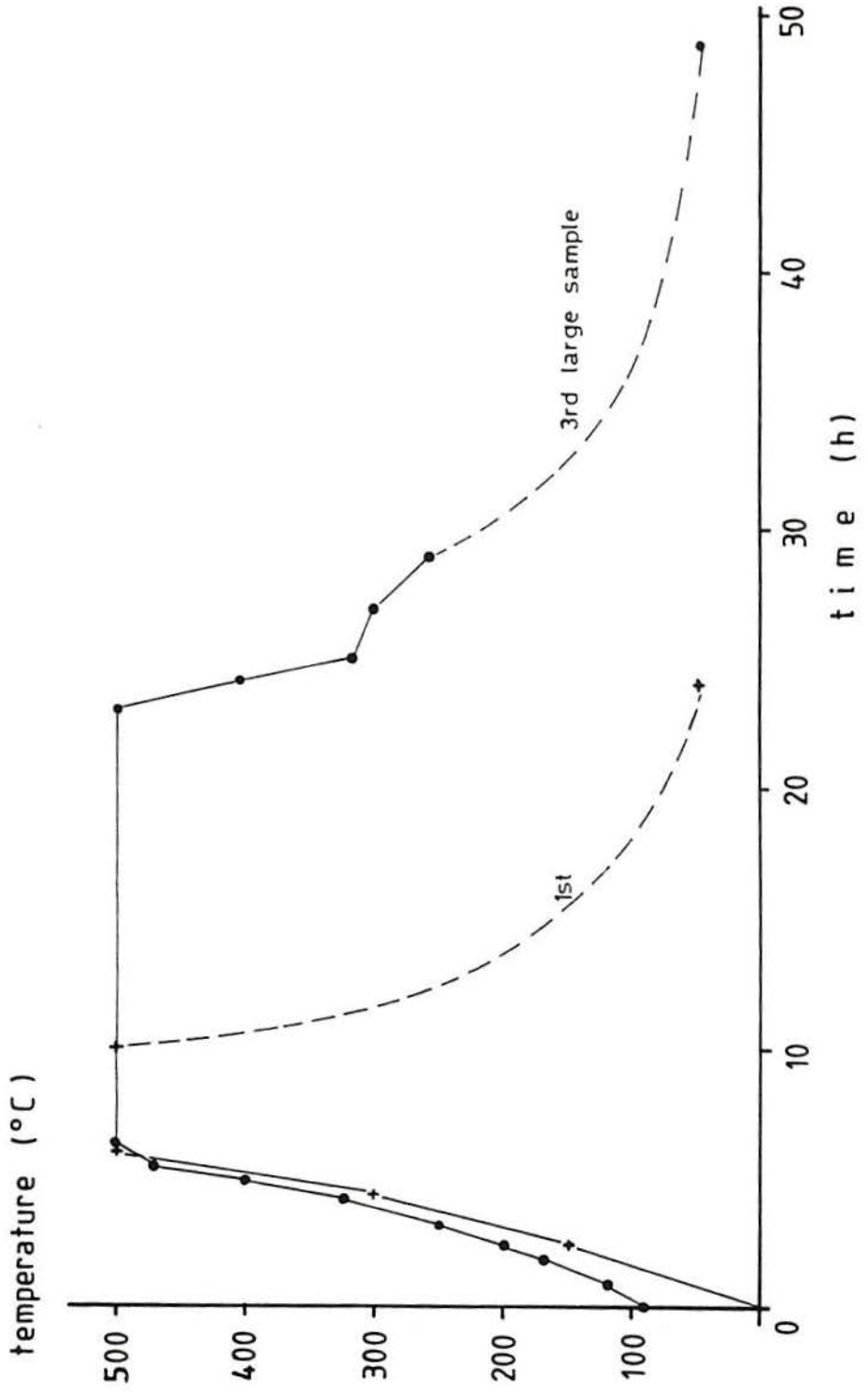

Figure 4.11 – Temperature history of two large samples (h=180 mm, D=100 mm)

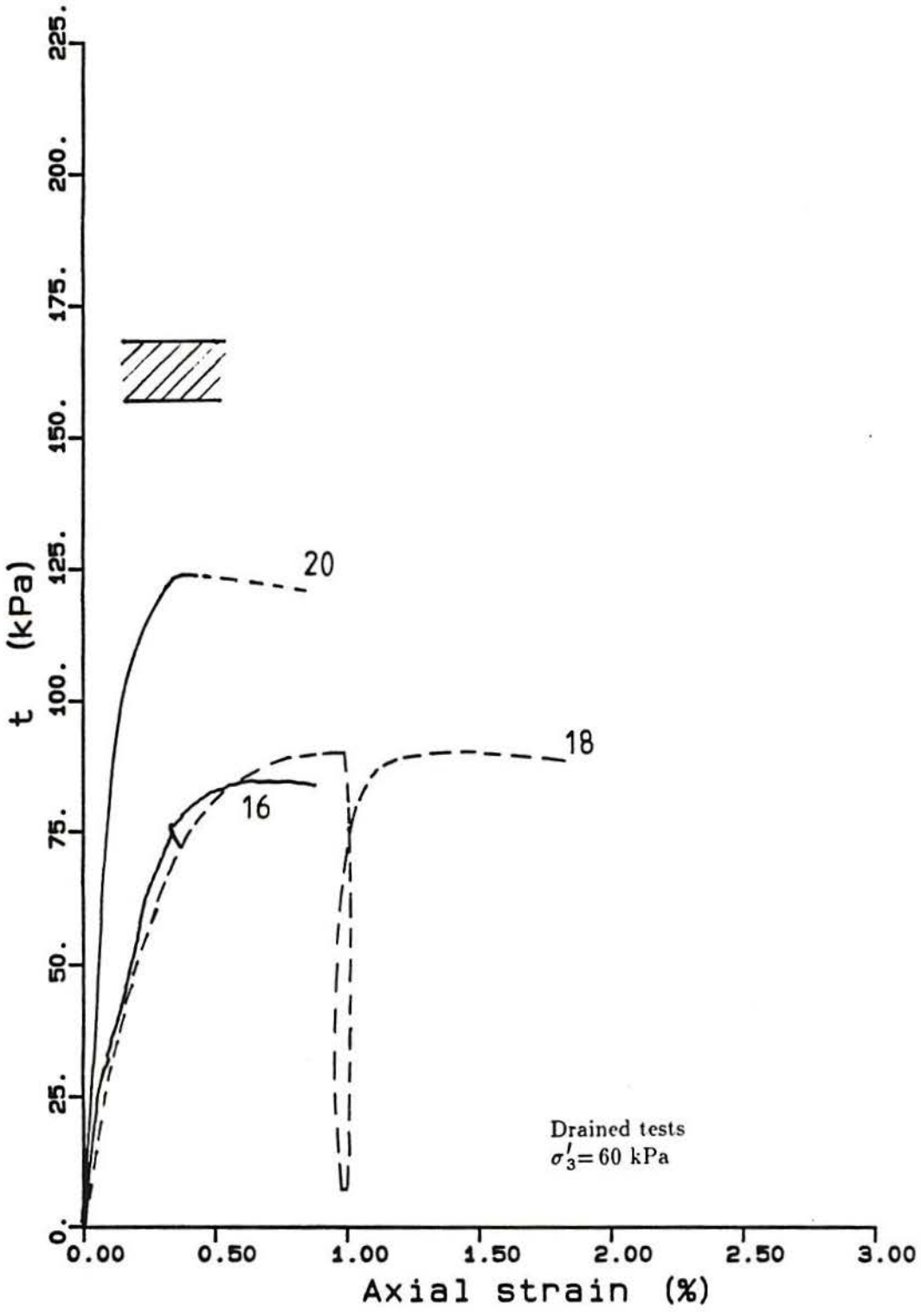

Figure 4.12 - Triaxial drained compression test results of soil 130087 (00 series). Influence of sample preparation size

5. ARTIFICIAL BONDED SOIL — 100 SERIES (void ratio $\simeq$ 1.5)

5.1 INTRODUCTION

The results of the second series of tests on the high void ratio material are presented in this chapter. Although occasional references are made to tests 101 to 109, most of the analyses will be based on tests 110 to 118 together with tests S100/1, S100/2 and S200. Table 5.1 contains some basic information: test name, void ratio, form of saturation, consolidation stress, the presence or otherwise of local measurements of axial strain and an indication of what kind of top cap arrangement had been used (Chapter 3). All twelve tests were initially drained and were subjected to isotropic consolidation before shearing. All of the samples were saturated by the dry vacuum method described previously.

5.2 REVIEW OF PREVIOUS WORK

All of the results discussed in this section were obtained by Maccarini (1987). The material used by Maccarini is the same as that used for the present study, but with a slightly higher void ratio (1.6). However, since the bonding is the main characteristic of the soil, it is considered that his results can be compared directly with those presented later.

5.2.1 Isotropic compression behaviour

Fig. 5.1 shows the results of isotropic compression tests on samples IL1 and IL2. Both samples were fired at 500°C for 5 hours. Their total void ratios were 1.58 and 1.60 respectively. The confining effective stress was increased at a constant rate of 0.8 kPa/min during the test. The arrows in Fig. 5.1 mark two points at which a change in behaviour was

observed. The first point was described as "an initial gentle yield", indicated by departure from an initial linear portion. At this point, the stress level was 95 kPa for samples IL1 and IL2. The second arrow, at 270 kPa, indicates the stress level at which marked deformation starts. This second point was designated "second yield".

The results of isotropic consolidation on a sample with a stronger bond (IL3, fired at 800°C for 3 hours) are plotted on the same figure. The same two stress levels were identified, using similar definitions. The first yield was identified at 320 kPa and the second at 660 kPa.

In all three samples, axial strain was measured locally. The measured volumetric strain was affected by membrane penetration into the sample and was therefore not used. All three samples were saturated by boiling.

5.2.2 Triaxial drained tests

Maccarini (1987) presented results of five triaxial drained compression tests on the artificial soil with void ratio 1.6 (Fig. 5.2) in which the axial strains were measured with local transducers.

At low confining pressures (8 and 50 kPa) the soil showed brittle behaviour. As the confining pressure increased the initial stiffness dropped in absolute value. Only test ILS8 exhibited any dilation, though its maximum dilation rate happened after peak deviator stress was reached. Test ILS50 showed a clear peak and it compressed throughout. In both cases the peak strength was little if at all affected by the energy component due to dilation as is the case for dense sands. Taylor (1948) proposed that the shear strength of a specimen is a sum of two components, one due to friction between particles and the other due to interlocking. His work was later expanded by Schofield and Wroth (1968). They formalized the energy equation for a direct shear test as

$$\tau \, A \, dx = \sigma'_v \, A \, dy + \mu \, \sigma'_v \, A \, dx$$

This expression relates the total energy expended in the shearing process (τ A dx) with the energy due to dilation (σ_v A dy) and due to internal friction ($\mu \, \sigma'_v$ A dx).

The initial stiffness obtained from the triaxial tests in the artificial soil was not a direct function of the confining pressure as is the case for unbonded soils. The less dense soil (e=1.6) showed a drop in stiffness when the confining pressure was increased beyond a certain level (Fig. 5.3).

A summary of all of the results obtained from tests on the less dense soil are presented in Fig. 5.4. The lines marked 1 to 5 correspond to the drained compression tests. Samples marked 7, 8 and 11 were tested under a constant ratio of σ_1'/σ_3' and line 9 was a one-dimensional compression test. The black points represent the main yield points obtained from such tests. There is little difficulty in defining these yield pressures for tests 6, 8 and 9 from the plot of axial strain versus average pressure. In the conventional compression tests the point of maximum curvature of stress-strain curves was adopted as the yield point. For tests 1 and 2, these coincide with the peak strength.

The behaviour of the one-dimensional compression test is worth special attention. Its stress path approximated to a straight line until close to the failure envelope, with small axial strain (0.5%). After that point the stress path starts to move in the direction of the unbonded soil stress path, accumulating strains (from 0.5% to 8.5%). After reaching this unbonded line its stress-strain behaviour becomes more or less linear.

5.3 TESTING DETAILS AND EQUIPMENT

The same basic equipment as described in Chapter 4 was used: a triaxial stress path cell and a constant rate of displacement triaxial cell both with the usual electronic transducers (volume gauge, internal load cell, external displacement transducer and cell and pore pressure transducers). However, two significant changes to the system were made in relation to the tests described before: a pair of electro-levels for local measurement of axial strain was made available and a loading button was used in all tests except test 115. The initial arrangement

used (described as "preliminary" in Table 5.1) was simply a loading button attached to the load cell and a flat surface top cap. Later this arrangement was modified to the system described in Chapter 3 (Fig. 3.8). The guided top cap can accommodate larger strains without excessive tilting. Filter paper discs were not used in any of the tests as they were not considered necessary.

During the investigation, the author also used a pair of local axial strain transducers based on the Hall effect device (see details in Chapter 3). Tests 113 and 114 are the same as those presented in Fig. 3.9 and 3.10. Specific details of each test are given when discussing the test results.

The main differences between the tests presented here and those of Chapter 4 are that these samples were all saturated by the dry vacuum method and that no effect of stress concentration in shear should be expected due to the loading arrangement used.

5.4 RESULTS OF ISOTROPIC COMPRESSION TESTS

5.4.1 The isotropic yield

A brief summary of specific test details is given when presenting the test results. Six consolidation tests were performed, the first two of which (110 and 111) were consolidated to pressures of around 430 kPa.

Test 110 was the last one in which no local instrumentation was used. The isotropic pressure was increased in steps up to 425 kPa. The second test, 111, had local measurements of axial strain and the effective confining pressure was increased at a constant rate of 0.27 kPa/min up to 430 kPa.

In test 110, in addition to measuring the volumetric strains externally, the vertical displacement of the top cap was measured at the end of each consolidation step. The procedure was to lower the load cell ram until the load cell attachment touched the top cap. A

nominal load of 2N was applied so that the load cell deflection was the same on each occasion. This assured a positive contact which would be difficult to guarantee by visual means only. These measurements allowed the calculation of the axial strain at each stress level. Naturally, there is a small error due to the true bedding as discussed previously.

In test 111, local instrumentation for measuring axial strain was used and the monitoring of the transducers allows the definition of a continuous line. The data are plotted together with results of test 110 in Fig. 5.5 and 5.6. Both sets of volumetric data seem to agree well, although the constant rate of stress increase sample exhibited stiffer behaviour at a stress level greater than 300 kPa. At the end of the test, the pressure was held constant, and the sample showed some creep from 9.8% to 11.2% volumetric strain, moving towards the volumetric strain of test 110.

Some problems were experienced with the local axial transducers in test 111. One of the pads glued onto the membrane fell off at around 350 kPa and they indicated negative strain measurement at the beginning. This negative strain may have been caused by a slight pushing of pads and membrane against the sample by the increasing pressure. This causes the transducer to register an apparent sample expansion. Such problems can be eliminated by applying suction to the sample before gluing the pads or, alternatively, by using a strip of membrane on top of them forcing contact with the sample from the beginning of the test. This latter solution was used in all subsequent tests.

In test 111 the same technique of measuring the axial strain externally was used. The results of seven such measurements are also plotted in Fig. 5.5. As the test was left running overnight no external measurements were taken in the range 30 to 290 kPa. The last two points represent the creep that the sample showed over a period of 91 hours. Also in Fig. 5.5, five points obtained from the incremental consolidation of another sample (112) up to 225 kPa are plotted. The external measurements give closely parallel lines of deformation before and after yield. The value for the pressure in which the first linear portion breaks can be assumed to be between 280 and 310 kPa. The same range is also indicated by the local measurements

(296 kPa by the lines intercept).

The plot of volumetric strain against confining pressure (Fig. 5.6) gives very similar values for the breaking point (yield). Test 110 gives a value of 280 kPa again and test 111 a value of 305-310 kPa.

Using the same data, a new plot was produced. In Fig. 5.7 the axial strain curves were shifted vertically so that they all gave a value of zero axial strain for 30 kPa effective stress. This pressure was chosen arbitrarily because the measurements of the small strains/pressures were not reliable. There is a close agreement between the curves before the yield.

The volumetric data is affected to some extent by membrane penetration. Although the resulting error can be evaluated for remoulded samples through special tests or different sample sizes and geometries (see Vaid and Negussey (1984) for details) this would be impractical or impossible for the undisturbed samples. A radial belt for measuring the radial strains directly is necessary. Maccarini (1987) used such a belt for testing and the author developed another one (see Chapter 6). The author's tests on the artificial soil with a void ratio of 1.1 gave corrections that are very close to those obtained by processing Maccarini's data from similar samples (Fig. 5.8). As no direct radial strain measurements were made on the high void ratio samples, the correction obtained from Maccarini's data for the less dense samples was applied to the results of tests 110, 111 and 112.

Fig. 5.9 shows the volumetric strain data with the membrane penetration error taken into account. The curves were shifted so that they read zero at 50 kPa (the membrane penetration error is very large up to this pressure). The agreement between the three test results is good in the range 50-275 kPa.

After the yield pressure the soil appears to be affected by the rate of stress increase. The incremental test (110) seems to be more compressible than the constant rate of stress increase test (111). The yield pressures obtained from this are 285 kPa (test 110) and 310 kPa (test 111) indicating some influence of the test procedure. As with the axial strain, in test 111 there was some continued volumetric strain under constant pressure at the end of the test.

An examination of the increment of volumetric strain against time for each step of pressure in test 110 can throw some light on this behaviour (Fig. 5.10). Curves are shown for pressures of 100, 165, 230, 280, 360 and 425 kPa. The first increment of 65 kPa is not shown. No corrections of any kind were applied. During the test the time for final consolidation was arbitrarily fixed at 2 hours so that all steps can be compared directly. The curves for the stresses of 100 and 165 kPa indicated that consolidation was complete within that time. The curve for 230 kPa shows that there was still some tendency to deform after 2 hours. At 280 kPa the sample had a different initial behaviour. Instead of a sudden jump in volumetric strain, associated with the material's high permeability, the sample showed a more gradual consolidation curve. The deformation had not stopped completely at 2 hours. At 360 kPa the sample deformed much more than previously and was still deforming after 2 hours (insert in Fig. 5.10). At pressures of 360 and 425 kPa, the initial deformation was less pronounced than at lower pressures. Creep of the structure due to internal redistribution of stress is the likely explanation. The rate of creep after the yield is known to increase dramatically on the artificial soil (Maccarini, 1987). The sample was left with the stress of 425 kPa for a total of 86 hours. It would appear that the creep starts somewhere before the yield pressure but that it only becomes significant after that pressure has been exceeded. Note that the pressure of 280 kPa was very close to yield pressure defined for the same sample (285 kPa), and so it is not surprising that the creep became noticeable at that increment.

5.4.2 Creep effects and initial yield

The results presented suggest that there is considerable creep after the yield pressure is exceeded and that the soil behaves linearly up to the yield pressure. There was no indication of a first yield as suggested by Maccarini (1987). The measurements presented, however, are subject to some errors and the behaviour up to 50 kPa was disconsidered in the analysis.

The consolidation phase of four other samples provided some useful information on the pre-yield phase. As stated above, some samples were tested using two pairs of local

transducers for axial strain determination (see Chapter 3 for details). In these tests, the pads were initially held in place by a membrane strip so that close contact was maintained with the sample before the confining pressure was applied.

Test 113 was consolidated isotropically to 160 kPa under two rates of stress increase. From 27 kPa to 98 kPa the effective stress was increased by 0.90 kPa/min. The rate was then increased to 3.6 kPa/min until the final pressure was reached. The axial strains obtained from the two pairs of local transducers are shown against pressure in Fig. 5.11.

From the results it is not possible to observe any significant influence of the rate of stress increase on the deformation of the sample and there is no evidence of any change in compressibility in the stress range covered by the test. The agreement between the two sets of measurements is satisfactory.

Sample S200 was consolidated isotropically to 200 kPa using two rates of stress increase: 0.16 kPa/min up to 137 kPa and 0.41 kPa/min from then on. As before, no influence of this change can be observed, nor is any first yield visible. On this test only one pair of local transducers was used.

Sample 114 showed different behaviour. The rate of stress increase was maintained constant throughout at 1.8 kPa/min. Initially, the sample showed large compressibility up to around 50 kPa and then a compressibility of the same order of magnitude as the other two samples. This behaviour was shown by the two independent local measurements. At the end of the test, however, one of the pairs of local measurements showed a creep of 0.1% strain over a period of 100 min when neither the other pair nor the volume gauge indicated such behaviour. There is no apparent cause for the initial high compressibility of sample 114.

The results presented so far show that the yield pressure determined by incremental stress increase is similar to that determined from a constant rate of stress increase (tests 110 and 111). The compressibility before yield is also little affected by changes in rate during the test. The rates used varied between 0.16 kPa/min (test S200) and 3.6 kPa/min (test 113).

The lack of sensitivity of the stiffness to the rate would suggest that the yield pressure

should also be unaffected by the rate. Unfortunately, this is not the case. Sample 115 was consolidated to an isotropic stress of 515 kPa at a quick rate (7.5 kPa/min). Having reached this pressure, the sample was left for a period of 118 hours. During the first 27 hours the pressure remained constant but it dropped from then on due to a undetected leakage in the pressure line [Fig. 5.12(a)]. The volumetric strain obtained during the loading of the sample is plotted in Fig. 5.12(b). The two lines represent the direct measurements and the measurements with the membrane correction taken into account (see Fig. 5.8). The points on the corrected plot indicate the pressures at which the error was calculated. Below 50 kPa the value of the error was similar to the value measured. There is a clear indication of yield at around 375 kPa which represents a 30% increase over the value obtained from the previous tests. It is interesting to note that yield occurs in a region in which the membrane error is constant with pressure, which means that it cannot have had any influence on the determination of yield pressure.

The axial strain determined from local transducers is shown in Fig. 5.13. However, the logging system did not start taking their readings until the effective pressure had reached 305 kPa. For this reason, the axial strain was assumed to be 1/3 of the volumetric strain at that pressure (ϵ_v=1.9%). The extrapolation back to origin provided a reasonable fit to the data, suggesting that the data can be relied upon. This plot again indicates a yield pressure of 375 kPa. This test also had another pair of local transducers. The results are not given here, but the same yield pressure can be inferred from them.

The fast rate used in test 115 (7.5 kPa/min) induced a greater value of the yield pressure than when using incremental consolidation or a slower rate (0.3 kPa/min, test 111). However, this rate influence seems to be important only before the yield. From Fig. 5.13 (or Fig. 5.12) it can be seen that the sample underwent considerable deformation under a constant effective pressure of 510 kPa. The creep was present for 18 hours, after which the sample seemed to stabilize. Six hours later the cell pressure started to drop due to the leakage for a period of 88 hours. The pressure was then further decreased to a value close to zero and

reloaded at a fast rate (7 kPa/min). The unload/reloading curves do not show any sign of being influenced by the rate and the small creep at the end of the consolidation was over in a period of 30 min.

5.4.3 Bulk stiffness

Bulk stiffness values were calculated from all of the test results wherever possible. The samples were assumed to behave isotropically.

(*a*) Pre-yield stiffness

(i) external axial strain – tests 110, 111, 112 (Fig. 5.7)

K = 9.3 MPa

(ii) local axial strain – tests 113, S200, 114 (Fig. 5.11)

K = 18 to 24.5 MPa

(iii) corrected volumetric strain

K = 15.4 MPa – tests 110, 111 (Fig. 5.9)

K = 20.2 MPa – test 115 [Fig. 5.12(b)]

(*b*) Post-yield stiffness

(i) external axial strain – tests 110, 111, 112 (Fig. 5.7)

K = 1.7 MPa

(ii) local axial strain – test 115 (Fig. 5.13)

K = 2.8 - 2.2 MPa

(iii) corrected volumetric strain

K = 1.8 MPa – tests 110, 111 (Fig. 5.9)

K = 1.8 - 2.3 MPa – test 115 [Fig. 5.12(b)]

Significantly, these measurements show a low scatter for the post-yield regions. In the pre-yield regions the measurements obtained using the external axial measurements gave values which are considerably lower than the others. That is not surprising as the strains are small and therefore the true bedding error is significant in such cases. It is quite clear however that

the bulk stiffness drops to a tenth of its value after the isotropic yield.

5.5 RESULTS OF TRIAXIAL COMPRESSION TESTS

A total of twelve tests were performed, the majority of which were carried out under drained conditions. Some tests were later converted to undrained tests, particularly after the drained yield had been defined. The strain rates were typically 1%/h at the beginning of the tests so that a large number of readings could be taken during the initial stages of testing. The rate was increased to 5%/h at later stages in some tests. This is the same rate as used by Maccarini (1987). A back-pressure of 200 kPa was used in all of the tests.

5.5.1 Yield in shearing

The determination of the yield surface in a soil is normally associated with the change in behaviour of that soil when loaded. The definition used by Maccarini in his work (the "second" yield) was the point of maximum curvature of the stress/axial strain plot obtained from drained compression tests. Vaughan (1988) suggested using log-log plots of stress against strain. These ideas will be tested here.

Previously results (Fig. 5.4) suggest that the yield curve of the artificial soil is centered around the isotropic axis. It was shown that there is an isotropic pressure at which a clear break point occurs (Fig. 5.7 and 5.9). These results also indicate that triaxial compression tests consolidated isotropically at pressures below about 250 kPa may show a yield in shear.

Four conventional triaxial compression drained tests were performed with pressures below that value (Fig. 5.14).

Test 118 was consolidated under a nominal isotropic effective pressure of 5 kPa and was sheared fully drained. The axial strain was measured with four local transducers. Initially the strain rate used was 1%/h up to an axial strain of 1.0%; it was then increased to 5%/h. The

test showed a clear drop in stress and a slight expansion after the initial peak. The sample developed a shear plane near and intercepting the pedestal which caused large overall displacements only partially measured by one of the local transducers.

Test 113 had also two pairs of local transducers. The test was carried out under drained conditions up to an axial strain of 1.0% when the drainage was closed. The rate used was 1%/h throughout. The isotropic consolidation pressure was 160 kPa.

Test 114 also had four local transducers and the initial isotropic stress was 200 kPa. The strain rate was 1%/h, later changed to 5%/h. Various cycles of loading/unloading were carried out after the yield region had been passed.

Test 112 was consolidated at 225 kPa. In this test no local instrumentation was employed. The external measurements were obtained as described in Chapter 3 but, nonetheless, may not be strictly comparable with the local measurements in the other tests.

Fig. 5.14 shows the curves of stress versus axial strain and volumetric strain versus axial strain obtained from these tests. Except for test 118 (σ'_3=5 kPa) all of the tests showed a compressive tendency under shear. Examination of the stress-strain curve indicates a clear region where the material shows a change in behaviour. In test 118 this region coincides with the peak strength. In the other tests, however, this region of stress occurs below the ultimate strength and the stress continues to build-up with further straining.

Using the point of maximum curvature of the stress/axial strain curves, the values of t at the yield points were defined as 25 kPa (118), 56 kPa (114), 67 kPa (112) and 82 kPa (113).

The other form of determining the yield would be to plot the stress/axial strain curves to log-log scales. These plots are shown in Fig. 5.15. Fig. 5.15(a) has the results of the two independent measurements of axial strain from test 118 plotted together. Both show a more or less linear portion from 0.01% axial strain up to a point where the sample showed a slight unloading. After this point the stress increases slightly to the peak and failure. The large difference between the two types of local measurements when compared with other tests was probably caused by the shear plane which became visible later on. All of the transducers were

supported by the membrane strip on the top pads and the contact was satisfactory as far as could be seen. At the end of the test however, the shear plane intercepted one of the Hall effect transducers. It is possible that the strain was concentrated there from the start of loading. The t value at the yield point, nevertheless, is clearly in the range 21-25 kPa as marked in the figure.

The two pairs of local axial strain transducers of test 113 had close agreement and the t value at yield determined from either of them is around 79 kPa.

The two measurements obtained from test 114 are in good agreement. The point at which there is a change from a more or less smooth curve to a straight line is at 57 kPa, very close to the value determined on the linear scales.

Test 112 had no local measurements of axial strain. However, the external measurements seem to have given reliable results. The t value at yield point from Fig. 5.15(d) is 67 kPa.

These results show that both definitions give similar yield points.

Apart from the conventional triaxial drained tests just described, some other tests were performed, following different stress paths. Three samples were loaded under conditions of constant s' and increasing t. The samples were first isotropically consolidated to an initial pressure and then tested under stress controlled conditions. The cell pressure was decreased at a constant rate of 0.7 kPa/min while the axial pressure was manually controlled so that the required path was followed. Two samples started at 100 kPa (S100) and one at 200 kPa (S200).

The first sample tested (S100/1) was sheared under stress control throughout. Near the end of the test it exhibited an acceleration of strains and uncontrollable failure. The second test (S100/2) was stress controlled up to t=48 kPa, after which it was strain controlled. The strain rate used was 1.2%/h. The test was later continued undrained.

Test S200 was stress controlled up to an axial strain of 1.45%. It was then switched to strain control under undrained conditions.

The stress-strain curves of the three tests (t against axial strain and axial strain against volumetric strain) are given in Fig. 5.16. To define the yield the same criteria as used above were applied to the data. It is interesting to note that the two samples S100 had very similar plots of strain up to the point where the second sample was switched to strain control. It seems that this sample was affected by this modification, and was unable to attain the same strength as the first.

Logarithmic curves were also prepared from the data [Fig. 5.17(a), (b) and (c)] and they show well defined straight lines. Test S100/1 showed three linear sections before the uncontrolled failure. From these, two yields can be defined: an initial yield (10 kPa) and another at 56 kPa. The yield determined from Fig. 5.16 corresponds to t=65 kPa. Test S100/2 also had three linear portions in log-log scales and the main yield is at t=56 kPa. From Fig. 5.16 the value is 59 kPa. Test S200 again showed three linear portions in the log-log plot. The main yield is around t=48 kPa which is very similar to the value obtained from the previous plot (50 kPa).

The yield points are plotted in Fig. 5.18 together with those obtained by Maccarini (1987). Also plotted in the figure are the yield points determined from tests 104 and 105 (Fig. 4.9) and the results of tests 116 and 117 which are discussed later (item 5.5.3). In general there seems to be a good agreement between the points obtained following different stress-paths, with the exception of test S200 (constant s' of 200 kPa).

The isotropic yield obtained in this work is slightly above the value obtained by Maccarini although an examination of Fig. 5.13 suggests that a value of 280 kPa could have been selected. The yield surface appears to be centered around the isotropic line. Although no extension tests have been carried out it is likely that a similar yield curve would be found, due to the isotropic formation of the soil. The yield curve drawn in the figure was extended to a negative s' value of -2.5 kPa, the tensile strength of this material as measured in the diametrical compression, or Brazilian test (Maccarini, 1987).

5.5.2 The ultimate strength parameters

Most of the tests described here were carried out under drained conditions until the change of behaviour indicated that the yield point had been reached.

Some tests were then changed to undrained in order to determine if a condition of constant deviator stress under increasing strain could be attained, and to ascertain the strength parameters in that condition. Not all tests could be strained far enough, generally because the electro-levels touched the base of the cell. Except for sample 118, all the others tended to show a drop in deviator stress and a large number of internal shear planes rather than a prominent single one. The samples were very soft at the end of the tests, rather like a cohesionless loose sand. Great care had to be taken to recover the whole sample for water content determination as the water tended to run out carrying particles with it.

In Fig. 5.19 five stress-strain curves of such tests are presented and their stress paths are given in Fig. 5.20 (together with the stress path of test 109). Test 114D was carried out on the same sample as test 114B. The first test (114B) was tested fully drained and taken to an axial strain of 6.5%. The sample was then re-consolidated to a higher stress and sheared again. The other samples were all sheared under a constant cell pressure first drained, then undrained.

All of the stress-paths tended towards a small region of the stress space. The increase of pore-pressure with the straining is notable in tests 112, 113 and 114D. In comparison, test S100/2 showed little variation of pore-pressure with straining, suggesting that its condition was not far from the so called critical state. Its initial undrained stress level was close to the ultimate failure line defined from the average of all mixtures of artificial soil (ϕ'=35°, see Chapter 7 or ϕ'=34° from Maccarini, 1987).

Test S200 also showed a large, but not smooth, change in pore-pressure. The rate of change with strain increased markedly when the ultimate failure line was approached. The sample showed a much more brittle behaviour than the others (Fig. 5.19).

At the end of test 114D the straining was stopped and the load decay monitored. The stress path of this section shows a drop away from the failure line with a small generation of

pore-pressure. After 80 minutes all decay seemed to have stopped. The sample seems to be able to withstand a stress ratio close to that at failure without further deformation.

The fully drained tests at higher stresses normally did not reach an ultimate stable condition even at axial strains of 20%.

In the lower stress range ($s' \leq 200$ kPa) there is a large number of test results to define the failure line. Fig. 5.21 shows the stress paths of tests in that range. In addition to the tests already shown in Fig. 5.20, two more are included: 118, fully drained, and 101 mostly undrained. Test 101 had no local axial strain instrumentation.

The test results generally seem to fall into two slightly different classes. Tests 113, 114 and 101 indicate a failure line associated with little or no cohesion for a friction angle of 34°. Tests 118, S100/2 and S200 on the other hand gave a higher strength envelope indicating that a cohesion intercept should be taken into account. A value of 7 kPa seems to be the upper limit. Tests 109 and S100/2 lie between these two classes. Test S100/1 had the highest strength of all of the tests, crossing the failure line defined by the others. The peak strength occurred at an axial strain of 0.76% and was followed by collapse.

5.5.3 Influence of stress-path on shear strength

The results presented in the previous section seem to indicate that the soil behaviour may be affected by the stress path prior to failure or yield. To test this influence, two tests were carried out in which the shear strength envelope was approached maintaining a constant deviator stress while s' was reduced. The initial axial strain due to isotropic consolidation was 0.41% for test 116 and 0.10% for test 117.

Test 116 was isotropically consolidated to 100 kPa. After the consolidation was finished the vertical stress was increased as in a normal triaxial compression test up to t=50 kPa. Afterwards, maintaining this value approximately constant, the pore-pressure was first reduced and then increased giving the stress path shown in Fig. 5.22. The rate of increase used for the pore-pressure was 0.17 kPa/min. The sample had an axial strain of 0.3% at point F and at

point G rupture occurred very quickly (the broken line). The final strain at which equilibrium was restored was 19.8% and t had dropped to 22 kPa. The stress-strain results of this test are plotted in Fig. 5.23 with the corresponding points A to G marked on it. No correction was applied to the volumetric data. Note, however, that the effective confining stress varied from 174 kPa to 49 kPa between points B and D. If the correction of Fig. 5.8 holds true in unloading, which may not be the case, it would imply that around 1.2% of the apparent volumetric expansion is erroneous. This is close to the value measured (1.1%).

The axial strain measured with local transducers shows very stiff behaviour when the mean stress was reduced. The incremental strain between points B and E was only 0.06%.

The sample was able to withstand a stress ratio well beyond any sample tested previously (point G), showing small deformation in comparison. Its failure was very quick and unregistered except by the final point which lies between the two failure lines discussed above.

Test 117 was performed under similar conditions. Starting from an isotropic stress of 60 kPa, the sample was subjected to conventional drained compression. When t=30 kPa, the test was continued with that value constant while the pore-pressure (and s') were changed. The radial effective stress was reduced to 3 kPa without any signs of sample failure. A conventional drained compression test with strain control was then carried out.

Peak stress and clear failure behaviour were observed with t reducing after reaching a peak. After this drop, the sample was reloaded in small arbitrary steps (see dotted line in Fig. 5.22) and finally sheared undrained (discontinuous line).

This sample was also able to withstand stress ratios well above the failure envelope defined previously. The failure was only achieved by straining the sample under quite low effective stresses. Once failed, however, the final points of the drained and later undrained stress-paths lie close to the envelope of ϕ'=34° and intercept t=5-7 kPa. This test is particularly interesting when compared with test 118 which could not withstand a value of t in excess of 26 kPa, and with test S100/1 already discussed.

These test results were used to define the yield line in the low stress range (Fig. 5.18).

They plot above the other test results and show the influence of bonding at that stress level.

5.5.4 Effect of cycles of unloading/reloading

The artificial soil has a very open structure which is held together by the bonding between grains. This structure is susceptible to damage due to cycles of isotropic loading (Chapter 4). Two tests were subjected to cycles of deviator stress loading/unloading to see whether the bonding could also be destroyed by these sort of cycles. Both samples were consolidated isotropically before the shearing phase. Test 114B was consolidated to 200 kPa and test 115 to 515 kPa. Test 114B (Fig. 5.24) was initially loaded at a rate of 1%/h until the yield was defined. It was left under load overnight with no additional external deformation and the sample showed load decay with some straining. The remainder of the test was carried out at a faster rate of 5%/h. Six cycles of unload/reload caused an increase in axial and volumetric strain but with no change in their ratio. The rate of stress change with further axial strain showed a moderate increase. This may have been the effect of the structure creep and the faster rate used. No degradation was noticeable.

Test 115 was subjected to only two cycles (Fig. 5.25). It showed some irrecoverable volumetric strain, producing two steps on its otherwise smooth curve of volumetric vs axial strain. Its stress increase with strain, however, does not show any significant change that could indicate degradation, for example. The effect of different strain rates can be seen on its stress vs axial strain curve. Between the axial strains of 2% and 5.7% the rate was 1%/h while for the rest of the test it was 5%/h.

5.5.5 Stiffness measurements

The use of four local transducers on some samples and the development of the technique of external measurement of strain described in Chapter 3 provide useful data for comparison. The secant stiffness was calculated manually from the stress-strain curves of the tests. This is important in selecting the correct origin of strains. An example of typical test data is given in

Fig. 5.26 (test 114B). The two local axial strain measurements are relatively close to each other and there is little problem in selecting the origin. On the other hand, care is needed in selecting the origin of the external corrected measurement.

Having selected the origin, the secant stiffnesses at strains as low as 0.01% were calculated and plotted against the logarithm of strain as suggested by Jardine et al. (1984). These results are plotted in Fig. 5.27(a) to (i) in order of increasing cell pressure. As discussed above, the external measurements tend to be more reliable for larger initial confining stresses. In test 118 there were large differences between the local and external measurements: this was also reflected in the stiffness. In test 116 the external displacements were not reliably measured. On most tests good agreement was obtained between the different measurements used.

With the exception of test 111 [Fig. 5.27(f)], all tests showed the same pattern of decreasing stiffness with increasing logarithm of strain. There is a clear tendency for very high stiffnesses at strains smaller than 0.01%.

Using the data from Fig. 5.27, the values of stiffness obtained from two different strain levels (0.01% and 0.1%) were plotted against the confining pressure (Fig. 5.28). The line-connected dots indicate the measurement variation of each particular test. In two tests only external measurements were available. The results obtained from the stress-strain curves presented by Maccarini (1987) are also plotted in Fig. 5.28(b). The similarity between the two graphs (a) and (b) is remarkable. The stiffness increases markedly with the effective stress up to 100 kPa. It then drops in absolute terms until a pressure level of 300-350 kPa when it again starts to increase with the pressure.

To eliminate the effect of the confining pressure on the stiffness, plots were prepared of the values of normalized stiffness (E/σ'_3) against the pressure [Fig. 5.29(a) and (b)]. There is a more or less similar trend in both plots, the normalized value reducing quite rapidly up to a level of 400 kPa. At the small effective stresses, the normalized stiffness can be as high as 8000-12000 (Table 5.2).

Jardine et al. (1984) presented data of normalized stiffness at 0.01% for four materials (Fig. 5.30). They normalized the stiffness by the mean effective stress p'_0 $[=(\sigma'_1 + 2\sigma'_3)/3]$. Most of the samples were anisotropically consolidated, some overconsolidated. The values obtained by them for OCR$\simeq$1 varied in the range 800-1500. The maximum value for soils, independent of the OCR was 2430. In two samples of chalk, however, the normalized stiffnesses were 11000 and 15500.

The results presented here show that the artificial soil exhibits a drop in normalized stiffness with pressure which is not common for soils. At low confining pressures the normalized stiffness was quite high and comparable to that of a soft rock.

5.6 RESULTS OF TESTS ON REMOULDED SOIL AND PERMEABILITY MEASUREMENTS

It is commonly stated that tests on remoulded soil can provide an indication of the magnitude of the influence of the structure on the strength and stiffness of a soil.

To do so, some of the samples which had been already tested were remoulded by hand to a homogeneous silty sand (the broken bonding providing the finer particles). A known amount of soil was poured inside a metal mould with a vacuum applied to stretch a membrane inside it.

Two samples were obtained following this procedure. The first had an initial void ratio of 1.18 (REM1). The second was poured into the mould slightly wet so that the particles formed clumps which made this sample less dense. An initial void ratio of 1.39 was obtained (REM2).

In order to verify the maximum and minimum void ratios attainable for this soil, a simple test was performed. A measuring cylinder with remoulded soil inside it was turned upside down a number of times. The minimum density obtained corresponded to a void ratio

of 1.88 (e_{max}). The same sample was then subjected to compaction by shaking and vibration wet and dry. The minimum void ratio was 1.13 (e_{min}). This minimum void ratio is remarkably constant and little effort is needed to achieve void ratios in the range 1.20-1.25. Note that although Maccarini obtained some samples with e=0.9 (intergranular void ratio=0.48), the samples were of a different initial material as the kaolin was still a plastic wet clay, not a silt size non-plastic fraction as is the case after remoulding it.

The two remoulded samples were instrumented with local strain transducers and they were saturated with back-pressure. Test REM1 was left to saturate for eight days and test REM2 was saturated in four days. Both samples had a back-pressure of 200 kPa.

5.6.1 Isotropic compressibility of remoulded soil

The remoulded samples showed a much more compressible behaviour than the intact material. Axial strain against pressure for the isotropic consolidation of test REM2 is plotted in Fig. 5.31. In the same figure the local measurements of tests S200 and 515 are also shown. It is clear that the bonding provided much of the initial stiffness. However, once the yield pressure is exceeded in the bonded soil, it tends to deform by an amount comparable to that of the remoulded soil.

Similar results are obtained from the volumetric strain (Fig. 5.32). The two lines correspond to the measurements as obtained and corrected by the membrane penetration error. The shaded area represents the results of tests 110 and 111.

Test REM1 showed less compressible behaviour, which is consistent with its lower initial void ratio. The axial strain measurements of the two remoulded tests are plotted together in Fig. 5.33. Both tests were subjected to cycles of loading/unloading and the results are similar to those described for loose sands.

In Fig. 5.34 the same local axial strain data is plotted against the logarithm of pressure. The local axial strain was chosen as it is a reliable measurement and it is not subject to any error. Both samples showed very similar stiff unloading/reloading stages and a noticeable

creep when the pressure was maintained constant (300 kPa for test REM1 and 600 kPa for test REM2) and they also show an apparent pre-consolidation pressure, caused by the saturation phase, in the range 50-60 kPa.

The influence of void ratio on the compressibility of unbonded soils is very well established in soil mechanics. To verify this influence some points have to be considered. Both samples are affected by the membrane penetration error described earlier. Although this error correction does not present difficulties, there are other considerable problems. The samples were assembled dry, or moist, to obtain the high void ratio required. Until they were fully saturated the volume measurements were of little or no use. The samples also deformed considerably during saturation when water was percolated through them and the effective stress was increased to 50 kPa. The sample dimensions were measured directly at the beginning of the test (under a vacuum of 10 kPa) and at the end of shearing phase. Using the last point as a reference, the volume was calculated backwards and the volume correction applied.

In test REM2, there is a large difference between the directly measured initial void ratio and the back-calculated value for the beginning of consolidation. The test results, however, indicate that such a difference may be caused by the initial stress application.

In Fig. 5.35 the results of the two tests are presented. They incorporate the membrane error and use the final void ratio as reference. The initial points measured during assembly are also marked on the figure (triangles). Test REM2 which had the highest initial void ratio showed very large compressibility. However, it is surprising that test REM1 was able to cross the line of the other test maintaining a higher void ratio for pressures above 300 kPa. This difference in behaviour can only be explained by the different structures created when the samples were formed. Test REM1 was poured dry and test REM2 was assembled slightly moist with the grains forming lumps. This may account for the difference not only in the compressibility but also in the void ratio/pressure curve obtained.

5.6.2 Triaxial compression test results on remoulded soil

Following the isotropic consolidation stages, the two samples of remoulded soil were sheared under fully drained conditions. Sample REM1 was slightly overconsolidated (OCR=1.2) but sample REM2 was overconsolidated to an OCR of 6.2. Their void ratios before shearing were 1.00 and 0.96 respectively.

The axial and volumetric strains are plotted in Fig. 5.36 and 5.37 together with the half deviator stress (t). Both showed compressive behaviour throughout and their volumetric strains seem to indicate that they achieve a more or less stable structure at the end of the test. The stress-strain curves do not show clear signs of failure, although the curve for test REM2 is relatively flat. If the maximum stresses in the tests are assumed to be close to failure, they plot close to the failure envelope defined above (Fig. 5.38). The straight line passing through the origin and the two maxima gives a corresponding ϕ' value of 35°.

The cycles for unloading/reloading in these samples are also of some interest. The two cycles carried out on sample REM2 caused no significant volume changes. In contrast, the one cycle carried out on sample REM1 caused a considerable volume change during unloading. This may be related to the different stress levels at which the two samples were tested, to the magnitude of the unloading or to the different OCRs of the samples.

The remoulded sample tests also provided the opportunity to examine the idea of yield determination using log-log plots. The half deviator stress, t, is plotted against the local axial strain in Fig. 5.39(a) and (b) for both tests. The curve obtained from test REM1 has hardly any change in slope or any other feature which could indicate a yield point. The same result is obtained if the normal scales are used (Fig. 5.36): there is no indication of yield from a clear point of maximum curvature. Test REM2 gives a different result. From the linear scales it is not easy to select a point, but, the log-log plot [Fig. 5.39(b)] indicate that at a stress level of t=40 kPa there is a yield. This yield may be associated with the overconsolidation of the sample.

The stiffnessess of these two samples were also determined for axial strains of 0.01% and

0.1%. The results are presented in Table 5.2. The comparison with the values obtained in the bonded soil is interesting (Fig. 5.40). Sample REM2, sheared at 100 kPa confining stress, gave stiffnesses values well below the values determined for the bonded soil at a similar void ratio. The overconsolidation ratio of 6.2 was not enough to increase its stiffness to the level of the bonded ones. Sample REM1, although lightly overconsolidated (OCR=1.2), gave much higher stiffnesses. When their normalized stiffness (E/p_0') is compared with the values given by Jardine et al. (1984) (Fig. 5.30) both samples have values which are close to half the expected values for their overconsolidation ratios: test REM1 has a normalized stiffness at 0.01% of 450 (OCR=1.2) and test REM2 has a normalized stiffness of 1000 with an OCR of 6.2.

5.6.3 Permeability measurements

Permeability tests were conducted on some triaxial samples of the artificial soil before testing in compression. Different pore-pressures were applied at the top and bottom drainage to generate a hydraulic gradient. Typically 10 kPa difference was maintained. Monitoring of the flow allowed the calculation of sample permeability. The results shown in Table 5.3 represent the average obtained from 5 to 8 determinations with continuous measurement of top and bottom pressures. Two of the bonded samples were tested before shearing and they have an average permeability of 2.5 x 10^{-6} m/s. The two remoulded samples had their permeabilities measured a number of times. Sample REM1 had a permeability reduction from 2.5 to 0.4 x 10^{-6} m/s due to consolidation.

The other remoulded sample reduced in permeability from 6.5 to 2.8 x 10^{-6} m/s. This difference in permeability between the two samples again indicates that their internal structure must be different, as the void ratio is so similar. One measurement of permeability was made on a partly saturated sample to determine how much it affected the measurement.

Sample	γd (kN/m^3)	e_0	σ_3' (kPa)	Local axial strain	Top cap arrangement
110	10.43	1.49	425	No	Preliminary
111	10.48	1.48	430	Yes	Preliminary
112	10.51	1.47	225	No[a]	Preliminary
113	10.64	1.44	160	Yes[b]	Preliminary
114	10.58	1.46	200	Yes[b]	Preliminary
115	10.54	1.47	515	Yes	No
116	10.35	1.51	100	Yes	Guided top cap
117	10.57	1.46	60	Yes[b]	Guided top cap
118	10.59	1.45	5	Yes[b]	Guided top cap
S100/1	10.58	1.44	100	Yes	Preliminary
S100/2	10.69	1.43	100	Yes	Preliminary
S200	10.50	1.48	200	Yes	Preliminary

$G_s = 2.65$
(a) Both local transducers fell off
(b) Four local transducers were used

Table 5.1 — Artificial bonded soil - 100 series (133057, 500°C/5h)

Test	σ'_3 (kPa)	E_{sec} at 0.01% (MPa)	E_{sec} at 0.1% (MPa)	$\frac{E_{0.01}}{\sigma'_3}$ ($\times 10^3$)	$\frac{E_{0.1}}{\sigma'_3}$ ($\times 10^3$)	$L = \frac{E_{0.1}}{E_{0.01}}$
118	5	32–64	24–38	6.4-12.8	5-7.6	0.6–0.8
117	60	112–160	56	1.8-2.7	0.9	0.3–0.5
116	100	220–250	80–94	2.2-2.5	0.8–0.9	0.36
113	160	190–220	76	1.2-1.4	0.5	0.36–0.42
114	200	140–210	50–60	0.7-1.1	0.25–0.30	0.27–0.36
112	225	250(c)	70(c)	1.1(c)	0.31(c)	0.28
110	425	154(c)	44(c)	0.36(c)	0.104(c)	0.29
111	430	95	45	0.22	0.105	0.48
115	515	110–134	54	0.21-0.26	0.105	0.40–0.50
114D	400	350	96	0.88	0.240	0.27
111C	430	58	56	0.14	0.130	0.93
REM1	605(a)	275	123	0.41	0.20	0.45
REM2	100(b)	100	59.5	0.95	0.57	0.60

(a) OCR = 1.2
(b) OCR = 6.2
(c) External measurement

Table 5.2 — Stiffness parameters of the 100 series tests and remoulded soil samples

Sample	e	k (m/s)	Observation
102	1.37	3×10^{-6}	bonded sample
103	1.39	2×10^{-6}	bonded sample
REM1	1.12	0.6×10^{-6}	partially saturated
	1.12	2.5×10^{-6}	saturated
	1.00	0.4×10^{-6}	after consolidation
REM2	1.19	6.5×10^{-6}	before consolidation
	0.97	2.8×10^{-6}	after consolidation

Table 5.3 — Results of permeability test on artificial soil samples

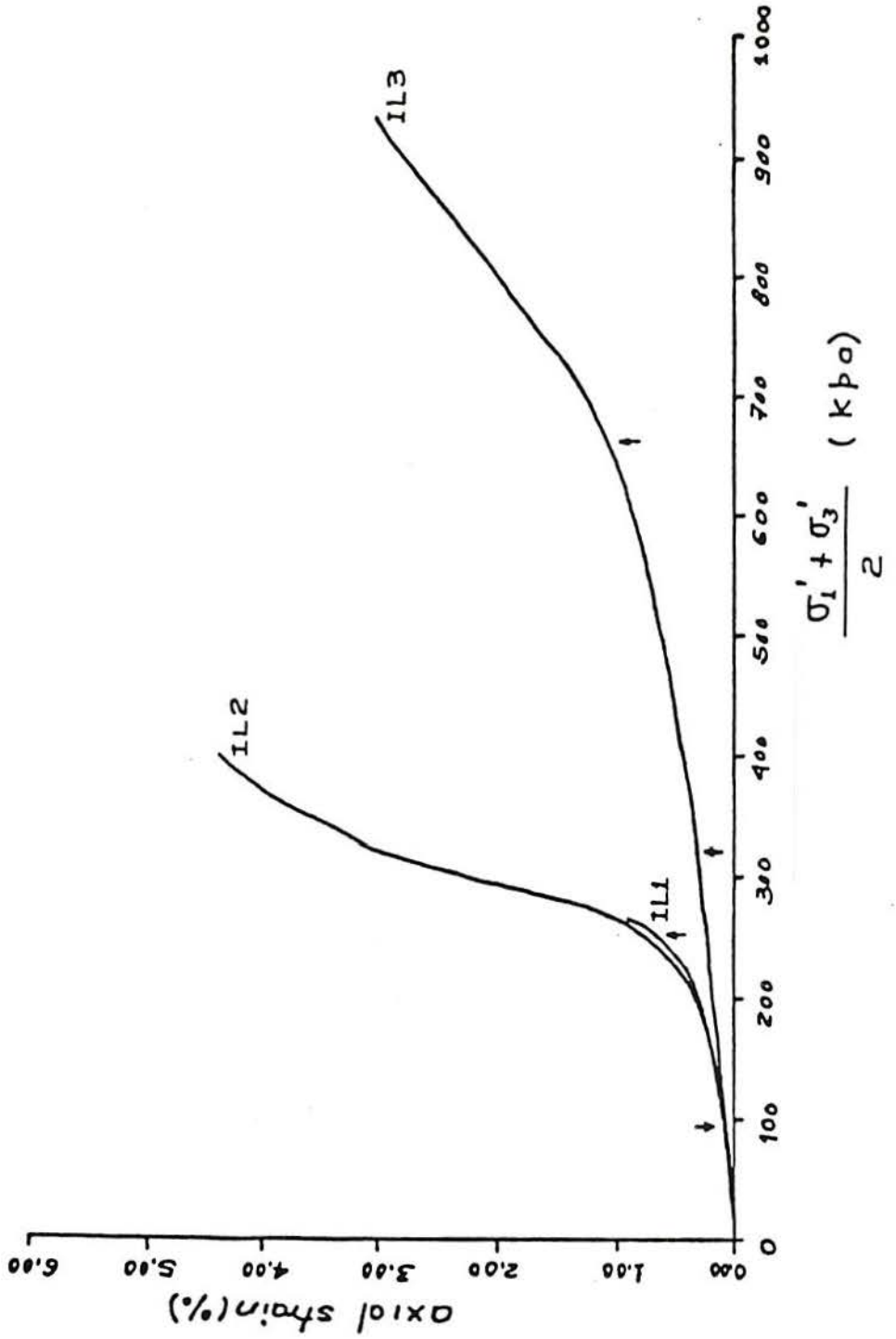

Figure 5.1 – Isotropic compression tests on artificial soil with e=1.6 (after Maccarini, 1987)

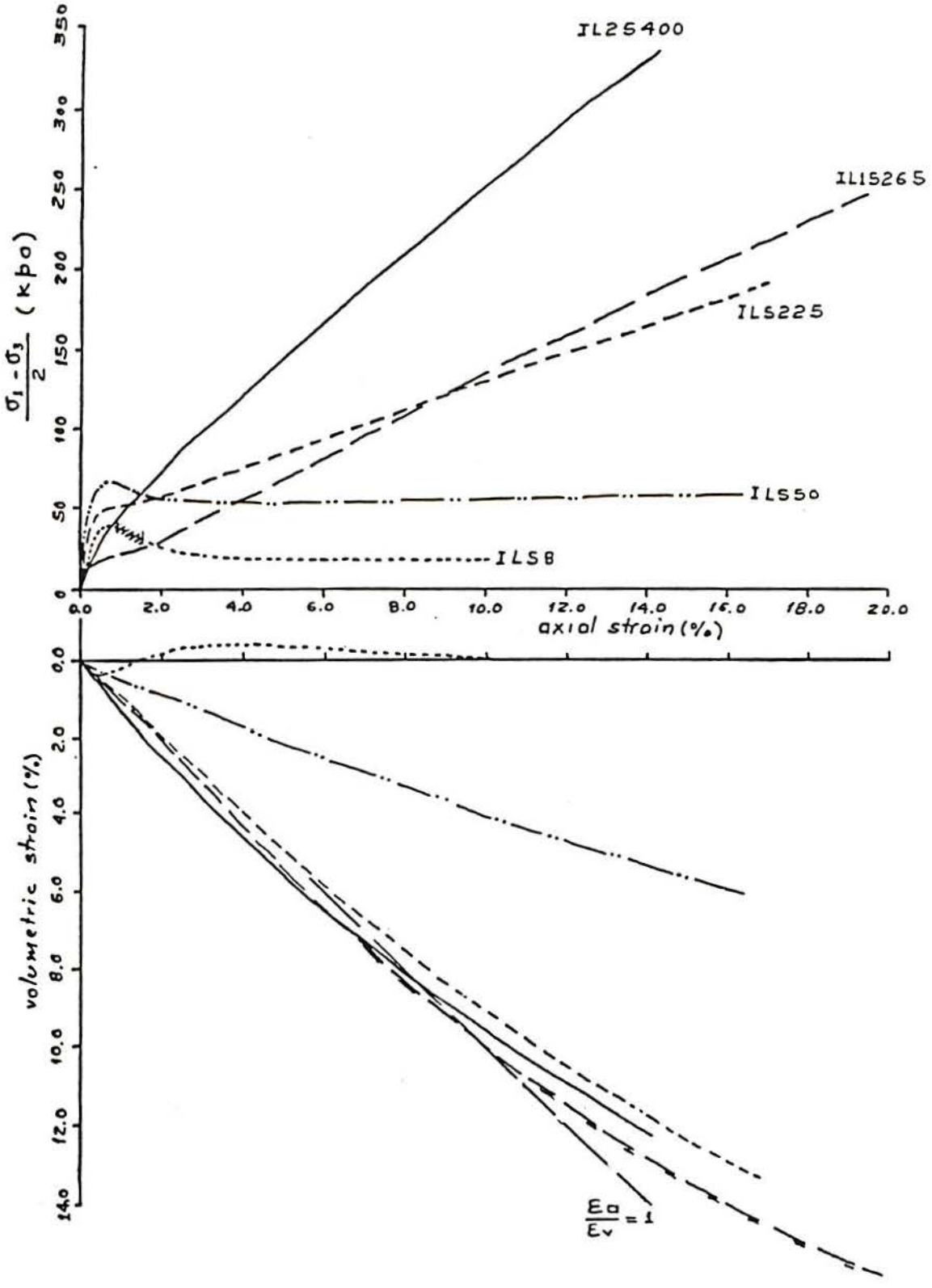

Figure 5.2 - Drained triaxial compression tests on artificial soil with e=1.6 (after Maccarini, 1987)

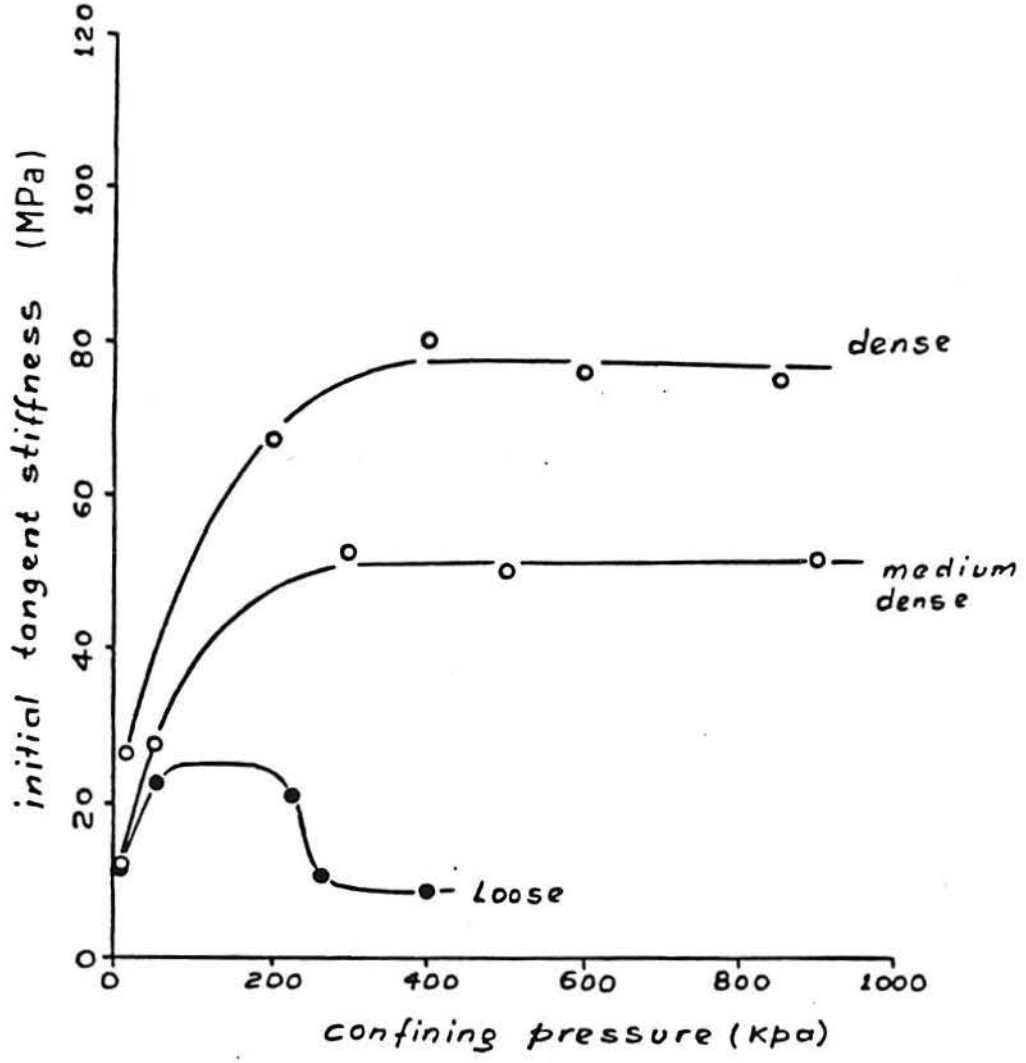

Figure 5.3 – Initial stiffness measured on triaxial drained tests on the artificial soil (after Maccarini, 1987)

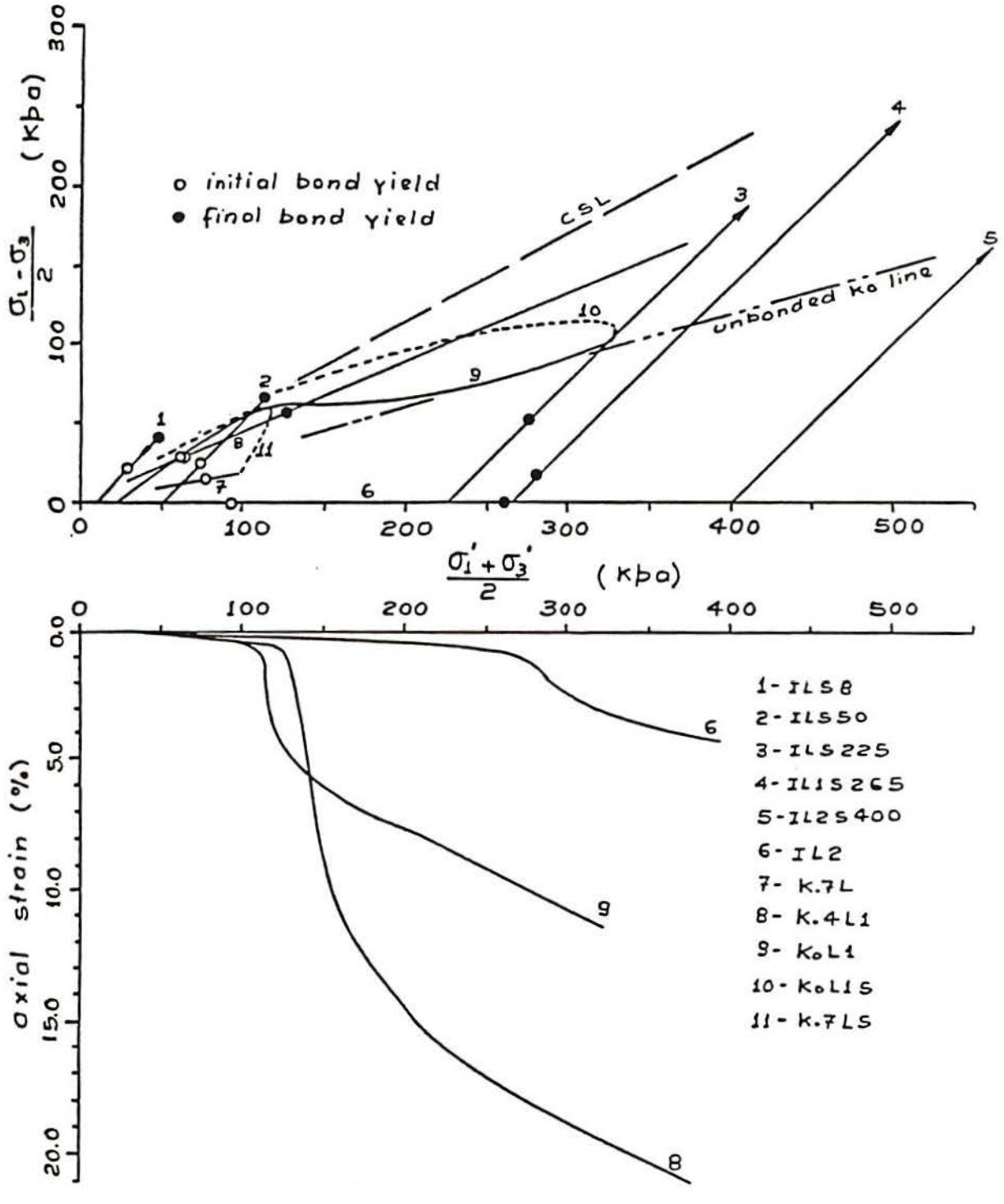

Figure 5.4 – Summary of all test results on the artificial soil with e=1.6 (after Maccarini, 1987)

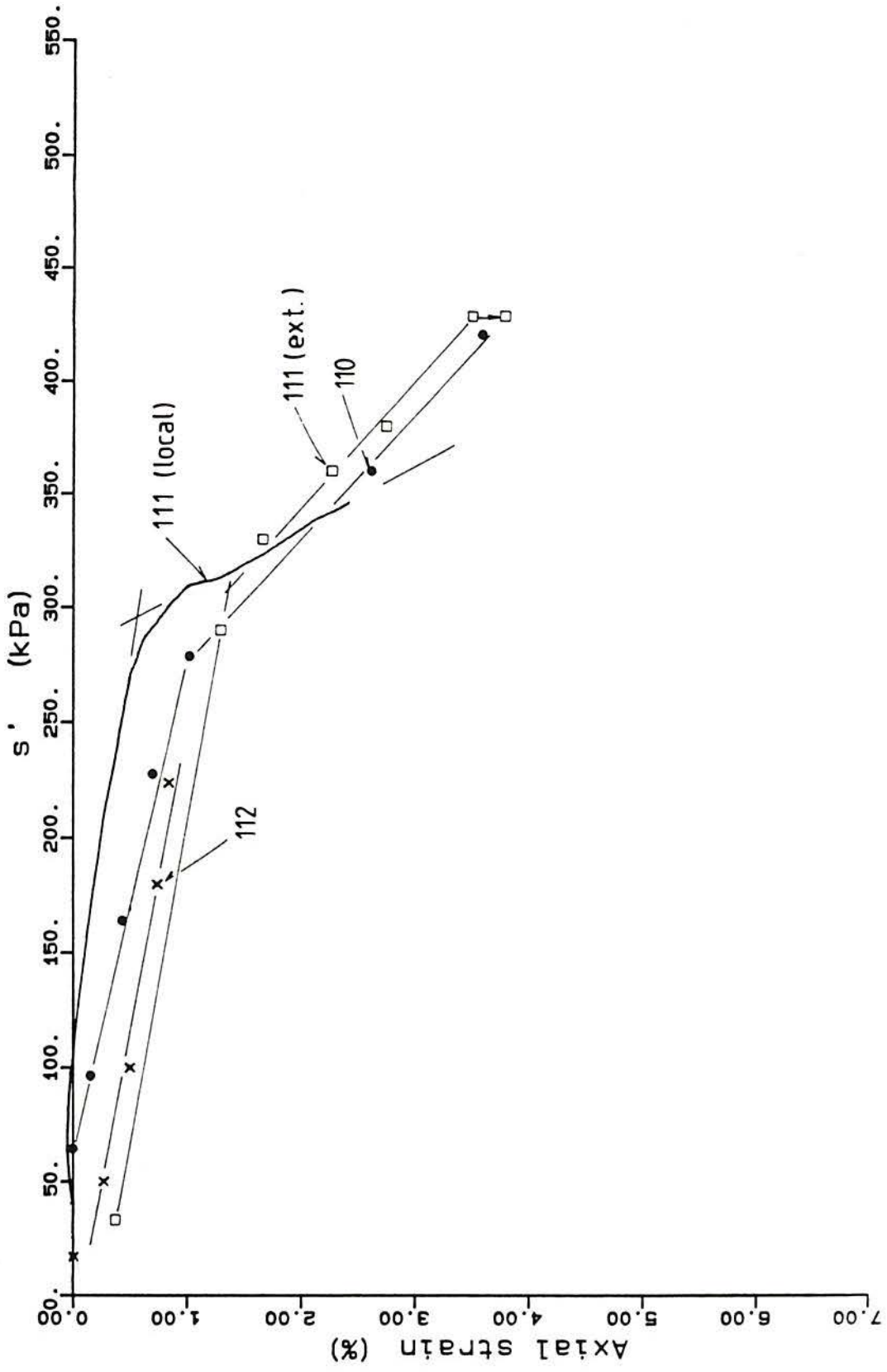

Figure 5.5 – Results of isotropic compression tests on artificial soil with e=1.5; axial strain versus s'

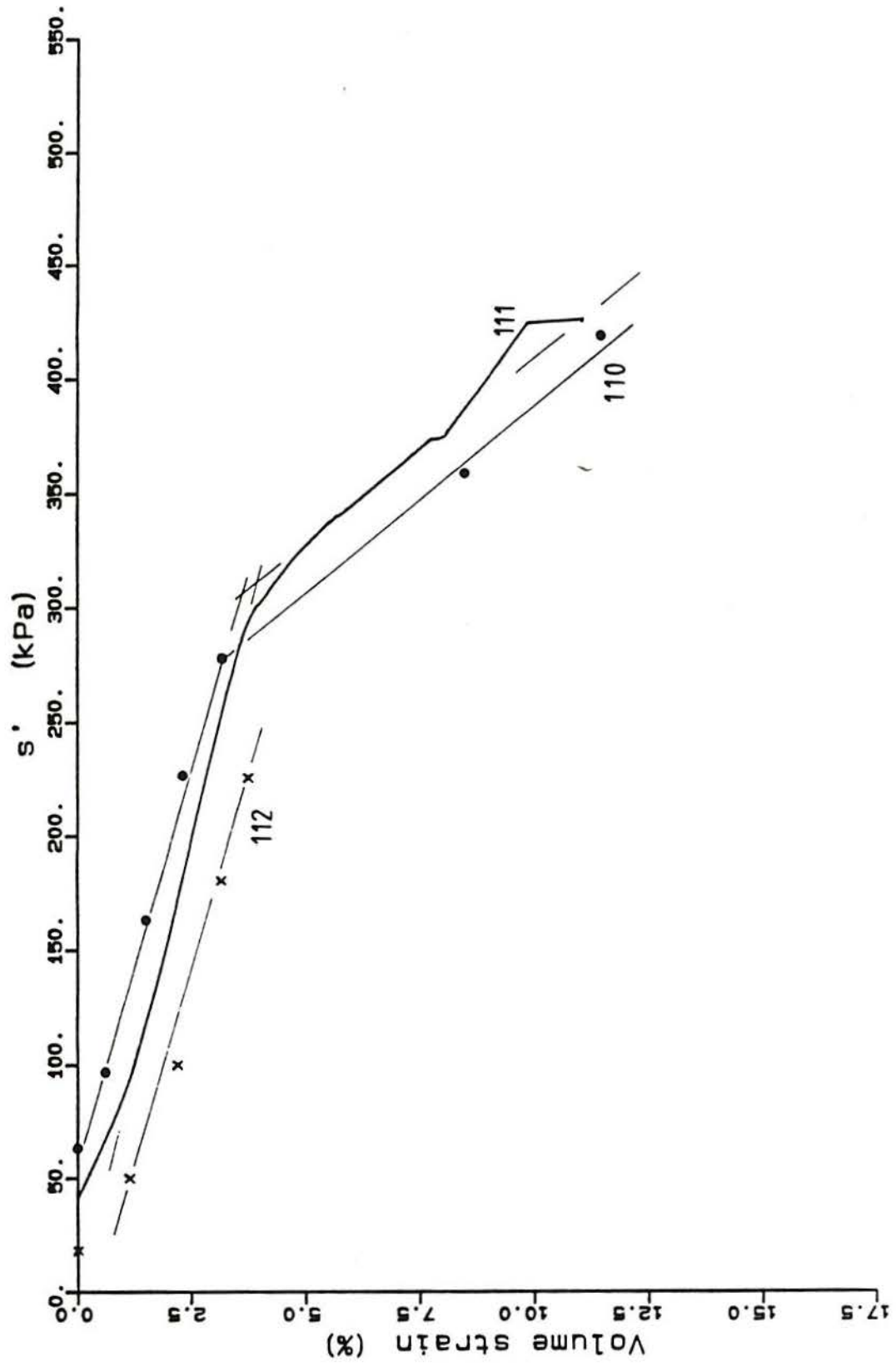

Figure 5.6 – Results of isotropic compression tests on artificial soil with e=1.5; volumetric strain versus s'

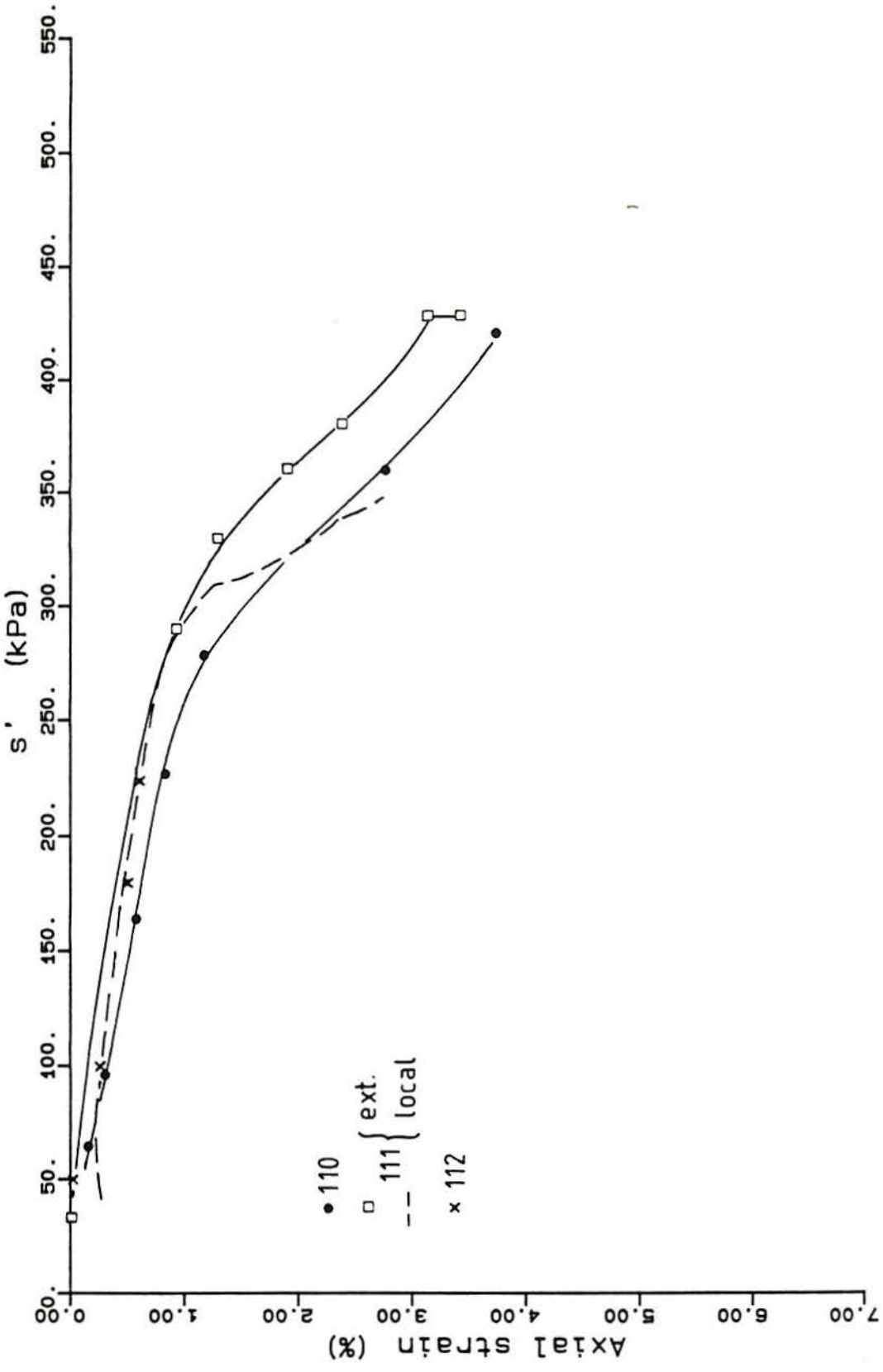

Figure 5.7 – Results of isotropic compression tests on artificial soil with e=1.5; shifted axial strain versus s'

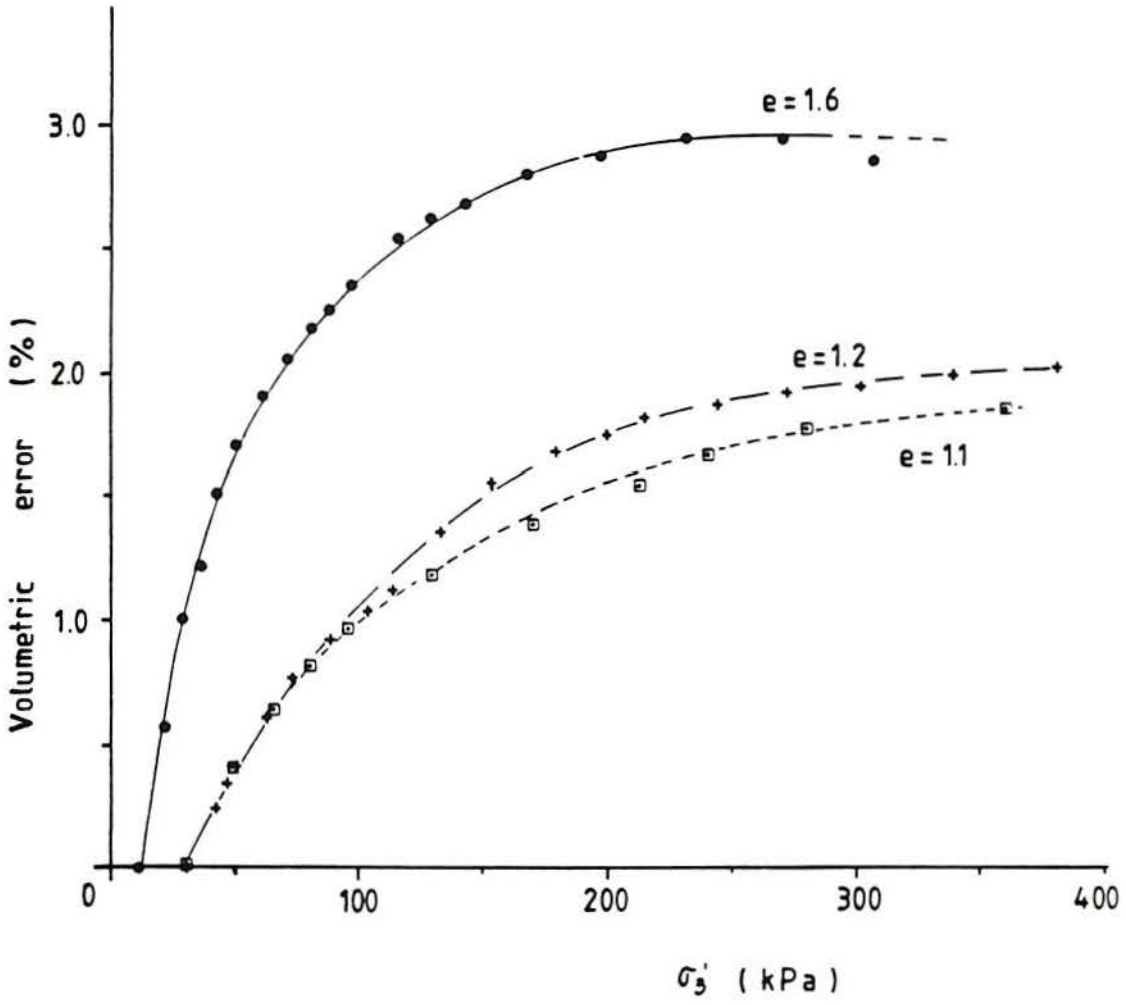

Figure 5.8 – Membrane penetration error (ϵv_r) versus confining effective pressure

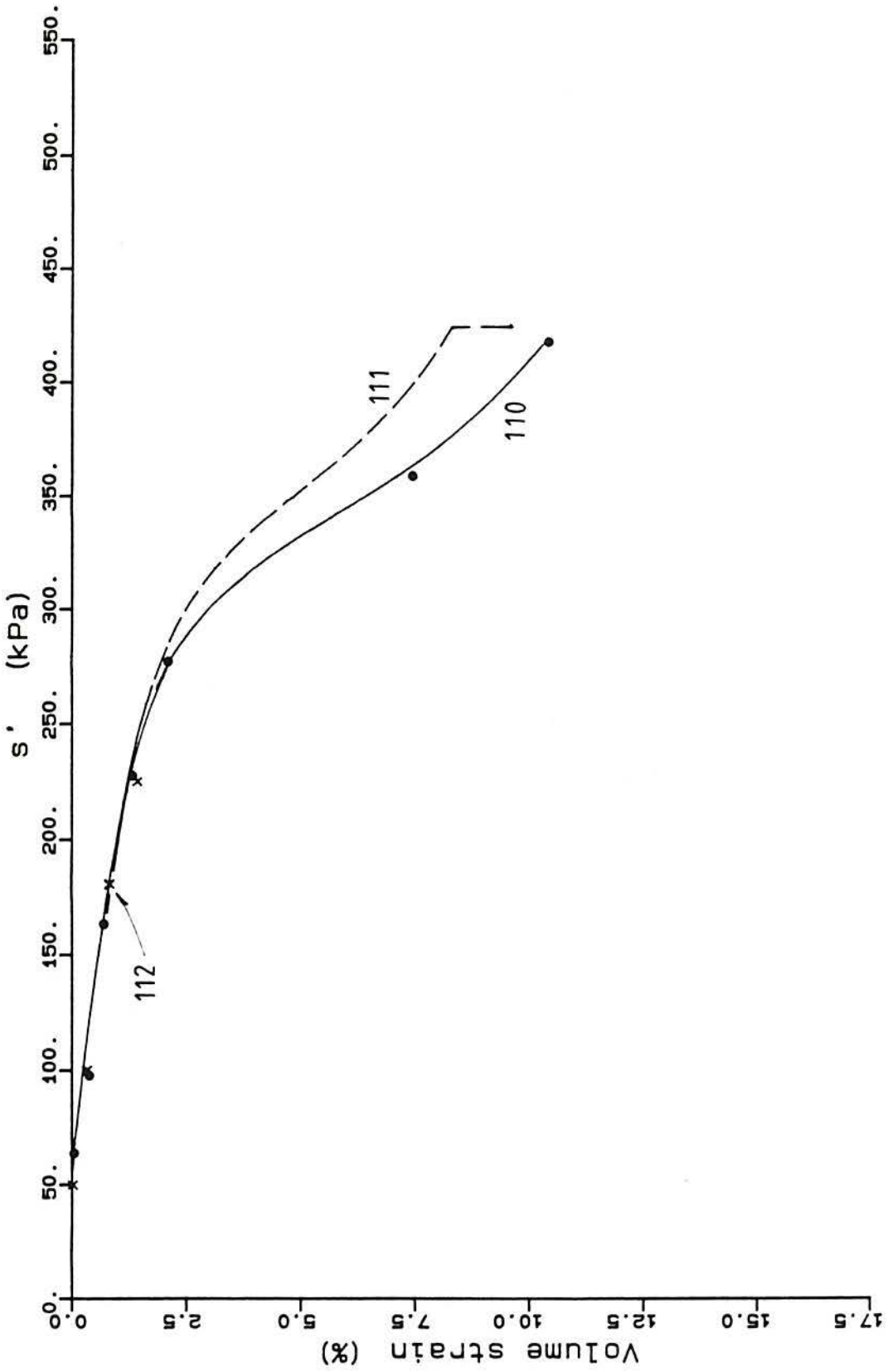

Figure 5.9 – Results of isotropic compression tests on artificial soil with e=1.5; corrected volumetric strain versus s'

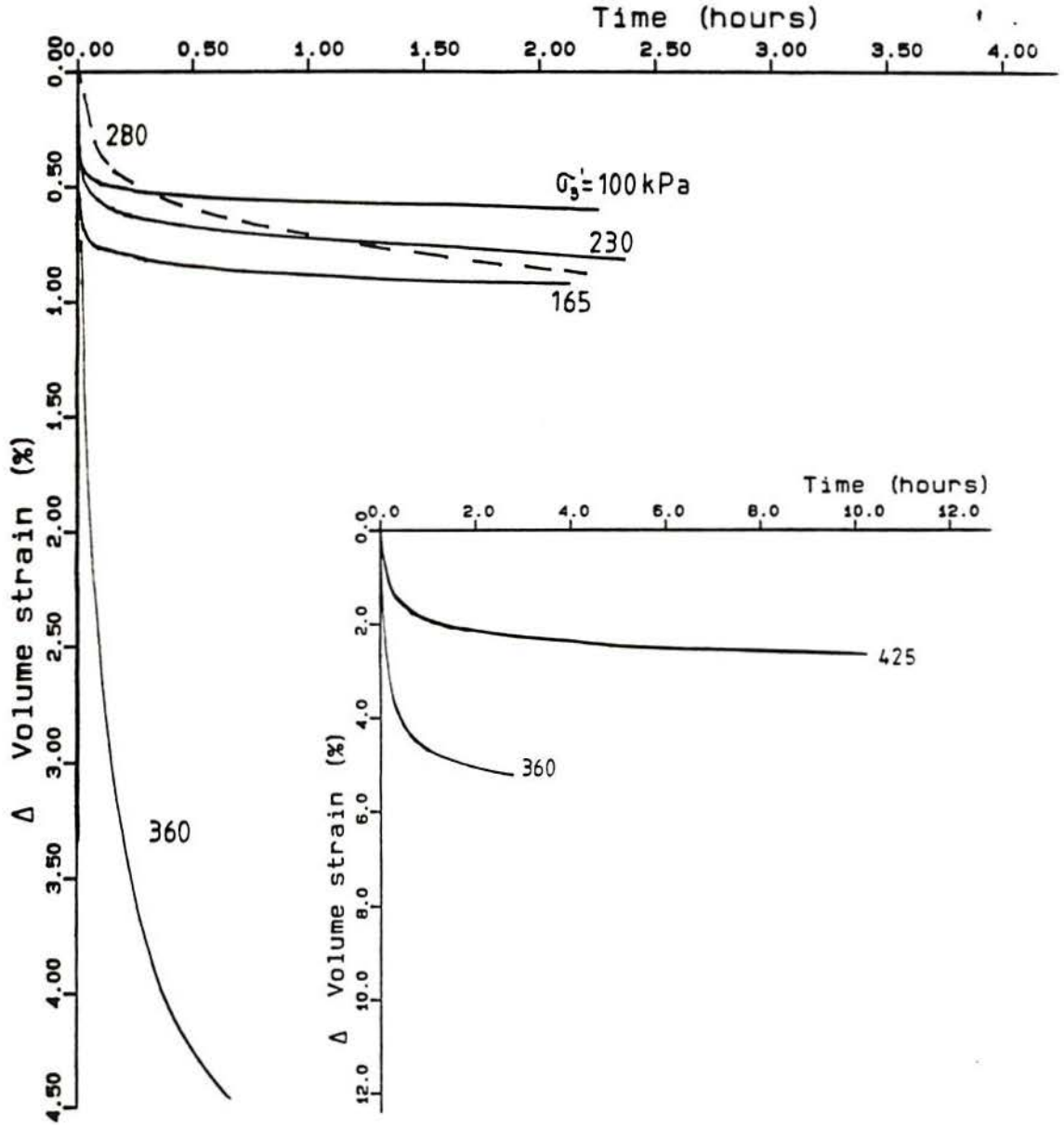

Figure 5.10 – Consolidation steps of test 110

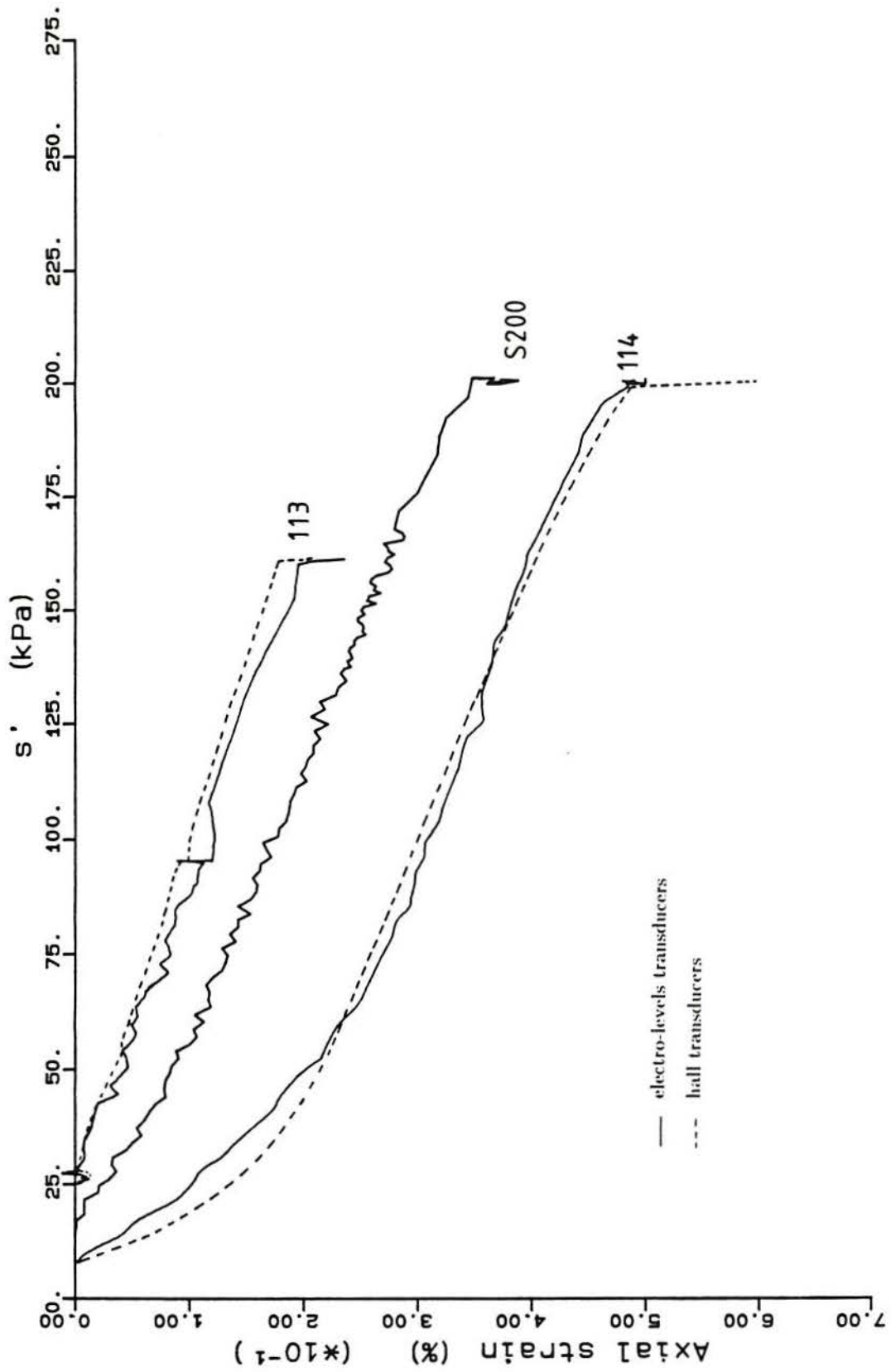

Figure 5.11 – Isotropic consolidation results of tests 113, 114 and S200. Local measurements of axial strain

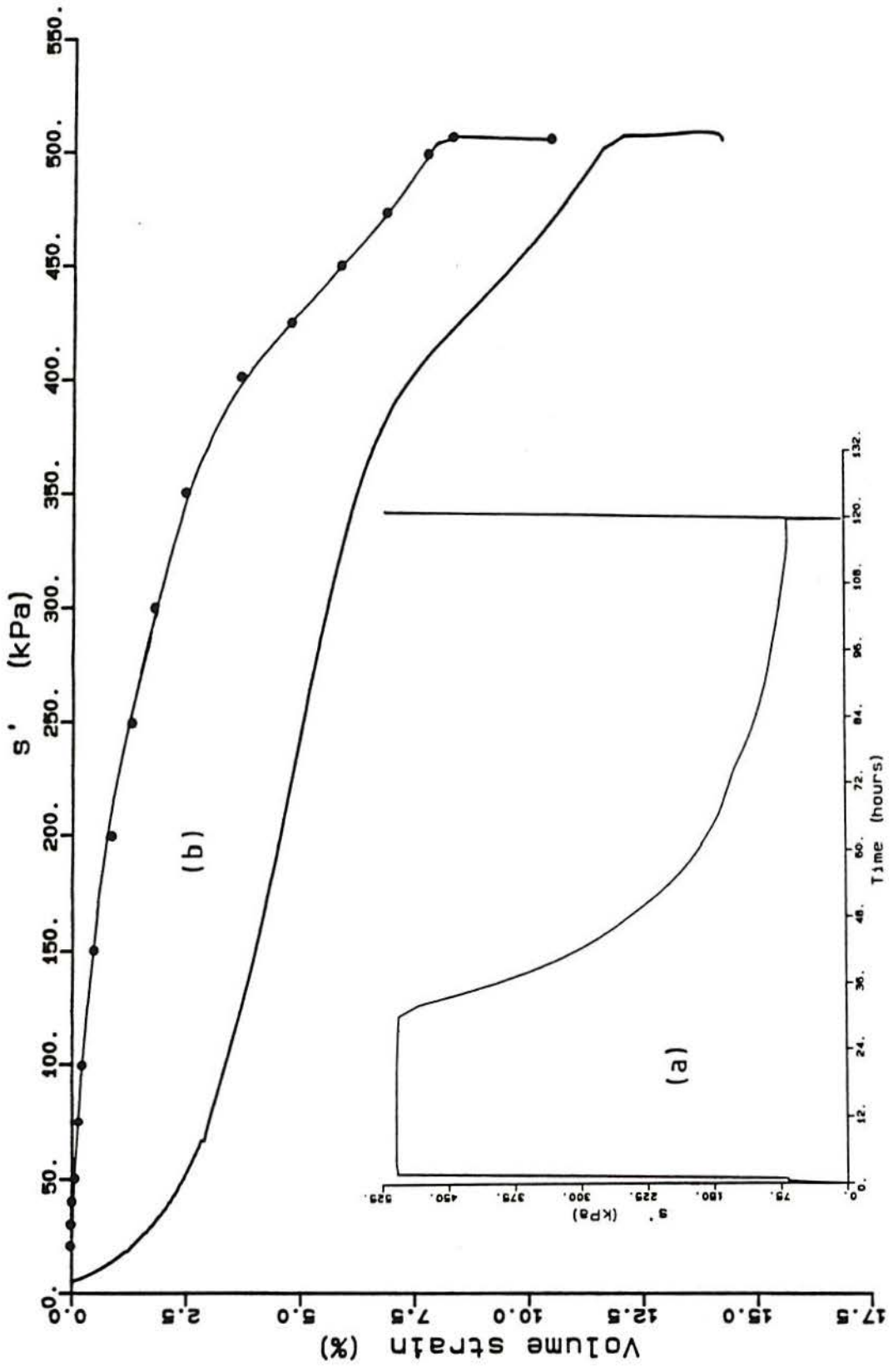

Figure 5.12 – Results of isotropically consolidated test 115. (*a*) variation of pressure with time; (*b*) volumetric strain versus pressure

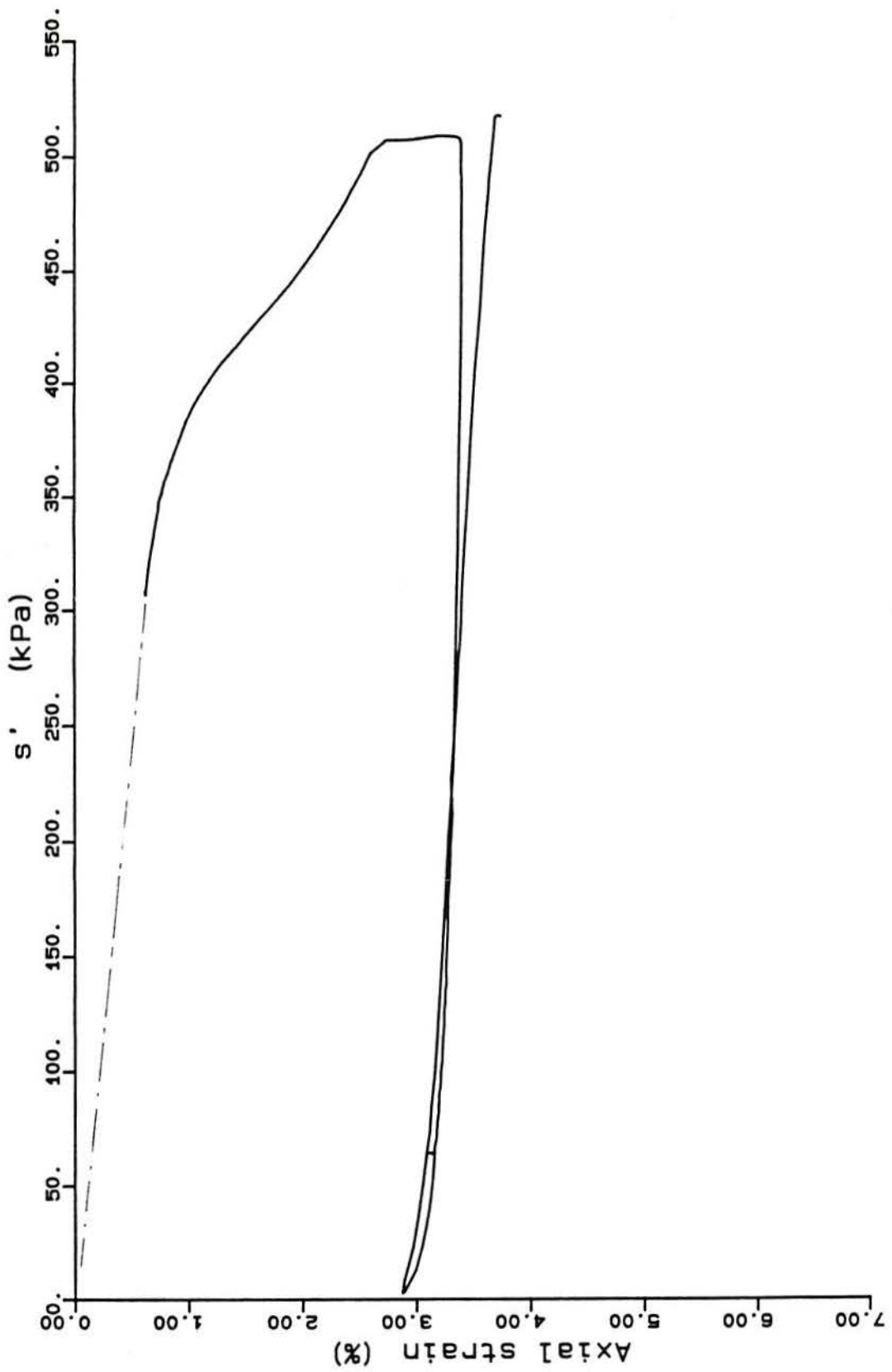

Figure 5.13 – Results of isotropically consolidated test 115; axial strain versus s'

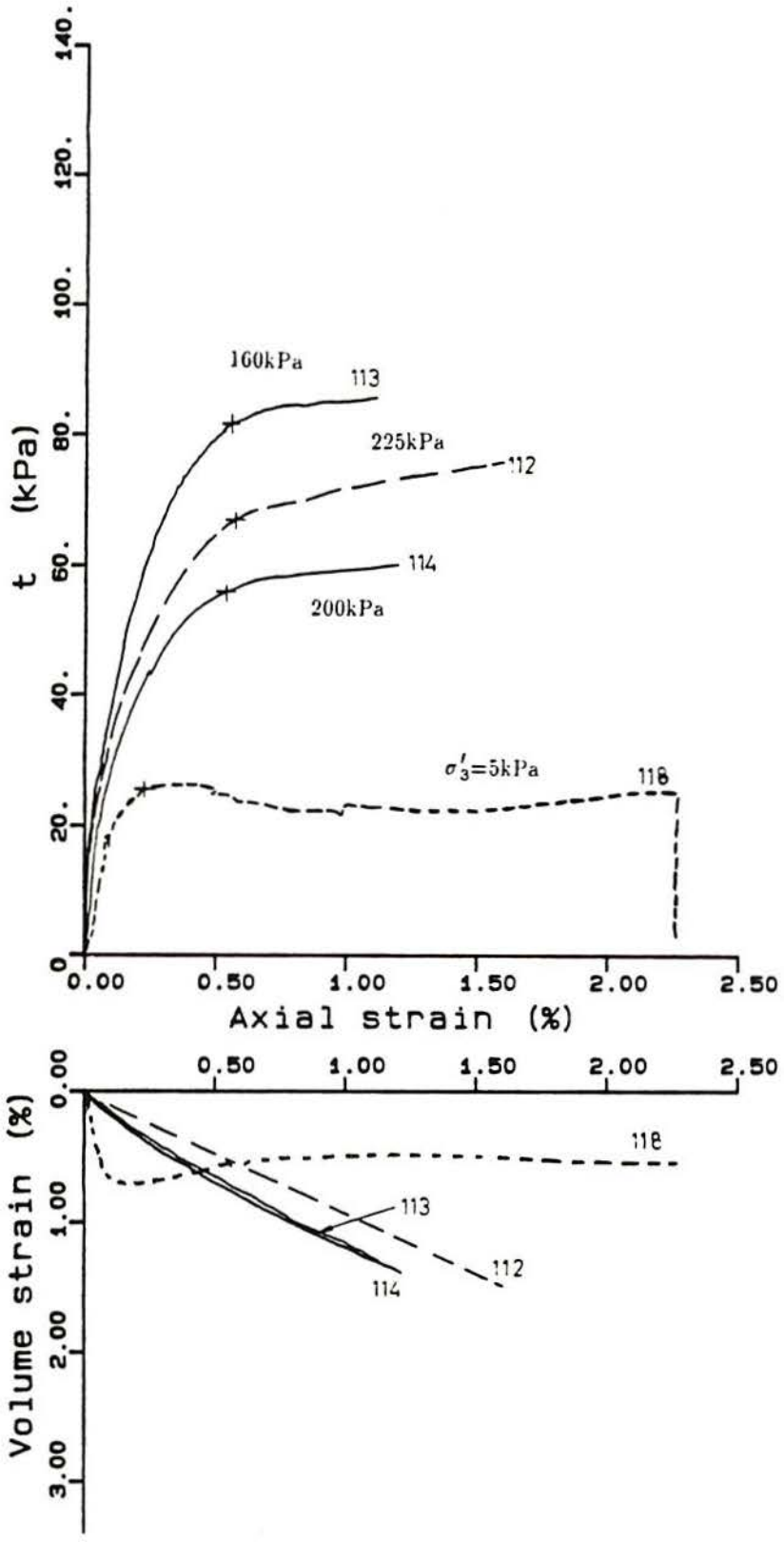

Figure 5.14 - Drained triaxial compression tests on artificial soil with e=1.5. Confining stresses of 5 kPa (118), 160 kPa (113), 200 kPa (114) and 225 kPa (112)

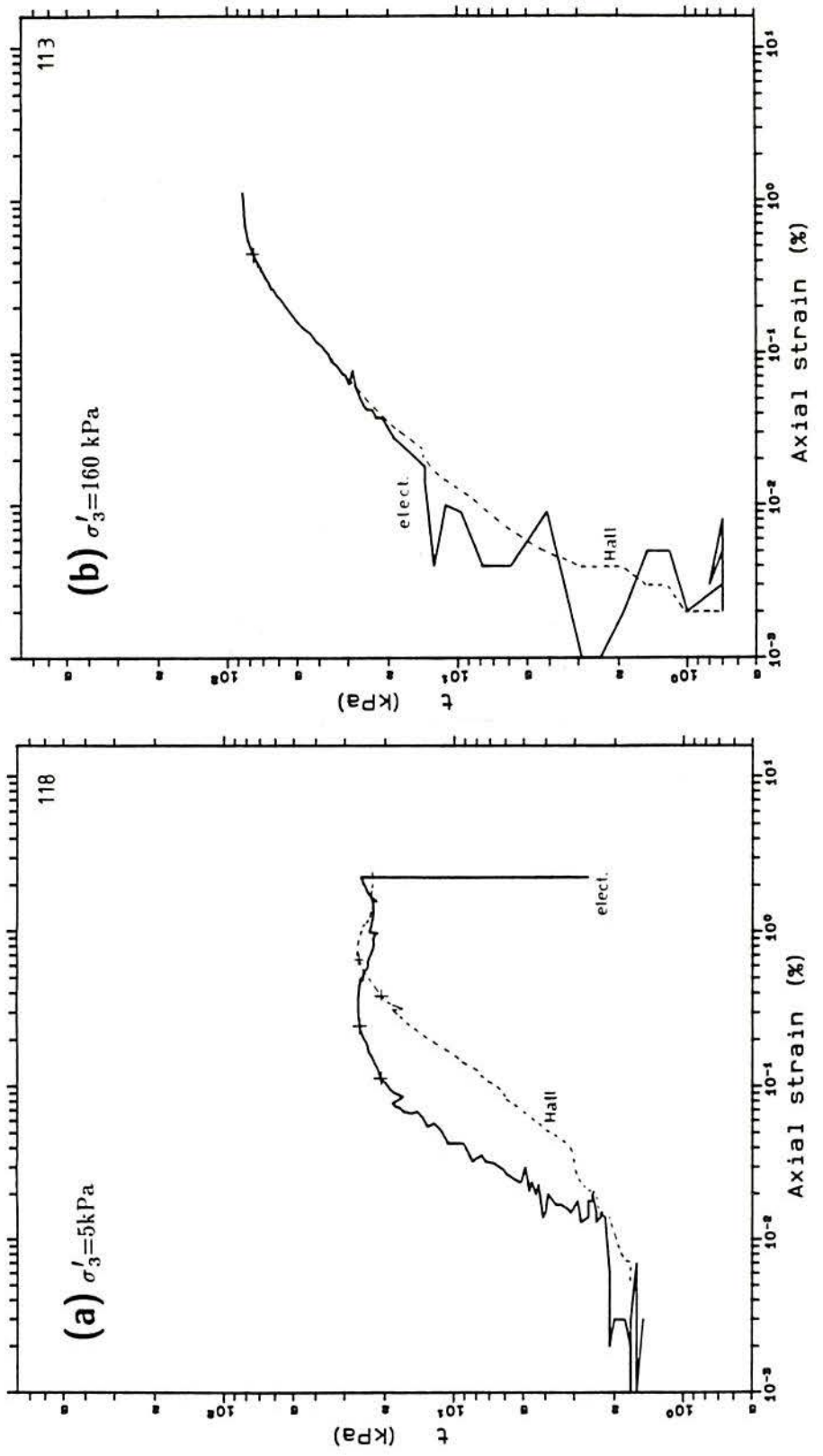

Figure 5.15 – Log-log plots of half deviator stress (t) versus axial strain of compression drained tests (e=1.5); (*a*) test 118; (*b*) test 113; (cont.)

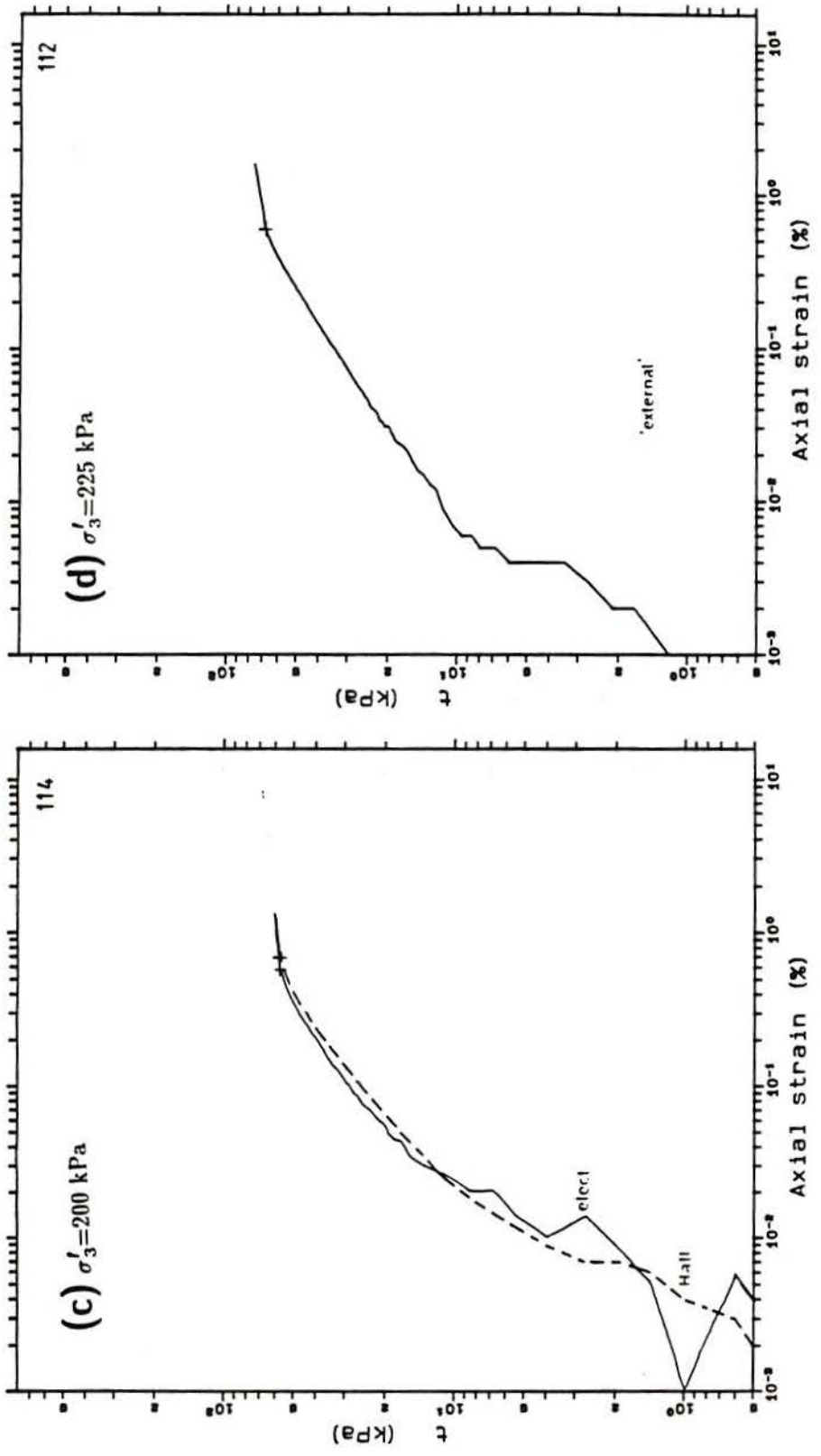

Figure 5.15 – (cont.) (*c*) test 114; (*d*) test 112

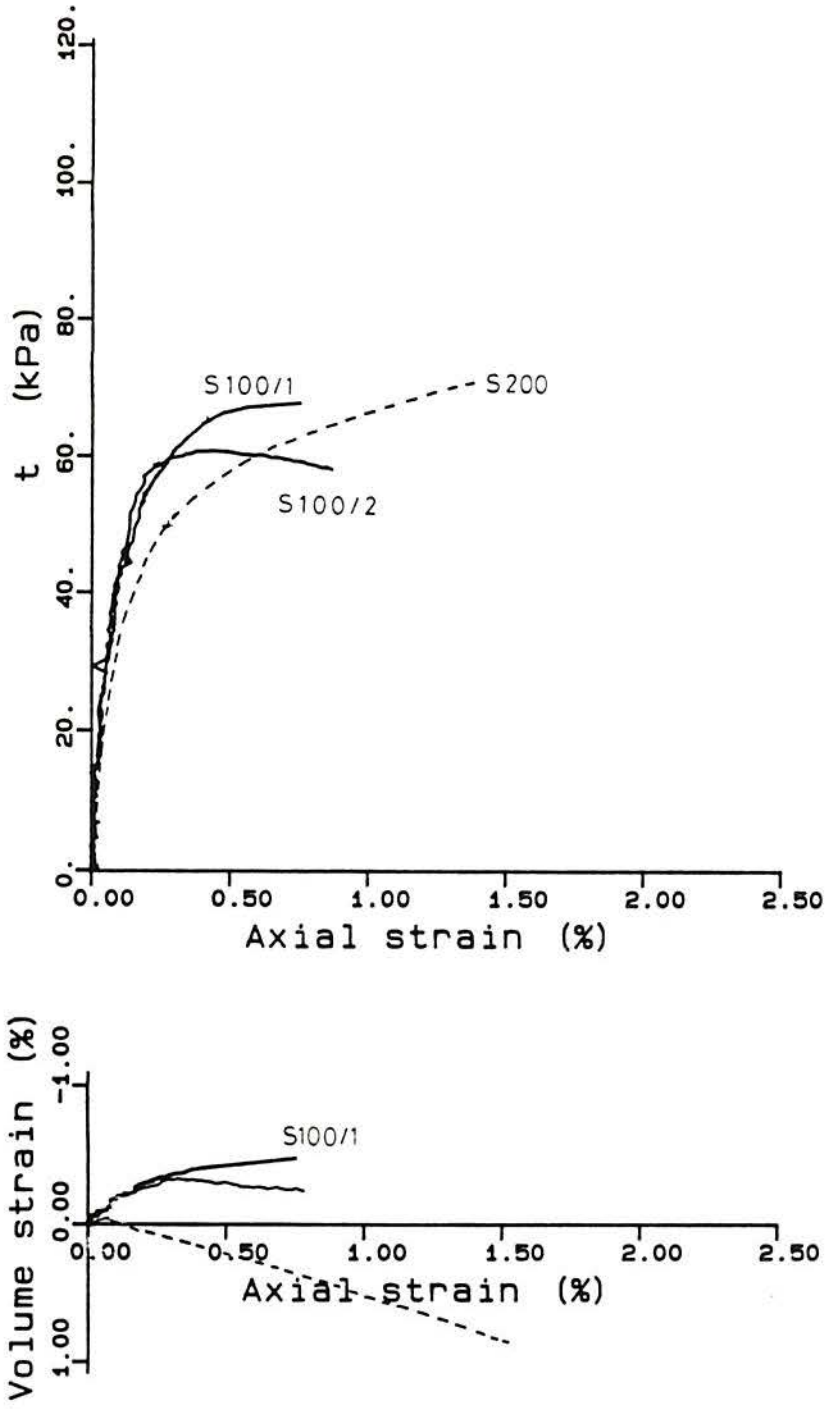

Figure 5.16 – Results of drained constant average stress s′ triaxial tests

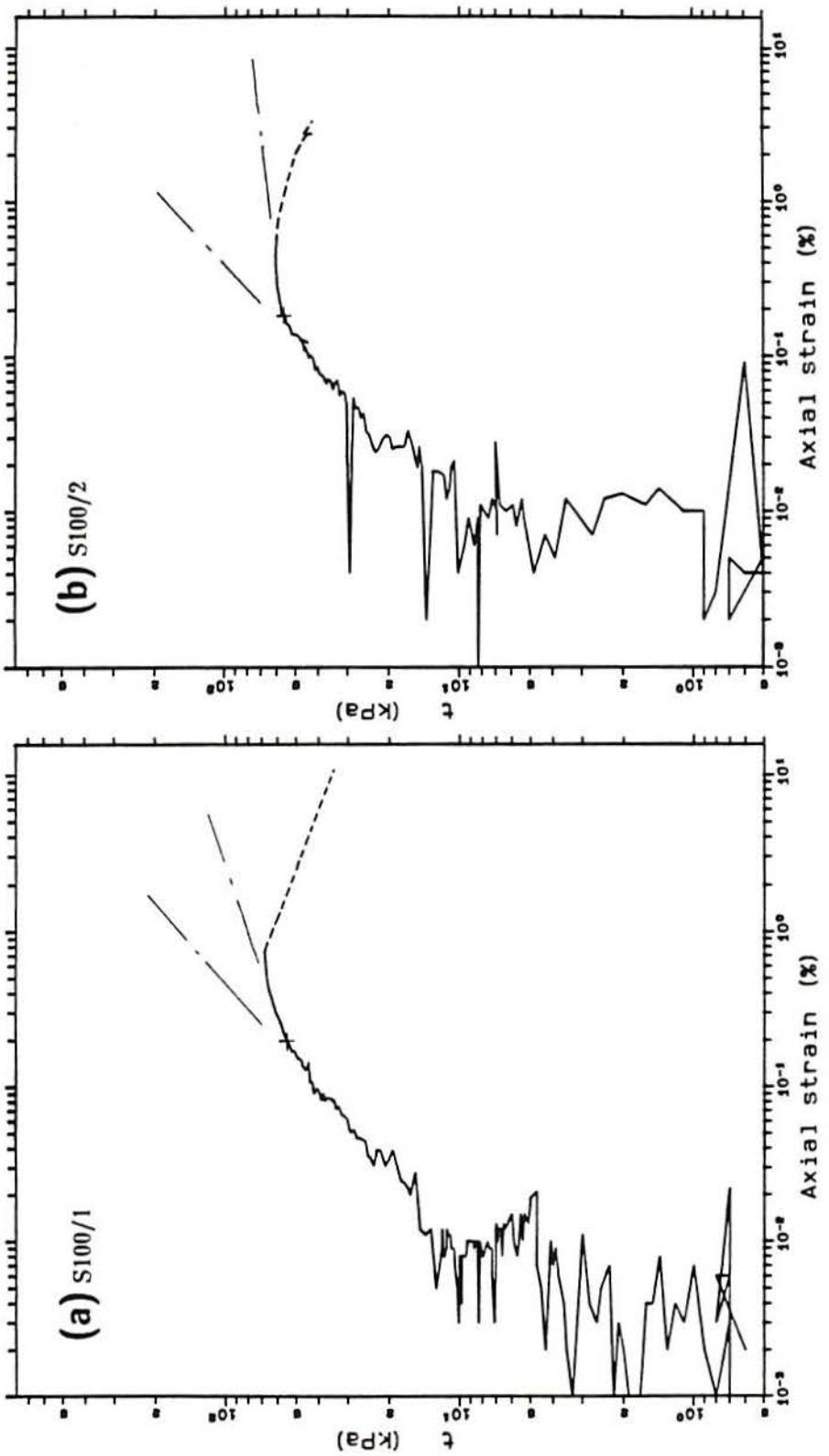

Figure 5.17 – Log-log plots of half deviator stress (t) versus axial strain for tests under constant s' (e=1.5); (*a*) test S100/1; (*b*) test S100/2; (cont.)

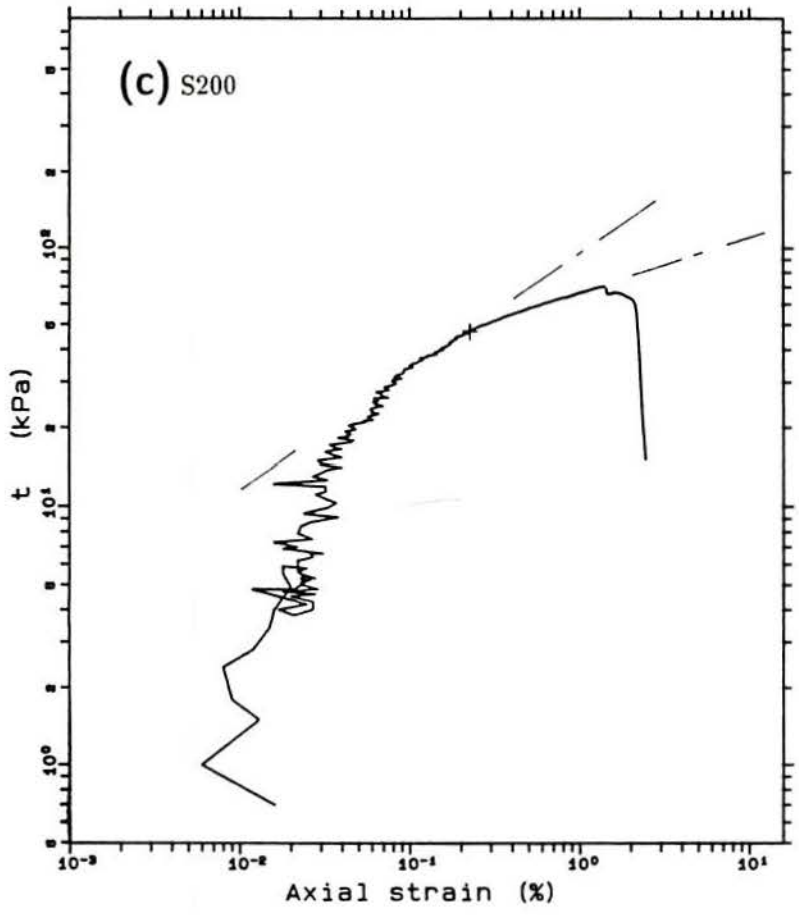

Figure 5.17 – (cont.) (*c*) test S200

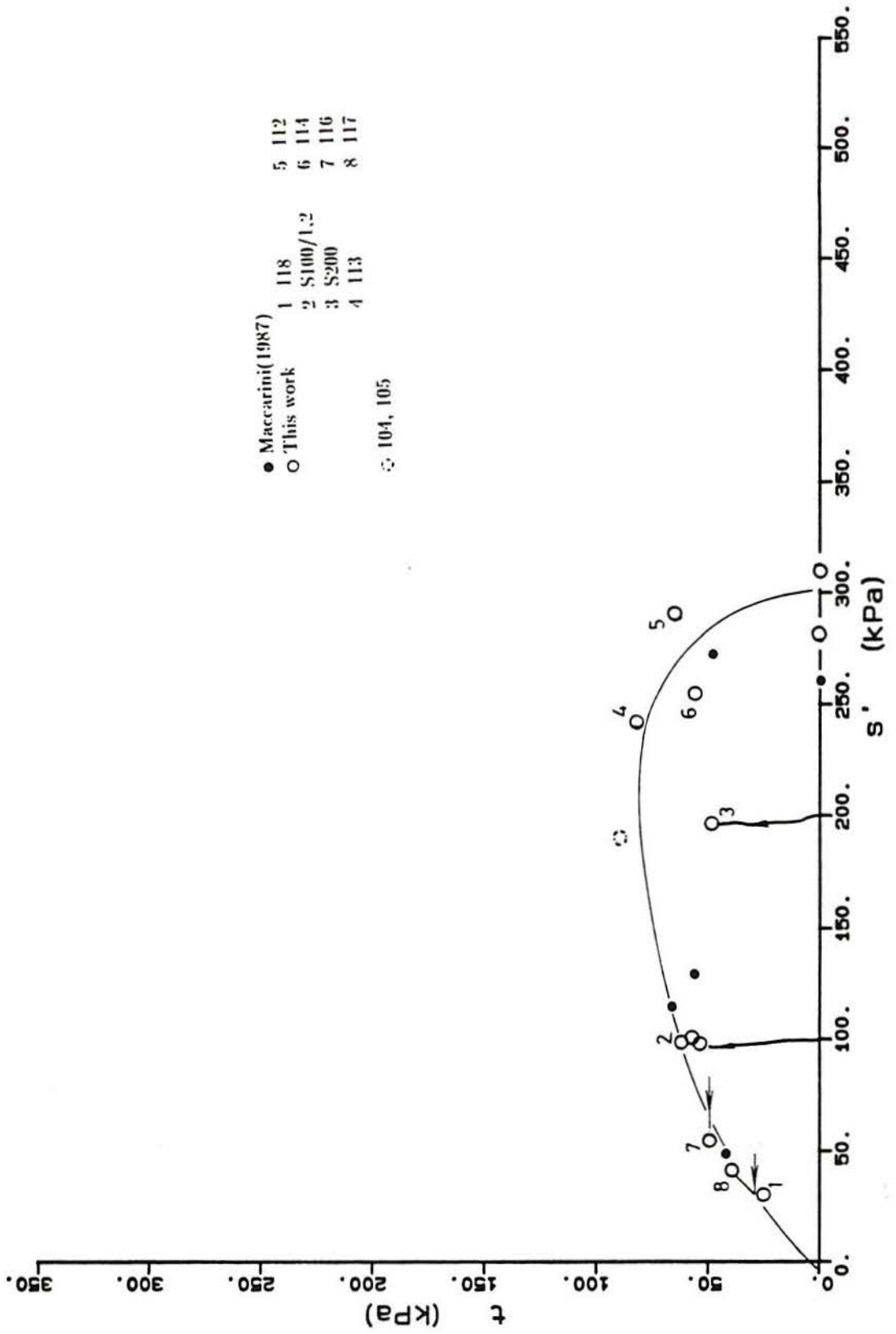

Figure 5.18 – Yield points determined from triaxial tests on artificial soil (e=1.5)

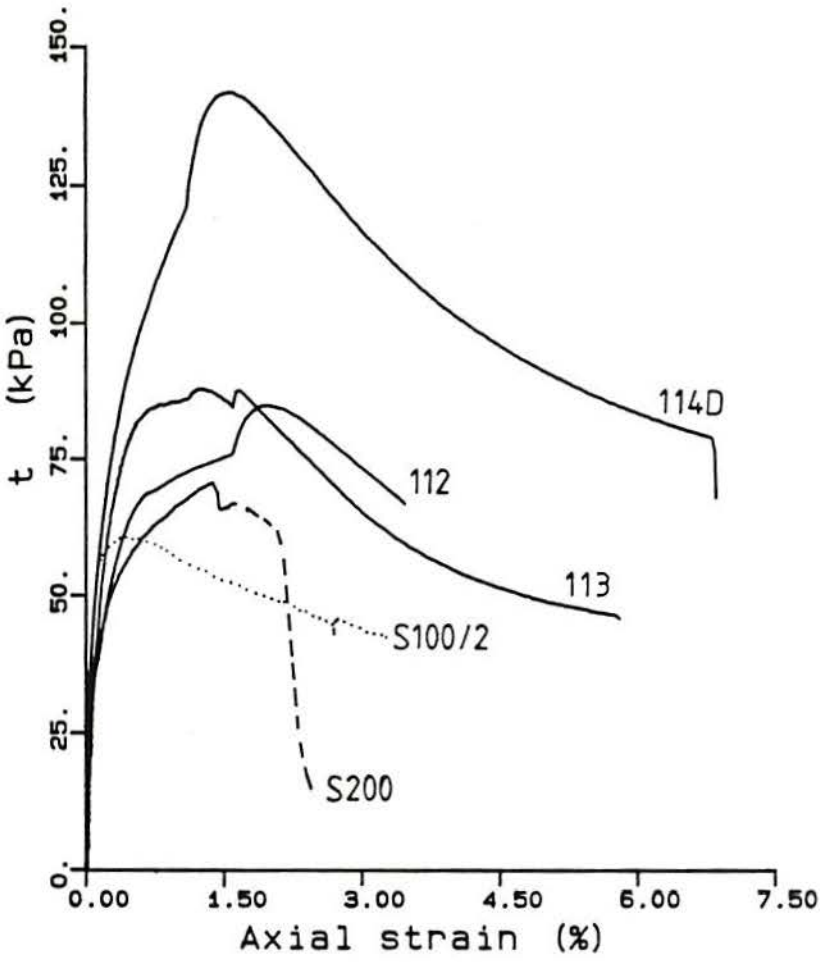

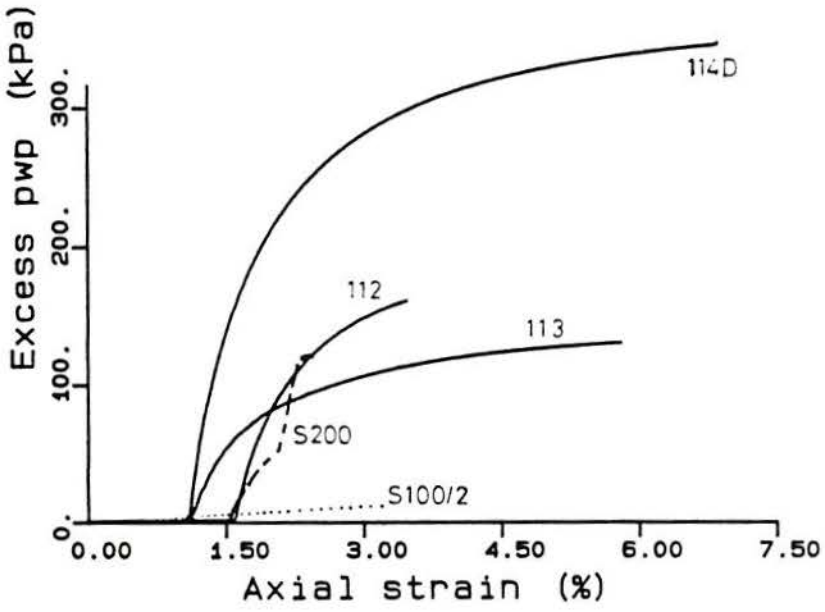

Figure 5.19 – Results of triaxial tests on artificial soil (e=1.5). Tests initially drained (see Fig. 5.18) and then undrained

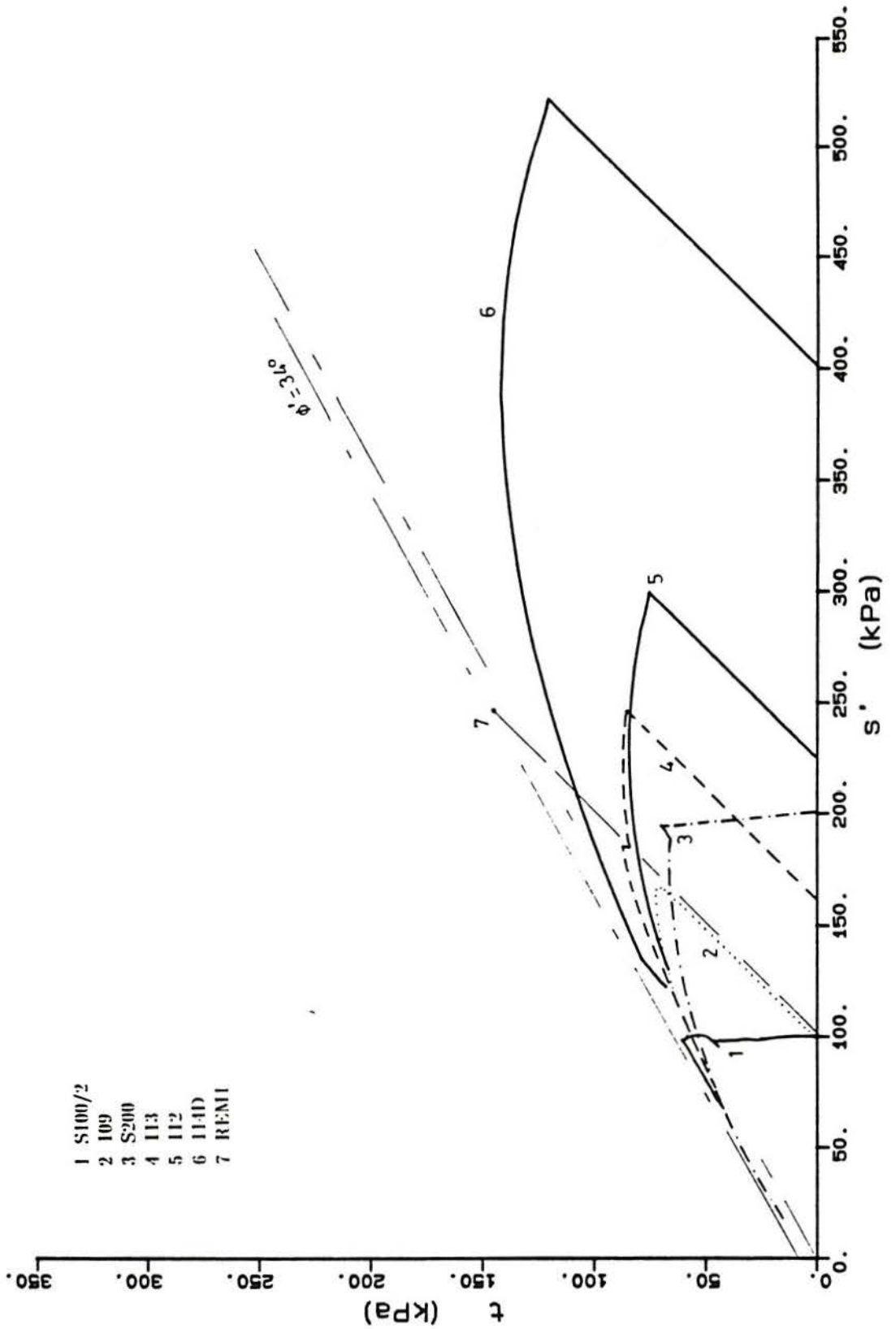

Figure 5.20 – Complete stress paths of some tests on the artificial soil (e=1.5)

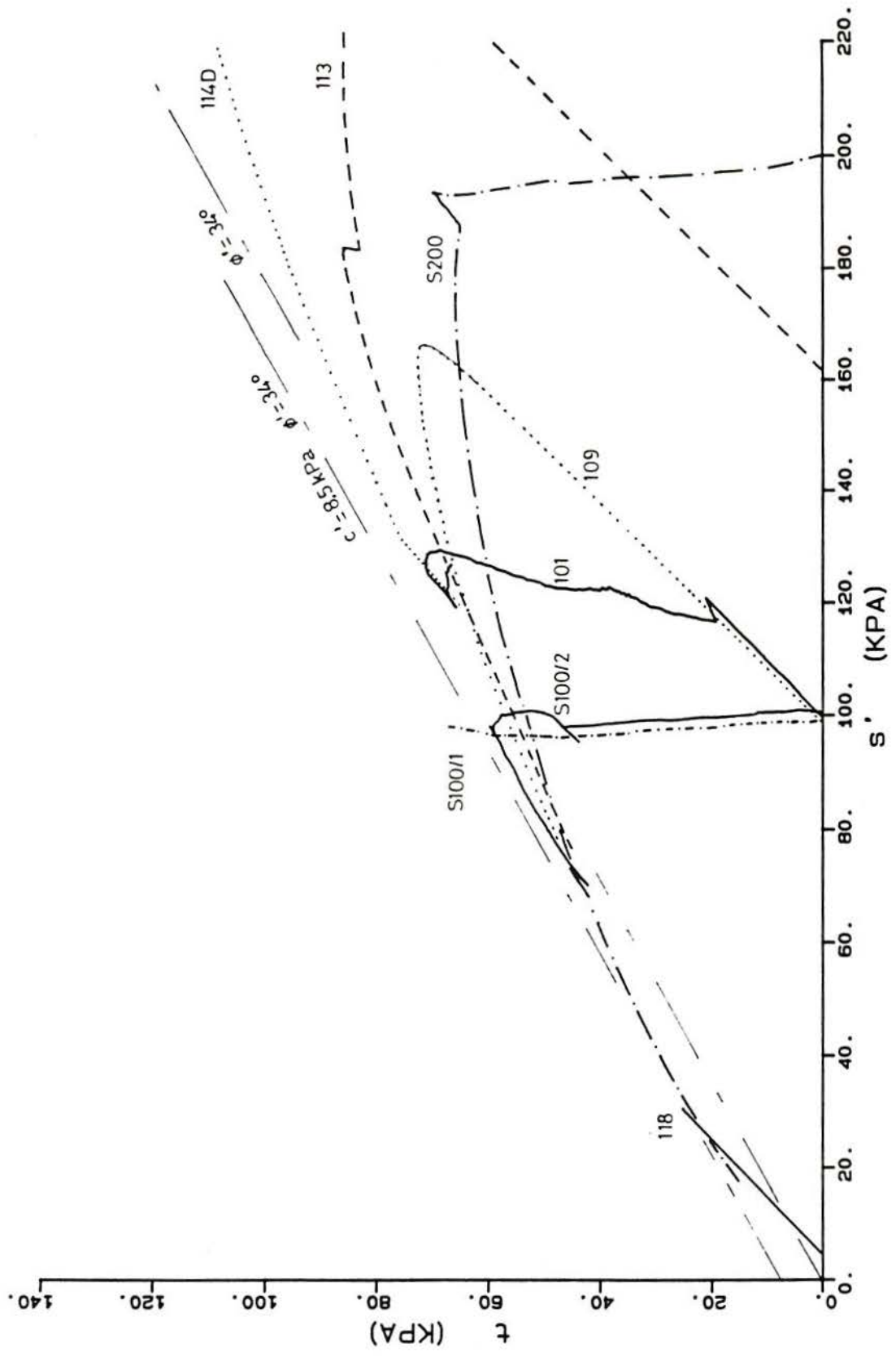

Figure 5.21 – Stress path of tests on artificial soil (e=1.5) at lower stress levels

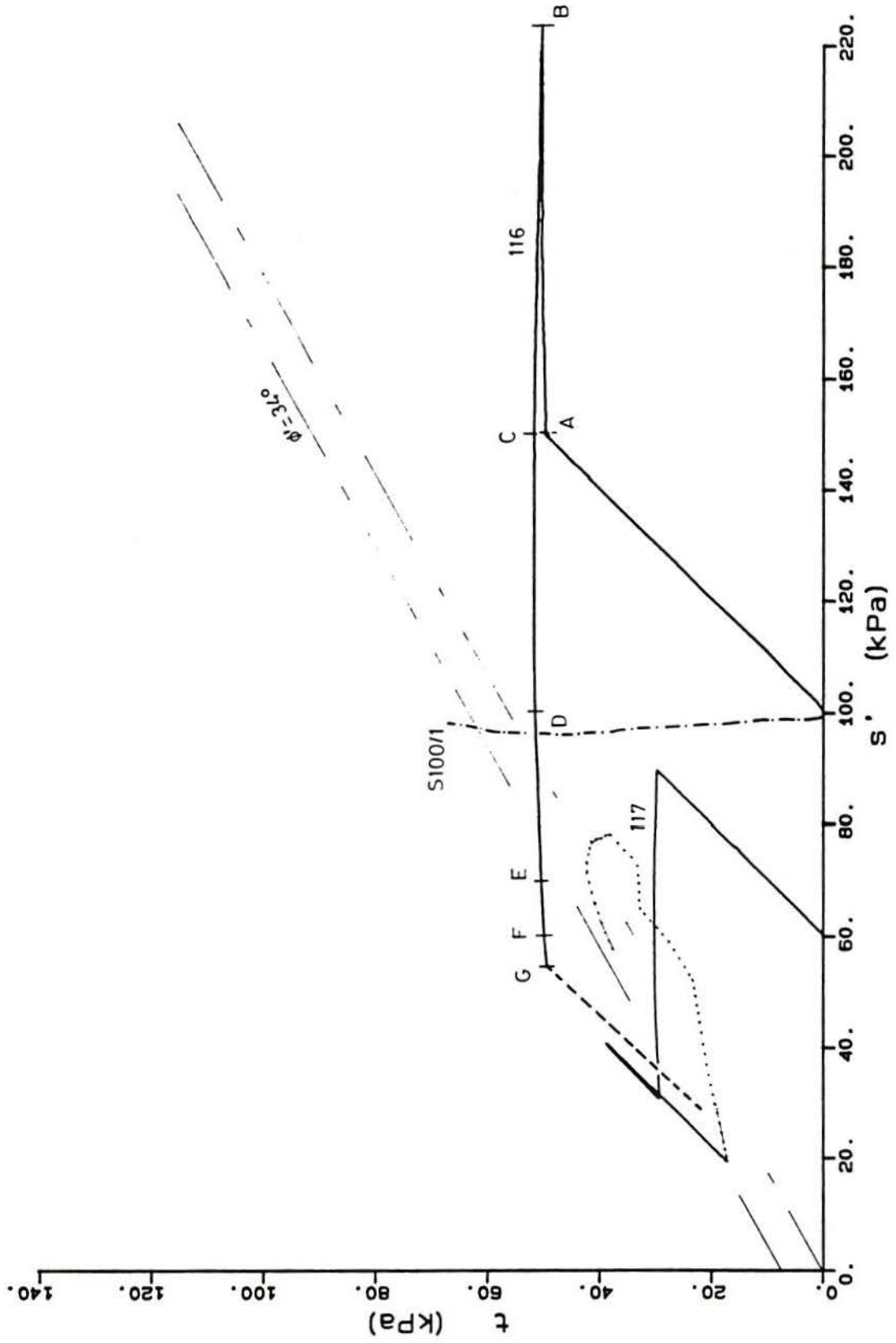

Figure 5.22 – Stress paths of triaxial drained tests with reduction of s' under constant deviator stress. Artificial soil, e=1.5

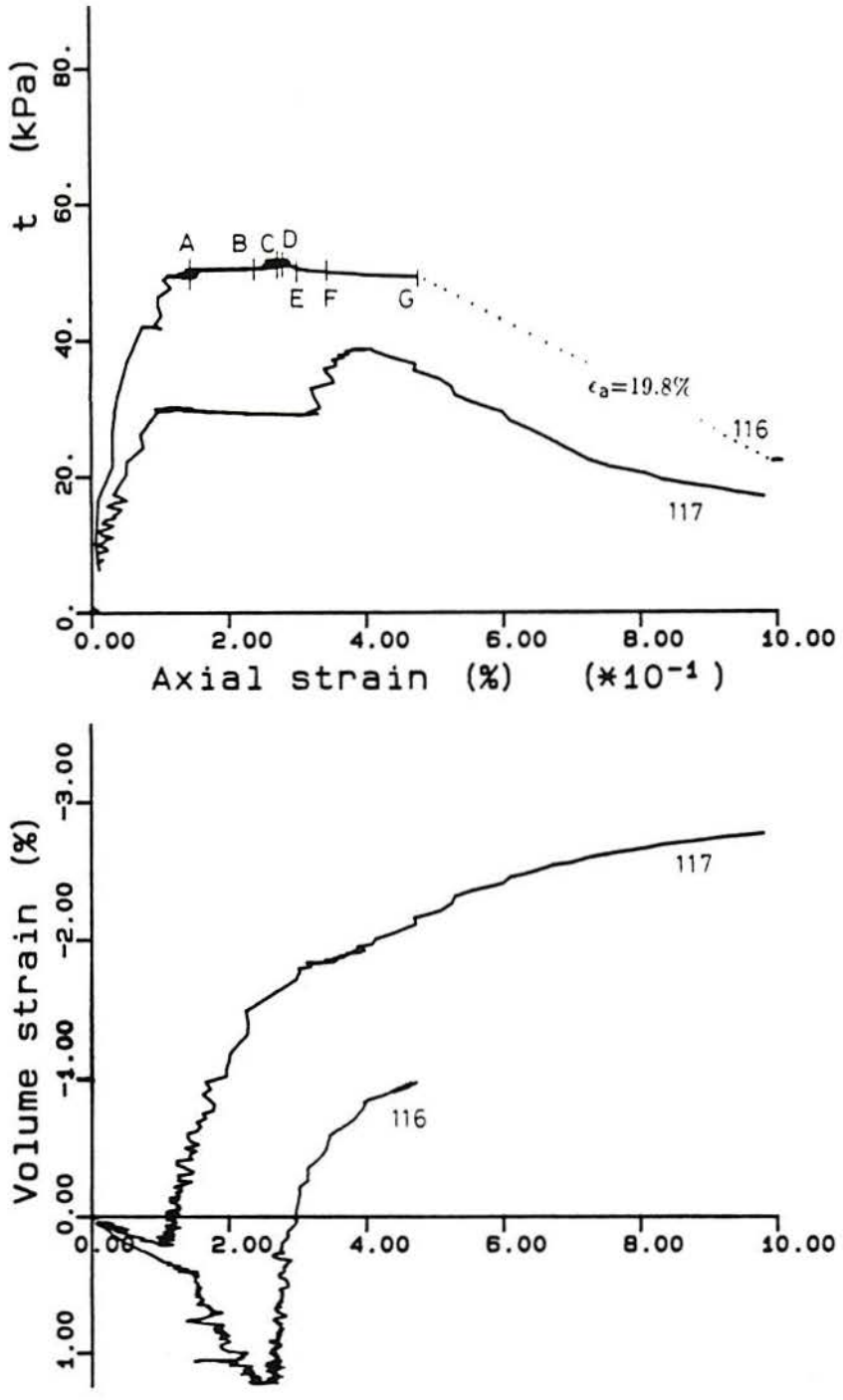

Figure 5.23 – Constant deviator stress and reducing s′ triaxial tests on artificial soil (e=1.5) (see Fig. 5.22)

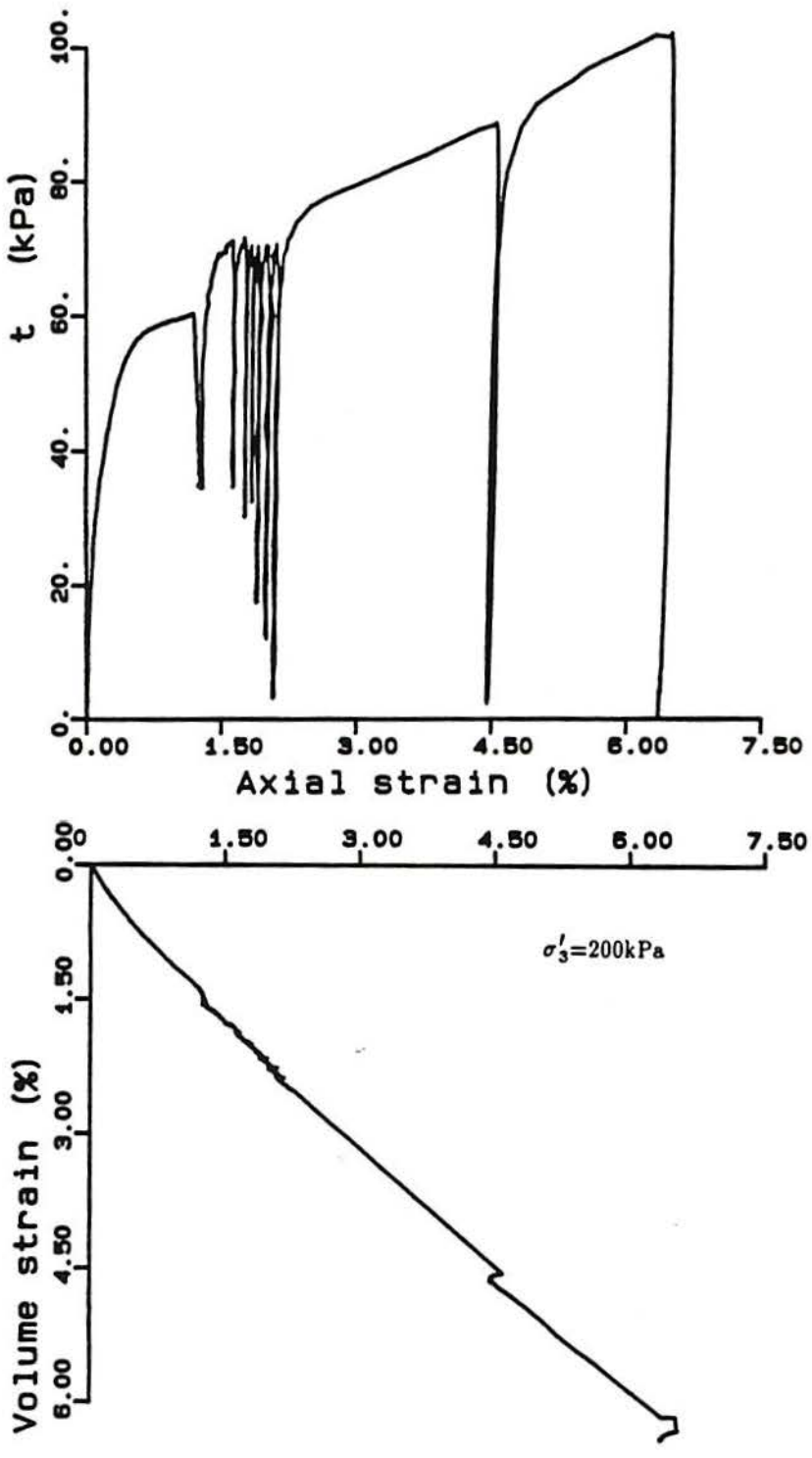

Figure 5.24 - Triaxial drained compression test on sample 114B (artificial soil, e=1.5)

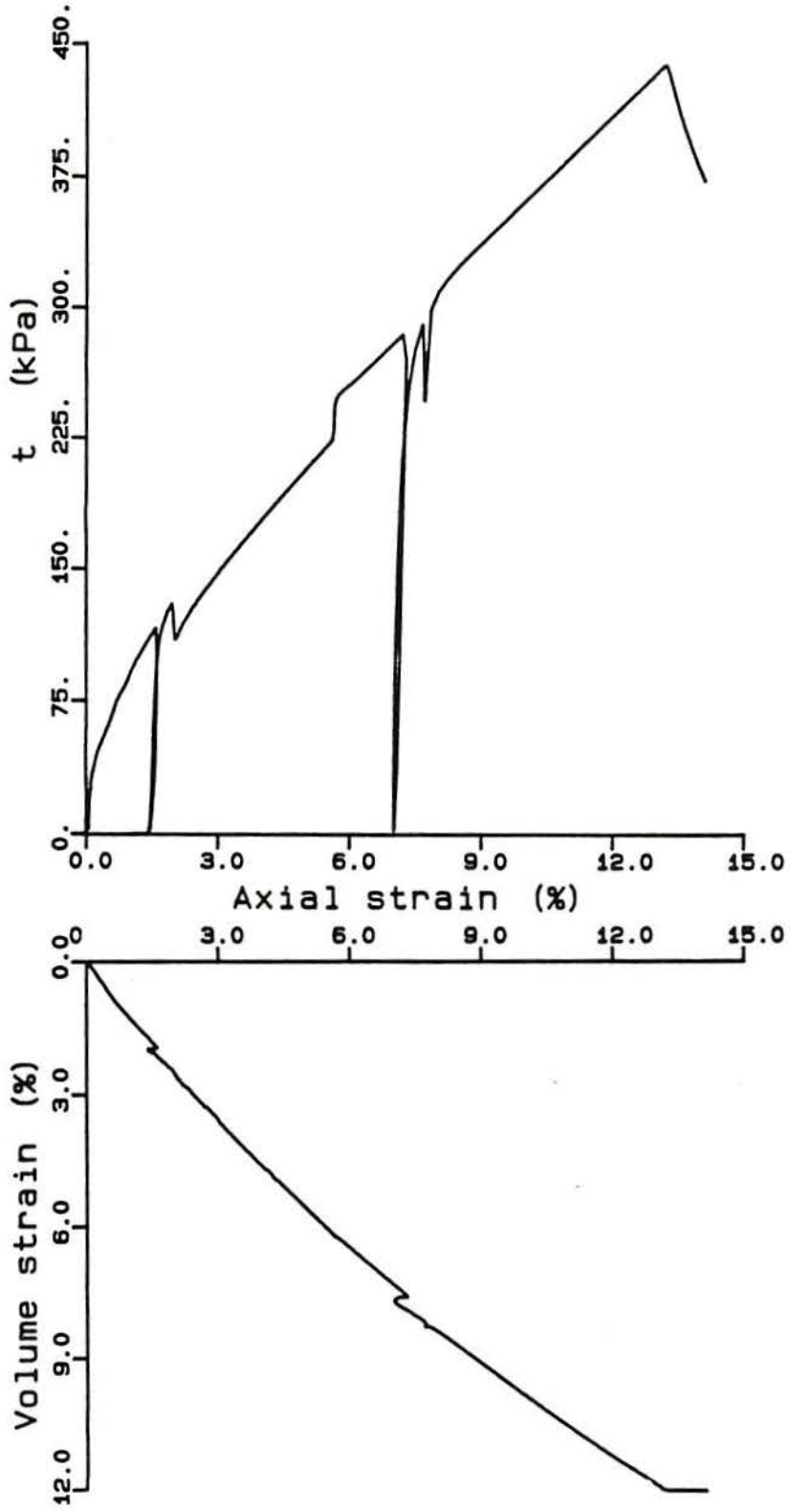

Figure 5.25 – Triaxial compression test on sample 115 (artificial soil, e=1.5)

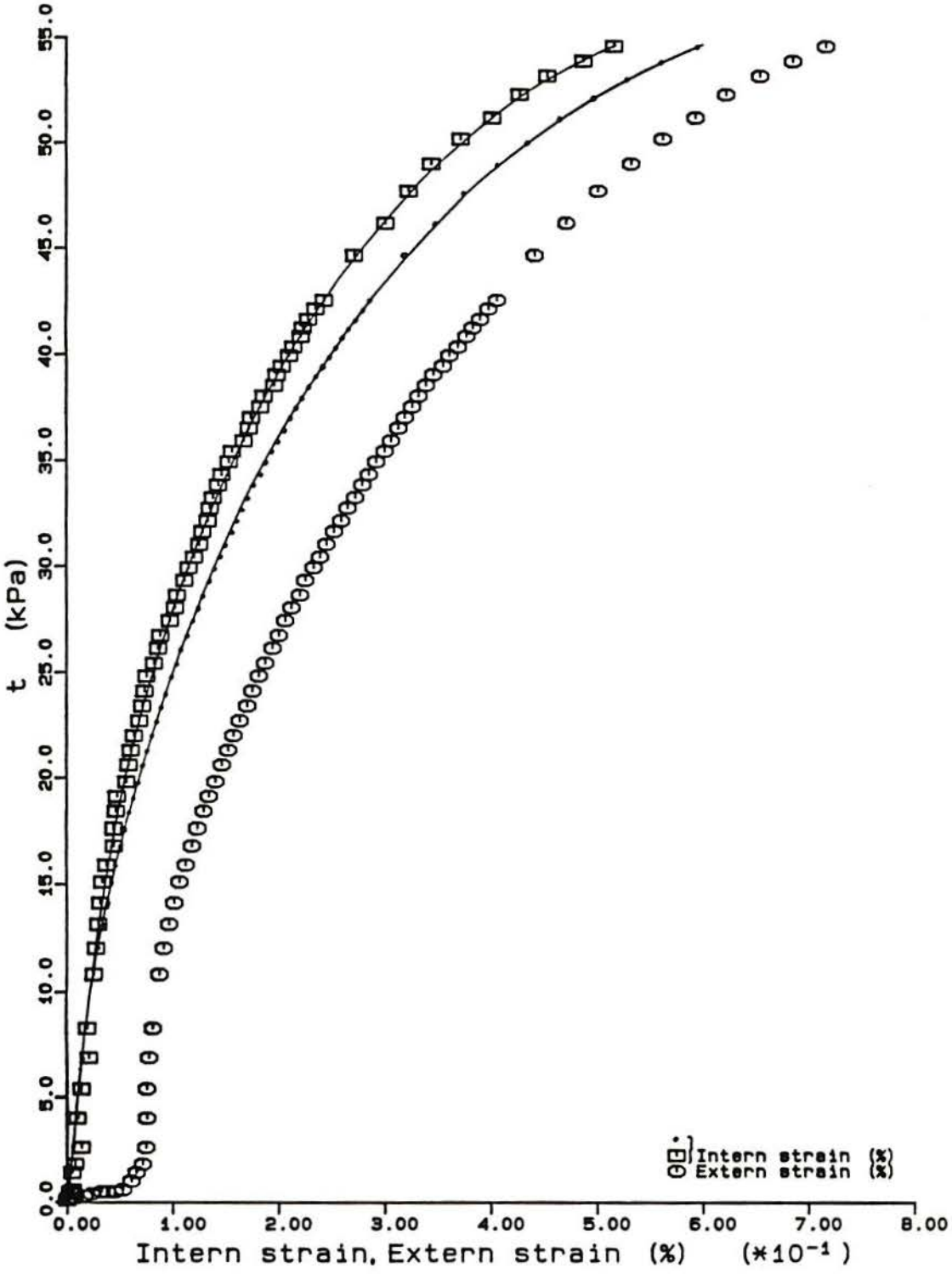

Figure 5.26 - Stress-strain results obtained from three different measurements on test 114B (σ'_3=200 kPa)

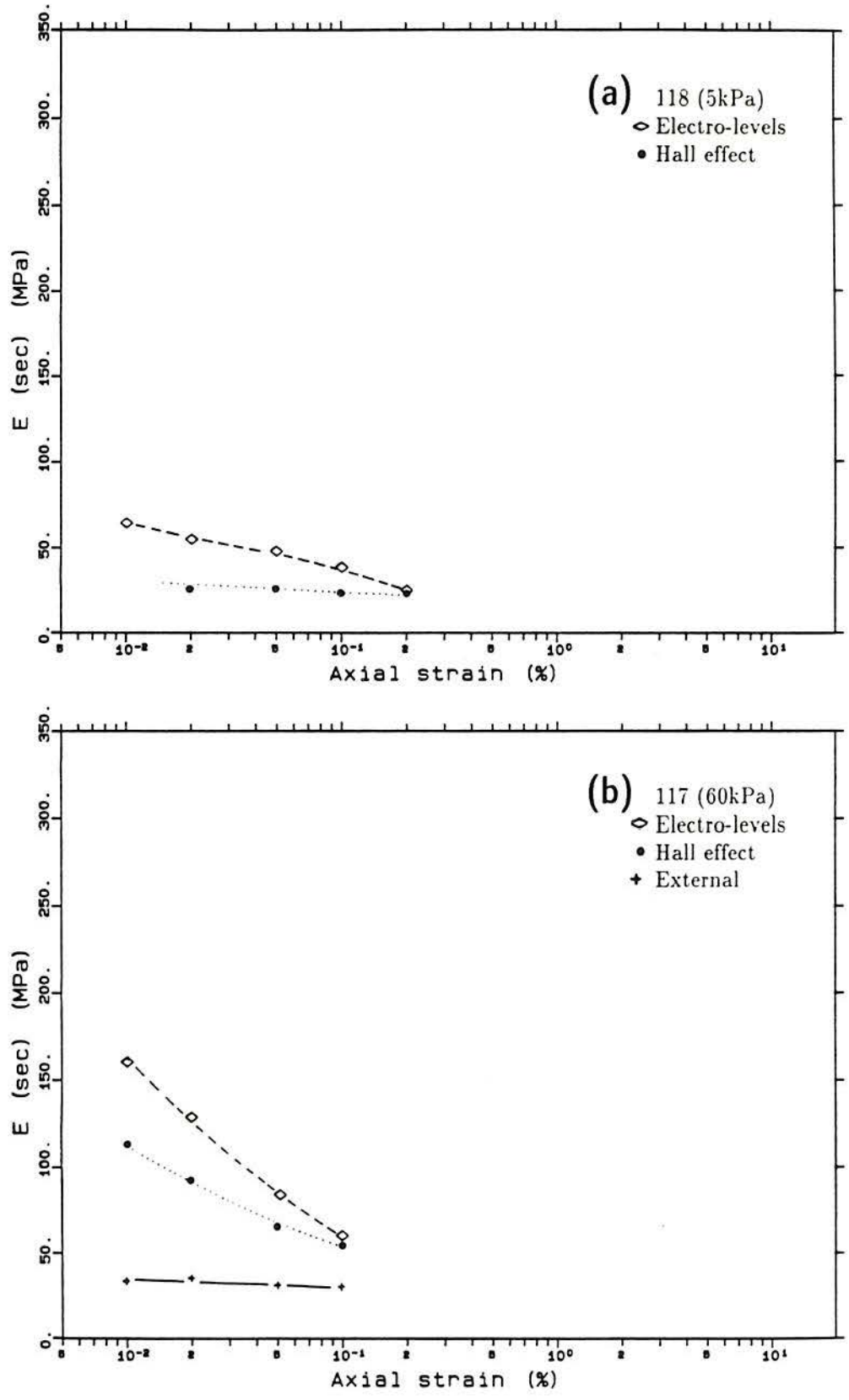

Figure 5.27 – Secant stiffness versus logarithm of axial strain obtained from different measurements. (*a*) test 118; (*b*) test 117; (cont.)

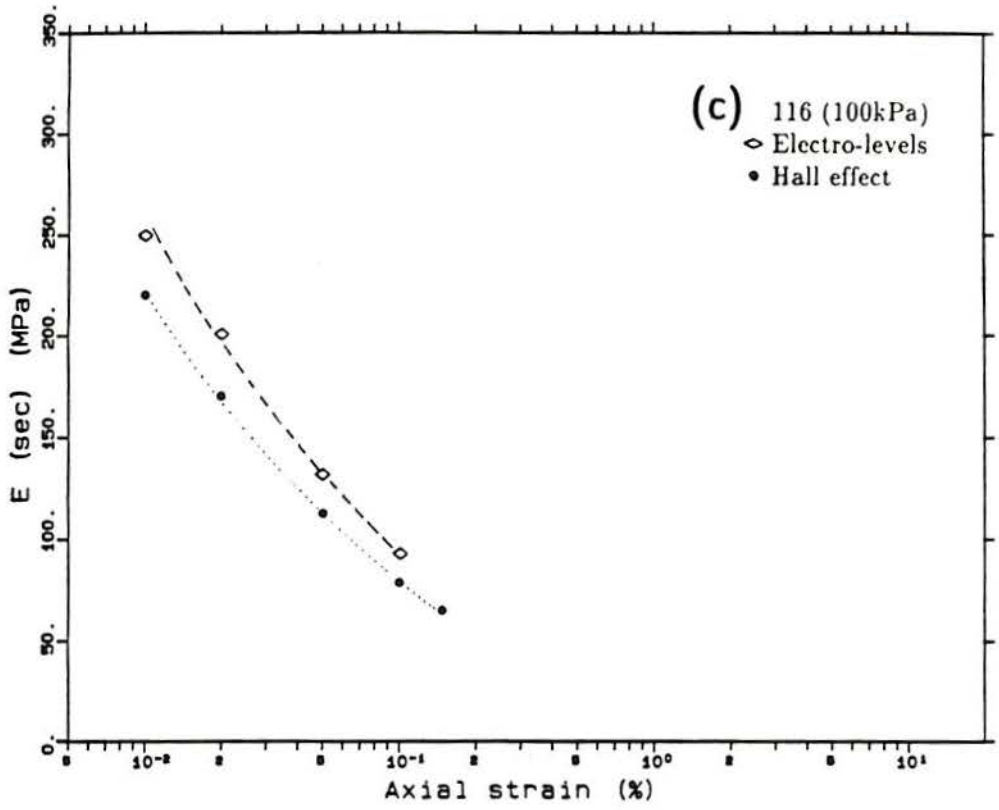

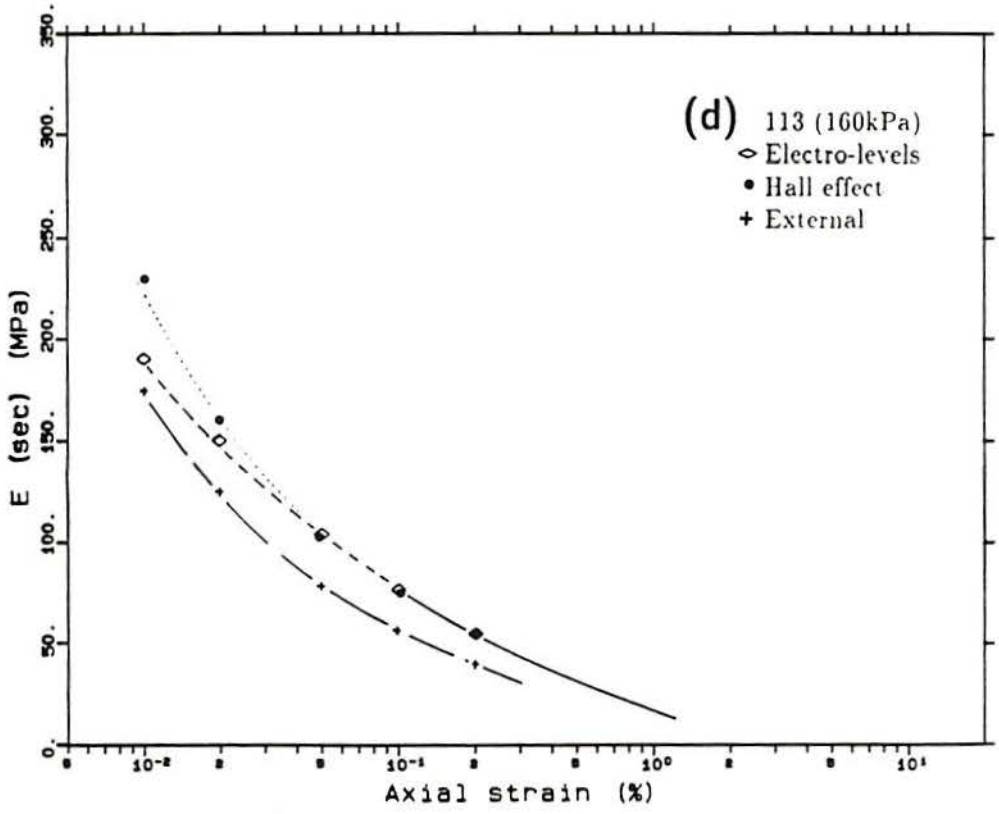

Figure 5.27 - (cont.) (*c*) test 116; (*d*) test 113; (cont.)

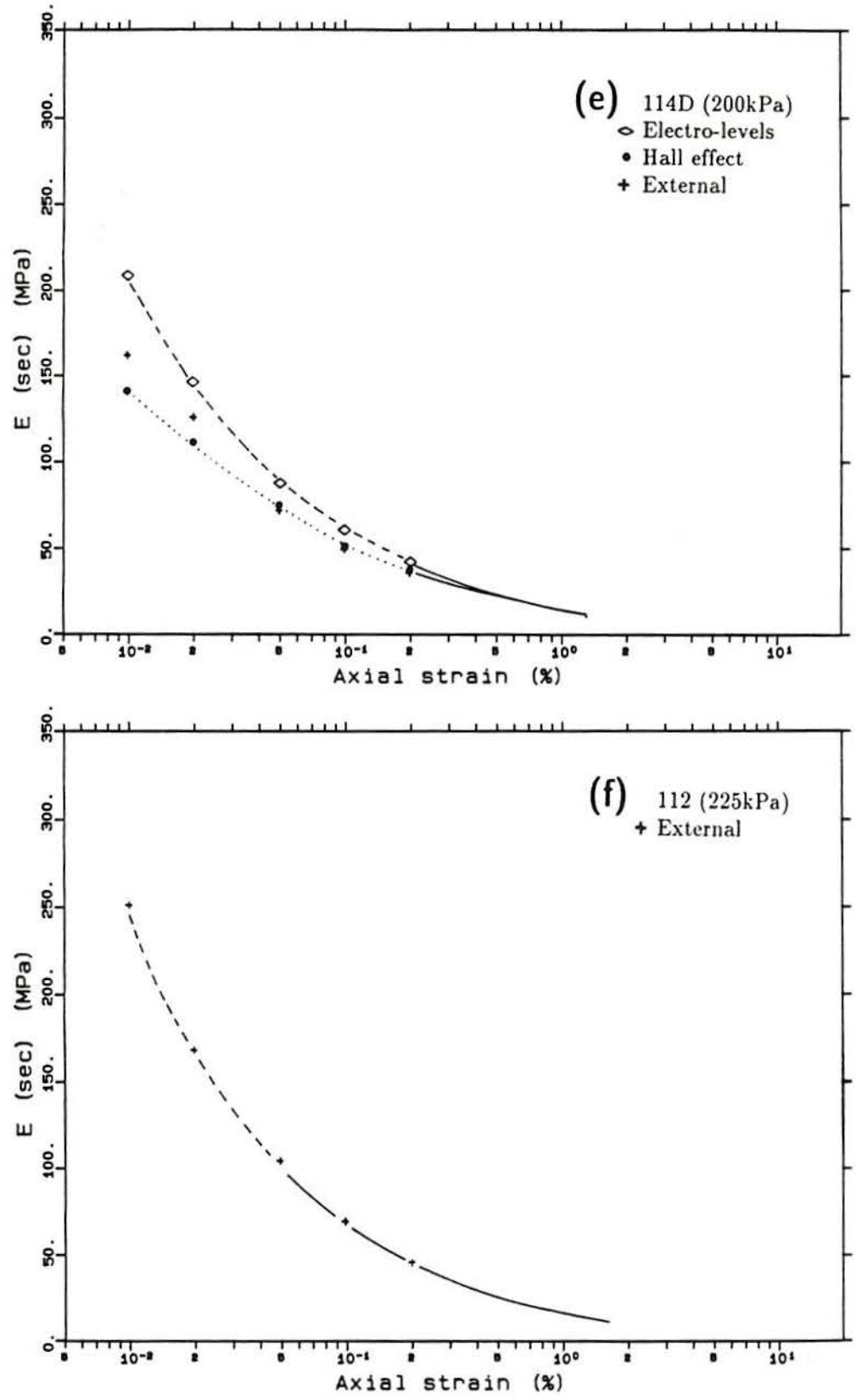

Figure 5.27 – (cont.) (*e*) test 114B; (*f*) test 112; (cont.)

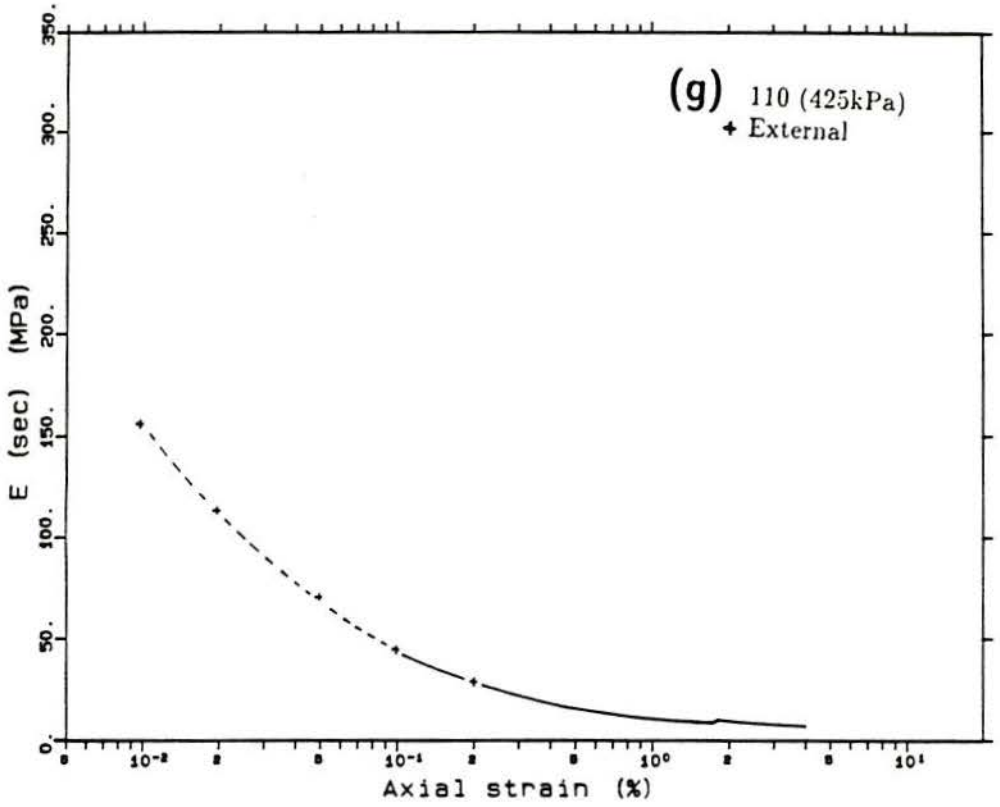

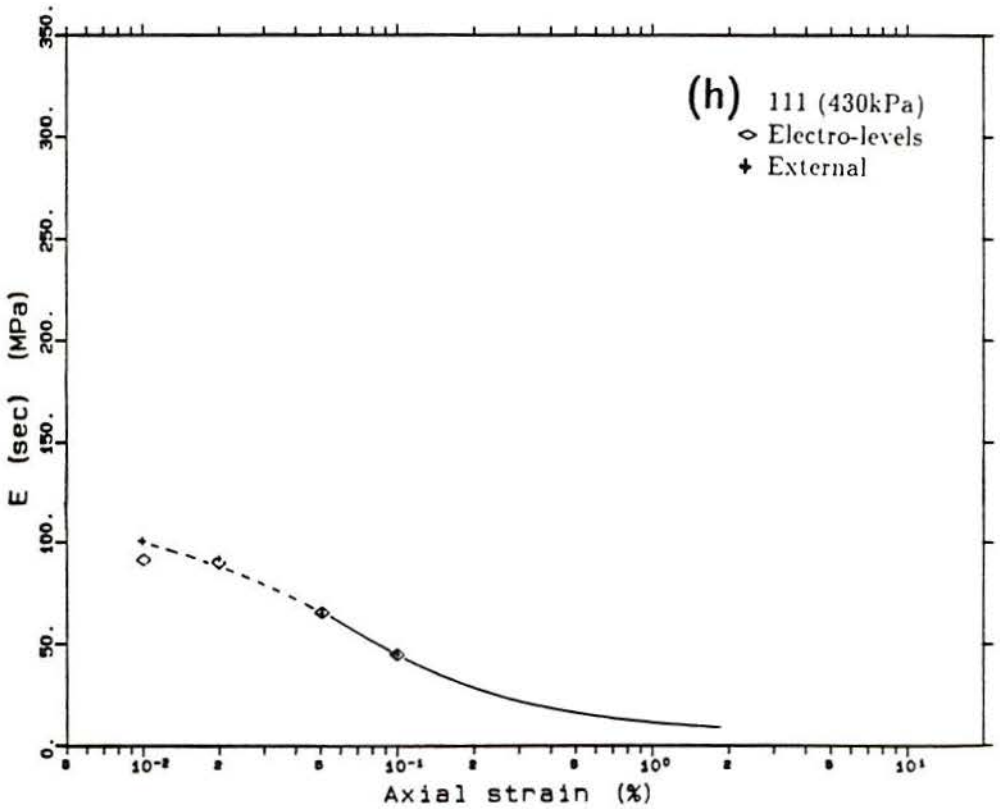

Figure 5.27 - (cont.) (*g*) test 110; (*h*) test 111; (cont.)

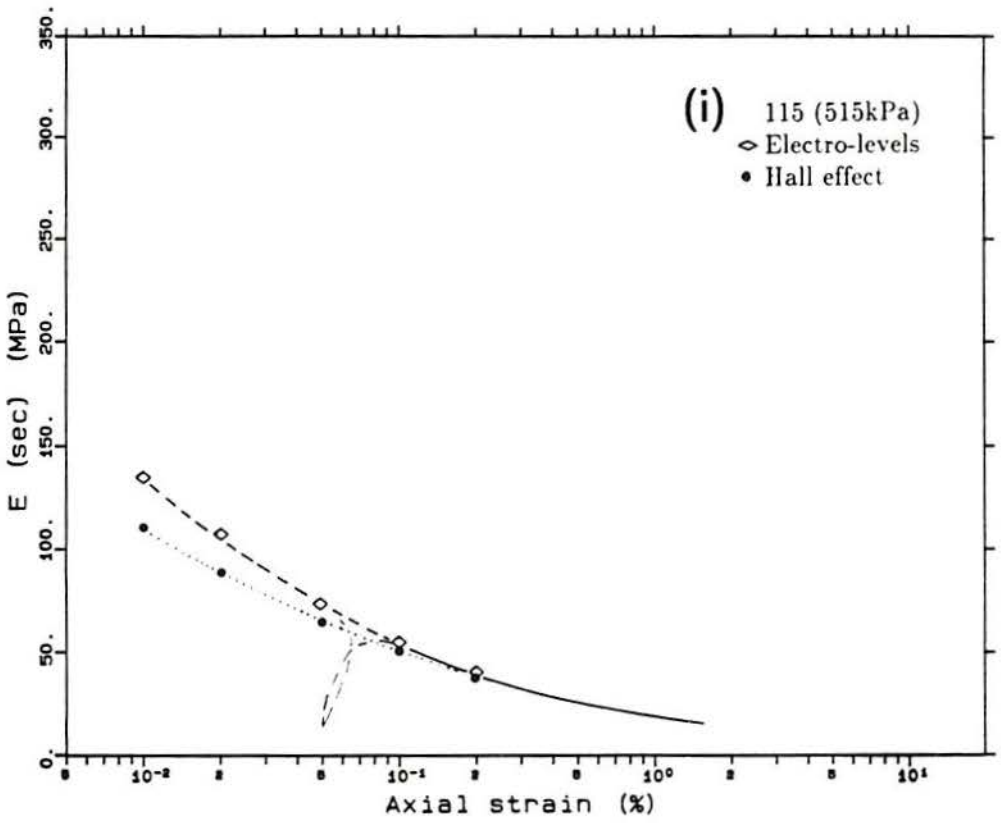

Figure 5.27 – (cont.) (*i*) test 115

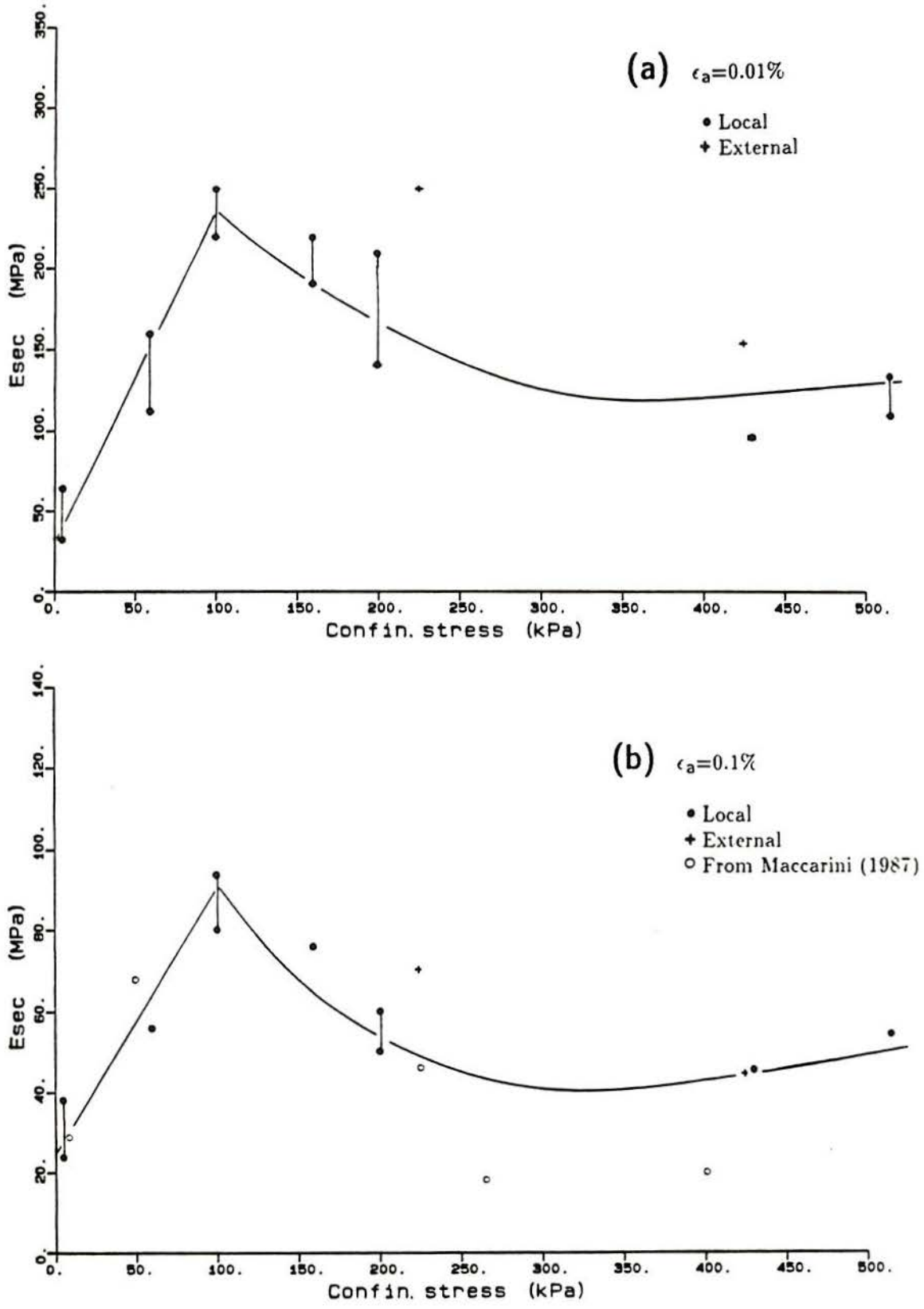

Figure 5.28 – Stiffness variation with confining pressure. (*a*) determined at ϵ_a=0.01%; (*b*) determined at ϵ_a=0.1%

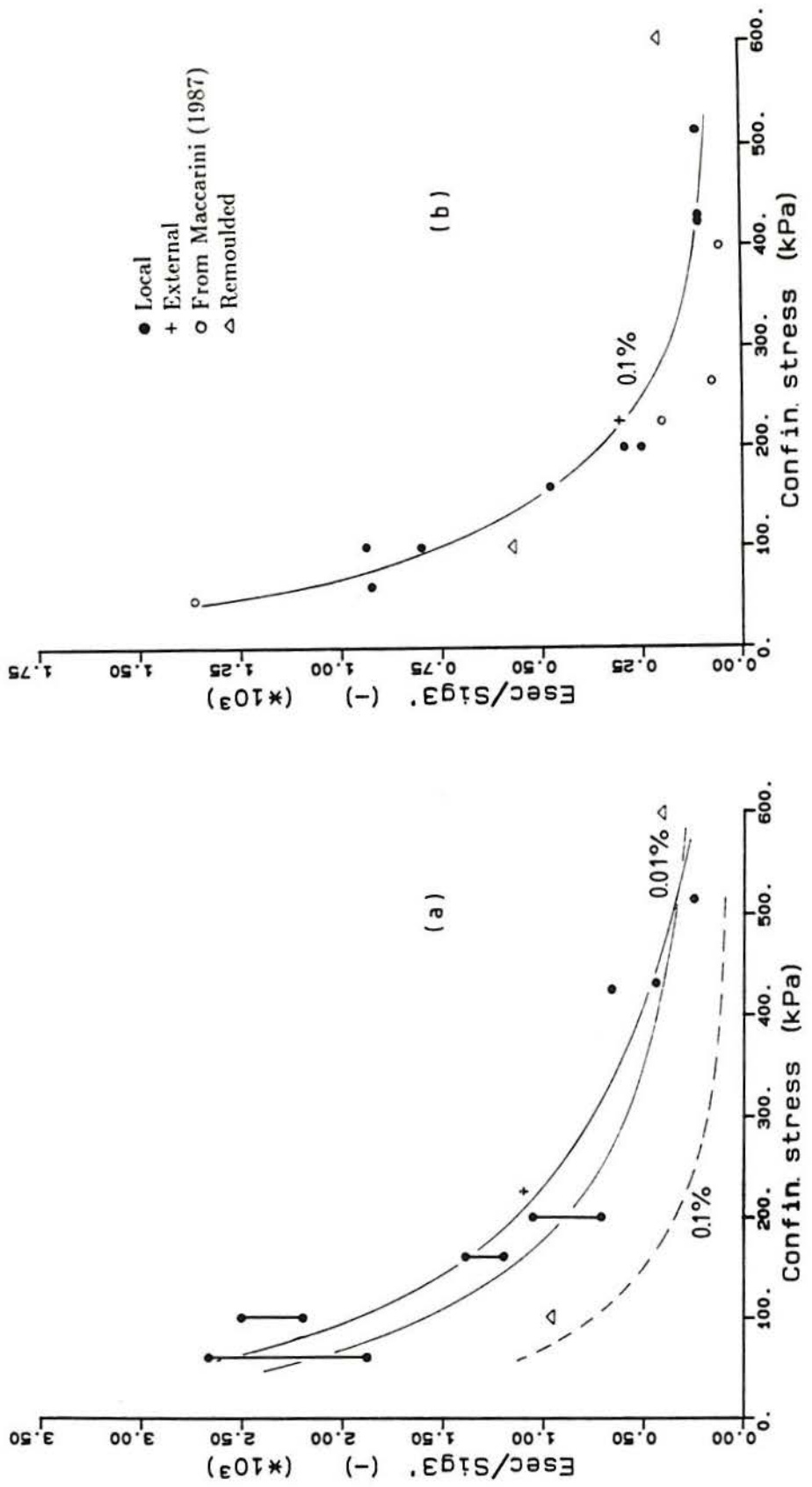

Figure 5.29 – Normalized stiffness versus pressure for two levels of strain. (*a*) at ϵ_a=0.01%; (*b*) at ϵ_a=0.1%

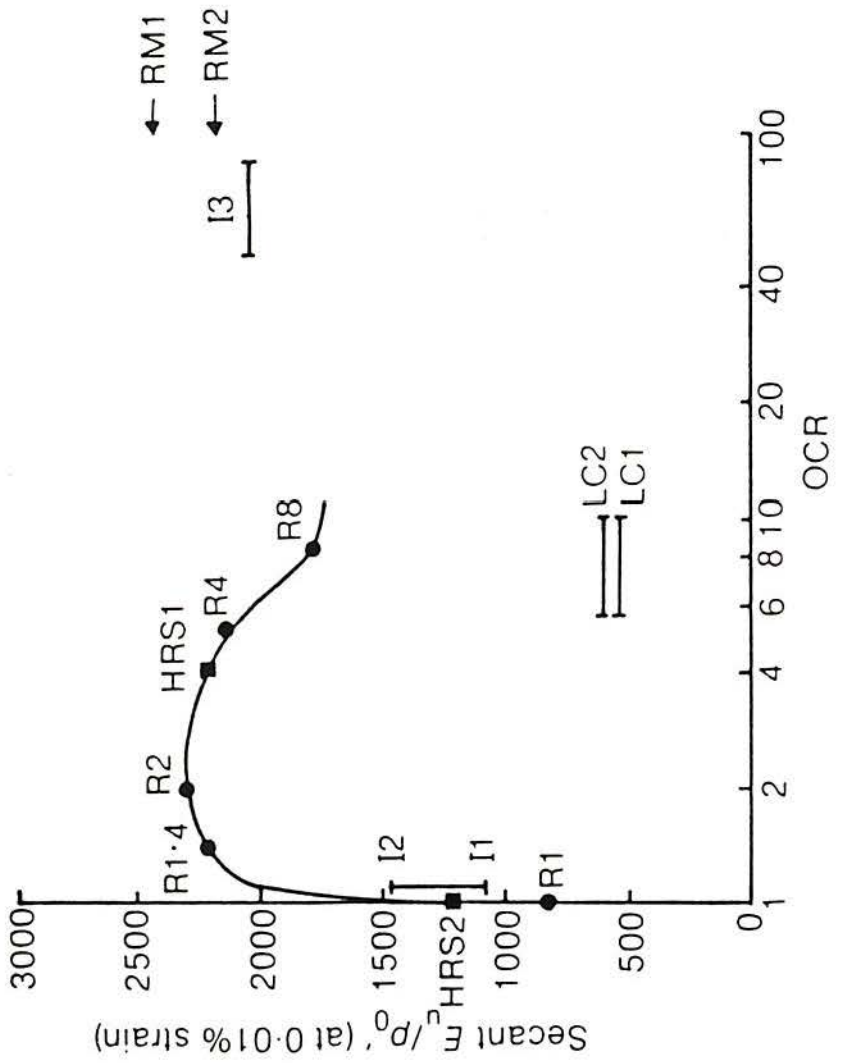

Figure 5.30 – Normalized stiffness determined from four soils (after Jardine et al., 1984)

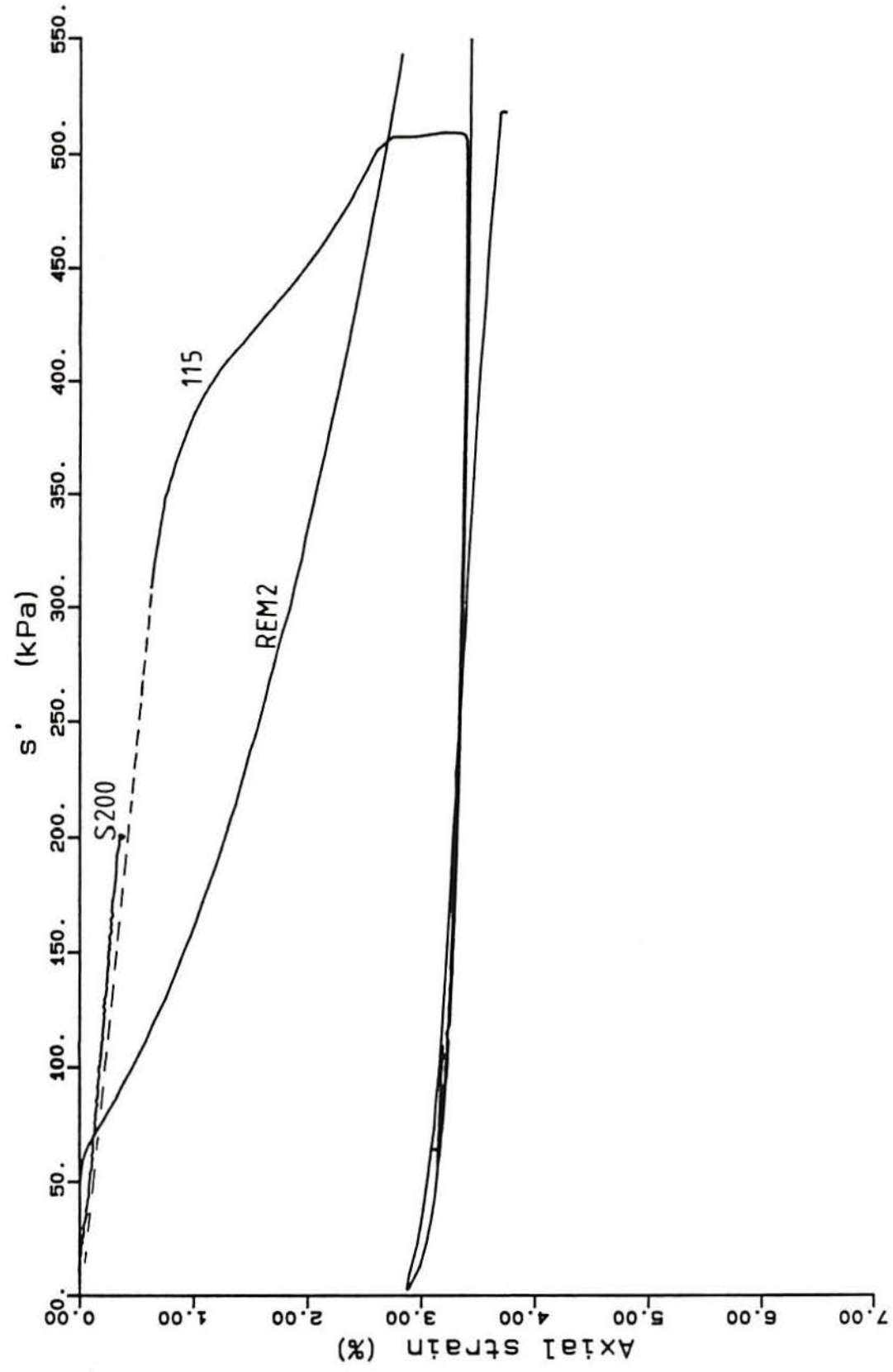

Figure 5.31 – Results of axial strain of test REM2 during isotropic consolidation compared with tests S200 and 115

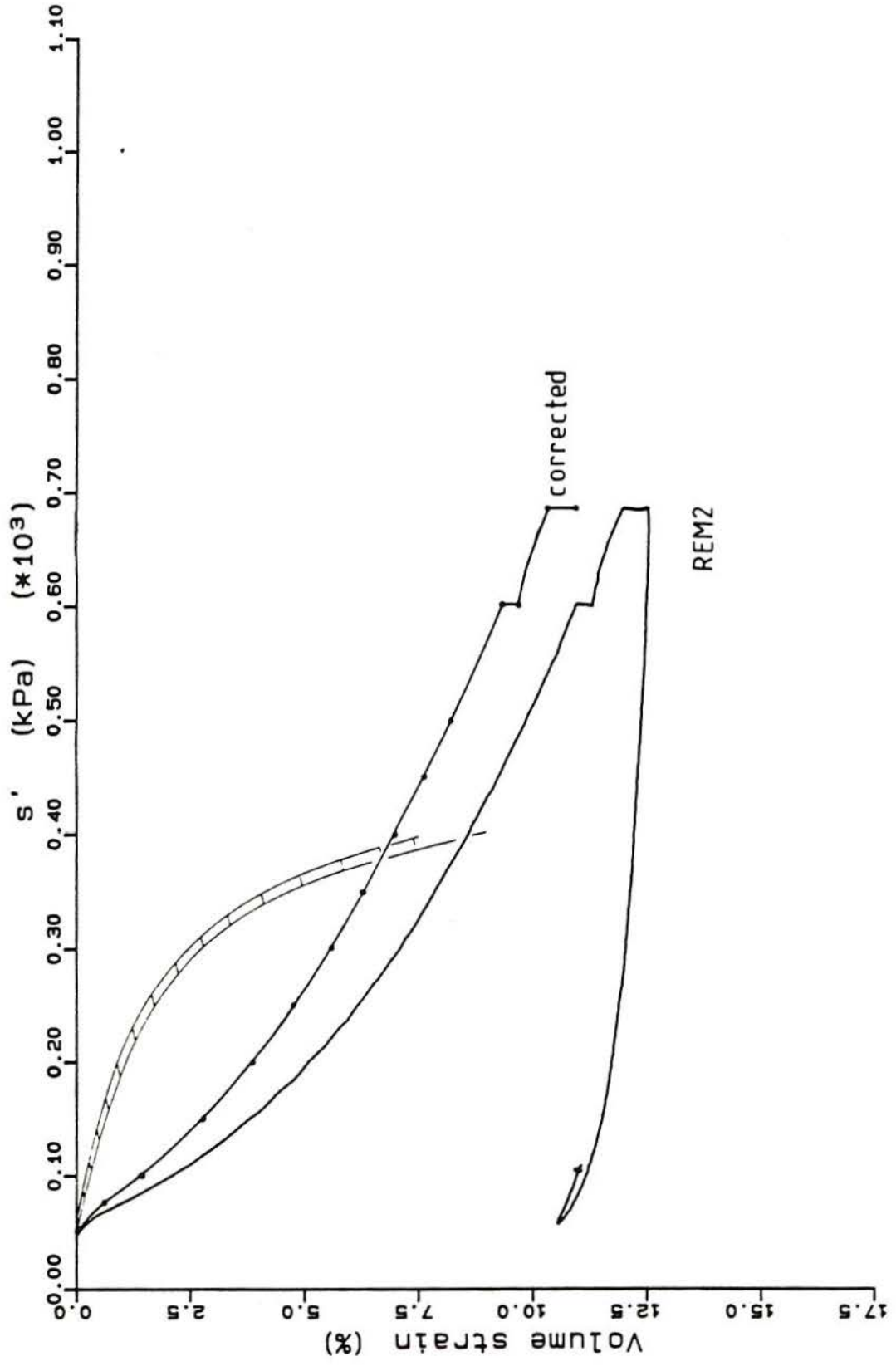

Figure 5.32 – Results of volumetric strain of test REM2 with and without membrane correction. Shaded area is the range of test results on bonded artificial soil

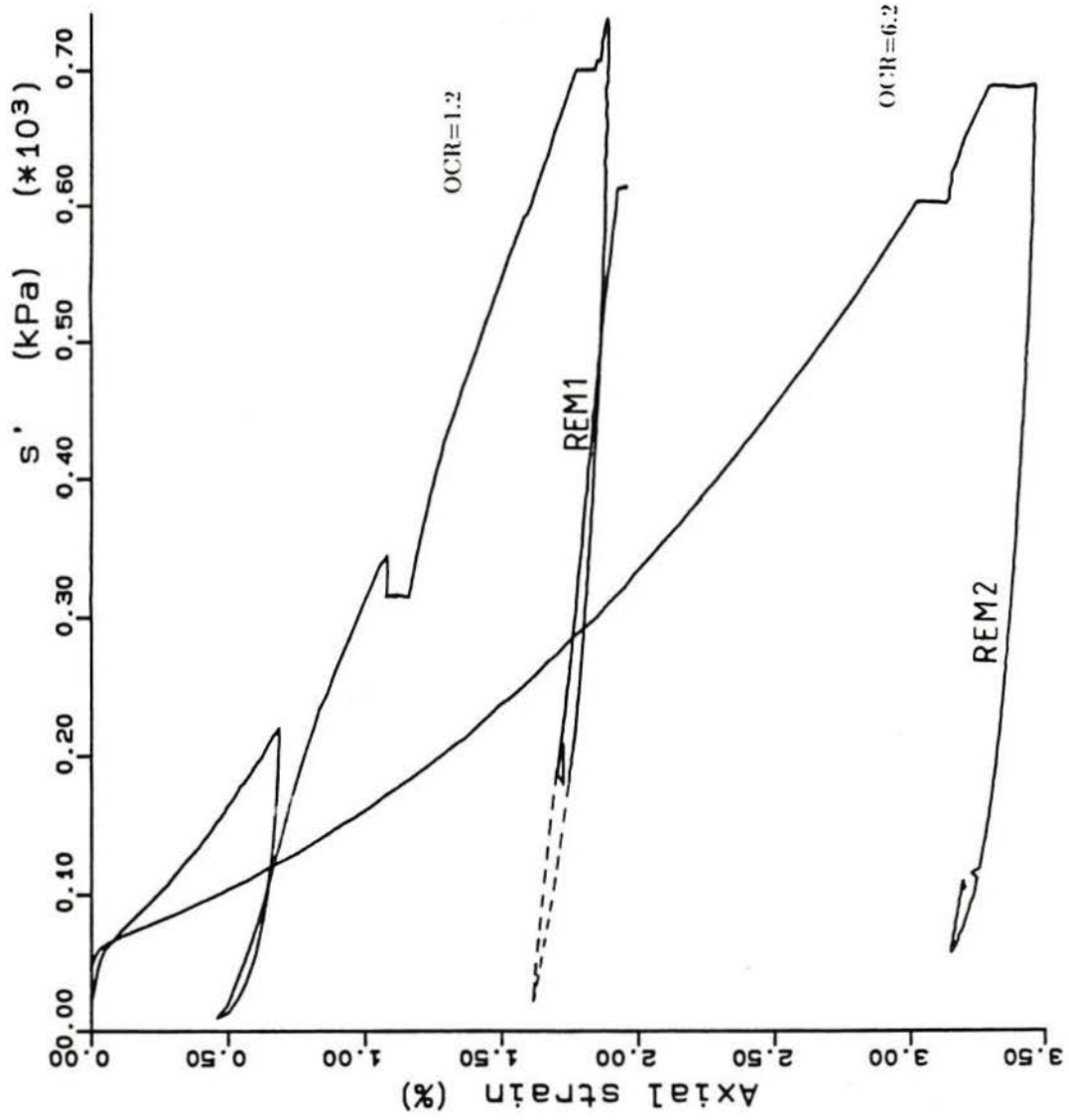

Figure 5.33 – Axial strain measurements obtained during isotropic consolidation in two remoulded samples

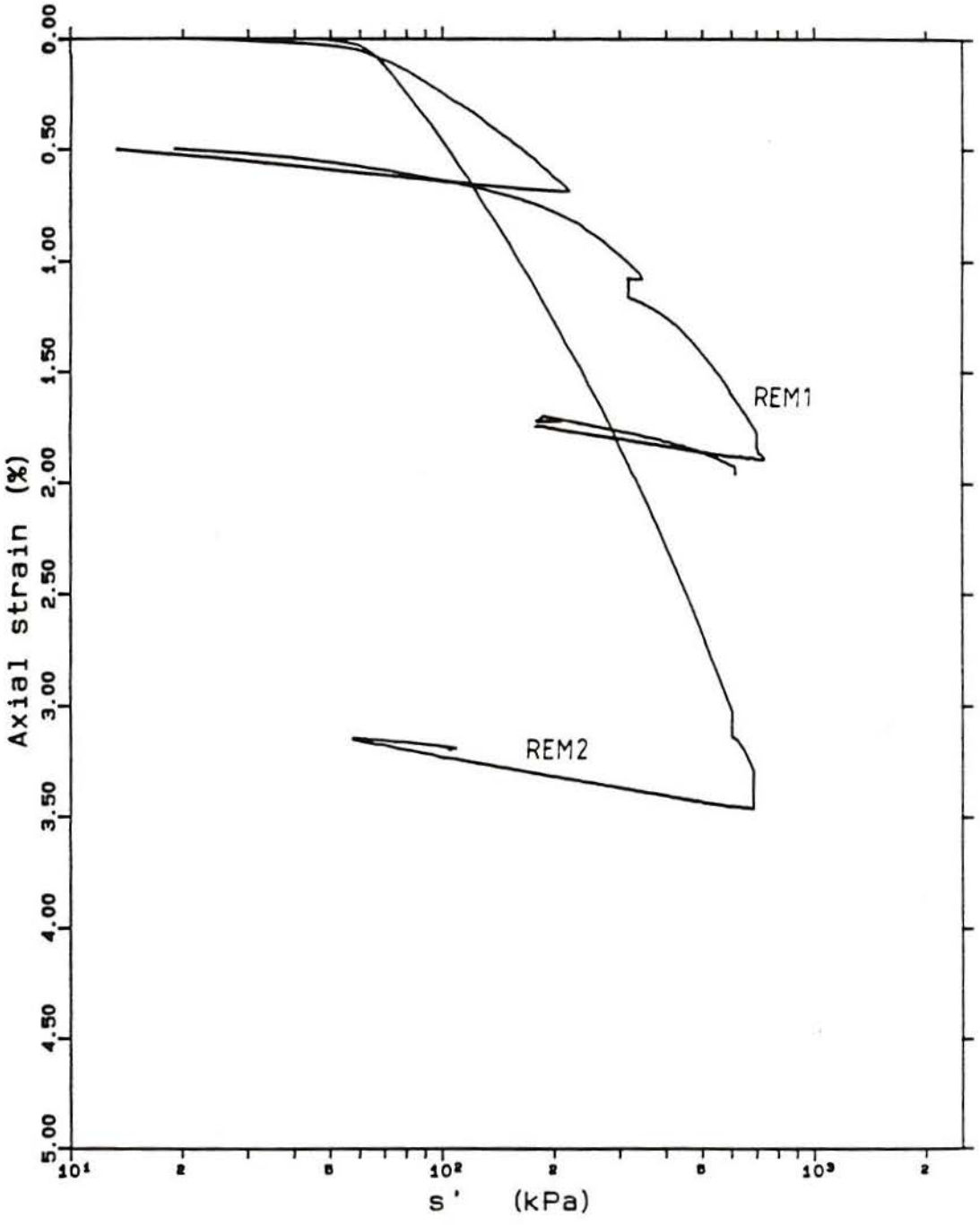

Figure 5.34 – Axial strain measurements versus the logarithm of isotropic pressure of remoulded soil samples

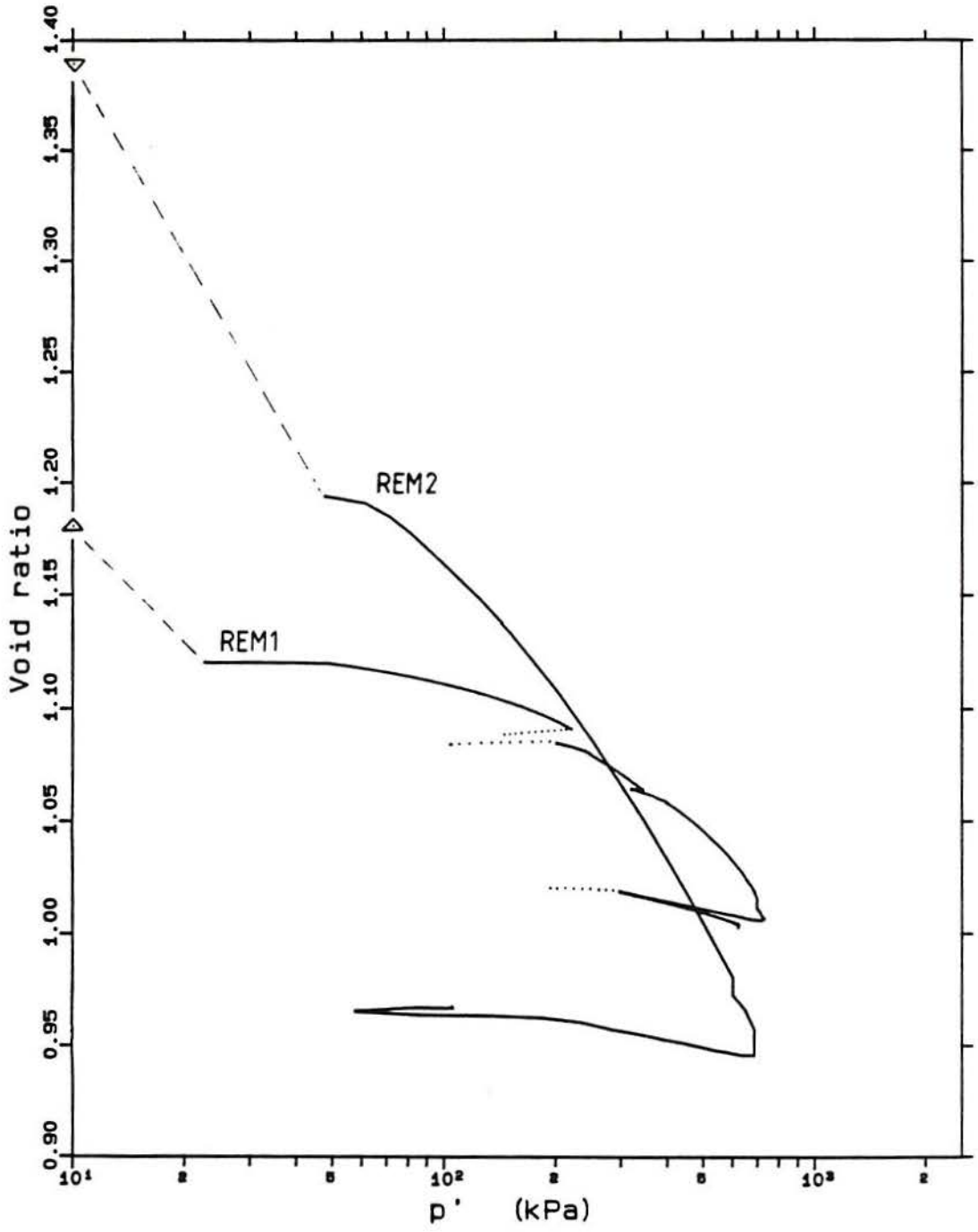

Figure 5.35 – Isotropic consolidation of two remoulded samples of artificial soil. The void ratios as assembled are marked

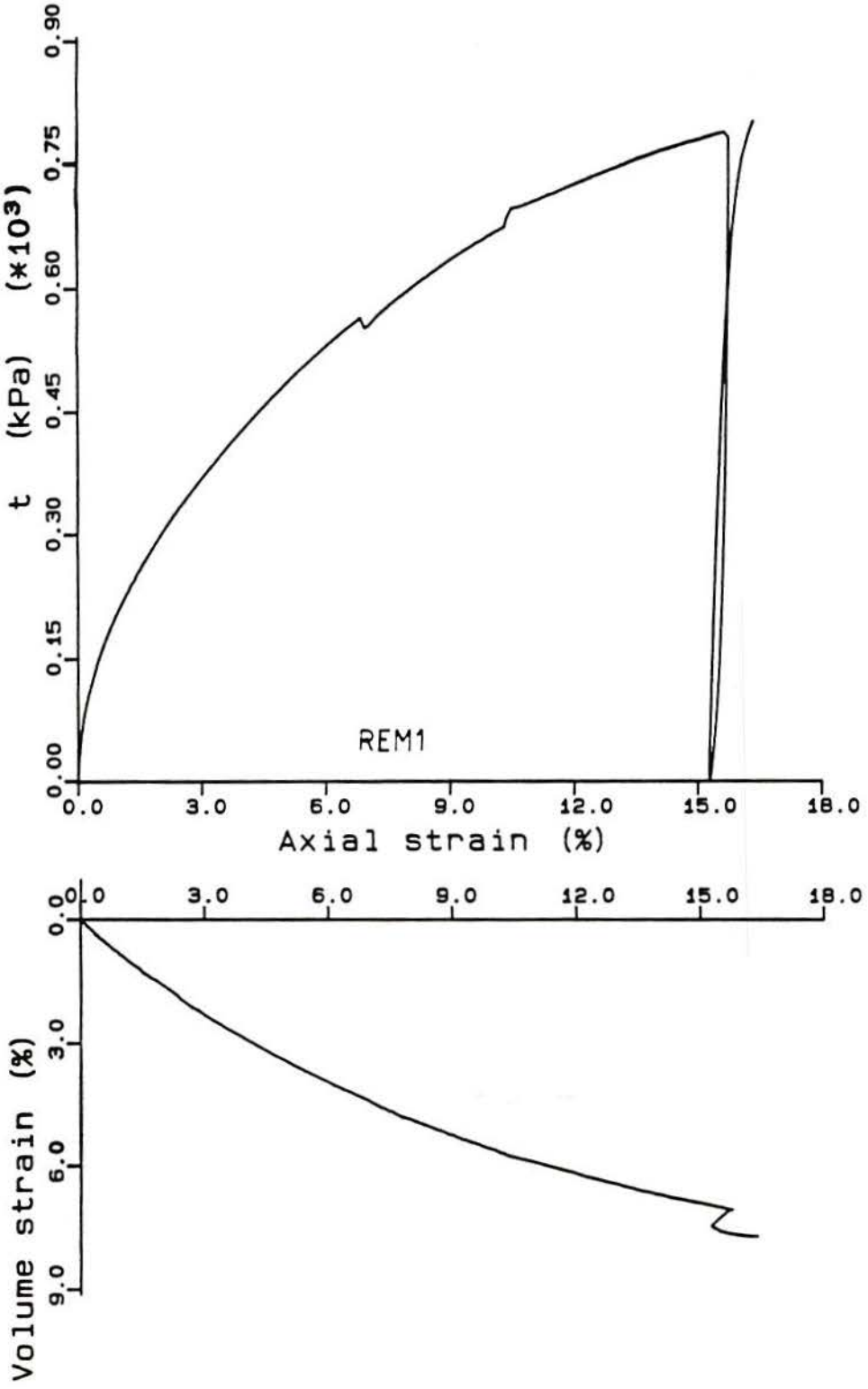

Figure 5.36 - Triaxial compression test on remoulded soil, sample REM1 (e=1.00). σ_3'=600 kPa, OCR=1.2

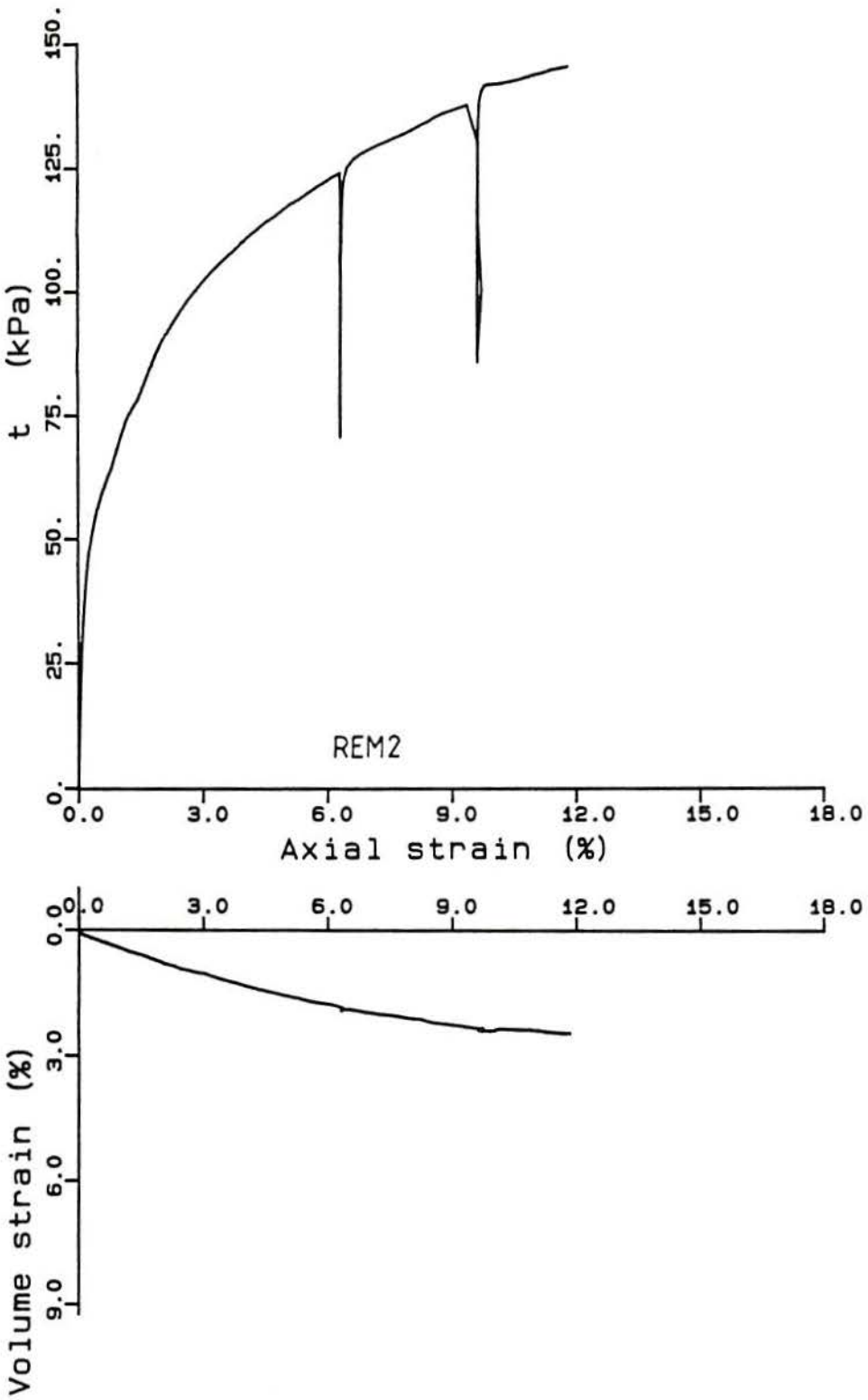

Figure 5.37 – Triaxial compression test on remoulded soil, sample REM2 (e=0.96). σ'_3=100 kPa, OCR=6.2

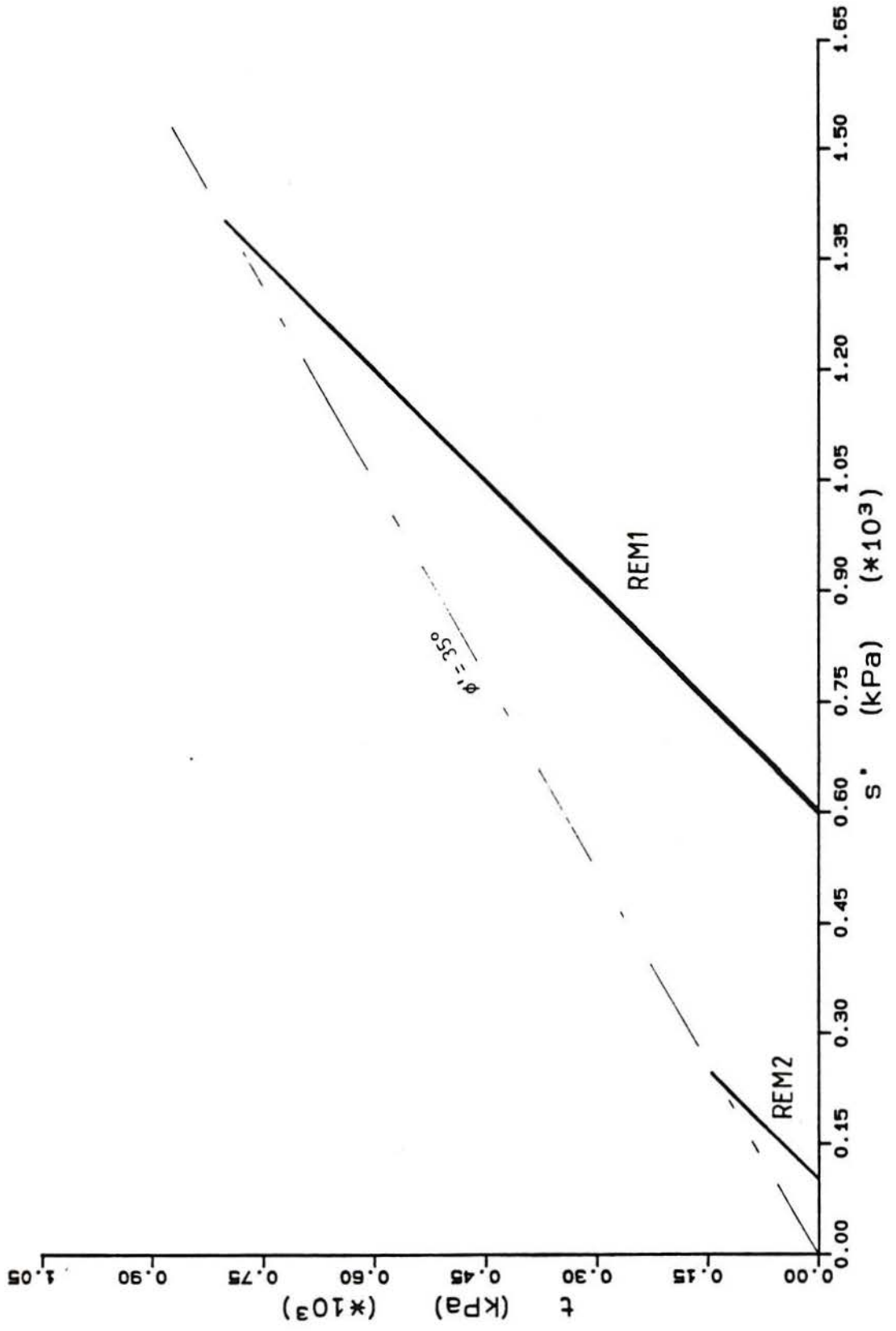

Figure 5.38 – Stress-paths and possible failure envelope for two remoulded soil triaxial tests

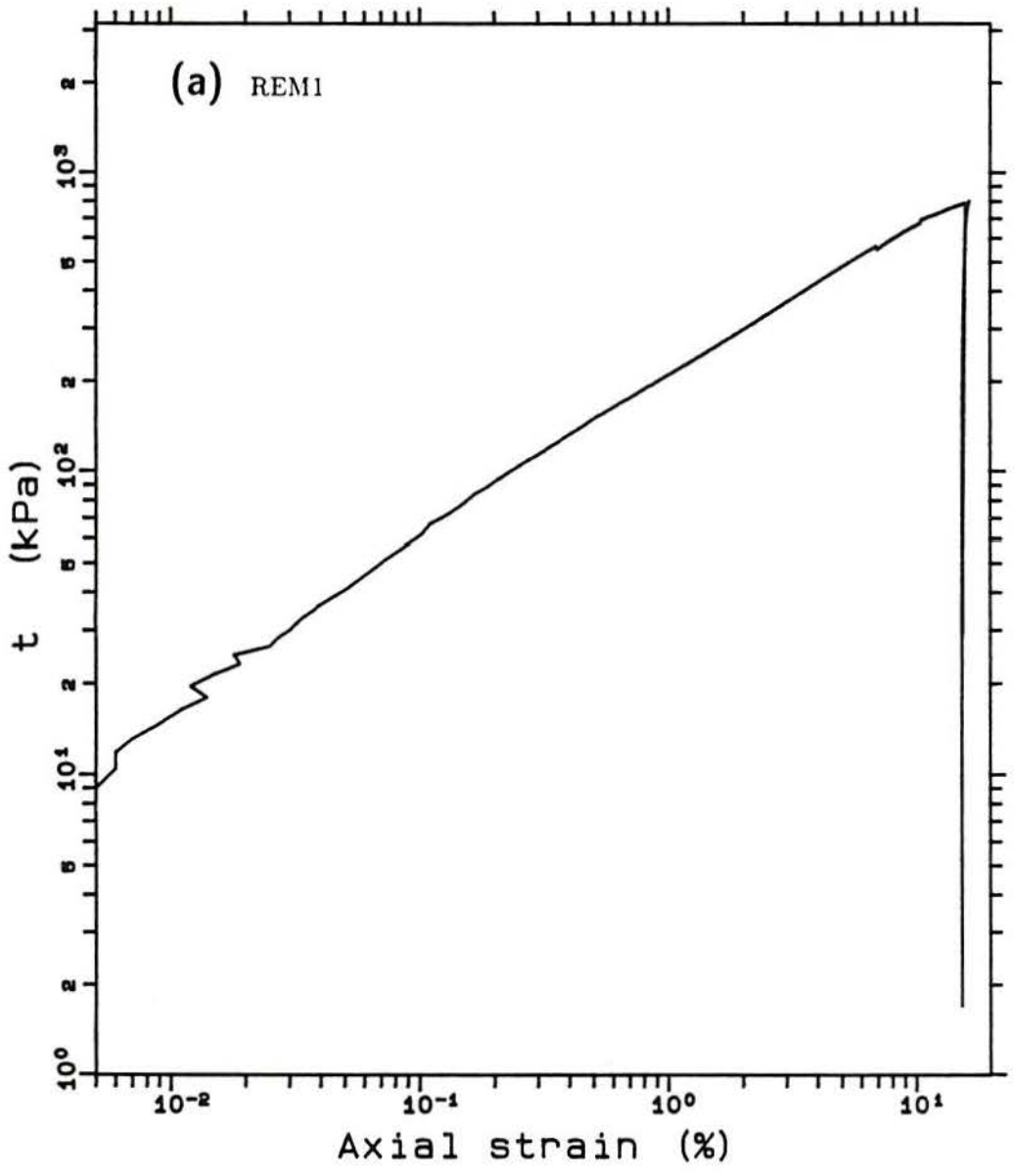

Figure 5.39 – Log-log plots of local axial strain versus t for triaxial tests in remoulded samples. (*a*) test REM 1; (cont.)

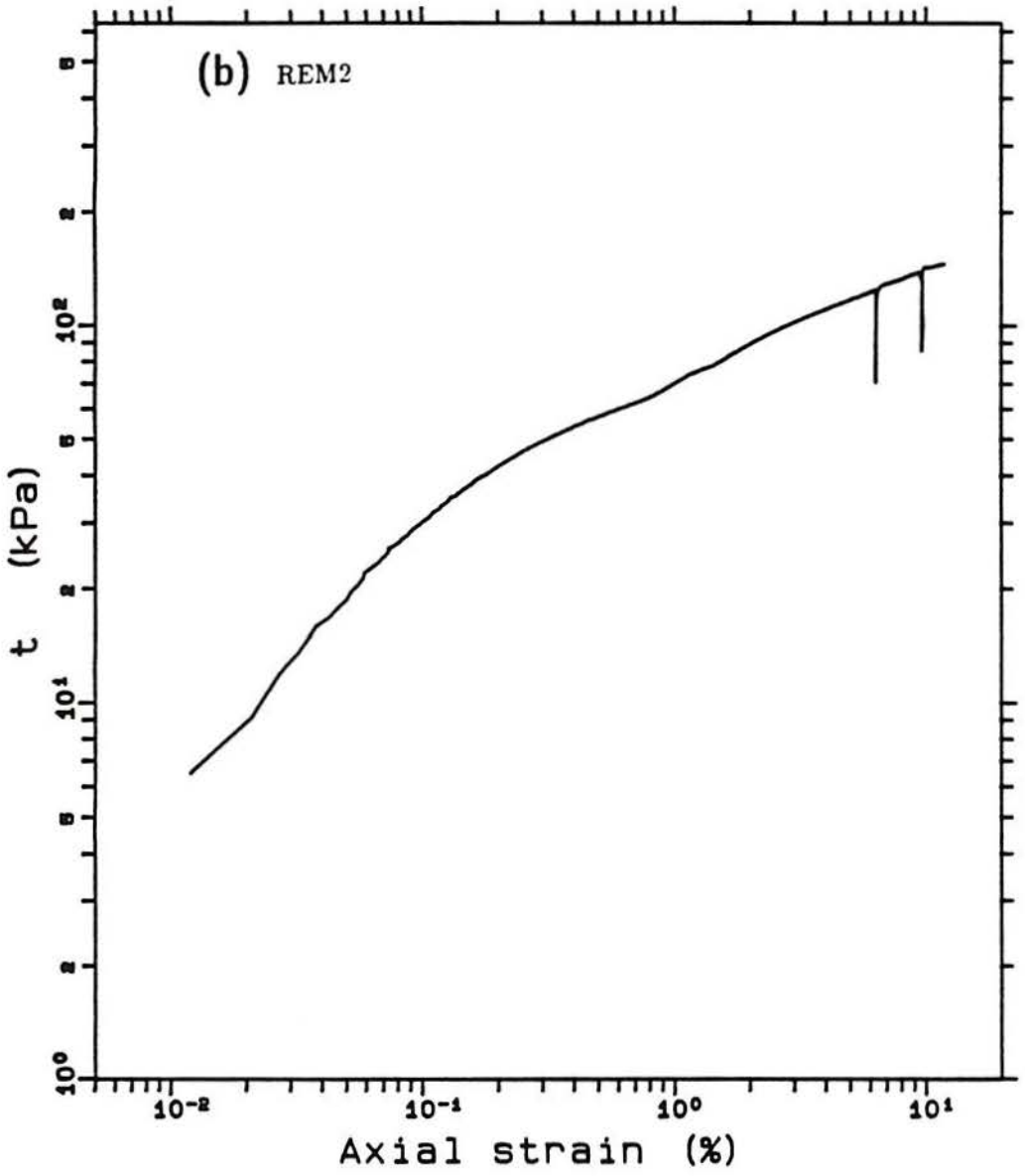

Figure 5.39 – (cont.) (*b*) test REM 2

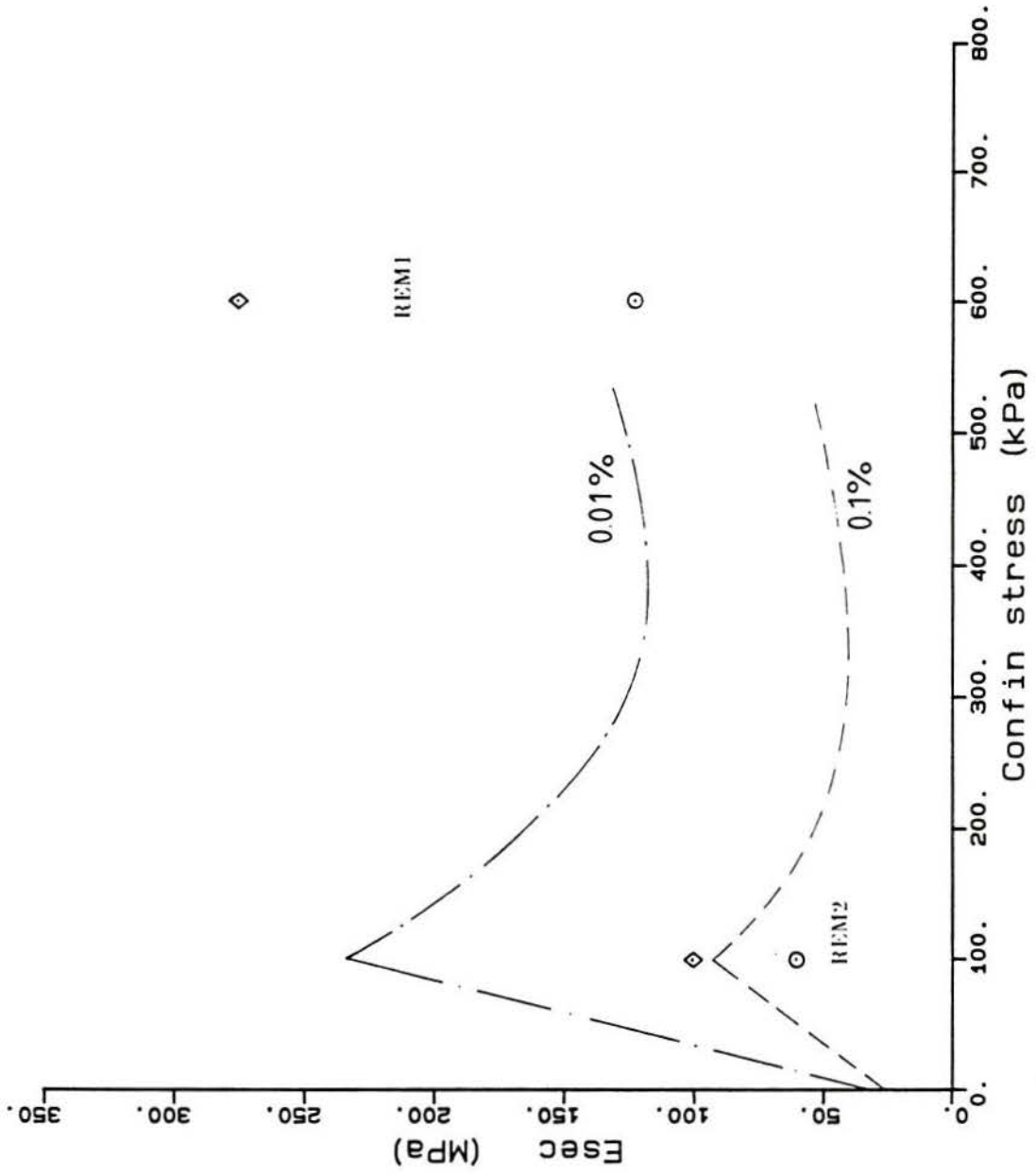

Figure 5.40 – Comparison between the values of stiffness determined from bonded and remoulded soil samples

6. ARTIFICIAL BONDED SOIL – 200 SERIES (void ratio = 1.1)

6.1 INTRODUCTION

This chapter presents the results of the second main series of test on the artificial soil. The results obtained by Maccarini (1987) from tests on the same material are briefly reviewed and later compared with the tests carried out during this work.

Two pieces of equipment are described: a radial belt for measuring radial strain on triaxial samples and a system for applying confining pressures of up to 3.5 MPa.

6.2 REVIEW OF PREVIOUS WORK

All tests referred in this section were carried out by Maccarini (1987) on the same material as that used in the 200 series.

6.2.1 Isotropic compression tests

Maccarini used two test procedures in loading samples: incremental and a constant rate of stress increase (CRSI). It has already been discussed (see Section 4.4.4) that the incremental tests, which were the first to be carried out, caused a degree of sample damage due to the back-pressure technique used for saturation. For this reason, these test results will not be discussed here.

The CRSI tests were performed at a rate around 0.8 kPa/min. The results from tests on three samples have been presented in Fig. 4.3 when discussing the influence of storage time. All three tests had local axial strain instrumentation. The void ratios of these samples were 1.19 (IM1), 1.18 (IM2), 1.19 (IM3) and the values of t at the yield points observed were 260

kPa, 280 kPa and 250 kPa respectively; all at around 0.2% of axial strain. There were insufficient data presented from tests IM4 and IM5 to obtain yield points.

6.2.2 Triaxial compression tests

Five triaxial drained compression tests were carried out at effective confining pressures of 10, 50, 300, 500 and 900 kPa (Fig. 6.1). The initial void ratios of the samples varied between 1.19 and 1.22. The behaviour of samples with higher stresses was contractant during the tests while at lower stresses (10 and 50 kPa), significant sample dilation occurred. However, as with the artificial soil of e=1.5, the maximum rate of dilation occurred after the peak strength had been reached (see item 5.2.2) which indicates that the dilation energy component of strength is not an important one.

Other triaxial drained tests were also carried out under constant stress ratio (σ'_3/σ'_1) and one-dimensional compression (K_0). In the latter, a radial belt was used to monitor the strains at the mid-height of the sample. A microcomputer continuously monitored the test adjusting the cell pressure as required to maintain constant radial strain constant.

The stress path of these drained tests are plotted in Fig. 6.2 together with the undrained shearing stages which followed most of them. Also indicated in the figure are the yield points determined from the stress-strain results.

6.2.3 Loss of bond strength with strain

Some of the most interesting results presented in Maccarini's thesis are from the measurements of tensile strength (diametrical compression test) of samples loaded along the same stress path but stopped at different levels of stress. His results were presented in terms of tensile strength loss (as a percentage) against mean effective stress [Fig. 6.3(a)] or volumetric strain [Fig. 6.3(b)]. The samples were loaded isotropically or with constant stress ratios of 0.4 and 0.7. From Fig. 6.3(a) it can be seen that the tensile strength was unaffected for pressures less than 280 kPa in all three kinds of tests. Larger pressures cause a gradual reduction to

around 20% of the intact strength for pressures around 900 kPa. There seems to be a faster reduction for the isotropic test after the level of 580 kPa is reached. The volumetric strain appears to be a good indicator of the tensile strength deterioration. For volumetric strains of less than 1.5% there is little or no reduction of the strength. This is followed by a gradual reduction for all stress paths followed. At a volumetric strain of 4.0% only about 20% of the original tensile strength remains.

Using these results a plot was produced (Fig. 6.4) in which the tensile strength percentages are expressed in t, s' stress space; also plotted are the lines of initial yield, at which the tensile strength seems to remain intact, and the final bond yield.

6.3 TESTING DETAILS AND EQUIPMENT

Twelve samples were prepared and tested in this series. All samples were saturated using the dry suction method, described in Chapter 4, before being assembled. The value of B measured at the beginning of the consolidation was always larger than 0.95. No filter paper was used in contact with the samples for the reasons given in Chapter 3.

Some physical parameters and testing details are given in Table 6.1 for the twelve samples tested.

Local instrumentation was used in most tests. A specially built radial strain belt (described later) was used to monitor sample diameter at mid-height during four tests.

The average void ratio of the samples was 1.07. This value is slightly lower than the void ratio of Maccarini's samples for which e=1.18.

The testing equipment consisted of the hydraulic stress path triaxial cell described before with full instrumentation (internal load cell, displacement transducer, external volume gauge, pore pressure and cell pressure transducers) and a modified cell for larger pressures (up to 3.5 MPa). Two pairs of local axial transducers were used: one based on electro-level

sensing devices and the other with a strain-gauged pendulum device.

6.3.1 Triaxial equipment for confining pressures of 3.5 MPa

In order to investigate the soil behaviour at pressures larger than the usual limit of the laboratory equipment (1 MPa), a triaxial cell was modified and an increased pressure source built. The only modification required for the triaxial cell was to replace the perspex tube (cell wall) with one of aluminium alloy (alloy 6082 - HE30TF). The analysis of the tube as a thin walled cylinder with internal pressure can be considered by the expression

$$\sigma_{ts} = \frac{p \cdot R}{t}$$

where σ_{ts} is the aluminium yield pressure in tension (with a factor of safety), p is the maximum internal pressure, R is the radius of the tube and t the wall thickness.

For the dimensions t=8.9 mm, R=193 mm, with p=3.5 MPa the factor of safety of the tube is 4 (the tensile strength of the alloy was quoted as 310 MPa). The factor of safety against failure of the six tie bars that maintain the top plate in place is somewhat lower at 3.6 which should not be overlooked when using the equipment. These tie bars must be thightened up carefully and uniformly before pressures are applied.

The high pressures tests were performed using the usual plastic tube connections used for testing over the conventional pressure range; no problems with leakages were encountered.

Three options for the pressure source were considered:

(*a*) pressure amplifier — based on a piston with two different areas working by equilibrium of forces. The primary pressure (air or liquid) acts on the larger piston face. The resulting force is counter-balanced by a higher pressure acting on the smaller face. If flexible diaphragms (e.g. Bellofram) are used the friction can be quite small but the maximum pressure is then limited to the safe working pressure of the diaphragms (typically 2.5 MPa). If O-rings are employed then there is no such pressure limit but the friction may be unacceptable. This system is relatively easy to build and versatile. Precision is variable, depending on the design (friction is the main factor).

(*b*) gas regulator — based on a simple one-way gas regulator using standard industrial compressed air bottles which are readily available and have a precision of ±5 kPa. The question of safety arises when considering possible leakage and explosion. The pressure cannot be reduced automatically with this system (only increased if necessary) and a continuous outflow is required which can be provided.

(*c*) servo-control motor and piston (the option chosen) — in this system the electric signal from a pressure transducer is continuously compared with a value set by the user. Any variation causes the control system to change the direction and/or the speed of a electric motor connected with a screw-piston pump. The pressure can be increased or decreased and there is no safety problem due to the use of gas.

The electronic servo-control used has been fully described by Hight (1983) where it was used to control the rate of stress increase through either the elevation of mercury pots or the control of an air pressure manostat. The electronic diagram of the servo-control is given in Fig. 6.5(a). The servo-control can actuate the motor either to maintain a constant electrical signal or to rotate at a constant velocity independent of the feedback signal. The constant signal mode was generally used with a pressure transducer being employed to provide the feedback signal. The servo-control drove the motor to maintain the signal close to the value pre-set by the user.

The system was sometimes used in the velocity mode in which case the control maintains the motor turning at a pre-set angular velocity, independent of the load. As the system compliance is almost constant with pressure, a relatively constant rate of stress increase could be obtained.

The mechanical arrangement is shown in Fig. 6.5(b). Mercury pots were used in the initial phase of the tests (with pressures below 1 MPa). Once the plastic tubing, the cell and the soil samples had all deformed, the servo-control was switched on and the mercury pot valve closed. At the beginning of each consolidation step, when fast volume variation had to be accommodated, the hand pump was used to avoid using up the travel of the screw pump. If

during the test the screw pump had to be refilled then this was achieved using the following sequence:

(a) the cell valve was closed;

(b) the servo-control was switched off;

(c) the pressure in the lines was reduced to 900 kPa (using the hand pump);

(d) the mercury pot valve was opened;

(e) the screw which connected the pump with the sliding turning rod was released and the pump screw was manually filled;

(f) increase the pressure to same value as before;

(g) perform steps (d) to (a) in reverse.

When the pump is driven near the limit of travel the electrical switches [ES, Fig. 6.5(b)] are actuated. They reverse the electrical current from the servo-control so avoiding damage to the pump.

Another safety measure adopted was to maintain the volume gauge connected to the sample drainage at a position such that if the sample membrane were perforated the volume intake of the transducer would be larger than the screw pump volume. This eventuality would then cause the pump to run to its mechanical limit triggering the electric switches (ES). Damage would not be caused either to the volume gauge by excessive pressure or to the pump.

The screw pump has a working volume of only 25 cc which was adequate for all tests. Pressures up to 3.5 MPa were successfully maintained though it is possible that such pressures could be close to the limit that some mechanical parts such as the pump thread, the gear box, and the bearings can withstand.

This system performed well maintaining a constant pressure under all conditions. Fig. 6.6 is a plot of cell pressure against time obtained from test 209. The nominal confining pressure was 1720 kPa and in the first 15 hours it oscillated by ± 2 kPa around this value. There was some increase in pressure later on, but overall the range was within ± 2.5 kPa or $\pm 0.15\%$ of the applied pressure. Larger oscillations occurred only when the pressure change

trend was reversed (e.g. during unloading/reloading) but it was always smaller than ±4.5 kPa in these cases. However, these measurements were not independent, as they were obtained from the same transducer whose electrical signal provided the feedback to the servo-control. It has been assumed that the transducer stability was reliable: its calibration, checks against other transducers, readings of pressures provided by the stable mercury pots and checks against a calibrated dial pressure gauge (accuracy of 3-5 kPa) all proved satisfactory. Its performance against another transducer in the pressure range of 220-790 kPa was also satisfactory (difference smaller than ±1.5 kPa at thirty different pressures).

6.3.2 Radial strain belt

The measurement of the variation of sample volume, during triaxial tests on soils with a rough surface such as the artificial soil, sands or residual soils, can be erroneous when using external gauges, due to membrane penetration error. This error can be eliminated by using techniques which evaluate its value and correct the measurement accordingly (see, for example, Vaid and Negussey (1984) for details).

A radial belt was developed to obtain direct measurements of the radial strain. Together with the local axial strain devices the belt enabled the volumetric strain of the samples to be calculated. The data were also used to correct the volumetric strain of other samples in which the radial belt was not used (see Fig. 5.8). The gauge was also used for performing one-dimensional triaxial tests (K_0) on the artificial soil and on the Corinth Marl.

The transducer was designed using a Hall effect sensor which gives an analogue electric output which is a function of the magnetic flux which actuates it. The output of the transducer is dependent on both the distance between the sensor and the magnet and their relative position sideways. The integrated circuit package contains the sensor itself, an amplifier which can compensate temperature effects, a voltage regulator and an output transistor. The energization can be chosen in the range 8 to 16 V (or 6 to 12 V in some cases) but must be stable. In this work a voltage of 15 V with a stability better than ±0.15%

(±0.023 V) was used to power the Hall sensor. The whole package weighs 0.35 g and its dimensions are 7.6 mm in width, 20 mm in length and 1.8 mm in height. The sensor does not need any physical contact with the magnets and there is no damage resulting from over-saturation by the magnetic flux, [for more details see Clayton et al. (1989) and the manufacturer's catalogue (Honeywell)].

After the experience with the local axial strain transducer (see Chapter 3) the slide-by configuration was thought to be easily adaptable for the radial belt. The idea is not new and has been used at the University of Surrey (Clayton et al., 1989). They used the radial belt first designed by Bishop (Bishop and Henkel, 1962) exchanging the visual mercury sensor and piston by the Hall sensor and magnet holder (Fig. 6.7). The transducer was designed for use on samples with 102 mm diameter. Uneven forces applied by the springs tend to twist the two semi-circles forcing the Hall sensor against the PTFE block and maintain the gap constant.

The radial belt constructed for this work was designed using the confining pressure as a means of support. The essential requirements which had to be incorporated into the design were that: the pads should be in close contact with the sample; they should have no slack in relation to the belt, and the belt should not offer any restriction to the sample movements.

These problems were overcome by some minor modifications to the original design (Fig. 6.8). The support of the belt and its rigid connections to the sample were provided by using pads which pass through the membrane [Fig. 6.8(b)]. The pads are circular with a recess for fitting an 0-ring seal. They contain a hole in which the belt adjusting beam pin fits. This arrangement creates a hinge with very little friction, a rigid non-slack connection and which holds the whole belt in place by gravity without the need of springs.

The pads are fitted by sliding the 0-rings into the grooves over the membrane. The membrane is then cut around the edges with a razor blade, while being held in place by the O-rings.

The pads need only to be glued onto the membrane for materials with a smooth surface (as shown by the pad represented on the left side of the figure). However, the instrument may

measure membrane deformation as well as that of the sample and care should be taken.

The integrated circuit package was put inside a metal box without top or bottom. A thin piece of microscope slide glass (0.1 mm thickness) cut to size was glued onto the top. The face of the circuit was glued to it with a thin layer of epoxy resin (Araldite). The same resin was used to glue the thin glass to the edges, the whole box was then filled with the epoxy resin and a glass plate 1.0 mm thick glued onto the underside.

Once installed on a sample, the relative movement of the pads is mechanically magnified 1.5 times by the belt. The sliding of the magnets in relation to the sensor is output as change in voltage. To maintain a constant gap between the magnets and the sensor, two measures were taken. The belt works in a plane orthogonal to the main hinge which is a close fitting stainless steel pin [Fig. 6.8(c)]. A compromise between tightness of fit and friction was adopted so that there is little possible mis-alignment of the two arms. The beam holder of magnets was also lightly pressed against the glass cover by using a rubber washer between the beam and its adjusting screw. This arrangement maintains a close contact between the PTFE (polytetra-fluorethylene) pin and the glass so providing a constant gap between sensor and magnets.

The transducer arrangement fits neatly inside the frames of the local axial strain transducers (Fig. 6.9). The tube carrying the electric wiring was moulded to a shape that did not interfere with any measurements. Unless restrained, the belt has a tendency to tilt towards the sensor box. This is best avoided for representative measurements of radial strain normal to the sample axis. The belt was therefore maintained in a horizontal position by gluing a small stop piece [Fig. 6.8(c)] onto the membrane at an appropriate position. This piece reacted against the belt pivot pin providing a positive restriction without interfering with measurements.

The whole transducer weighs 20 g and the pads plus the "balancing piece" another 4.5 g. This weight was not considered excessive and no counter-weights were used for the soils tested.

During the initial phase of testing and calibration it was observed that the lateral movement of the magnet holder had an important influence on the electrical output. A satisfactory solution was achieved by simply gluing a stainless steel guide pin onto the sensor container box [Fig. 6.8(a)] so that the beam is forced to follow a central path.

The calibration of the belt was carried out a number of times to verify its performance and to obtain the best accuracy possible for the test measurements. They were carried out using the same rig as normally used for calibration of the local axial transducers (Fig. 6.10). The rig was put in a horizontal position and the pads fixed to its measuring parts. A displacement dial gauge with resolution of 2.54 μm was used for the input readings. The calibrations were all of the same general pattern as those presented in the literature (Fig. 6.11). There is a near linear central portion which should be aimed at when setting up the test and two curves at its extremes. Observe that the signal trend reverses with further displacement.

The transducer signal had a resolution of the order of 0.2-0.6 μm during the tests and the central portion has a range of 1.6 mm.

The transducer sensitivity to cell pressure variation was examined by using dummy samples and also at the end of test 208. This sample was isotropically unloaded/reloaded four times. This variation of effective pressure was achieved either by changing the total cell pressure or by changing the back-pressure (Fig. 6.12). The sample showed some hysteresis in compression after the initial expansion but the results do not indicate any tendency of the measurement being affected by the total cell pressure variation. The final cycles are very similar to each other, and are independent of the method of stress variation employed.

6.4 RESULTS OF ISOTROPIC COMPRESSION TESTS

Thirteen triaxial tests were carried out on samples of the 200 series (Tables 6.1 and 6.2). Two of the samples did not have local instrumentation installed as they were exploratory tests

at high pressures. The final consolidation pressures indicated on Table 6.2 were the ones applied just before shearing. Two samples were overconsolidated: sample 206 consolidated to 3200 kPa and sheared at 600 kPa and sample 207 consolidated to 3120 kPa and sheared at 1200 kPa.

The test results and the relevant test details will be presented individually. All samples were prepared following the description given in Chapter 4 and they were fired for 5 hours at 500°C. They were then cut to size and saturated by the vacuum dry method.

The analysis of the test results during consolidation is considered in two sections relating to axial strain, obtained from local measurements in most tests, and volumetric strain.

6.4.1 Compressibility for pressures up to 500 kPa

Seven consolidation tests with a constant rate of stress increase were carried out at pressures of 450 kPa or more. The results from three of them are presented in Fig. 6.13(a). The tests were set-up with a initial pressure of 20-30 kPa so that initial readings could be taken. The rate of stress increase was 1.0 kPa/min for tests 207 and 209 and 2.1 kPa/min for test 208 (Table 6.2).

The three tests showed a clear bi-linear compressibility with the changing point occurring in the region 100-135 kPa. The initial higher compressibility may be due to the closing of internal cracks and small fissures, similar to those which occur in rocks (see Fig. 3.6 of Goodman, 1989). The compressibility of the second portion (from 100 kPa to 500 kPa) seems quite linear. Assuming an isotropic behaviour, the bulk stiffnesses of three samples (207, 208 and 209) were calculated as 60, 51.5 and 49.5 MPa respectively. Apart from the initial higher compressibility, there was no other significant deviation from linearity.

In Fig. 6.13(b) the results of four other tests are presented using the same scales. In the first tests (201 to 205) the local transducers were glued onto the membrane with the sample at zero effective stress. A membrane strip stretched over the top pads provided the initial support. This led to some uncertainty of the measurements as the transducers sometimes

indicated a lengthening of the sample with increasing pressure. For this reason, the results from tests 201 and 202 were calculated using data from only one transducer and should be used with caution. In all the latter tests (207-212) the instrumentation was glued onto the membrane after a suction of 10 kPa had been applied to the sample. This made the initial readings much more reliable and no lengthening was observed.

In Fig. 6.14 results of test 212 are plotted together with those from tests 201, 207, 209 and 211. The sample compressibility in this test was slightly higher in its linear portion but the initial compressibility was much higher than observed in any of the other tests and this initially high compressibility continued to a confining pressure of 150 kPa.

The bulk stiffness values indicated on Table 6.2 were calculated from the linear portion of the test results and isotropic behaviour was assumed. The variation of the stiffness ranged from 42 to 60 MPa in most tests. Tests 201 and 204 gave the highest values (170 and 110 MPa).

Before judging these results it is worth examining the volumetric strain results obtained from the same tests.

Fig. 6.15 shows the experimental points obtained from test 201 using the external volume gauge; also shown are the measurements corrected for membrane penetration error (as plotted in Fig. 5.8). This correction was obtained from the results of test 212 in which the radial belt was used to measure the true volumetric strain of the sample. The error is large due to the roughness of the sample surface. A pressure of 50 kPa was adopted as the origin for volumetric strain because the error is very large at lower pressures.

Using the same kind of correction for each of the tests, a set of corrected curves was build from the original data. All these results are presented in Fig. 6.16 with the exception of test 201. The result of test 212, in which the measurements were made directly with local transducers (axial and radial strains) is also plotted in the same figure.

The results have some scatter in terms of compressibility; some tests indicate bi-linear, or even tri-linear behaviour. Test 212, the only one with local measured volume, shows a

decrease in compressibility after 400 kPa. Tests 201, 207 and 209 have similar results and seem to have an increase in compressibility at around 300 kPa. Although less compressible, tests 207 and 208 also indicate a similar pattern. This change was most clearly shown by the two stiffer samples, 204 and 211.

The tests can be divided in two groups: one formed by the two stiffer samples (204 and 211), with a clear change in compressibility, and the other with more compressible behaviour and less well defined change in stiffness. Both groups, however, present this change at around 300 kPa.

It is worthy mentioning that the two incremental tests are each on a different group (samples 206 and 211), indicating that the form of loading has no influence on the results. Note also that the two stiffer samples (204 and 211) appeared to be so for both measurements (axial and volumetric strain).

Using the linear portion of the volumetric strain versus pressure plots the values of bulk stiffness were calculated (Table 6.2). The stiffer samples have values of 60 and 68 MPa, the others are in the range 20-30 MPa. The ratio of the bulk compressibilities calculated from both measurements has also been calculated (Table 6.2). These ratios seem to indicate that the samples are more compressible radially than axially.

The axial measurements from test 202 should be used with caution as there is great discrepancy between the sample behaviour in terms of volumetric strain and the axial strain. All other tests show a reasonable agreement between the axial and volumetric strains. However, the volumetric strains indicate a yield for most tests at around 300 kPa while the axial measurements do not.

6.4.2 Compressibility for pressures of 500 kPa to 3000 kPa

The behaviour of samples tested at pressures below the normal limit of 1000 kPa was not conclusive in terms of yield. The results obtained previously (Fig. 6.2) suggested that it might be necessary to go to higher pressures to obtain an isotropic yield as obtained from the

100 series.

One of the first tests at high pressures was carried out with sample 206 which was consolidated incrementally up an effective stress of 3300 kPa. No local instrumentation was used for fear of damaging it. Thirty stress increments were applied to the sample and the results of this test are presented in Fig. 6.17 and 6.18. The volume strain was corrected by the membrane penetration error but this correction had no influence for pressures above 400 kPa. The axial strain presented in both figures was obtained by measuring the displacement necessary for the load cell attachment to touch the guided top cap, at the end of each consolidation step. However, these measurements are not reliable at low stress levels because of sample roughness but can be satisfactory for larger pressures. For the first unloading/ reloading cycle, the measurements of axial strain from the two devices were 1.24% and 1.25% at 700 kPa and 1.11% and 1.10% at 400 kPa, which indicates a good degree of accuracy.

The two membranes punctured after some time under the effective pressure of 3300 kPa. The volume change was being continuously measured and so could be used in the calculations but the axial deformation, which required manual reading, could not. When the cell was opened to change the external membrane the new sample dimensions could be measured directly. These were used to calculate the strains at the beginning of the reloading as marked in the figures. It is interesting to observe that in this case the reloading was more compressible and to achieve the same level of pressure reached before (3200 kPa), the volume strain increased from 12.2% to 17.1% and the axial strain from about 4.8% to 6.6%. It seems that the structure of the sample was changed by the large unloading/reloading cycle. This was not the case in the first cycle at around 700 kPa.

In Fig. 6.18 the data is presented using the traditional logarithmic pressure scale. This plot emphasizes the difference in compressibility between the two unloading/reloading cycles and also turns an almost linear compression line into a very curved one.

Other tests were also consolidated isotropically to pressures above 500 kPa and some had local measurements of axial strain. In Fig. 6.19 the results of local measurements of axial

deformation of three tests are presented for the range 0-2750 kPa. Test 211 was consolidated incrementally to 1500 kPa and tests 207 and 209 were consolidated under constant rate of stress increase with continuous monitoring of strain. In test 209 no measurements were taken in the stress interval of 545 to 1190 kPa due to problems with the data acquisition system. Nevertheless the dotted line does seem to agree well with the measured data. The external measurements obtained from test 206 are included on the plot for comparison. The smooth curve of test 207 seems slightly disturbed at the pressure of 2500 kPa, and a more compressible linear behaviour starts at around 1600 kPa. The overall range of stress used is represented in Fig. 6.20(a) and (b). The yield pressure of 1600 kPa for test 207 does not appear in the log-log plot but the influence of the unloading-reloading cycle is apparent.

Using this larger scale, the volumetric strain results of six tests are plotted in Fig. 6.21. Although there are some differences at lower stresses, there is a general agreement in their trend. Also, there is no clear change in compressibility as that which occurred with the artificial soil of higher void ratio. The bulk stiffness of sample 207 was 30 MPa which is quite close to the values calculated at lower pressures.

Fig. 6.22 shows the results from four tests of volumetric strain versus the logarithm of pressure. The volume strains were corrected by the membrane error for pressures smaller than 400 kPa. On this scale, the agreement of the data is quite satisfactory. Using the classical methods of pre-consolidation pressure determination (Casagrande method for example), a value of 1600 kPa can be selected from such a graph. The axial strain results versus the logarithm of the pressures are plotted in Fig. 6.23. If the local axial strain results of tests 207 and 209 are used to determine the pre-consolidation pressure, a value of 1700 kPa is likely to be chosen. However, there is not a clear yield point for stresses greater than 500 kPa, only an almost continuous compression. This may indicate that no sudden structural rearrangement or breakage of bonding occurs. Some data suggest that in the region 1600-1700 kPa a gentle yield can be defined.

6.5 RESULTS OF TRIAXIAL SHEARING TESTS

6.5.1 Yield in drained compression

Most of the samples were sheared in compression under drained conditions following isotropic consolidation. Some samples were later further sheared under undrained conditions.

The curves of stress-axial strain and axial-volumetric strain from the tests are presented in Fig. 6.24 and 6.25. All samples show a compressive behaviour throughout this phase. Two of the samples were overconsolidated (206, OCR=5.5 and 207, OCR=2.6) and they showed a less compressible tendency than the others and their initial stiffnesses were greatly increased. Naturally, their initial void ratios were smaller than the void ratios of other samples (Table 6.3) due to the overconsolidation.

In order to identify any yield points in the tests the stress-axial strain curves were examined as for the 100 series (Chapter 5). In Fig. 6.26 the enlarged t versus axial strain results of tests carried out at lower pressures are presented. The crosses marked on the curves represent the points of maximum curvature (or yield as defined here). It is clear that test 206 was very much affected by its overconsolidation. Test 210, with an effective confining stress of 100 kPa had its yield point very close to the stress at failure. The others, however, showed a yield well below the maximum failure stress.

The results of tests carried out at higher pressures are plotted in Fig. 6.27. The yield points are marked on the figure as before and they are well below the failure line. Two of the test results (203 and 205) show a remarkable discontinuity on the stress-strain curves at about their level of yield stress (also coincident with that from test 213).

The experimental points of these tests are plotted individually in the discontinuity region in Fig. 6.28. Two of the tests show clearly that there is a change in slope immediately after such breaking points, especially test 205. In test 213 there is only a very slight drop of load at that level, only detectable because of the small logging interval used, and no change of slope occurs.

However the plots that show most clearly the change in behaviour are the stress versus radial strain curves, presented in Fig. 6.29. Test 205 shows a very clear alteration in the radial strain after reaching the stress level discussed above (marked on the curves by the small circles). Test 203 also showed some variation although it was less well defined than test 205. In test 213 the point is close to the onset of dilation.

It is important to note that these radial strains were determined using the measurements of external volumetric strain and axial strain. In test 203 the axial strain was calculated from external measurements and this makes its radial strain less reliable.

The same kind of plot can also be produced for the lower stress range, but a certain margin of error may be expected. Although the confining stress remained constant for all tests, the bedding of the sample ends can cause variations in the volume measured outside. It is important to note that 0.01% of radial strain corresponds to $\pm$ 0.008 cc which is close to the resolution of the volume gauge transducer. There are two tests however in which the radial strain was directly measured with the radial belt. The results of these tests (210 and 208) are presented in Fig. 6.30. Two curves are shown for each test: one measured directly and the other calculated from the results of volumetric and axial strain as explained above. Test 210 was consolidated under an effective stress of 100 kPa and it should be expected that the bedding error is more significant at this level. The examination of the strain curves obtained directly shows that the yield points selected before (Fig. 6.26) are in the region where the sample behaviour starts changing radically.

The results of the other tests are presented in Fig. 6.31, together with the yield points chosen from Fig. 6.26. Although in tests 206 and 201 the axial and the volumetric strain were both determined from external measurements, the change in behaviour at the yield points is quite clear.

These results, obtained from external measurements, can give only a general indication of the changes and must be used with caution. Nevertheless, they may provide a positive indication of structure change and this may be especially true for soils in which the bedding

error is small.

Finally, plots of stress and strain using logarithmic scales were prepared [Fig. 6.32(a) to (d)] as for 100 series. The tests were separated by groups which are more or less comparable. Note that samples 202, 203 and 206 had their axial deformations measured externally. The yield points were determined from the intersection of two lines fitted to the data. Such line fitting was easily performed for tests 201, 207 and 208 and the values obtained are indicated in Table 6.3, between brackets.

Fig. 6.33 was prepared using the results obtained from the natural and logarithmic scales. The drained stress path followed by the tests is indicated and different symbols are used to differentiate the method of yield pressure determination. A different symbol was also used for the overconsolidated samples. It must be pointed out that the stress-radial strain plots were used only to provide a confirmation of sample behaviour and of the yield stress defined before. They were not used as a third alternative to define the yield pressures.

Analysis of the figure indicates that the agreement between the two determinations is quite satisfactory for tests carried out at the lower range of pressures. However, for tests 203 and 213 there is quite a large difference. It appears that test 205 marks the threshold of two processes. One which tends to decrease the yield stress level as the average effective stress increases and the other which maintains it almost constant with the increasing pressure. The reader is referred back to Fig. 6.27 and 6.28 to verify the difficulty in selecting one stress level as a yield definition for tests 203 and 213. The log-log plots provide a more positive indication.

For the overconsolidated samples there is little doubt that the yield point is pushed beyond the limit defined by the other tests and this is especially clear from test 206 which has been consolidated to 3250 kPa. The likely yield curve associated with the overconsolidated tests 206 and 207 is indicated in the figure.

Fig. 6.34 presents these yield points together with the points defined by Maccarini (1987) on the same soil with a slightly larger initial void ratio (e_0=1.2). They do agree

satisfactorily with the data presented here, especially for the low pressure range.

6.5.2 Results of a test performed under constant t whilst reducing s'

Having defined a yield curve with reasonable confidence in the region of low stress from compression drained tests, it was necessary to verify the influence of the stress path on the yield strength surface, in the same manner as for the results obtained from the 100 series tests.

A test was carried out on sample 204 after isotropic consolidation to 580 kPa. It was loaded drained as in a normal compression test to a stress level of t=279 kPa (Fig. 6.35 and 6.36). The sample was then allowed to creep freely for 2 hours by which time the load had dropped to t=237 kPa (point B). The testing of the sample was carried out by reducing the effective confining stress while maintaining manually a relatively constant value for t of 250 kPa. The effective stress was reduced from point B to point D at a rate of 2.40 kPa/min. The value of s' was reduced from 830 kPa (point B) to 440 kPa (point C) with very little straining. From that point to point D it was not possible to maintain a constant value of deviator stress and the strain increased considerably. When the average effective stress was reduced below 483 kPa the sample deformed by a large amount. Finally, at point E (ϵ_a=2.68%) the effective confining stress was held constant and the test was continued under constant rate of straining up to ϵ_a=7.0%. The yield point of this test is clearly somewhere between points C and D.

The complete stress-path of test 204 is plotted in Fig. 6.37(a) and (b) together with the results presented before. There is good agreement between the yield curve previously defined and the result of test 204. For this void ratio it seems that the artificial soil is unable to cross the yield (and failure) line for the level of stress employed, contrary to what happened with the 100 series tests.

6.5.3 Results of one-dimensional compression test

The development of the radial strain belt described earlier was useful in showing the characteristics of deformation of tests 208 and 210 and especially their radial strain pattern in

relation to yield as defined by the deviator stress versus axial strain. However, test 208, which was a normal compression drained test, showed no radial strain up to a stress level of 400 kPa approximately (Fig. 6.30). This led the author to speculate what the stress path of an one-dimensional compression test would be starting from a relatively high isotropic stress, instead of a more conventional low initial stress level.

Using local instrumentation for measurement of axial and radial deformations, a sample was initially consolidated isotropically to 580 kPa effective stress (sample 212). The test was then continued with a constant rate of axial strain imposed by the triaxial machine. The radial strain belt was monitored continuously and the effective radial stress was modified as required to keep the radial strain constant. The transducers were monitored for 16 hours before the test during which time the belt showed an oscillation smaller than 1 μm (or 0.0026% of radial strain). This indicates that its readings can be relied to that precision which is satisfactory (note that its resolution was 0.4 μm).

The rate of straining used was 1%/h to allow easy control of the radial strain, also this was the rate used in most tests. The test was performed in two days and the sample was unloaded slightly before the control was released overnight. The load dropped a little further during that period due to creep and in the morning the radial strain had changed to 0.016% (radial compression). The test was re-started and carried on to the limit of pressures available in the stress-path cell (950 kPa). Finally, it was unloaded whilst still under one-dimensional conditions.

Throughout the test, the radial strain was maintained within a tolerance of $\pm 0.004\%$ (Fig. 6.38), except for the uncontrolled overnight period. The stress path rises steeply up to t=300 kPa (Fig. 6.39). This agrees well with the behaviour observed in test 208. From that stress onwards the stress path continued increasing and became linear. If this linear portion is used to calculate the ratio σ_3'/σ_1' (K_0 under these conditions), the value of 0.47 is obtained.

The axial strain obtained has a relatively smooth increase with pressure. The deformation during the cycle of loading/reloading is similar to that observed in other soils

under the same conditions. There is one point though that warrants attention. When the deviator stress reached t=375 kPa the sample showed a rapid unloading with a small increase in axial strain and change in the radial belt. The radial pressure was reduced to restore the radial strain and the load started to increase again. A change in behaviour occurred at that level, as can be seen from the stress path direction. It is likely that a structural rearrangement may have occurred causing the sudden unloading and variation of the strains.

A comparison of this test with others is made in Fig. 6.40(a) and (b). The yield line and experimental yield points presented previously are plotted together with the stress paths of three tests: the constant t test (204), the one-dimensional test presented here (212) and the one-dimensional test carried out by Maccarini (1987) – (k0M1).

The results of the two one-dimensional compression tests seem to show the same tendency of following a straight stress-path after an initially steeper start. Both tests show yield stresses that are lower than those obtained from normal compression drained tests. The results of test 212 also indicate that within the stress range employed there is no tendency to drop to a lower stress path as happened with the higher void ratio artificial soil (Maccarini, 1987). The value of 0.47 for the ratio of σ'_3/σ'_1 is a higher value than those obtained from the well known expressions relating $K_0(\sigma'_3/\sigma'_1)$ with the effective friction angle ϕ':

$$K_0 = 1 - \sin \phi'$$

or

$$K_0 = 0.95 - \sin \phi'$$

Assuming that ϕ' is in the range 35° to 36° (see 6.5.5), these expressions give values of 0.38 and 0.44 for the K_0 ratio.

6.5.4 Stiffness measurements

The thirteen tests carried out cover a relatively large range of stress and any tendency of stiffness variation with pressure can be studied with some confidence. The secant stiffnesses derived from plots of deviator stress versus axial strain were calculated at a number of strain levels. The local instrumentation was employed in most tests and the stiffnesses were

calculated from these measurements and from the corrected external deformation measurements. All samples except sample 209 were tested with the guided top cap and loading button following the techniques described in Chapter 3. When analysing the results, the general characteristics of the external measurements should be considered: (*a*) at low confining pressures measurements are affected by the bedding of the sample ends, and (*b*) there is better agreement between the local and external strains in the small strain range.

The results of secant stiffness calculations at 0.01% and 0.1% axial strain are plotted against confining pressures for a range up to 1000 kPa on Fig. 6.41(a) and (b). In Fig. 6.41(b) results of stiffness at 0.1% axial strain which were calculated from the figures presented by Maccarini (1987) are also plotted. The numbers indicate the test (8 for 208, 12 for 212, etc.) and a line connects the results obtained from the same test using the two methods. At small strain levels (0.01%) the external strain sometimes gives a higher value of stiffness than the local measurements. There are various possible reasons for this but it is most likely due to the choice of the strain origin. Nevertheless, the tendency of both plots and both kinds of measurements indicates a steady increase in stiffness with pressure.

To examine the behaviour over the whole range of confining pressures, stiffnesses calculated at 0.01%, 0.1% and 0.2% axial strain are plotted against confining pressure (Fig. 6.42 to 6.46). The stiffnesses at 0.1% and 0.2% were also calculated from the results of Maccarini (1987) and are incorporated into the figures. In the discussion that follows, test 209 is considered a special case and its results were not used for drawing the band represented on the figures; the reasons for this are discussed later (item 6.5.6).

Fig. 6.42 shows the results of all stiffnesses obtained at 0.01% axial strain. Two of the tests were overconsolidated before shearing and they have a stiffer behaviour. The others seem to fall inside a band which again indicates a linear increase of stiffness with confining pressure.

The stiffnesses calculated at 0.1% and 0.2% are plotted on Fig. 6.43 and 6.44. The incorporation of Maccarini's data helps to define a different behaviour at low pressures. Although the tendency of increasing stiffness with pressure remains, it is no longer linear. It

seems that up to 200 kPa the stiffness has a rapid increase with pressure, it then remains almost constant and from 600 kPa onwards another increase occurs but less pronounced than the initial one.

Note that this tendency is not the same as that presented before for the artificial soil (Maccarini (1987) and Fig. 5.3). The result obtained from the sample at 900 kPa has not been considered here when drawing the lines. The test gave a low value of stiffness and the reason for this may be the same as for test 209 (see 6.5.6).

An increase in stiffness with confining pressure leads to the idea of its normalization in relation to the pressure and the resulting plot is presented in Fig. 6.45. Very high values of normalized stiffness were obtained at low confining stresses indicating that the stiffness is greatly influenced by the bonding. As the pressure increases this influence lesses and the pressure has a larger role. The drop is very marked up to 200 kPa after which a much slower reduction occurs for quite large variations in pressure.

The same pattern of behaviour may be better visualized in Fig. 6.46. In that figure the normalized stiffness was plotted on a logarithmic scale and the pressures on a natural one. It seems that up to 600 kPa the reduction in the logarithmic value of the normalized stiffness is more noticeable.

6.5.5 The ultimate strength parameters

Considerable examination has been made of sample behaviour in terms of yield pressures. Nevertheless, it is important to know if the parameters that define the failure at large strains remain the same over the whole range of pressures.

All tests were carried out initially drained with the exception of test 211. Some tests were, at a later stage continued undrained so that the failure envelope could be reached with the strains obtainable in the triaxial test. Although the rate of strain was 1%/h initially, this was increased in most cases to 5%/h later on. The latter was also the rate used by Maccarini (1987) in all his tests.

The results of tests carried out at lower pressures are presented in Fig. 6.47. Samples 201 and 202 had their strain rate increased during the test to 5%/h at around 5% axial strain. Sample 206 had it increased on the second reloading. There is a considerable variation in the volumetric strain between the test 202 (s_0'=450 kPa) and test 201 (s_0'=600 kPa) but even more so when test 206 is compared with test 201. The overconsolidation had a large effect in the stiffness and volumetric behaviour of sample 206 . Sample 210 was sheared to an axial strain of only 2.2% as a well defined shear plane had already developed at that stage.

Fig. 6.48 contain the results of the higher pressure tests. Two of the samples had been tested initially drained and then undrained. Sample 203 had a constant rate of shearing of 5%/h and samples 205 and 207 a constant rate of 1%/h. Sample 213 was initially sheared at 1%/h and after the first unloading its drainage was closed and its rate increased to 5%/h.

The volumetric strains for three of the tests are very similar and the effect of overconsolidation can be clearly seen from the results of test 207.

It is interesting to note that the cycles of loading imposed on samples 206 and 207 did not cause any significant change in the volumetric variation either in tendency or in the instantaneous value. The axial stress behaviour was also unaffected, except when the rate was increased (test 206, second cycle).

The stress paths from all tests are presented together in Fig. 6.49(a) and (b). In addition to the tests referred to above, the paths of the drained test 204 and the undrained test 211 are also included. The fully drained tests (conventional stress paths) are represented only by their maximum point (crossed circle).

The results indicate a unique strength envelope which, for the pressure range presented, is quite linear. The parameters for the envelope indicated in the figure are ϕ'=36.2°, c'=17.5 kPa.

The drained tests 202, 205 and 207 seem not to have been able to reach final strength and this agrees well with the results presented in Fig. 6.47 and 6.48. Test 210, on the other hand, shows that the envelope is higher at lower stresses, as is expected for bonded soil.

The undrained paths of tests 201, 203 and, particularly, tests 211 and 213 are interesting in terms of the strength envelope. The second unloading/ reloading that was carried out undrained on test 213 has a noteworthy stress-path. On reloading it climbed back to the failure envelope and then followed it very closely with increasing stress. After reaching a maximum, the deviator stress started dropping but the stress path continued along the failure line.

6.5.6 Undrained tests

Although some of the tests were sheared undrained mainly to define the failure line, some of the results warrant closer attention. Two samples were consolidated isotropically to 1500 kPa and sheared in drained compression up to around ϵ_a=15%. They were unloaded and reloaded undrained and strained to large strains (around 28%). The results of both tests are presented in Fig. 6.50 and 6.51.

The difference between the test results is quite significant and test 209 did not even fail on the same envelope as the others. An examination of Table 6.1 shows that both samples were prepared in exactly the same way (temperature and void ratio) and saturated with the dry vacuum method. The only difference was that test 209 was carried out without the load cell attachment as used in all other tests. This may induce large concentrations of stress on the sample if the top cap and load cell are not parallel (see further discussion in Chapter 4). Such concentrations were thought to affect the stiffness measurements, even when local transducers were used, but not the ultimate strength parameters. Test 213 was carried out specifically to make a comparison with test 209. The final portions of both tests are plotted in Fig. 6.52. The same testing procedure was followed: after the unloading the drainage was closed and the rate of shearing increased to 5%/h. The pore pressure rose sharply up to a point where it stabilized for awhile. The deviator stress decreased uniformly after reaching the stress level previously applied. A characteristic of both tests is that the stress paths of the undrained reloading are very similar in shape and show a very sharp bend where the deviator

stress reaches the level previously attained in the drained portion, showing that the drained loading has a very marked influence on the sample behaviour at later stages of the test.

Another test to compare with test 209 is test 211. The sample was also consolidated isotropically to 1500 kPa and had very similar initial conditions (Table 6.1). The test was carried out under undrained conditions from the beginning and large pore pressures were generated (Fig. 6.53). A cycle of unloading/reloading shows that the stress path is very much affected by the previous loading, as in the drained tests. There is, however, very little doubt about its final strength. In fact, a small unloading/reloading caused the stress path to travel along the failure line (Fig. 6.54). The main results are plotted together with the other undrained (or partly undrained) tests on Fig. 6.53 and 6.54. It again reinforces the conclusion that sample 209 clearly failed very much differently than any other sample and analysis of Fig. 6.52 does not necessarily indicate that the sample was not strained far enough.

It was briefly noted that the stiffness could be affected by the concentration of stress. This also seems to have happened in test 209. For this reason its stiffness results were not taken into consideration when drawing the limit lines in Fig. 6.42, 6.43 and 6.44. The results presented in Fig. 6.50 only confirm this point.

It may be argued that an unseen factor may be responsible for such a drop in stiffness and strength. However, this sample showed very similar isotropic compressibility to the others (see for example, Fig. 6.19) and in every other aspect the test was carried out in the same manner as the others.

It is possible that the same effect has occurred on the test carried out by Maccarini (1987) at 900 kPa, as he did not use the loading button in his tests. The reason as to why the other samples did not suffer from the same effect can only be speculated upon.

Sample	γd (kN/m^3)	e_0	Saturation	Local measurements	Load cell attach.
201	12.66	1.053	suction dry	(1)	Yes
202	12.41	1.094	suction dry	(1)	Yes
203	12.61	1.061	suction dry	No	Yes
204	12.51	1.077	suction dry	(1)	Yes
205	12.67	1.052	suction dry[a]	(1)	Yes
206	12.53	1.075	suction dry	No	Yes
207	12.74	1.040	suction dry	(1), (2)	Yes
208	12.49	1.081	suction dry	(1), (2)	Yes
209	12.54	1.073	suction dry	(1)	No
210	12.55	1.072	suction dry	(1), (2)	Yes
211	12.52	1.077	suction dry	(1)	Yes
212K_0	12.73	1.042	suction dry	(1), (2)	Yes
213	12.43	1.091	suction dry	(1)	Yes

$G_s = 2.65$
(a) Small oscillation of vacuum pressure during saturation
(1) Axial strain
(2) Radial strain
Tests 210 and 212 were the only ones with reliable radial belt measurements (see text)

Table 6.1 — Artificial bonded soil — 200 series (133057, 500°C/5h)

Test	Consol. (kPa)	Rate (kPa/min)	Bulk stiffness[a] (MPa)	$k(\epsilon_a)/k(\epsilon_v)$
201	20-600	1.0	(ϵ_a) 48.8[b]	
			(ϵ_v) 22	2.2
202	25-450	1.0	(ϵ_a) 170	
			(ϵ_v) 18 & 25	-
203	5-585	0.7	(ϵ_v) -	
	585-1700	2.8		-
204	25-600	3.0	(ϵ_a) 110[b]	
			(ϵ_v) 60.3 & 26.1	1.8-4.2
205	20-1200	increm.	(ϵ_v) -	-
206	25-3300-600	increm.	(ϵ_v) 23.9	-
207	25-480	1.0	(ϵ_a) 60.0	
	480-3120	0.8	(ϵ_v) 29-33	1.8-2.0
208	25-750	2.1	(ϵ_a) 51.5	
			(ϵ_v) 22-29	1.8-2.3
209	25-1500	1.0	(ϵ_a) 49.5	
			(ϵ_v) 25.7	1.9
210	25-100	19	-	-
211	25-1500	increm.	(ϵ_a) 77	
			(ϵ_v) 68.5	1.1
212	25-580	2.1	(ϵ_a) 42.5	
			(ϵ_v) 29.2[c]	1.4
213	1500	increm.	-	-

(a) Considering isotropic behaviour and for pressures in the range 100-500 kPa
(b) Only one local transducer
(c) Calculated with radial belt

Table 6.2 — Isotropic consolidation of 200 series tests. Pressures below 500 kPa

Table 6.3 — Summary of triaxial test results of 200 series (133057, 500°C/5h)

Test	σ'_{H_0}	e_i	Drainage	Yield pressure[a]		Failure		$E_{SEC\ 0\text{-}1}$(MPa)		$E_{SEC\ 0\text{-}2}$(MPa)	
				t (kPa)	s' (kPa)	t (kPa)	s' (kPa)	local	ext.	local	ext.
201	600	1.00	drain./undr.	450 (440)	1050 (1040)	474[g]	791	187	182	142	128
202	450	1.06	drained	405 (400)	855 (850)	575	1025	-	116	-	91
203	1700	0.95	drain./undr.	565	2265	897[g]	1507	-	360	-	234
204[b]	600	1.05	drained	236	382	236[g]	382	180	164	129	116
205	1200	0.94	drained	581	1781	1480	2680	295	285	208	187
206	600[c]	0.68	drained	655 (580)	1255 (1180)	852	1452	-	405	-	313
207	1200[d]	0.84	drained	695 (510)	1895 (1710)	1610	2810	615	516	438	393
208	750	1.06	drained	550 (500)	1300 (1251)	-	-	208	196	157	140
209[e]	1500	0.95	drain./undr.	306/585 (261)	1806/2085 (1761)	753[g]	1550	220	150	151	110
210	100	1.08	drained	203 (190)	303 (290)	212	312	104	58	85	52
211	1500	0.98	undrained	-	-	401[g]	649	394	351	297	261
212K_0[f]	580	1.00	drained	-	-	-	-	168	141	128	104
213	1500	1.05	drain./undr.	581 (110)	2081 (1610)	-	-	291	235	205	167

(a) From arithmetic and (log-log) plots
(b) Constant t test
(c) OCR = 5.5
(d) OCR = 2.6
(e) Only test without load cell attachment
(f) One-dimensional compression test
(g) Maximum σ'_1/σ'_3

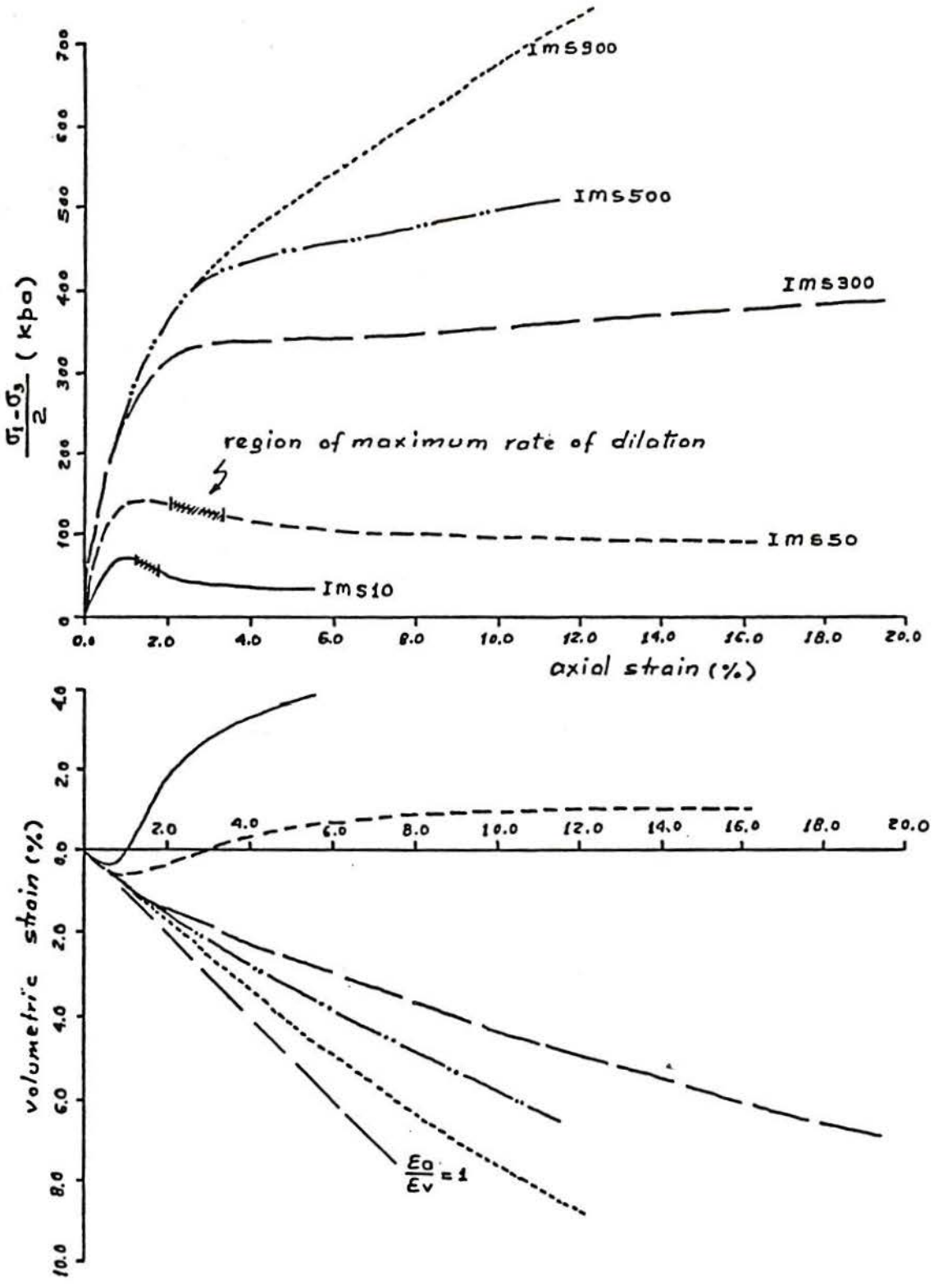

Figure 6.1 – Results from triaxial compression tests performed by Maccarini (1987)

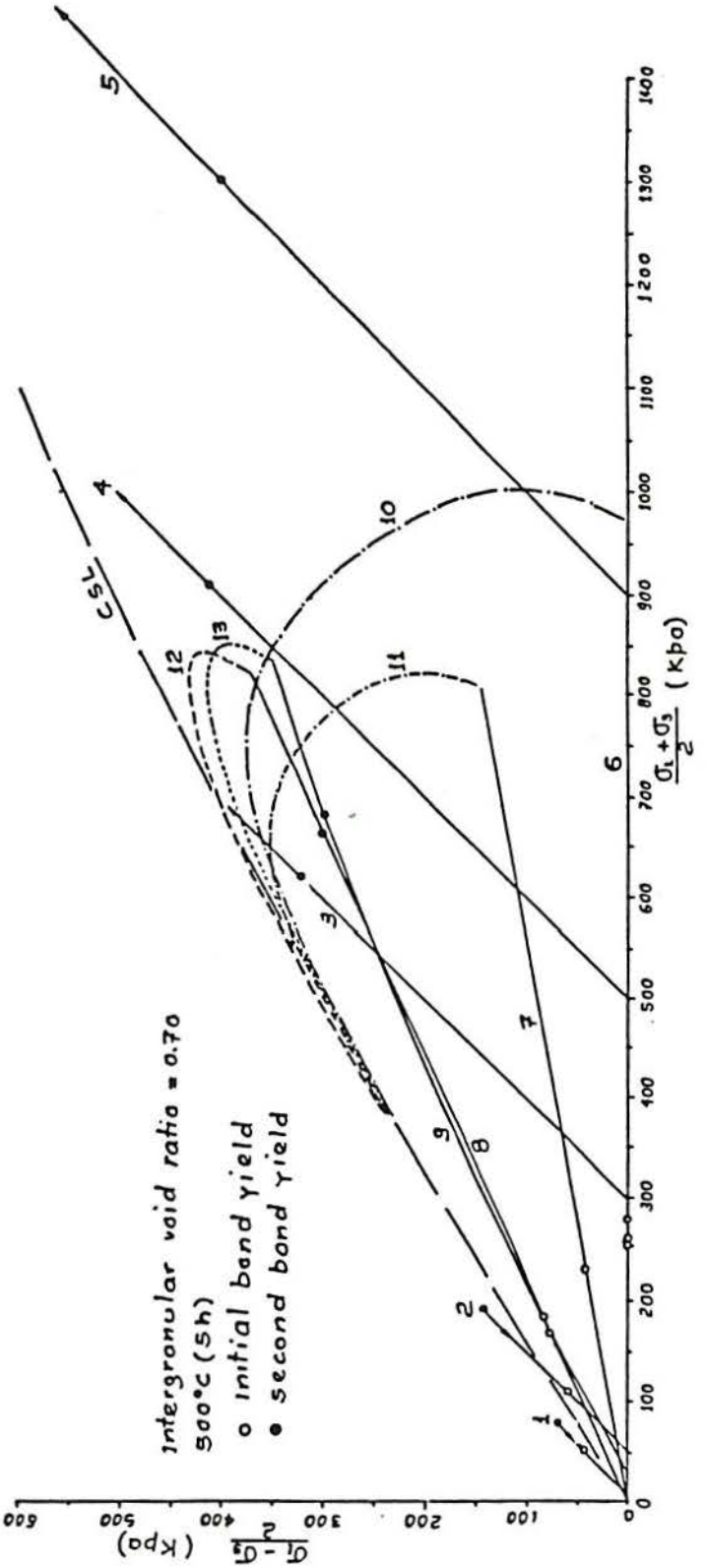

Figure 6.2 – Test stress-paths and yield points determined by Maccarini (1987)

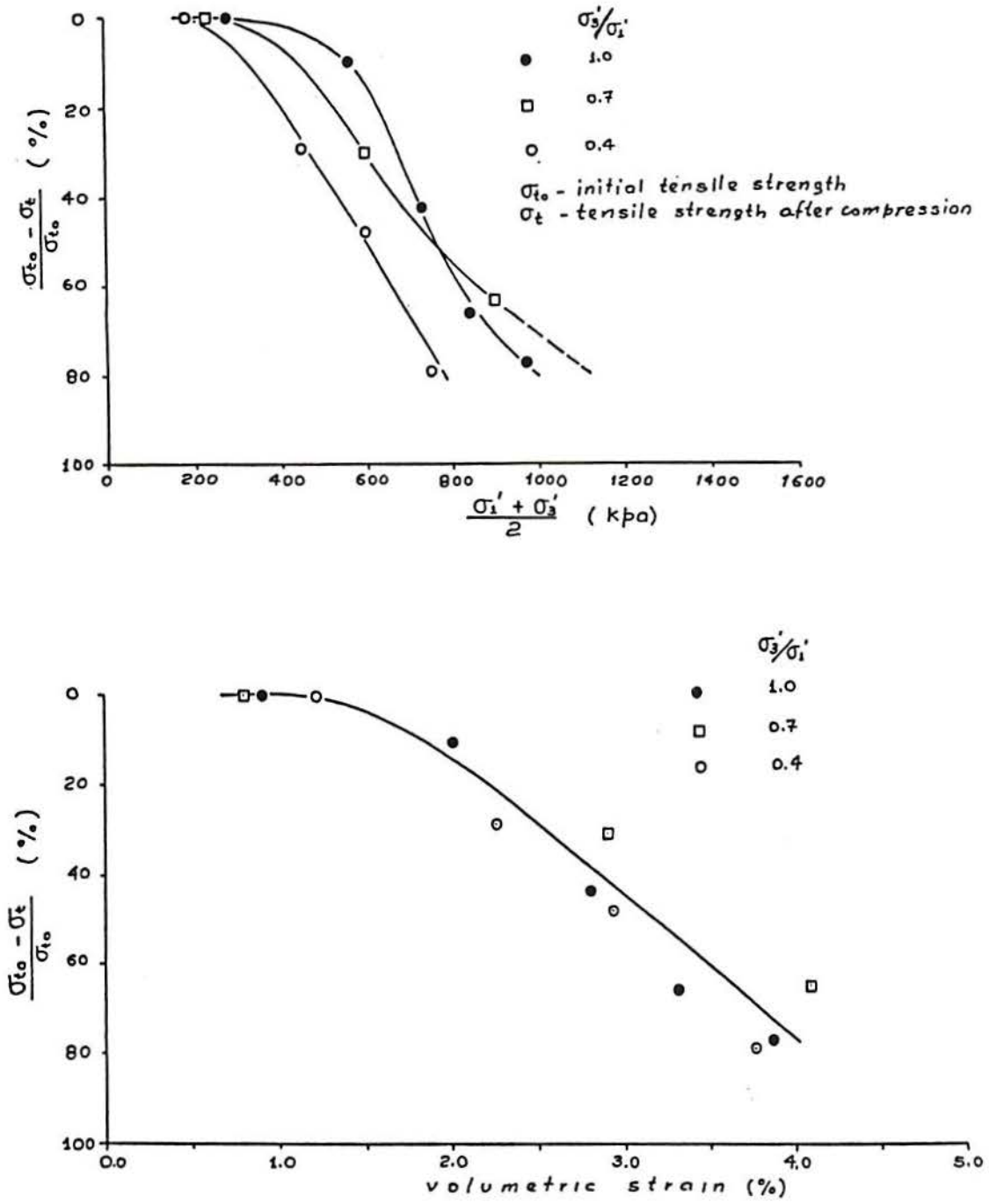

Figure 6.3 – Loss of tensile strength versus (*a*) mean effective stress, and (*b*) volumetric strain (after Maccarini, 1987)

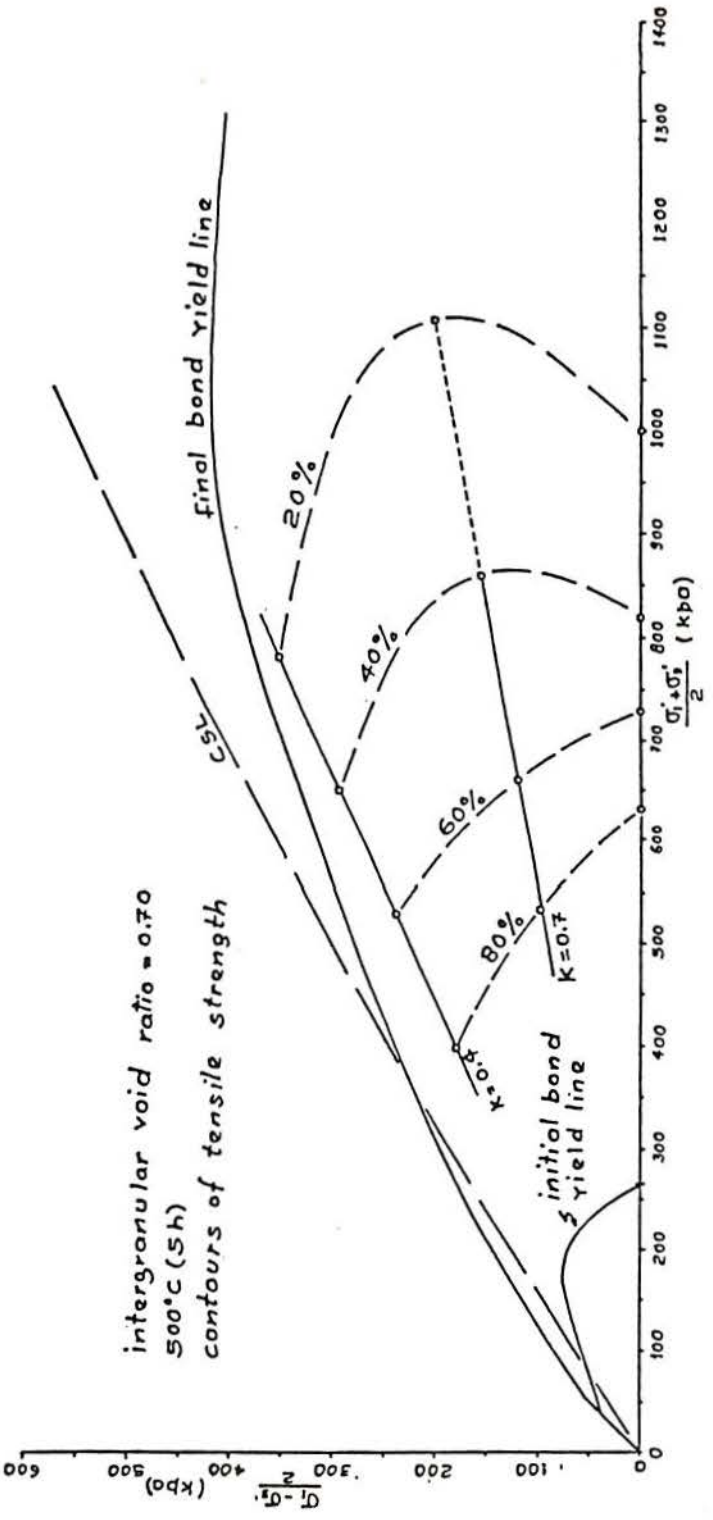

Figure 6.4 – Contours of tensile strength for the artificial soil in t, s′ space (after Maccarini, 1987)

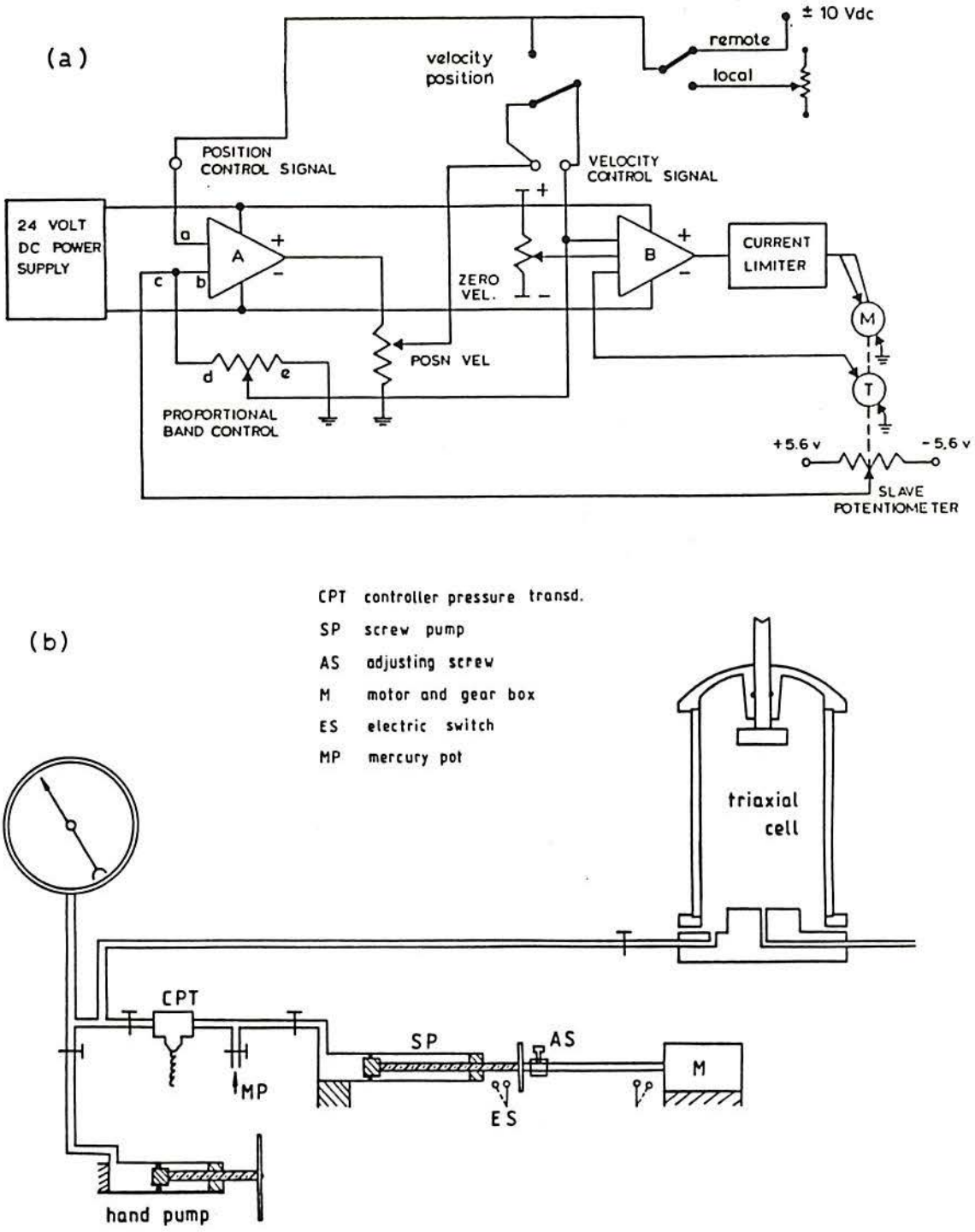

Figure 6.5 – Servo-control system for applying confining pressures of up to 3.5 MPa. (*a*) Electric diagram (after Hight, 1983); (*b*) Mechanical arrangement

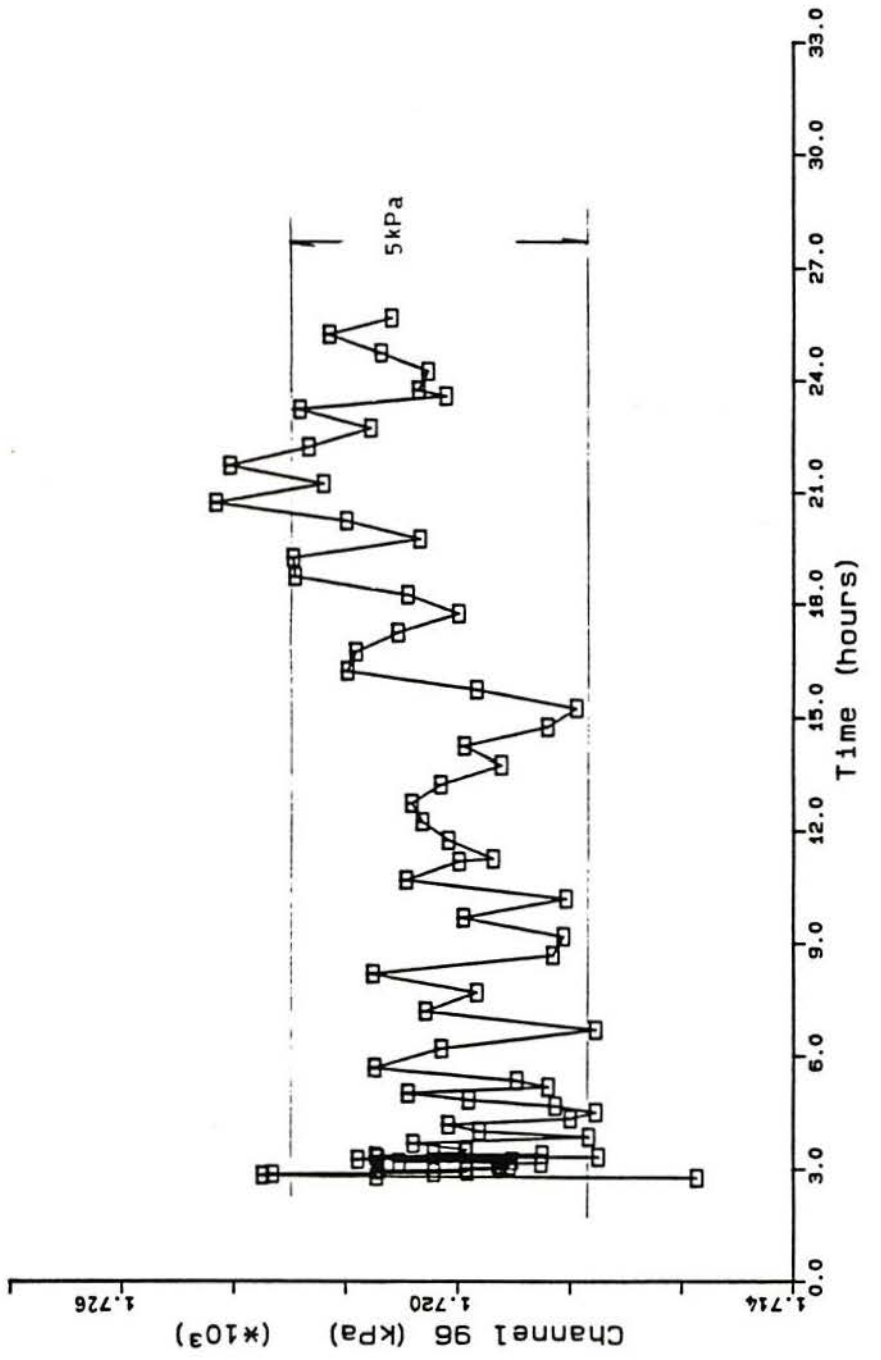

Figure 6.6 - Variation of cell pressure versus time – servo-control screw pump

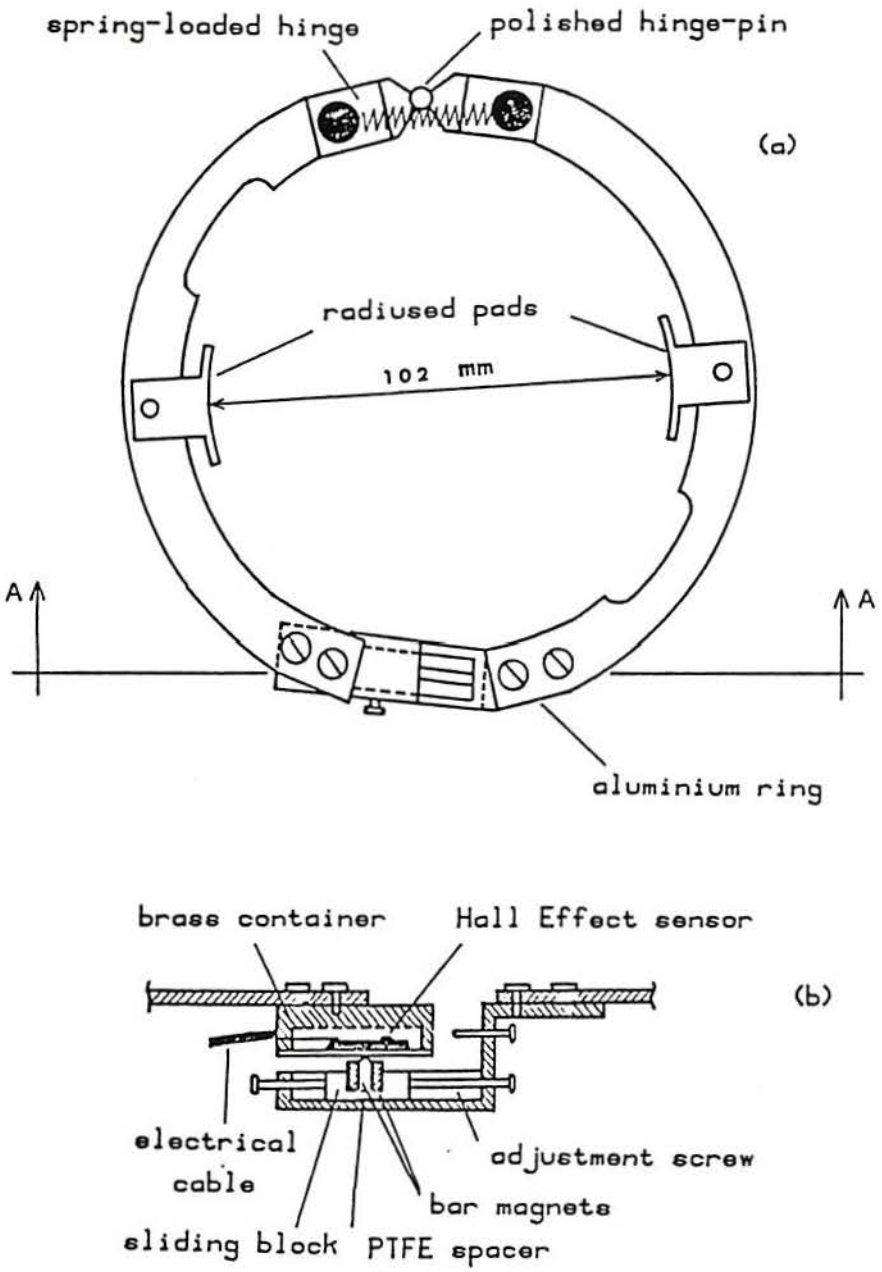

Figure 6.7 – Radial belt proposed by Clayton et al. (1989)

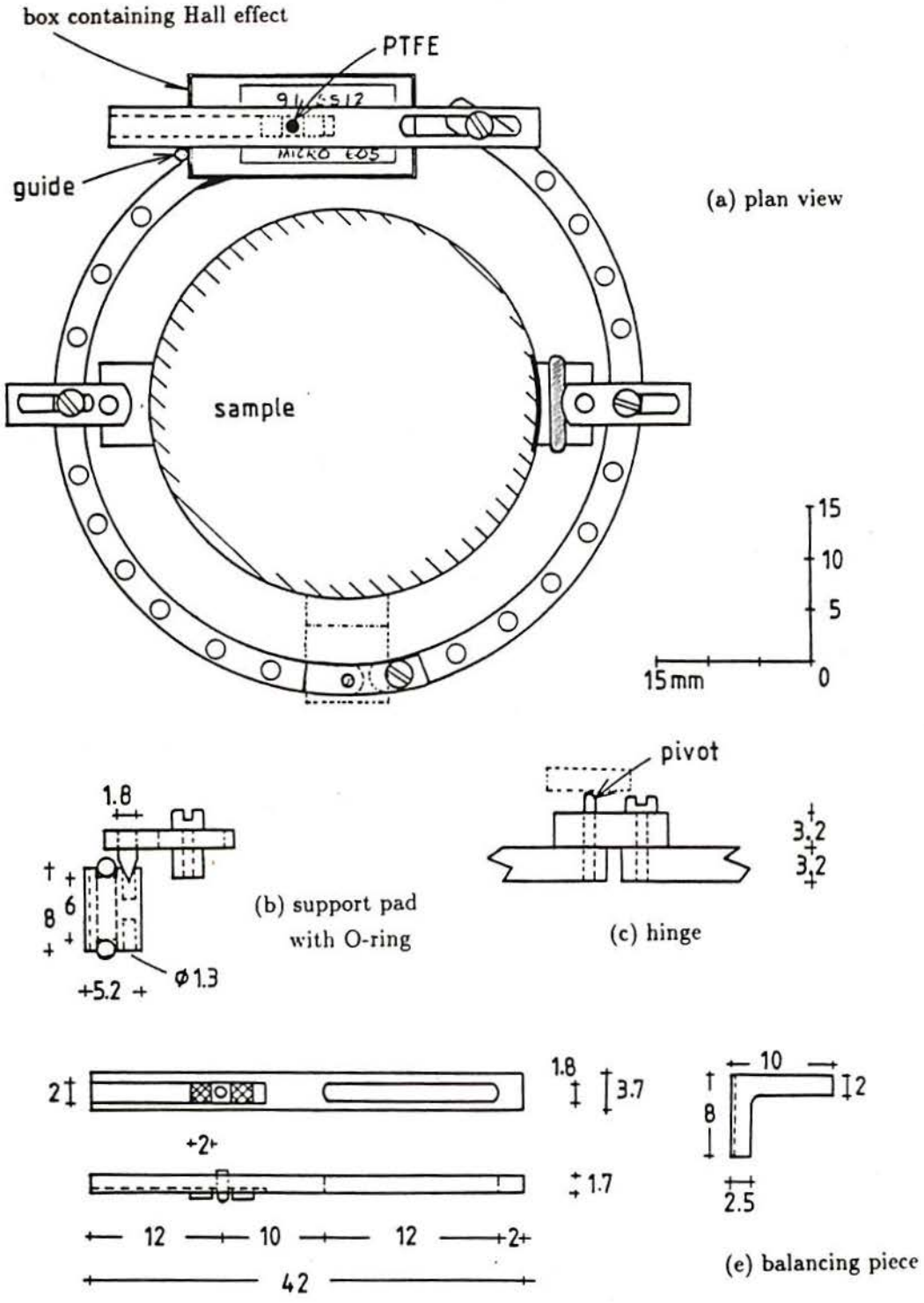

Figure 6.8 – Radial belt developed using a Hall effect sensor

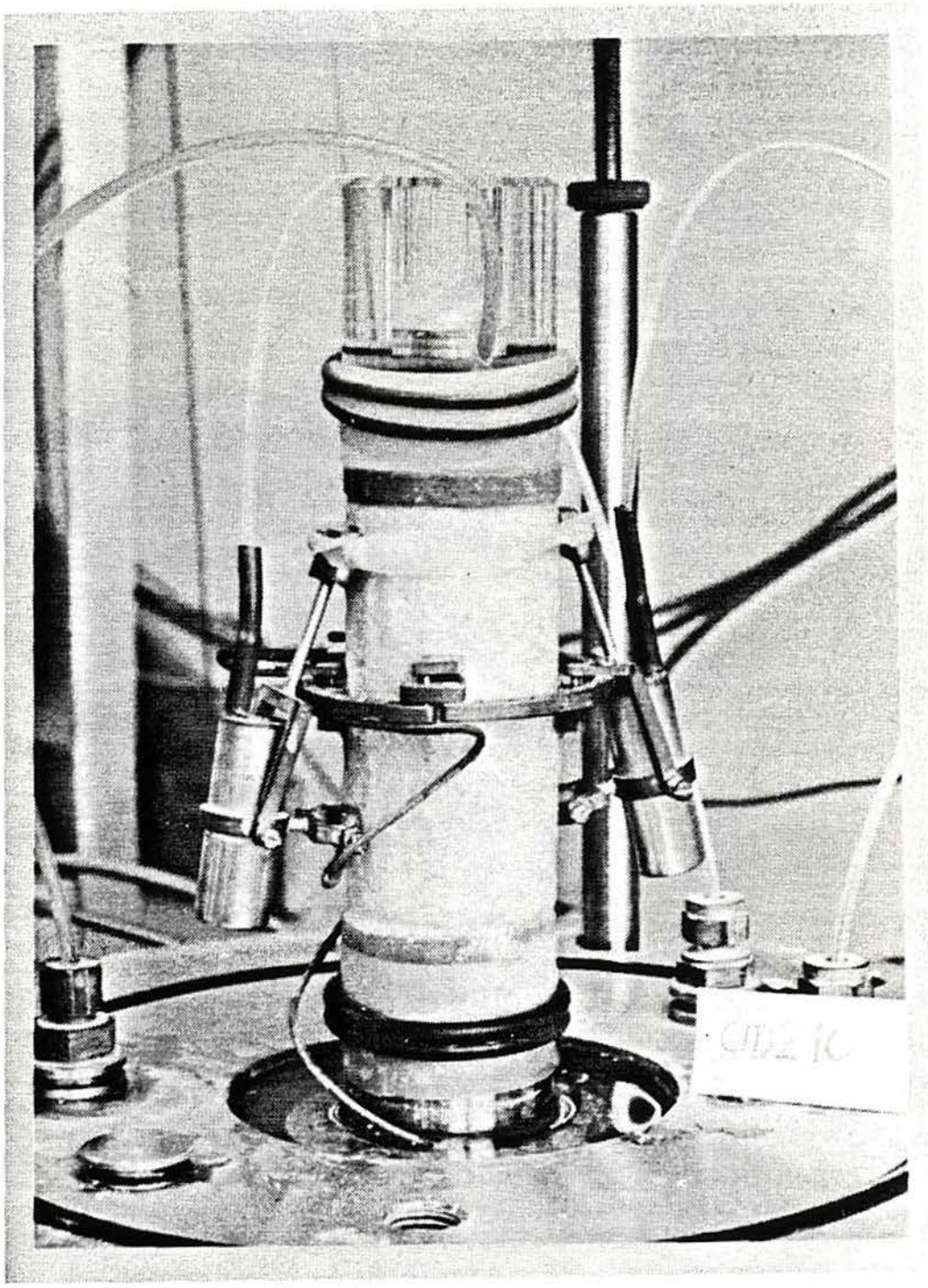

Figure 6.9 – Assembly of local transducers for axial and radial strain measurements

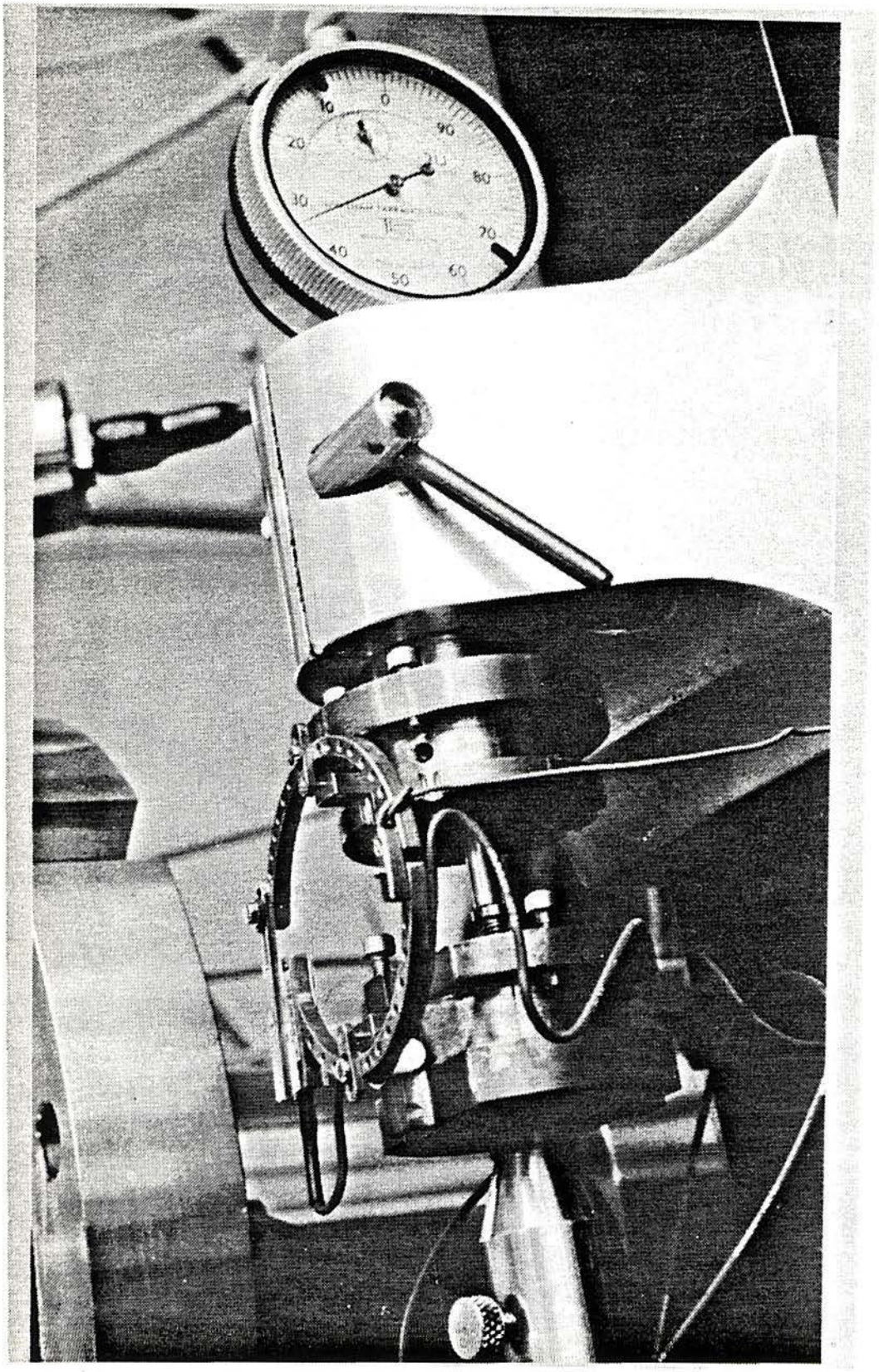

Figure 6.10 – Arrangement for the calibration of the radial belt

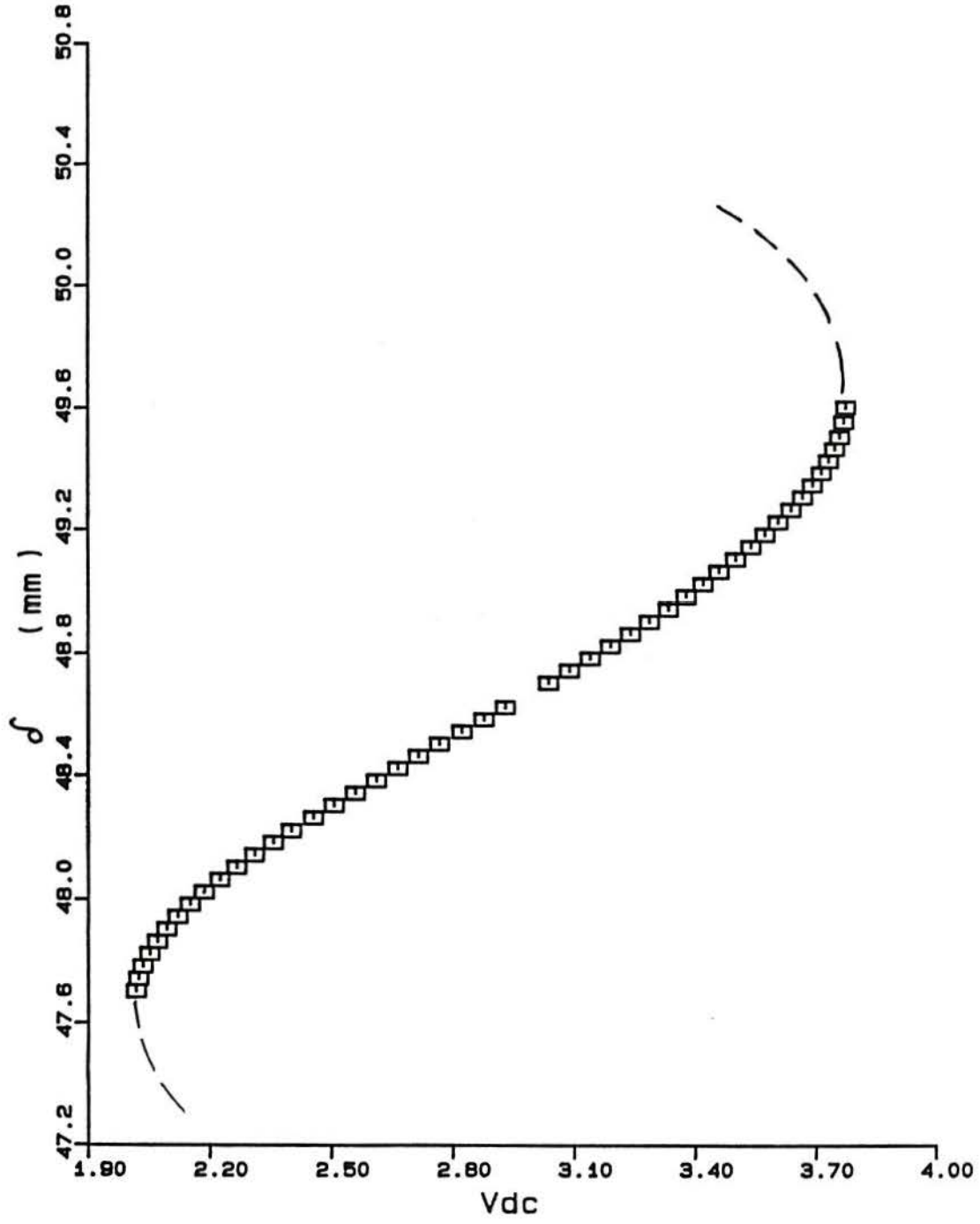

Figure 6.11 - Calibration curve for the radial belt

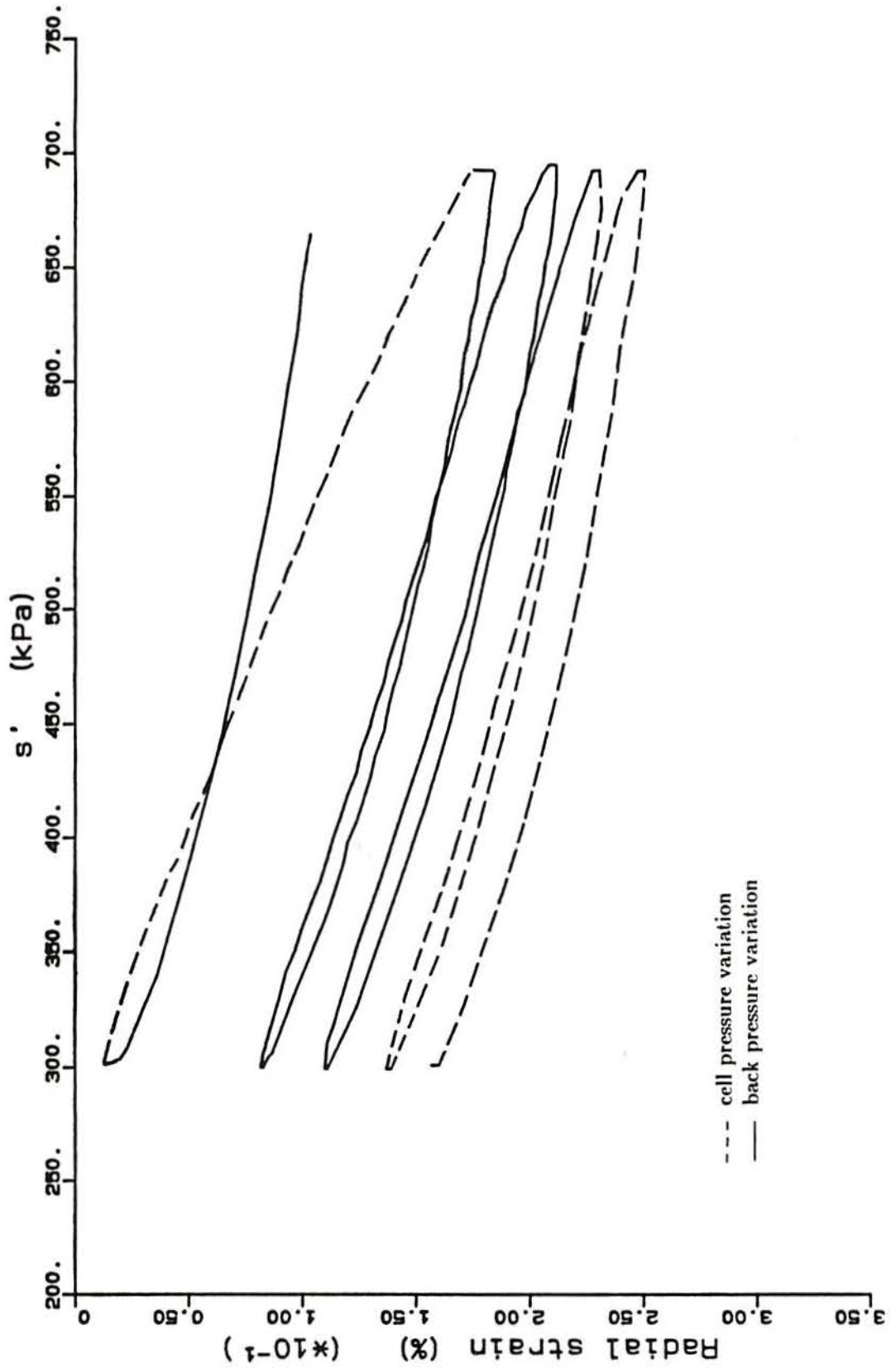

Figure 6.12 – Influence of cell pressure on the radial belt — isotropic cycles with two forms of effective confining stress variation

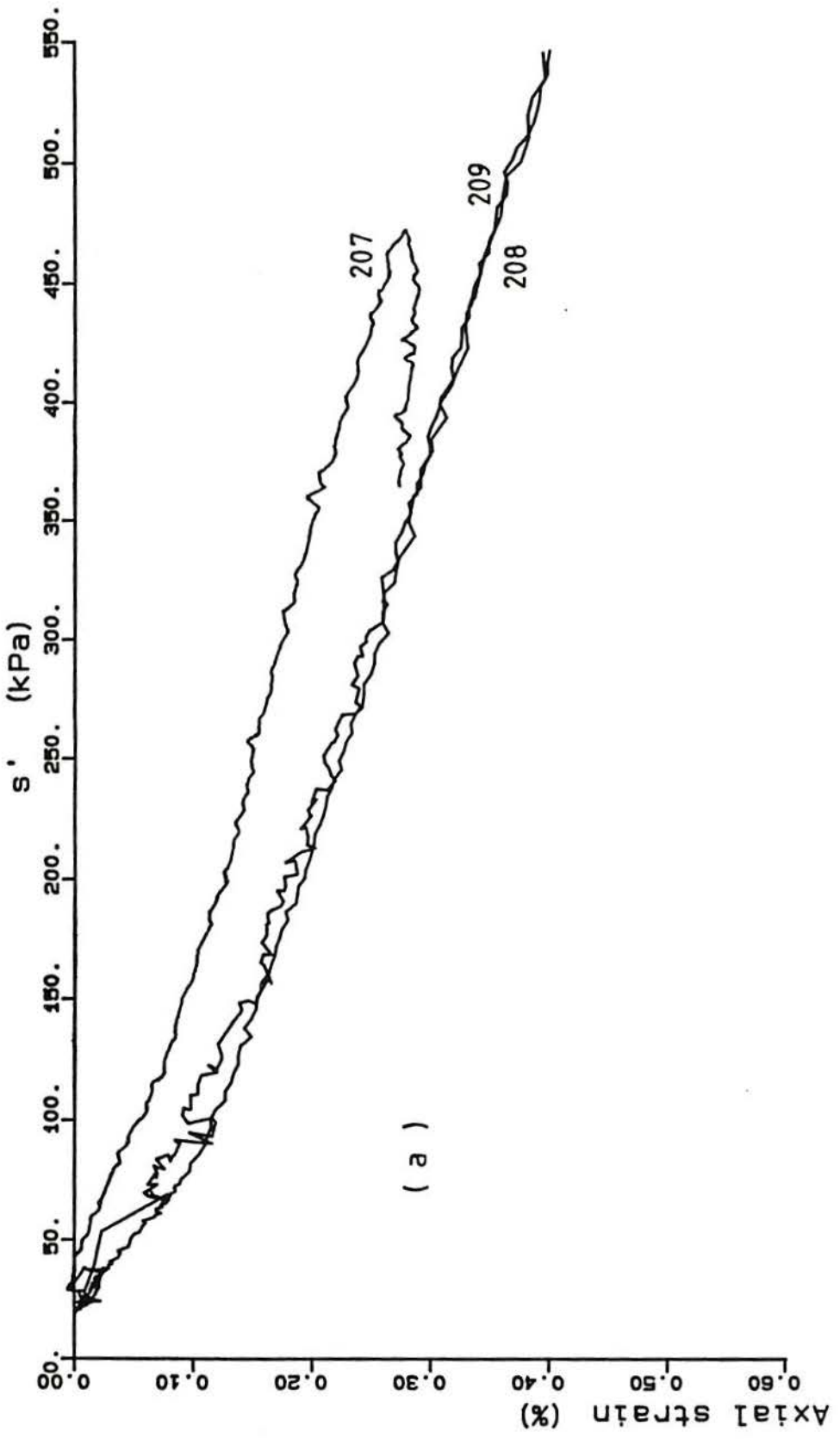

Figure 6.13 – Isotropic consolidation of 200 series — axial strain (local) versus confining pressure (a) tests 207, 208 and 209; (cont.)

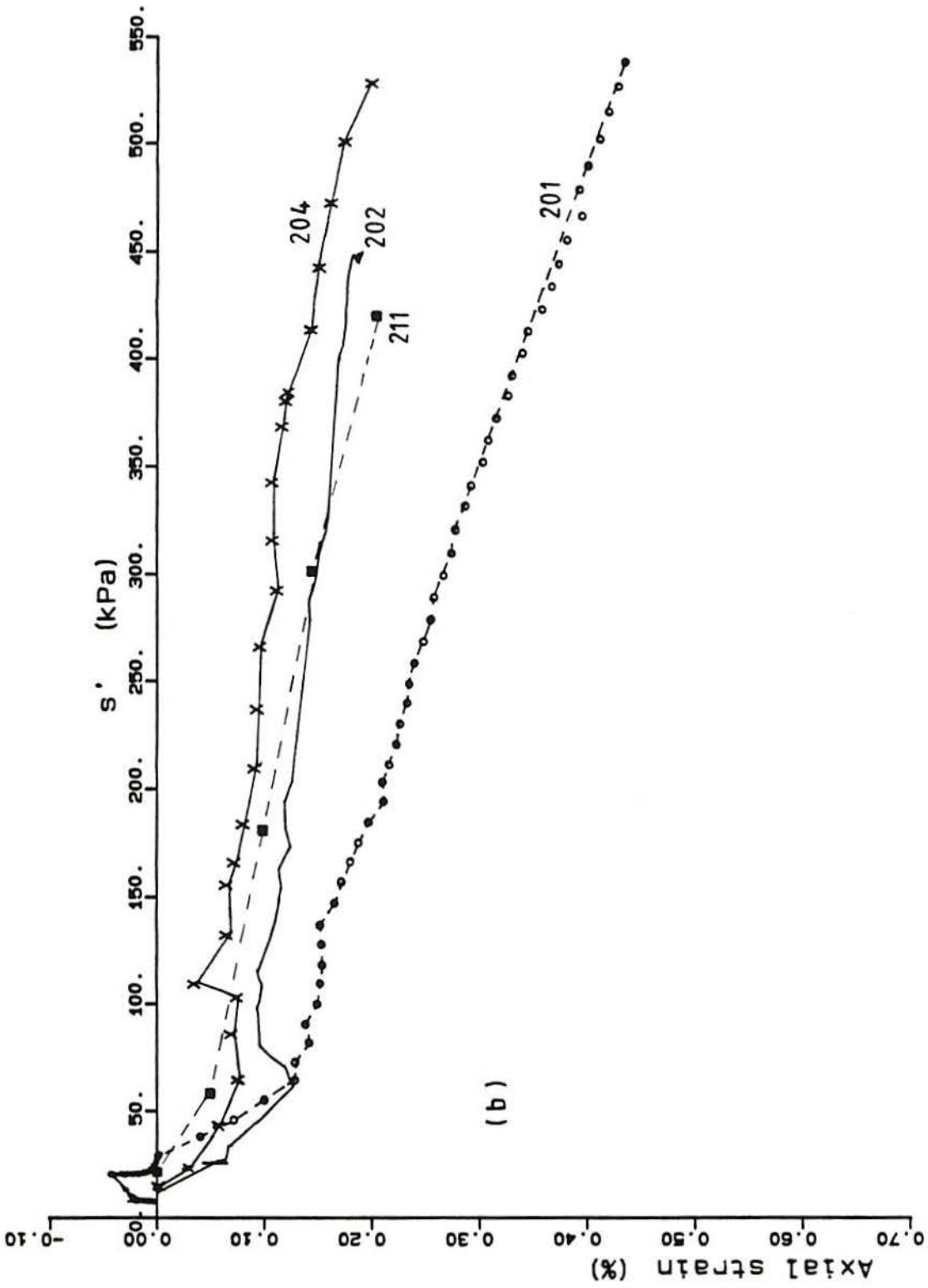

Figure 6.13 – (cont.) (*b*) tests 201, 202, 204 and 211

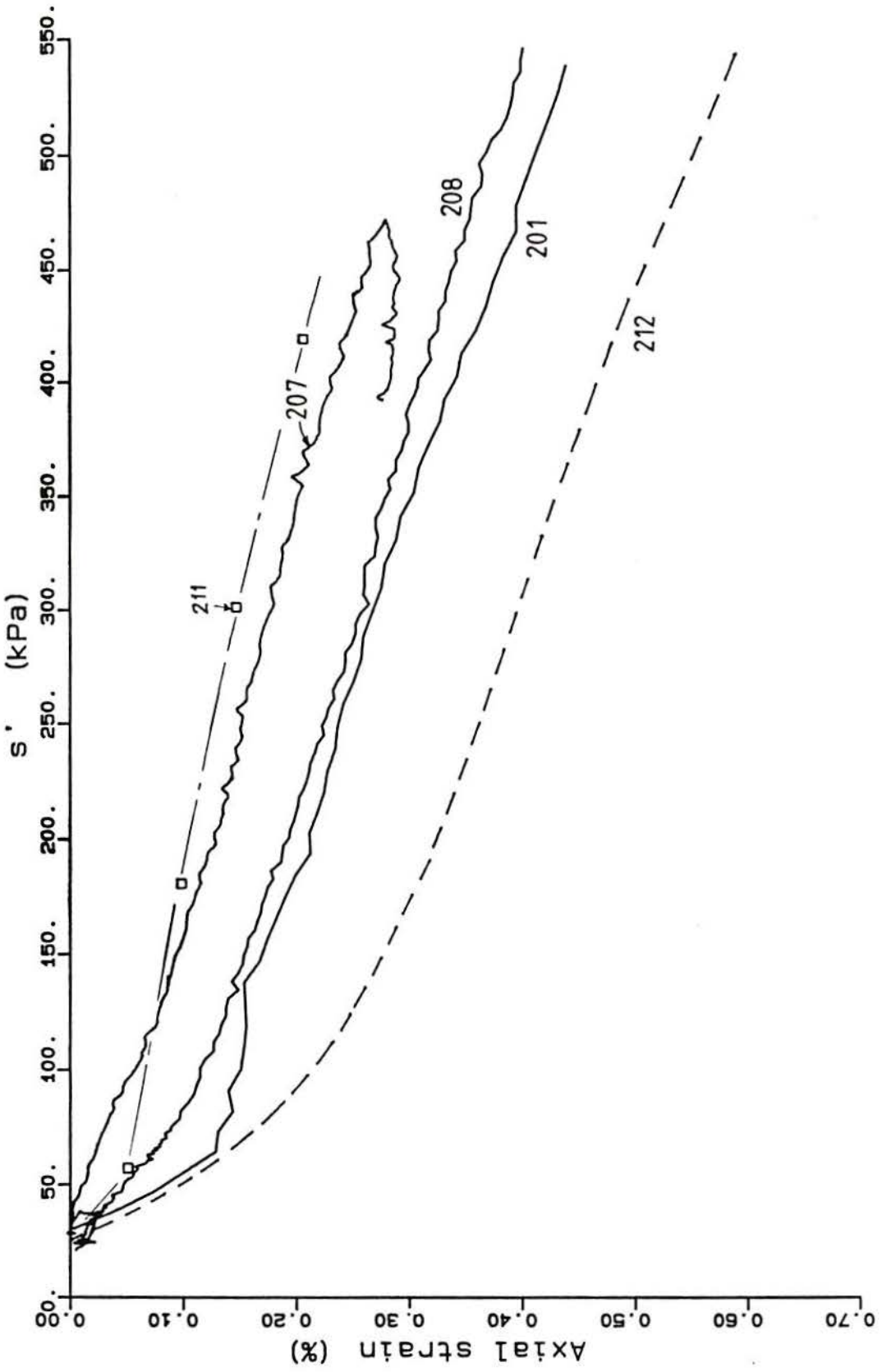

Figure 6.14 – Isotropic consolidation test results of 200 series – summary

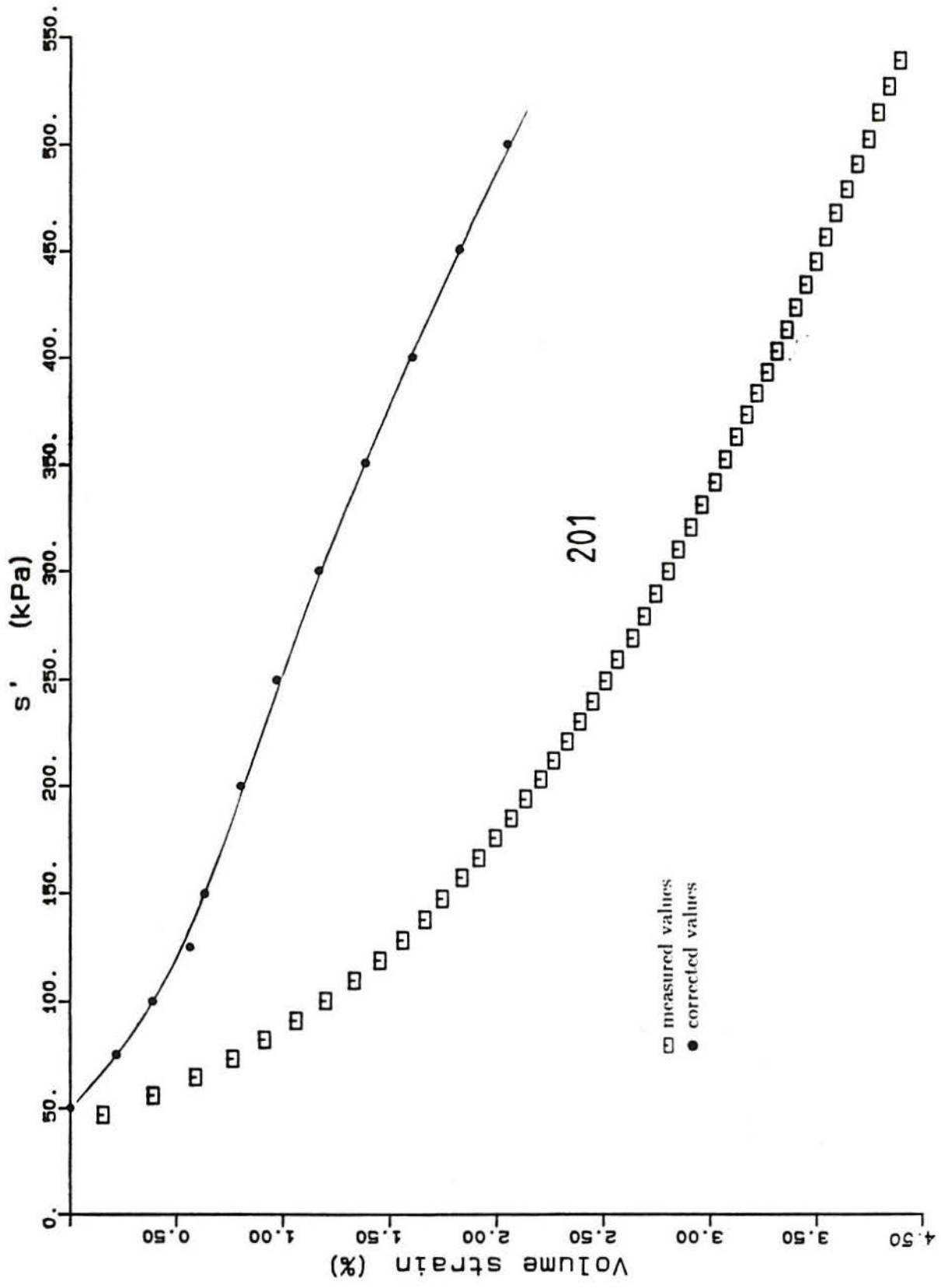

Figure 6.15 – Example of volumetric strain obtained in the 200 series; as measured and corrected for membrane penetration error

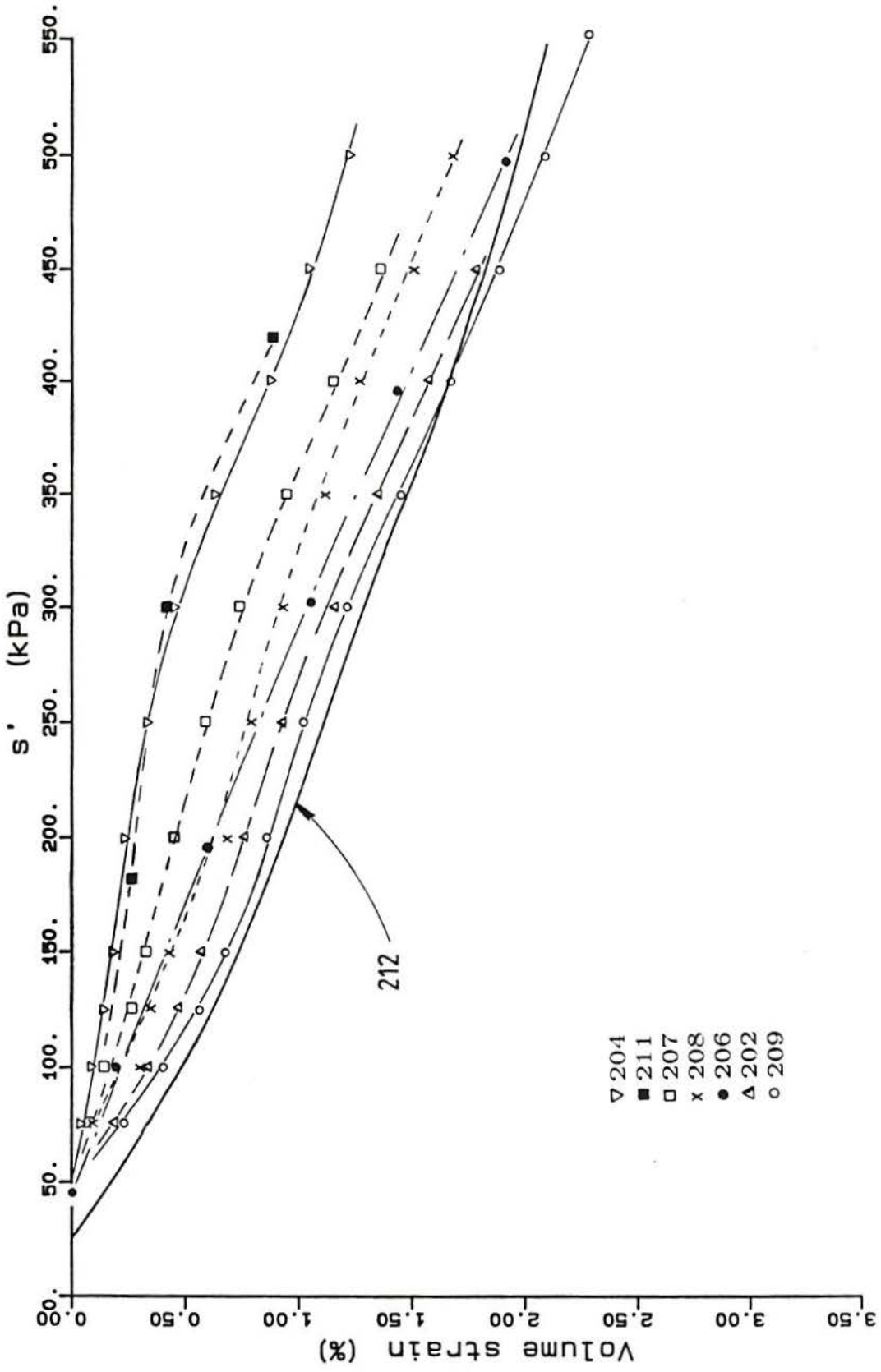

Figure 6.16 – Volumetric strain of isotropic compression tests, 200 series

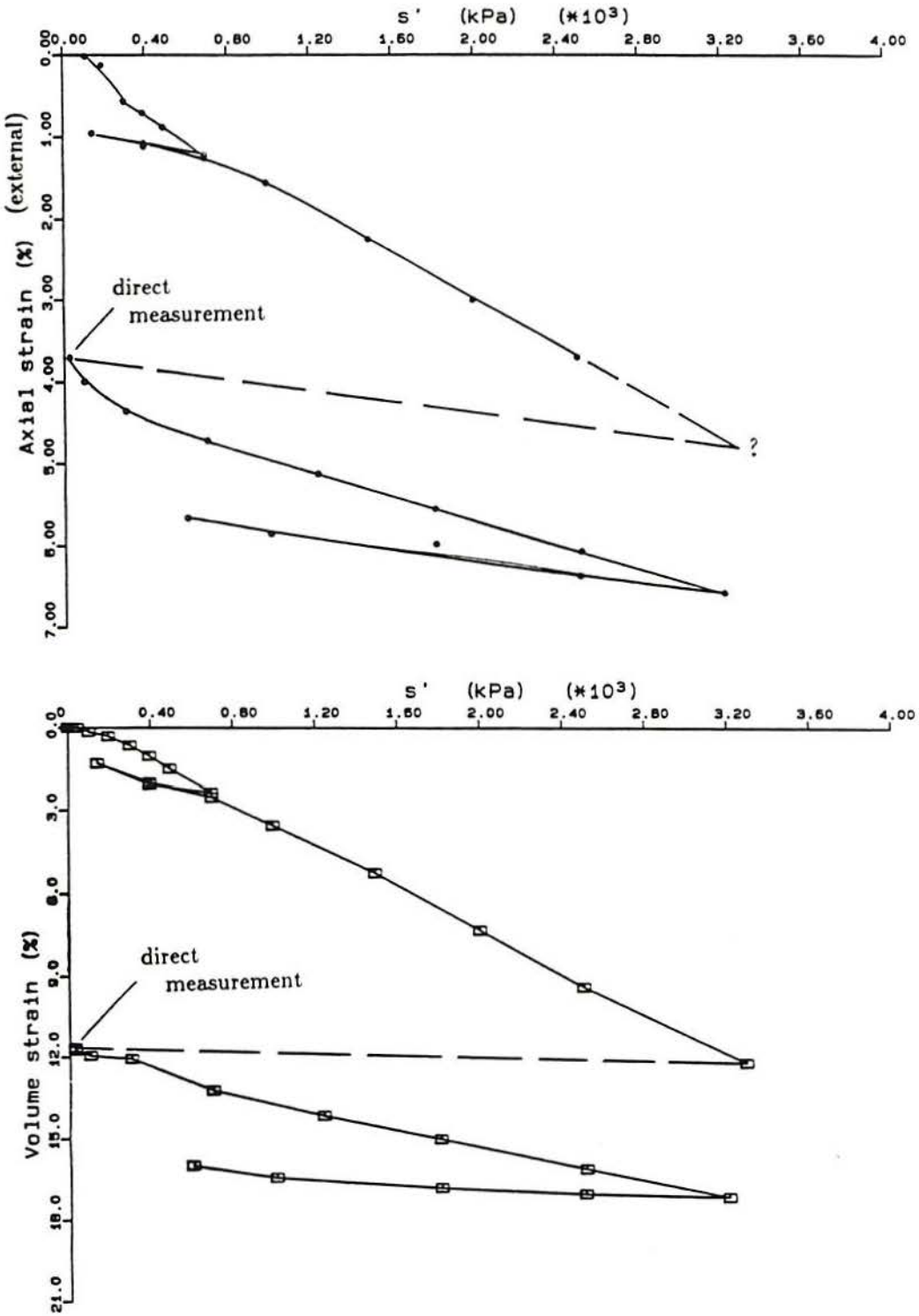

Figure 6.17 – Results of isotropic consolidation test of sample 206, natural scales

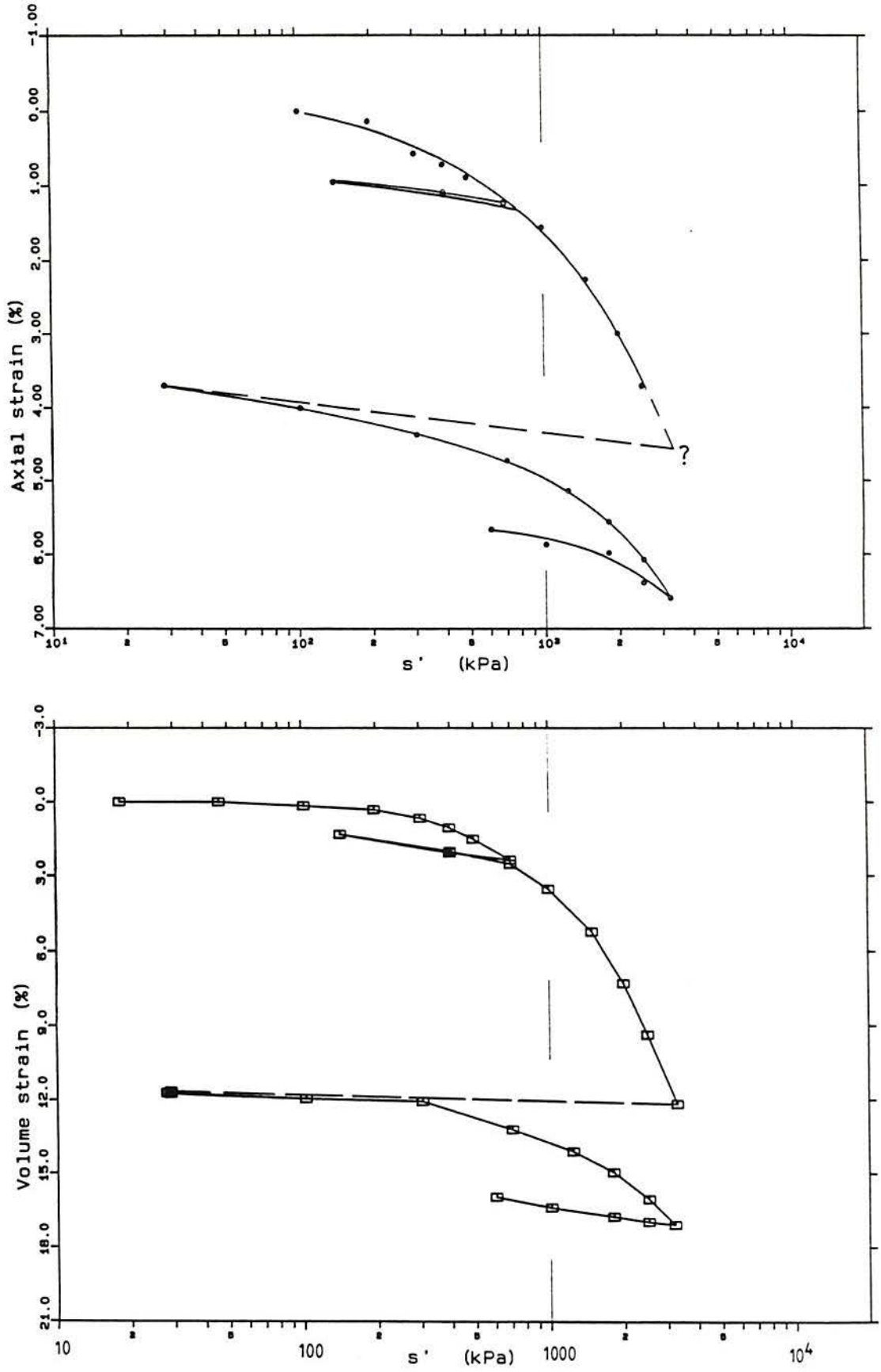

Figure 6.18 – Results of isotropic consolidation test of sample 206, logarithmic scale of stress

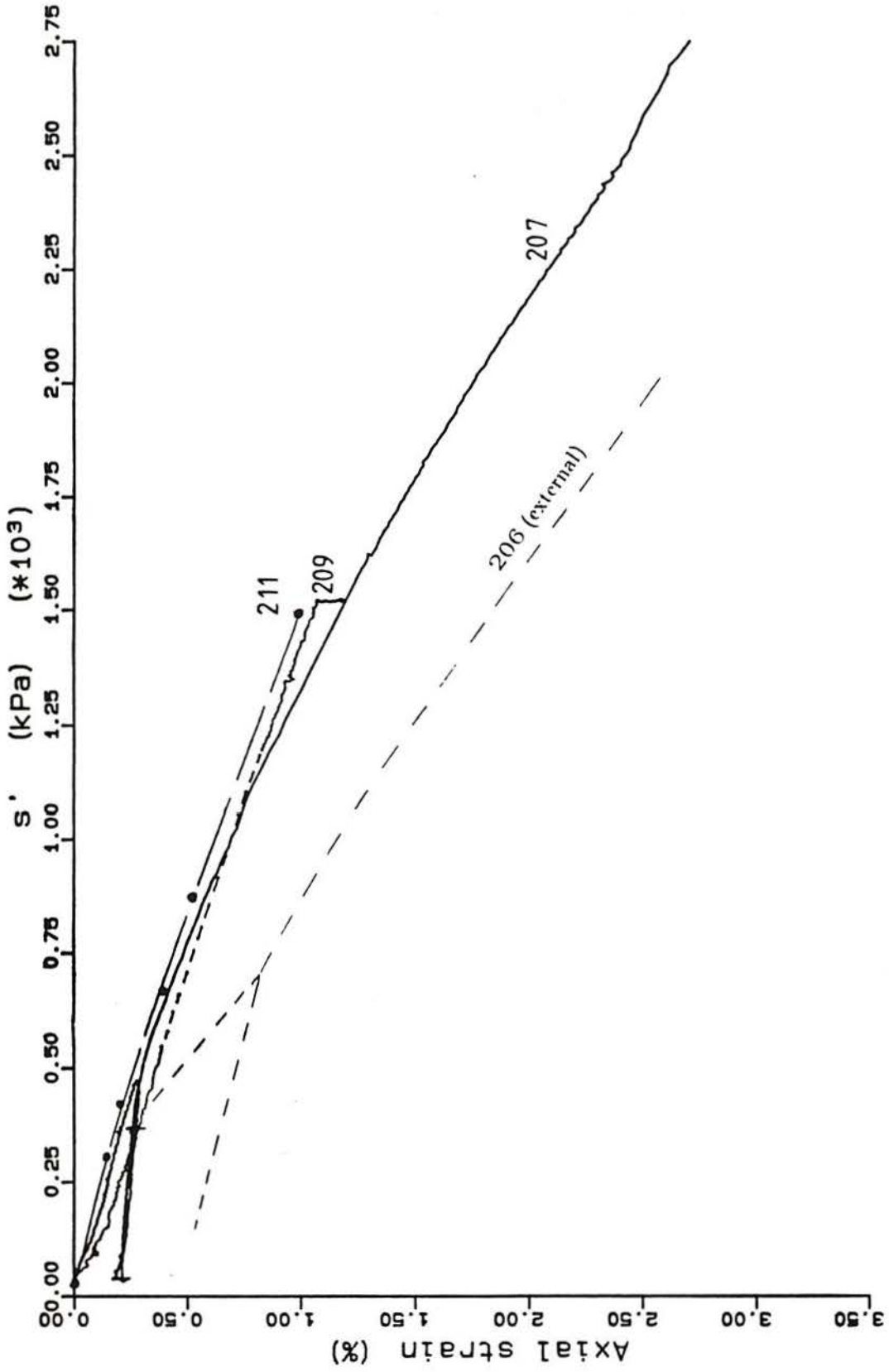

Figure 6.19 - Results of isotropic consolidation tests with axial strain measured locally (pressure scale 250 kPa)

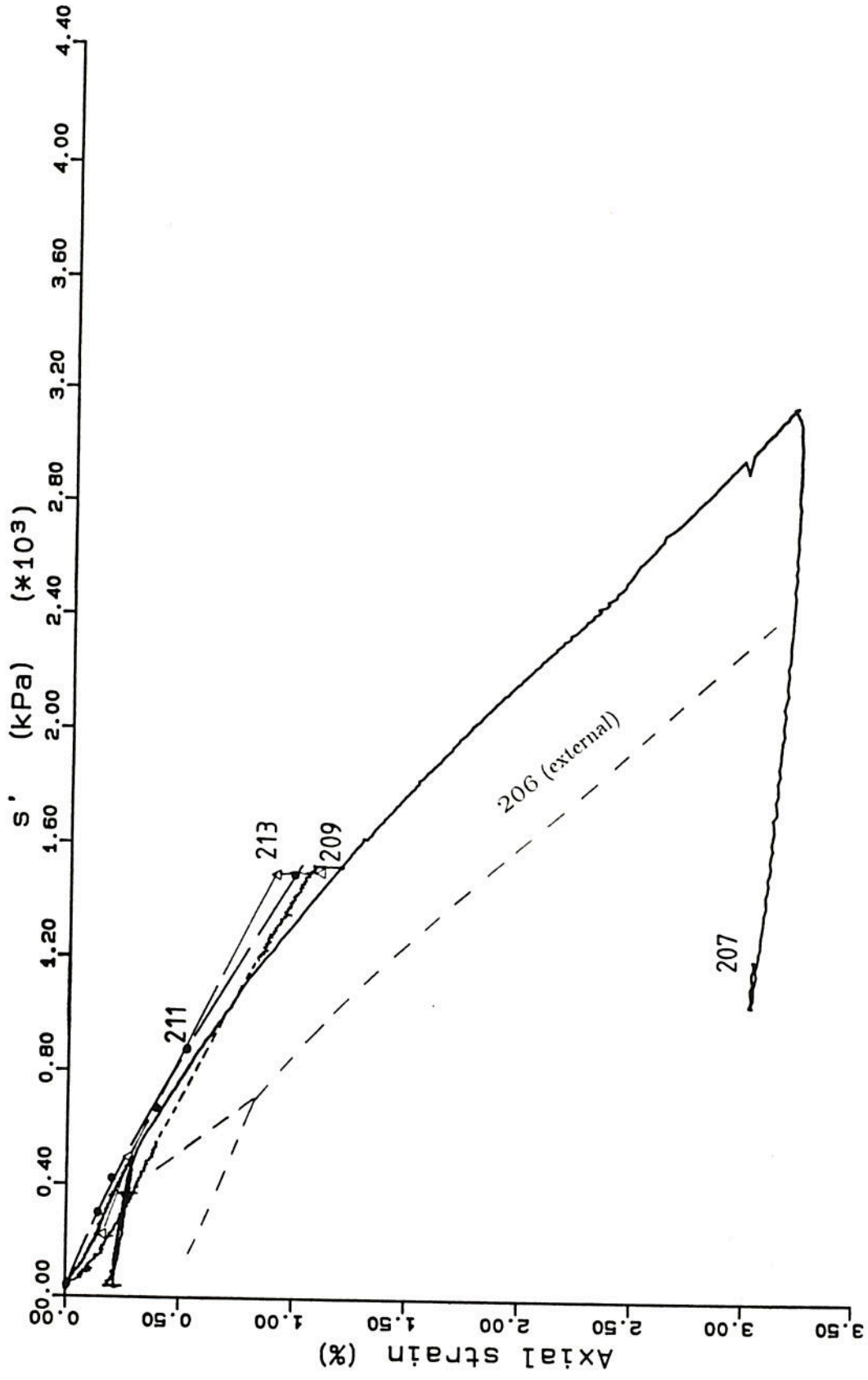

Figure 6.20 – Results of isotropic consolidation tests with axial strain measured locally (*a*) natural scales; (cont.)

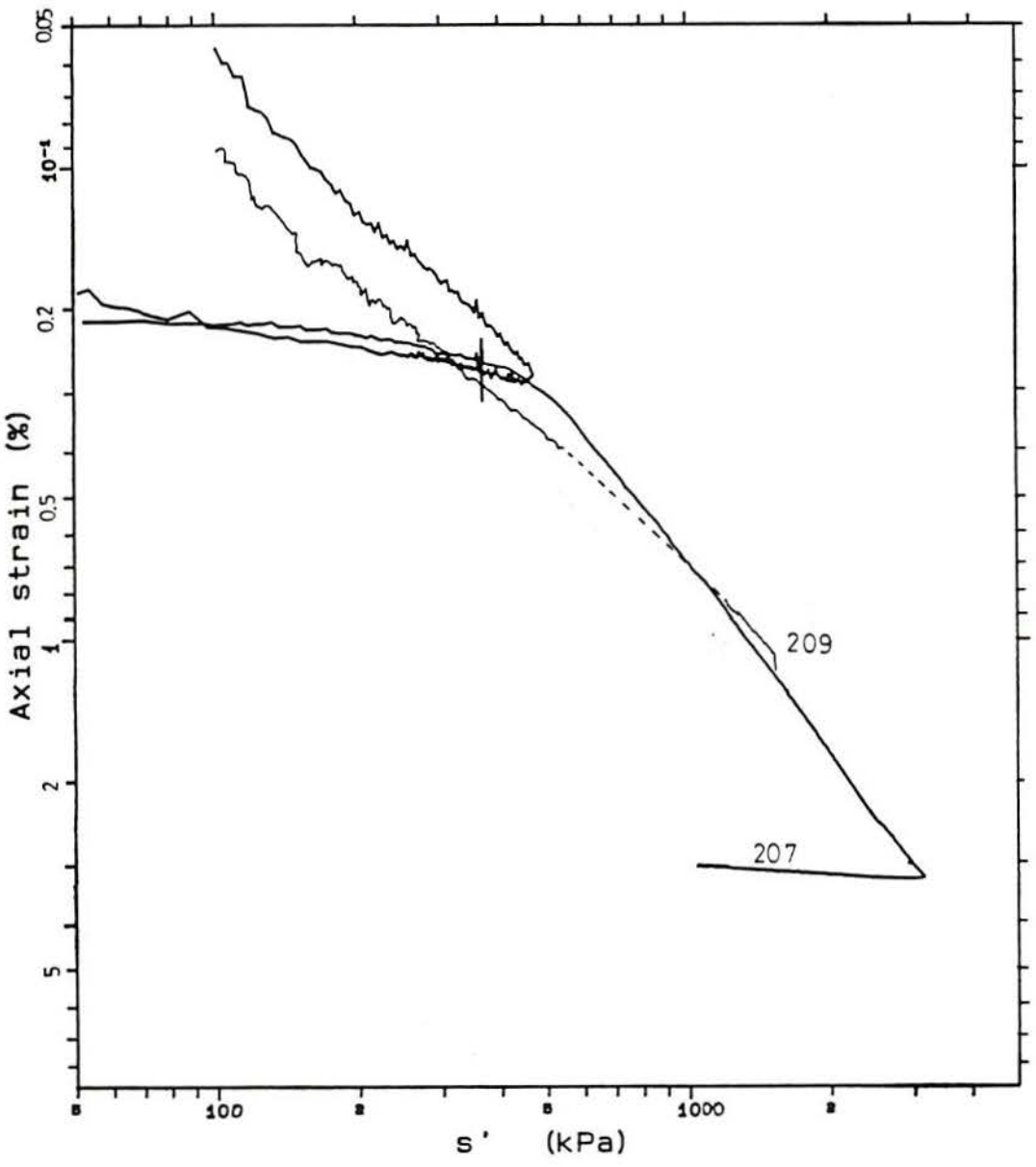

Figure 6.20 – (cont.) (*b*) logarithmic scales

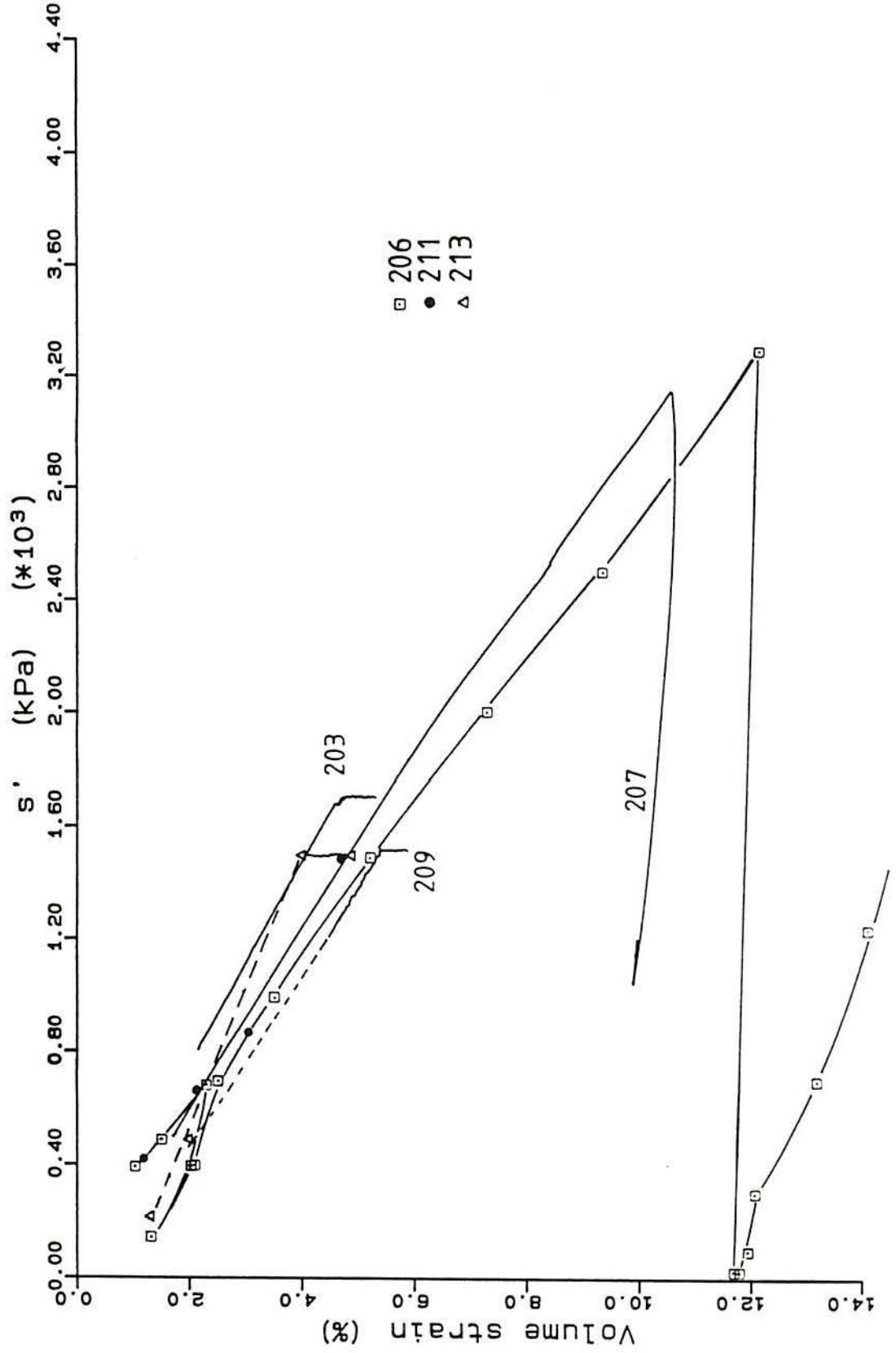

Figure 6.21 – Results of isotropic consolidation tests; corrected volumetric strain versus effective stress

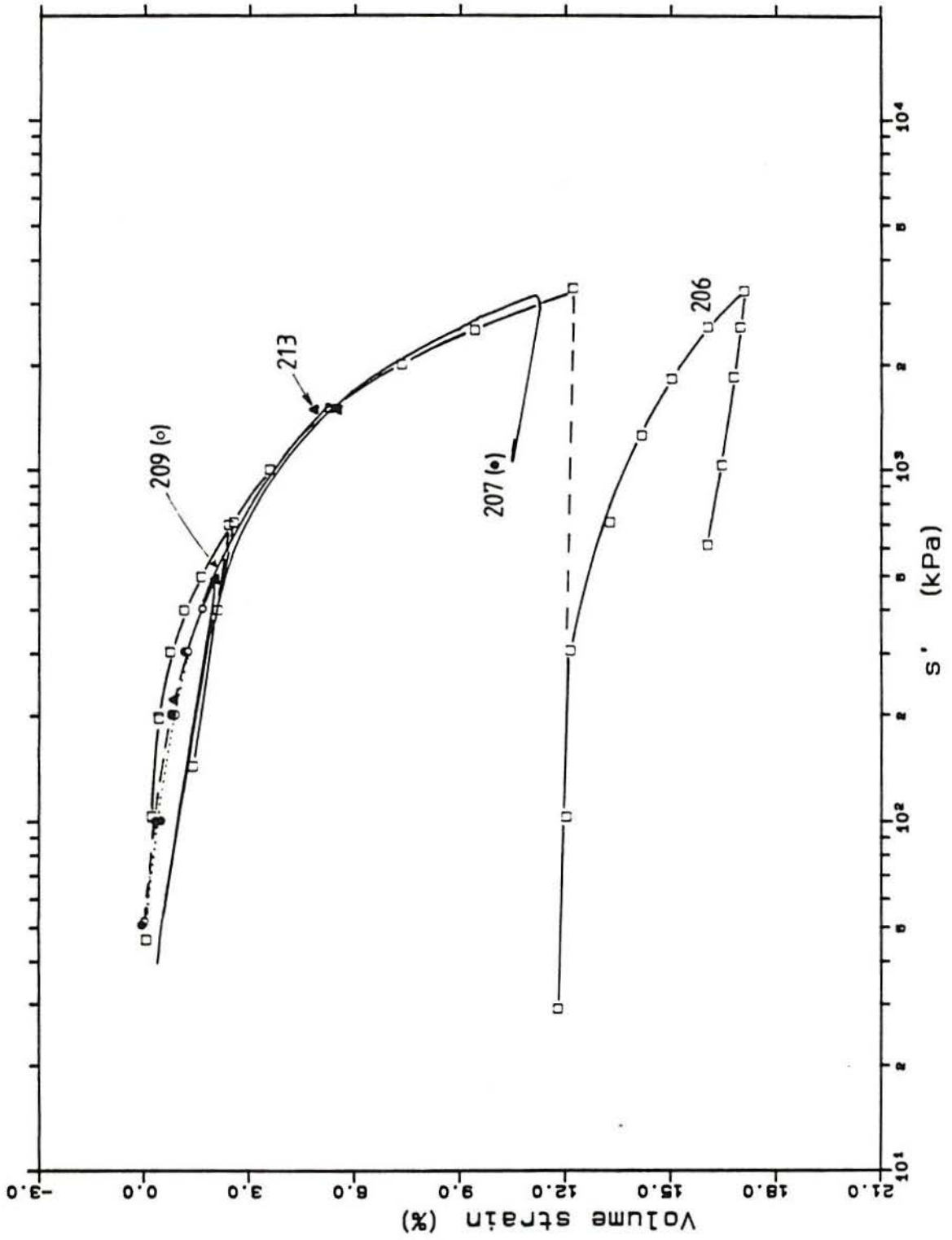

Figure 6.22 – Results of isotropic consolidation tests; corrected volume strain versus the logarithm of pressure

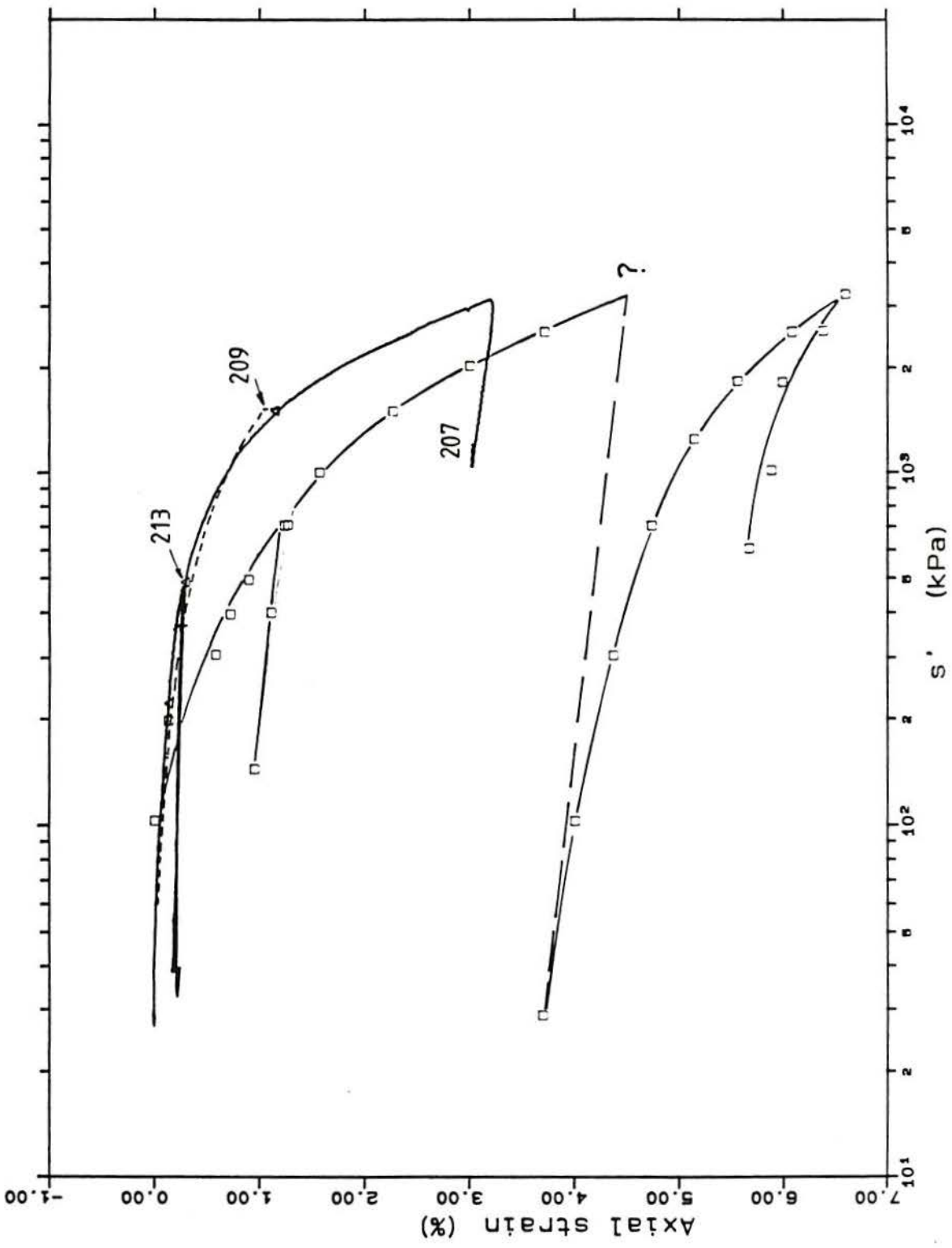

Figure 6.23 – Results of isotropic consolidation tests; local axial strain versus the logarithmic of pressure

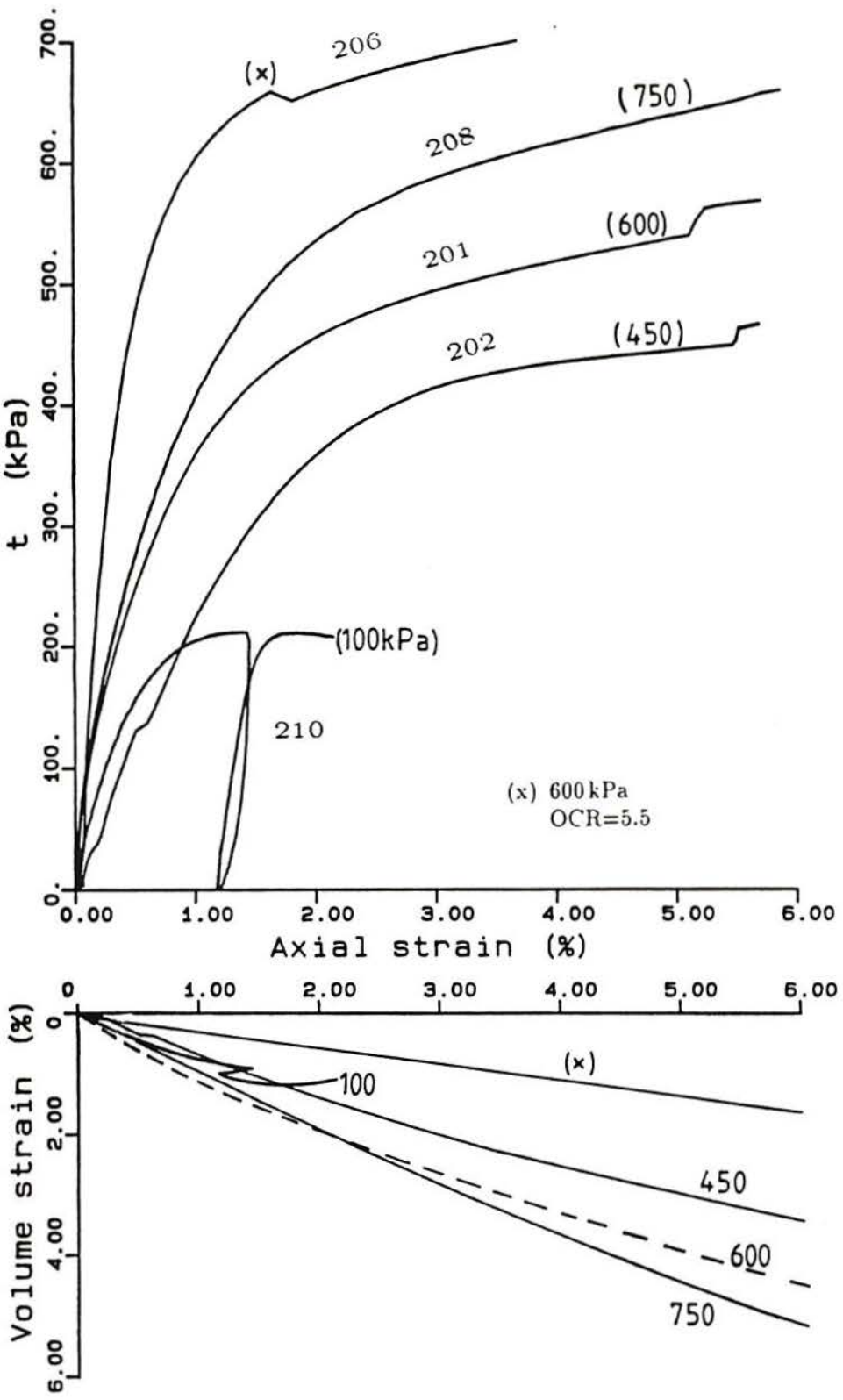

Figure 6.24 - Results of triaxial compression tests 210 (100kPa), 202 (450kPa), 201 (600kPa), 208 (750kPa) and 206 (600kPa, OCR=5.5)

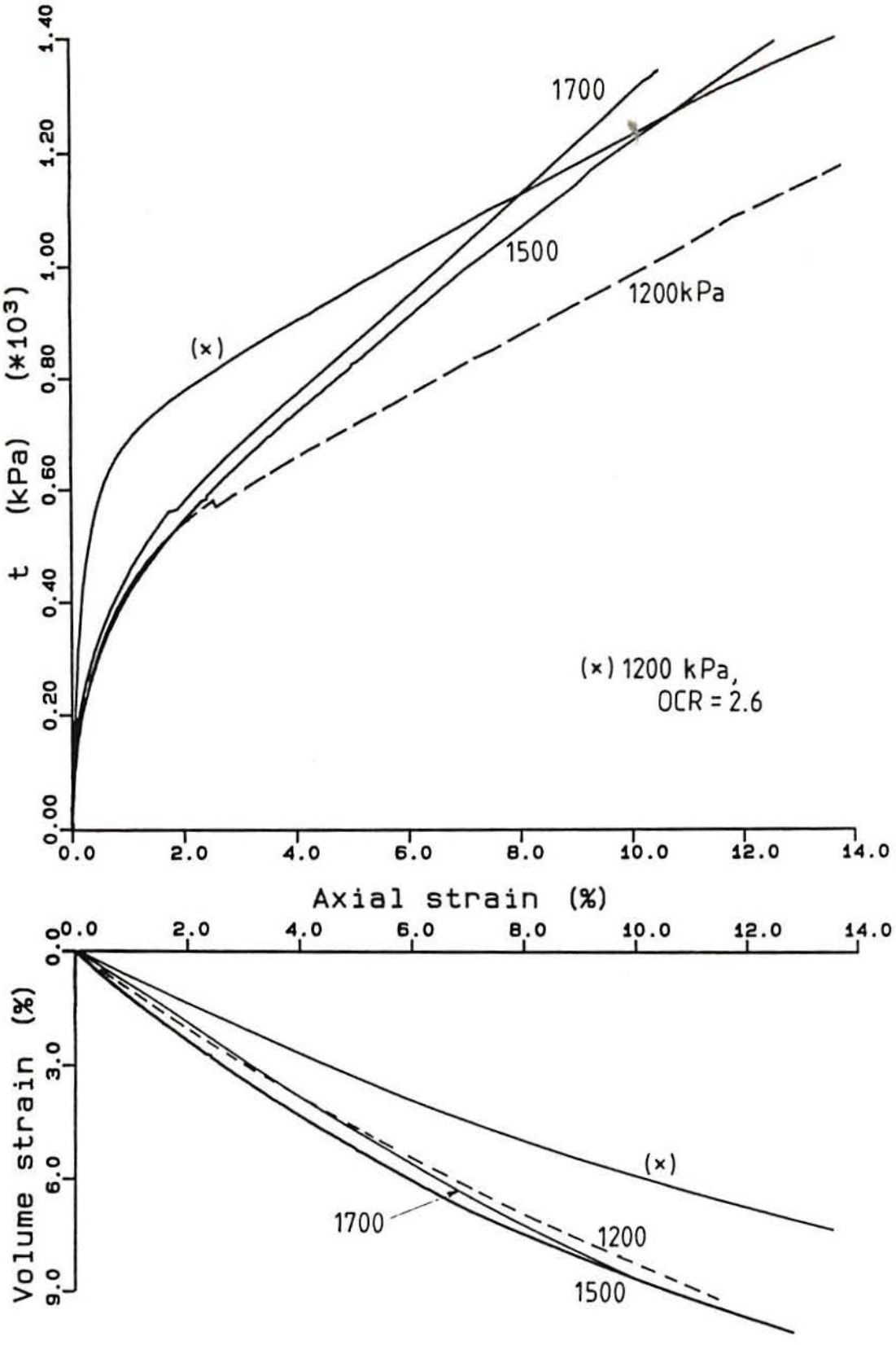

Figure 6.25 – Results of triaxial compression tests 205 (1200kPa), 207 (1200kPa, OCR=2.6). 213 (1500kPa) and 203 (1700kPa)

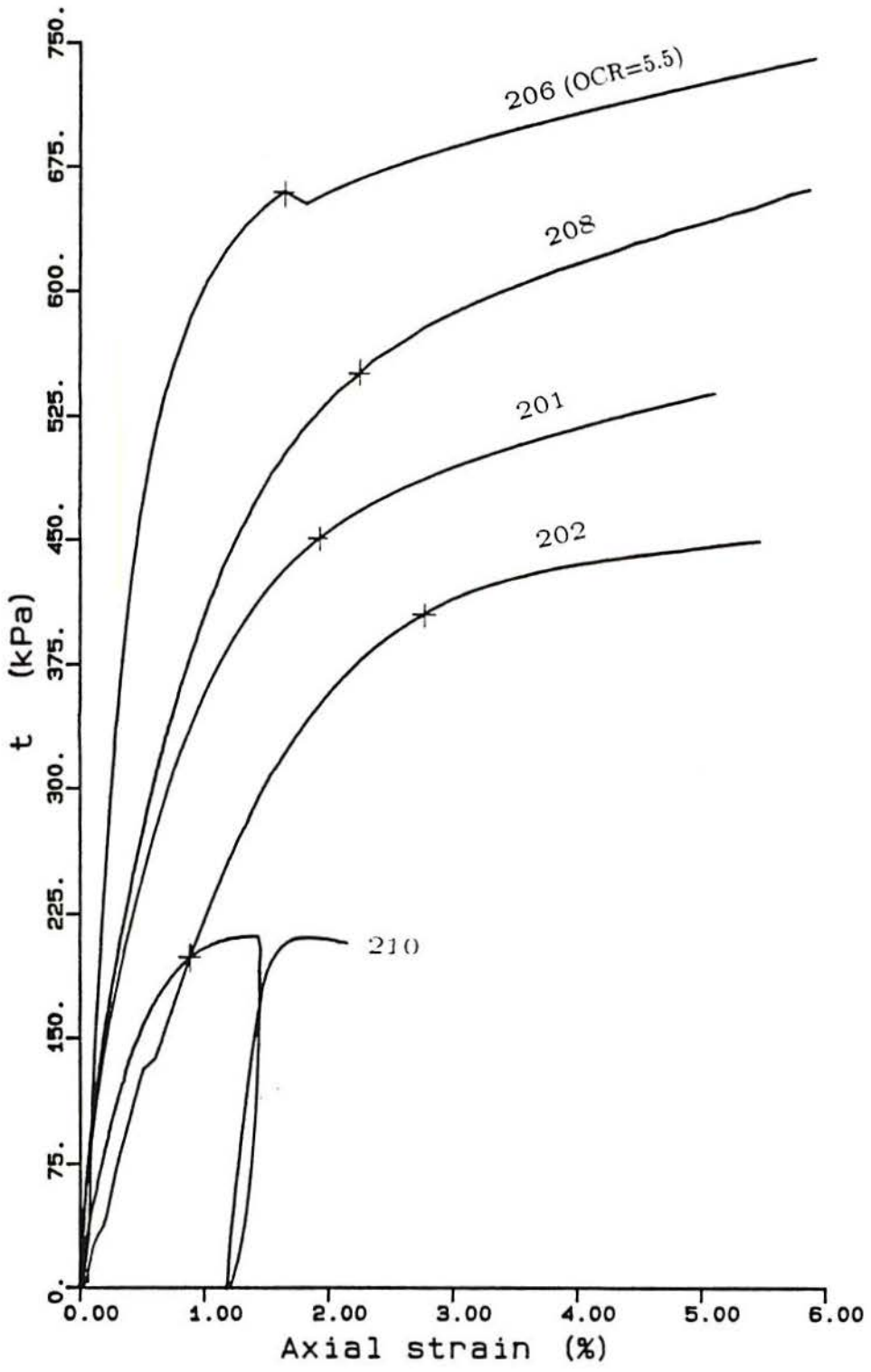

Figure 6.26 – Results of drained triaxial compression tests of 200 series at lower confining pressures

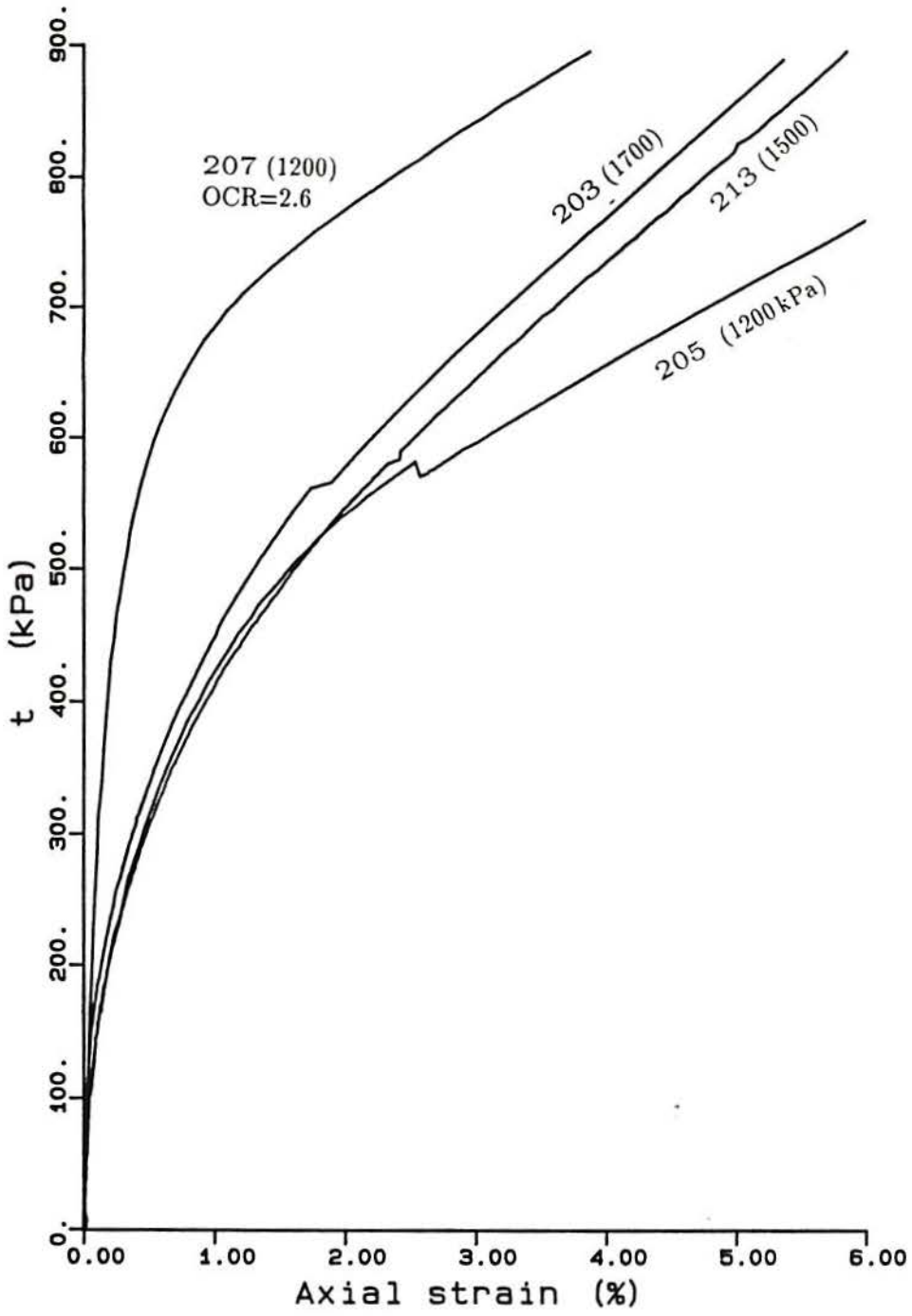

Figure 6.27 – Results of drained triaxial compression tests of 200 series at higher confining pressures

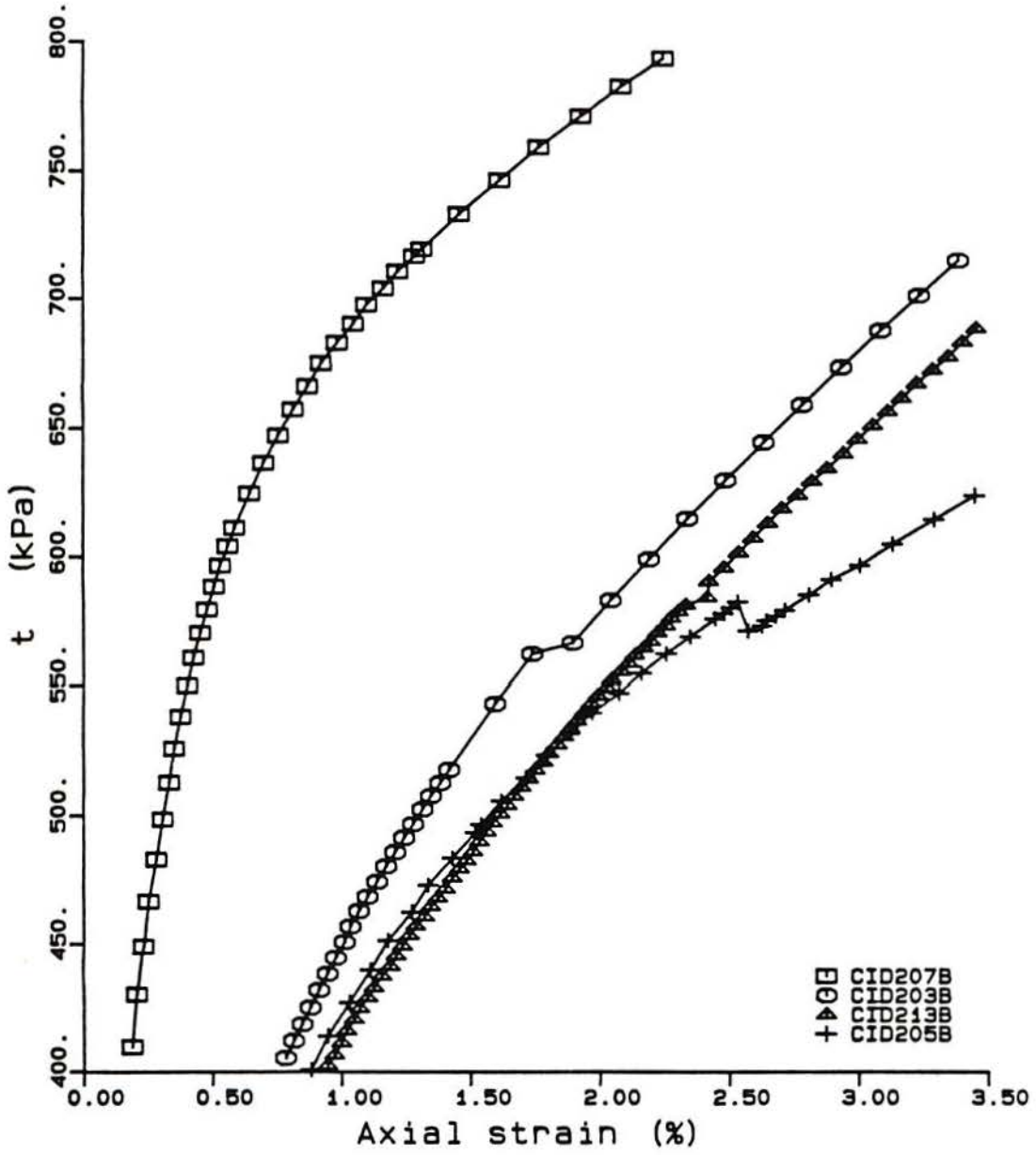

Figure 6.28 – Detail of stress-strain region of discontinuity of tests 203, 205, 207 and 213 (all experimental points represented)

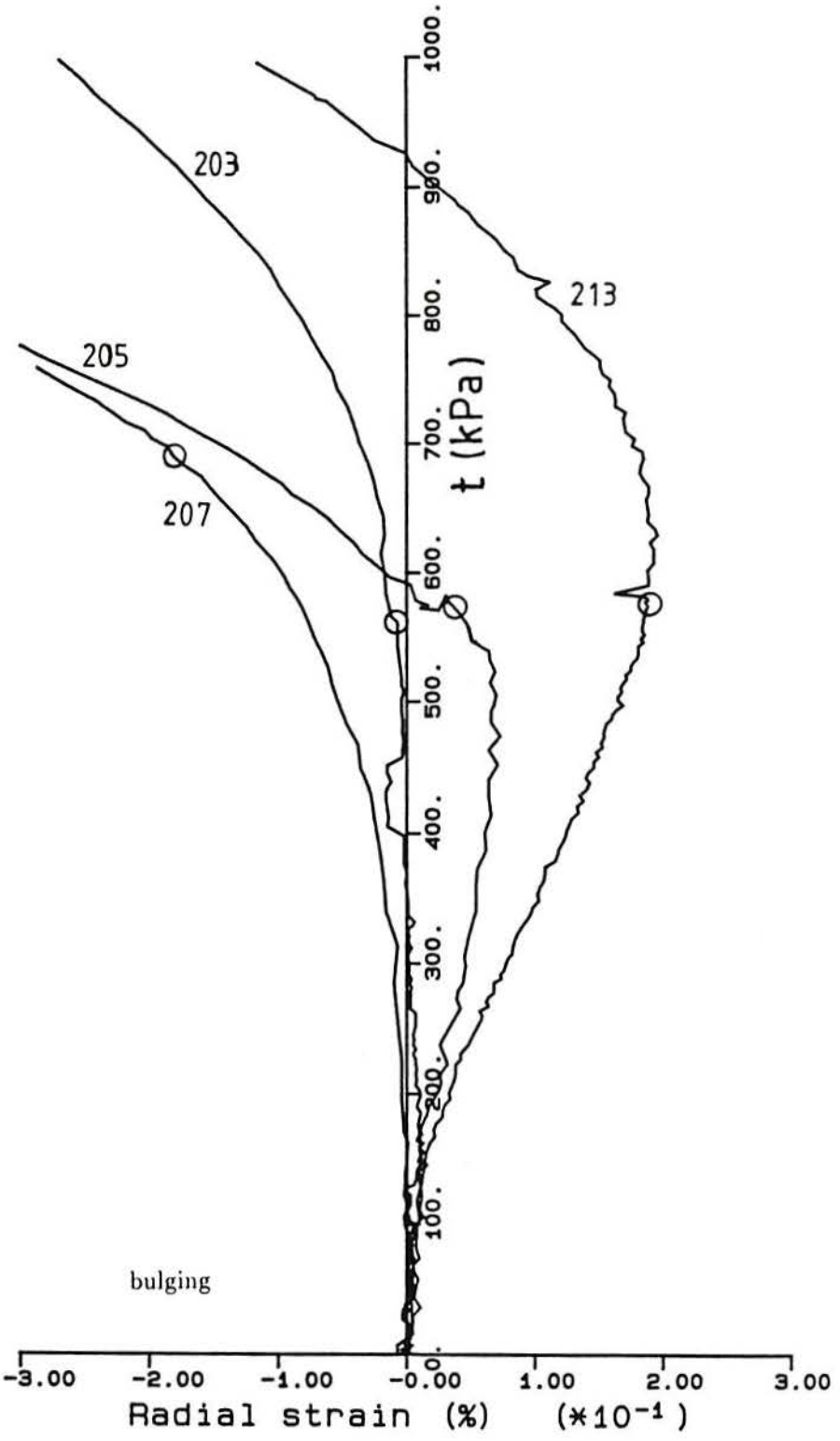

Figure 6.29 – Stress versus radial strain of samples sheared at higher confining pressures

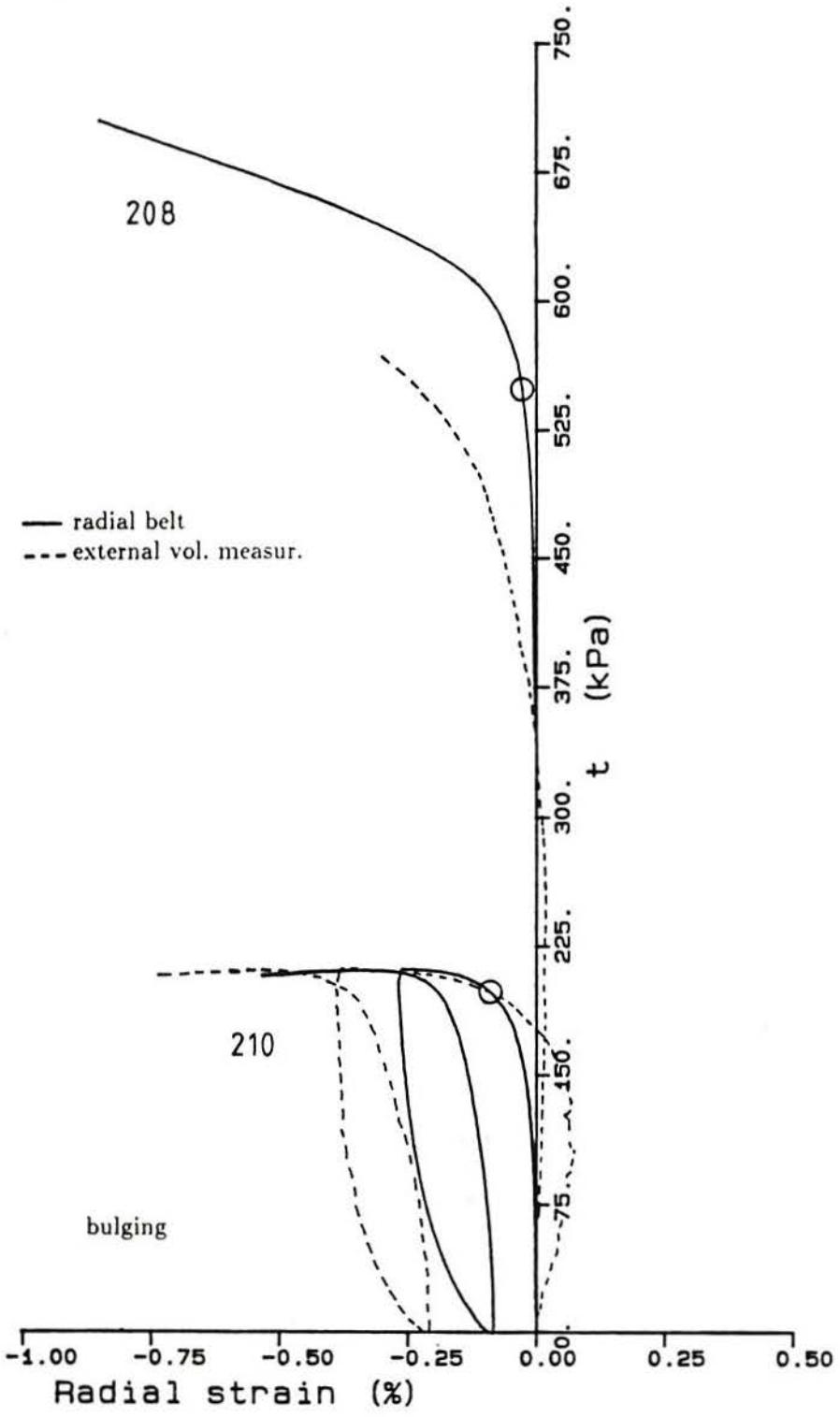

Figure 6.30 - Results of stress versus radial strain measured on tests with radial belt (208 and 210)

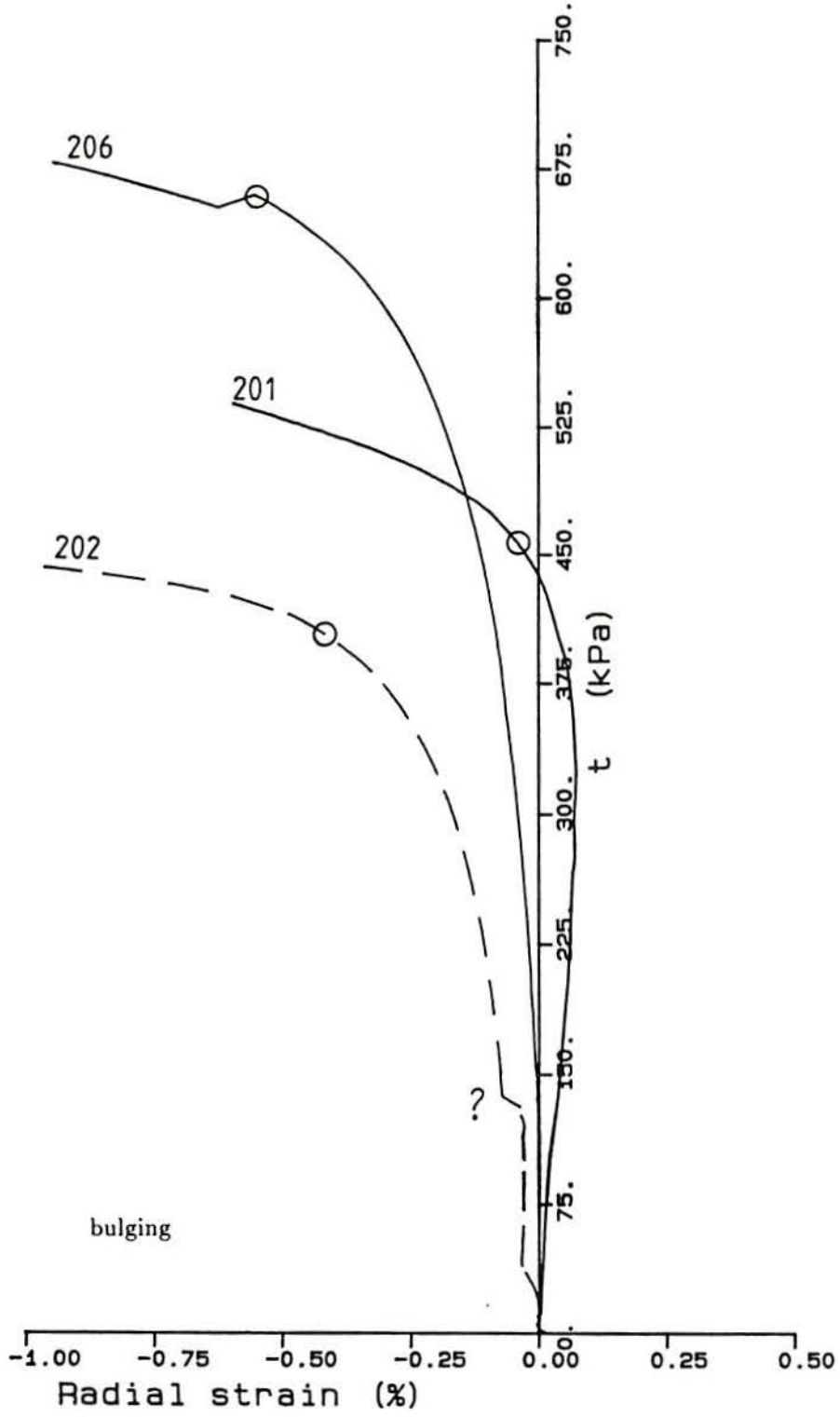

Figure 6.31 – Results of stress versus radial strain calculated from external measurement of volume

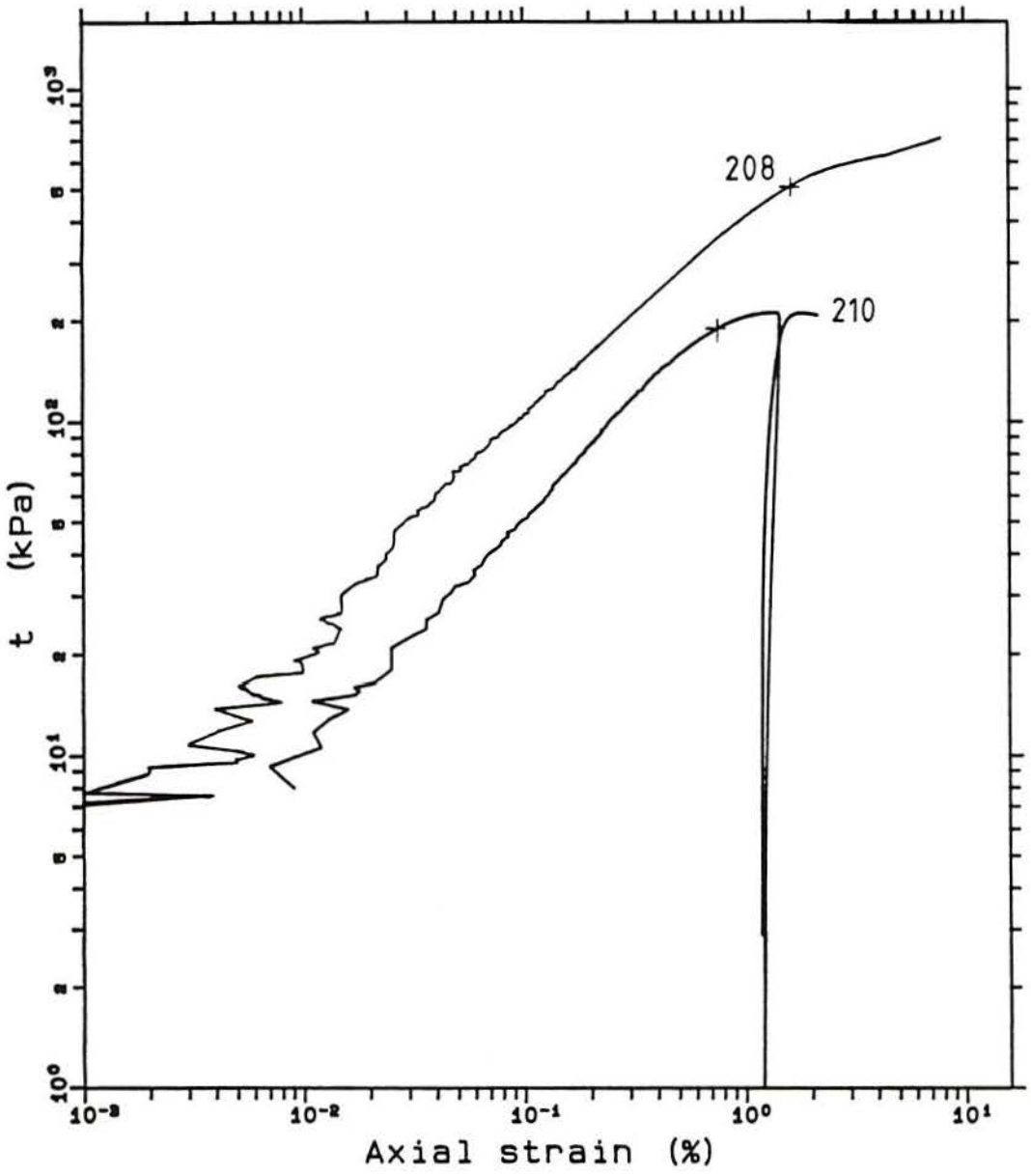

Figure 6.32 – Stress-strain plots using logarithmic scales for determination of yield. (*a*) tests 208 and 210; (cont.)

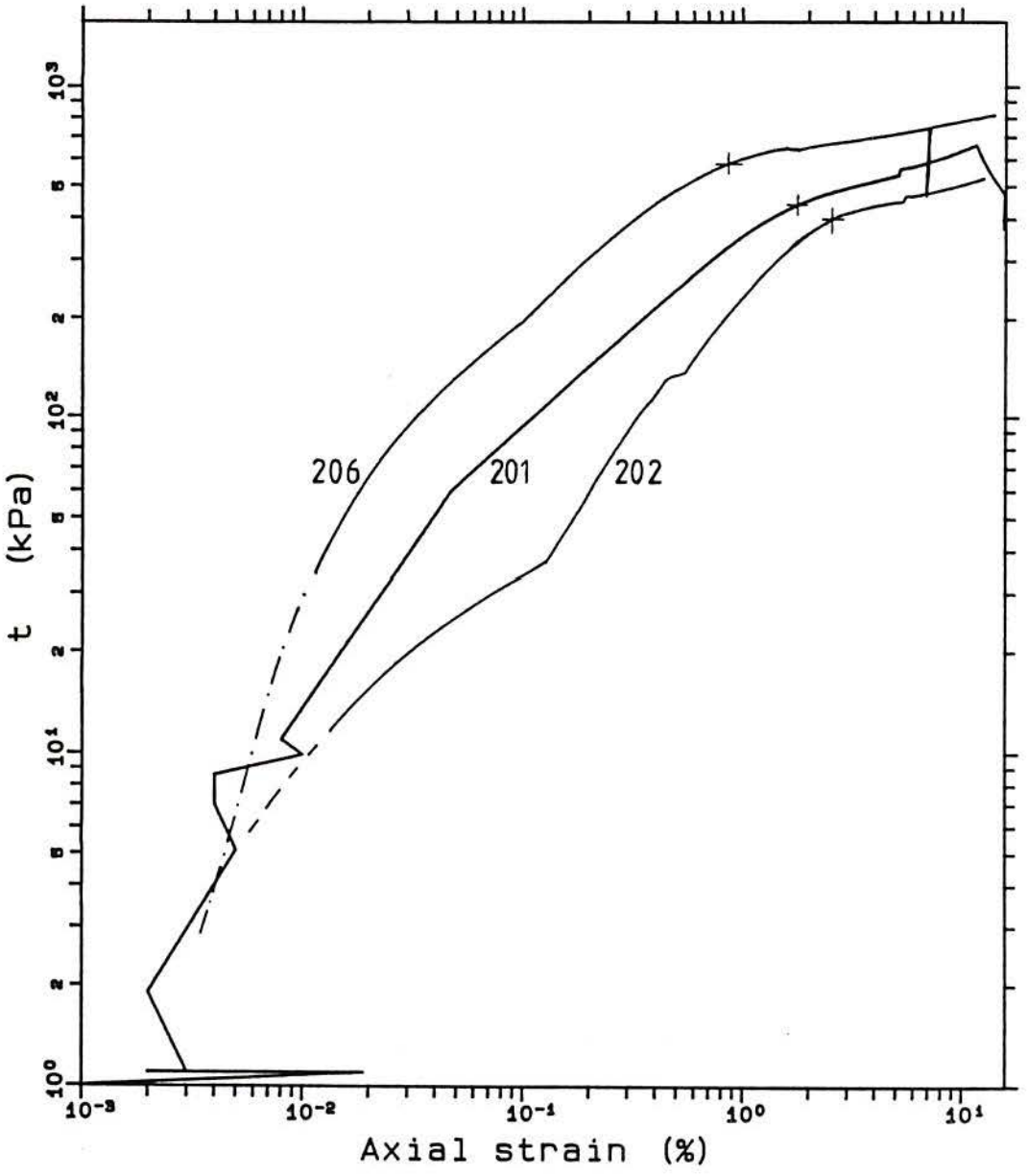

Figure 6.32 – (cont.) (*b*) tests 201, 202 and 206; (cont.)

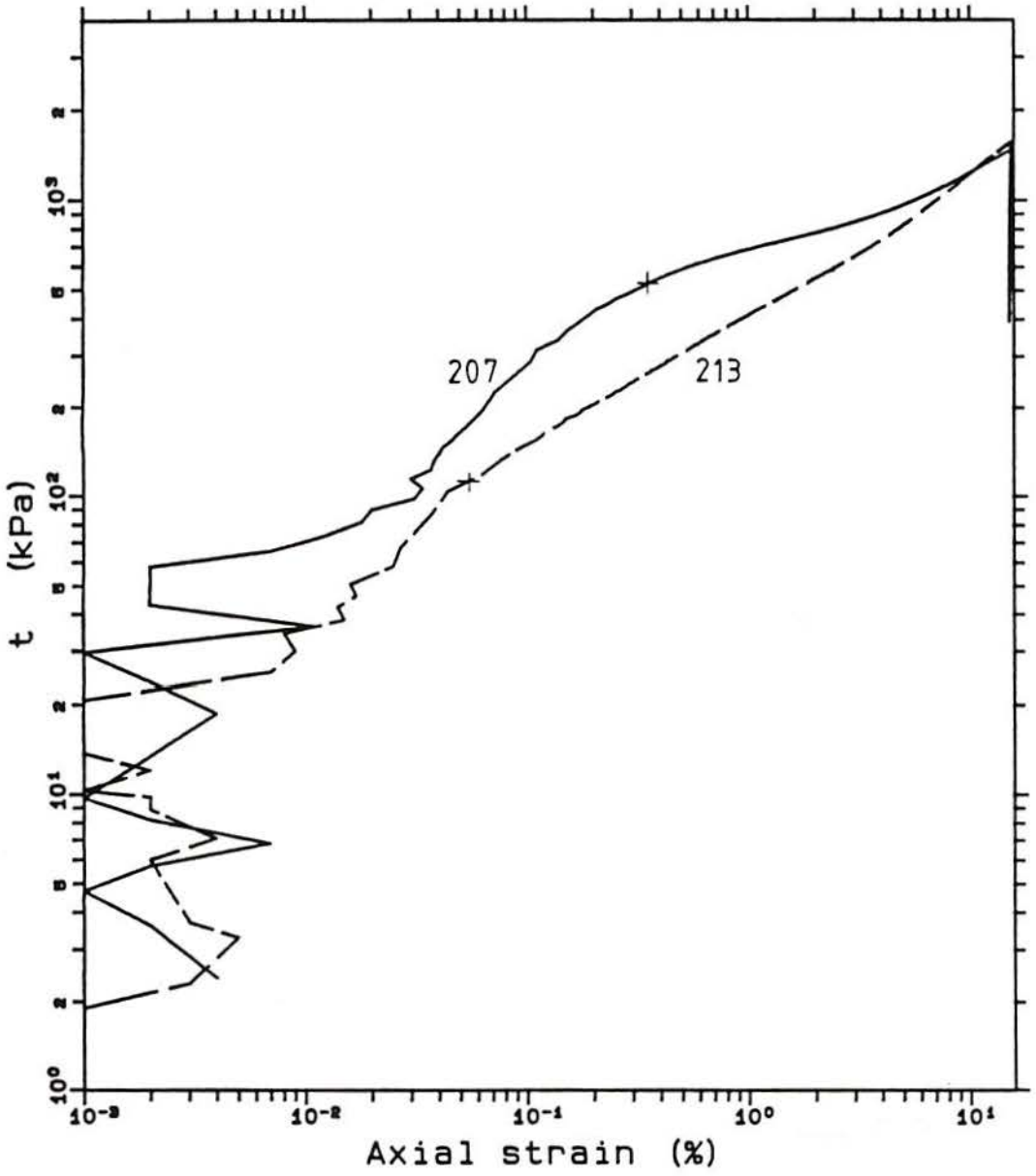

Figure 6.32 – (cont.) (*c*) tests 207 and 213; (cont.)

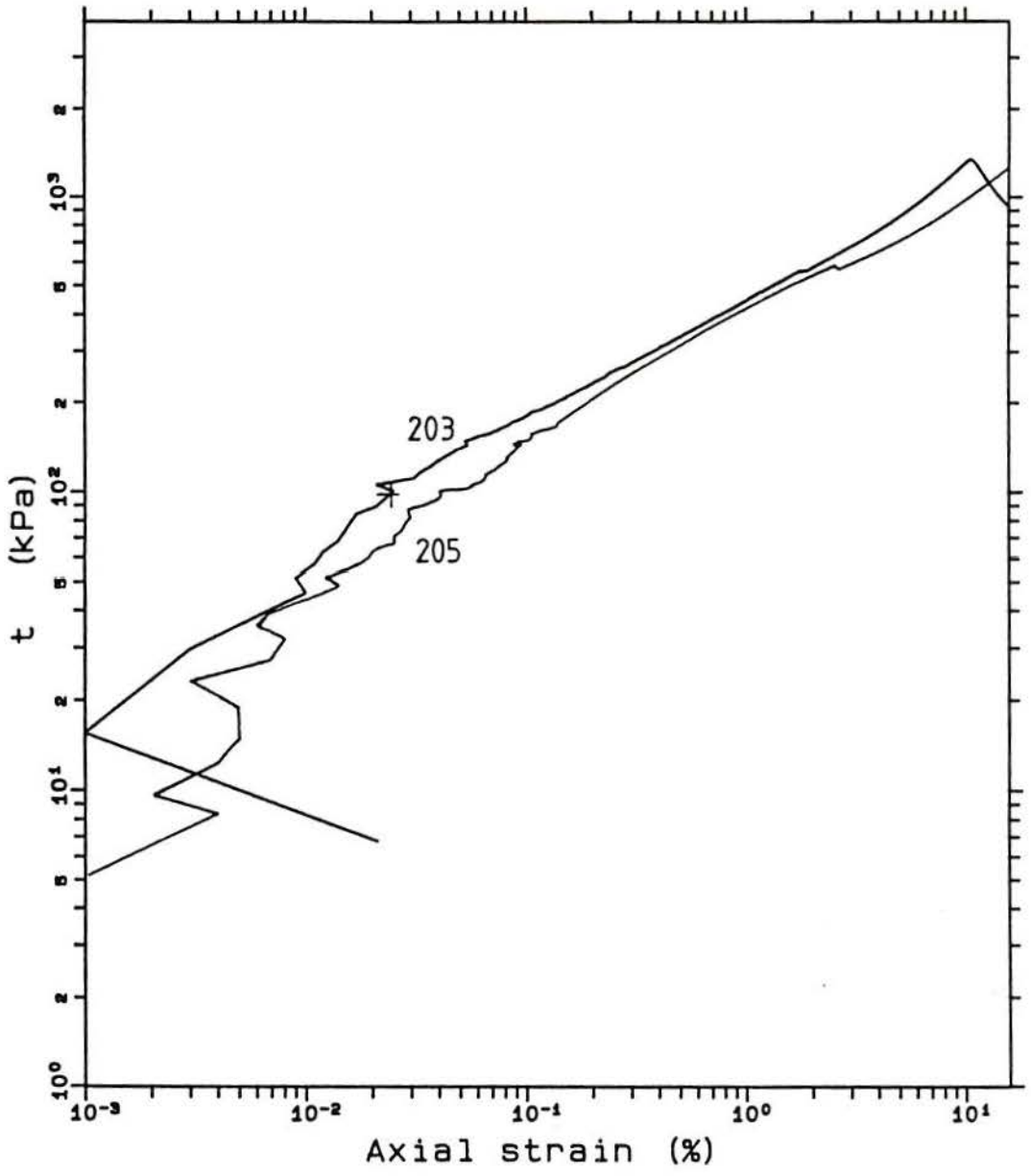

Figure 6.32 – (cont.) (*d*) tests 203 and 205

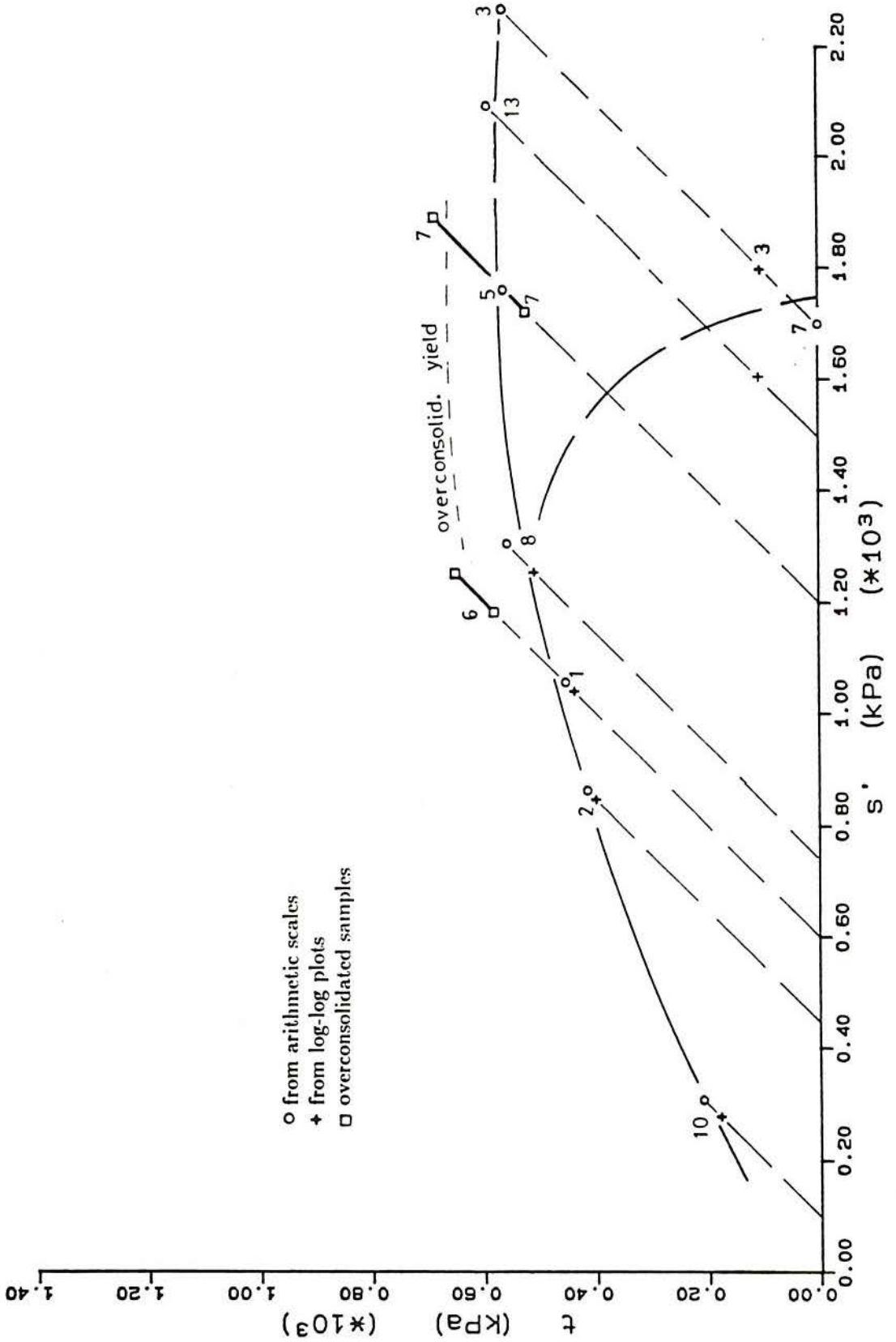

Figure 6.33 – Yield pressures obtained from stress-strain curves for 200 series

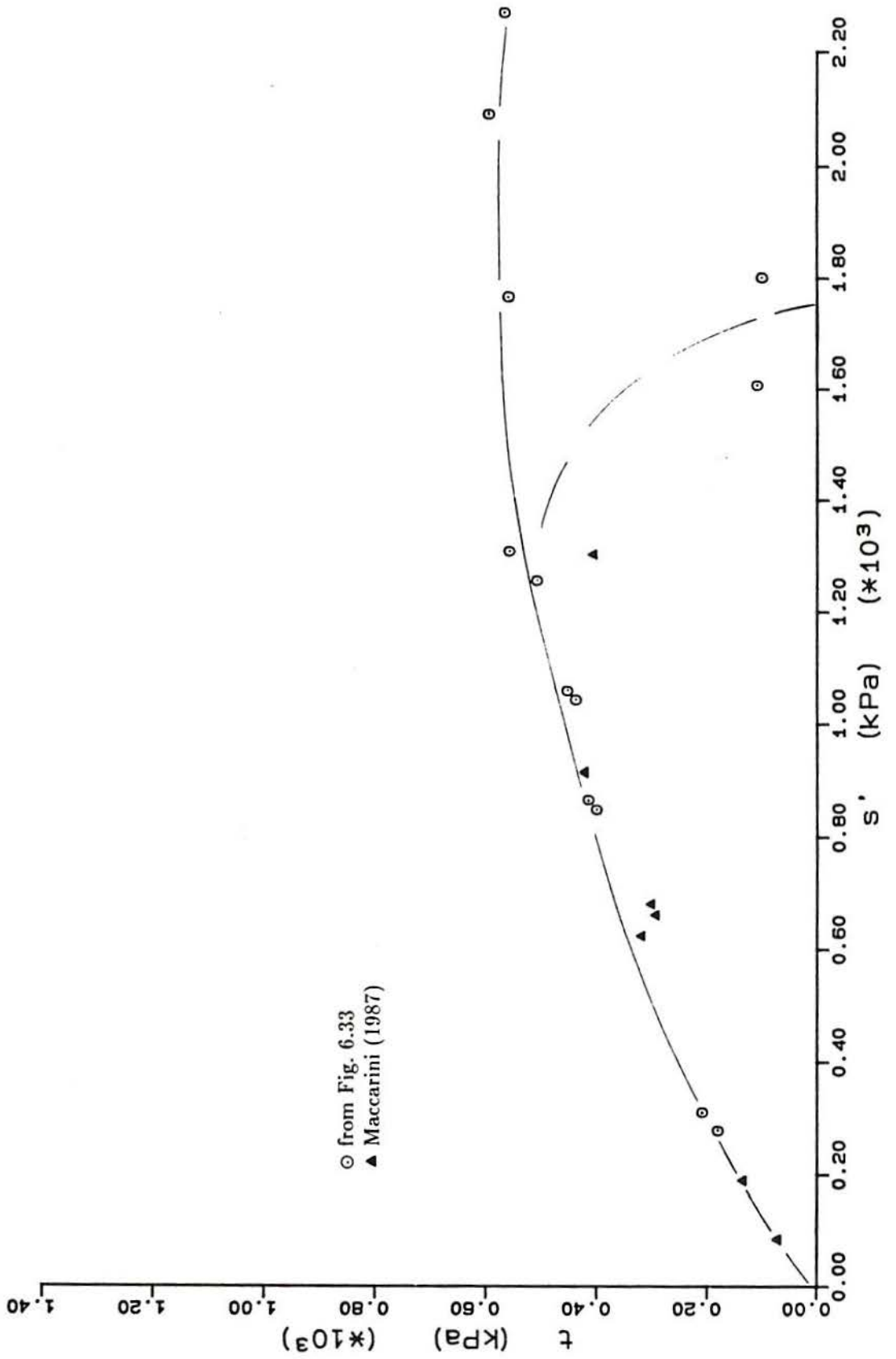

Figure 6.34 – Yield points of artificial soil of initial void ratio $\simeq$ 1.1

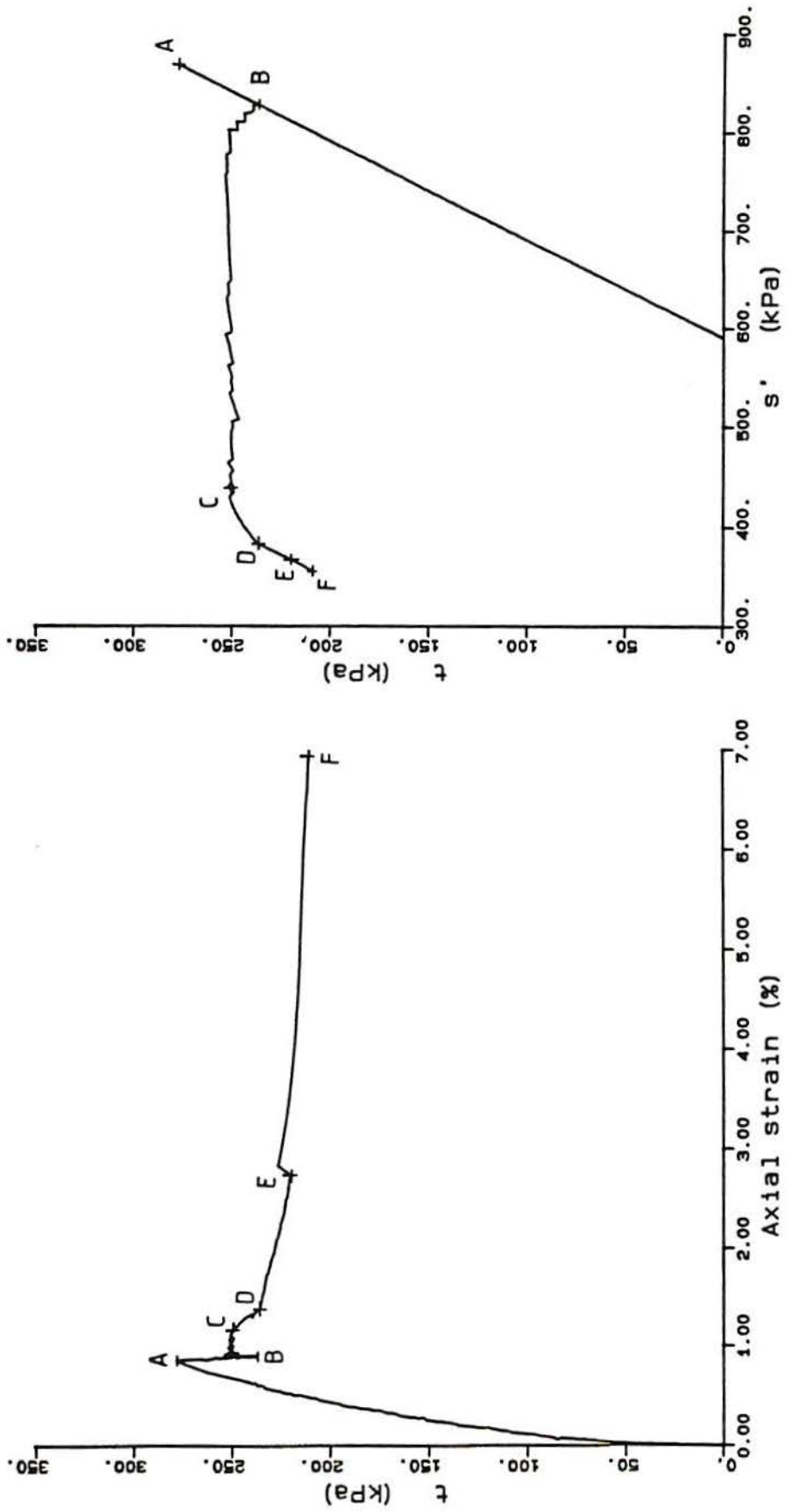

Figure 6.35 – Stress-path and deviator stress versus axial strain results of test 204 (constant t and reducing s′)

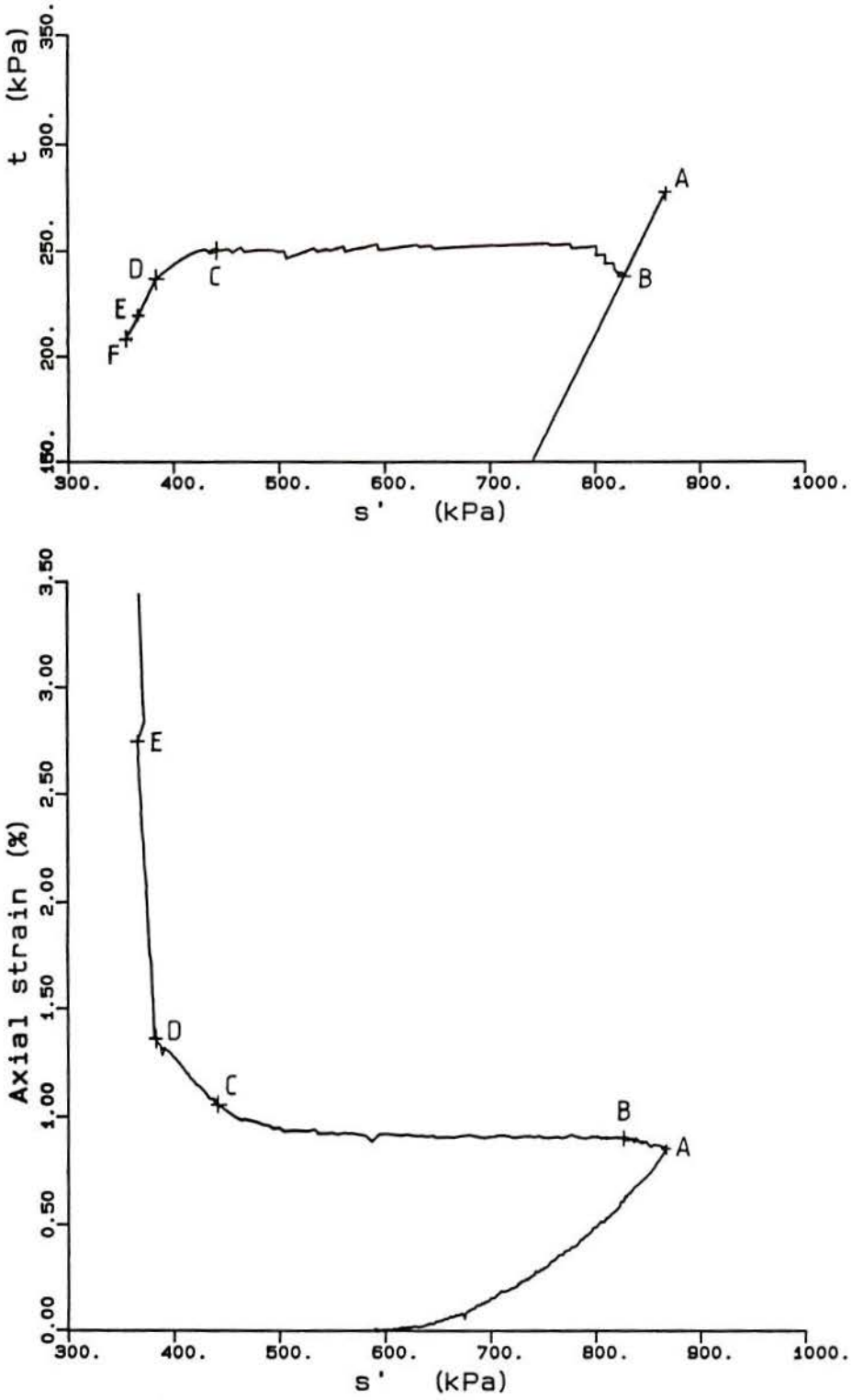

Figure 6.36 – Stress-path and average stress versus axial strain results of test 204 (constant t and reducing s')

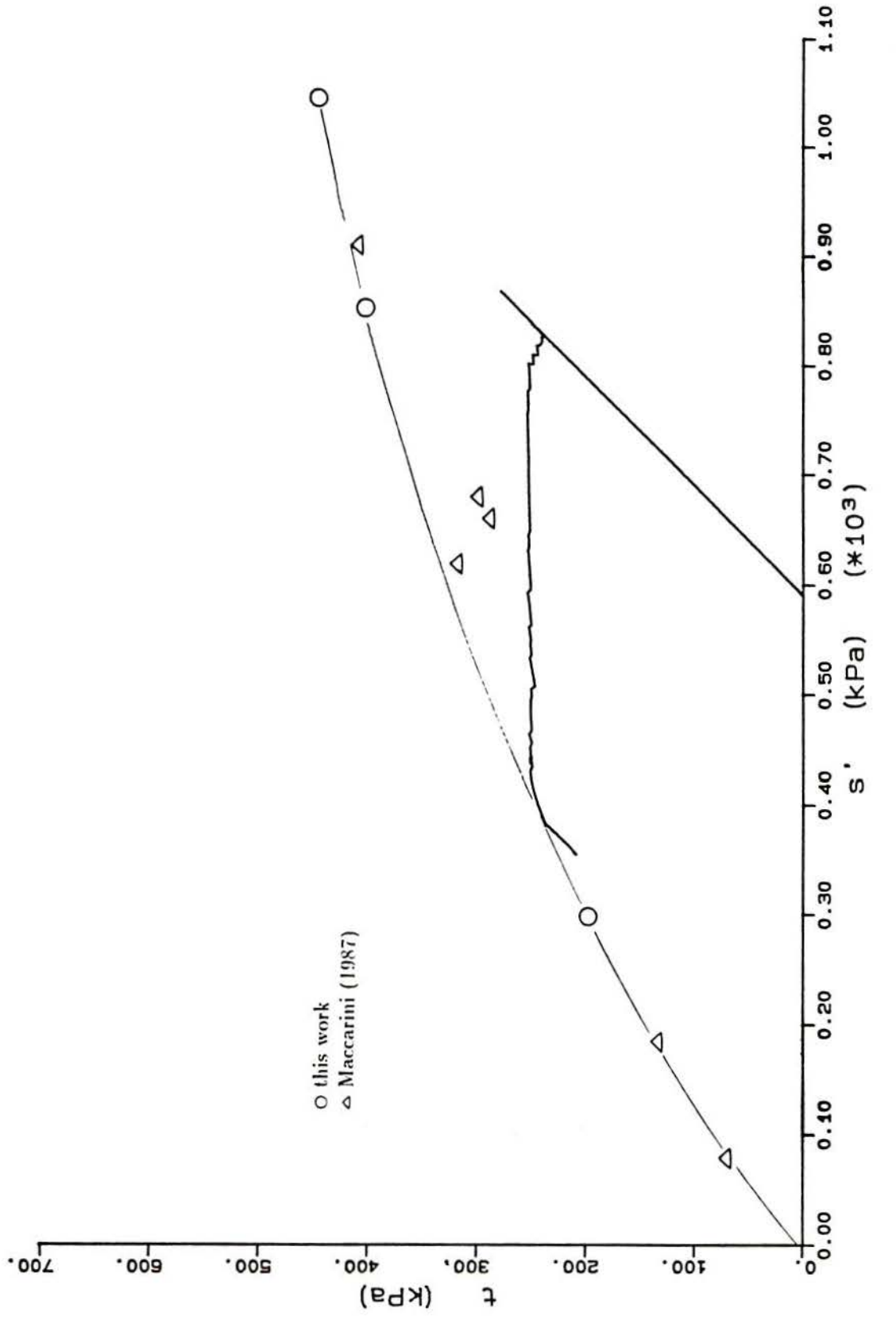

Figure 6.37 - Comparison between the yield curve obtained from drained compression tests and test 204 (*a*) $s' \leq 1000$kPa; (cont.)

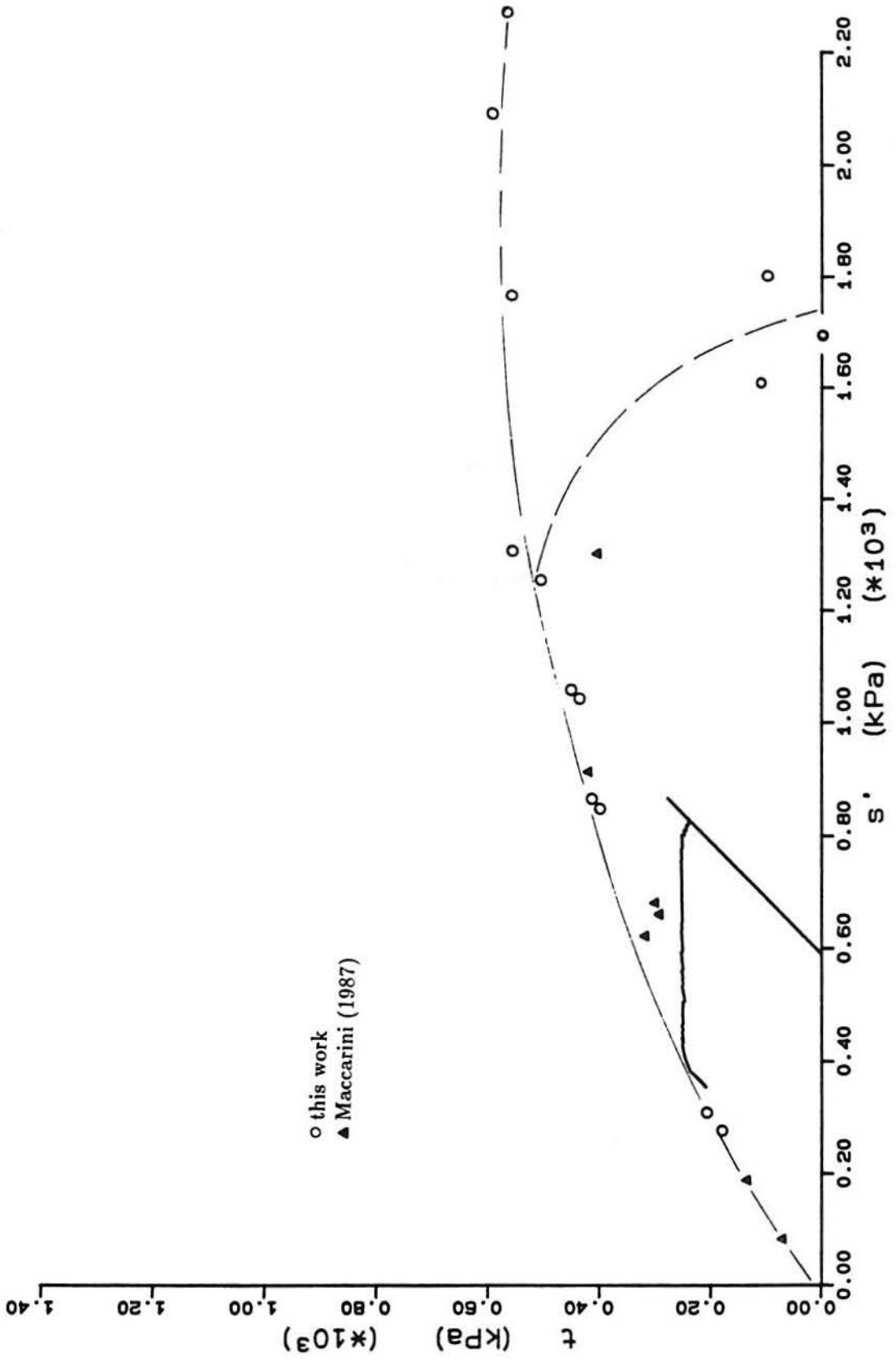

Figure 6.37 – (cont.) (*b*) complete range of results

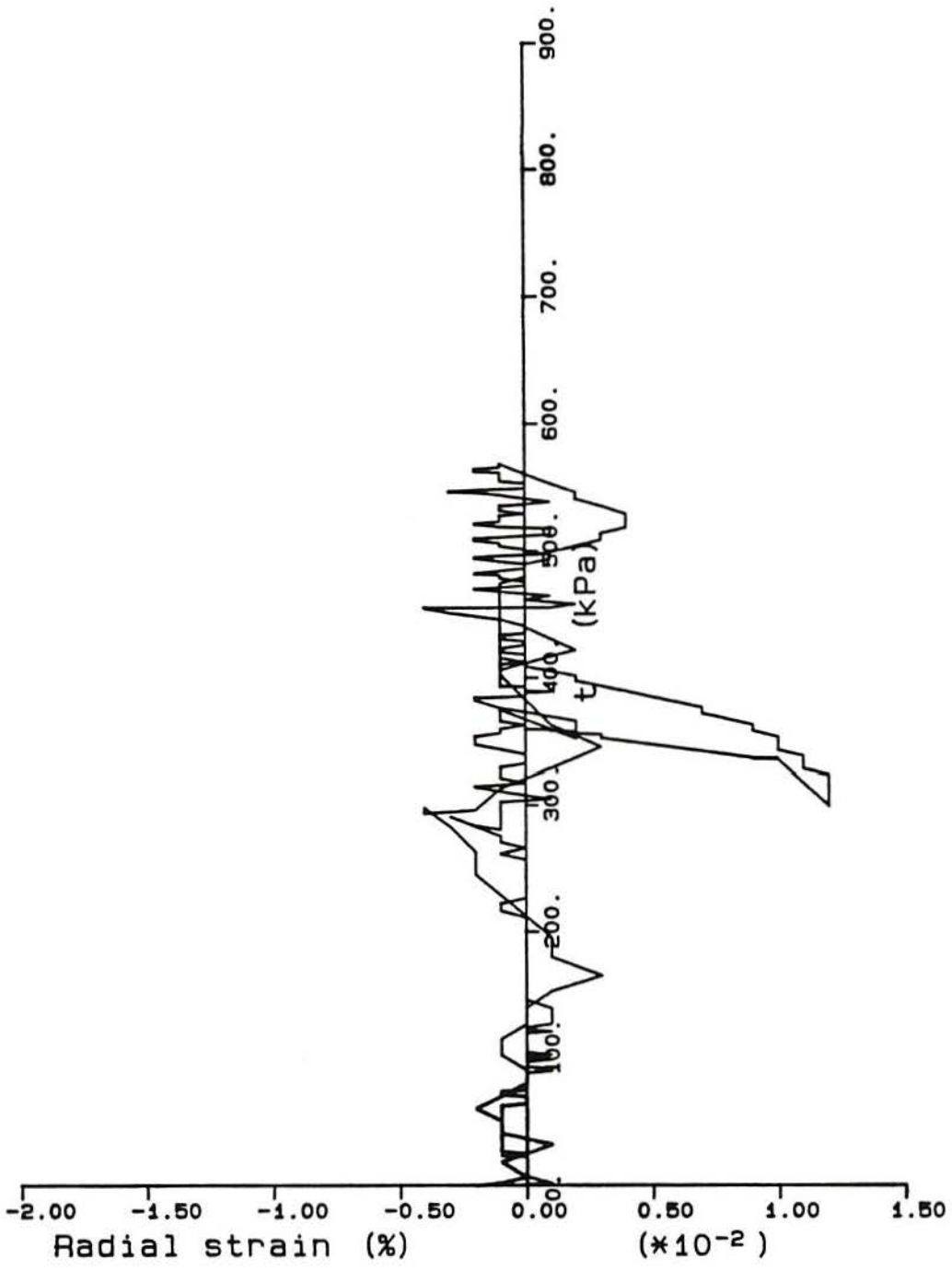

Figure 6.38 - Radial strain oscillation during test 212, one-dimensional compression (scale 0.005%)

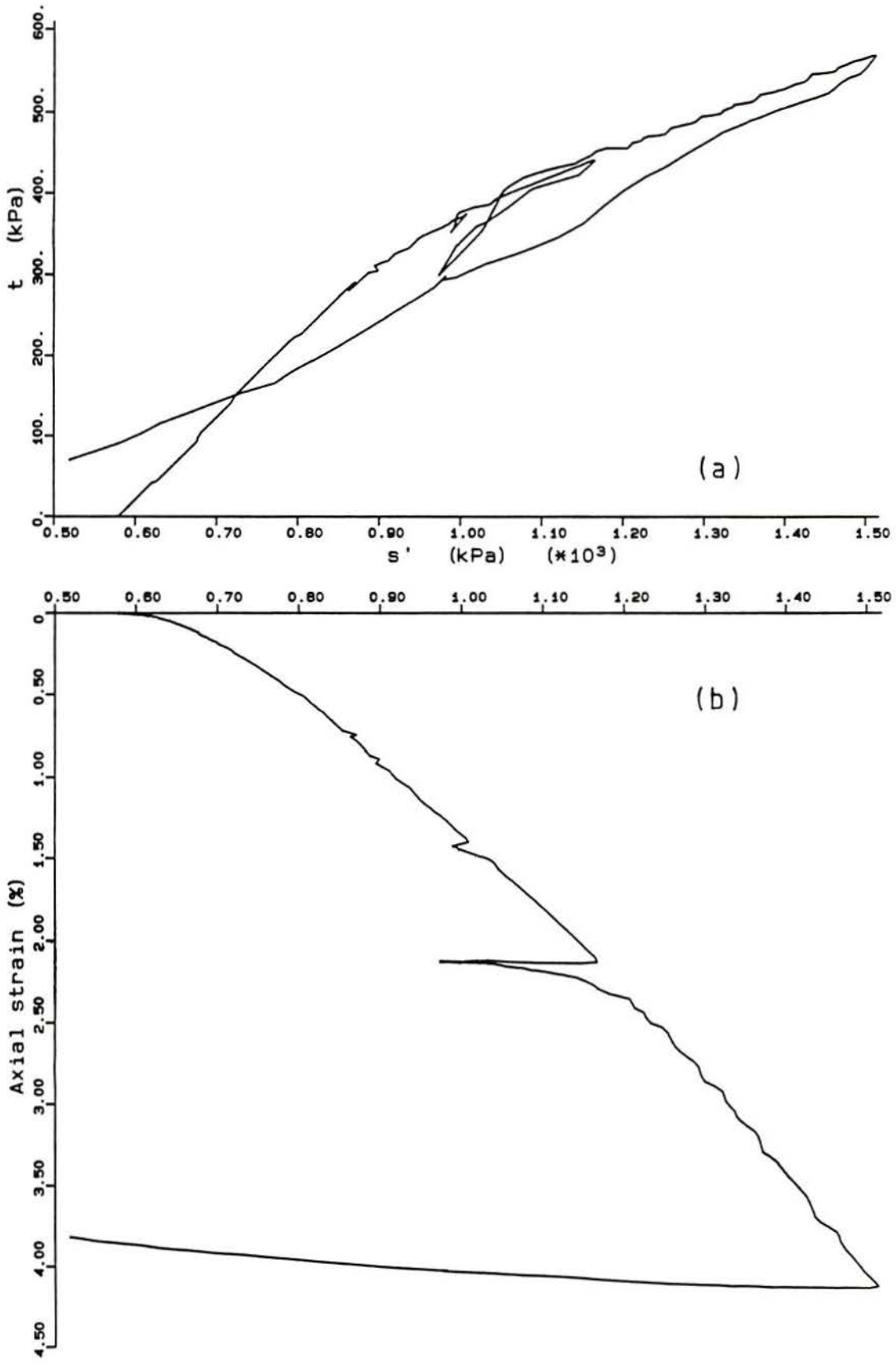

Figure 6.39 – Results of one-dimensional compression test, sample 212. (*a*) stress-path; (*b*) average stress versus axial strain

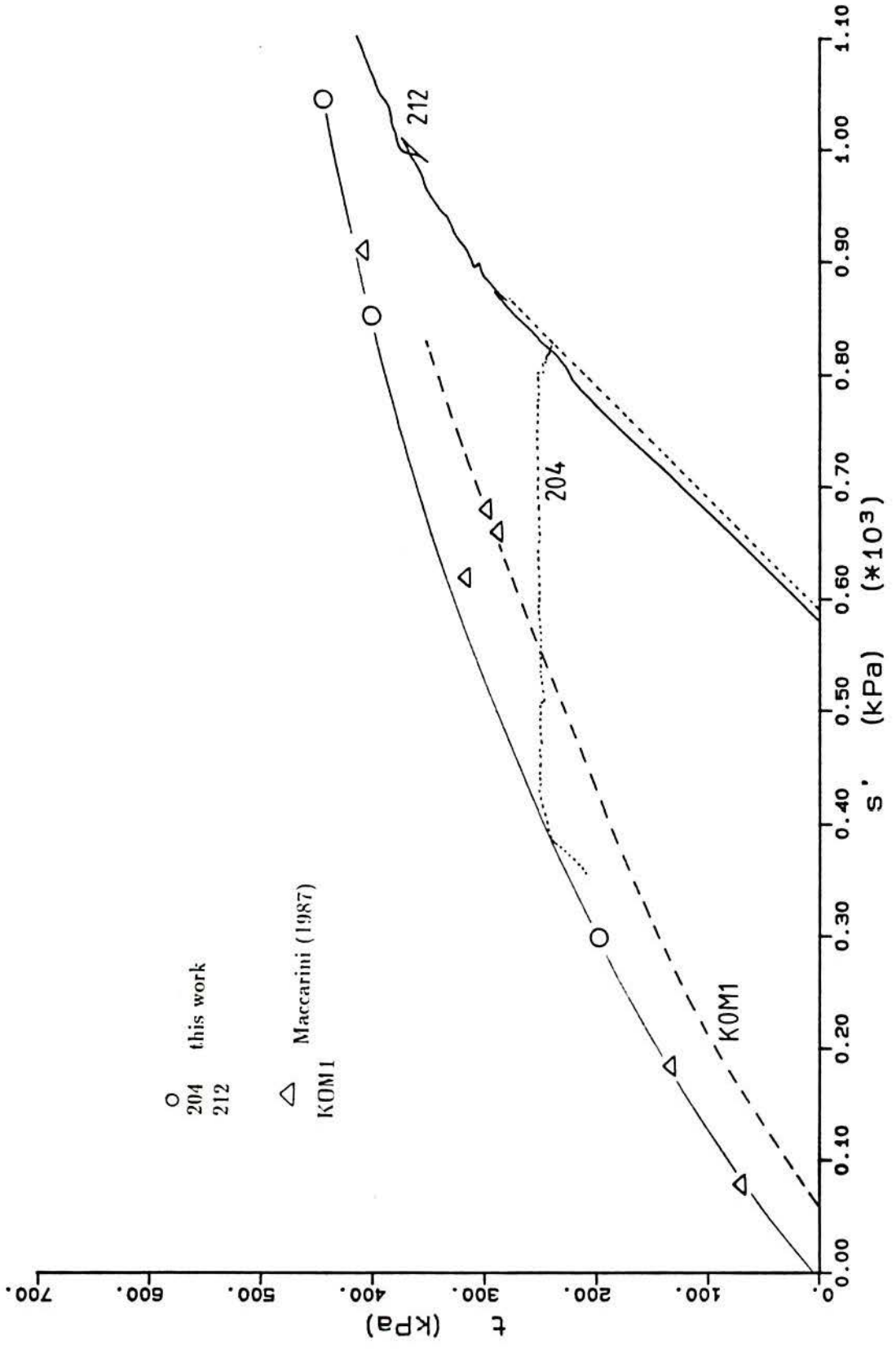

Figure 6.40 - Comparison of one-dimensional compression tests and yield line. (*a*) lower stress region; (cont.)

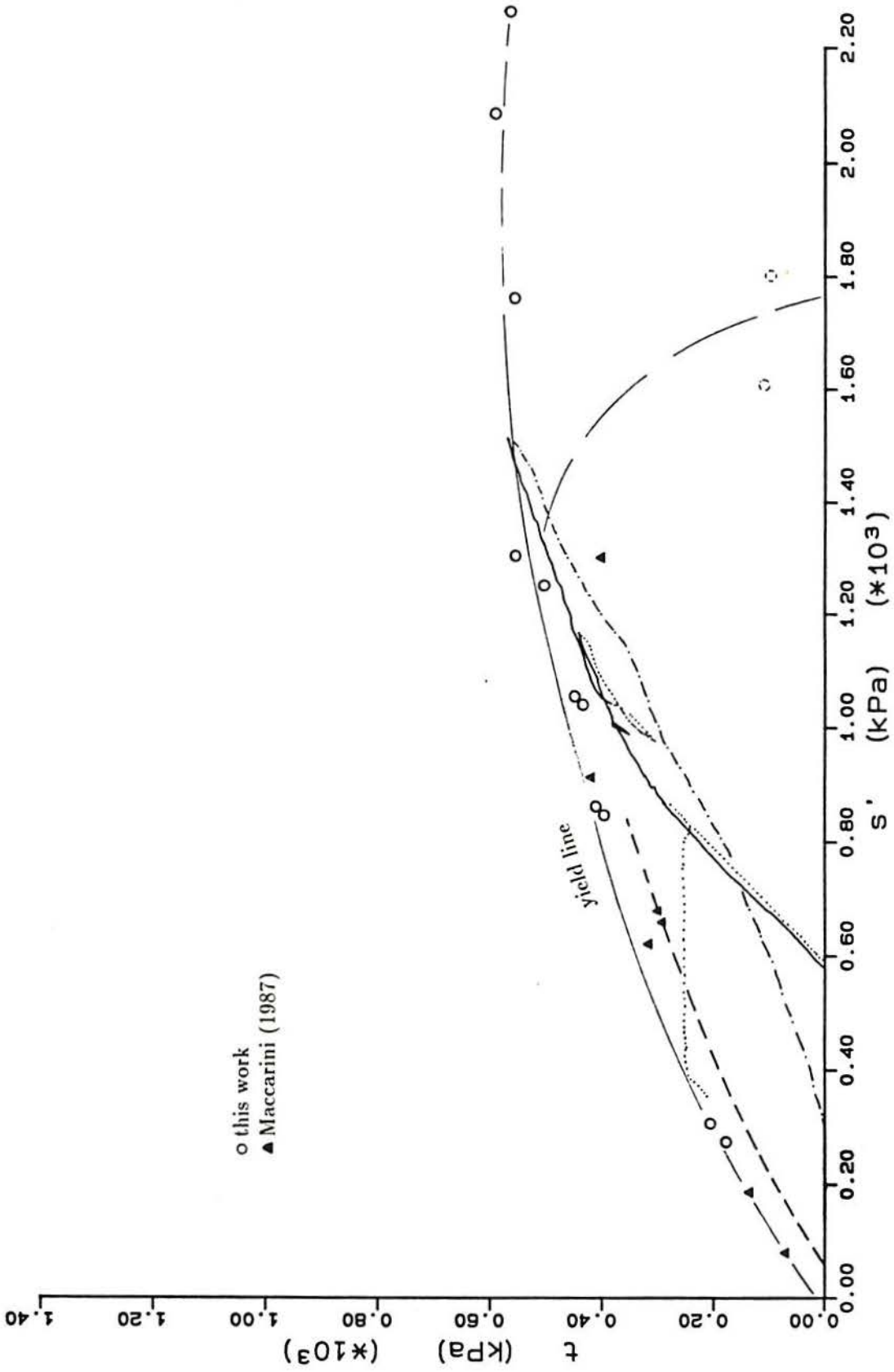

Figure 6.40 – (cont.) (*b*) higher stress region

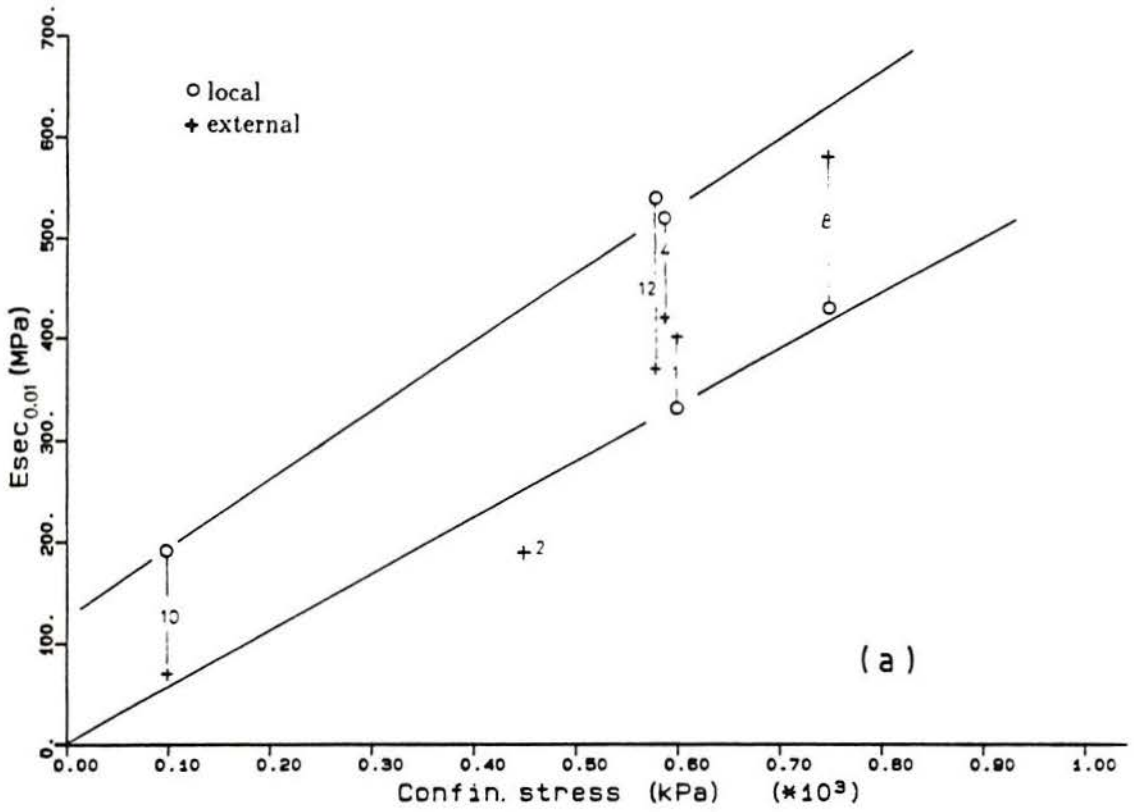

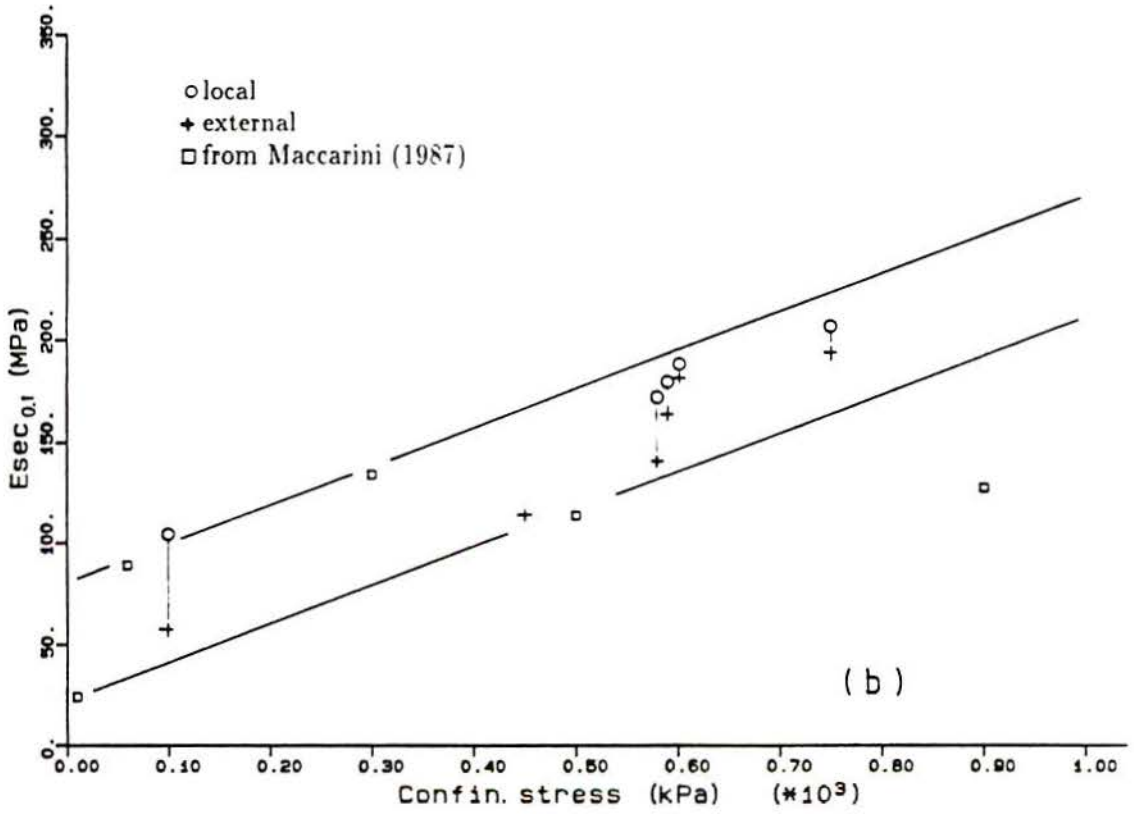

Figure 6.41 - Secant stiffness versus confining pressures up to 1000 kPa. (*a*) at 0.01%; (*b*) at 0.1%

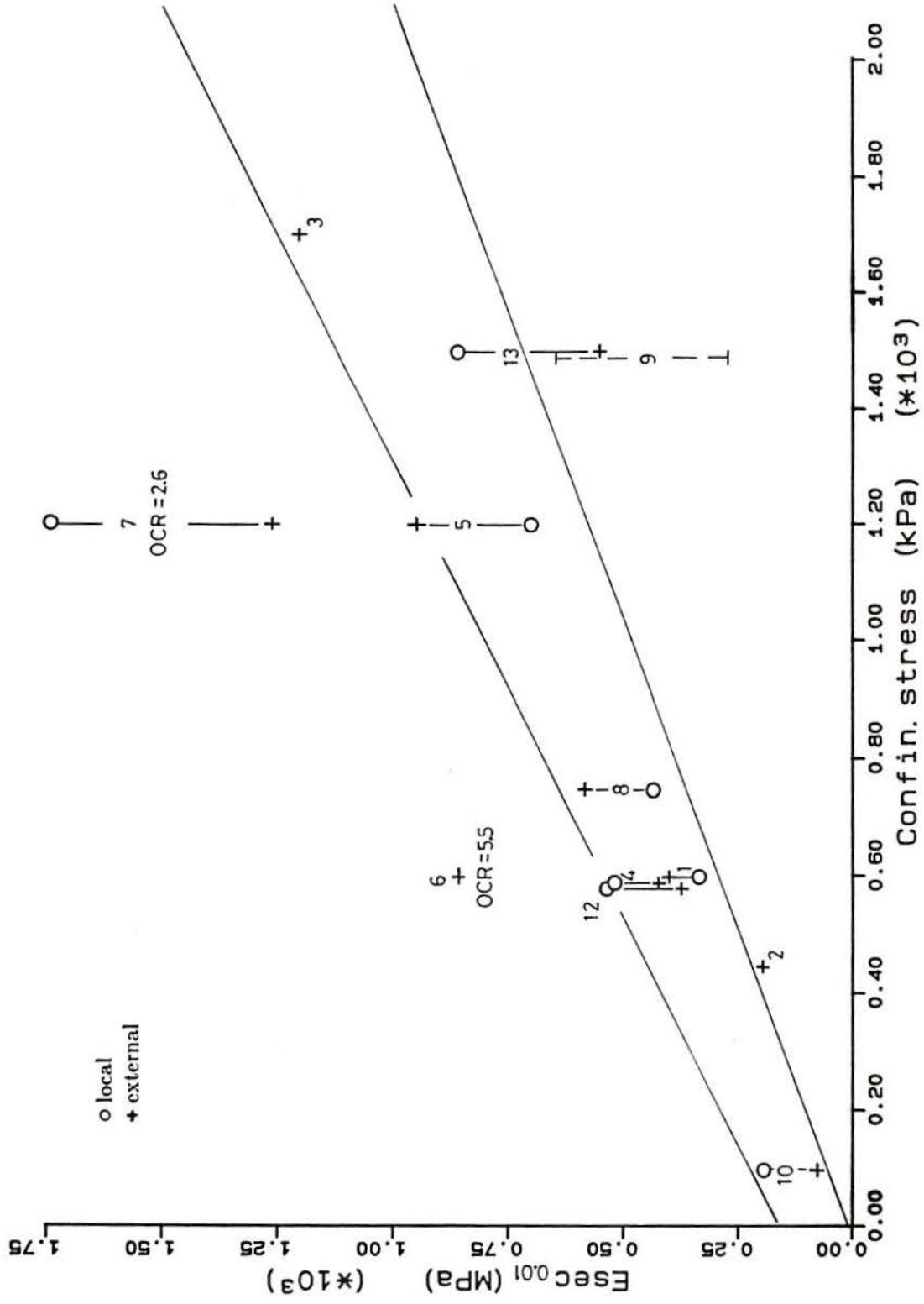

Figure 6.42 – Secant stiffness at 0.01% axial strain versus confining pressure - all tests

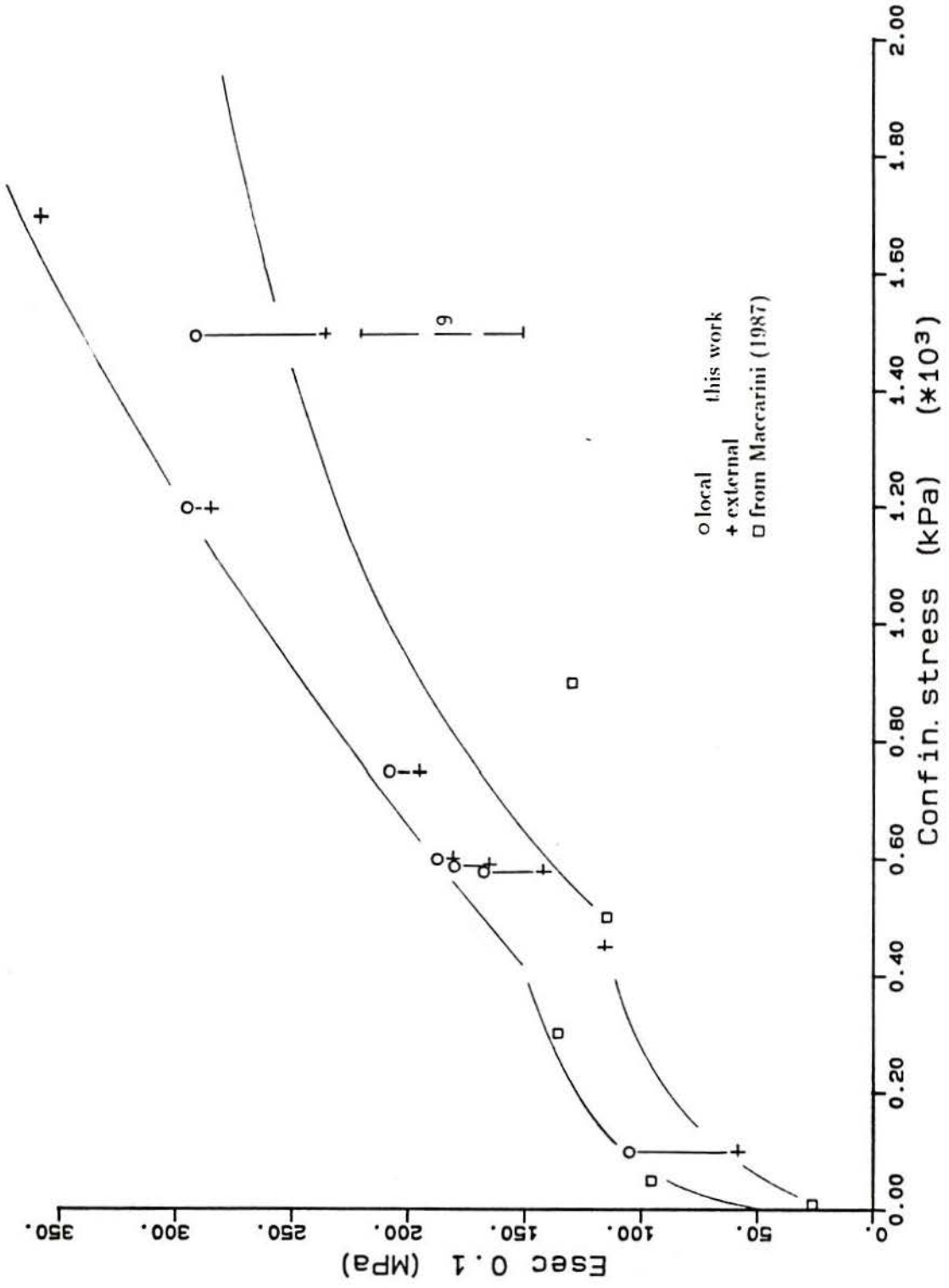

Figure 6.43 – Secant stiffness at 0.1% axial strain versus confining pressure - normally consolidated tests plus results calculated from Maccarini (1987) data

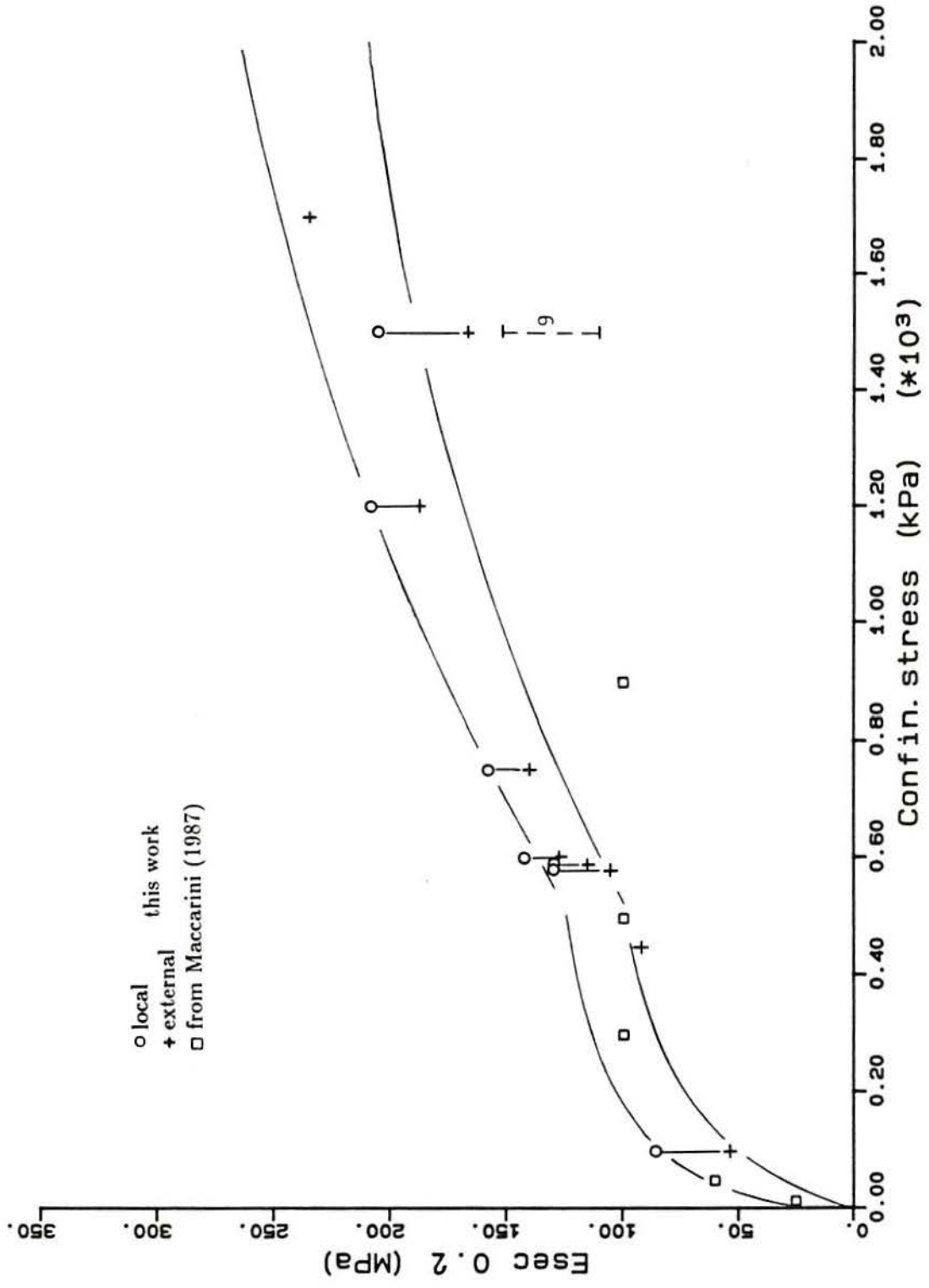

Figure 6.44 – Secant stiffness at 0.2% axial strain versus confining pressure - normally consolidated tests plus results calculated from Maccarini (1987) data

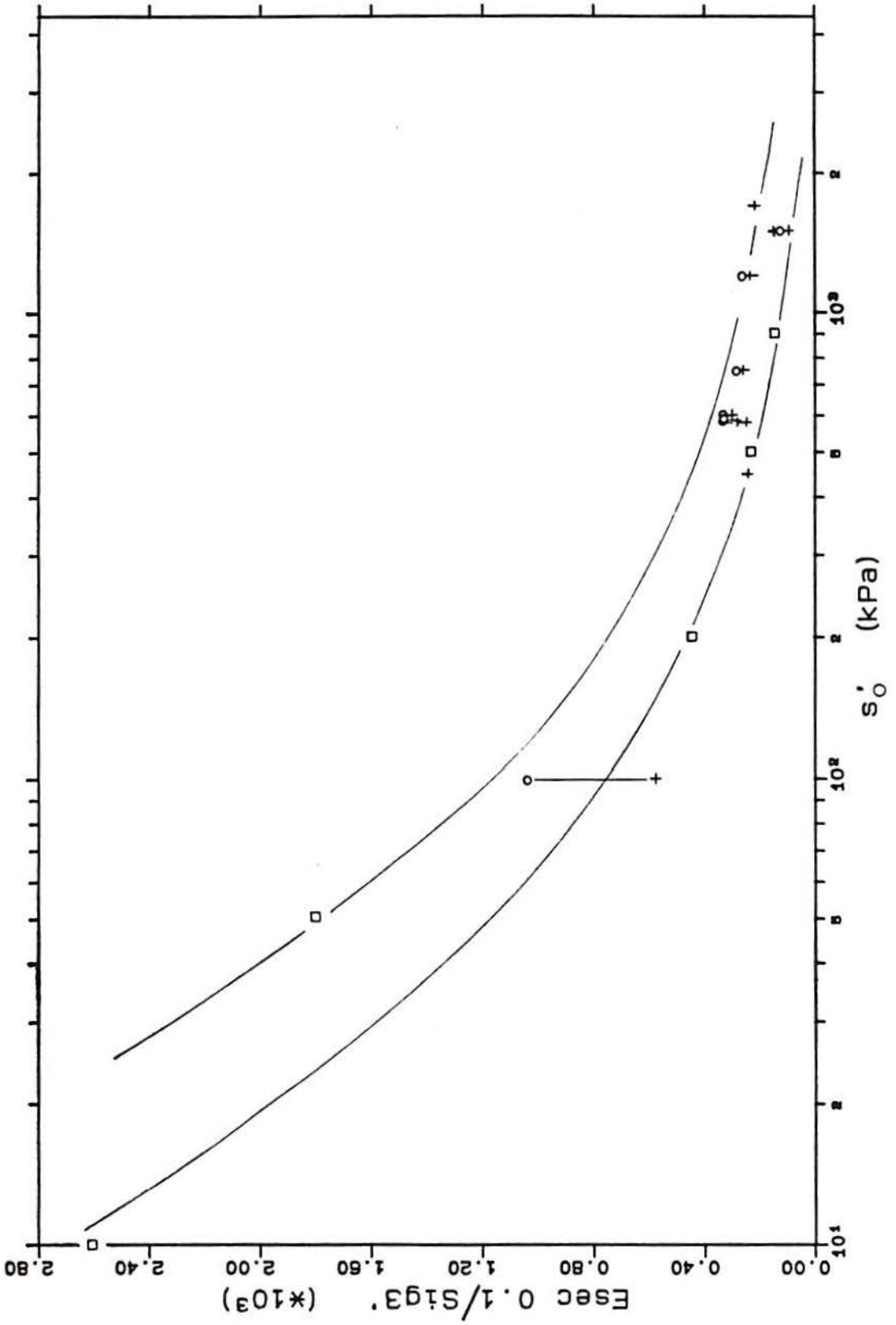

Figure 6.45 – Normalized stiffness versus the logarithm of average initial pressure

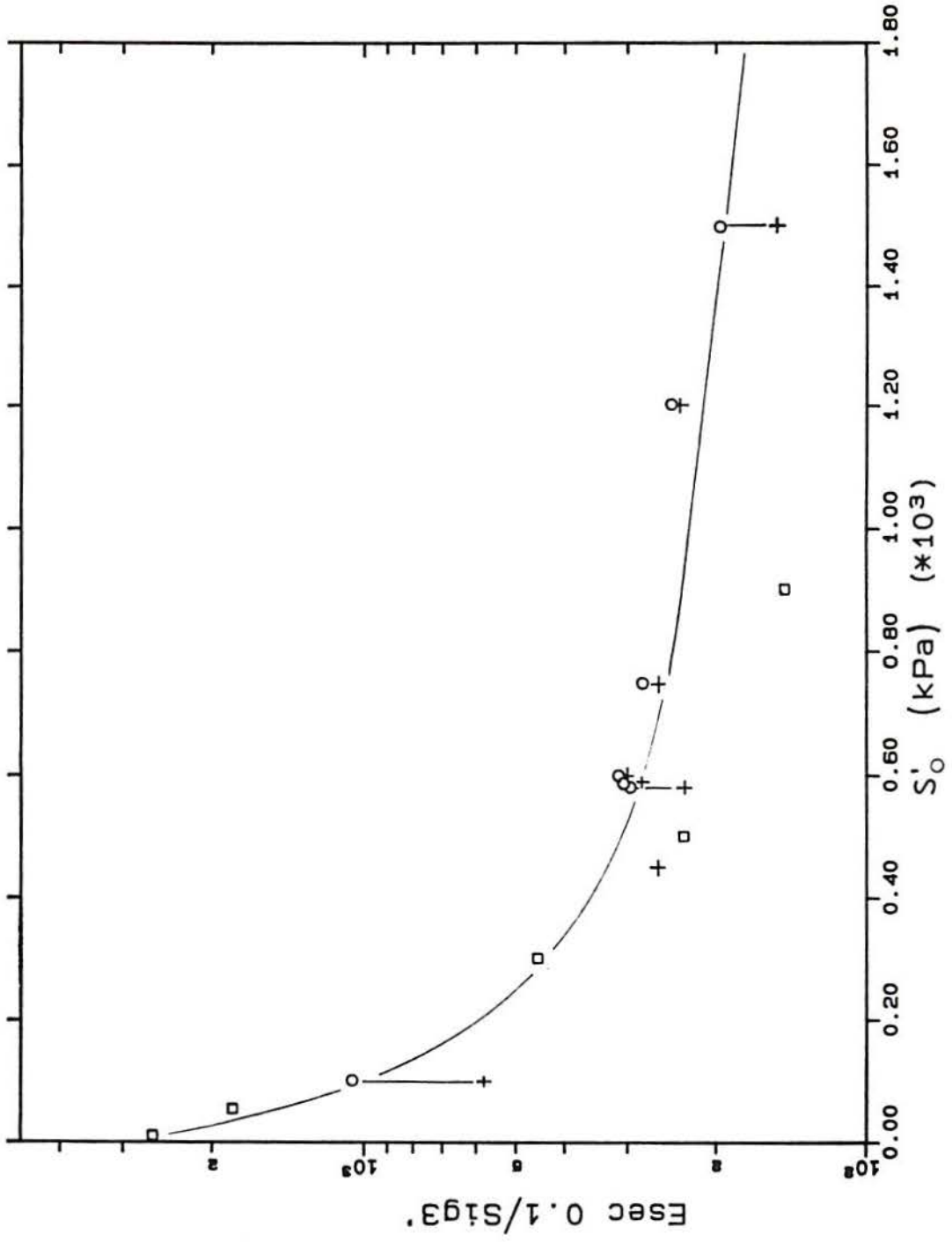

Figure 6.46 – Logarithm of normalized stiffness versus the average initial pressure

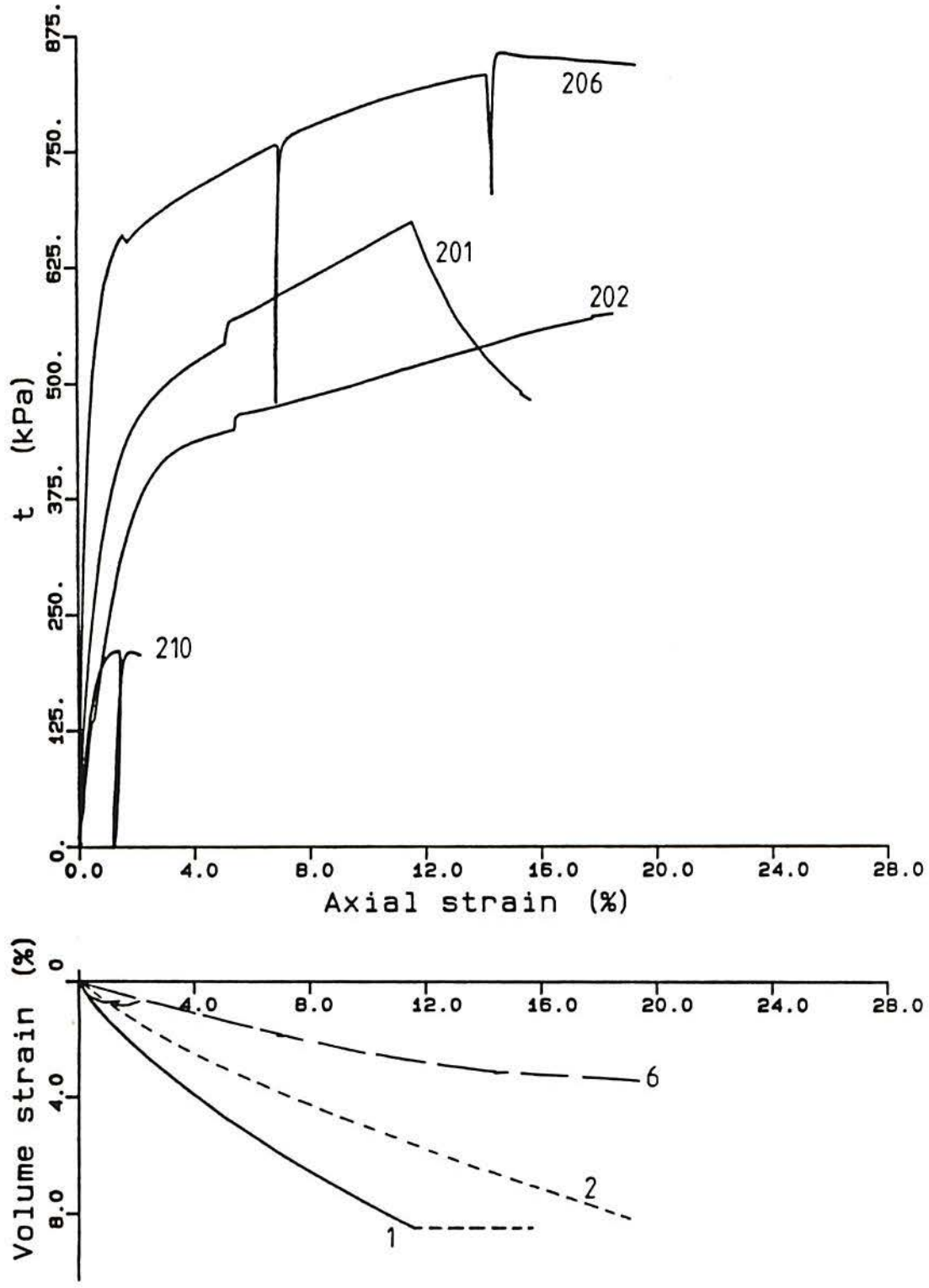

Figure 6.47 - Complete test results carried out on samples 201 (drained/undrained), 202, 206 and 210

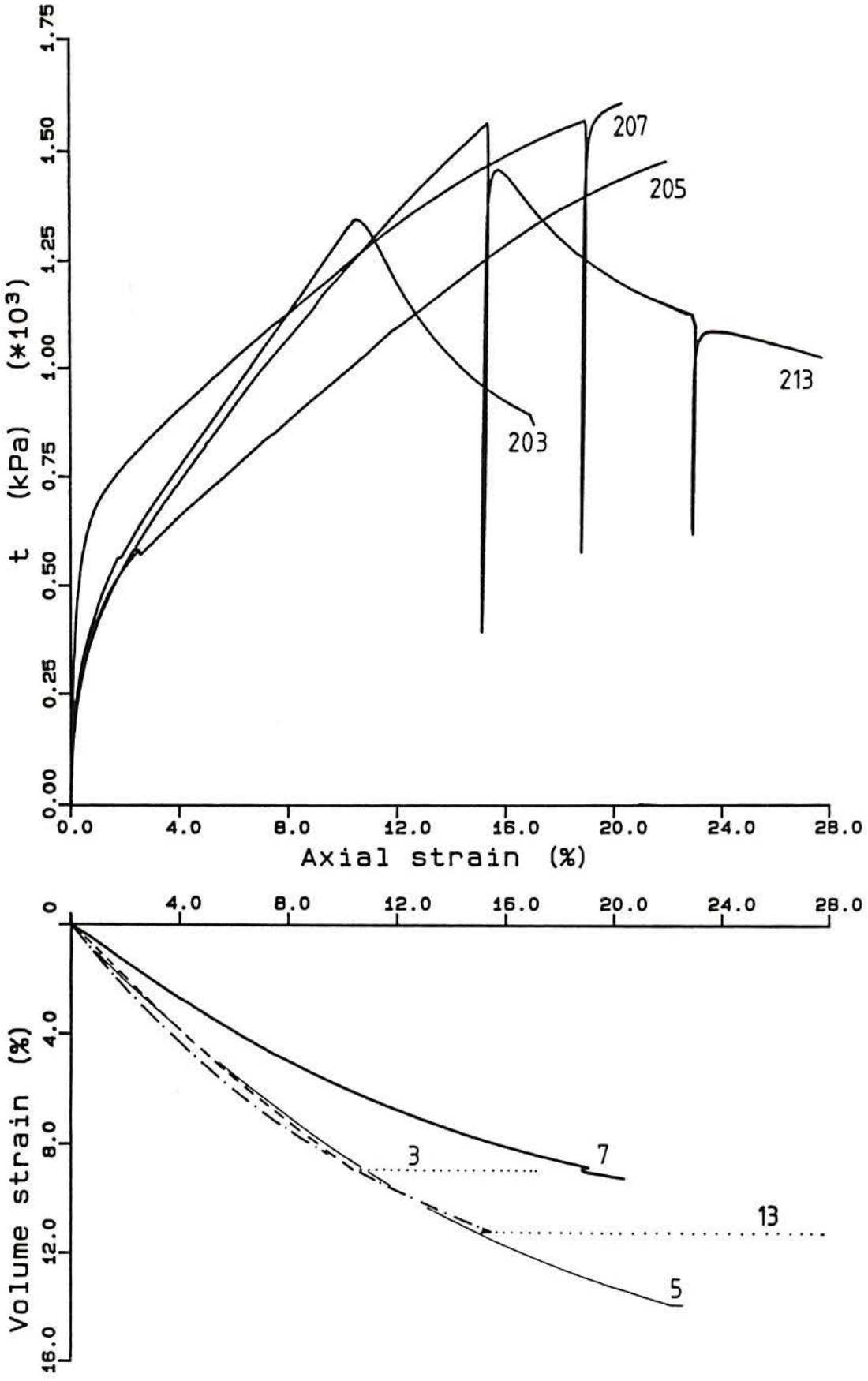

Figure 6.48 – Complete test results carried out on samples 203 and 213 (drained/undrained), 205 and 207

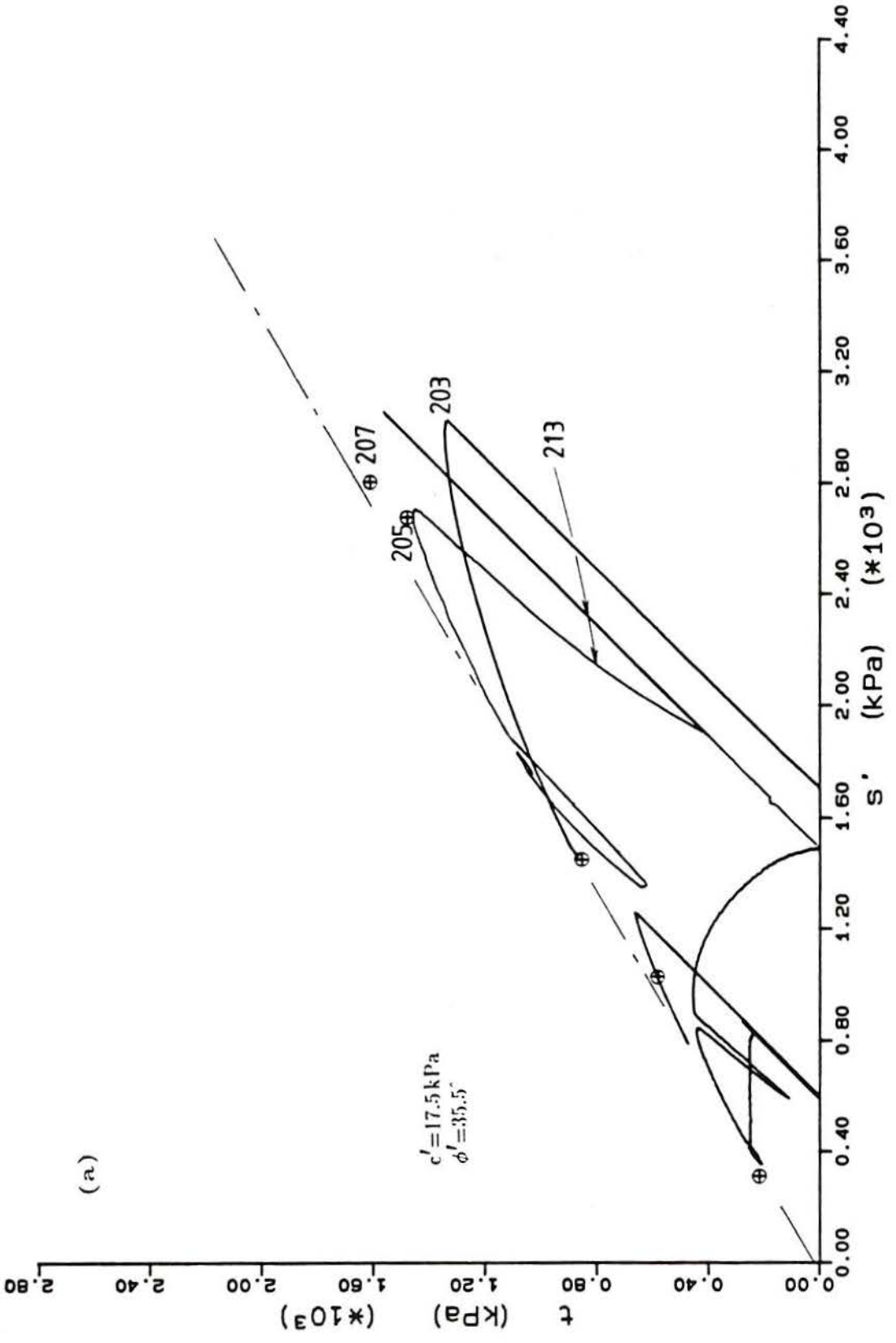

Figure 6.49 – Failure envelope and stress-paths of tests on artificial soil (*a*) the complete set: (cont.)

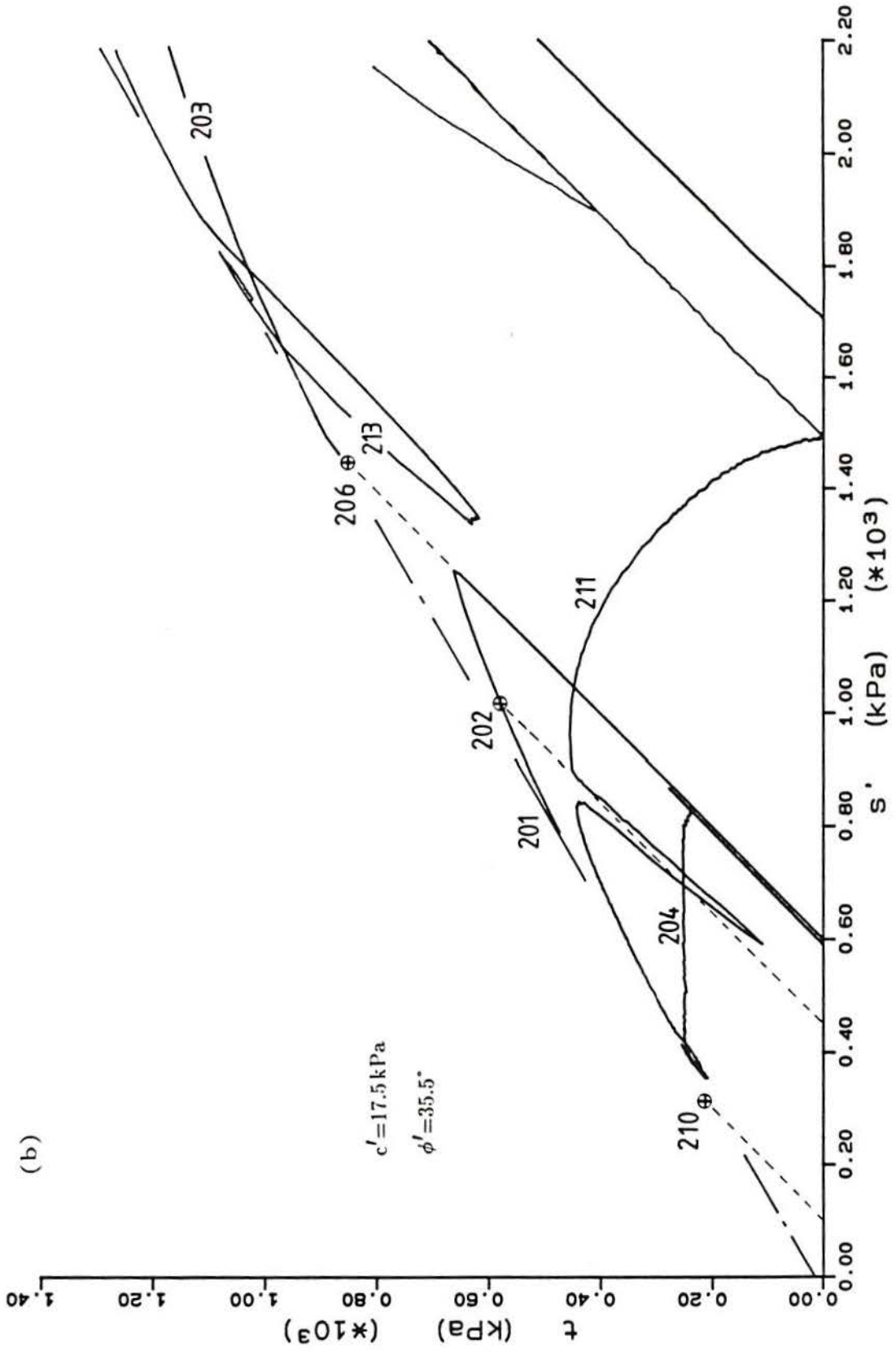

Figure 6.49 – (cont.) (*b*) low pressures region

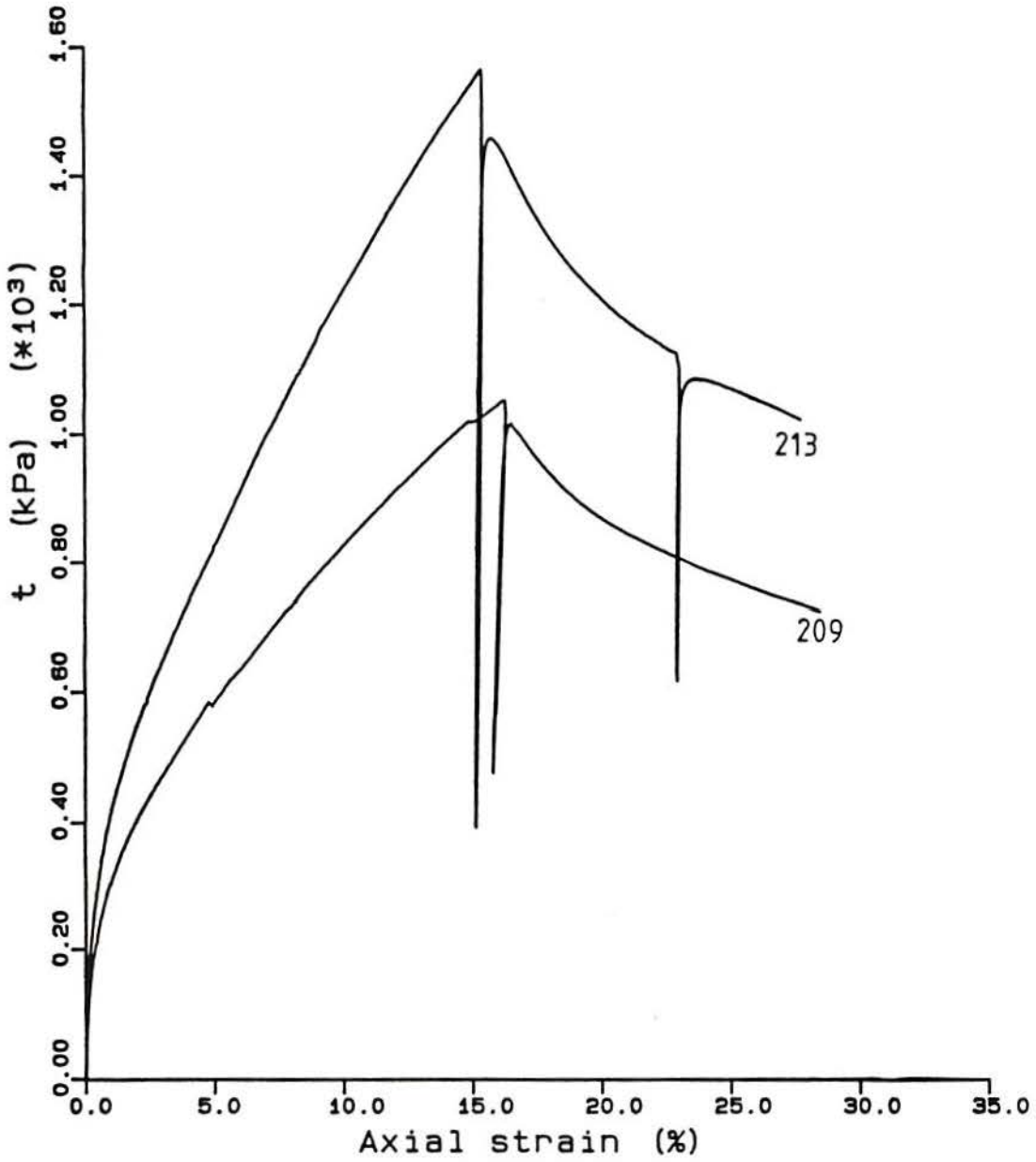

Figure 6.50 - Comparison between two tests initially consolidated at 1500 kPa

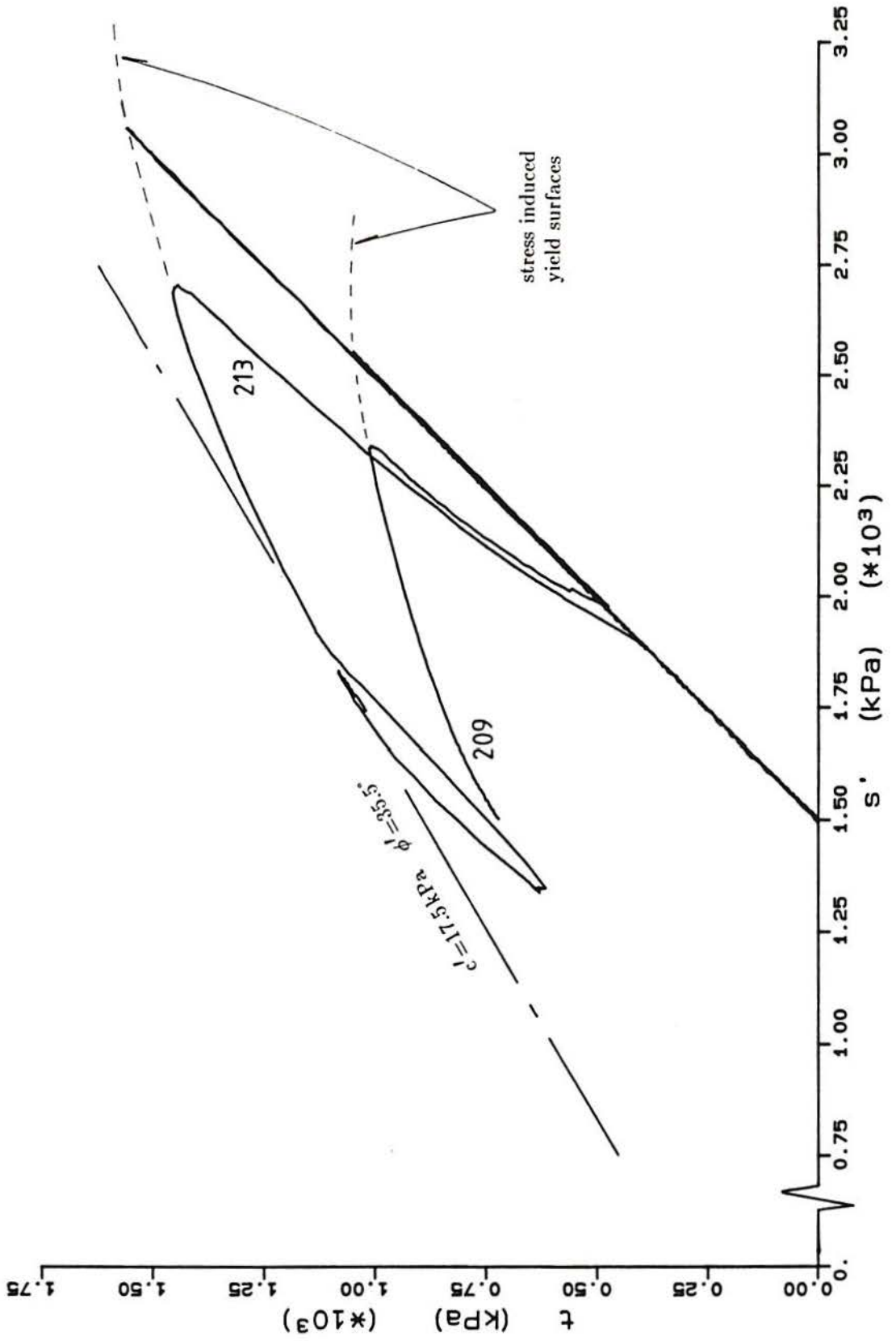

Figure 6.51 – Stress-paths of two tests initially consolidated at 1500 kPa

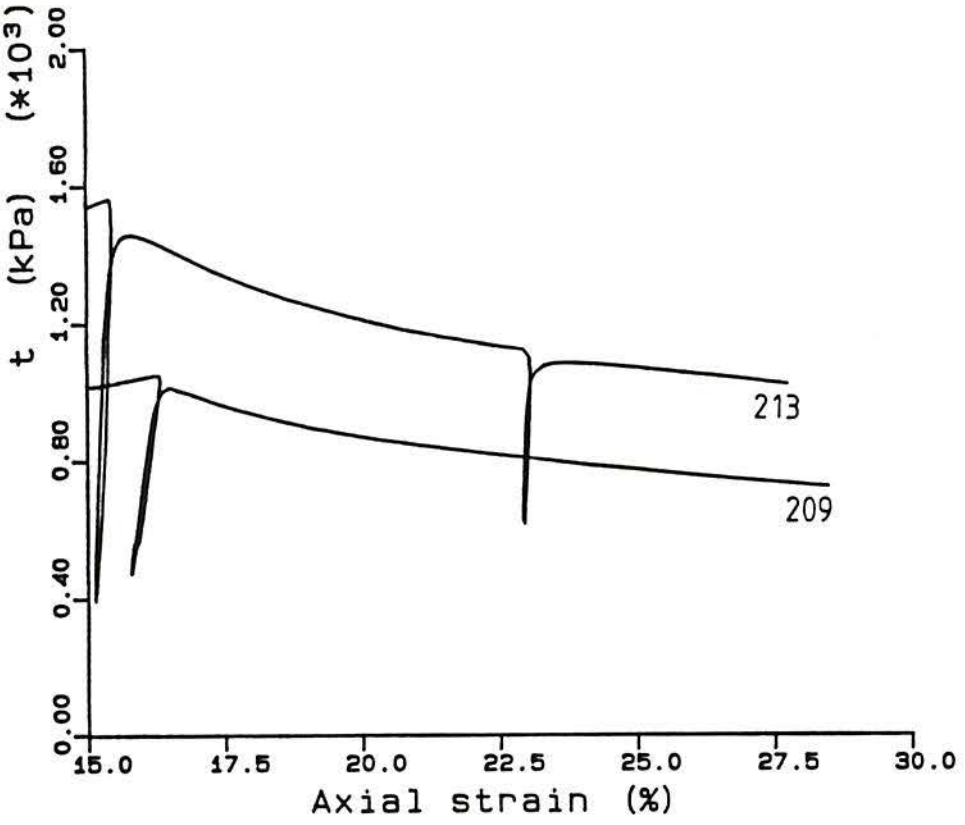

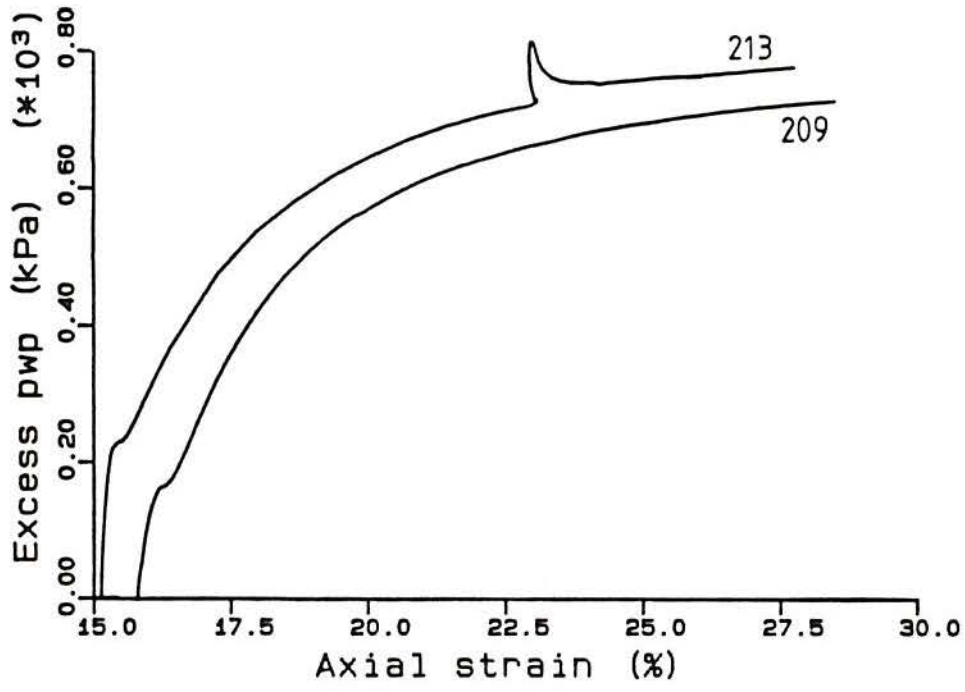

Figure 6.52 - Comparison of the undrained portions of tests 209 and 213

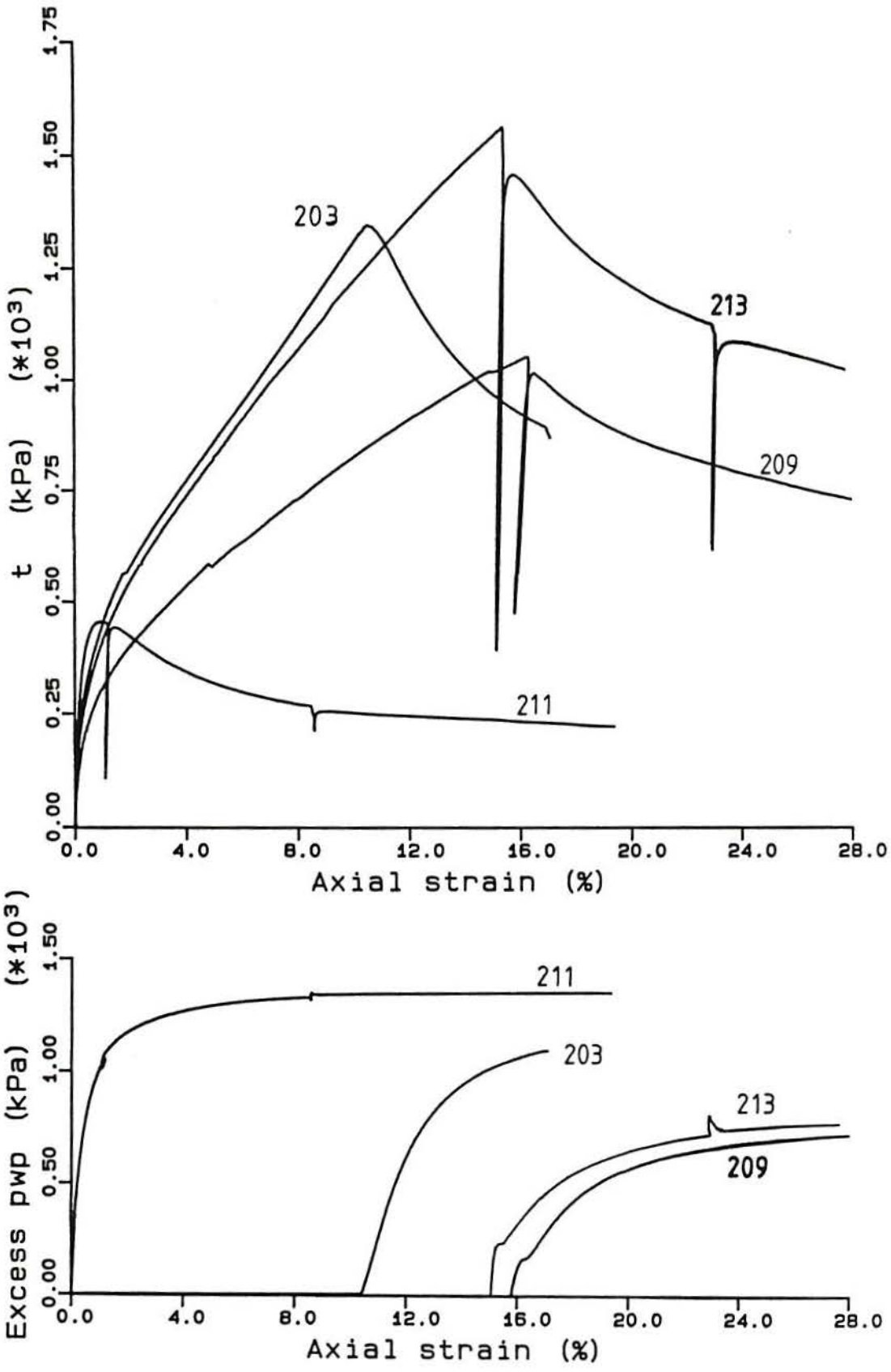

Figure 6.53 – Results of undrained (or partially undrained) tests

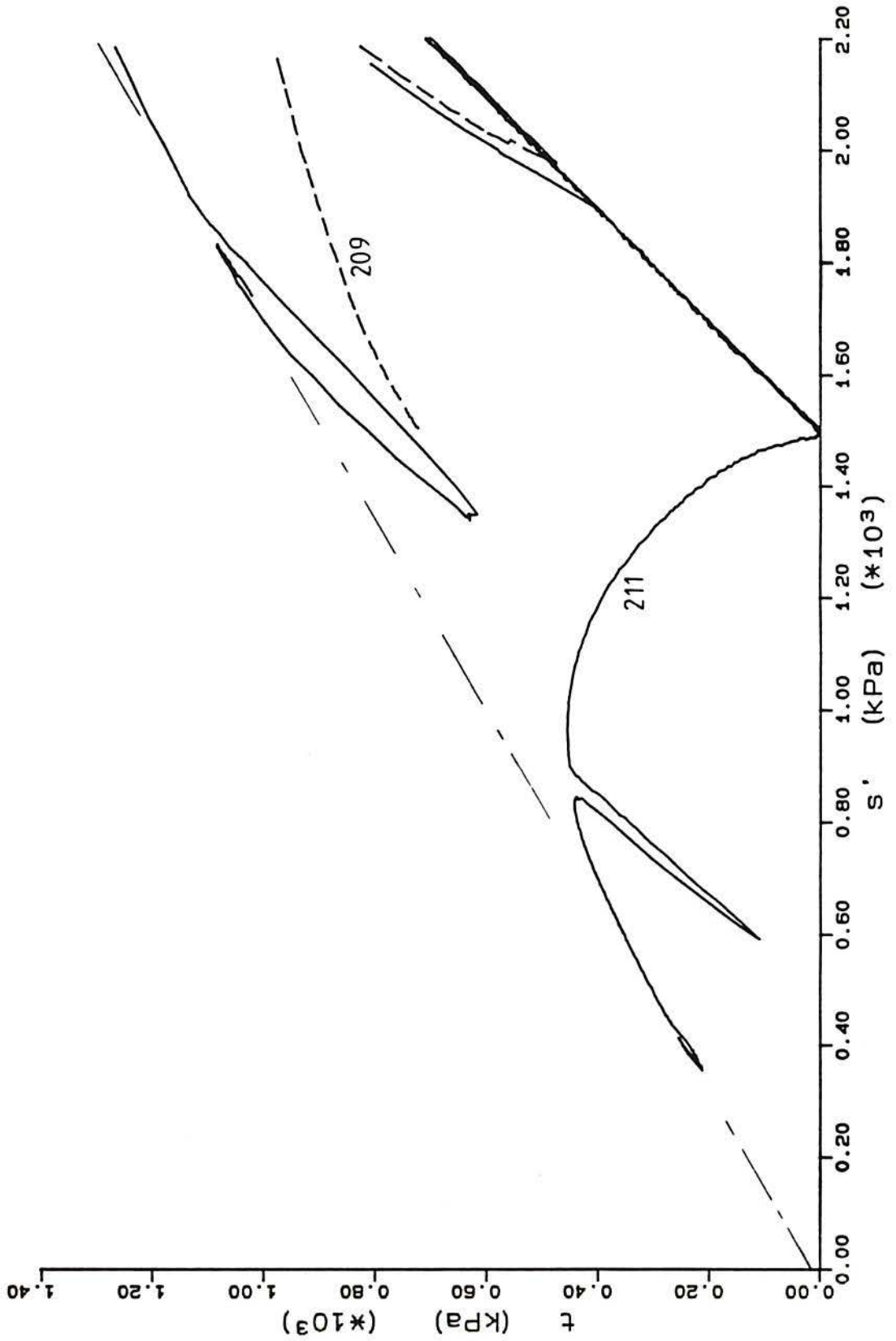

Figure 6.54 - Stress-paths of tests 209, 211 and 213

7. ARTIFICIAL BONDED SOIL – COMPLEMENTARY SERIES AND COMPARATIVE STUDY

7.1 INTRODUCTION

This chapter describes tests made on three different mixtures of artificial soil. One mixture had no quartz sand (300 series), other had no CFK (00 series) and another had a stronger bonding (600 series). The purpose for these changes was to investigate the influence of each factor and throw some light on how the factors interact.

An investigation of the structural arrangement is attempted with the use of micro-photographs taken on an electron microscope.

7.2 ARTIFICIAL SOIL 00 SERIES

This series was used during the preliminary study described in Chapter 4 and provided some useful results. The soil was composed of 13% of kaolin (bonding) and 87% of quartz sand (no CFK fraction is included). All samples were fired at 500°C for 5 hours.

The samples were saturated using the dry vacuum method and they were loaded using the guided top cap and loading button arrangement. Sample 22, however was loaded with the conventional arrangement.

The initial void ratio of the nine samples (Table 7.1) was close to 0.64 and they were isotropically consolidated before shearing. Test CIU1 was the only sample sheared undrained from the start.

7.2.1 Review of previous work

Fig. 7.1 presents the stress paths followed in the undrained tests carried out on soil 130087 by Maccarini (1987). The dotted line represents the result of a test on a remoulded soil with a similar intergranular void ratio. The peak values obtained from drained triaxial compression tests are also presented (open circles). The void ratio was close to 0.71 (see Appendix 1 for details).

The failure line defined by the remoulded test is very close to a straight line passing through the origin with ϕ'=32.5°. The peak strengths of the undrained and drained tests on the undisturbed soil lay well above this line in the range of 0 to 800 kPa. After the peak the stress path of the undrained tests tends to drop to the failure line defined by the remoulded sample. An examination of drained stress-strain curves (Maccarini, 1987) shows that they also tend to the same envelope after their peak. These tests were carried out without local strain measurement and hence no data on stiffness is available.

7.2.2 Triaxial test results – shearing strength

The tests only covered the normal range of stresses used in soil mechanics (σ'_3<1000 kPa, Table 7.1). Fig. 7.2 presents a summary of the test results. Only one of the four tests carried out at 60 kPa is presented. The dotted section of test 27 (500 kPa) represents the likely behaviour because no data was recorded during that period. All tests were sheared at a rate of 1%/h until the peak was well defined.

The axial and volumetric strain results for these tests are presented on Fig. 7.3 and 7.4. For the purpose of comparison test 25 has been presented on both plots. Four tests were carried out at 60 kPa (tests 21 to 24) as a continuation to the preliminary series (Chapter 4). Test 22 was carried out without the guided top cap to examine its influence on the stiffness behaviour. Initially all the samples suffered considerable compression, the onset of dilation being almost coincident with the peak strength.

The failure points of the tests are plotted together in Fig. 7.5(a) and (b). The full

circles represent the peak strength obtained on the drained tests and the crosses indicate the strength at the end of the tests (tests 25 and 27).

The failure line which passes through the origin agrees with the peak strength of test 28 and with the strength at the end of tests 25 and 27. This line is the same as that obtained on the remoulded soil by Maccarini (1987) (see Fig. 7.1, $c'=0$, $\phi'=32.5^{\circ}$). The peak strength envelope is curved up to $s'=900$-1000 kPa, after which it appears to be defined by the straight line just referred to. The curved envelope of Fig. 7.1 has also been indicated. At pressures up to 500 kPa it agrees well with the test results but for higher pressures it drops slightly below.

There are three special tests worthy of mentioning. Test 26 was carried out as a normal compression drained test up to t=220 kPa. It was subsequently unloaded laterally whilst maintaining a constant deviator stress. Failure occurred close to the previously defined envelope. Tests 21 and 24 were carried out as normal drained tests up to their peak strength (see Fig. 7.3). Once the peak had been well defined, the effective confining stress was increased to 170 kPa and 245 kPa respectively. Test 21 proceeded undrained from then on and test 24 was sheared drained until it once again showed signs of failure at which point the drainage was closed. The resulting stress-paths are presented in Fig. 7.5 and the corresponding stress-strain and pore pressure curves are given in Fig. 7.6. The interesting point about these stress paths is that they define very well the shear envelope of the soil. The undrained test carried out from an isotropic stress of 60 kPa (CIU1) is also presented in Fig. 7.5 (dotted line). The stress path of the test was initially curved to the left (positive pore pressure) and then gradually moved up and to the right, with failure occurring close to the curved failure envelope. The sample exhibited a vertical shear plane.

7.2.3 Triaxial test results – stiffness measurements

Values of secant stiffness were calculated from the local measurements of axial strain for all tests, except CIU1. The results of these calculations at 0.1% axial strain are plotted versus the initial confining stress in Fig. 7.7. The stiffness at 0.1% axial strain was chosen because at

that strain its determination is not so sensitive to oscillations in the transducers output or the choice of axial strain origin. All of the tests were drained at that strain. The stiffnesses calculated from external measurements showed a similar pattern but were typically 20 to 30% less than the locally measured values. The results in Fig. 7.7 suggest an increase in stiffness with increasing confining pressure, the rate of increase dropping above 300 kPa. At 60 kPa there is some scatter with a few samples showing an upward concave stress-strain curve. As this was locally measured it is believed to have been caused by the closure of small internal fissures.

A plot of the normalized stiffness versus the confining pressure is approximately linear when plotted on a vertical log scale (Fig. 7.8).

7.3 ARTIFICIAL SOIL 600 SERIES

The 600 series consisted of only four samples of artificial soil fired at 800°C for 3 hours. Apart from the higher firing temperature, and associated higher bonding strength, the soil is similar to 200 series in composition and void ratio (e=1.1).

Table 7.2 contains the main physical characteristics of the samples and the instrumentation used during the tests. All of the samples were saturated using the dry vacuum method.

7.3.1 Triaxial test results – shear strength

The results of axial strain and deviator stress are shown in Fig. 7.9. All of these tests were initially sheared under drained conditions. Two were later sheared under undrained conditions (601 and 602). Test 604 was the only sample which showed dilatancy but its peak strength occurred at a time of almost no dilation. This was the only sample in the series to have a visible shear plane passing through the middle of the sample (62° to 65° to the

horizontal). The tests carried out at higher confining stresses underwent compression throughout the test. Test 603, which was performed with an effective confining stress of 2300 kPa, did not seem to have approached the failure line and was still showing a steep increase in stress with strain at the end of the test.

The undrained stress paths of tests 601 and 602 are shown in Fig. 7.10(a) and (b) together with the maximum shear strength of test 604. The yield points are indicated as circles. The failure envelope found for 200 series is also shown. The undrained stress path of test 601 (σ'=750 kPa) agrees very well with the results of 200 series but test 602 (σ'_3=1510 kPa) lies well below it even after considerable axial straining.

7.3.2 Triaxial test results – stiffness measurements

The four samples were tested using the guided top cap and both local and external corrected axial strain measurements were used to calculate the stiffness at various strain levels. The resulting plot of stiffness variation versus the initial confining pressure is presented in Fig. 7.11. The two lines relate to the stiffnesses calculated from measurements made locally (open circles) and from those made externally (crosses). The behaviour seems well defined with both sets of results having a similar trend. It is apparent that there is a large increase in stiffness for confining pressures below about 750 kPa and that after this it drops slightly.

7.4 ARTIFICIAL SOIL 300 SERIES

Five samples in this series were tested in triaxial compression. The only sand used in this artificial soil was crushed fired kaolin fired at 500°C, instead of the usual 1000°C. No quartz was included in the mixture. The preparation procedure was the same as for the previous series except that the amount of water was increased and more kaolin was added (16% by weight). The increase in the quantity of water was required to obtain a mixture with a

similar consistency. All samples were again saturated using the dry vacuum method. The main characteristics of the five samples are presented in Table 7.3.

7.4.1 Triaxial test results – shear strength and yield

All of the results in this series are presented in Fig. 7.12. The tests were carried out fully drained and the rate of strain was initially 1%/h. Following an unloading sequence tests 302 and 303 were sheared at a faster rate (5%/h) on reloading. All samples showed compression during shear except test 302 which underwent a small post peak dilation. This sample together with samples 304 and 305 had a visible shear plane.

The samples would seem to have been strained far enough to reach their ultimate strength since their stress-strain plots appear to have stabilized. The maximum peak strength of each of these tests is shown as a full circle on the stress plot of Fig. 7.13. An interesting failure envelope appears to define the shear strength for this series. For s' smaller than about 900 kPa, the strength is close to that defined for the 200 series (c'=17.5 kPa, ϕ'=35.5°). However, for larger pressures this strength drops dramatically. Tests 305 and 301 (σ'_3=500 kPa and 750 kPa, respectively) are on the threshold between the two failure envelopes. Test 303 (σ'_3=1200 kPa) had a clear indication of ultimate failure being reached (Fig. 7.12) and it lies on a lower failure line. A line passing through the origin with ϕ'=22.5° (indicated in Fig. 7.13) may represent the de-structured material 300.

The analysis of the results presented in Fig. 7.12 gives no indication of any obvious yield points and hence log-log plots were produced as shown in Fig. 7.14(a) and (b), to help in their identification. Tests 301 and 305 showed bi-linear behaviour with a yield value of t close to 40 kPa. Test 305 also showed another change of linearity at t=560 kPa. For tests 302 and 304 only the failure or near failure stress appears to deviate from an otherwise straight line. Test 303 on the other hand showed a very concave initial curve and an irregular shape thereafter, the drop in stress at around 90 kPa being very noticeable at the time (a loud noise and the load dropped quickly).

If a yield point were to be selected for each test it would be almost coincident with the failure load for tests 302 and 304. Tests 301 and 305 showed a near bi-linear behaviour in the region close to 3-4%, with values of 400 kPa and 560 kPa respectively for the yield stresses. Test 303 showed a disturbance at small load (100 kPa) and tests 301 and 305 showed also what could be called an initial yield. The three most evident points were plotted in Fig. 7.13 and a speculative dotted line drawn through them. Although it seems clear that more points are required to define the surface better, its general form and agreement with the change in strength behaviour is encouraging.

7.4.2 Triaxial test results – stiffness measurements

These artificial soil samples had different characteristics in comparison to the others because they do not have the hard grains of quartz. The resulting surface of the trimmed samples was much more regular since the trimming wire was capable of cutting the grains. This led to a reduction in the errors associated with the sample roughness and the external stiffness can be relied upon with more certainty. The results of secant stiffness from local and external measurements at 0.1% axial strain are presented in Fig. 7.15. The stiffness seems to have a very small increase with increasing pressure up to 500 kPa followed by a drop in value at larger pressures. The external measurements show the same general trend but with a larger variation on both sides of the peak.

7.5 COMPARATIVE STUDIES

The testing of different soil compositions, different firing temperatures (bonding strength) and void ratio provides an opportunity to compare the effect of some of these factors on the soil behaviour. As described before, in some samples the weaker grains (CFK) were eliminated (00 series), whereas in others the strong quartz grains were not present (300 series)

and in one series the bonding strength was increased (600 series). Their behaviour is compared below.

7.5.1 Shear strength and yield stresses

The failure envelopes obtained during this work are presented in Fig. 7.16. These envelopes are related to 200 and 600 series (line a), 00 series (line b) and 300 series (line c). The results of 100 series (void ratio=1.5) gave a value that is closest to line (a) and the shear strength envelope of 300 series at higher pressures is much lower than the others. The shear envelopes of 00, 200 and 300 series are close together in the curved region at lower stresses (up to 1000 kPa). It seems that the bonding is the main factor in controlling the strength in this region and that the mineralogy does not have a significant influence on it. The strength is higher for the 600 series (stronger bonding) as shown by the result of test 604 (Fig. 7.17), however the envelope for this series was not defined properly in this region.

In Fig. 7.17, 7.18 and 7.19 the results of tests from each series which were performed at similar effective confining pressures are plotted together. At 100 kPa (Fig. 7.17) the influence of the bonding is very clear. The remoulded sample REM2 had a void ratio of 0.96 and an overconsolidation ratio of 6.2 and still it failed at a much lower stress than the bonded samples, which were isotropically consolidated (OCR=1.0), with void ratios of 1.1 (samples 210 and 604) and 1.4 (sample 302). The bonding was the same on samples 302 and 210 (500°C/5h) and stronger on sample 604 (800°C/3h). The stronger bonding gives the highest strength (sample 604) and the two bonding strengths have a marked effect on the stiffness in relation to the remoulded sample.

The behaviour of samples 210 and 302 is also interesting. Here the bonding strength is identical and the overall sample strengths are very similar even though the grain mineralogies differ. However, it is difficult to compare the strength without considering the void ratio: the intergranular void ratio formula gives values of 0.56 (sample 210) and 0.33 (sample 302) (see Appendix 1).

In Fig. 7.18 the results of tests carried out at 750 kPa effective confining stress are presented. Test 208 could not be strained further so its final strength cannot be compared with the others. There is a large difference in strength between sample 301 (no quartz grains) and sample 601. The same observation can be made for tests 303 and 602 (Fig. 7.19), performed at larger confining pressures. It is unlikely that the bonding has much influence at these confining pressures and the difference in strength may be caused by the different mineralogical composition of the samples.

The yield surfaces for the different series are plotted in Fig. 7.20. In the low stress region the yield stress level is quite close to the peak strength and hence the yield would appear to be a function of the bonding strength there. However, as the stress increases the behaviour changes. The most dramatic change occurred when the void ratio was altered whilst maintaining the same material composition and bonding strength. The yield surfaces of 100 and 200 series represent such case.

The influence of an increase in bonding strength while maintaining the same void ratio and mineralogy can be examined by comparing the yield surfaces of 200 and 600 series. There is a considerable increase in the area encompassed by the yield curve but the increase is not as dramatic as that corresponding to a change in void ratio (100 and 200 series).

For confining pressures larger than 1.5 MPa it is not clear where the yield occurs in 200 series (two dotted lines). However, a clear pattern exists for 300 series. Its yield pressure is higher than 200 series at 1000 kPa but a dramatic drop occurs thereafter. It seems that the kaolin fired at 500°C (the only constituent in this series) changes its behaviour at higher pressures. The quartz sand and the CFK of 200 series seem to provide an extra strength to the mixture at higher pressures.

7.5.2 Stiffnesses

The secant stiffness measured at 0.1% of axial strain provided perhaps the clearest pattern of behaviour for the different mixtures. The values of stiffness are plotted against the

confining stresses in Fig. 7.21(a) and (b). In the first figure, the influence of the softer grains of CFK in the soil can be seen when comparing the curves of 200 and 00 series. The two series have the same bond strength (500°C/5h) and a similar structure as measured by the inter-granular void ratio (0.56 and 0.65, respectively).

The 00 series shows a large increase in stiffness with pressure up to 500 kPa after which it levels off. 200 series on the other hand increases in stiffness quickly up to around 200 kPa, is approximately constant between 200 kPa and 500 kPa following which it starts to increase again. The 600 series has a stronger bonding than 200 series and this increased strength shows its influence for pressures between 200 kPa and 1000 kPa. 600 series is, nevertheless, much less stiff than the 00 series, which does not have CFK.

All the experimental points of the series with CFK are shown on an enlarged scale in Fig. 7.21(b). The top shaded area represents the upper limit of the stiffness values of 200 series, which were mostly derived from local measurements. Different symbols were used for each series.

The following interesting observations are made:

(a) For the same soil constituents (mineralogy) and bonding strength, a change in void ratio can have a large influence on the stiffness behaviour with pressure but, surprisingly, this is not evident at low stresses. For example, at 100 kPa the stiffness is 105 MPa for 200 series (e=1.1) and 90 MPa for 100 series (e=1.5). The behaviour was totally modified, though, for confining stresses larger than 100 kPa for the high void ratio 100 series.

(b) For the same void ratio (structure) and mineralogy, an increase in bonding strength makes the soil stiffer at intermediate pressure levels. For low pressure levels, though, the stiffness is surprisingly close. For example, at 100 kPa the stiffness is 115 MPa (600 series) and 105 MPa (200 series). As the pressure is increased the weaker bonded soil seems to pass through a change of behaviour. First a more or less constant stiffness value and subsequently at larger pressures the stiffness starts to increase again. The same behaviour may well occur with 600 series for pressures in excess of 2000 kPa.

(c) When the results of 300 series are compared with those from 200 series (same bonding strength) it is evident that both series have similar behaviour for pressures up to 500 kPa: for a 100 kPa confining stress the stiffness is 115 MPa (300 series) and 105 MPa (200 series) whereas for 300 kPa they are 125 MPa and 135 MPa respectively. The two series also show a similar range of pressures at which the stiffness tends to stabilize, but 300 series has a drop in stiffness for pressures above 500 kPa whereas the stiffness of 200 series presents another increase. It seems clear that the behaviour of 200 series has been influenced by the presence of quartz and CFK grains which had a stiffening influence under increasing pressure. The 300 series seems to have been disturbed and its structure was unable to present further increase in stiffness. Note that the inter-granular void ratio of 300 series is 0.33 whilst its mineralogy is composed of only one material.

These observations correspond well with those made in respect of strength and yield pressures. An illustration of the stiffness variation can also be seen in Fig. 7.17 and 7.18.

The sample behaviour under isotropic consolidation was also examined. The deformation of 300 series is approximately linear in nature (Fig. 7.22) with an average bulk stiffness of 24.2 MPa. Test results of 600 series are shown in Fig. 7.23. All of the tests followed a similar pattern with a strongly curved initial part. As the pressure increased they behaved in a more linear way. The bulk stiffness of the latter line is close to 89 MPa. Although not many results were gained for these two series, the patterns seem very well established.

The results of 300 and 600 series are plotted along with those obtained from 200 series in Fig. 7.24. Although some of the samples in 200 series presented an initially curved compressibility line the pattern is more pronounced for 600 series and it is almost inexistent on 300 series. It is likely that this higher initial compressibility corresponds to the closure of fissures and cracks created by the firing process (see microphotographs later). The mineralogical uniformity of 300 series seems to have prevented any significant crack formation. In 200 and 600 series the fissures were probably formed by the different thermal expansion

properties of the quartz and kaolin. This hypothesis agrees well with the observation that an increase in temperature (600 series) caused a larger initial compressibility. Nevertheless, once the cracks had closed, the influence of the higher bond strength was noticeable in the stiffer behaviour of 600 series (Fig. 7.24).

7.5.3 Permeability

The permeability of some of the samples was measured whilst the sample was in the triaxial cell. Previous research has related the change in permeability to structural changes and it may help to indicate such changes here.

The measurements made on samples from 100 series and on the remoulded samples gave values of 2.5 $\times$ 10^{-6} m/s for the former and between 0.4 and 6.5 $\times$ 10^{-6} m/s for the latter (Table 5.3).

Sample 601 had its permeability measured at different stages and the results were as follows:

k = 5.5 $\times$ 10^{-6} m/s	(initial, e = 1.1)
k = 0.8 $\times$ 10^{-6} m/s	(after consolidation at 750 kPa, e = 0.96)
k = 0.1 $\times$ 10^{-6} m/s	(ϵ_a = 15.5%, drained, e = 0.81)
k = 0.07 $\times$ 10^{-6} m/s	(end of undrained test, ϵ_a = 20.5%, e = 0.81)

Sample 302 presented the following permeabilities:

k = 0.2 $\times$ 10^{-6} m/s	(initial, e = 1.4)
k = 0.02 $\times$ 10^{-6} m/s	(end of test, shear plane, ϵ_a= 5.9%, e = 0.81)

7.6 MICROPHOTOGRAPHS OF ARTIFICIAL SOIL

The microphotographs presented here were taken using a scanning electron microscope in the Department of Geology, Imperial College. The samples to be examined were

impregnated with epoxi resin, cut in half and mounted on a glass plate, then ground down to the thickness required for the examination. The assembly was carried out in the Department of Geology workshop. All images were produced using the back scattered electron image technique.

Fig. 7.25 shows the images obtained from an undisturbed sample of 100 series for two amplifications: x30 [Fig. 7.25(a)] and x100 [Fig. 7.25(b)]. The three soil components can be identified easily by the different shades of grey. The white grains are quartz sand, the pale grey grains are the crushed fired kaolin which was fired at 1000°C and the dark grey areas are the bonding kaolin which had been fired at 500°C. The black spaces are voids and their irregular form is due to their different origins, i.e: wax sand that occupied some of them; air bubbles trapped in the original wet mixture (circular ones); voids originally water filled.

The figure shows that the spatial arrangement of the grains is maintained by bridges of the bonding which tend to coat all of the particle surfaces. There are few direct grain-to-grain contacts and some areas present a larger proportion of voids than others.

Fig. 7.25(b) is an enlarged detail of the same area shown in (a) (bottom left corner). The quartz grain shown has a direct contact with one of the CFK grains but all of the other grains seem to be coated. It is interesting to note that there are a large number of fissures in the contacts between the bonding and the grains. The most likely cause of this was contraction due to cooling following the firing process. Despite the occurrence of fissures the bonding material is present between most of the grains, locking them spacially in place.

Some of the quartz grains also show internal cracks. These may have been caused either by the heating/cooling process or by the grinding of the samples. They are, however, in general very thin and they do not appear to have had any significant influence on the sample behaviour as it will be shown later.

Microphotographs of an undisturbed sample from 200 series are shown in Fig. 7.26(a) and (b) with the same magnifications as before. The image of the quartz grains has been over-exposed in the higher magnification (pure white grains). The detail in Fig. 7.26(b) represents

the central part of the first microphotograph.

In this sample the cracks were fewer in number but the general characteristics of the artificial samples are once again evident i.e.: bonding bridges and coating of the grains. There are far fewer voids in relation to the previous sample since no wax was used in the mixture.

Three other samples of artificial soil were prepared and photographed in the same way after being tested in triaxial shearing. Fig. 7.27 and 7.28 are the images of one sample from 100 series and one from 200 series respectively. Both samples were tested at an effective stress of 100 kPa and loaded to approximately ϵ_a=2.0%.

There is little difference between these two images and those obtained from the equivalent undisturbed samples. A higher concentration of cracks in the bonding and in the grain contacts seems to have occurred but this effect is difficult to quantify. The relatively small strain to which the samples were subjected did not significantly change the soil structure, although the test results have clearly shown the yield stresses.

The second sample from 200 series to be photographed after testing was isotropically consolidated to 3250 kPa and then unloaded to 600 kPa and sheared. The shearing stage subjected it to a strain of ϵ_a=22% and its final void ratio was 0.62 (sample 206). The denser structure is easily seen in the microphotograph (Fig. 7.29). The test procedure caused widespread distortion and breakage of the CFK grains and shattering of the bonding material in many places. The quartz grains on the other hand were unaffected by the loading.

Test	γd (kN/m^3)	e_0	σ'_3 (kPa)	Local axial strain	Guided top cap
21	15.62	0.653	60	(a)	Yes
22	15.62	0.653	60	Yes	No
23	15.53	0.663	60	Yes	Yes
24	15.57	0.658	60/245	Yes	Yes
25	15.66	0.649	200	Yes	Yes
26	15.69	0.645	300	Yes	Yes
27	15.90	0.623	500	Yes	Yes
28	15.77	0.637	700	Yes	Yes
CIU1	15.81	0.632	60	No	Yes

$G_s = 2.631$
(a) Four local transducers

Table 7.1 — Artificial soil 00 series (130087, 500°C/5 h)

Test	γd (kN/m^3)	e_0	σ_3' (kPa)	Local axial strain	Guided top cap
601	12.37	1.102	750	(a)	Yes
602	12.27	1.118	1510	Yes	Yes
603	12.59	1.065	2300	Yes	Yes
604	12.45	1.088	110	(a)	Yes

$G_s = 2.65$
(a) Axial and radial measurements

Table 7.2 — Artificial soil 600 series (133057, 800°C/3h)

Test	γd (kN/m^3)	e_0	σ_3' (kPa)	Local axial strain	Guided top cap
301	10.14	1.428	750	Yes	Yes
302	10.25	1.402	100	(a)	Yes
303	9.89	1.490	1200	Yes	Yes
304	10.25	1.402	300	Yes	Yes
305	10.24	1.405	500	Yes	Yes

$G_s = 2.51$
(a) Axial and radial strain measurements

Table 7.3— Artificial soil tests 300 series (168400, CFK fired at 500°C, bonding at 500°C/5 h)

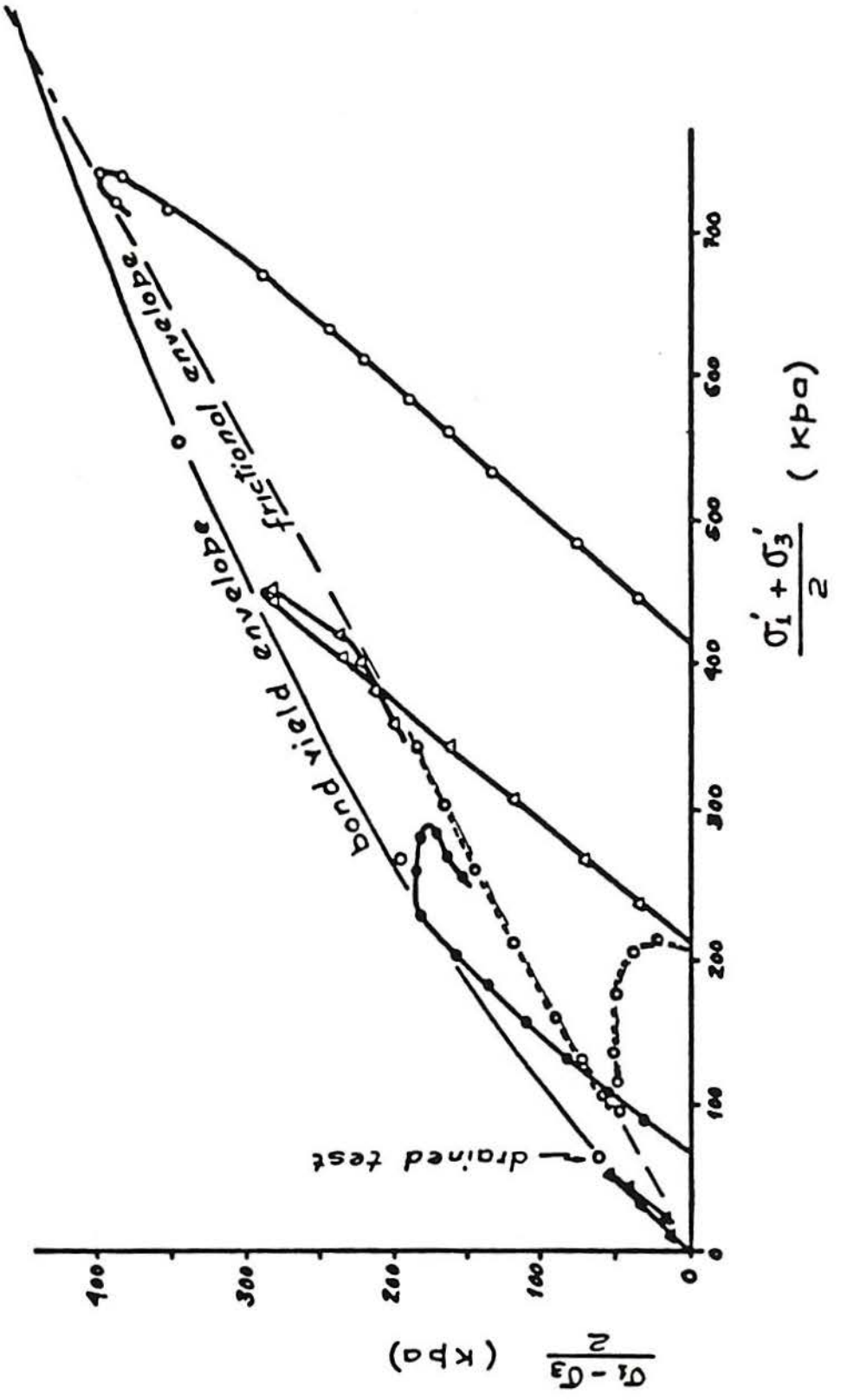

Figure 7.1 – Results of tests on soil 130087 (after Maccarini, 1987) e=0.71

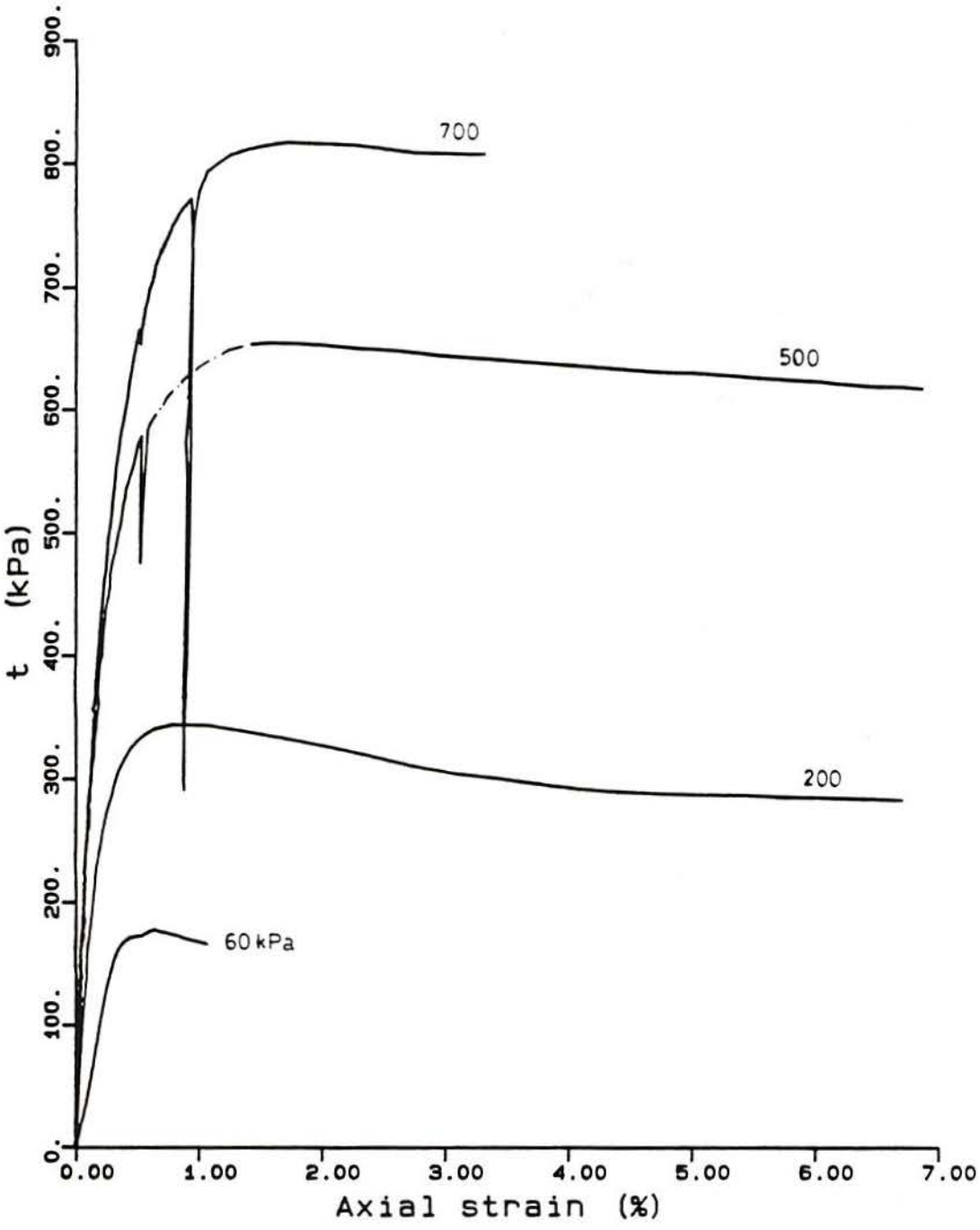

Figure 7.2 - Stress-strain curves of tests in 00 series — summary

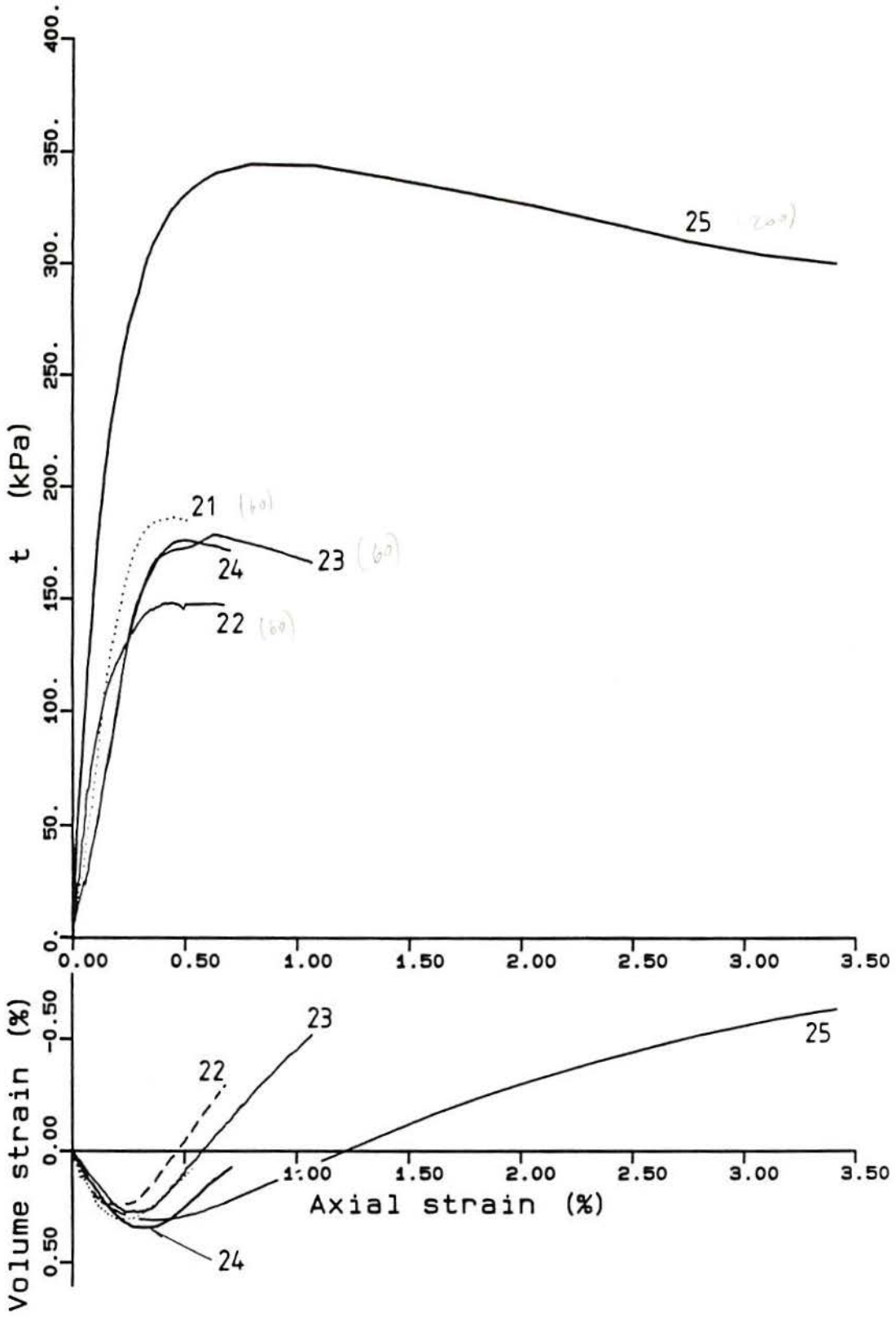

Figure 7.3 – Stress-strain test results of artificial soil 00 series — samples 21 to 25

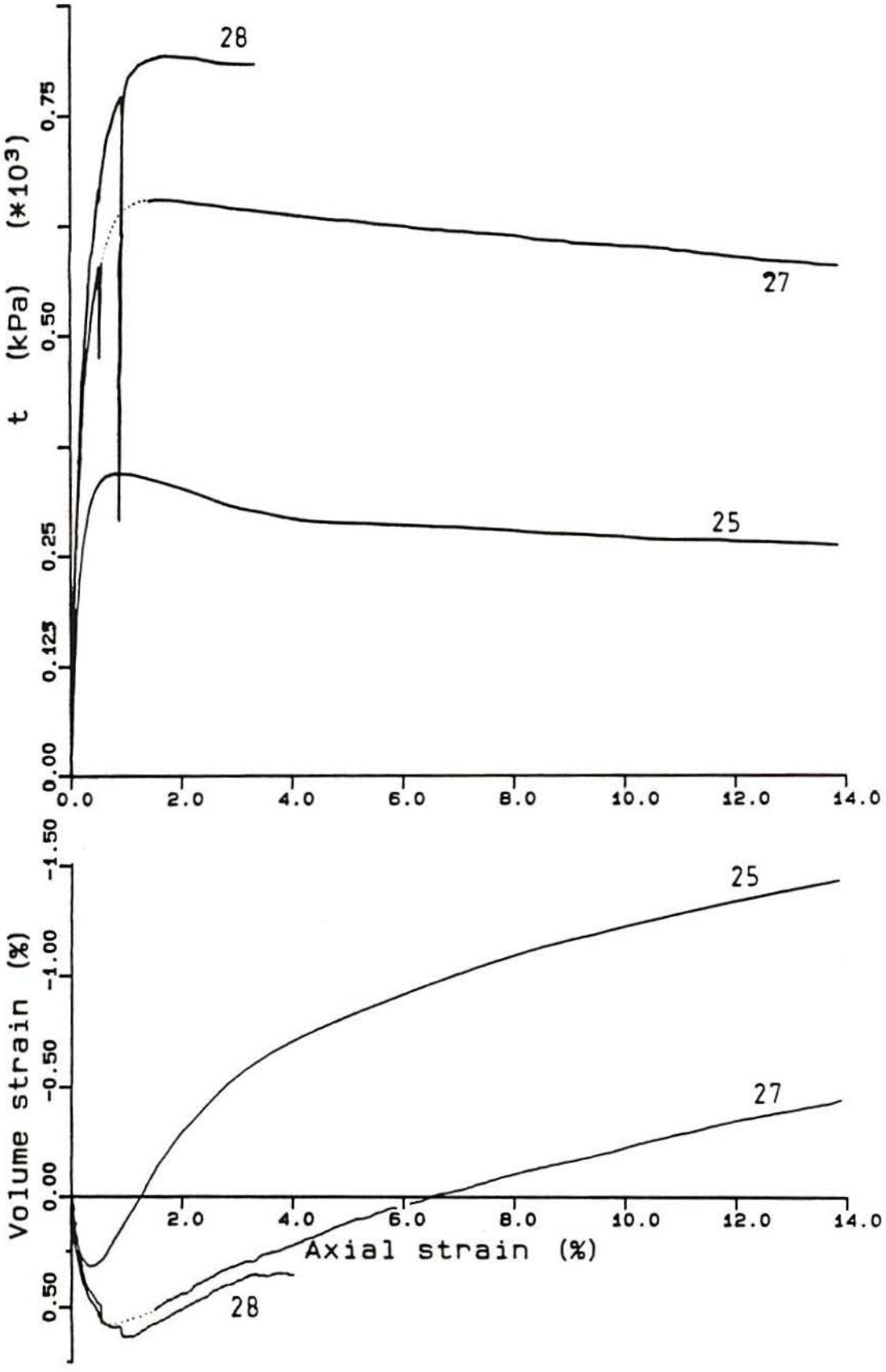

Figure 7.4 – Stress-strain test results of artificial soil 00 series – samples 25, 27 and 28

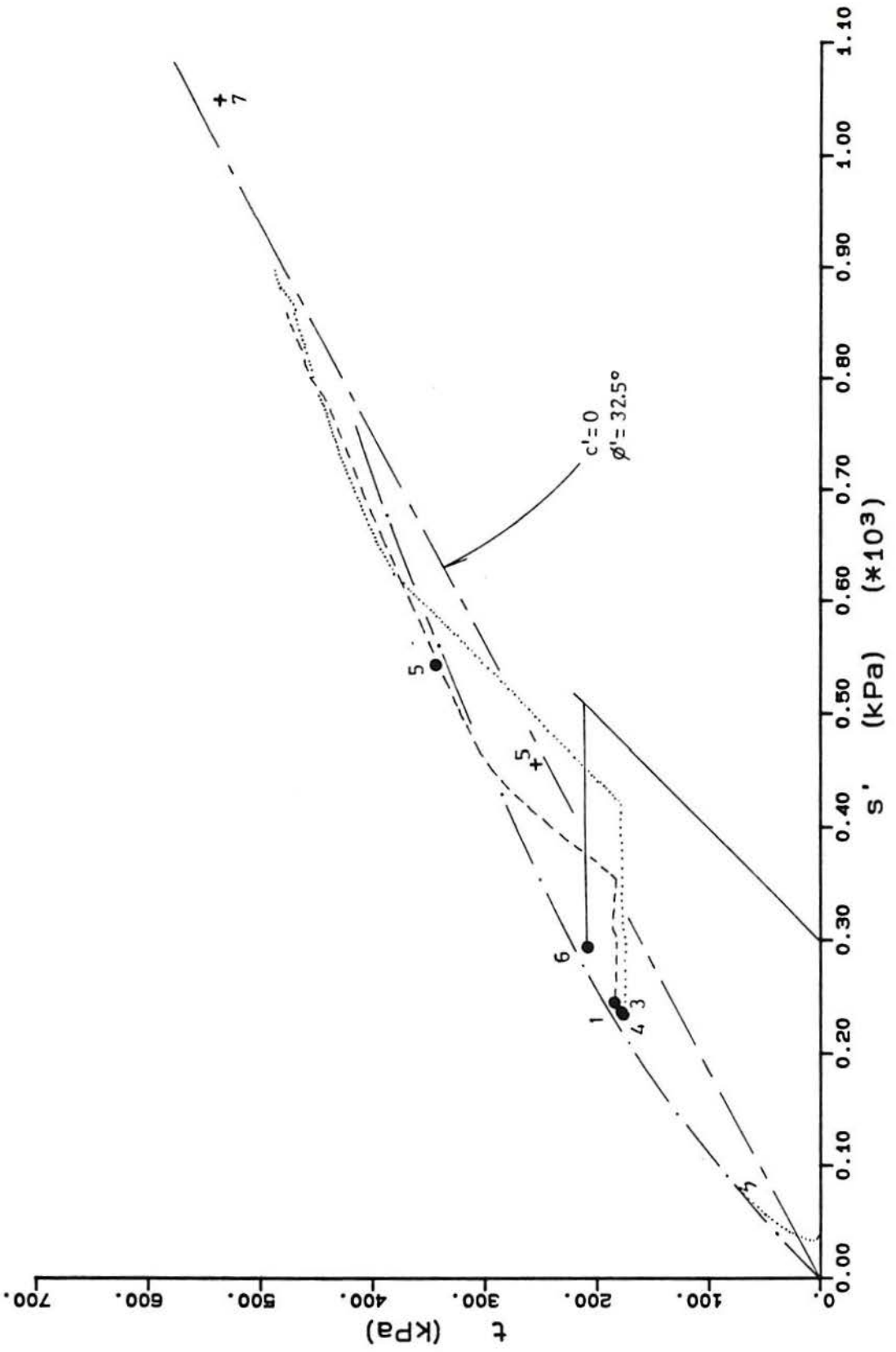

Figure 7.5 – Shear strength envelope of 00 series – (130087) (*a*) Low stresses (cont.)

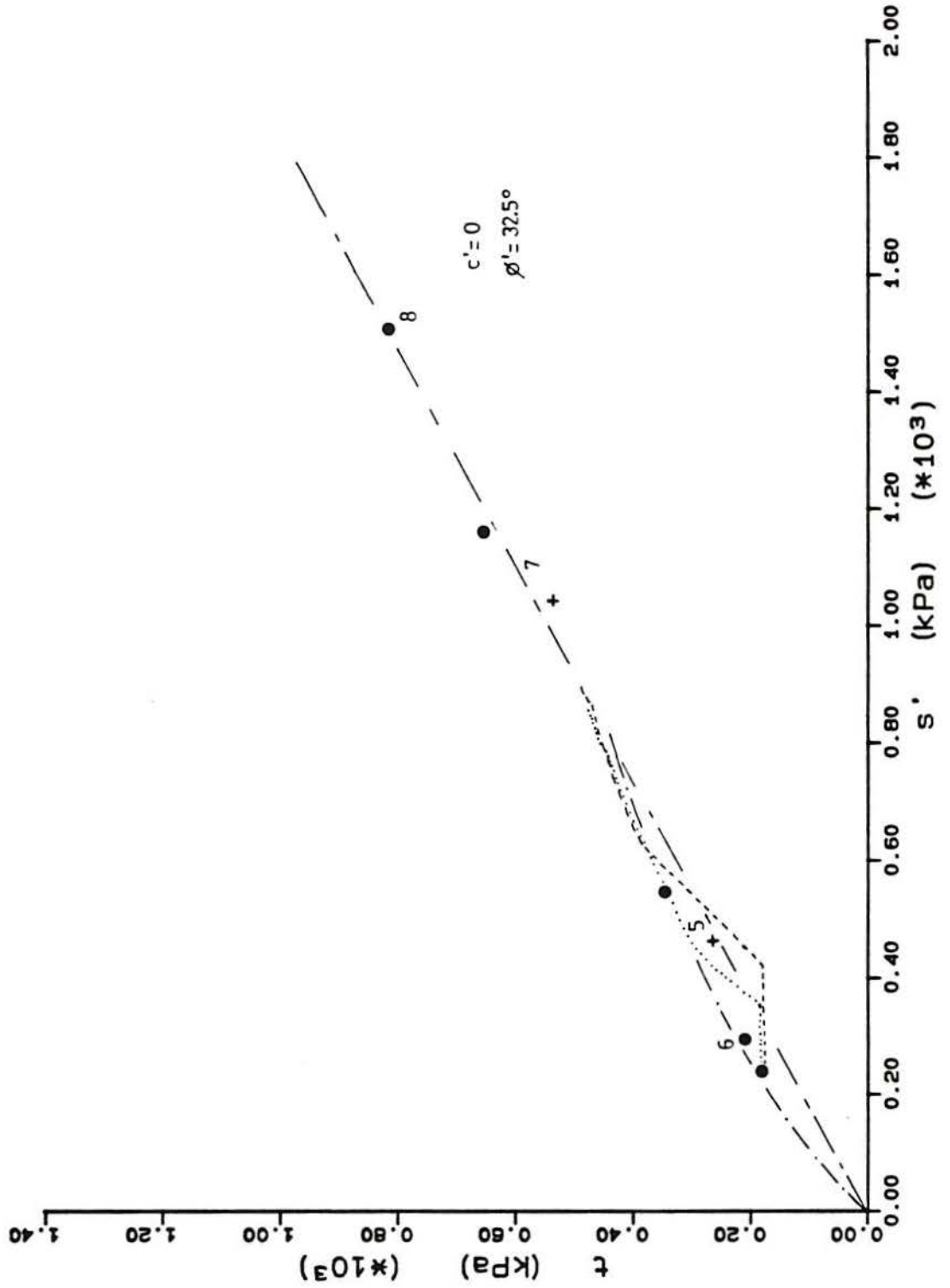

Figure 7.5 – (cont.) (*b*) Intermediate stress

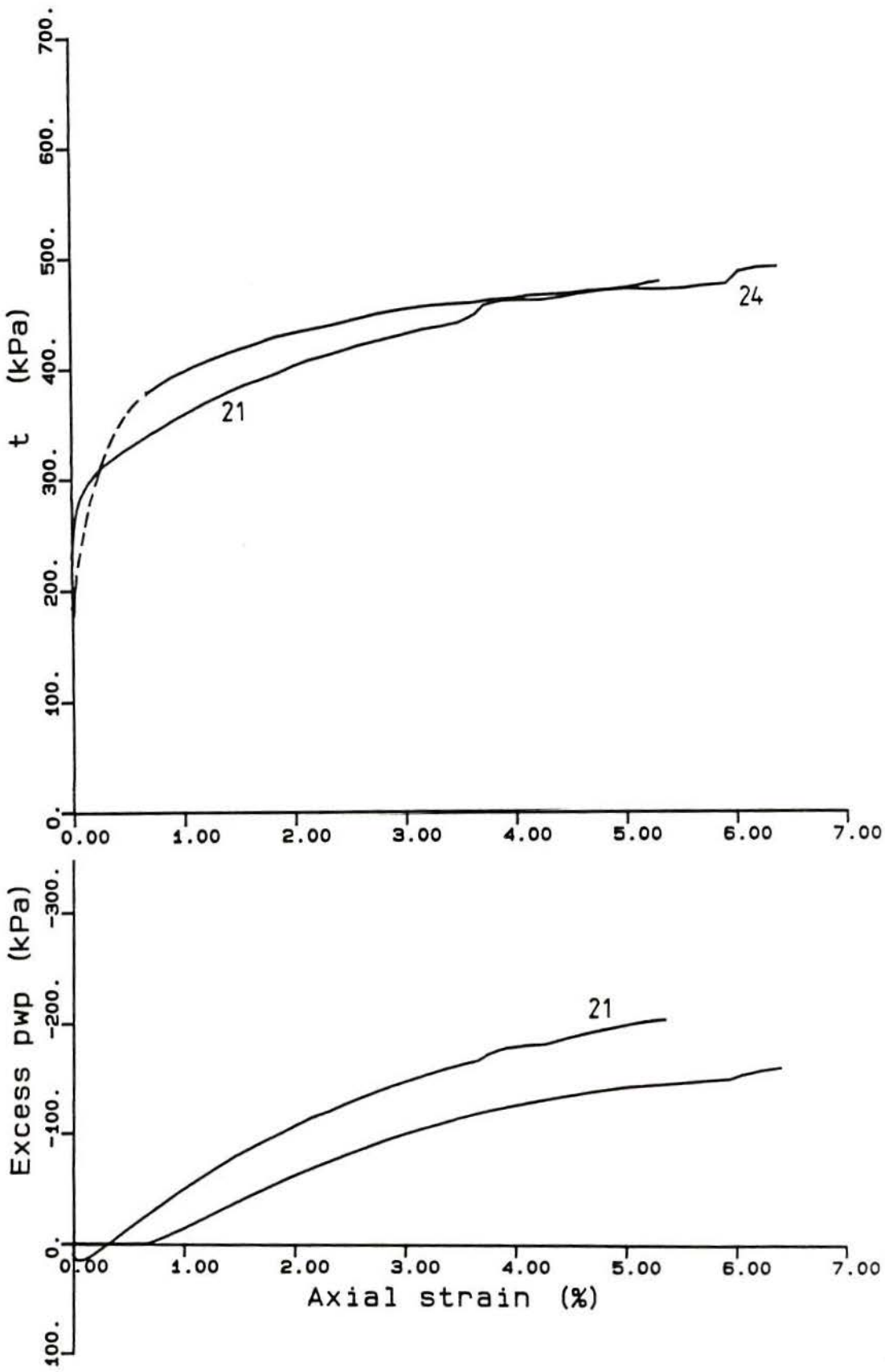

Figure 7.6 – Stress-strain and pore pressure curves of tests 21 and 24 after re-consolidation

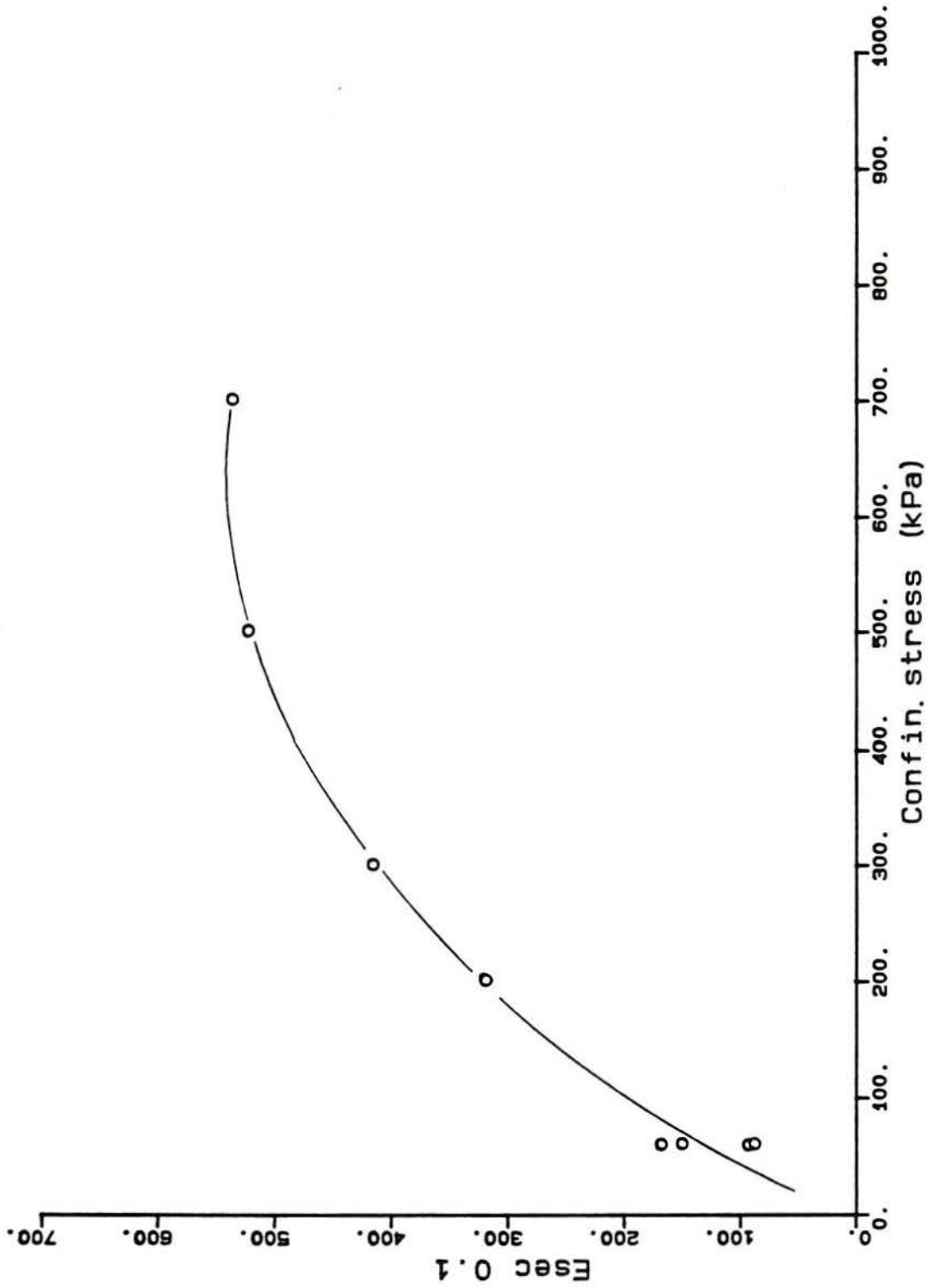

Figure 7.7 – Secant stiffness at 0.1% axial strain versus confining pressure – artificial soil 00 series

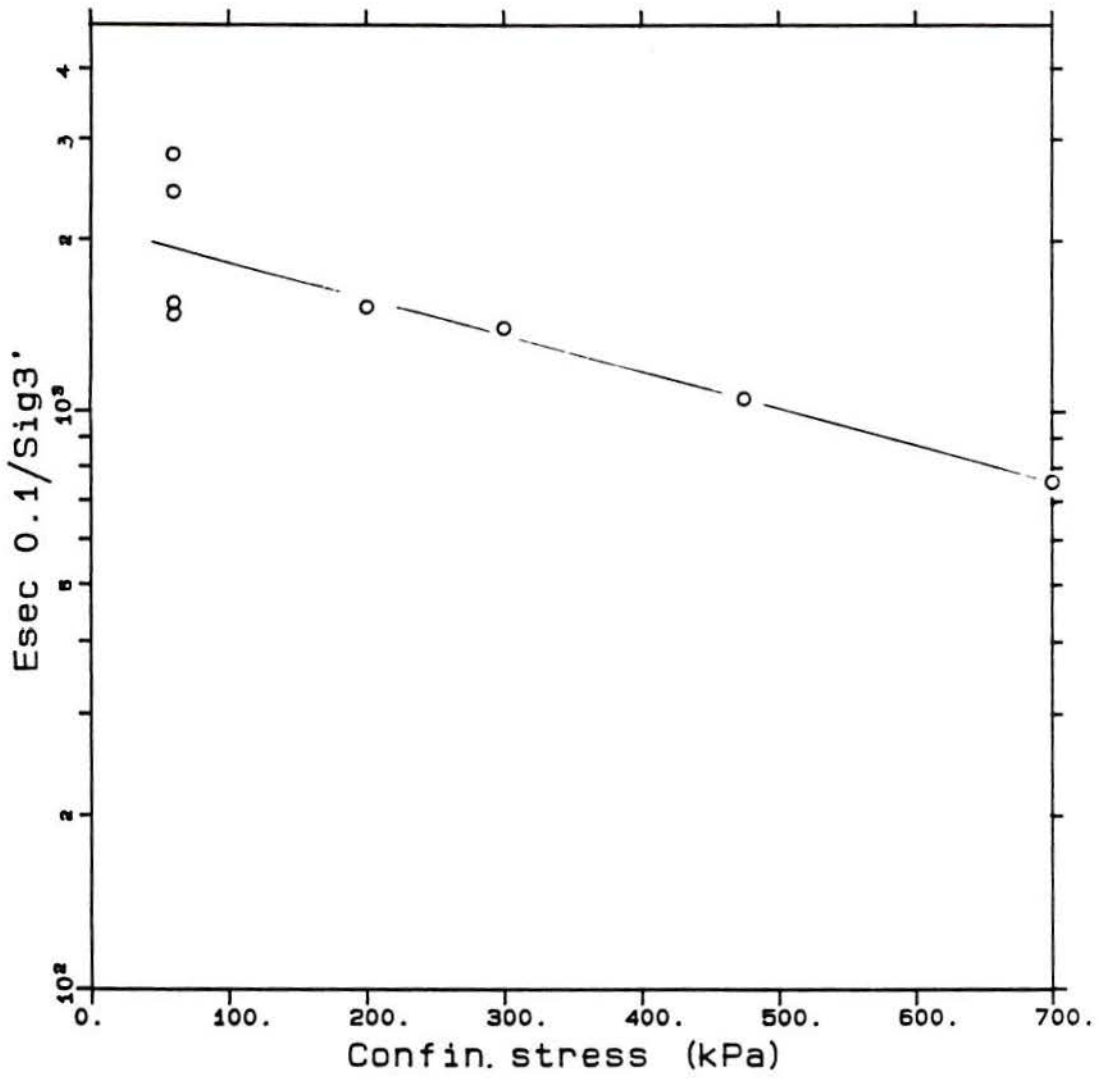

Figure 7.8 – Normalized secant stiffness at 0.1% axial strain versus confining effective pressure – artificial soil 00 series

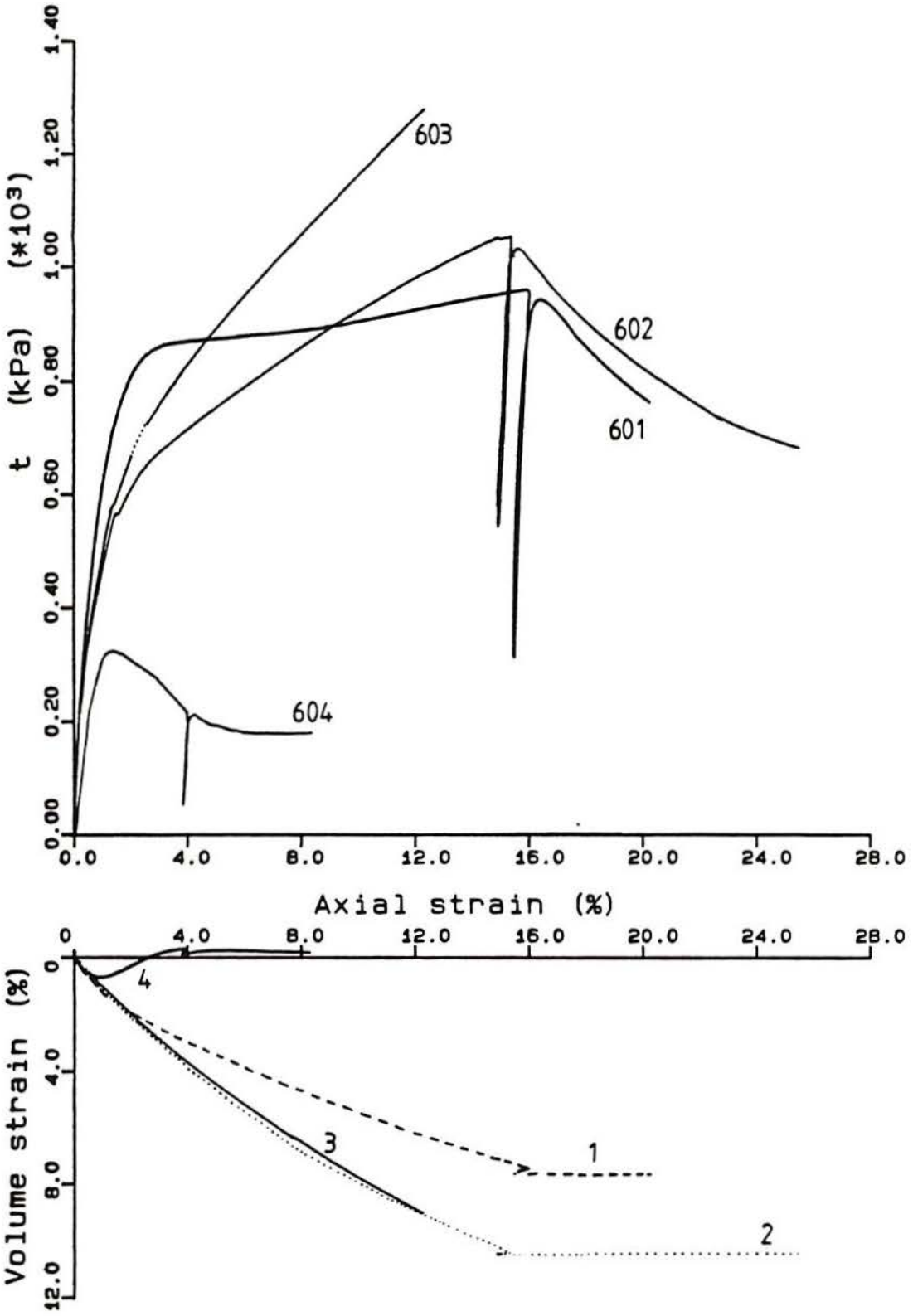

Figure 7.9 – Stress-strain test results of artificial soil 600 series

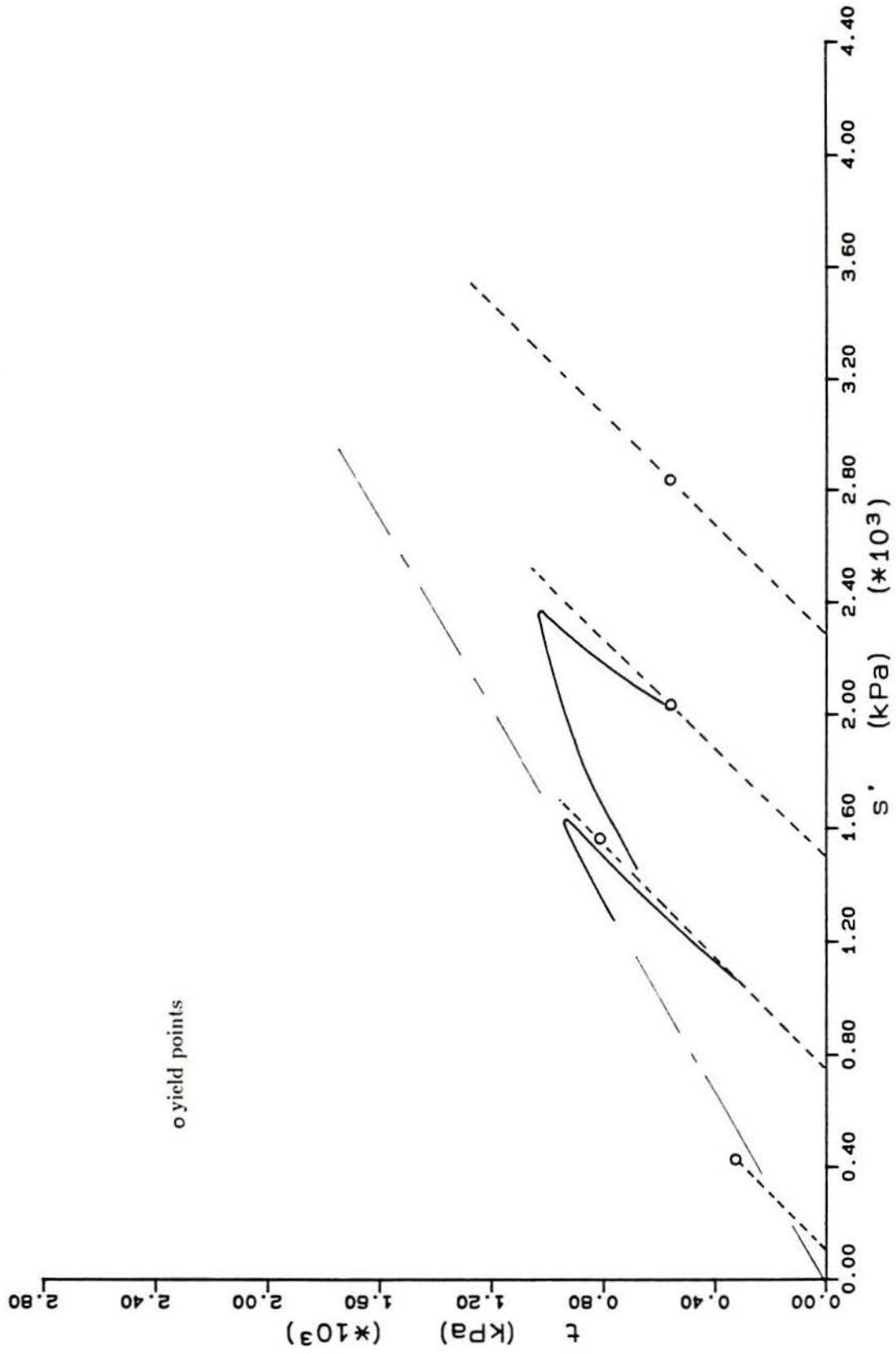

Figure 7.10 – Stress path, maximum shear strength and yield points of 600 series. (*a*) Full range of stresses (cont.)

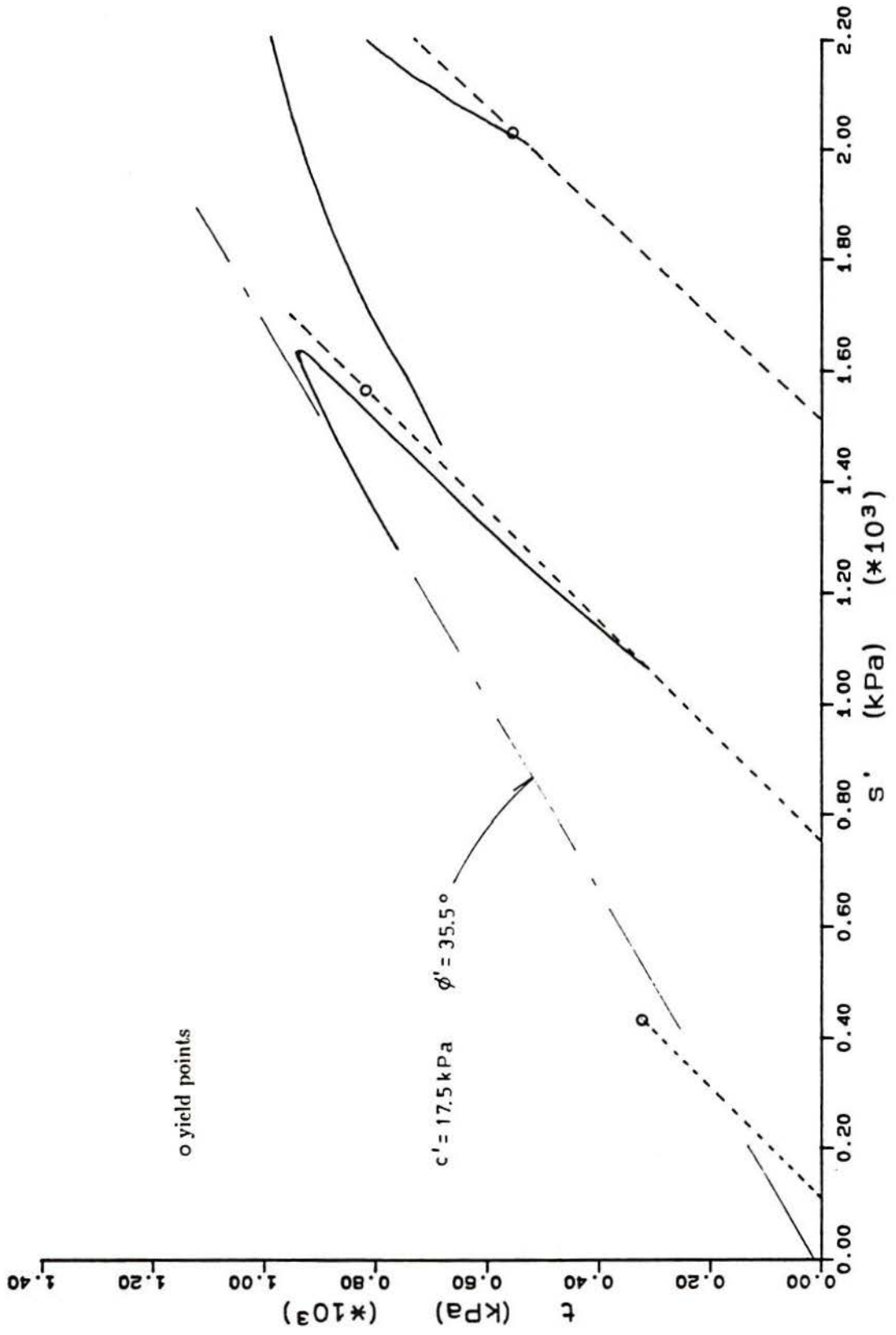

Figure 7.10 – (cont.) (*b*) Stresses up to 2000 kPa

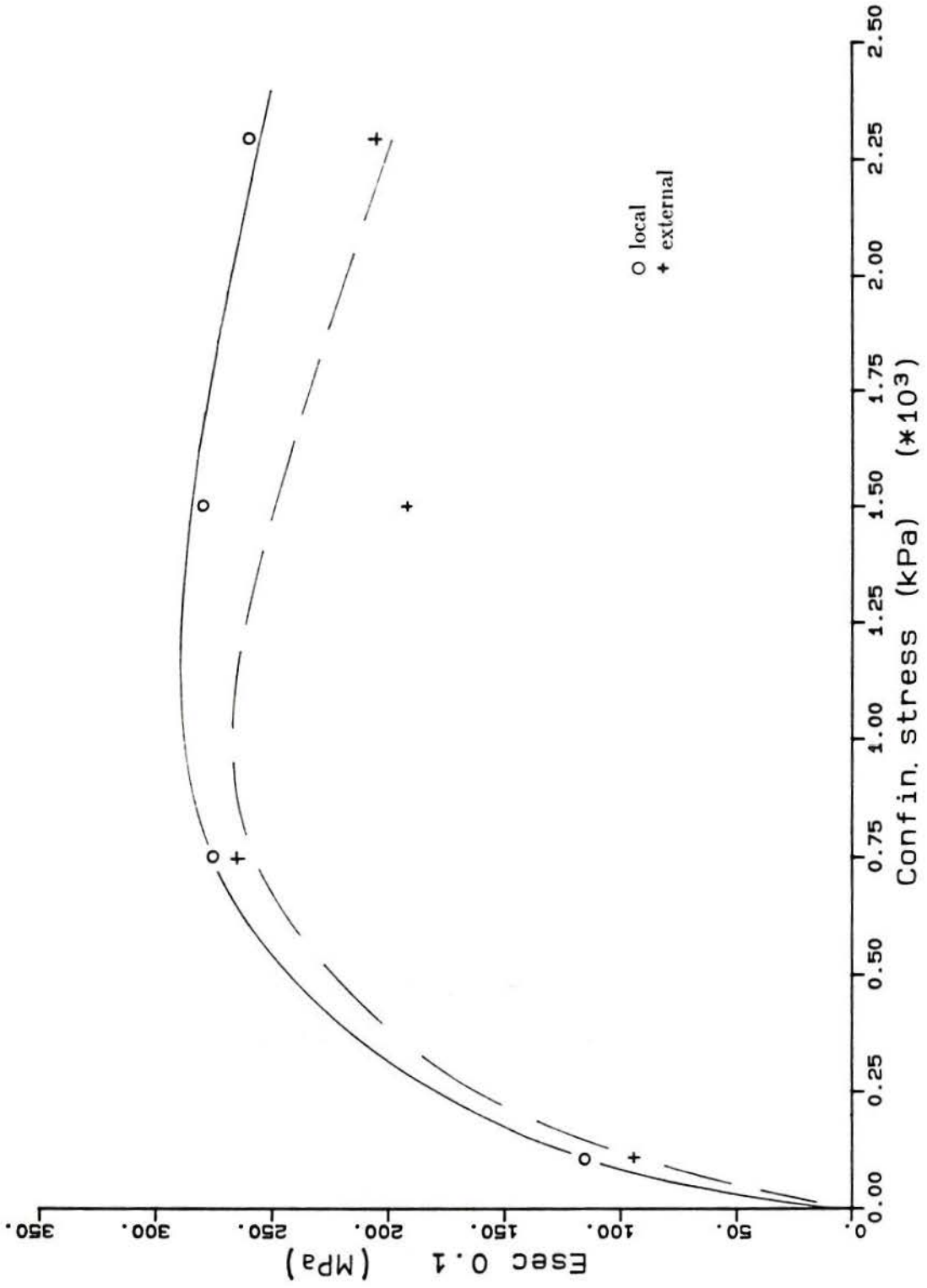

Figure 7.11 – Secant stiffness determined at 0.1% axial strain versus initial confining pressure – 600 series

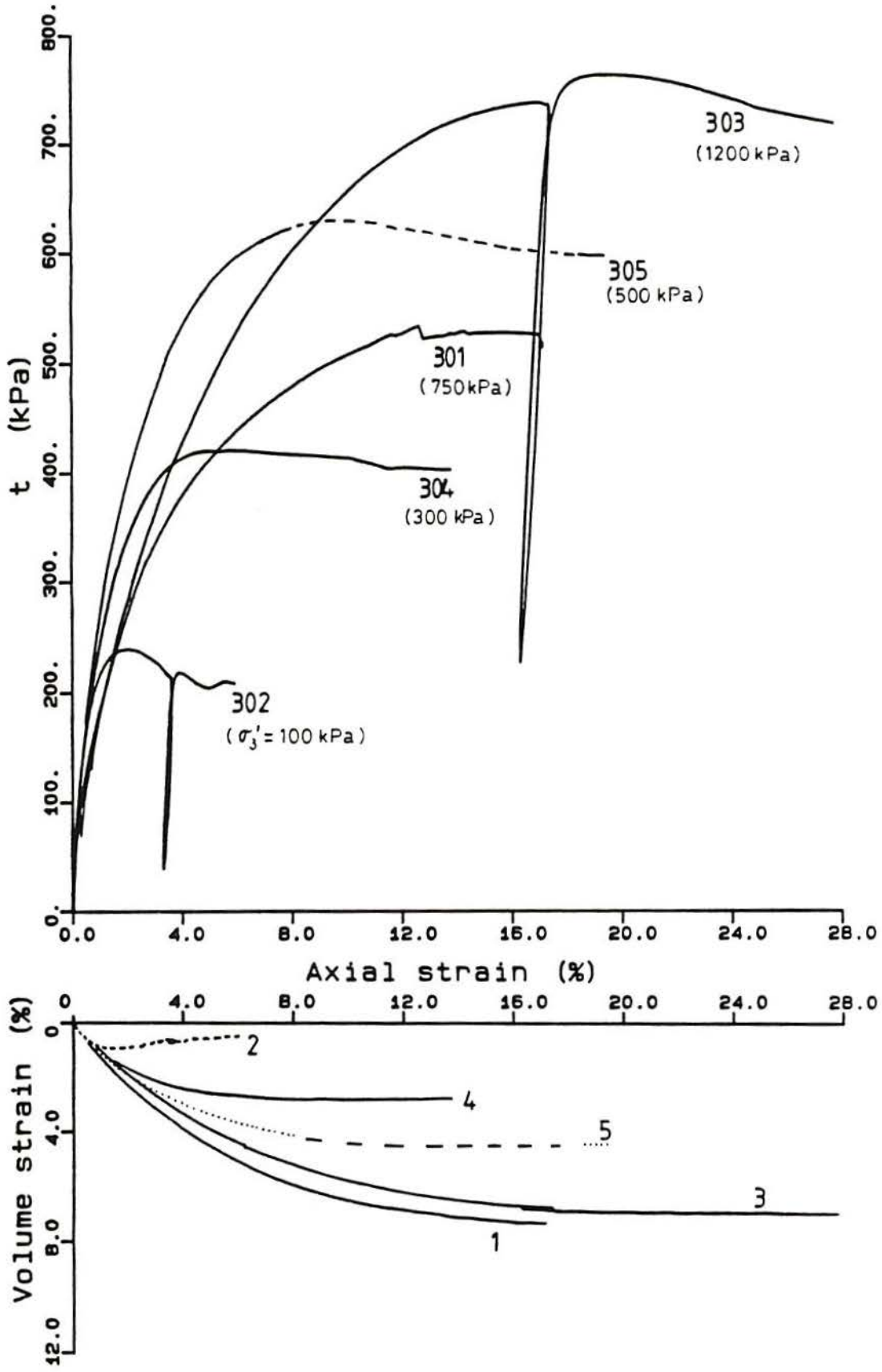

Figure 7.12 – Stress-strain triaxial results of artificial soil 300 series

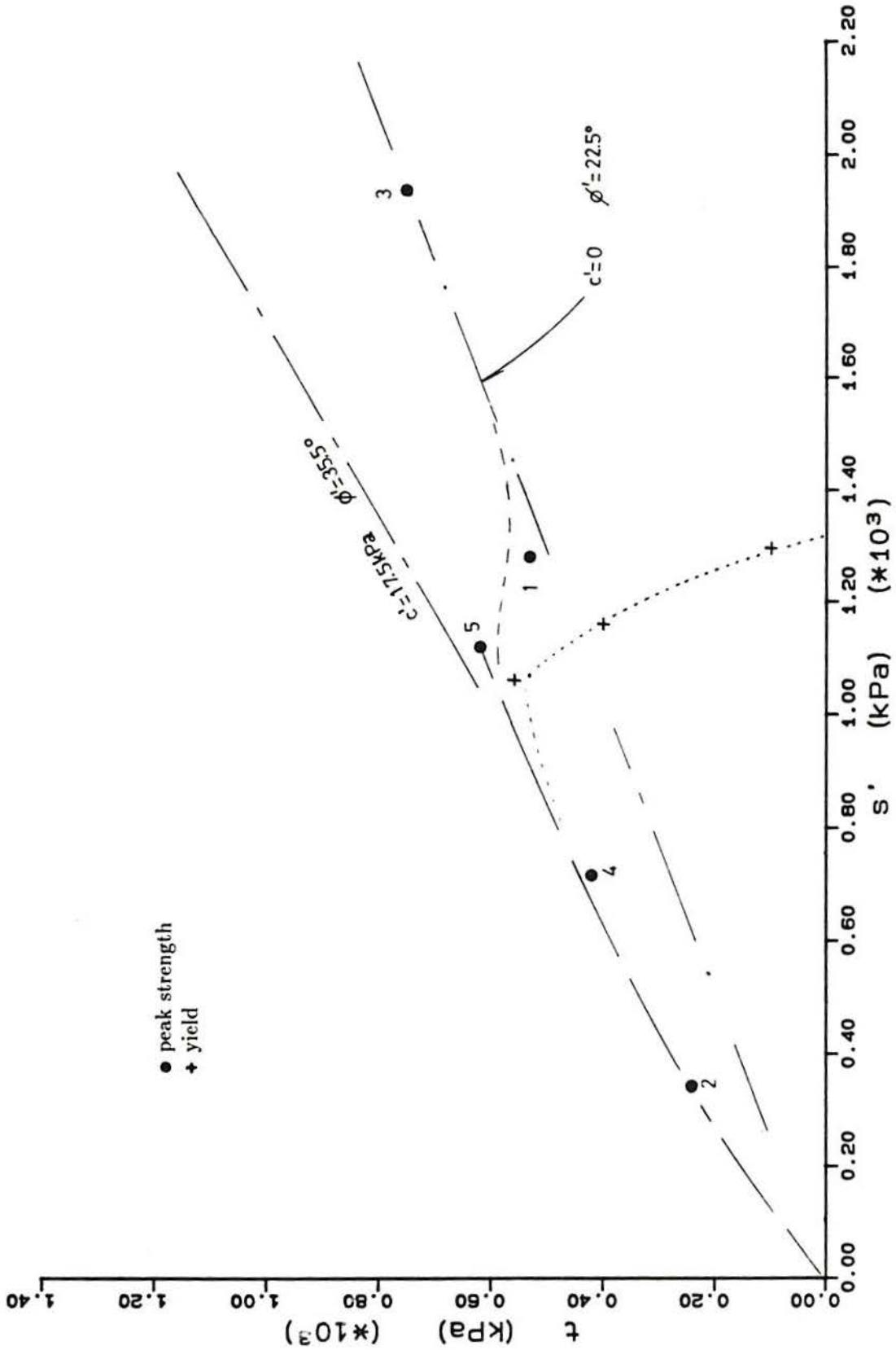

Figure 7.13 – Shear strength envelopes for artificial soil 300 series – drained test results

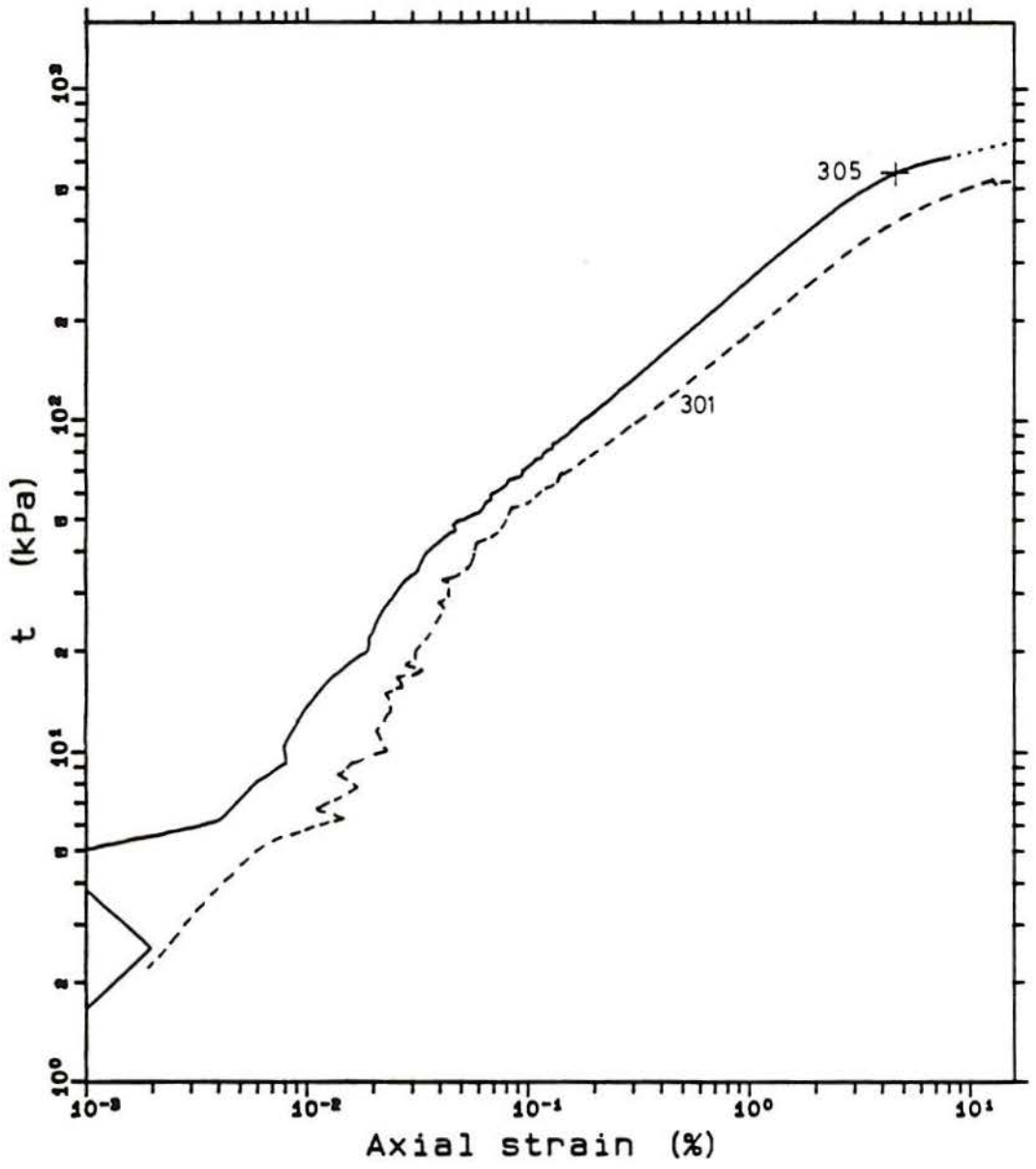

Figure 7.14 – Stress-strain plots using logarithmic scales – artificial soil 300 series.
(*a*) Tests 301 and 305 (cont.)

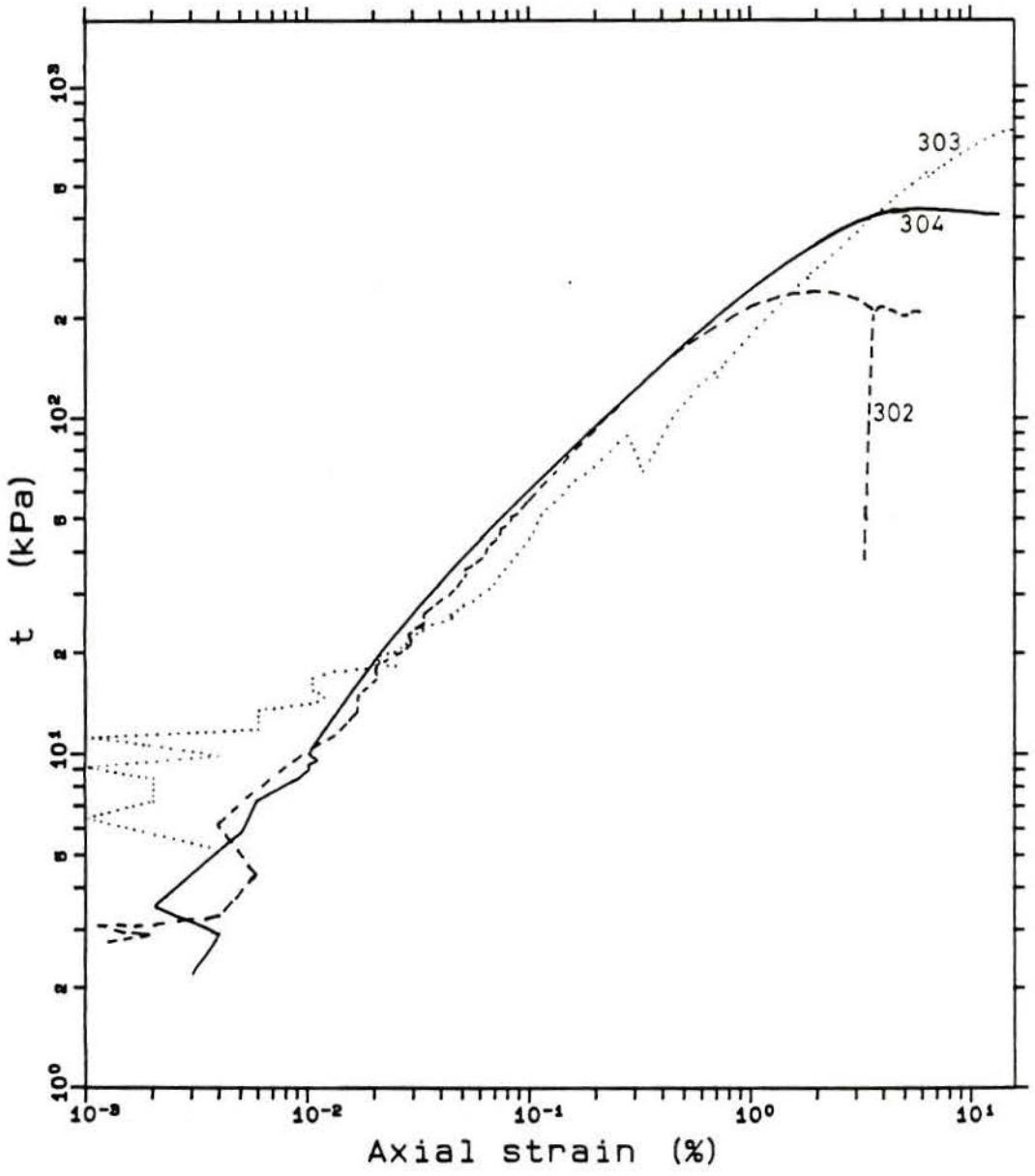

Figure 7.14 – (cont.) (*b*) Tests 302, 303 and 304

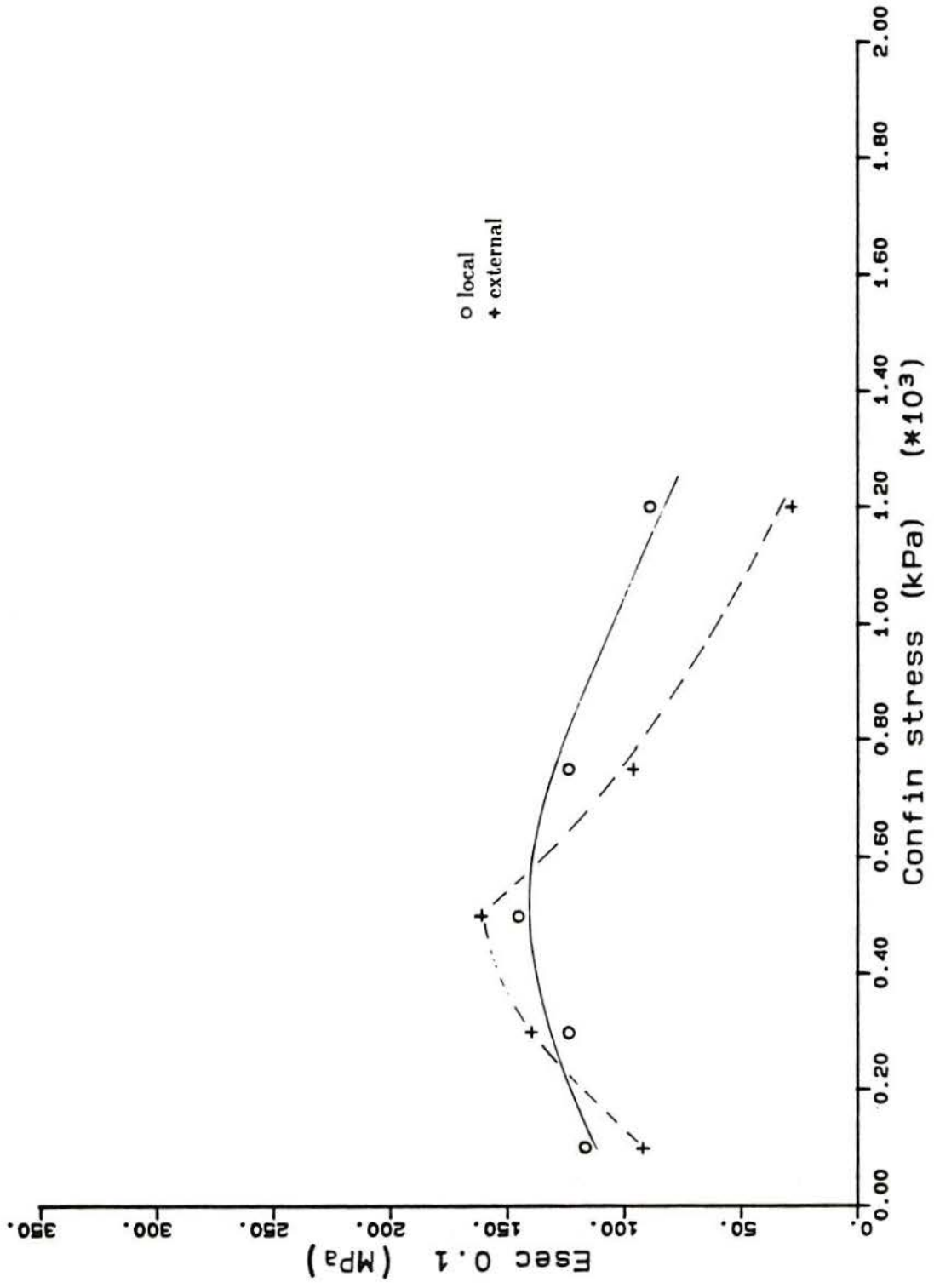

Figure 7.15 – Secant stiffness at 0.1% axial strain versus confining pressure for 300 series

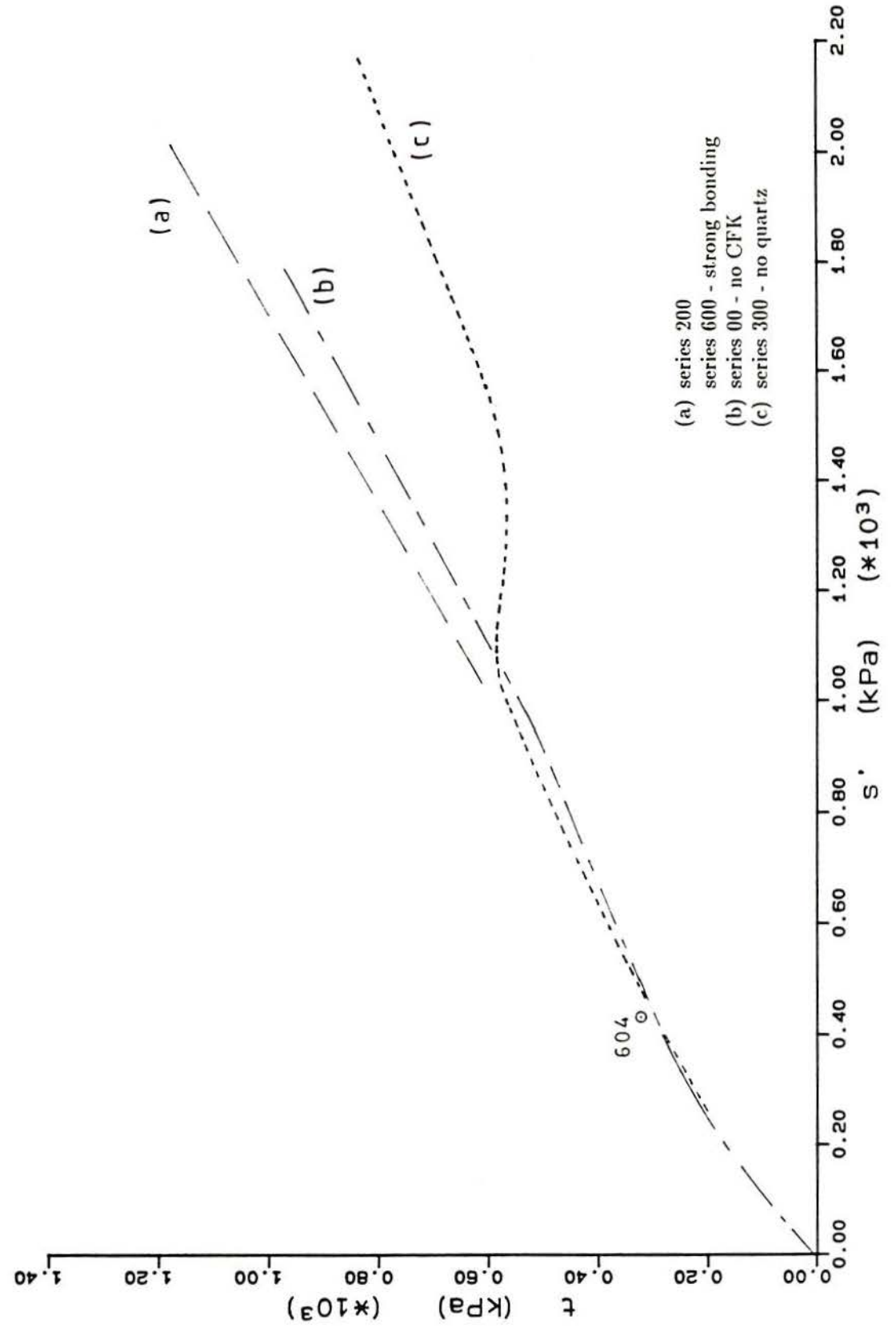

Figure 7.16 – Strength envelopes of the different artificial soil mixtures. (*a*) 200 and 600 series; (*b*) 00 series; (*c*) 300 series

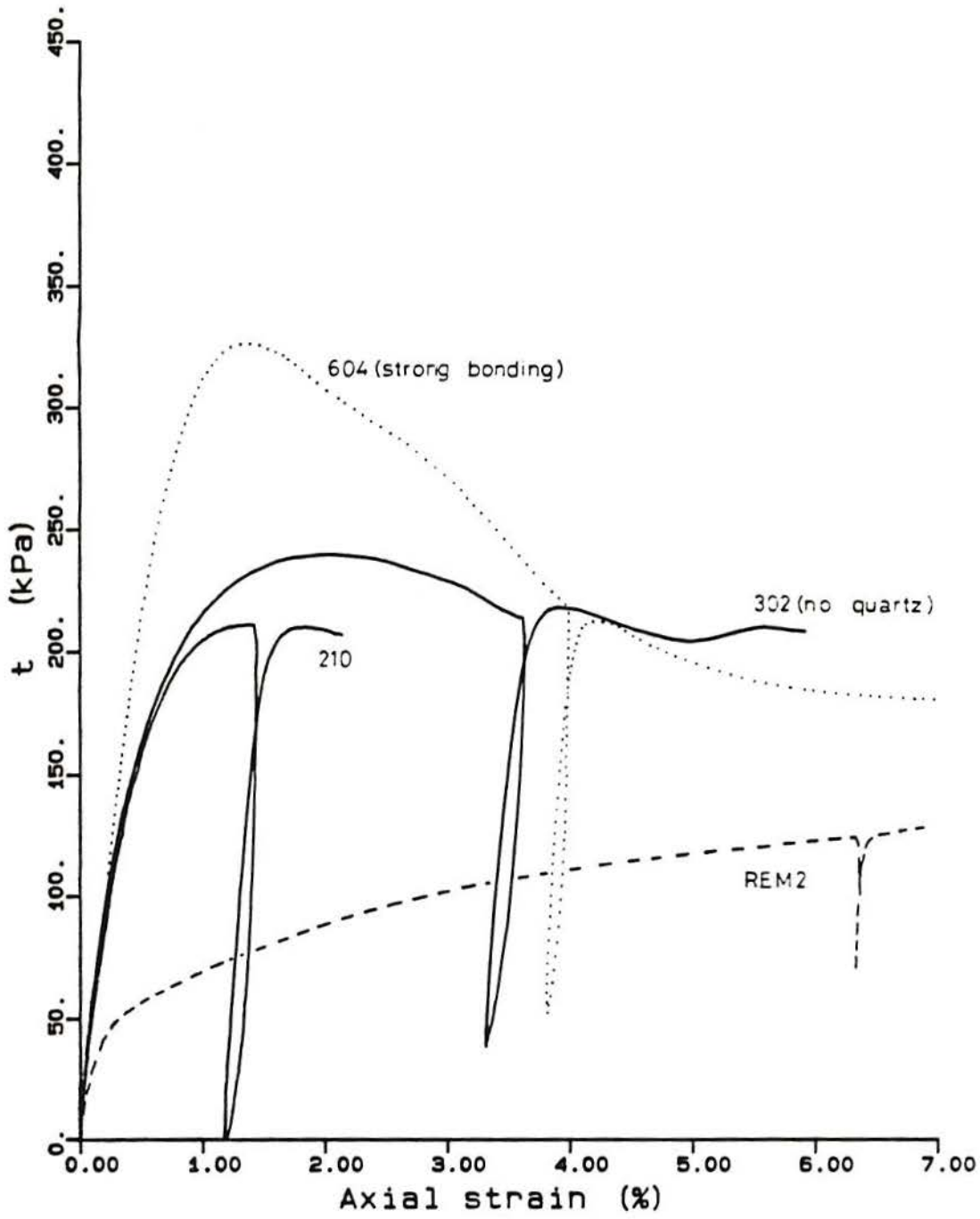

Figure 7.17 – Comparative behaviour of soil samples sheared at 100 kPa effective confining stress

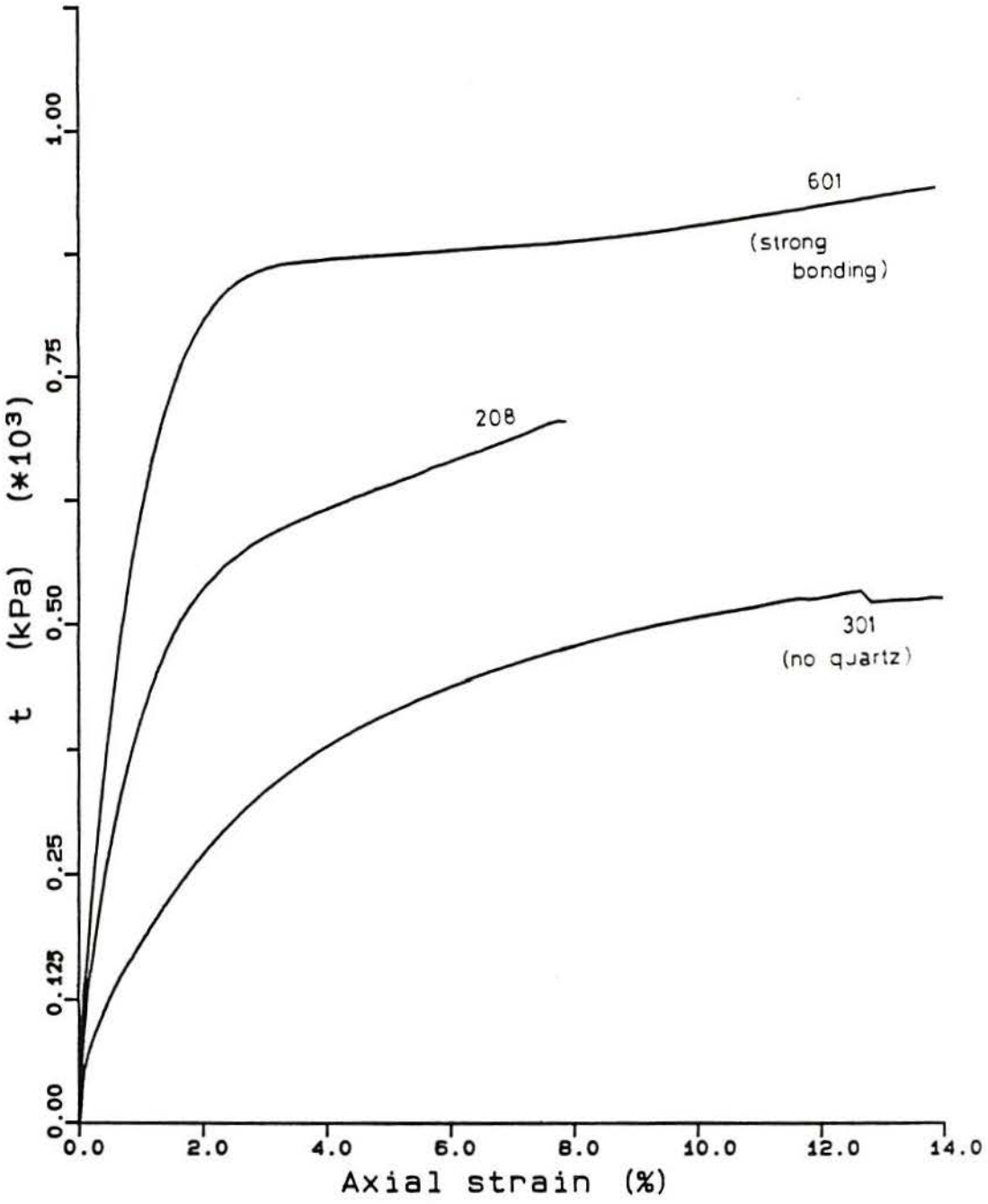

Figure 7.18 – Comparative behaviour of soil samples sheared at 750 kPa effective confining stress

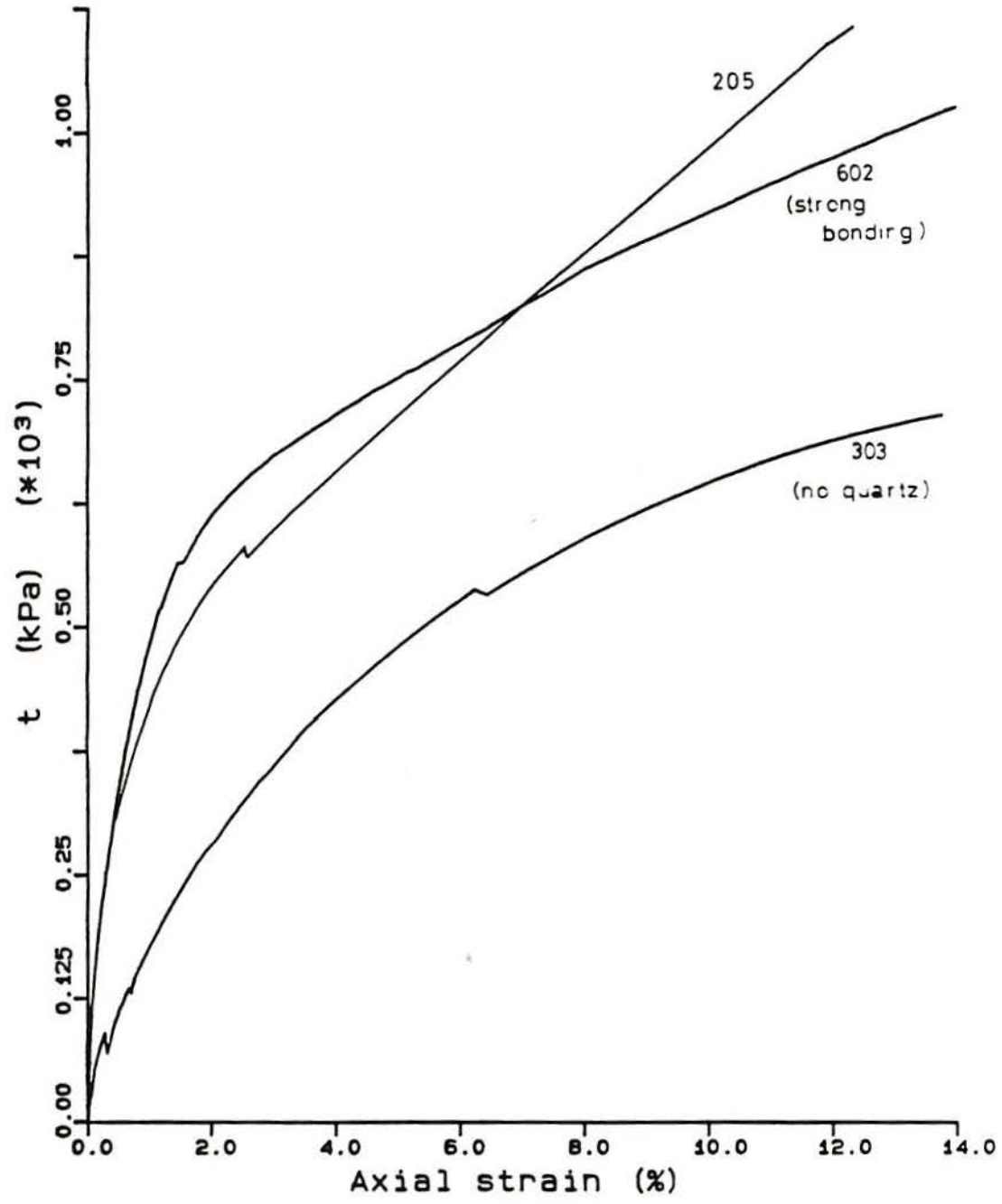

Figure 7.19 – Comparative behaviour of soil samples sheared at 1200 kPa (205 and 303) and 1510 kPa (602) effective confining stress

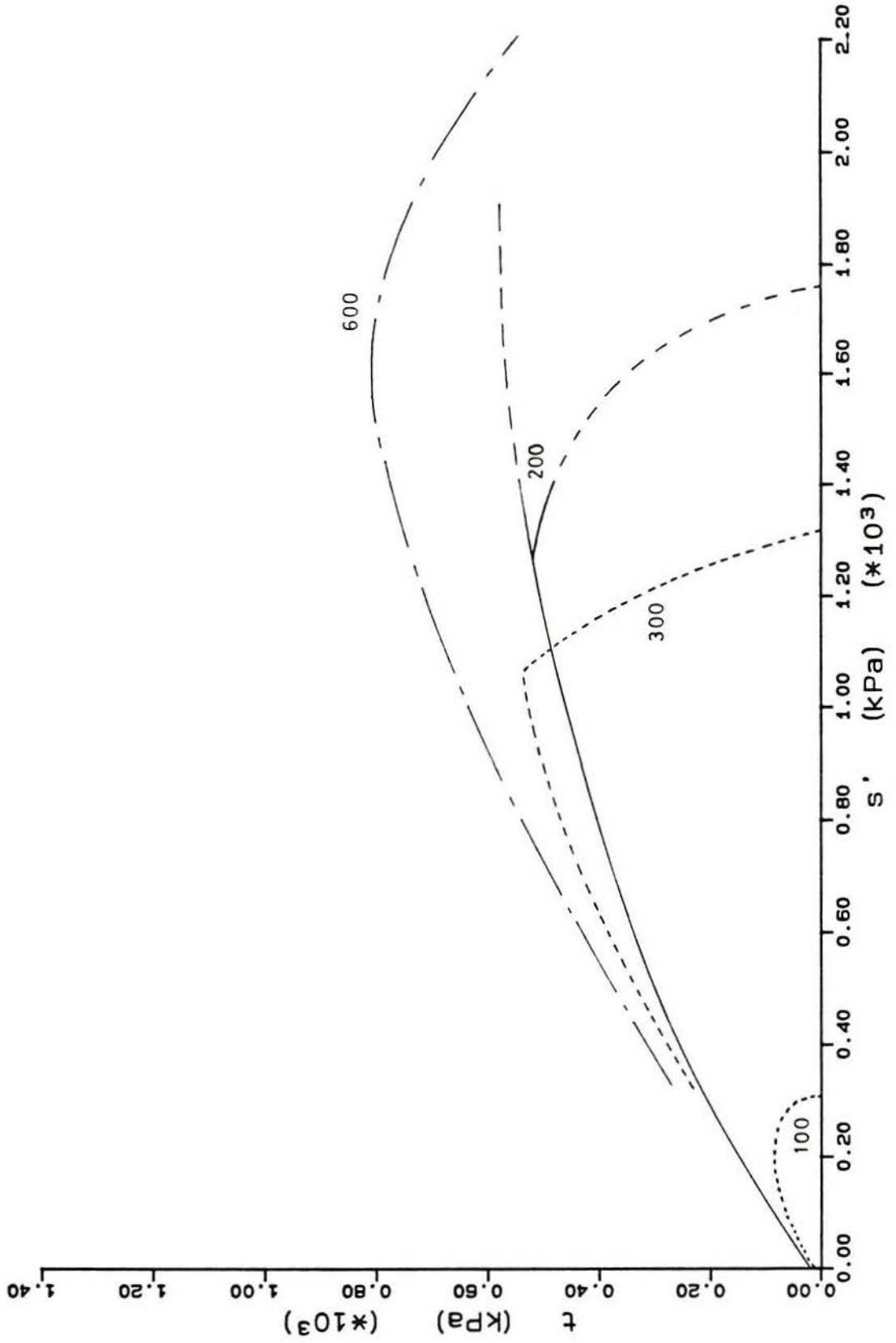

Figure 7.20 – The different yield surfaces for three of the artificial soil tested

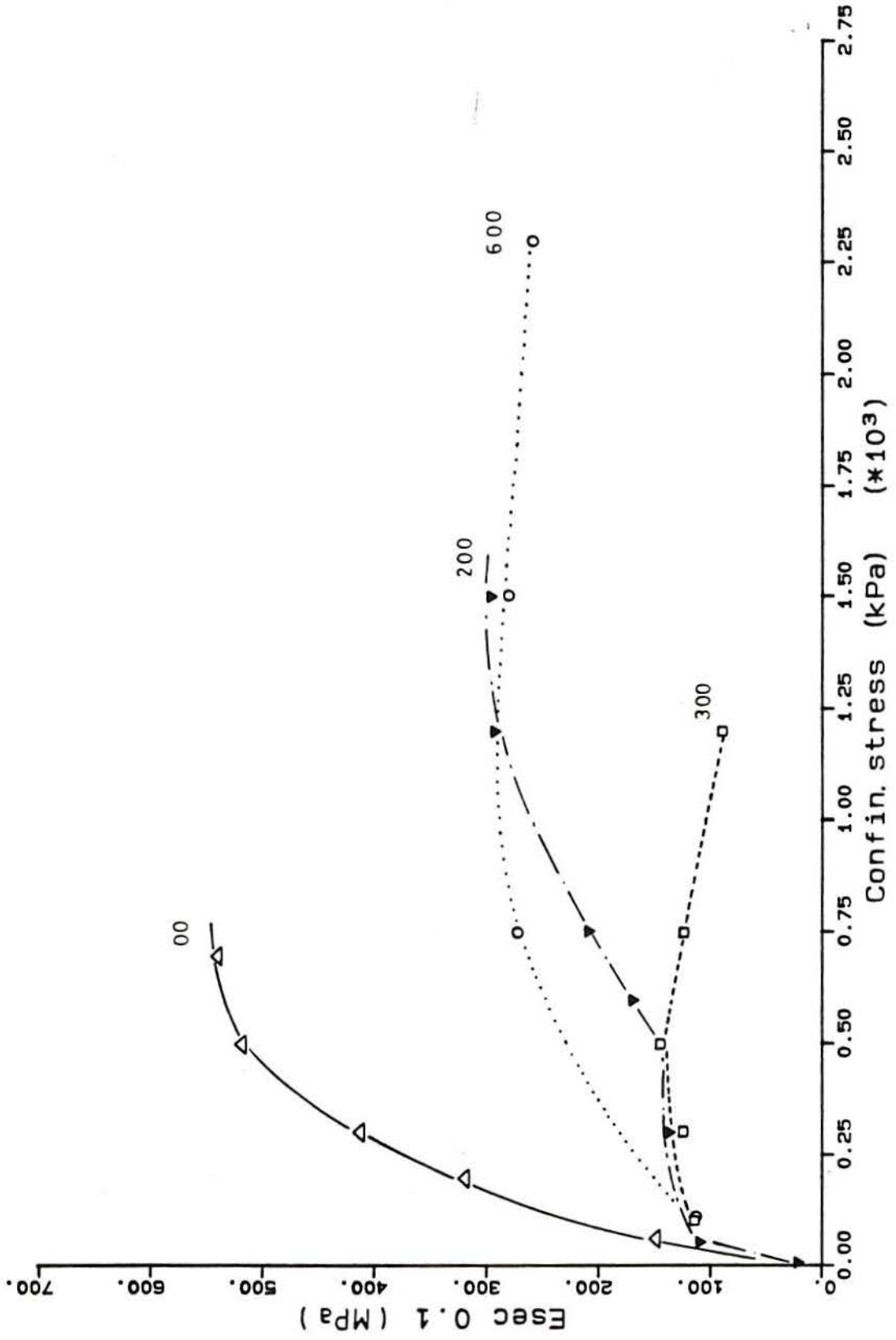

Figure 7.21 – Secant stiffness at 0.1% axial strain versus confining effective pressure for the artificial soil series. (*a*) Stiffness scale of 100 MPa (cont.)

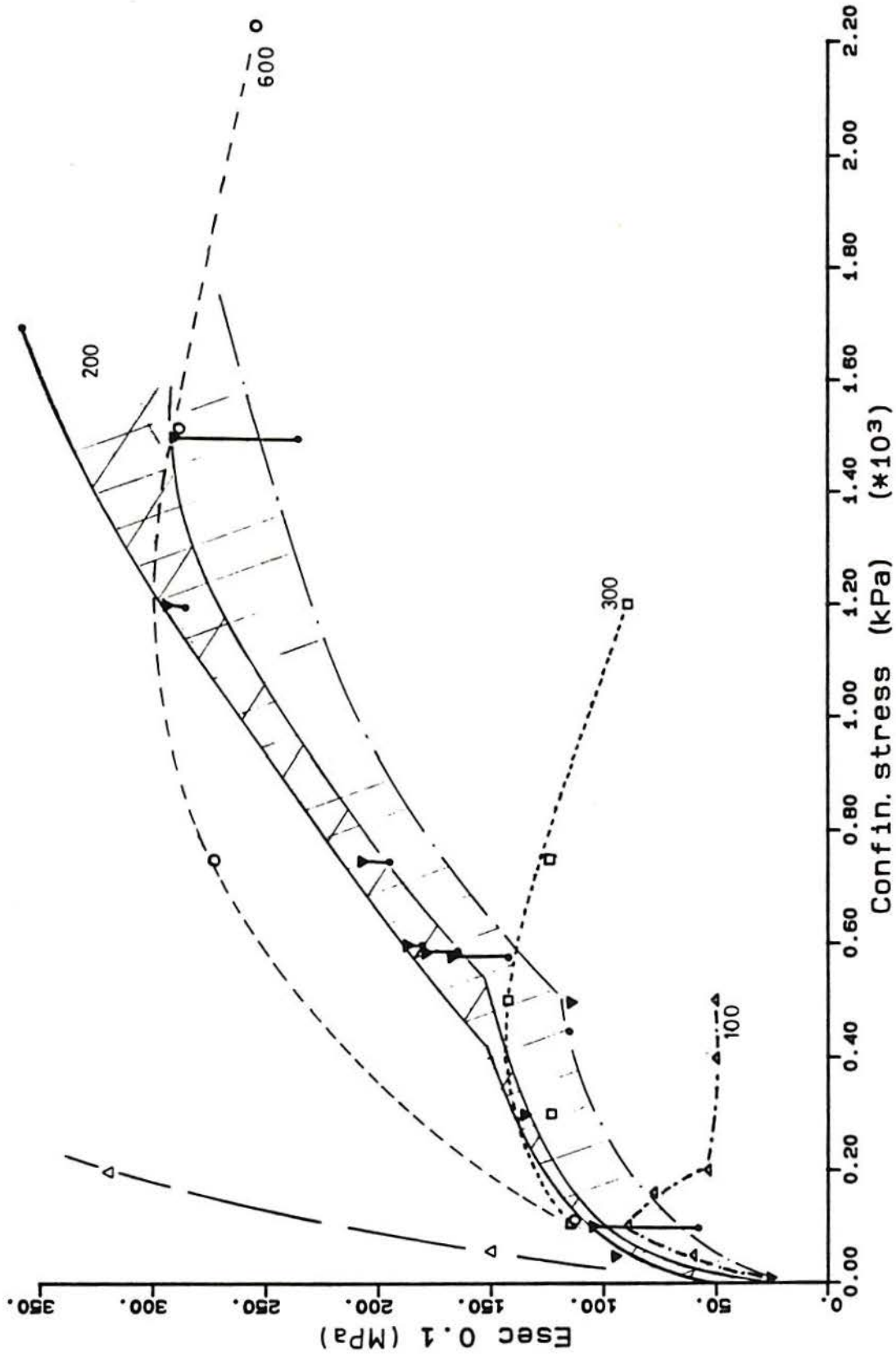

Figure 7.21 – (cont.) (*b*) Stiffness scale of 50 MPa

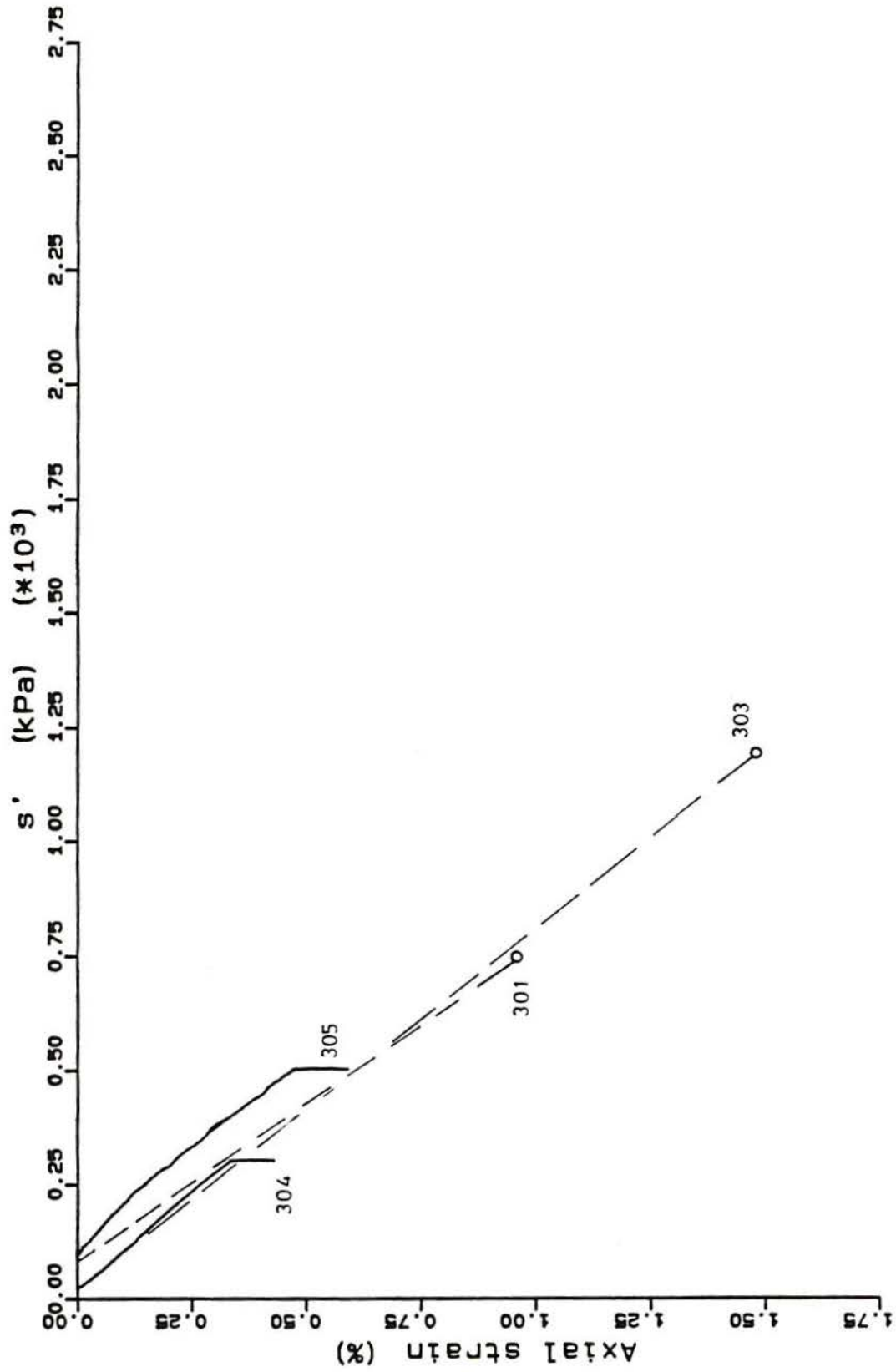

Figure 7.22 - Axial strain versus isotropic consolidation stress of samples of 300 series

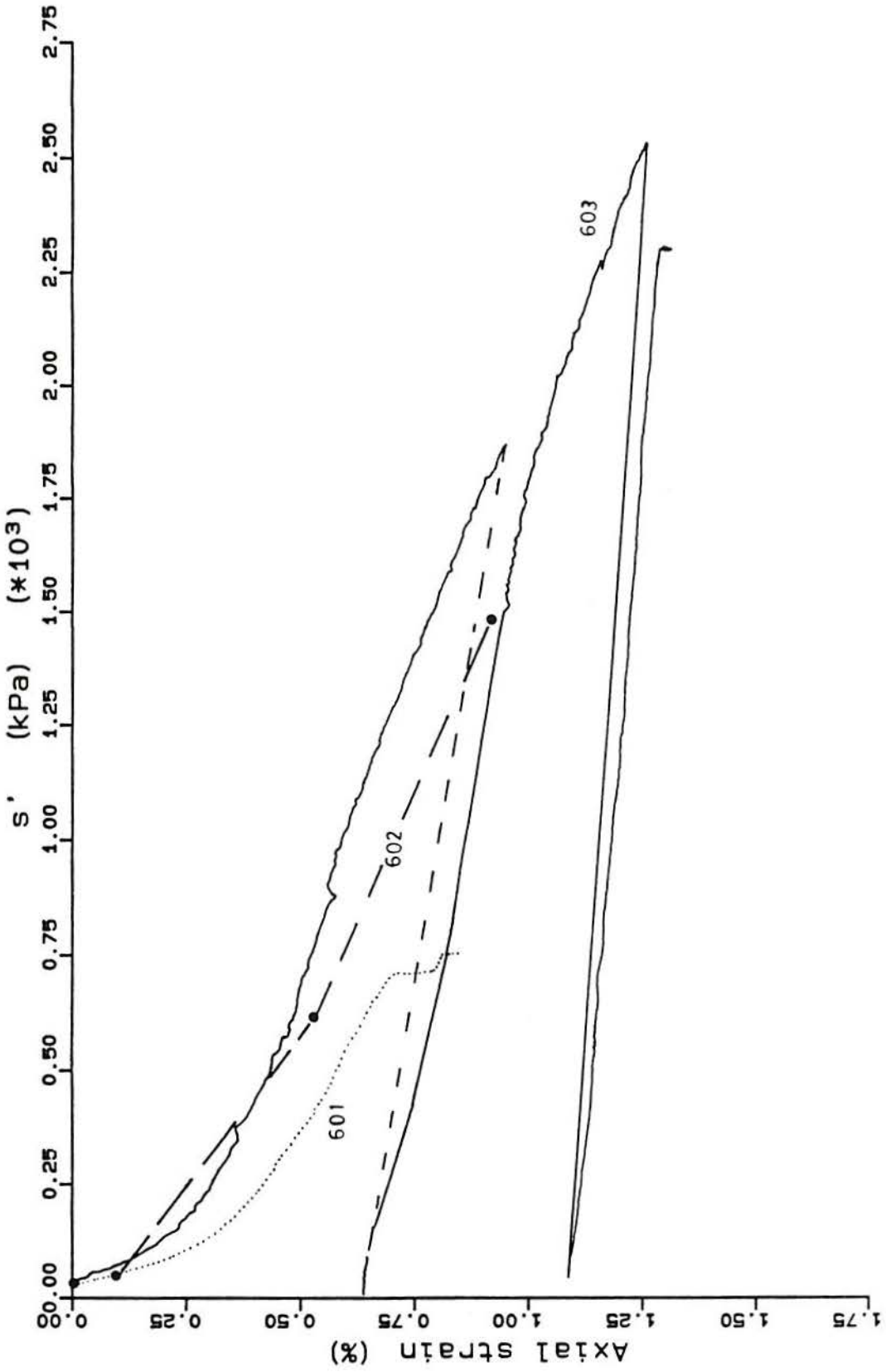

Figure 7.23 – Axial strain versus isotropic consolidation stress of samples of 600 series

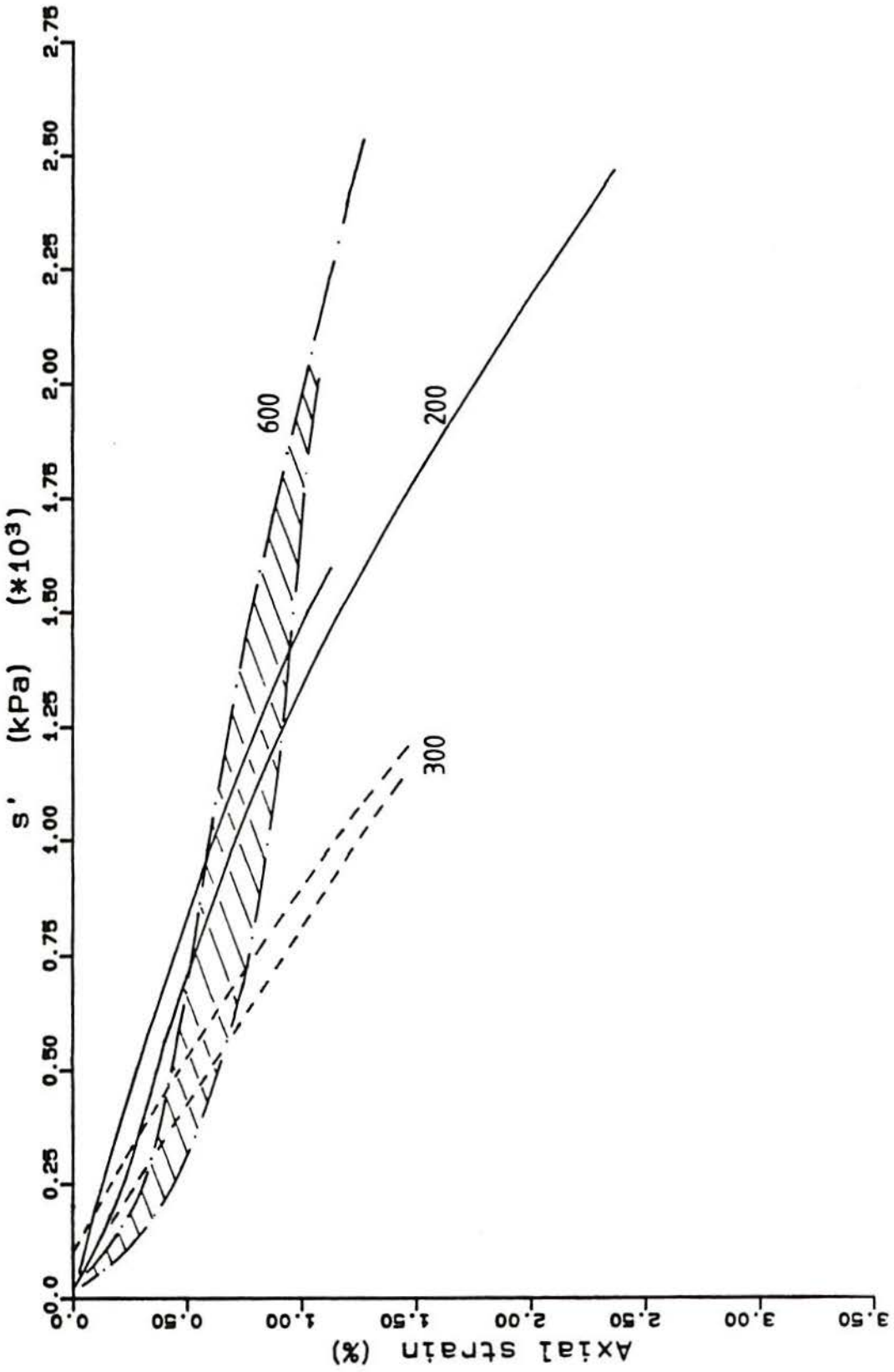

Figure 7.24 – Comparative behaviour of artificial soil series during isotropic consolidation

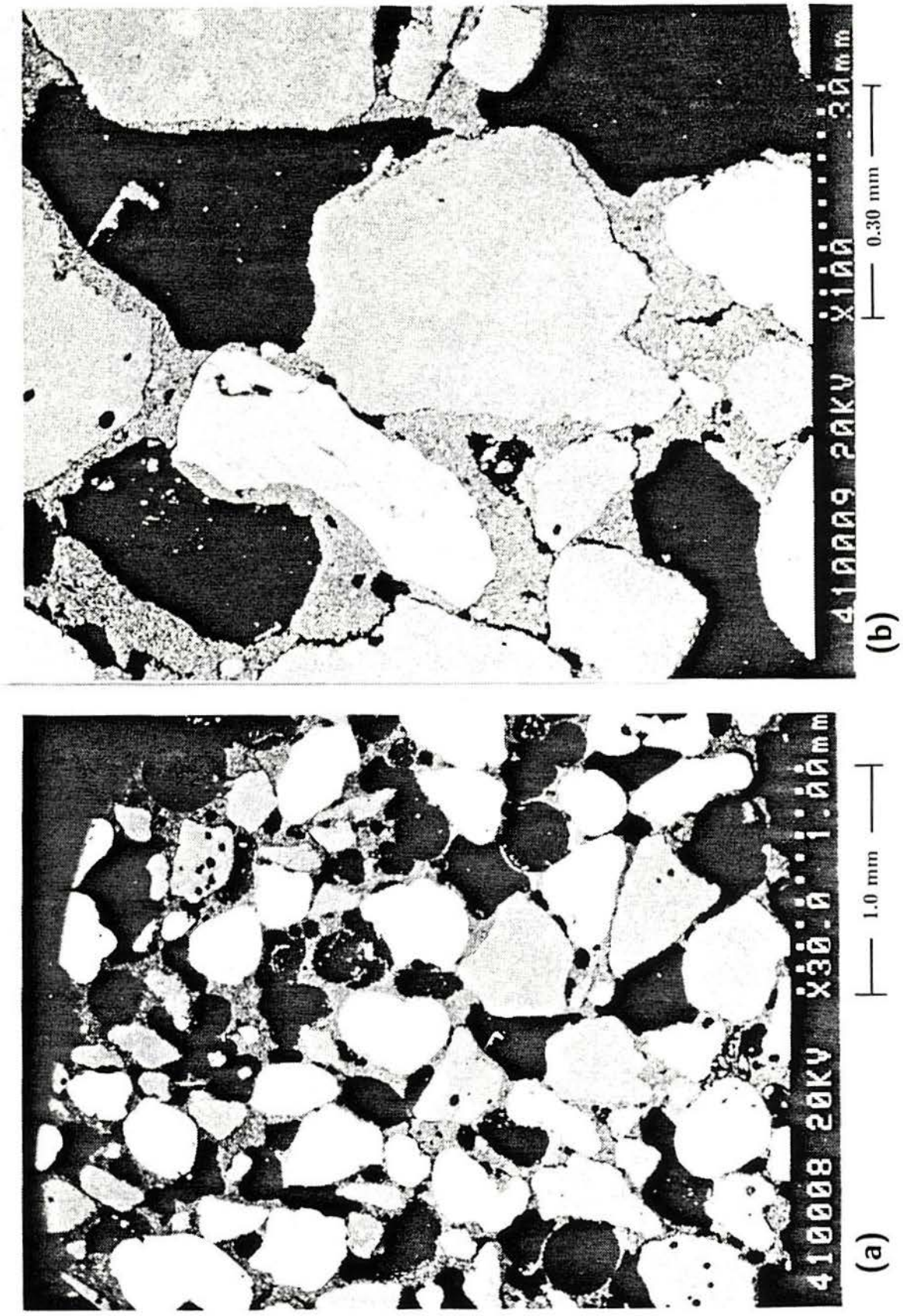

Figure 7.25 – Microphotographs of undisturbed sample of artificial soil 100 series: (*a*) x30; (b) x100

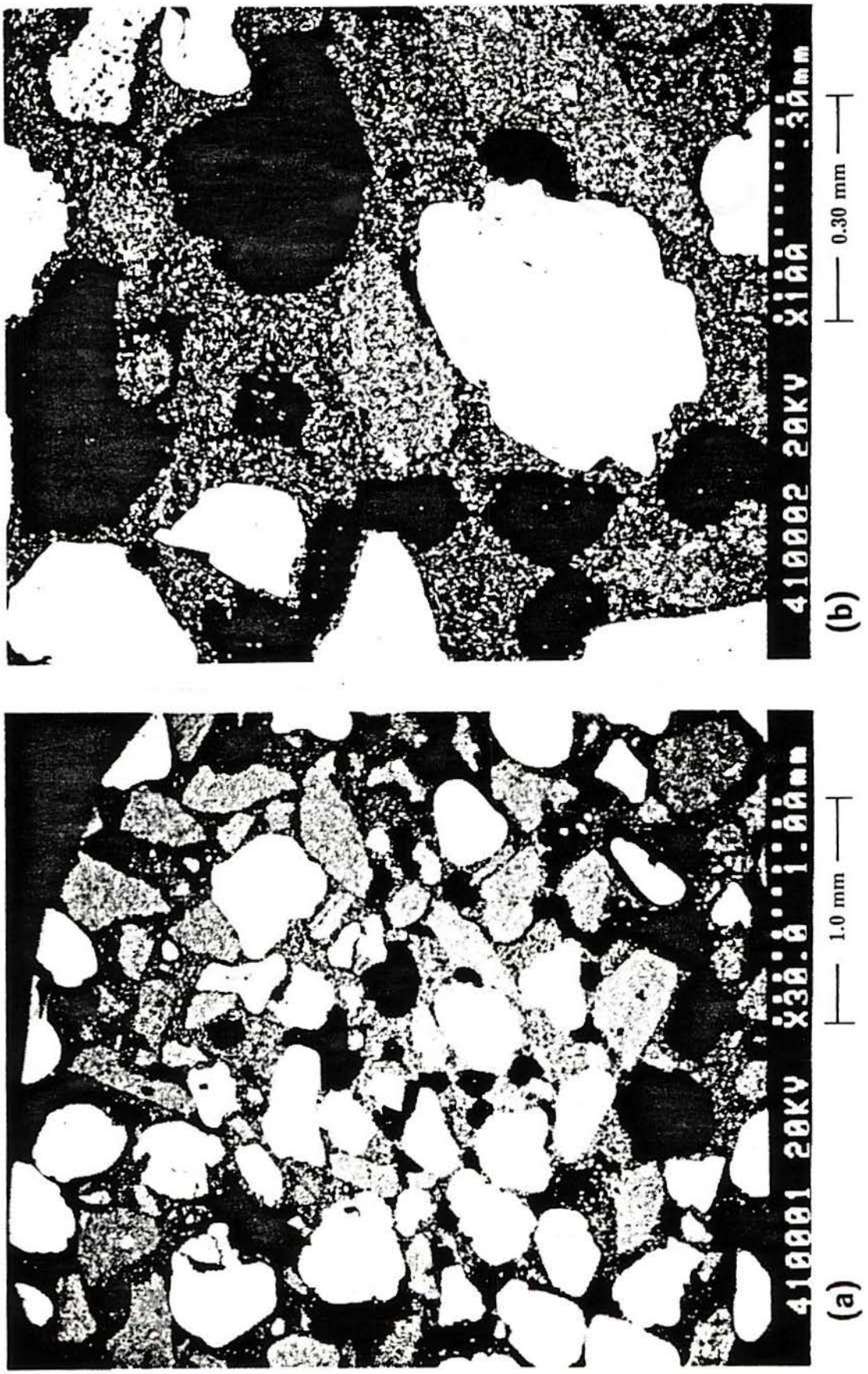

Figure 7.26 – Microphotographs of undisturbed sample of artificial soil 200 series; (*a*) x30; (*b*) x100

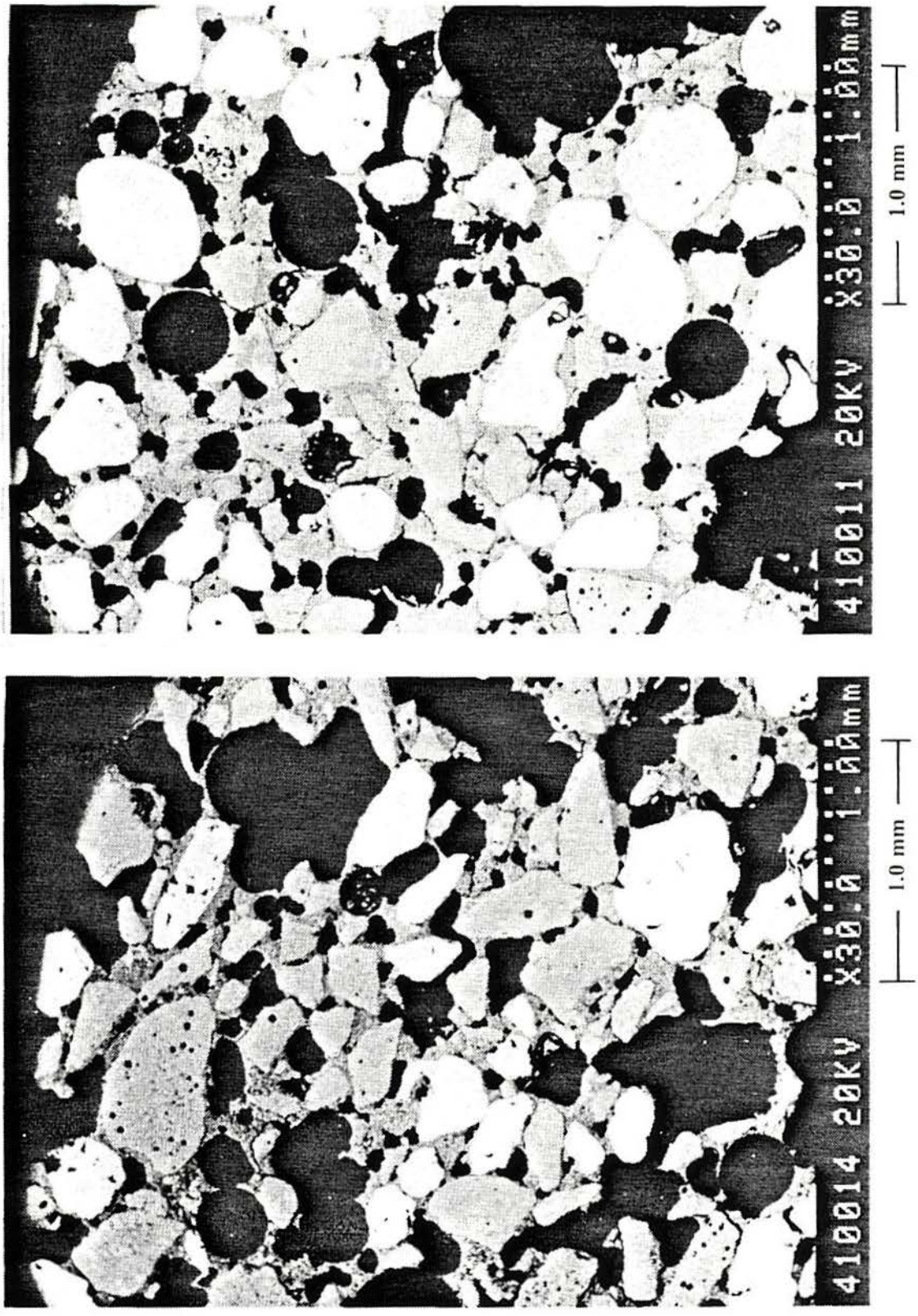

Figure 7.27 – Microphotographs of sample 106 after triaxial testing (σ'_3=100 kPa, ϵ_a=2%, e_f=1.23)

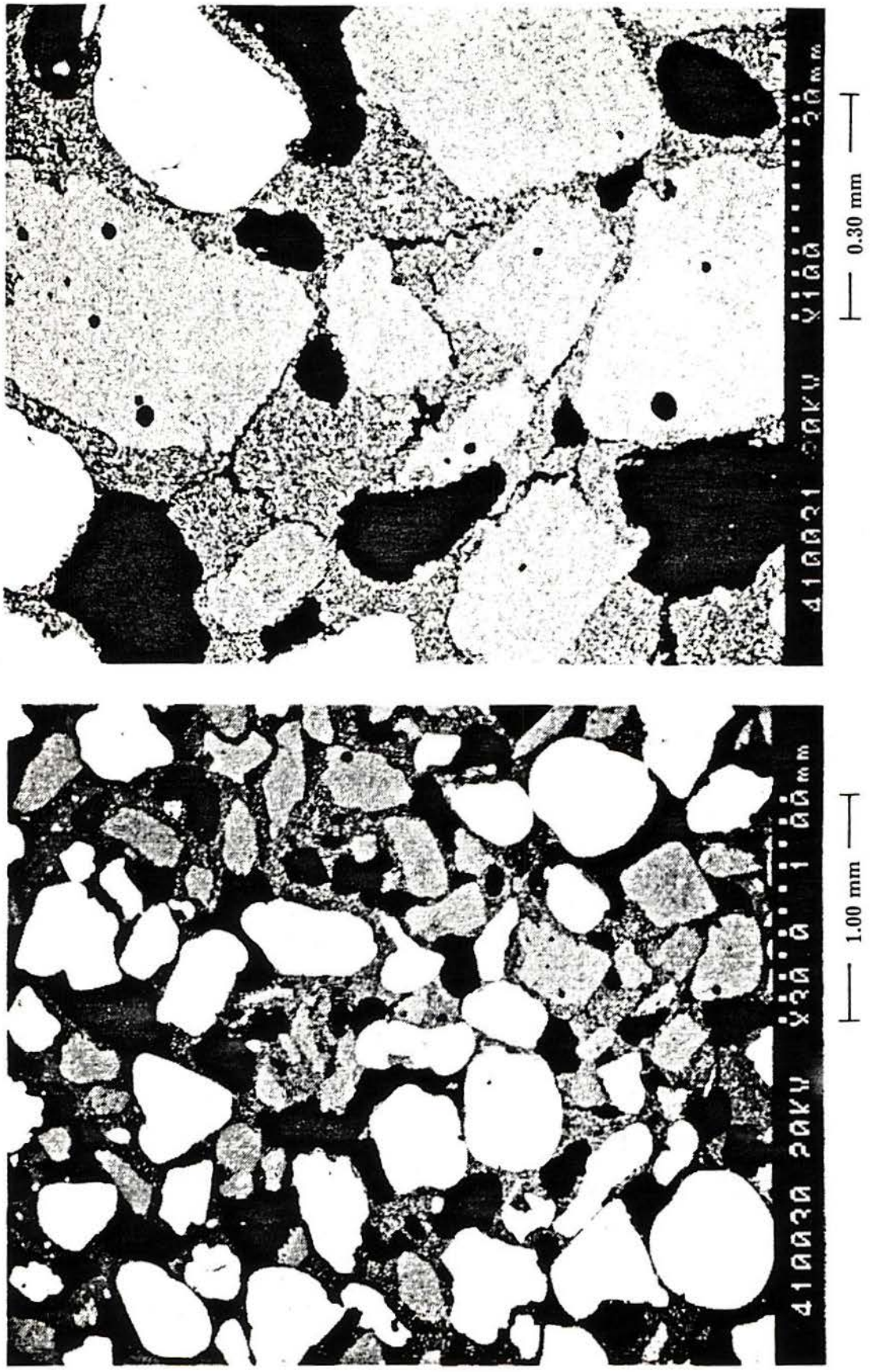

Figure 7.28 – Microphotographs of sample 210 after triaxial testing (σ'_3=100 kPa, ϵ_a=2%, e_f=1.07)

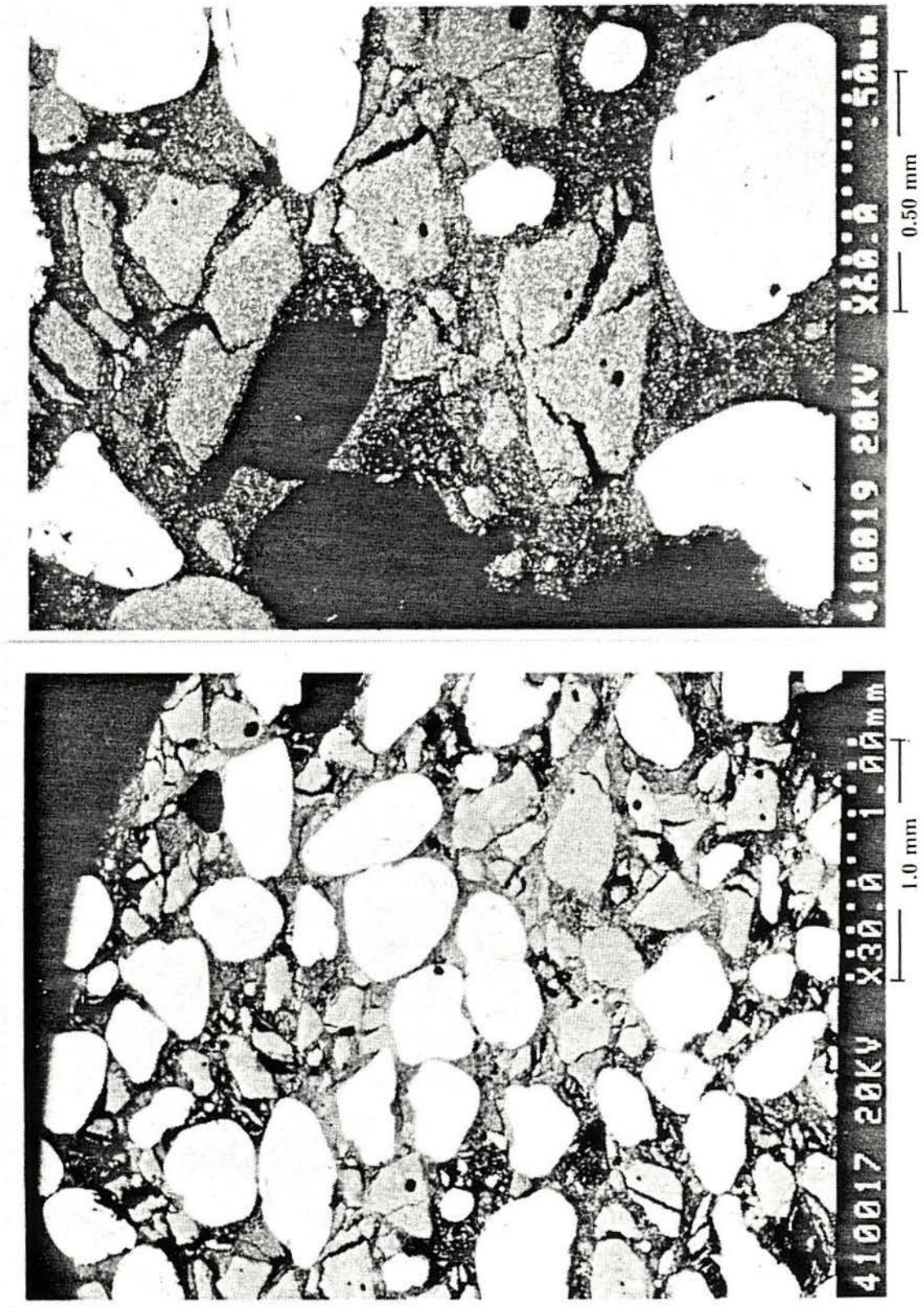

Figure 7.29 – Microphotographs of sample 206 after triaxial testing (σ'_3=600 kPa, OCR=5.5, ϵ_a=22%, e_f=0.62)

8. CORINTH MARL

8.1 INTRODUCTION

The study of the Corinth Marl started after contacts between Prof. A. Anagnostopoulos of the National Technical University (NTUA), Athens, Greece, and Imperial College (IC). An arrangement was made in which fresh samples were collected under the supervision of Prof. Anagnostopoulos, trimmed to triaxial sample size and sent to the author to be tested. Agreement was also made concerning the testing programme: conventional triaxial drained tests would be carried out at NTUA and IC covering the effective confining pressures range of 0-4 MPa. Special stress-paths tests were also considered in order to examine the failure line close to the origin. Nine conventional drained tests were carried out at NTUA and another seven special stress-paths tests were performed at the Research Centre Laboratory of the Ministry of Public Works (KEDE), also in Greece. The results of these tests were sent to the author by Prof. A. Anagnostopoulos and they are included in this thesis, together with the results of the fifteen tests performed by the author at IC. The material has some interesting mechanical characteristics, as will be shown, and some resemblance to the artificial soil behaviour.

In the description of the results, the two series are presented so that they are clearly identified. In most respects, the results are directly compared as the samples are from the same site and were tested under similar conditions. Note, however, that the NTUA results were all obtained using external strain measurements, whereas the IC results were obtained using local axial strain instrumentation.

8.2 LOCATION AND GEOLOGY

The Corinth Canal is an important navigational feature in Greece connecting the Corinthian and Saronic Gulfs. The canal was completed in 1893 and it has a maximum height of 75 m above water level (8 m depth of water) and its walls have slopes of 75°-80° (5:1). The canal is 6.3 km in length and, although subjected to earthquakes on a number of occasions, it has a satisfactory performance in terms of stability (Christoulas et al., 1984). The broader area of the isthmus of Corinth belongs to the sub-Pelagonian geotectonic zone of Greece.

Using the X-ray diffraction method and chemical analyses, Anagnostopoulos (1989) obtained the average composition shown in Table 8.1 for a number of samples of marl at different depths in the Corinth region. The grading (Fig. 8.1) from oven-dried samples shows a clay size fraction ($<2\mu$m) of 13-24%. It seems likely that this fraction contains some calcite and quartz as there is a smaller percentage of clay minerals (<10%) (Table 8.1). Liquid and plastic limits were determined from oven-dried samples. The liquid limit varied between 25% and 37% and the plasticity index between 3% and 12%.

Tests made at NTUA by Anagnostopoulos (1989), on samples collected from the same location as those used in this work gave the following results:

Chemical analysis: Calcite 56%, quartz 24%, illite 10%, plagiocase 5%, chlorite 2%, kaolinite 2%, and muscovite 1%.

Other properties: LL 28%, PL 20%, G_s=2.72, WC=19-21%, percentage passing 0.074 mm sieve = 98%, degree of saturation = 90%.

There are some differences in the amount of quartz, calcite and illite present in the Corinth canal samples compared with those collected around the area (see above) but the Atterberg limits are within the same range.

8.3 PREVIOUS WORK

Anagnostopoulos (1989) presented the results of a series of triaxial tests on the bluish grey marls of the Corinth Canal. They were performed on 38 mm diameter samples which were sheared undrained after isotropic consolidation. Cell pressures of up to 3.5 MPa were used with back pressure used for saturation. The maximum Mohr circles obtained are shown in Fig. 8.2.

The failure envelope shows some curvature and tends to ϕ'=30° at confining pressures greater than 2 MPa. He also presents data on residual strength of the marl, obtained from a ring shear apparatus such as described by Bromhead (1979). Twelve of these tests were performed with vertical pressures in the range of 50-400 kPa. The residual friction angles were all between 31° and 32°.

The stress paths of these triaxial tests were sent to the author by Prof. Anagnostopoulos during this research (Fig. 8.3). A straight failure line can be assumed with values of ϕ'=26.2° and c'=300 kPa. The shapes of the stress paths are interesting: the samples consolidated at pressures less than 1.5 MPa showed remarkably little increase in pore pressure up to failure.

Although all the samples had been saturated before shearing, they had been allowed to dry prior to testing due to inadequate storage (Anagnostopoulos, 1989), and this may have influenced the results.

More recently Kavvadas (1990) analysed data from tests from a new sample batch. Block samples were taken just above water level from the canal wall and trimmed to size in the laboratory. He also performed some tests on de-structured material (remoulded and reconsolidated, and slurry samples), both in terms of strength and compressibility. It is important to note that the samples are from the same location as those used in this thesis.

Fig. 8.4 shows consolidation curves for intact and reconsolidated samples, together with the results from a sample consolidated from a slurry, obtained from both isotropic and one-dimensional compression tests. There is a very large difference in behaviour even when the

initial void ratios are similar. Kavvadas (1990) indicated two yield points: at 3250 kPa and at 4000-5000 kPa, following Vaughan (1985) . Note that even after this second yield the intact sample still remains at a considerable higher void ratio (0.545) than the de-structured sample (0.408).

Fig. 8.5 shows the results of five drained triaxial tests on the intact marl. The samples consolidated at 98 kPa and 294 kPa isotropic effective stress showed a clear peak followed by a gradual reduction in stress. Kavvadas noted that the maximum dilation rate occurs at approximately the same stress as the peak stress. At higher stresses, the samples compressed throughout the test and the compression rate was more or less proportional to the consolidation pressure.

The maximum deviator stresses obtained from the complete set of drained tests are plotted in Fig. 8.6, together with the yield points, defined as the point of abrupt change in stiffness during the tests. The yield curve defined closely resembles those found for the artificial soil and, as the others, seems to be centered on the isotropic axis.

The stress-paths of a number of consolidated undrained triaxial tests carried out on the intact material are shown in Fig. 8.7. Tests carried out from consolidation pressures larger than 2 MPa exhibit a different behaviour from those started at lower consolidation pressures, due to excess pore-pressure generation. The peak strength points of all of the samples are plotted in Fig. 8.8. Kavvadas (1990) suggests a straight line failure envelope for pressures below 2000 kPa with parameters ϕ'=26.5° and a'=300 kPa (or c'=335 kPa), and ϕ'=33.4° and c'=0 for higher pressures.

Although Kavvadas says that the latter are the same parameters for the de-structured material (ϕ'=33.4°, c'=0), the data presented in his paper indicate otherwise (Fig. 8.9). The final normalised strength, $(\sigma_1-\sigma_3)/2\sigma'_3$, for the drained tests lies in the range 1.6 to 1.92, corresponding to ϕ' of 38° to 41°, considerably higher than the value mentioned previously.

All of the yield points determined from drained and undrained tests for the intact material are plotted on a graph of q ($=\sigma_1-\sigma_3$) versus p' ($=\sigma'_1+ 2\sigma'_3/3$) (Fig. 8.10) and they

define an ellipse centered on the isotropic axis.

8.4 TEST RESULTS

8.4.1 Sample preparation and testing procedures

All samples tested at NTUA were trimmed from blocks to a very closely specified size. Filter paper strips were used around the sample but leaving a clearance (8 mm) between the strips and the bottom porous stones. For pressures up to 1500 kPa two 0.3 mm thick membranes were used. For higher pressures, two thicker membranes (0.55 mm) were used. Saturation started with an isotropic effective stress of 20 kPa with a back-pressure of 10 kPa for 2-3 hours. The pressures were then increased to 440 kPa and 410 kPa over a period of four days. Three pilot tests gave B values of 0.95-0.97. The pressure used in consolidation was applied undrained as a further check of the saturation (again, B=0.95-0.97 typically). The end of consolidation was obtained from plots of ΔV versus $\sqrt{t}$. During drained shear a constant strain rate of 0.71%/h was used.

For tests carried out at IC a similar procedure was employed. While the high pressure system was being developed some tests were performed in a conventional triaxial cell, limiting the maximum value of back-pressure used. The samples were saturated by use of back-pressure with the cell pressure and back-pressure increasing simultaneously at 1 kPa/min up to back-pressures between 300 kPa and 500 kPa. These pressures were typically held for 3-4 days. Filter paper was not used. Values of B=0.95 were obtained after the first step of consolidation/saturation (normally σ'_3=100 kPa). The strain rates used were 0.18%/h and 1%/h during the shear stages, the former being used in all initial parts of drained tests.

8.4.2 Consolidation behaviour

Two consolidation tests were carried out at NTUA. The first was a normal oedometer

test in a sample with dimensions H=19 mm and ϕ=70 mm. The results are shown as vertical strain versus the logarithm of vertical pressure in Fig. 8.11(a) and the vertical strain versus the pressure to natural scales in Fig. 8.11(b). From plot (a) it is difficult to identify the point of maximum curvature necessary to obtain the maximum pre-consolidation pressure, but it appears to be in the order of 2-3 MPa. Note that the compression above this pressure is not linear in the log scale. From plot (b), three near linear portions can be identified. The deformation tends to increase with pressure at about 2.4 MPa. The vertical stiffness then remains constant up to 5.0 MPa when there is further increase in deformation. This behaviour is not common in soils and the two yield points may be associated with the breaking of bonding/structure and the breaking of individual particles.

One isotropic compression test was also carried out. The results are shown in Fig. 8.12 on both logarithmic and natural scales. In this test the change in compressibility is more gradual although it shows a change in behaviour at around 2-3 MPa.

Physical characteristics of the samples sent to IC are given in Table 8.2. The natural water content was measured from the trimmings of each sample. It underestimated the water content of the whole sample by 1.2% on average. This indicates that the samples were well kept during the storage period. Some of the samples had high degrees of saturation.

Volumetric and axial strain were plotted versus pressure in Fig. 8.13 and 8.14 using the results of the isotropic consolidation phases of the tests carried out at IC. All of the samples swelled (as measured by the negative axial strain) at pressures smaller than 100 kPa. Unfortunately, the volumetric strains could not be measured accurately at the beginning of the tests due to simultaneous intake of water for saturation. The zero reference value was adopted after full saturation in the first step of consolidation. Otherwise, no corrections have been applied to the results as the membrane penetration error is negligible due to the smoothness and uniformity of the samples' surfaces.

The results of different tests shown similar trends, especially for volumetric strains. The scatter is surprisingly small considering that the data came from eight different samples. Test

I11 showed some creep after the normal period of consolidation and was left for 90 h (the arrow indicates this creep). If the logarithmic stress scale is used [Fig. 8.13(a)] it is possible to define an isotropic yield between 2300 and 2500 kPa. The same data plotted on natural scale gives a yield between 2400 and 2750 kPa [Fig. 8.13(b)]. In this plot the scatter is larger, especially for tests 2 and 3.

Using the results of local axial strain measurements, a second figure of strain versus pressure was produced [Fig. 8.14(a) and (b)]. The results of test 2 were considerably different to the others and it was not considered in defining the yield pressure. The shaded areas in Fig. 8.14(a) and (b) represent the likely limits of axial deformation and the intersections of these lines give values of 2300-3200 kPa (logarithmic scale) and 2350-3250 kPa (natural scale).

Using Fig. 8.13(b), a bulk compressibility of 260 MPa can be obtained for the pre-yield phase. The post-yield value drops to 35-48 MPa.

8.4.3 Strength characteristics

8.4.3.1 Failure parameters from conventional tests

The author performed fifteen triaxial tests on intact samples of Corinth Marl: seven undrained compression tests and six drained compression tests were carried out after isotropic consolidation; two other samples were tested in one-dimensional compression. The main details of these tests are shown in Table 8.3.

Fig. 8.15 and 8.16 show the results of drained tests carried out on the marl. All of the tests were sheared initially at 0.18%/h and later some had the rate increased to 1%/h. This change has a marked local effect on the stress-strain curves (showing a sudden increase in stress) but it does not seem to significantly affect the ultimate strength (see tests I1, I8, I10, and I11). Test I6 was not taken to failure, but was instead unloaded and, after a stabilization period, carried out as an undrained test (test I7). All of the drained tests, except test I1, compressed throughout the test with volumetric strain variation being more or less

proportional to the confining stress applied. Even after well defined failure at large strains, tests I10 and I11 continued to show some increasing volumetric strain. The other surprising feature of these tests was the occurrence of well defined shear planes together with general bulging on samples I10 (2750 kPa) and I11 (3250 kPa) and bulging of sample I1 (525 kPa) when the opposite would be expected (Farmer, 1983; Goodman, 1989). In test I1 the maximum rate of dilation occurred simultaneously with a more or less constant load.

Seven undrained shear tests were also carried out. Five of the test results are shown in Fig. 8.17. All of the samples were initially sheared at a strain rate of 0.18%/h. However, samples I2 and I12 had the strain rate increased to 1%/h later, and for the sample I2 this had a significant effect on the pore-pressure generation and the resulting stress-strain curve. Shear planes were observed on samples I4, I5 and I12, while the others showed slight bulging. The shear planes of both tests sheared starting from σ'_3=100 kPa intersected the pedestal, having developed near the base and not at the sample mid-height. The shear planes were at angles of 67° and 60° to the horizontal for tests I4 and I12 respectively. The different behaviour of test I4 to the others is quite striking and will be discussed later.

Using the peak strength from both drained and undrained tests, a straight failure line with ϕ'=33.8° and c'=60 kPa seems well defined over a large range of stress (Fig. 8.18). The same failure line fits the data well in the s' range 0 to 1000 kPa (Fig. 8.19) with the significant exception of test I4 which attained a stress ratio (t/s') higher than any of the other tests. It is remarkable that the stress paths of three undrained tests (I2, I3 and I5) converged so closely.

Table 8.4 gives the main characteristics of the samples and results from the tests carried out at NTUA. Note that these samples are all from the same batch as those tested by the author at IC.

Fig. 8.20 shows the results of the eight drained tests performed at NTUA. Like test I1, sample N8 (505 kPa) was the only one to show any dilation during the test and it also had the peak strength coinciding with the onset of dilation and not with the maximum dilation rate. The compression of the samples seems to increase with the initial consolidation pressure.

Comparing the peak strength of these tests with the ones carried out at IC it seems that the NTUA results showed a larger scatter, with a tendency to exhibit lower strengths [Fig. 8.21(a) and (b)]. However, the straight line defined above seems adequate in describing the strength of all of the tests.

8.4.3.2 Failure envelope at low stresses

The data presented so far seems to indicate a linear failure envelope for all drained tests and for most of the undrained ones, the notable exception being test I4. In order to check the results of this test, it was considered necessary to perform some special tests. Six tests (N1 to N6) were carried out in Greece, at the soil mechanics laboratory of the Ministry of Public Works (KEDE), at the request of Prof. A. Anagnostopoulos. Samples from the same batch as those tested by the author were used. The samples were isotropically consolidated at a range of stresses between 150 and 900 kPa. Four samples were loaded conventionally in drained compression and then, while maintaining the value of t constant by manual control, were laterally unloaded until failure. The resulting stress-paths and failure points are shown in Fig. 8.22. The results of the two other tests, sheared at constant p', are also shown in the figure. Test N6 almost reached the line of zero lateral stress and had to be loaded further as a conventional drained test. All of the failure points of these tests are well above the previously defined failure line.

Another test was then carried out at IC (I13) to verify this behaviour. The sample was consolidated isotropically to 490 kPa, loaded drained to t=710 kPa and partially unloaded. This reduces the creep and allows better control of the constant load part of the test. A value of t=500 kPa was held constant while the effective radial stress was reduced at 1.6 kPa/min (Fig. 8.23). The sample was able to sustain a stress ratio larger than the limit defined by the conventional tests. The effective cell pressure dropped to 10 kPa (point A in the figure) and the sample was then strained further under this constant cell pressure and at a constant rate. A clear shear plane developed later (point B) which intersected the pedestal, with an angle of

approximately 75° to the horizontal. The apparent reduction of axial strain after point B was due to stress relief of the two separate blocks each containing one local transducer. The external axial strain increased by 0.4% from point B to the end.

The results of the tests carried out under a constant t are plotted together with the stress-path of test I4 in Fig. 8.24. Parts of the stress paths of tests made at KEDE are sketched. Also marked on the figure are two failure lines; one represents the overall behaviour of most of the samples (ϕ'=33.8° and c'=60 kPa), the other is the line proposed by Kavvadas (1990) (ϕ'=26.5°, c'=335 kPa).

The line with parameters ϕ'=33.8°, c'=60 kPa seems to represent the basic strength of the intact material as it seems to be valid over quite a large range of stress. It is interesting that it marks the lower bound of most undrained tests at values of s' less than 1.5 MPa and it represents the limit for all conventional drained tests carried out for this thesis, regardless of the pressure range.

To investigate the shear strength of the material for pressures below 1.0 MPa, it seems necessary to carry out special tests with reducing lateral pressures. They appear to be the most effective way to define the maximum stress ratio attainable repeatably. Occasionally an undrained test may reach the same ratios, as was the case for test I4. However, this is rather fortuitous as demonstrated by the results of test I12 which failed at a much lower stress ratio despite having a similar void ratio and test conditions to I4.

The curved failure envelope obtained from the special drained tests at KEDE together with tests I13 and I4 has a close resemblance to that obtained from the results of tests on the artificial soil: it can only be assessed properly with special stress-path tests and indicates, because of its curvature towards the origin, that the tensile strength is small.

8.4.3.3 Tensile strength

To investigate the tensile strength of the intact Corinth Marl directly, five cylindrical samples were tested in the Brazilian test (diametrical compression). Two samples originally

trimmed for triaxial testing were cut to produce small cylinders for testing. Three of these cylindrical samples were put inside a conventional triaxial cell for saturation with back-pressure in the same way as the triaxial samples. After saturation they were assembled in the testing rig described by Maccarini (1987), submerged in water and loaded at a constant rate of strain. The three tests gave the following values of tensile strength (samples saturated and submerged):

(a) sample 1 — 9.0 kPa

(b) sample 2 — 16.0 kPa

(c) sample 3 — 15.0 kPa

Such fine grained material may also develop large suctions when partially saturated. To test this influence, two more tensile tests were carried out in which the samples were also saturated with back pressure as described above. However, they were tested in air, so that suction could develop both by evaporation of the water from the surface and due to the sample dilation during testing.

The first sample tested this way (sample 4) gave such a high apparent tensile strength that a second modified test was carried out. The sample was loaded with the surface dry up to a certain load level when it was wetted on the outside via a plastic bottle nozzle (the arrow on test 5, Fig. 8.25). The stiffness was clearly affected and the final apparent strength is an intermediate value between the previous set of results (submerged) and the surface dry one (test 4). The results obtained are (both samples were saturated):

(c) sample 4 — 73 kPa (dry surface)

(d) sample 5 — 29 kPa (wet surface)

These results indicate that the drained tensile strength is comparable with that of the 200 series artificial soil and that its value is consistent with the curved envelope of Fig. 8.24. It also shows that the suction developed due only to the dry surface can considerably increase the available strength and may play some role in the field stability.

8.4.4 Yield

The test results obtained at IC and in the Greek laboratories (NTUA and KEDE) were analysed to verify if yield occurred in the same way as for the artificial soil.

The tests carried out at IC had local strain instrumentation installed on the samples and this allowed a much closer examination of their small strain behaviour. Their stress-strain results are shown in Fig. 8.26 and the points of change in behaviour, adopted as yield points, are indicated by dots. An important result was obtained from test I11 (σ'_3=3250 kPa) as it shows a clear yield point much lower than those shown by others tested at lower confining stresses.

The same yield points can also be defined when log-log plots are used (Fig. 8.27). The tests show a bi-linear behaviour, except for test I1 which had a yield almost coincident with failure. Values of the yield pressure were obtained from the intersection of the two straight lines for each test.

The same kind of construction and criteria were applied to the results of tests carried out in Greece. Fig. 8.28(a) and (b) shows the natural scale results and the yield points selected and Fig. 8.29 the plots using logarithmic scales. It is interesting to note that, although the small strains are unreliable on these tests, both kinds of plots show relatively clearly defined yields. The results of test N15 show a different pattern to those of the other tests, especially in log-log scales, where it does not show bi-linear behaviour.

The radial strain behaviour of the samples tested at IC was also examined and the results are plotted as t versus radial strain in Fig. 8.30. The yield points selected from Fig. 8.26 are also marked on the test curves. In most of the tests they are in a region of clear change in behaviour and this is particularly so for tests I6, I8, I9, and I10. The result of test I11 is clearly different to the others and its yield point is in a region where there is no change in radial strain.

Although this plot is useful for confirming the yield points selected, it would be difficult to select them using this plot alone. It is worth also mentioning that the errors in radial strain

are relatively small for the Corinth Marl due to the smoothness of the surfaces.

The yield points determined from all of the triaxial tests are plotted in Fig. 8.31. The isotropic yield is also marked (range 2800-3250 kPa) taken from the results shown in Fig. 8.13 and 8.14. The results obtained at IC seem to plot slightly above the Greece results. As the samples are identical, the most likely explanation for this difference would be the conventional loading ram/top cap arrangement used in the Greek laboratories and the stress concentration associated with it (see Chapter 4).

The yield curve obtained seems less centered on the isotropic axis than those found for the artificial soil (Chapters 5 and 6) or for the Corinth Marl by Kavvadas (1990). Although there are few results of isotropic consolidation at high pressures (at IC the maximum pressure applied was 3250 kPa) the results of isotropic tests presented here seem to indicate the same range of yield pressure mentioned above (Fig. 8.13 and 8.14).

8.4.5 Secant stiffness

It seems evident from Fig. 8.26 and 8.28(a) and (b) that the secant stiffness from individual drained triaxial tests increases with effective cell pressure up to 3500 kPa. For the IC tests the stiffness dropped substantially in the test with the highest confining pressure (test I11). A similar effect was observed in tests N15 and N16. The secant stiffnesses of the IC tests are plotted versus initial confining stress in Fig. 8.32(a) and (b) . Results of both drained and undrained tests are given on each plot. The pattern of stiffness variation seems well defined and for the larger strain (ϵ_a=0.2%) there is a clear drop in the stiffness for the test at 3250 kPa. The normalized stiffness follows the same pattern as for the artificial soil, having a tendency to stabilize at large confining pressures (Fig. 8.33). However, at the highest pressure the stifness is smaller than might be expected.

The results of the tests carried out in Greece cannot be used to obtain stiffnesses at such small strains, but by using stiffnesses at ϵ_a=1.0%, a reasonably clear picture emerges (Fig. 8.34). Although they all have similar stiffnesses, the variation with the confining pressure

appears to be well defined. It is probably more than just coincidence that the test at 3500 kPa showed a drop in stiffness consistent with the results obtained at IC.

8.4.6 One-dimensional compression tests

Two samples were loaded in one-dimensional compression using the radial belt described in Chapter 6 to monitor the radial strain. The first sample ($I14K_0$) was tested using conventional triaxial equipment. The stress-path triaxial cell was used and this limited the maximum effective cell pressure used to 950 kPa. The second test ($I15K_0$) was carried out in the higher pressure triaxial cell described in Chapter 6. The test was carried out up to an effective cell pressure of 3250 kPa. The radial belt withstood this high pressure and its behaviour during the whole test was satisfactory.

The first test was carried out with manual control of the effective cell pressure so as to maintain the radial belt readings within a certain tolerance. The control was successful in maintaining the radial strain smaller than $\pm$ 0.001% ($\pm$0.4 μm) for most of the test. On only three occasions the radial strain went as far as $\pm$0.005% but it was quickly restored. A cycle of unloading/reloading was carried out and the results in terms of stress-path and strain are smooth and similar to those for artificial soil (Fig. 8.35 and 8.36). The stress-path climbed steeply to near the failure line and then bent to the right. Note that this test was started after the isotropic consolidation/saturation had finished, with σ'_3=250 kPa.

Although the result seems to agree well with the general pattern described in Chapter 2 (Fig. 2.8), the final part did not define this trend clearly, as the stress-path seems to be curving down. To investigate the behaviour of the material at higher pressures test $I15K_0$ was carried out. The one-dimensional test started after isotropic compression to an effective stress of 500 kPa. The electrical signal from the radial belt was used as feedback for the pressure control source, thus making the test automatic. Occasional operator intervention was necessary to keep the strain inside tolerance during the initial loading. Later, while left unattended for some time, the control mis-functioned and the radial strain was not kept constant until manual

control was re-restablished, bringing the strain back within the limits. The test also had a cycle of unloading and reloading. During most of the test the radial strain was maintained typically inside $\pm 0.003\%$ ($\pm 1.1\,\mu$m), particularly on the unloading/reloading cycle. However, during the uncontrolled part, the sample compressed radially to $\epsilon_r = +0.045\%$ ($17\,\mu$m).

The results of the test are plotted in Fig. 8.37 and 8.38. At point A the manual control was restored and the steep increase in load from A to B was necessary to return the radial strain to its previous value. At that point the sample showed a considerable axial deformation and some vertical unloading was necessary to keep the radial strain constant. Because the axial strain was so large, the test was unloaded under one-dimensional conditions to zero deviator stress and the triaxial cell was opened for sample inspection. This procedure was done to ensure that no localized shear plane or other such feature had developed which could have influenced the sample deformation. The sample was found to be intact and the test was continued to a second cycle of reloading/unloading (Points C and D).

The results of the two tests are plotted together in Fig. 8.39. It is clear that the tests showed considerable differences in behaviour, both in terms of the stress-path and the compressibility. Test I14K_0 climbed much more steeply in the t-s' stress space and, as a consequence, showed larger deformation for the same values of s'. This test also showed a very good agreement between the stress-paths of the two loading cycles. The second test had a stiffer behaviour but its stress-path was flatter than the other test indicating a lower K_0 value. A comparatively large deformation occurred when the sample was loaded to its maximum value of t (point B).

These results are interesting when compared with the yield points presented above (Fig. 8.40). The yield curve is shown with a more pronounced tip, passing through the points defined by the IC tests. The stress-path of test I14K_0 climbed steeply until it approached the yield line and followed it quite closely thereafter. The second test (I15K_0) showed large deformation when its stress-path reached the yield defined by the conventional triaxial drained tests (point B). It seems that the one-dimensional behaviour is strongly influenced by the

same factors which originate the yield curve. These factors are a function of the bonding strength, as demonstrated for the artificial soil.

8.5 MICROPHOTOGRAPHS

Three samples were sent to the Department of Geology at IC, for preparation of micro-slides. The samples were impregnated with epoxy resin and mounted in glass slides for later examination on a scanning electron microscope at that Department. The microphotographs were taken using a back scattered electron image technique.

The three samples prepared in this way were:

(a) undisturbed sample, e = 0.620 (estimated),

(*b*) sample tested as I2; consolidated at 525 kPa, sheared undrained to $\epsilon_a = 8.5\%$, $e_f = 0.618$,

(*c*) sample tested as I11; consolidated to 3250 kPa, sheared drained to ϵ_a =2 2.8%, $e_f = 0.425$.

On a first examination at low amplification (50-100 times) the Corinth Marl seems a featureless uniform mass. It was necessary to examine the slides at magnifications of 200 times or more to see some of its composition in more detail.

The undisturbed sample provided a control against which the disturbance present in others could be assessed. The general appearance of the undisturbed material can be seen in Fig. 8.41(a) and (b). The darker grains are quartz and the lighter ones with roughly the same size (6 to 25 μm) are calcium. Small very bright particles are pyrite. The main feature of the two figures are the fossil remains which were deliberately emphasized as they give the best indication of disturbance.

The second sample examined (I2) had failed by bulging but the slide examination showed little apparent disturbance. An examination of the whole slide failed to find any shear

plane or preferential structure orientation. There was indication of some calcium grains slightly dislodged or with open fractures, like the one on the top right of Fig. 8.42, but no grain crushing was observed.

The breaking of grains is much clearer on the third sample as it was subjected to much higher stresses and shear strains. The sample naturally looks denser than the others [Fig. 8.43(a)] and the calcium grains are more clearly broken and dislodged [left bottom corner of Fig. 8.43(a)]. The most visible sign, though, was given by the broken fossil of Fig. 8.43(b). It was not possible to find any broken fossils or grains in either the undisturbed sample (Fig. 8.41) or in I2, even though both of these samples contained many intact fossils.

Although these microphotographs are not conclusive, as they only cover two extreme situations, they indicate that the yield at high confining pressures is somehow related to the grains' strength. The collapse of the individual weaker grains seems to contribute to the large distortion of the whole soil structure.

Mineral	% of weight
Calcite	73-77
Quartz	13-17
Feldspar	2-4
Illite	1.5-3
Chlorite	1-7
Illite-Montmorillonite	<1
Pyrite	<1

Table 8.1 — Mineralogical analysis of marls from the Corinth area (after Anagnostopoulos, 1989)

Test	WC_{nat} (%)	WC_0 (%)	γd (kN/m^3)	S_0 (%)	e_0
I1	-	22.45	16.26	95	0.641
I2	-	23.51	16.44	100	0.623
I3	-	21.90	16.24	93	0.644
I4	17.79	18.24	16.57	81	0.610
I5	-	21.57	16.66	97	0.602
I6/7	19.03	21.11	16.25	89	0.643
I8	18.95	20.57	16.53	91	0.614
I9	17.56	19.13	16.63	86	0.605
I10	19.04	20.36	16.70	92	0.599
I11	-	21.18	16.55	94	0.612
I12	21.00	22.47	16.56	100	0.611
I13	18.23	18.90	16.59	84	0.608
I14	21.20	22.54	16.59	100	0.609
I15	18.79	19.06	16.49	84	0.619

WC_{nat}– Water content from trimmings
WC_0 – Water content of the sample as received at Imperial College

Table 8.2 — Characteristics of Corinth Marl samples

Test	σ'_{3_i} (kPa)	e_i	Drainage	Failure[a] (kPa) t	s′
I1	525	0.641	drained	785	1324
I2	525	0.618	undrained	845	1445
I3	740	0.635	undrained	825	1430
I4	100	0.610	undrained	461	582
I5	520	0.602	undrained	725	1184
I6/7	1800/1800	0.633	drain./undr.	1747	3200
I8	1500	0.608	drained	1871	3372
I9	2250	0.588	drain./undr.	1828	3204
I10	2750	0.591	drained	3509	6242
I11	3250	0.574	drained	4133	7379
I12	100	0.611	undrained	210	309
I13	490	0.599	drained[b]	441	454
I14K_0	250	0.634	drained	-	-
I15K_0	480	0.619	drained	-	-

$G_s = 2.72$
(a) Maximum σ'_1/σ'_3
(b) Test with constant t and reducing s′

Table 8.3—Main characteristics of Corinth Marl samples tested in triaxial compression at Imperial College

Test	σ'_{3i} (kPa)	e_i	Failure (kPa) t	s′
N8	505	0.599	830	1335
N9	905	0.574	1150	2055
N10	1200	0.559	1580	2780
N11	1500	0.574	1760	3260
N12	1800	0.607	1960	3760
N13	2120	0.569	2720	4840
N14	2500	0.564	2990	5490
N15	4000	0.539	4560	8560
N16	3500	-	-	-

$G_s = 2.72$

Table 8.4—Corinth Marl samples tested in triaxial drained compression at NTUA

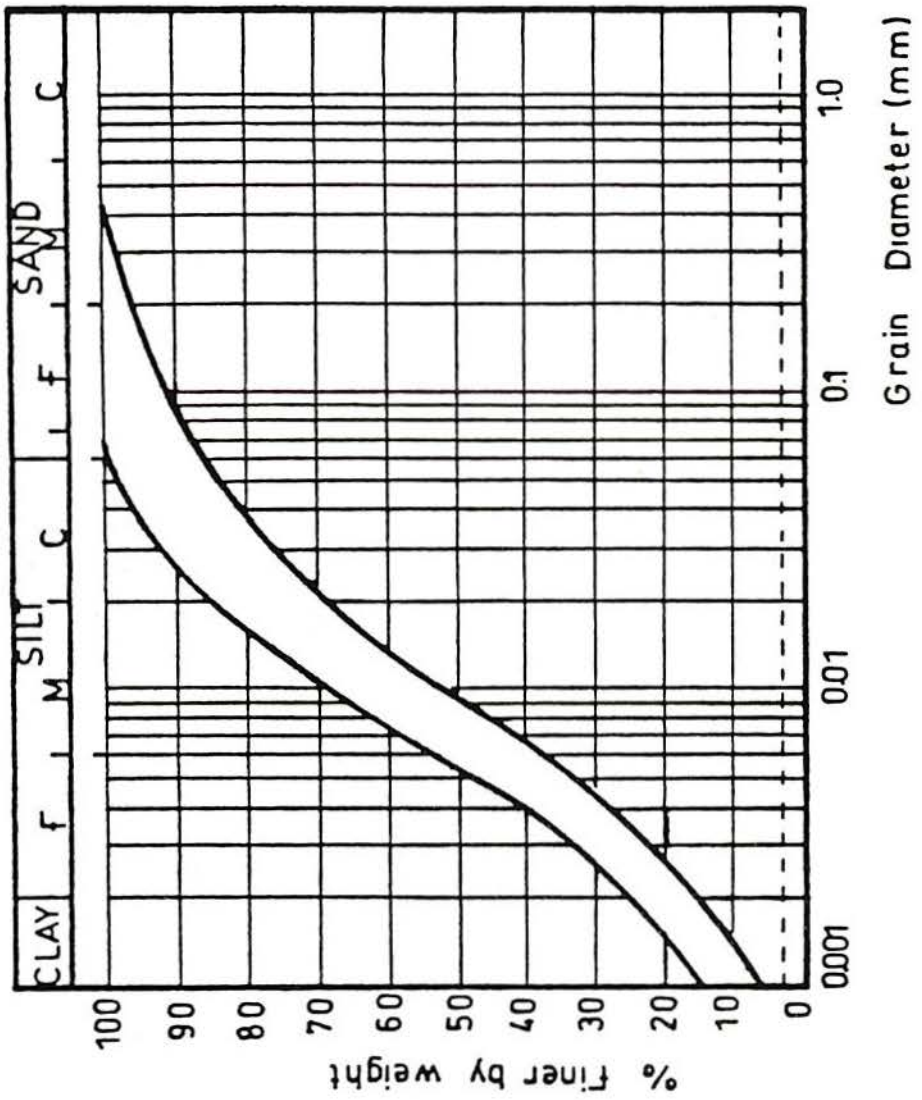

Figure 8.1 – Grading curve envelope for samples of various marls from the Corinth region (after Anagnostopoulos, 1989)

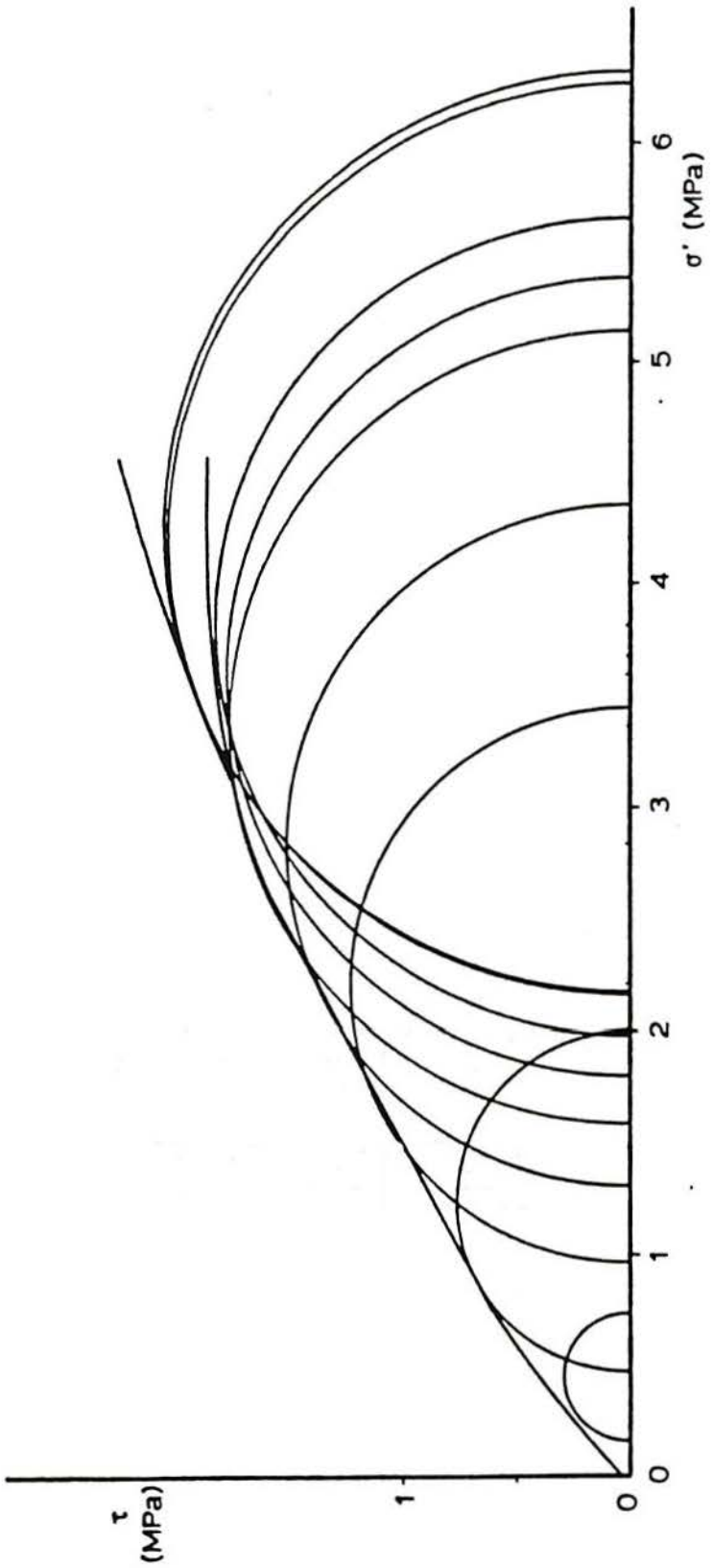

Figure 8.2 - Maximum Mohr-circles of stress for undrained tests on Corinth Marl (after Anagnostopoulos, 1989)

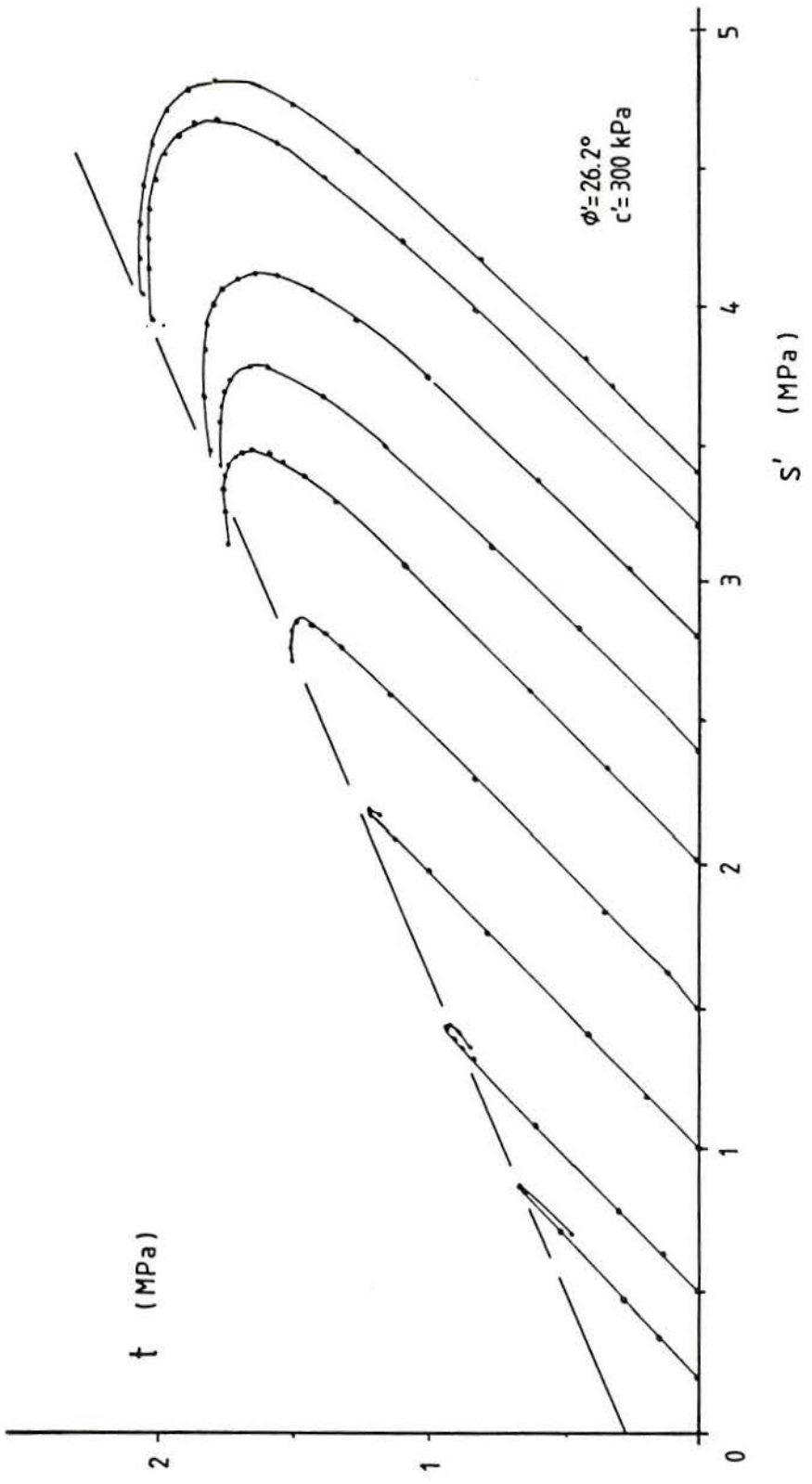

Figure 8.3 – Stress-paths of undrained tests on Corinth Marl (after Anagnostopoulos, 1989)

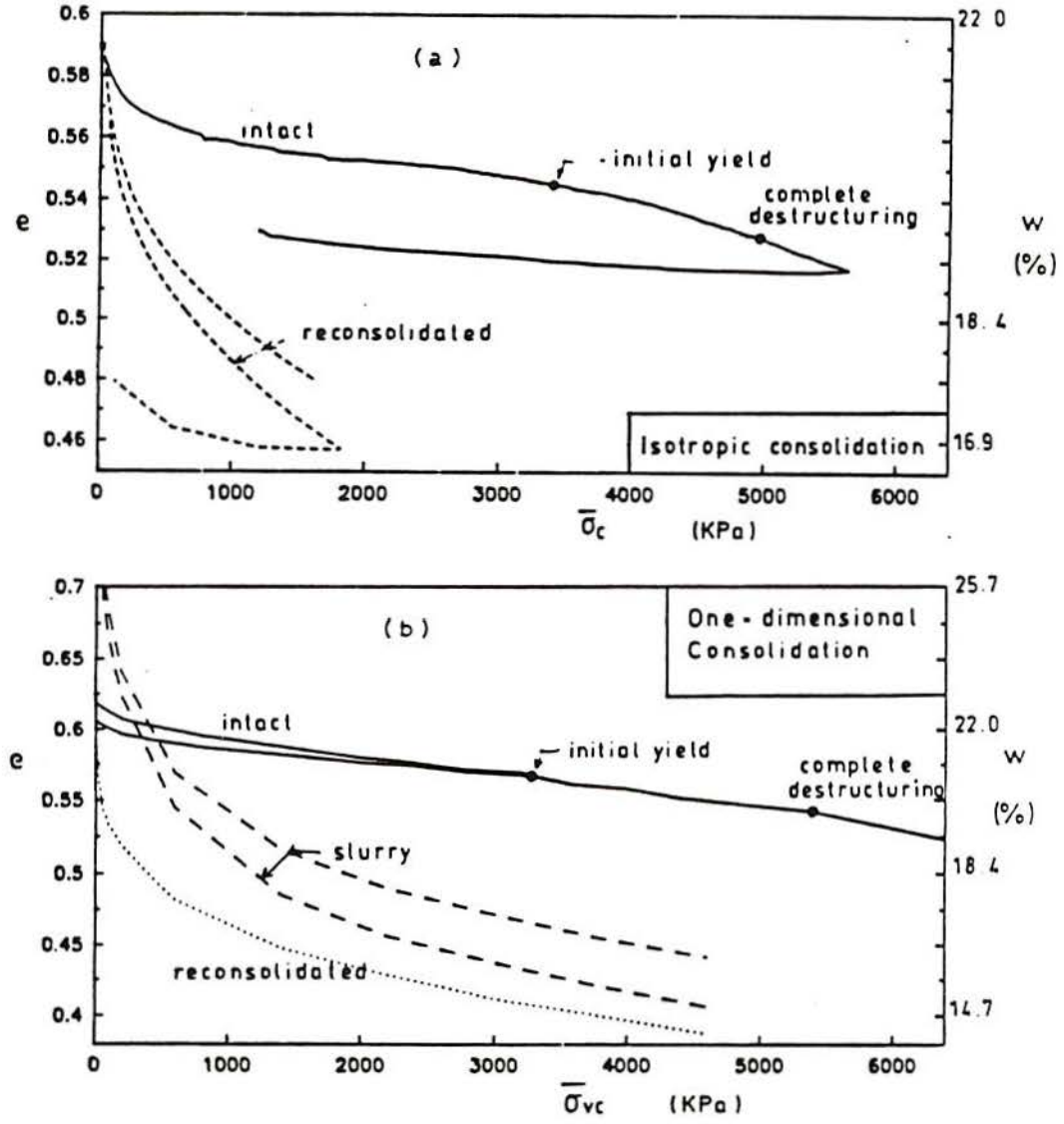

Figure 8.4 – Results of consolidation tests on different samples of Corinth Marl (*a*) isotropic consolidation; (*b*) one-dimensional consolidation (after Kavvadas, 1990)

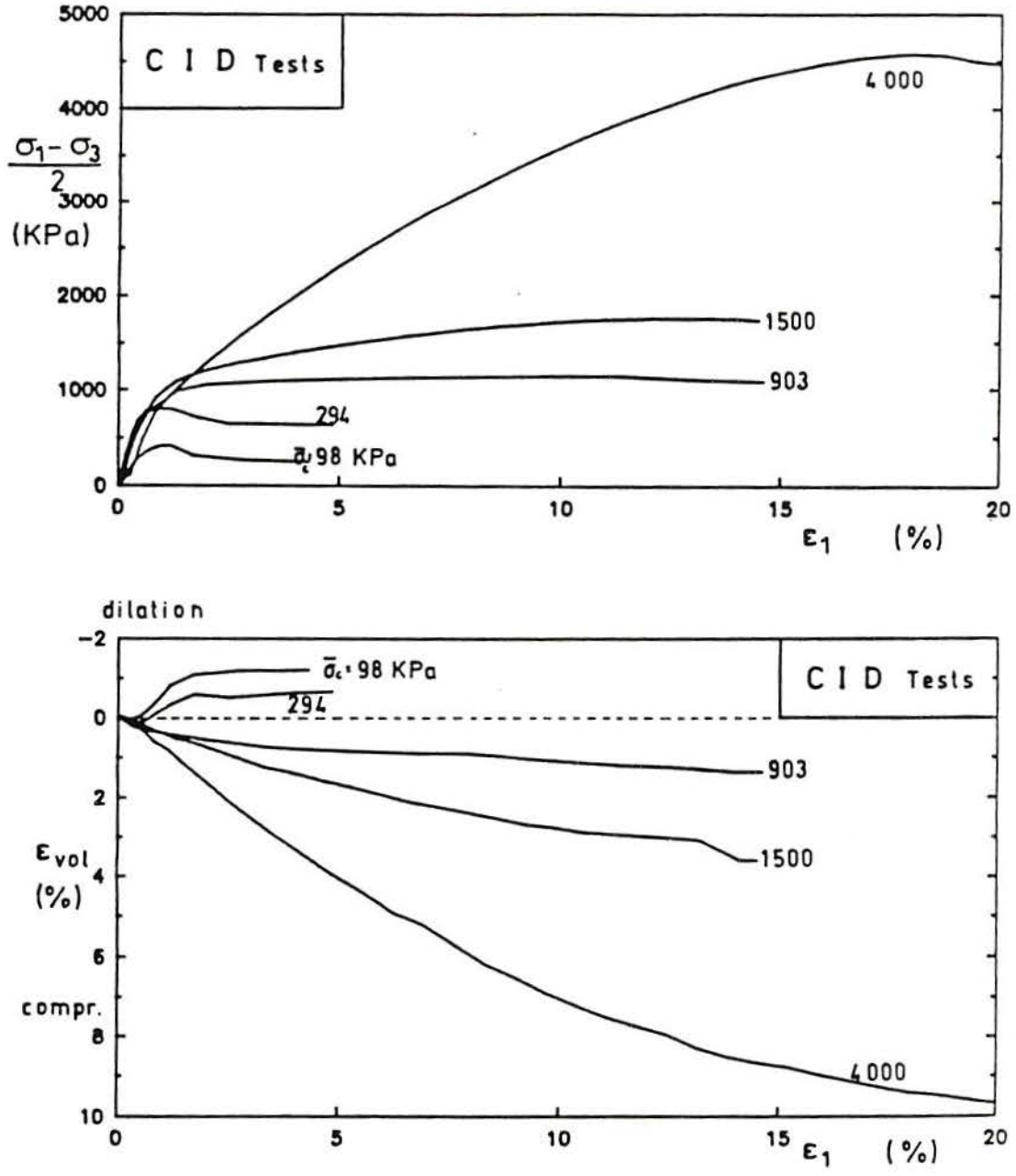

Figure 8.5 – Results of drained triaxial compression tests on Corinth Marl (after Kavvadas, 1990)

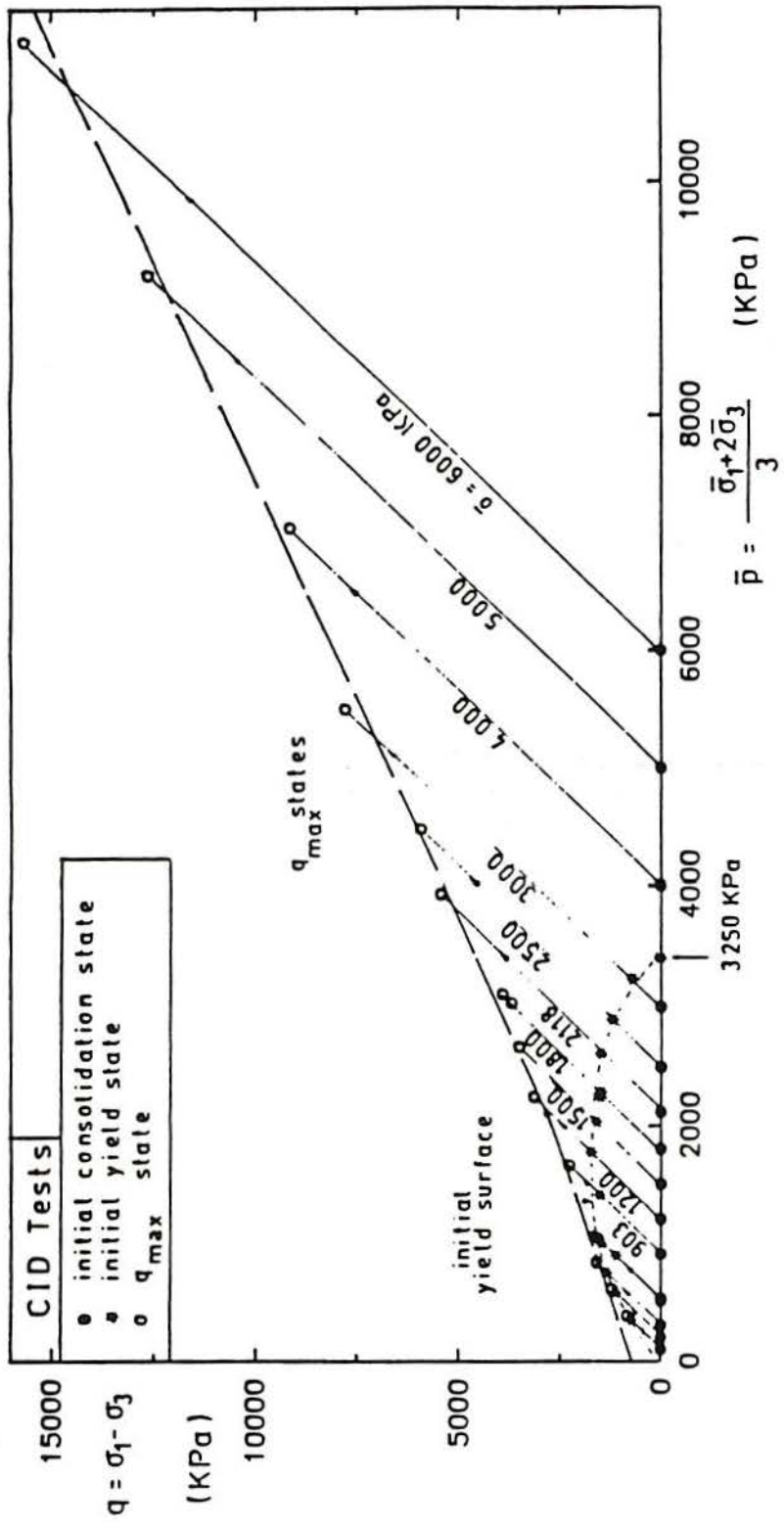

Figure 8.6 – Maximum deviator stresses obtained from drained triaxial tests by Kavvadas (1990)

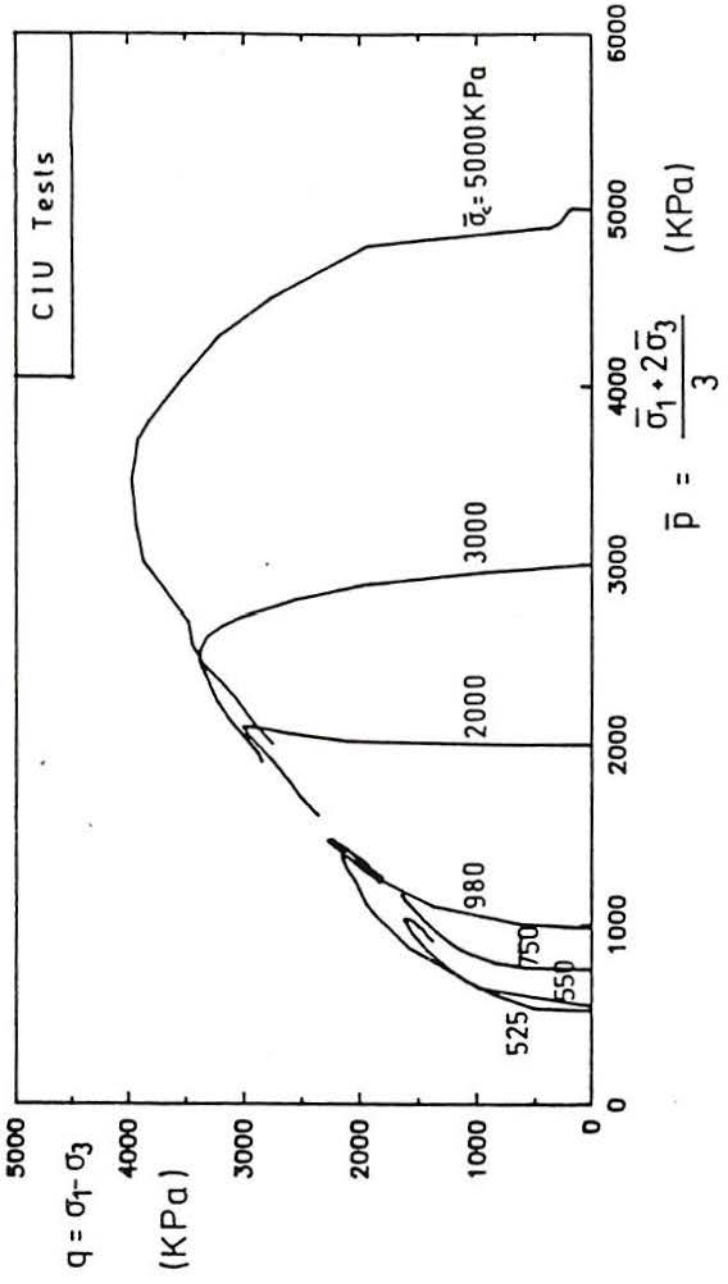

Figure 8.7 – Stress-paths of undrained tests carried out on Corinth Marl (after Kavvadas, 1990)

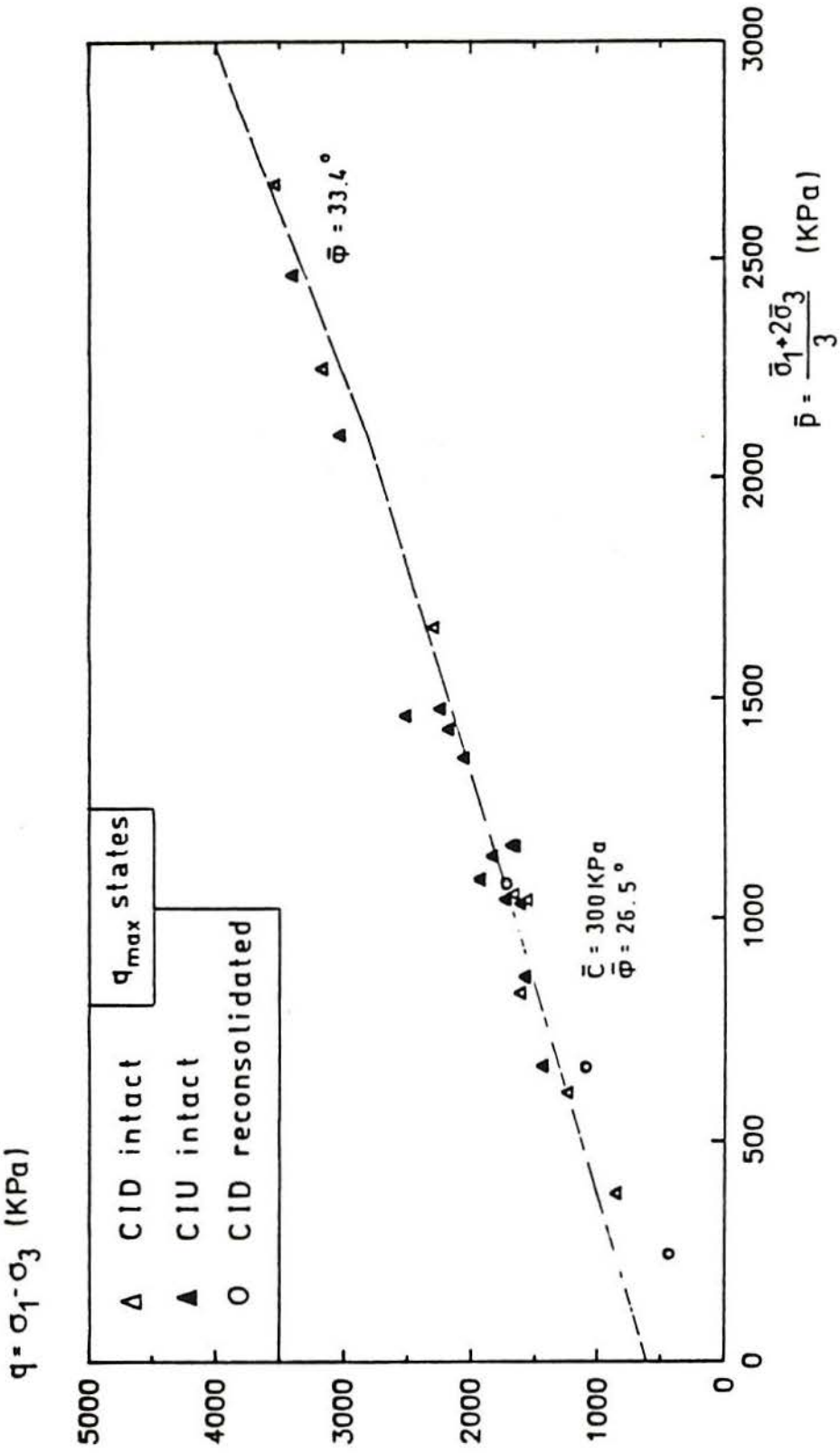

Figure 8.8 – Peak strength points of all tests on Corinth Marl (after Kavvadas, 1990)

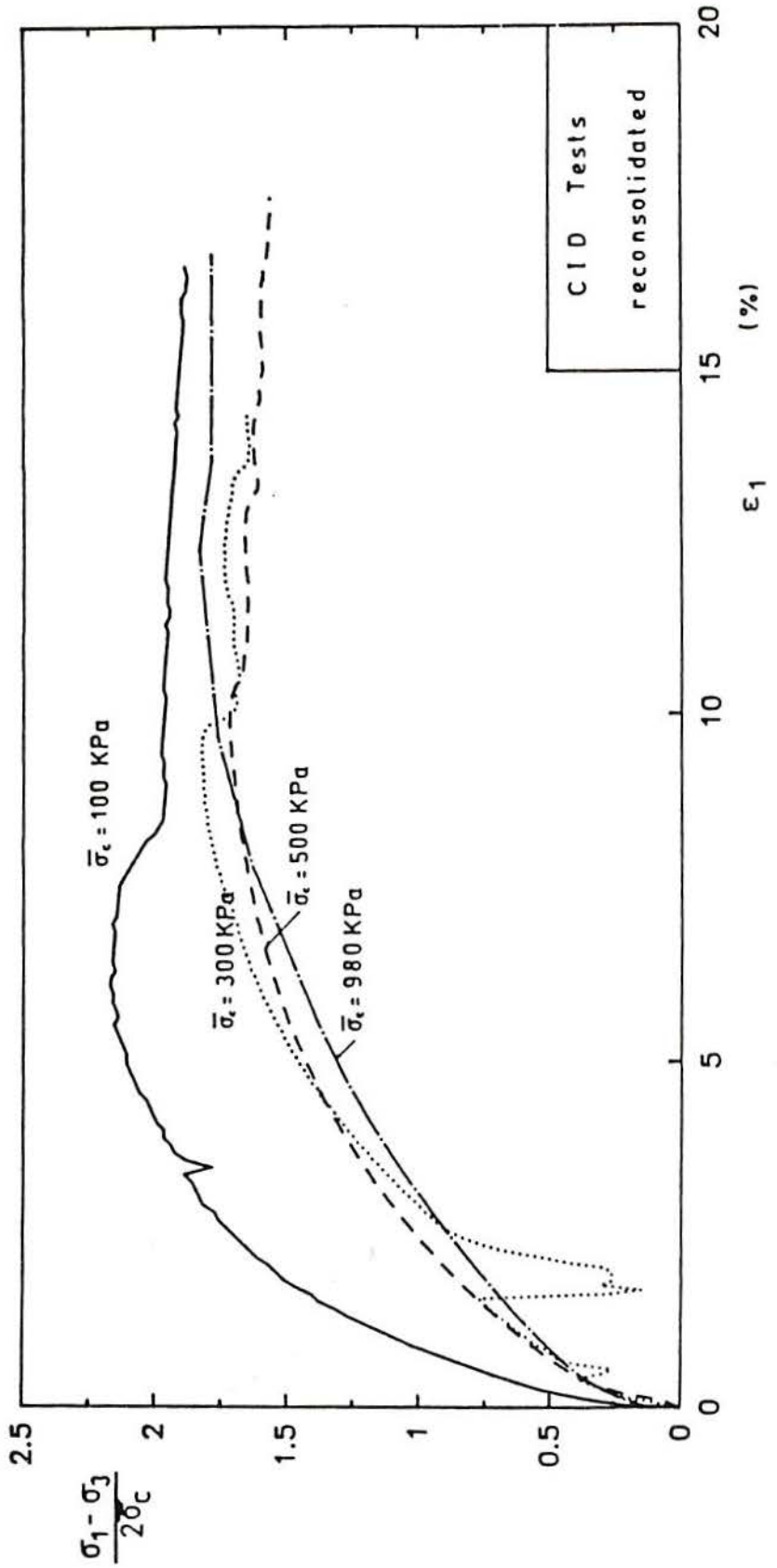

Figure 8.9 – Normalized stress-strain plots of drained triaxial tests on reconsolidated samples of Corinth Marl (after Kavvadas, 1990)

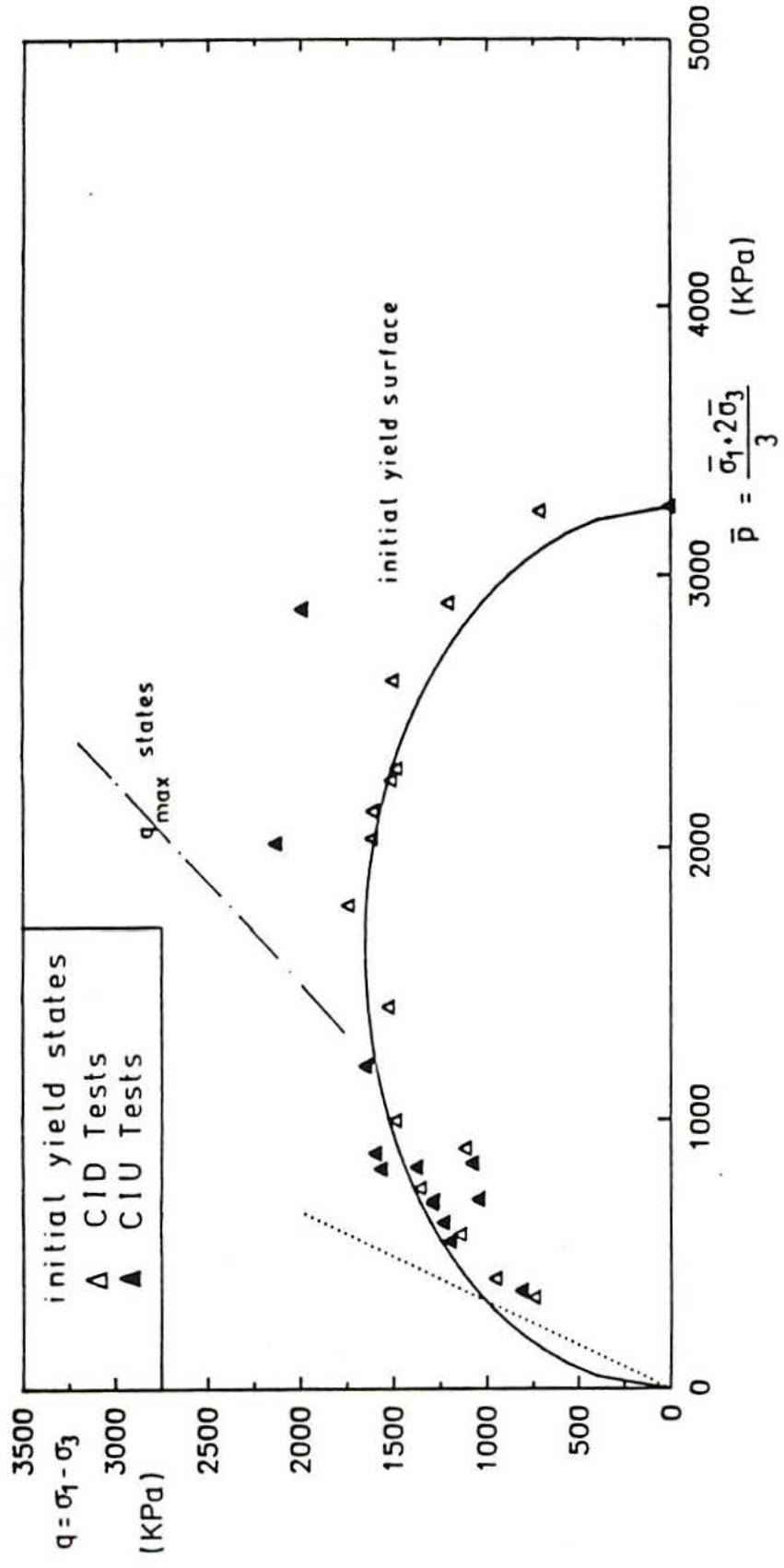

Figure 8.10 – Yield points determined from drained and undrained tests for Corinth Marl (after Kavvadas, 1990)

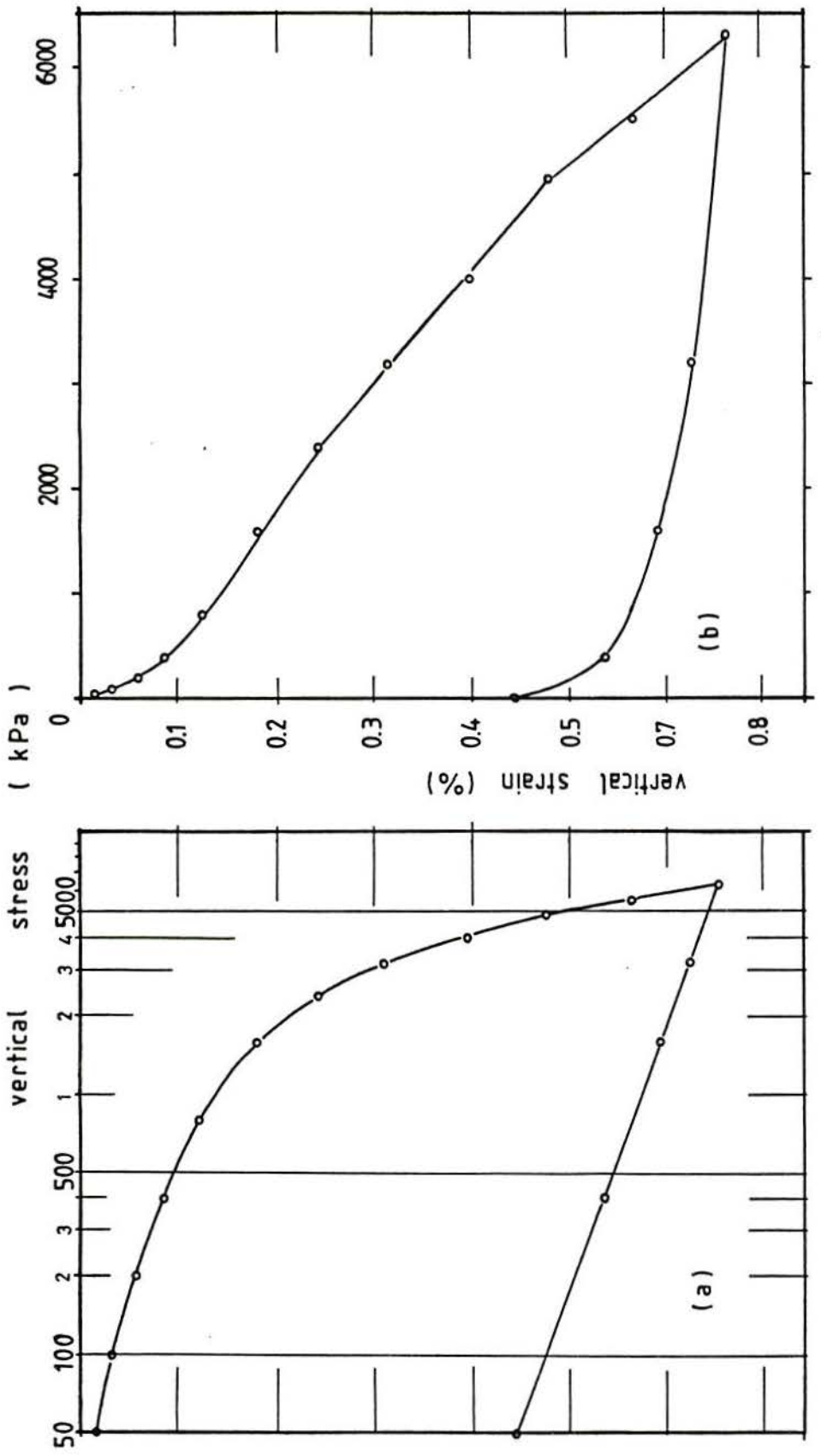

Figure 8.11 – Oedometer test results on intact Corinth Marl (*a*) logarithmic scale; (*b*) natural scale (after Anagnostopoulos, 1989)

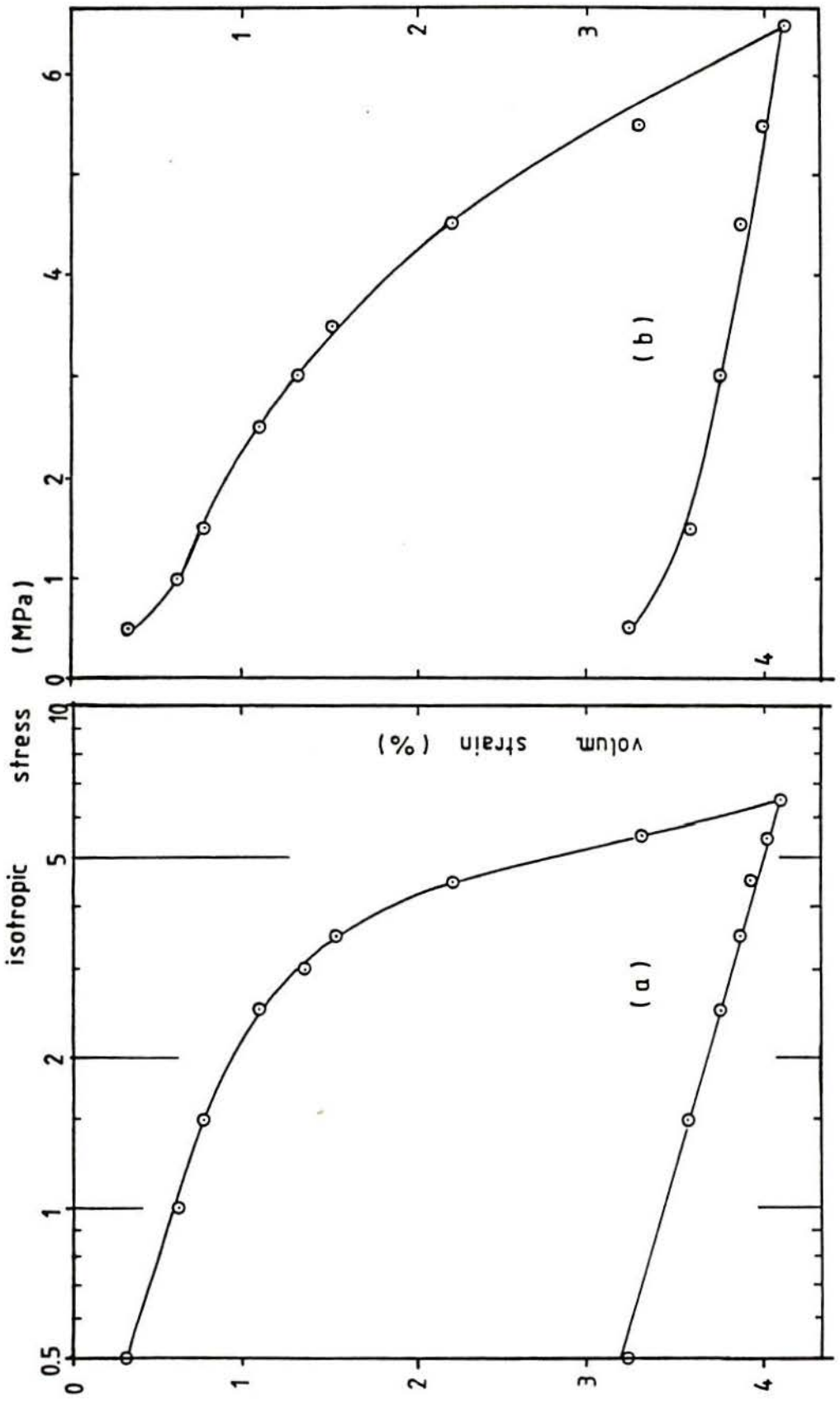

Figure 8.12 – Isotropic compression test results on intact Corinth Marl (*a*) logarithmic scales; (*b*) natural scales (after Anagnostopoulos, 1989)

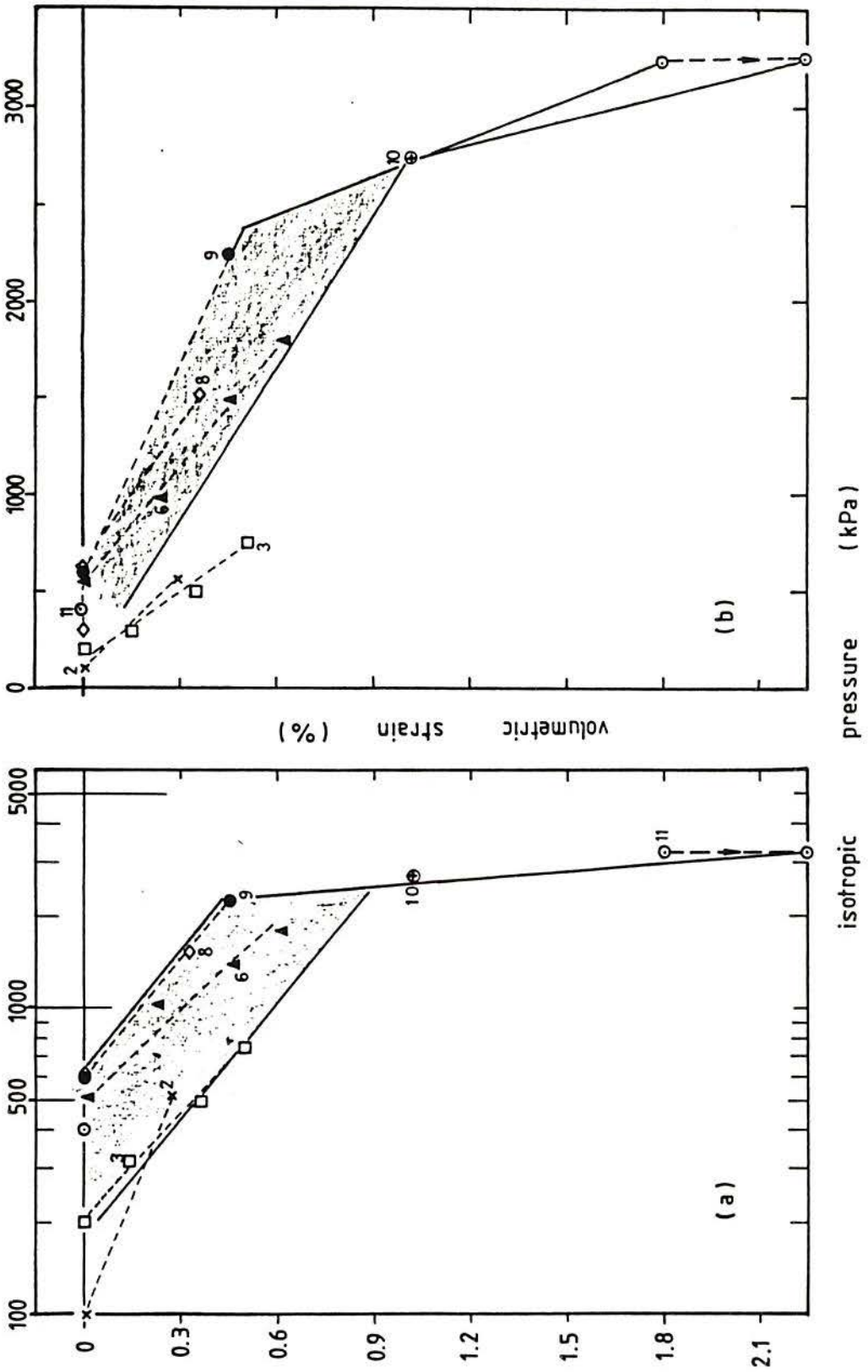

Figure 8.13 – Volumetric strain versus stress results of isotropic consolidation tests carried out at IC; (*a*) logarithmic scales; (*b*) natural scales

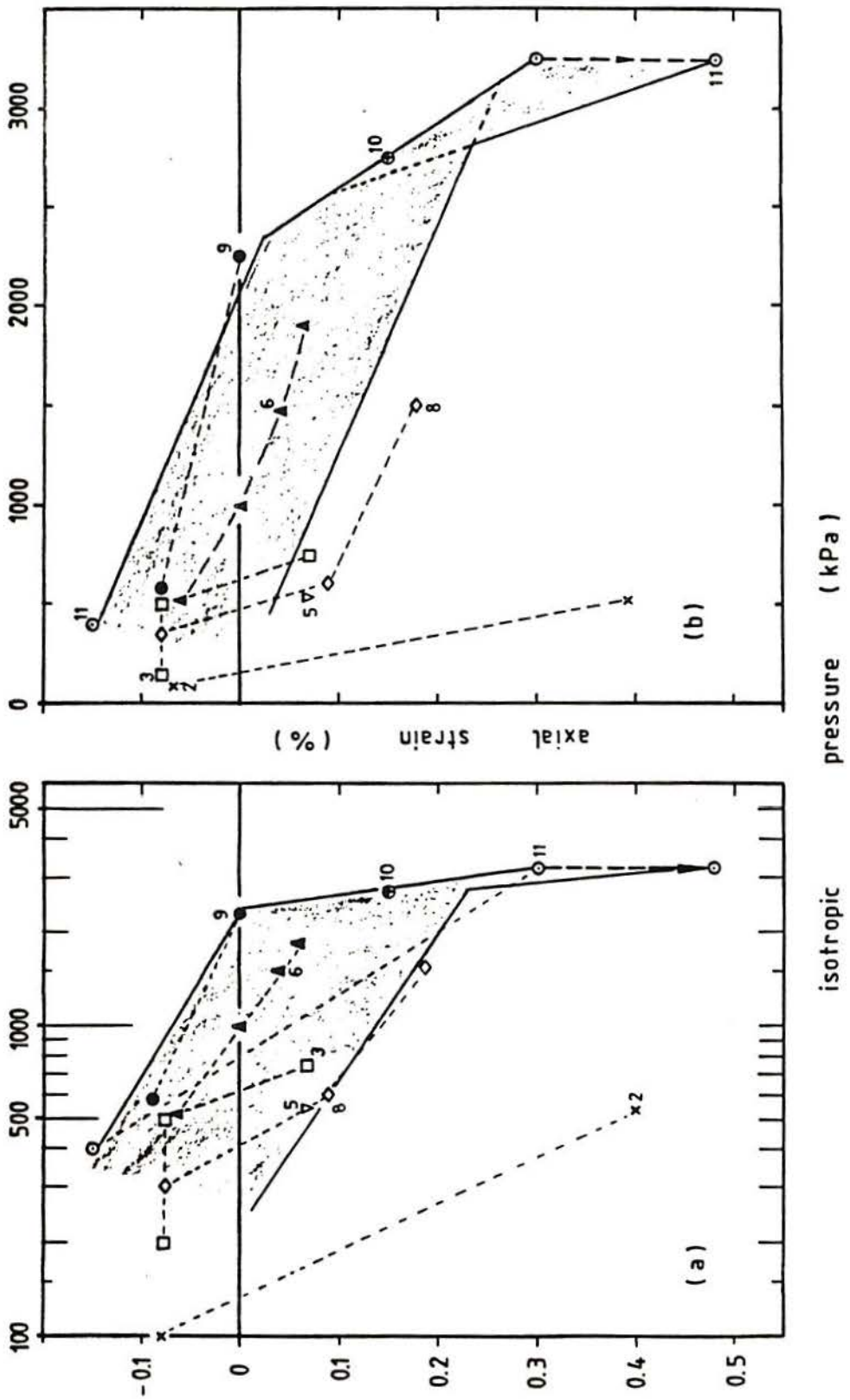

Figure 8.14 – Axial strain versus stress results of isotropic consolidation tests carried out at IC; (*a*) logarithmic scales; (*b*) natural scales

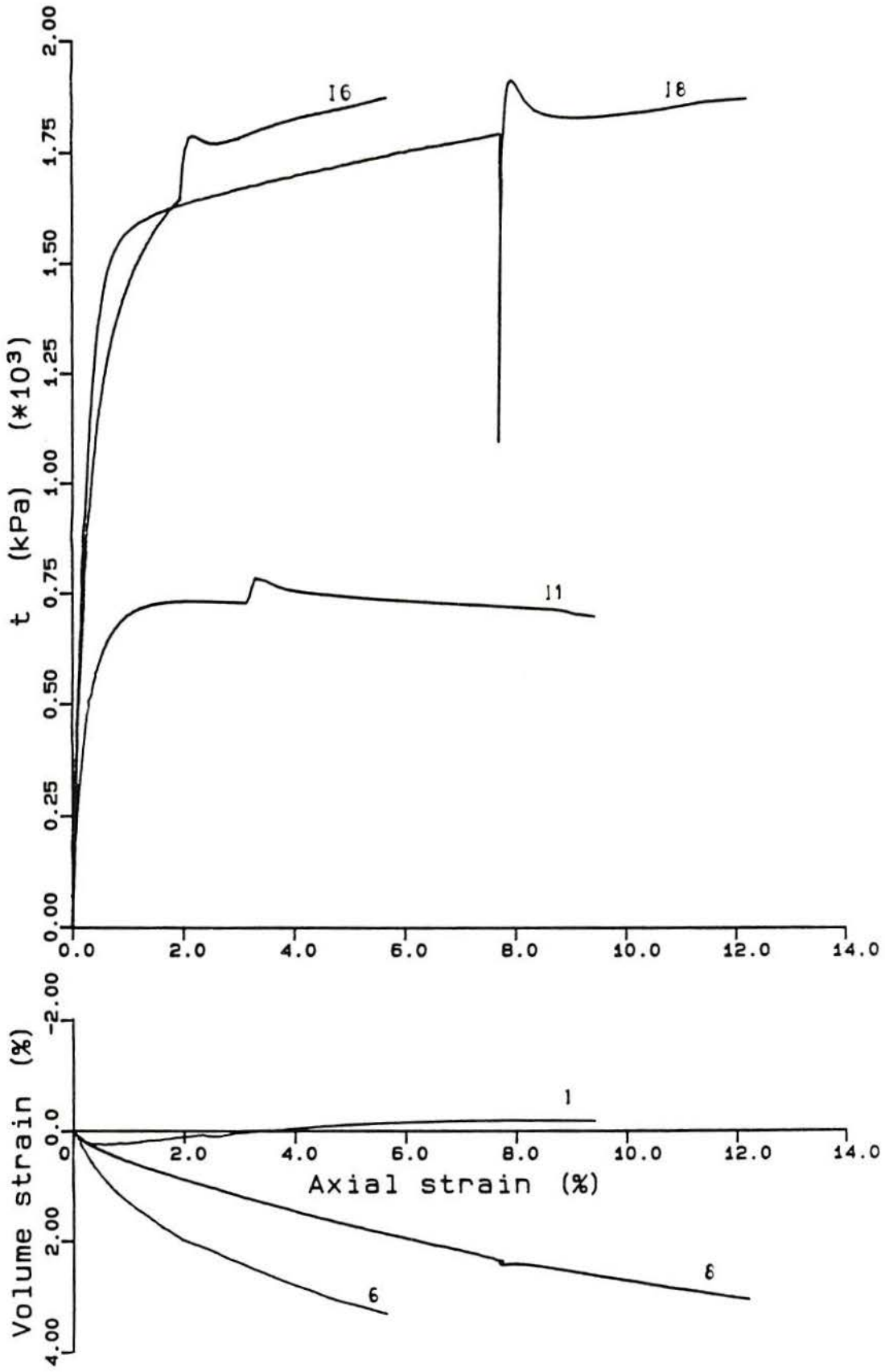

Figure 8.15 – Results of drained triaxial tests on samples I1 (525 kPa), I6 (1800 kPa) and I8 (1500 kPa)

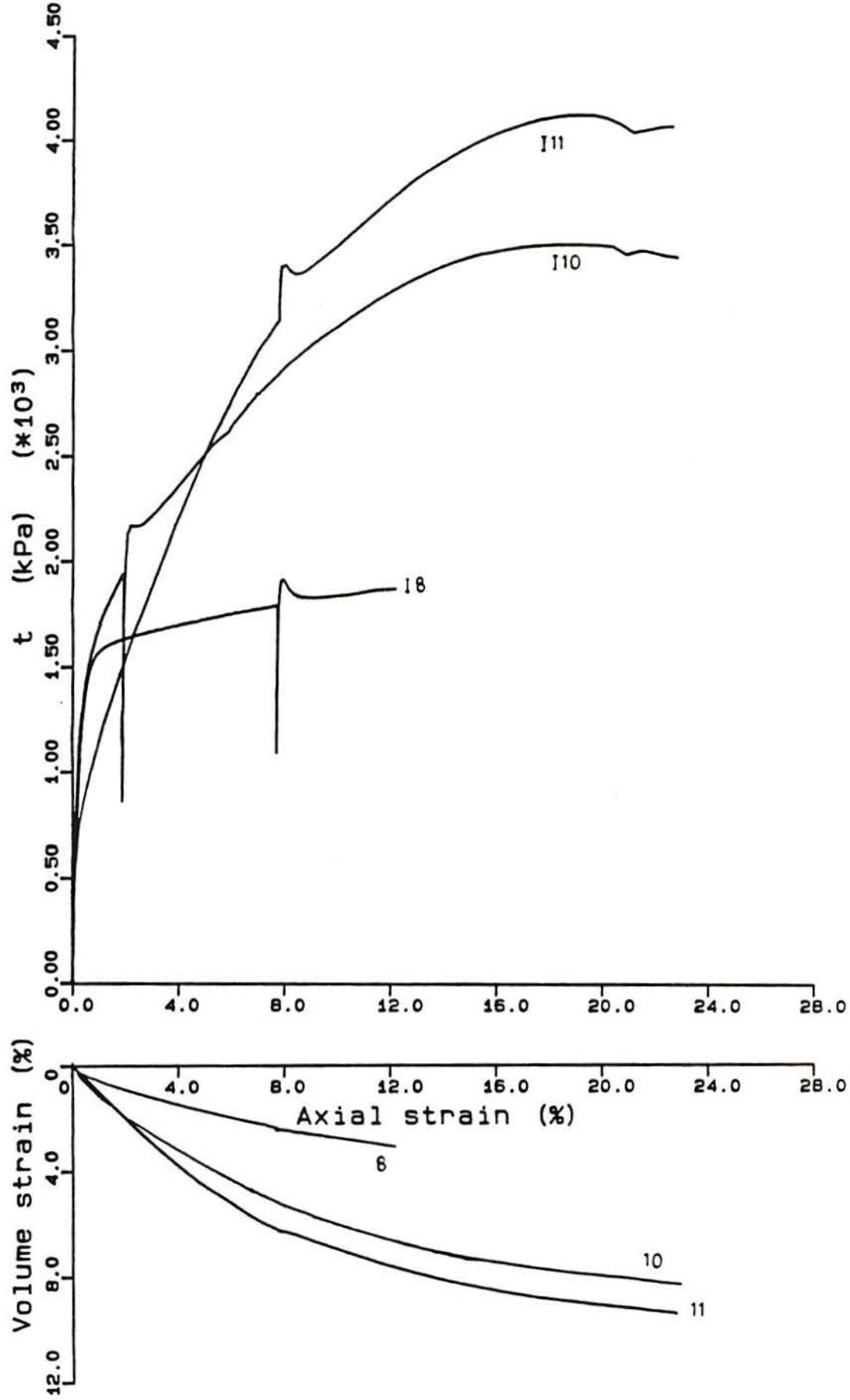

Figure 8.16 – Results of drained triaxial tests on samples I8 (1500 kPa), I10 (2750 kPa) and I11 (3250 kPa)

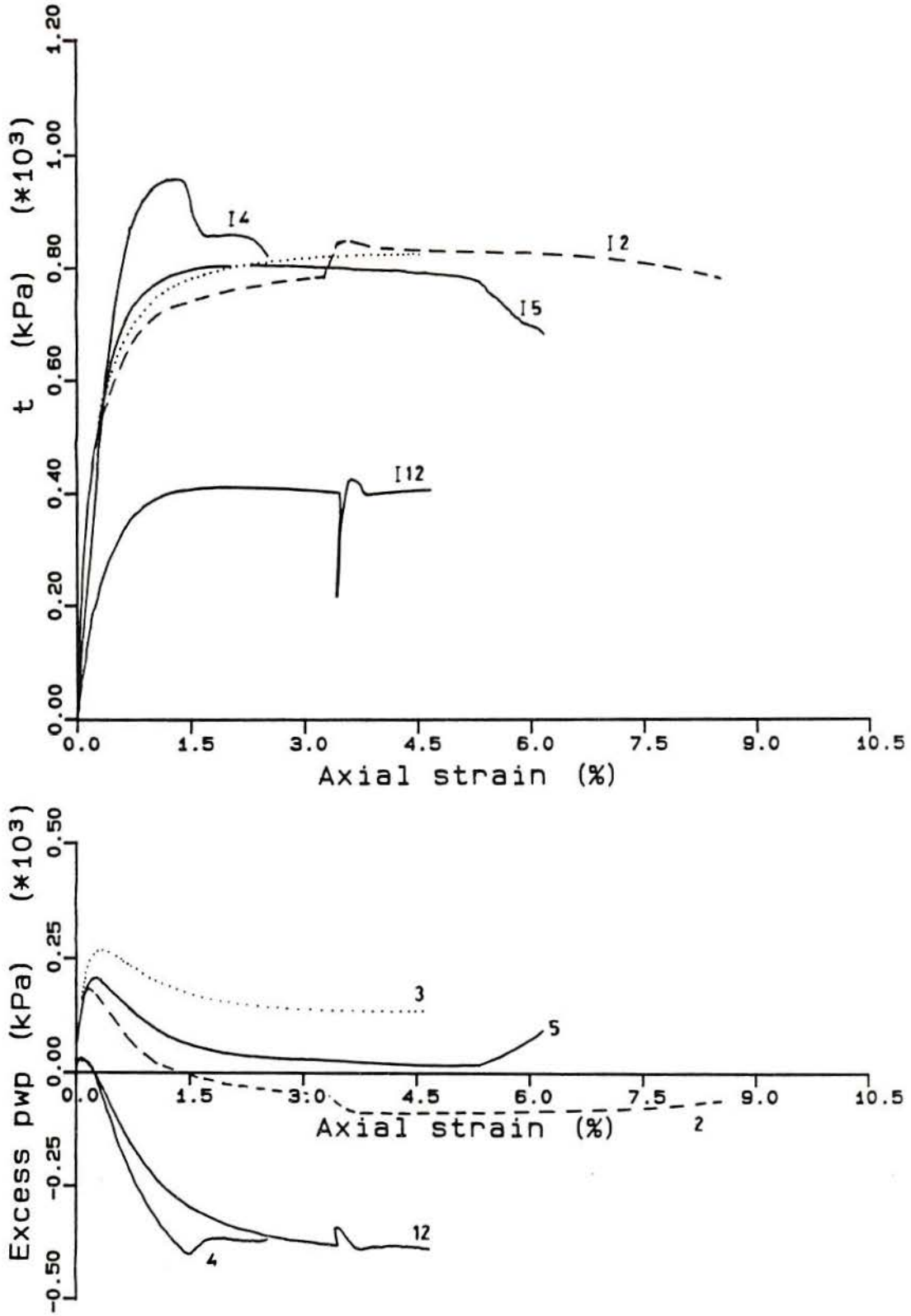

Figure 8.17 – Results of undrained triaxial tests on samples I2 (525 kPa), I3 (740 kPa), I4 (100 kPa), I5 (520 kPa) and I12 (100 kPa)

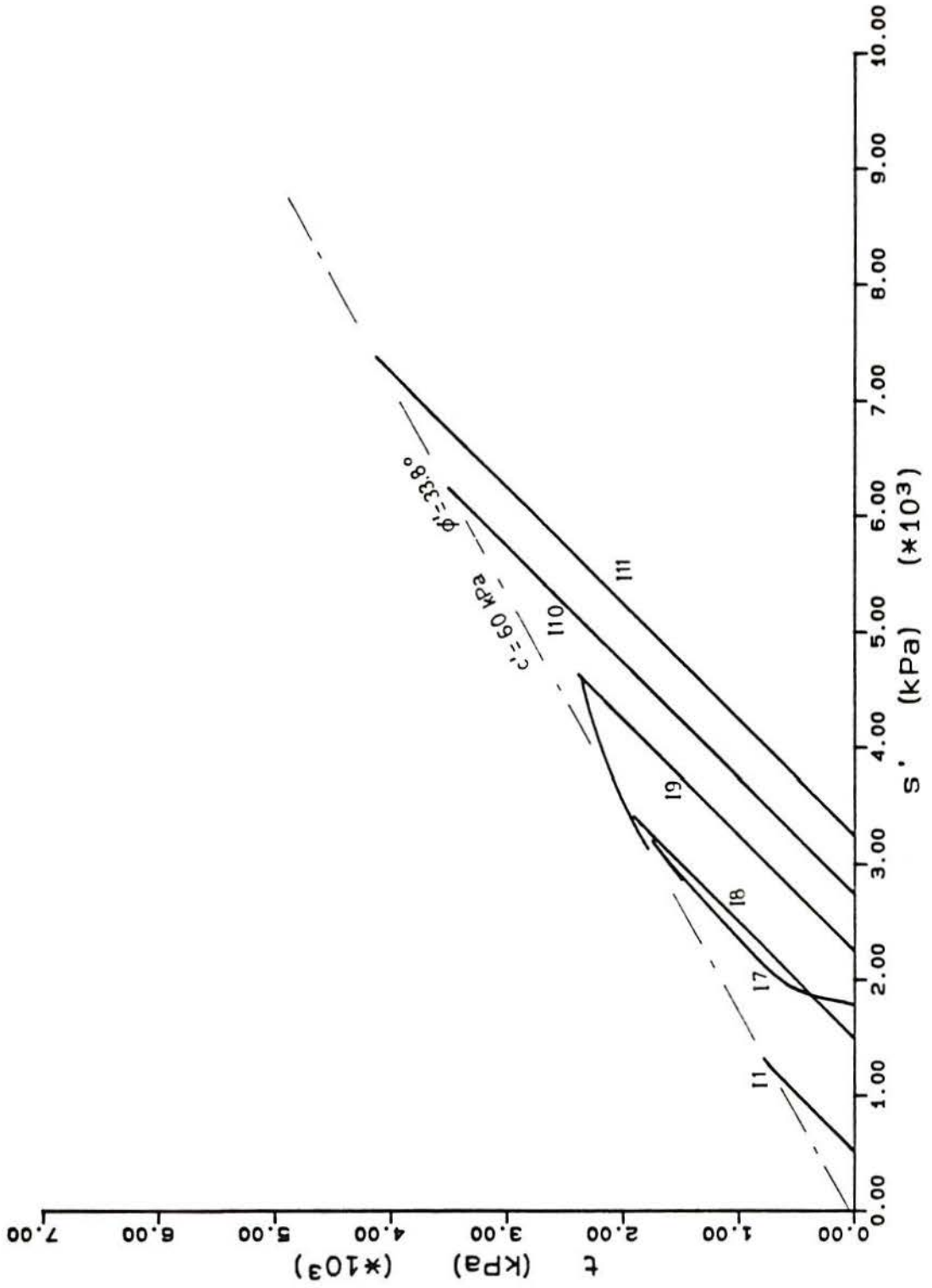

Figure 8.18 – Test results and failure line for entire stress range (IC tests)

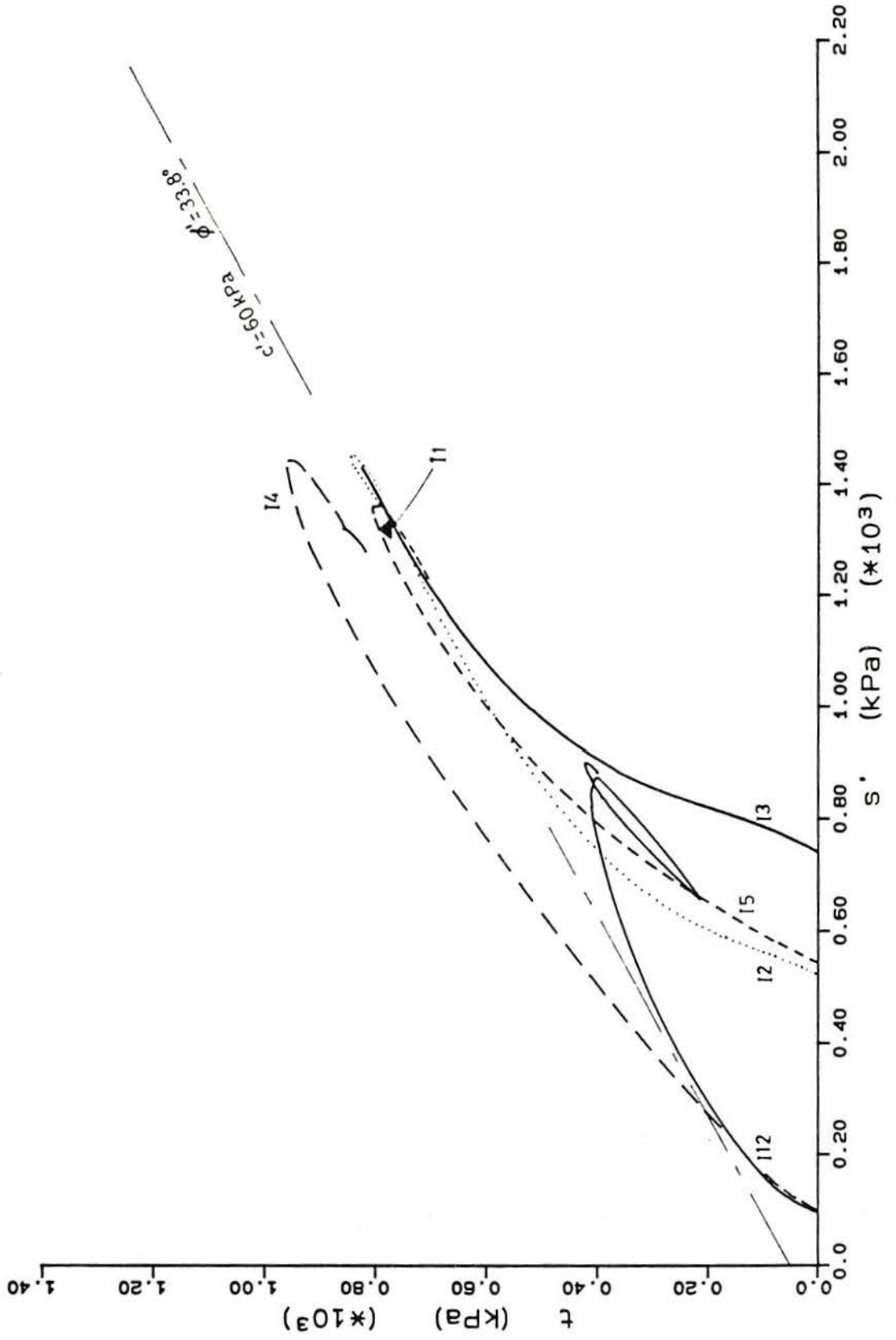

Figure 8.19 – Test results and failure line for s′ less than 1.5 MPa (IC tests)

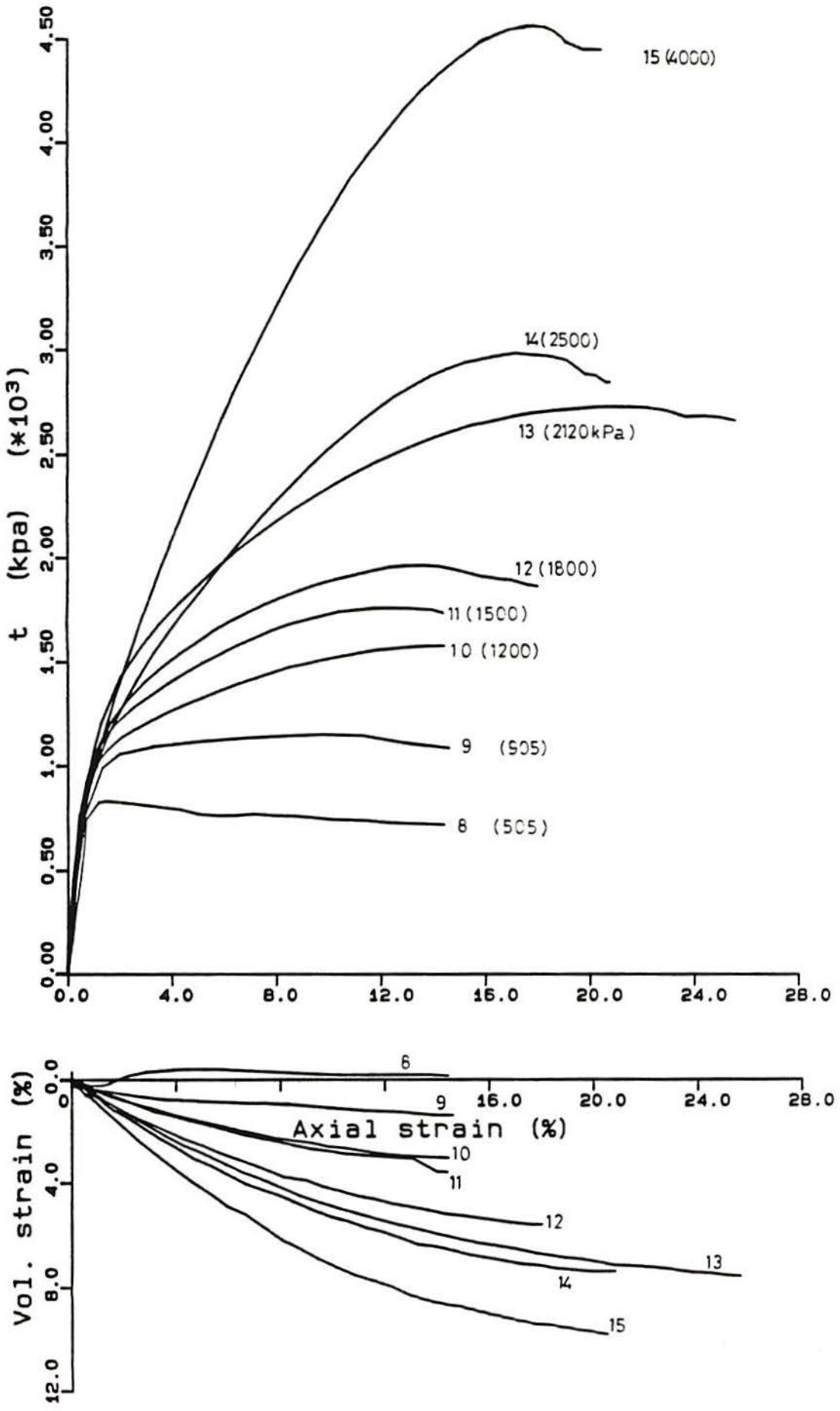

Figure 8.20 – Results of drained triaxial tests carried out at NTUA

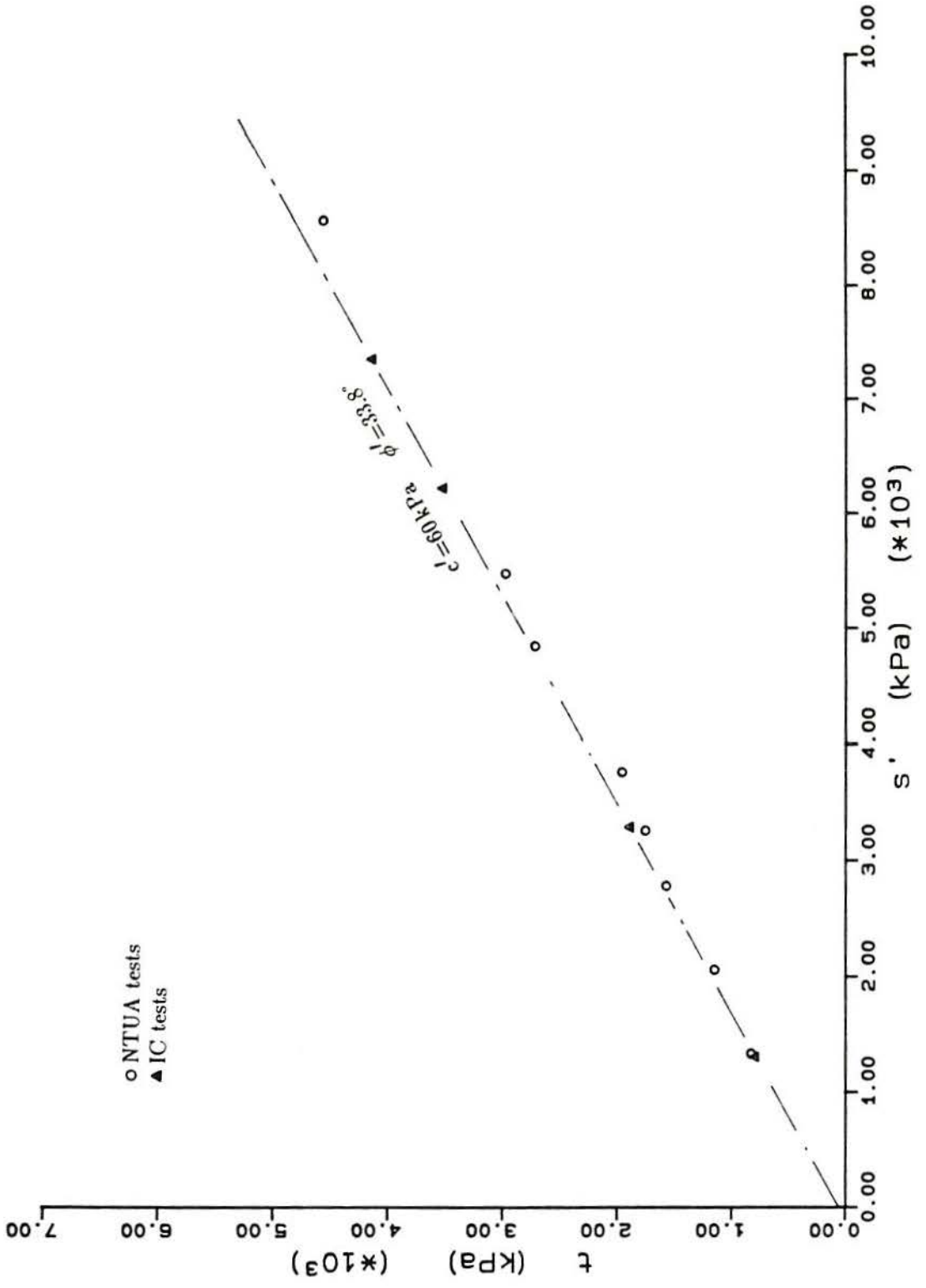

Figure 8.21 – The peak strength of triaxial tests – results of NTUA and IC tests; (*a*) whole range of stress (cont.)

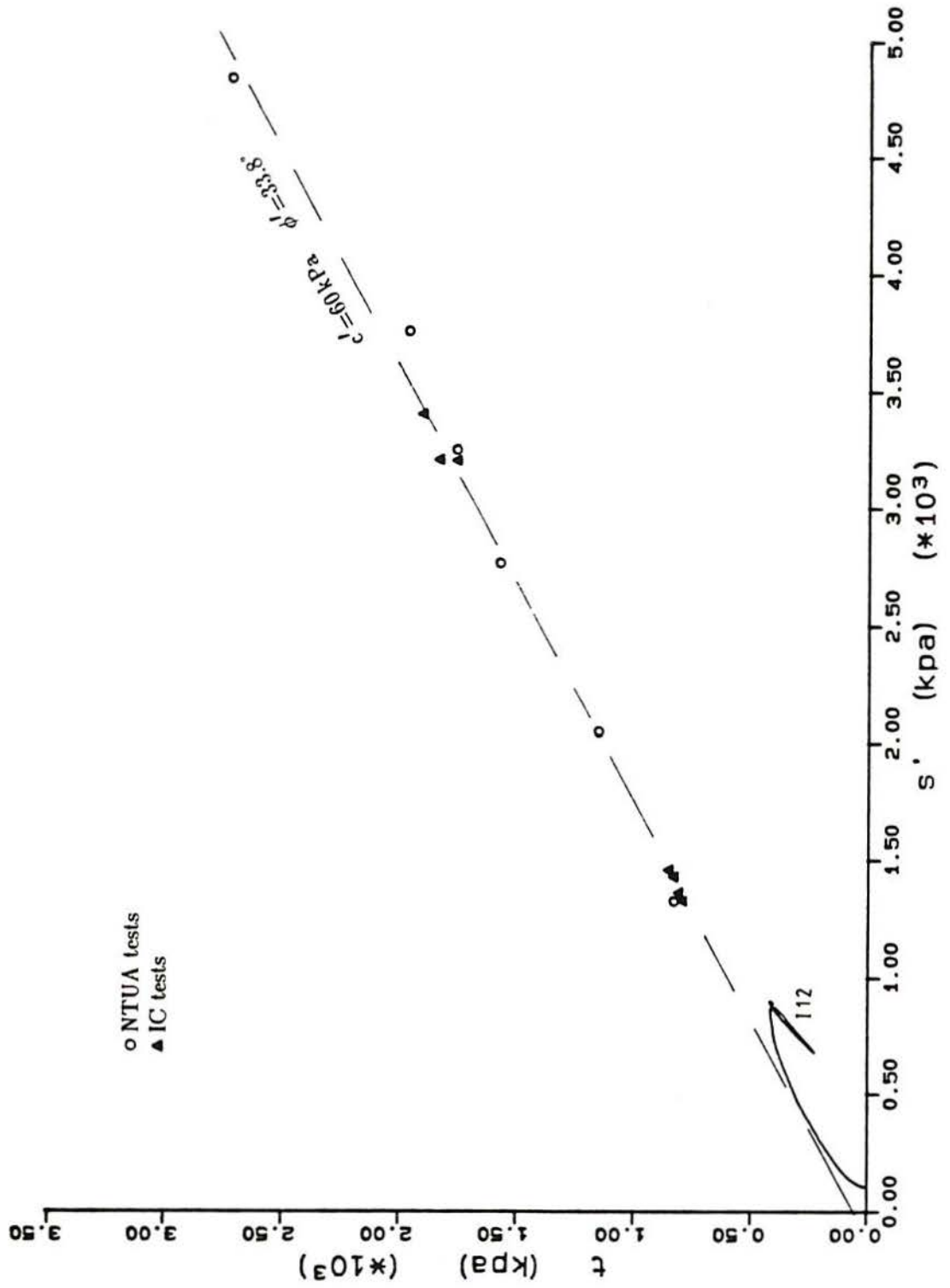

Figure 8.21 – (cont.) (*b*) s′ less than 5.0 MPa

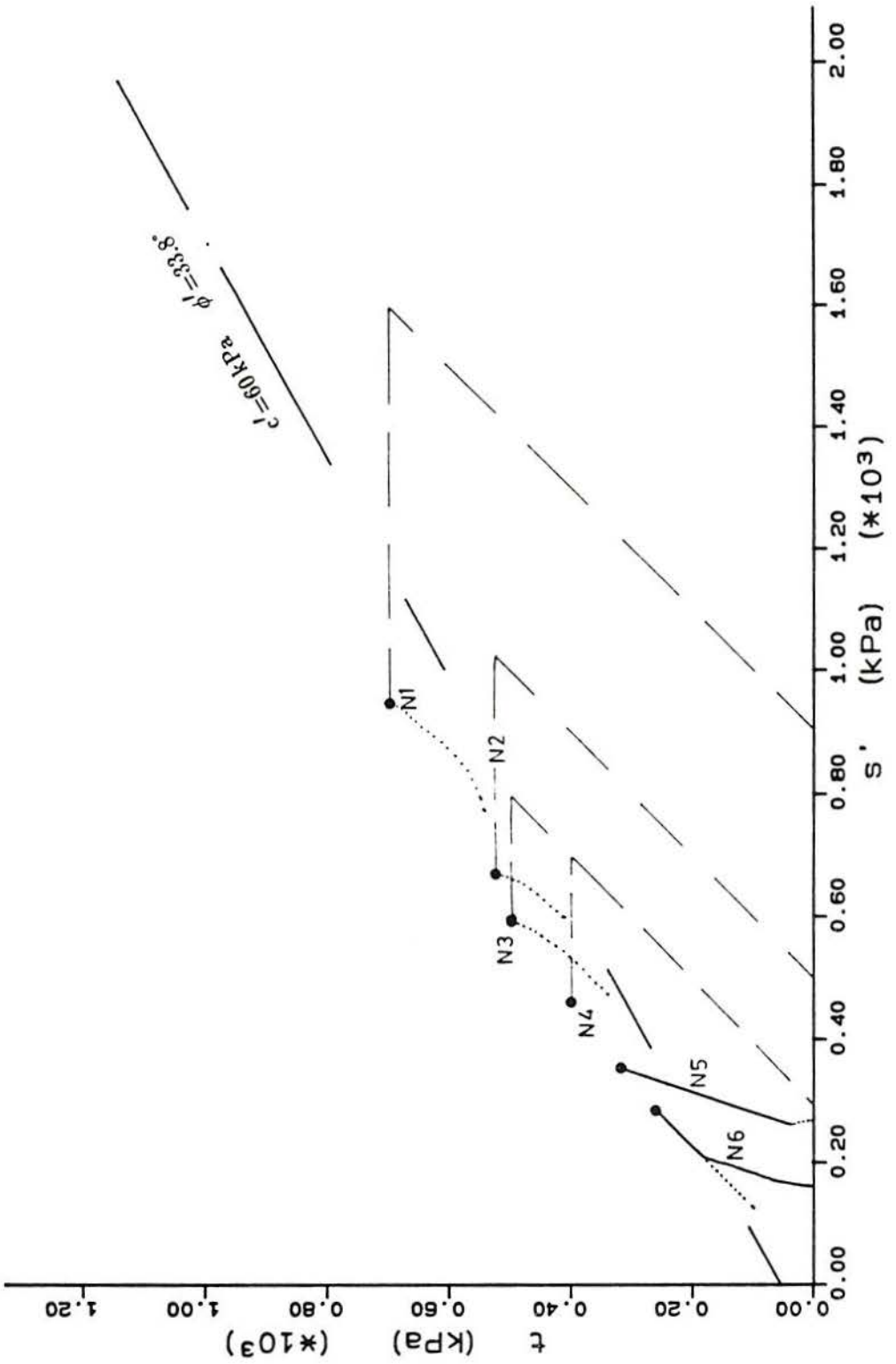

Figure 8.22 – Results of special triaxial tests carried out at KEDE, Greece

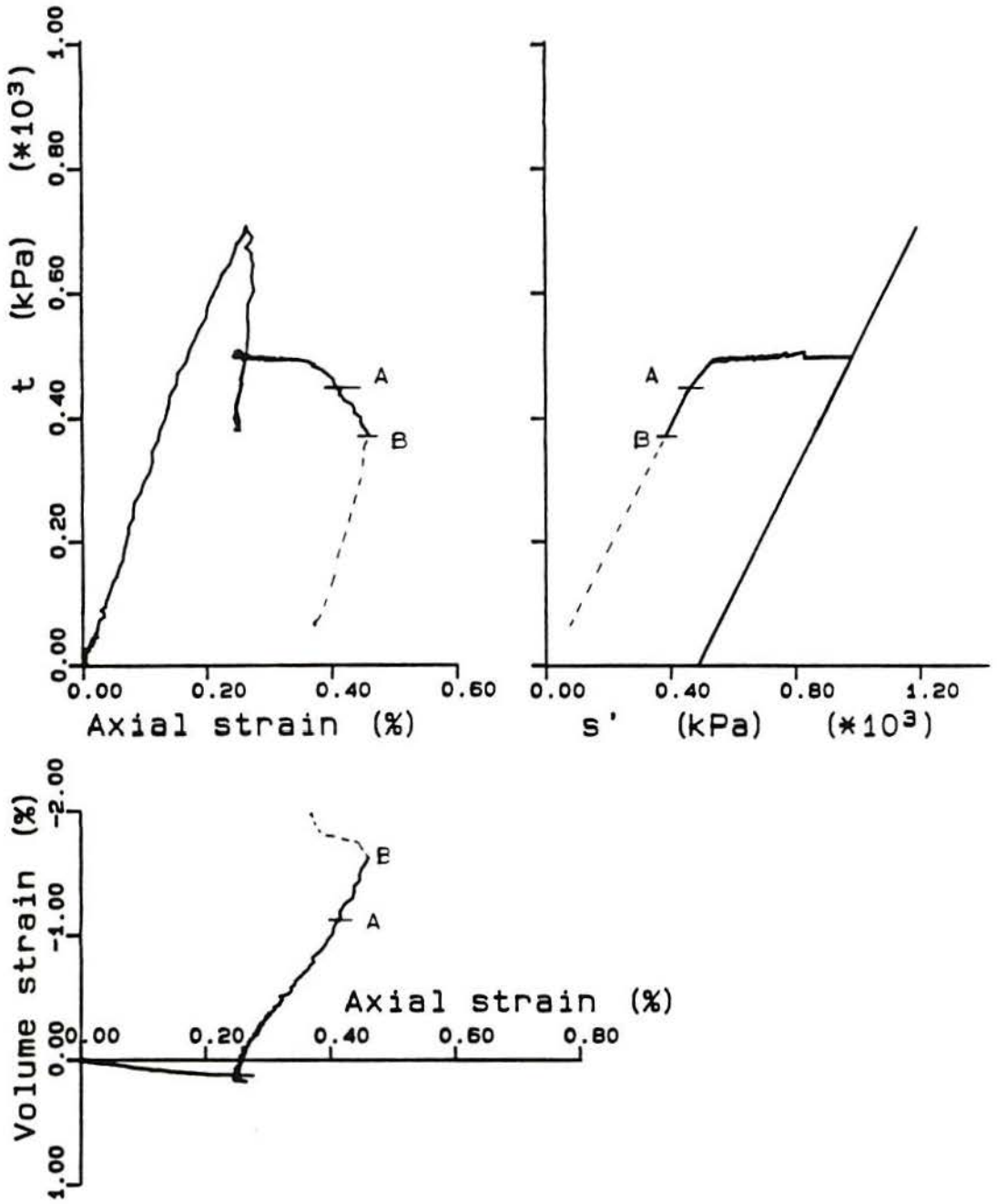

Figure 8.23 – Results of test on sample I13 (lateral unloading)

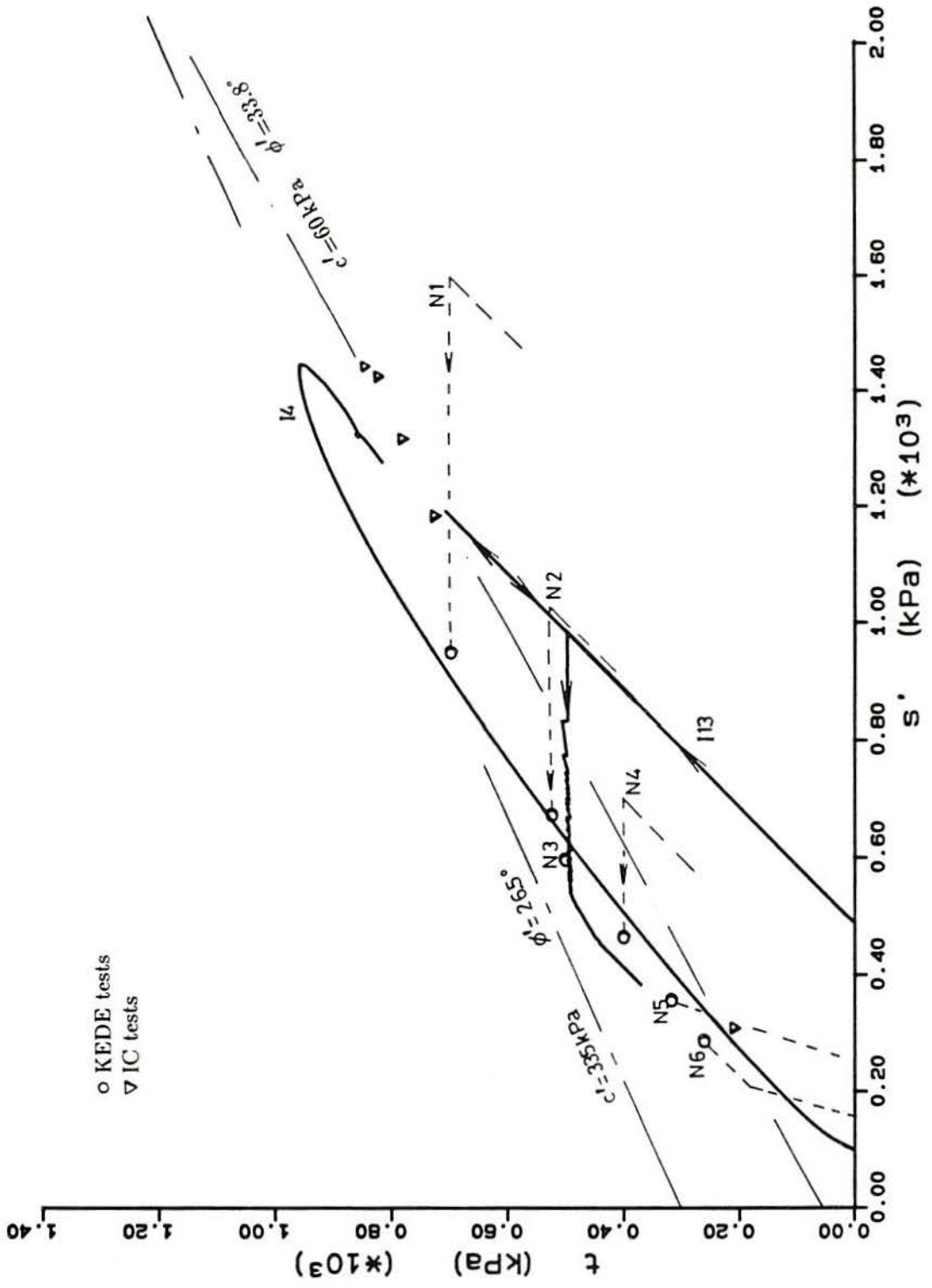

Figure 8.24 – Failure lines and failure points from different tests (*a*) s′ less than 2000 kPa (cont.)

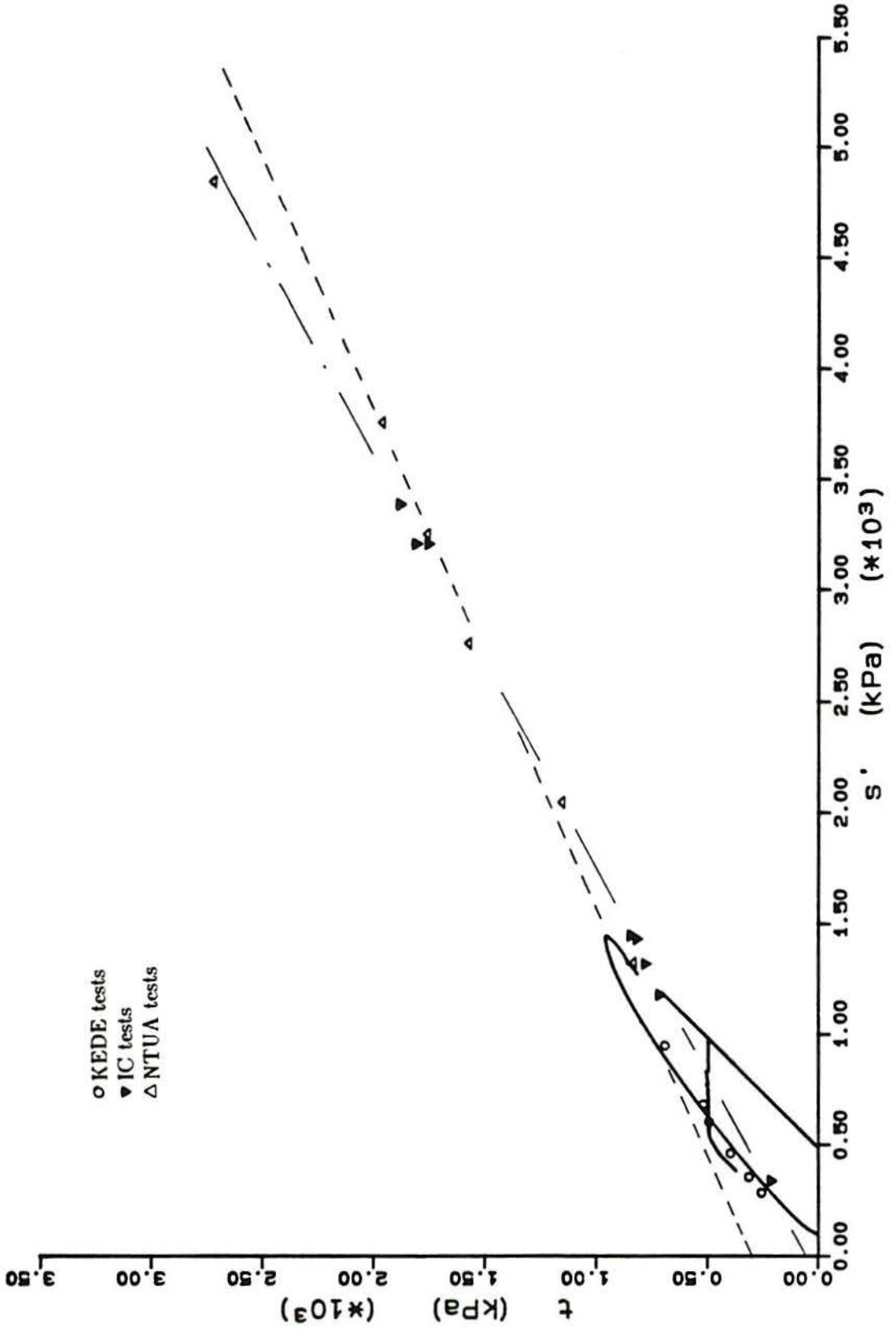

Figure 8.24 – (cont.) (*b*) s′ less than 5 MPa

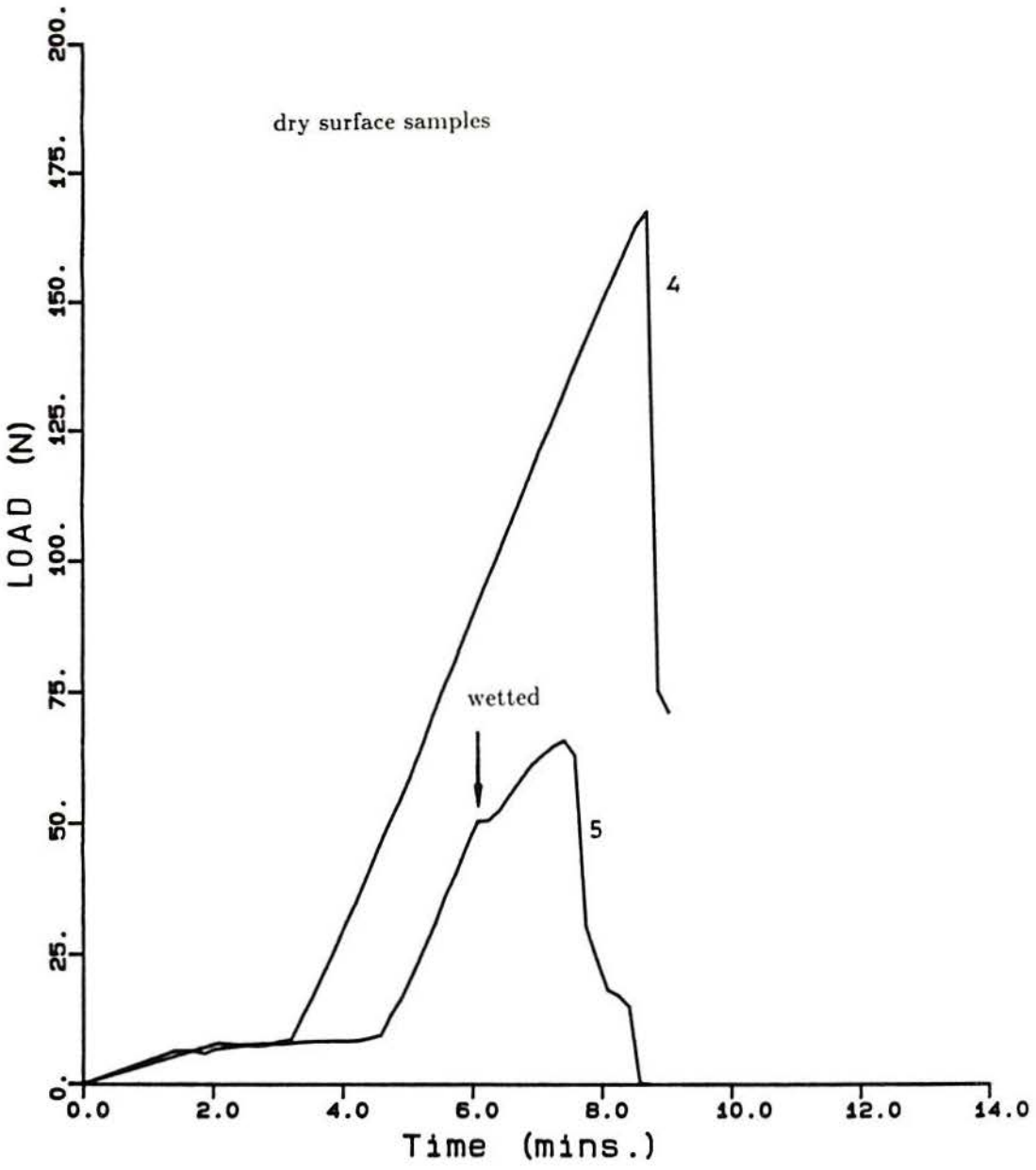

Figure 8.25 – Tensile test results on two saturated surface dry samples of intact Corinth Marl

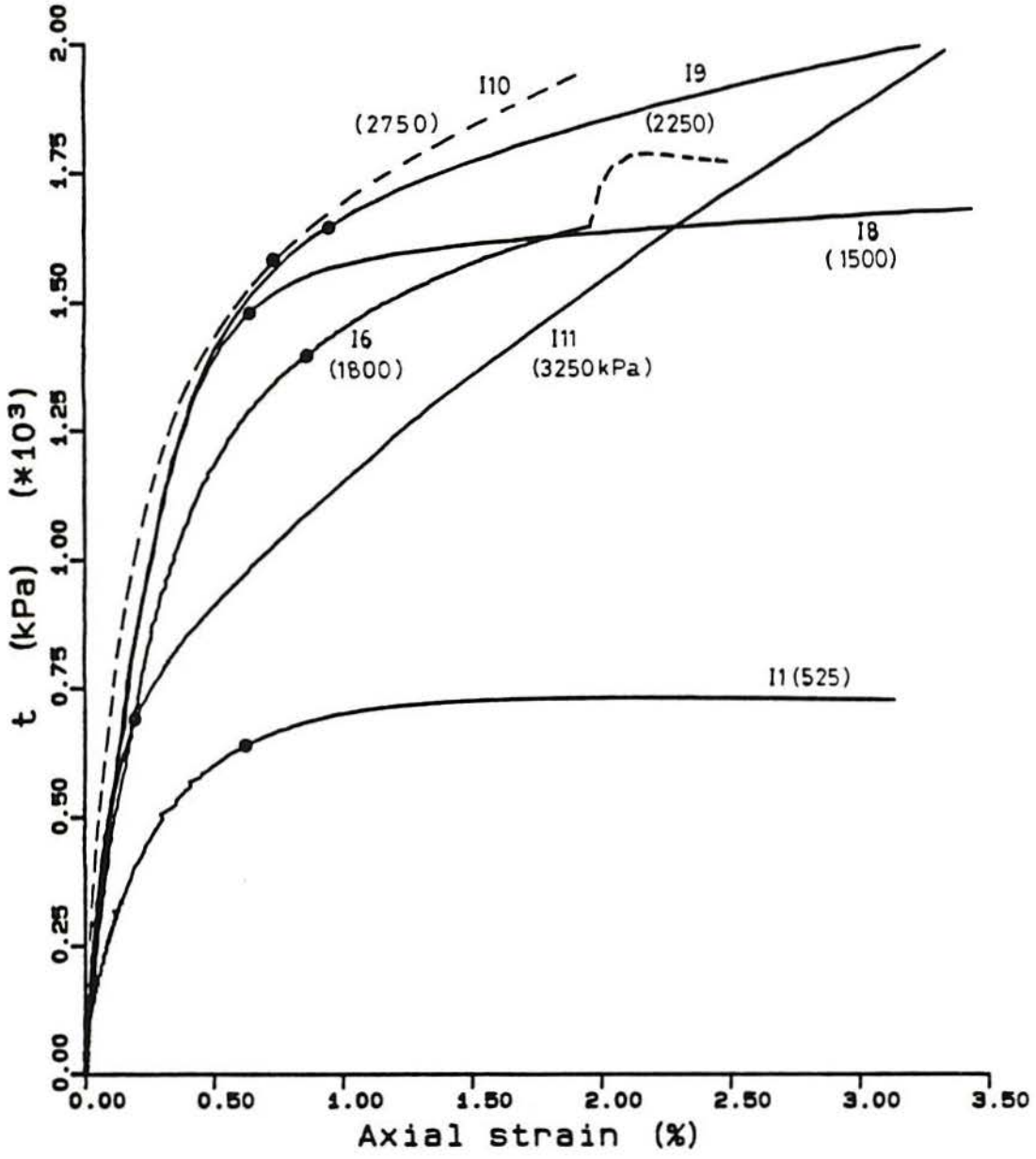

Figure 8.26 – Stress-strain test results carried out at IC; natural scale, yield points

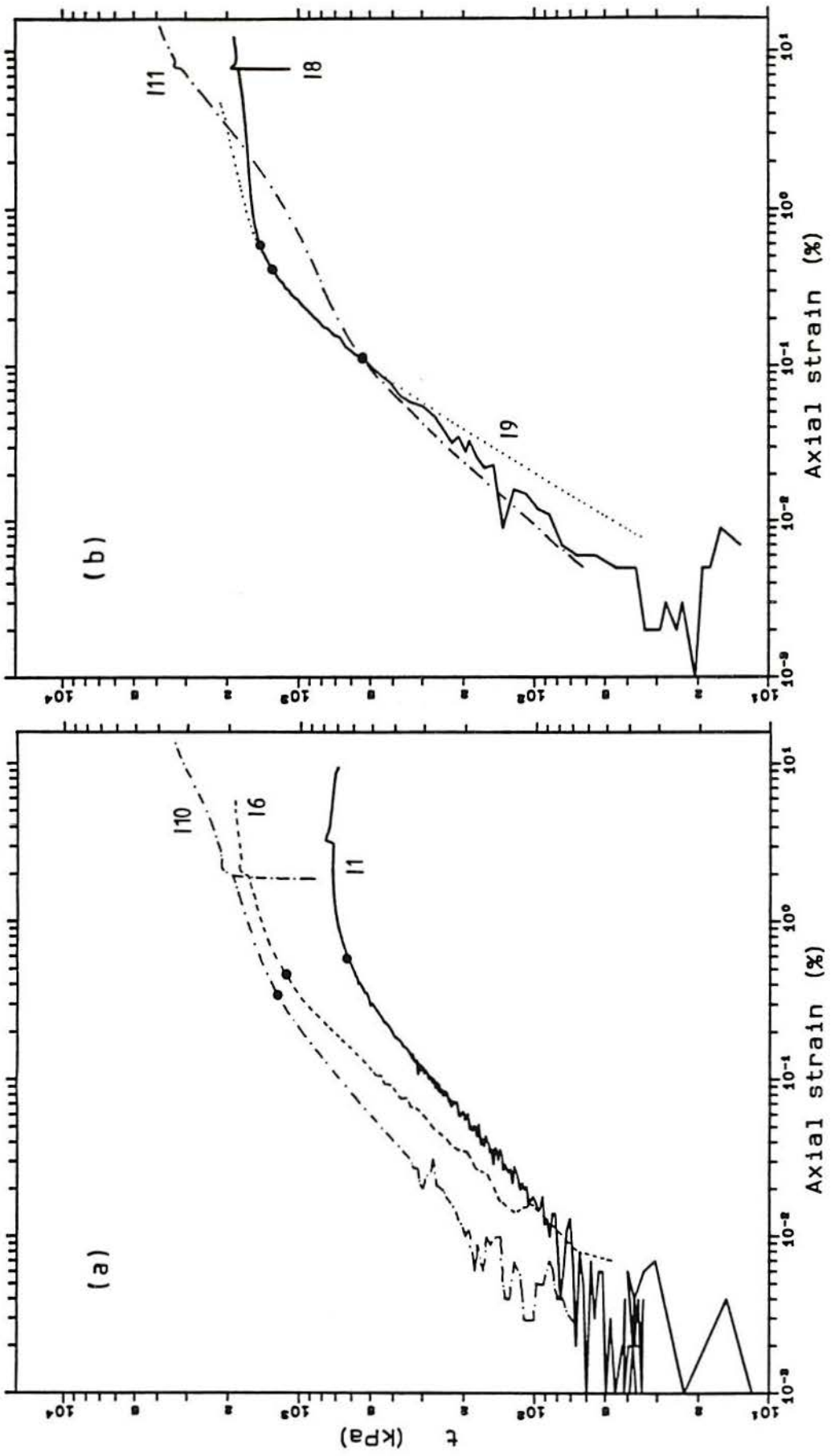

Figure 8.27 – Stress-strain test results carried out at IC; log-log scales

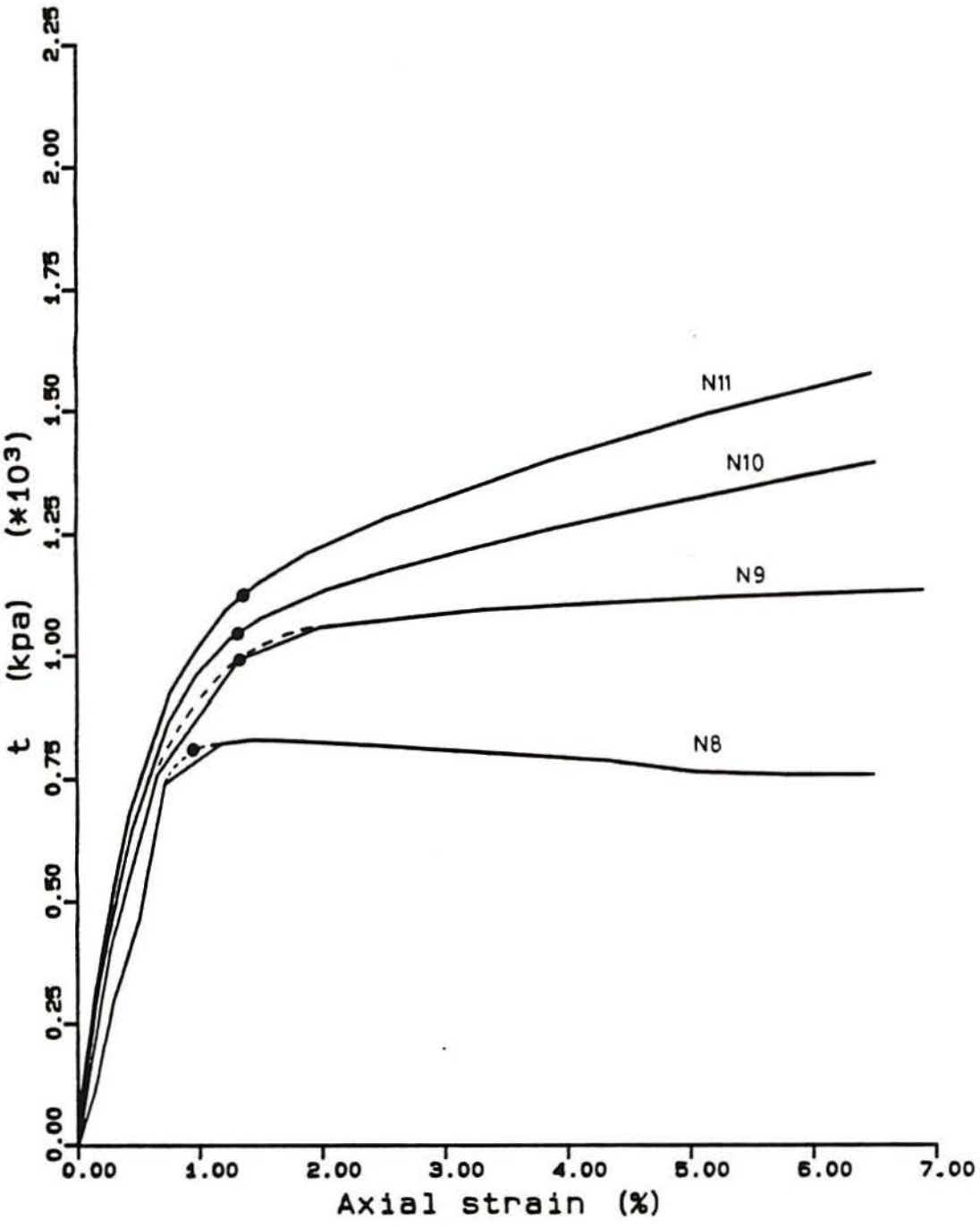

Figure 8.28 – Stress-strain test results carried out in Greece; natural scale, yield points; (*a*) Tests N8-N11 (cont.)

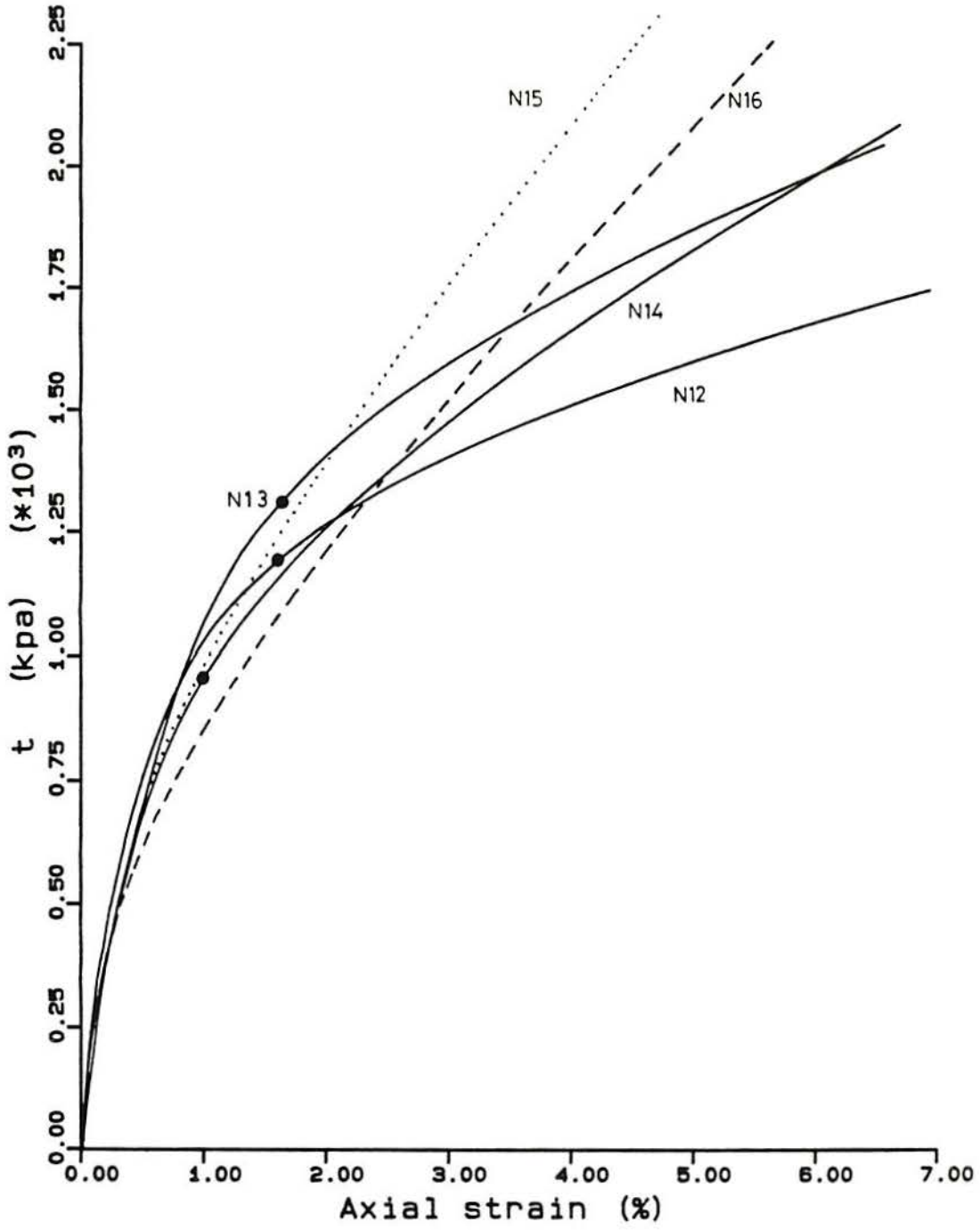

Figure 8.28 – (cont.) (*b*) Tests N12-N16

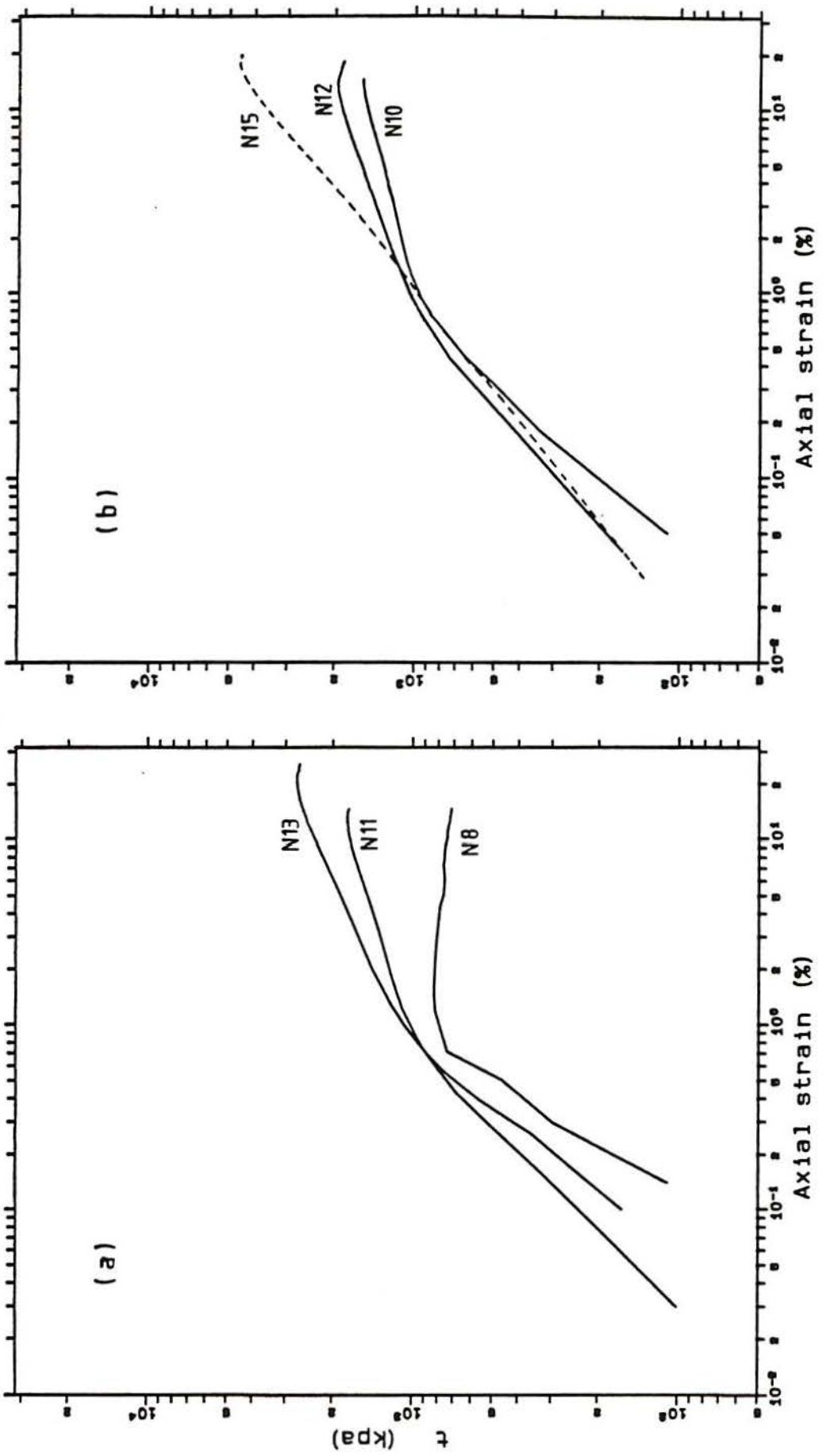

Figure 8.29 – Stress-strain test results carried out in Greece; log-log scales

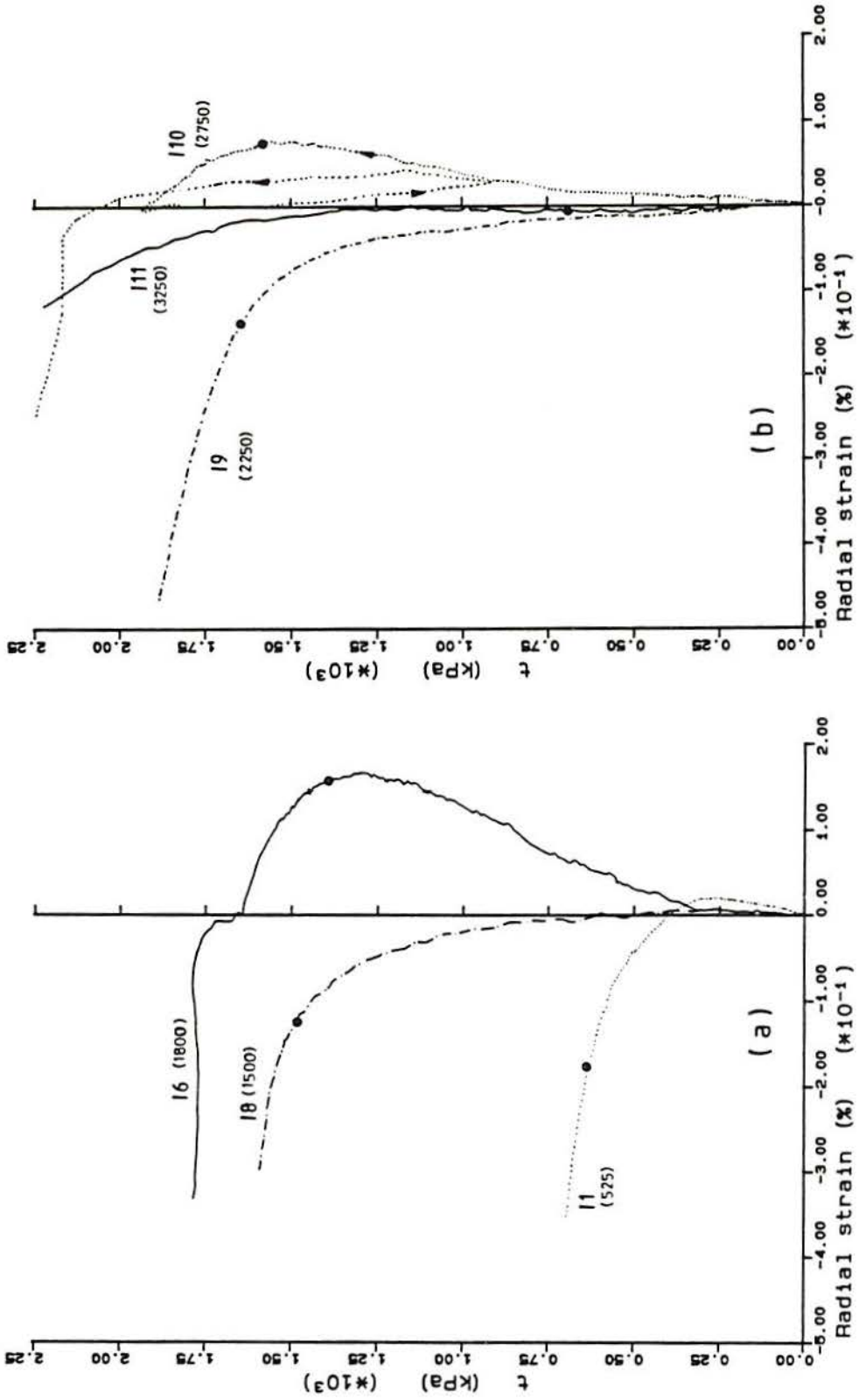

Figure 8.30 – Results of stress versus radial strain for tests carried out at IC

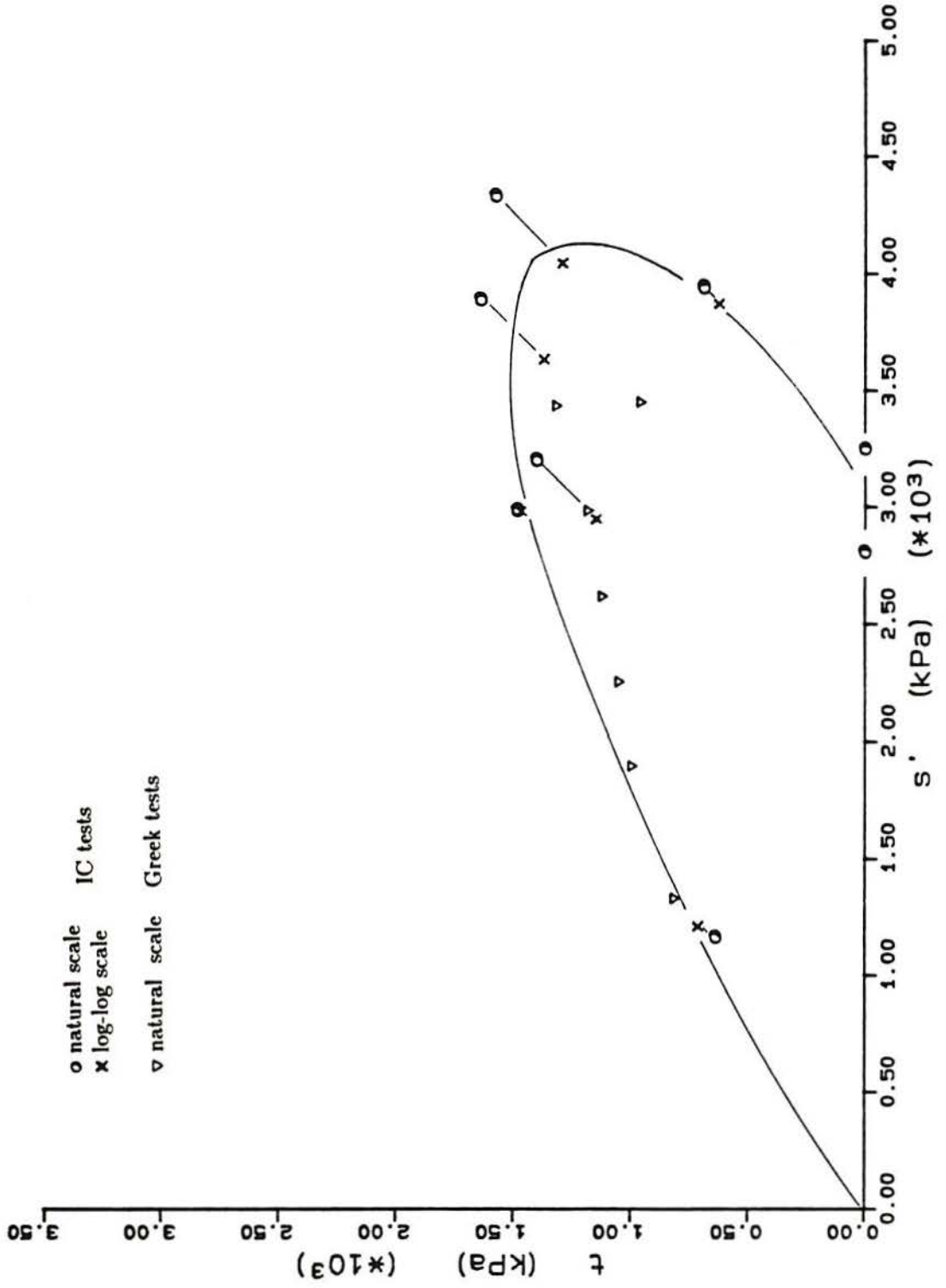

Figure 8.31 - Yield points of Corinth Marl

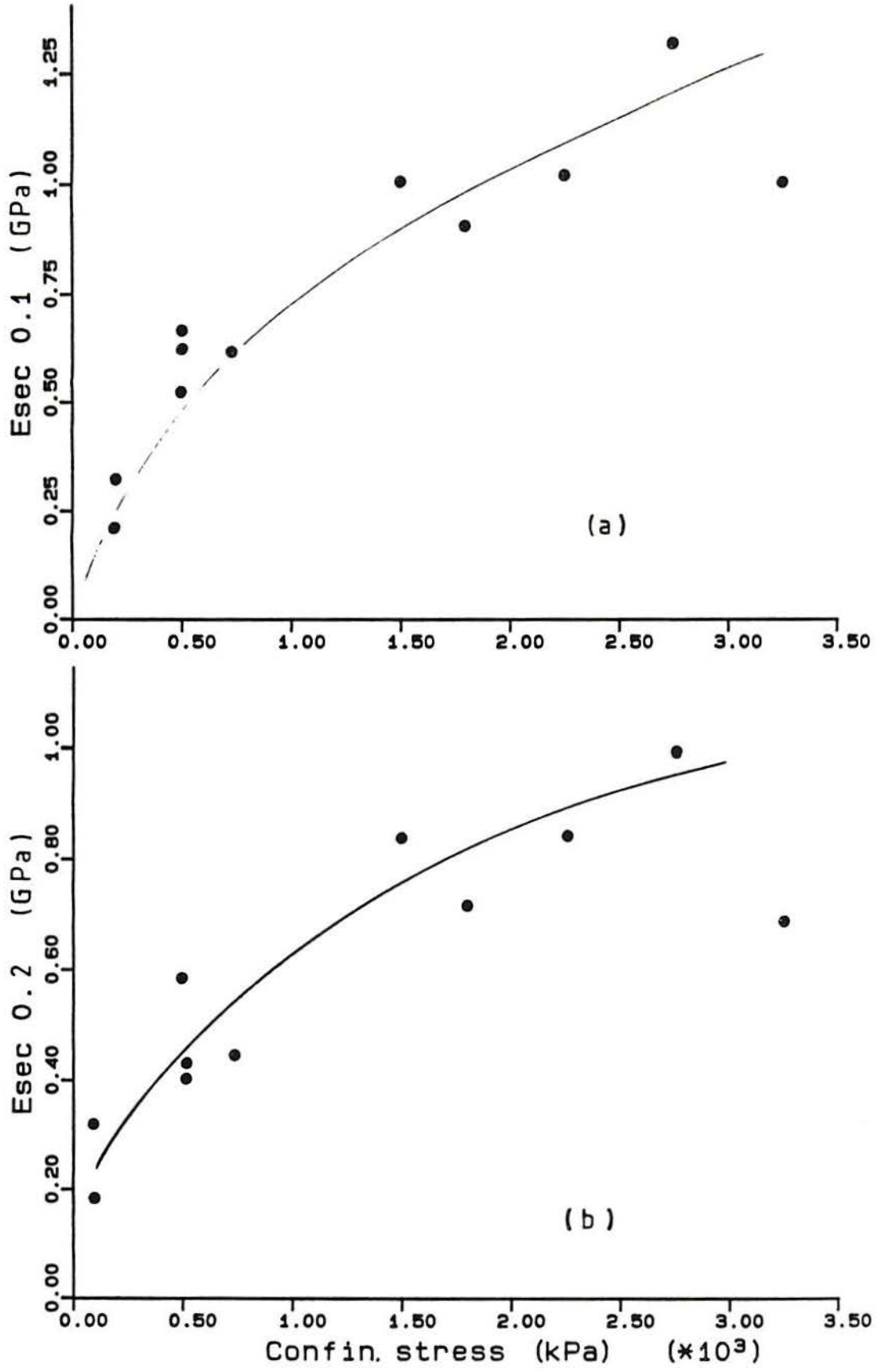

Figure 8.32 – Secant stiffness of tests carried out at IC; (*a*) at ϵ_a=0.1%; (*b*) at ϵ_a=0.2%

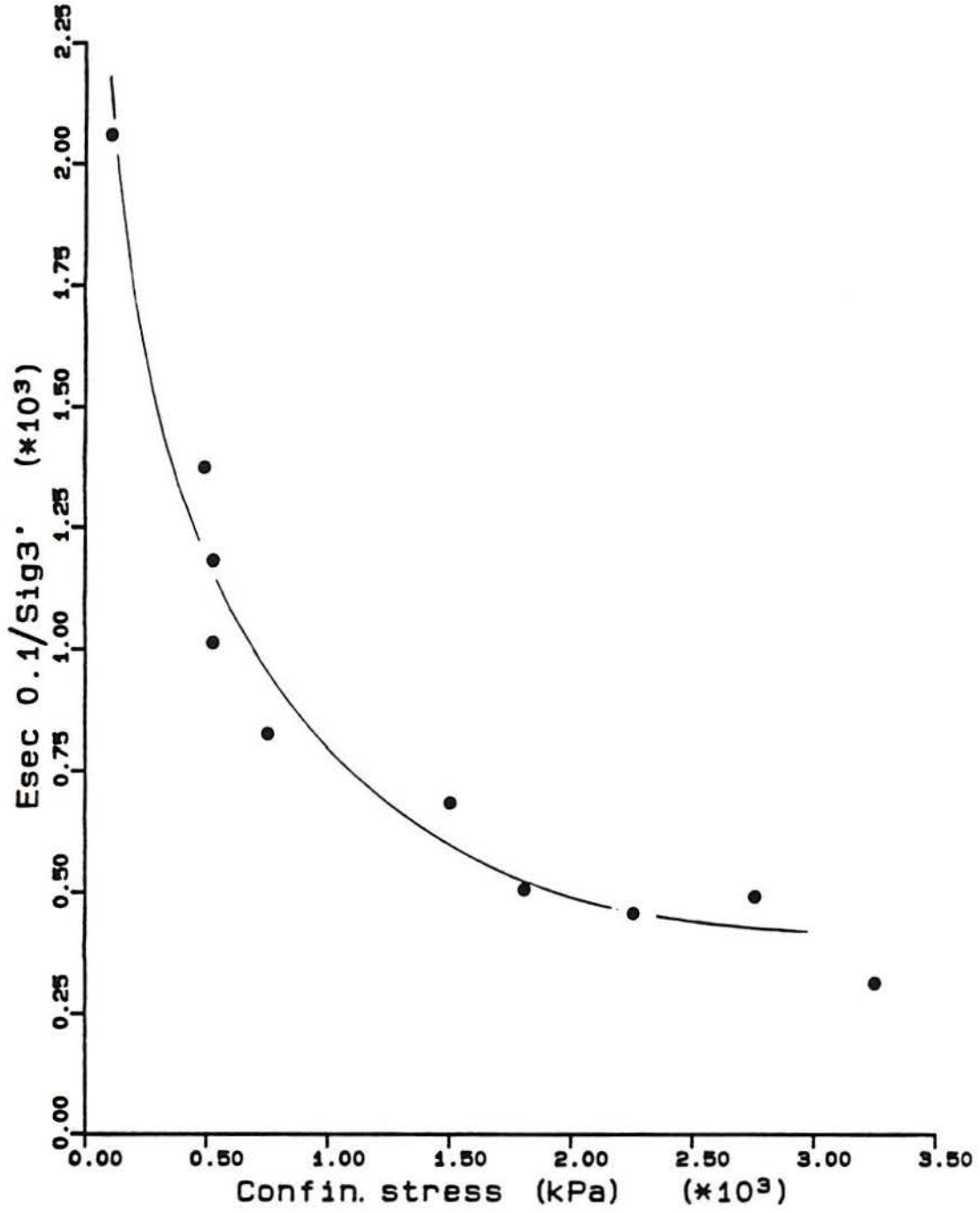

Figure 8.33 - Normalized secant stiffness of tests carried out at IC at ϵ_a=0.1% versus confining stress

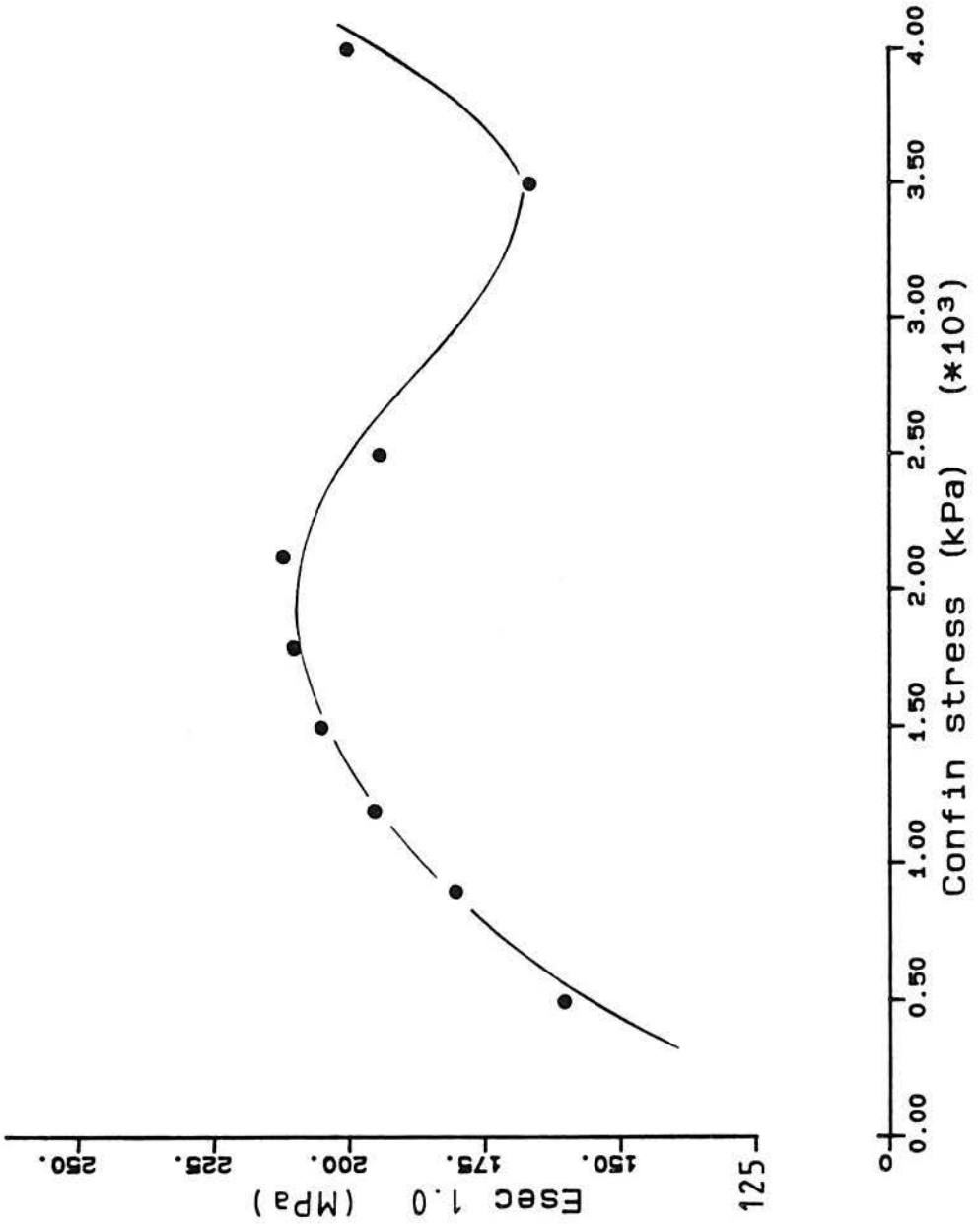

Figure 8.34 – Secant stiffness of Greek drained tests at ϵ_a=0.1% versus confining stress

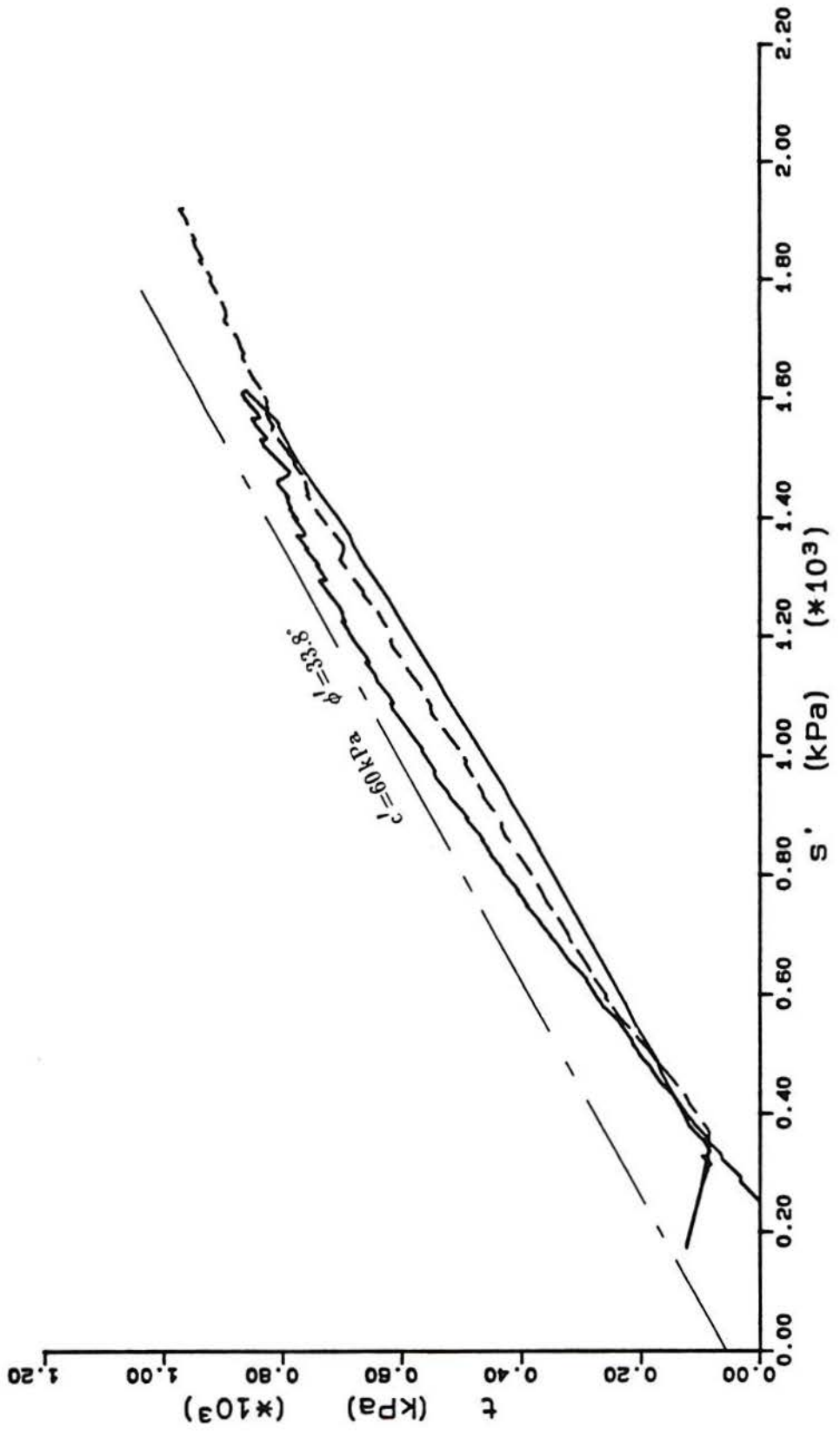

Figure 8.35 – Stress-path of the one-dimensional test I 14 K_0. The discontinuous line represents the second loading

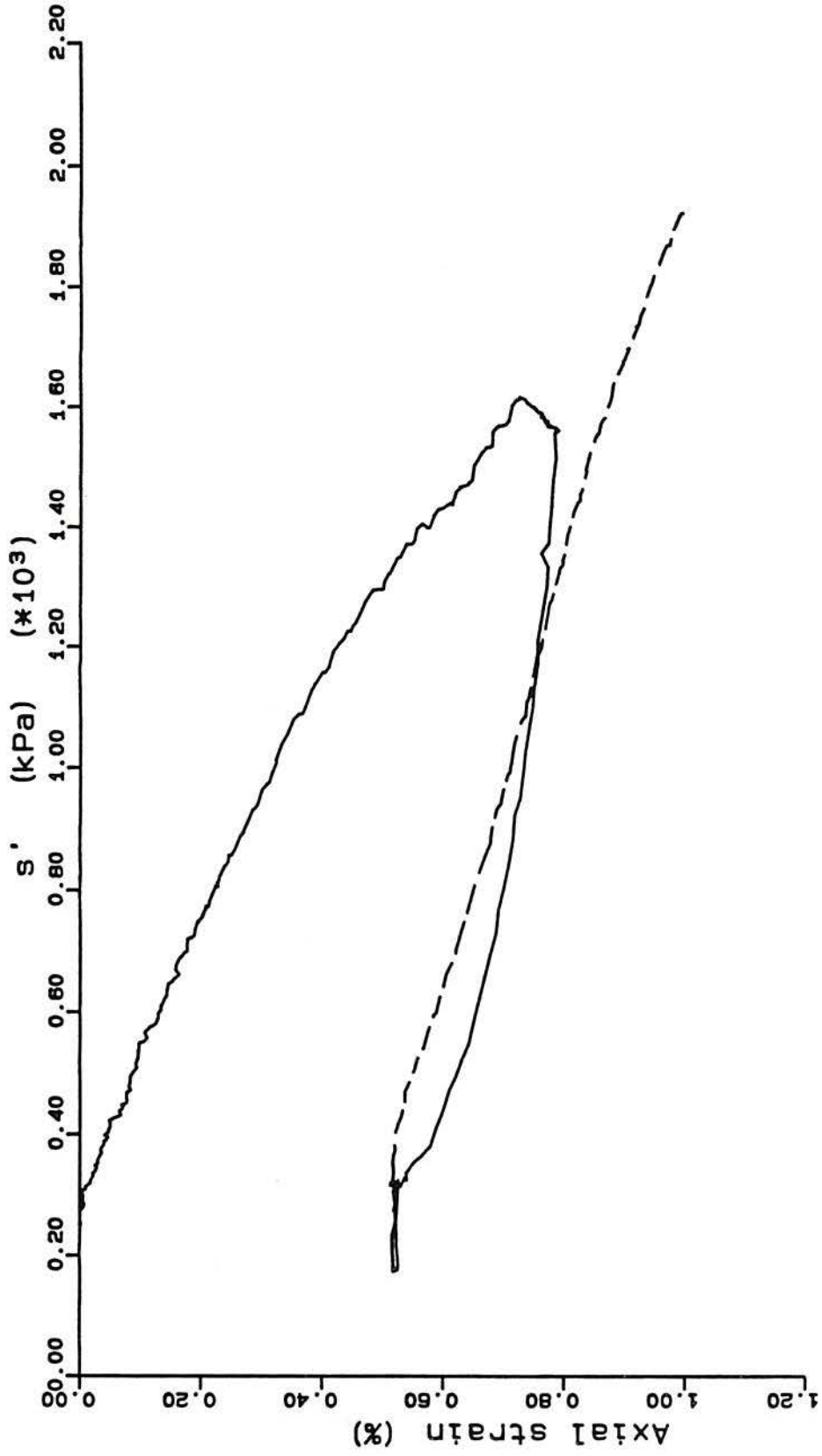

Figure 8.36 – Axial strain versus s′ of one-dimensional test I 14 K_0

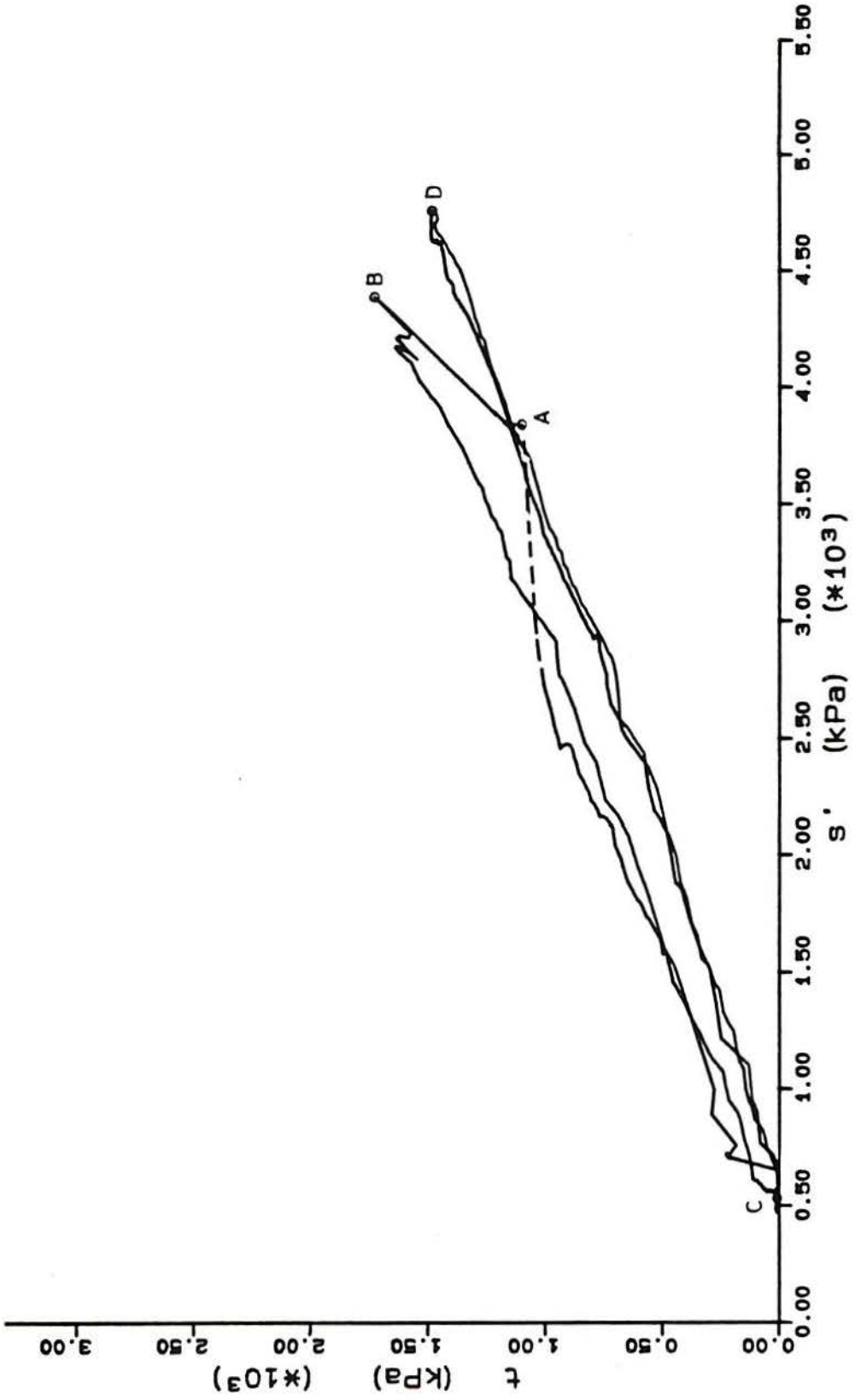

Figure 8.37 – Stress-path of the one-dimensional test I 15 K_0. The discontinuous line represents the uncontrolled part of the test

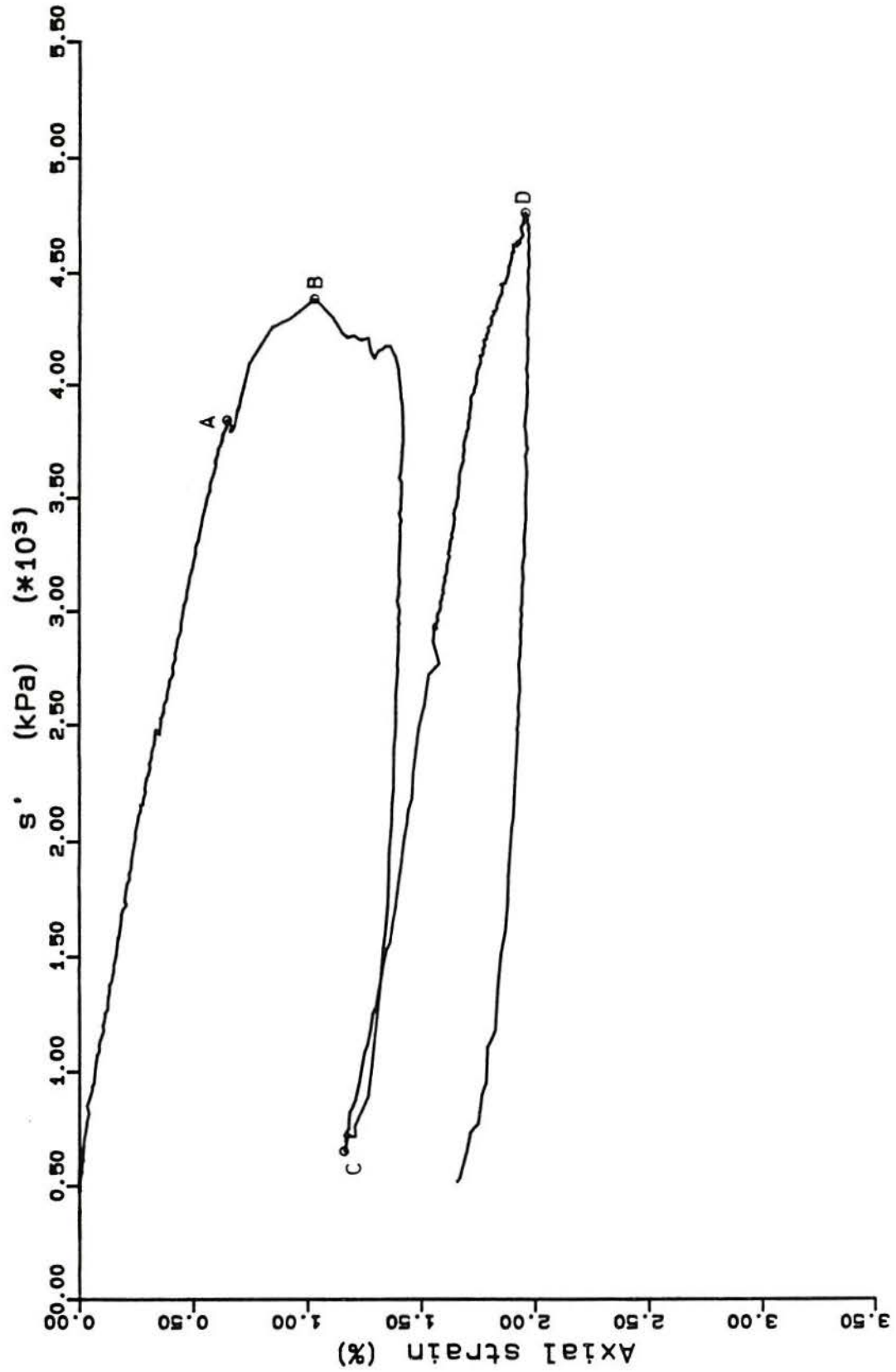

Figure 8.38 – Axial strain versus s′ of one-dimensional test I 15 K_0

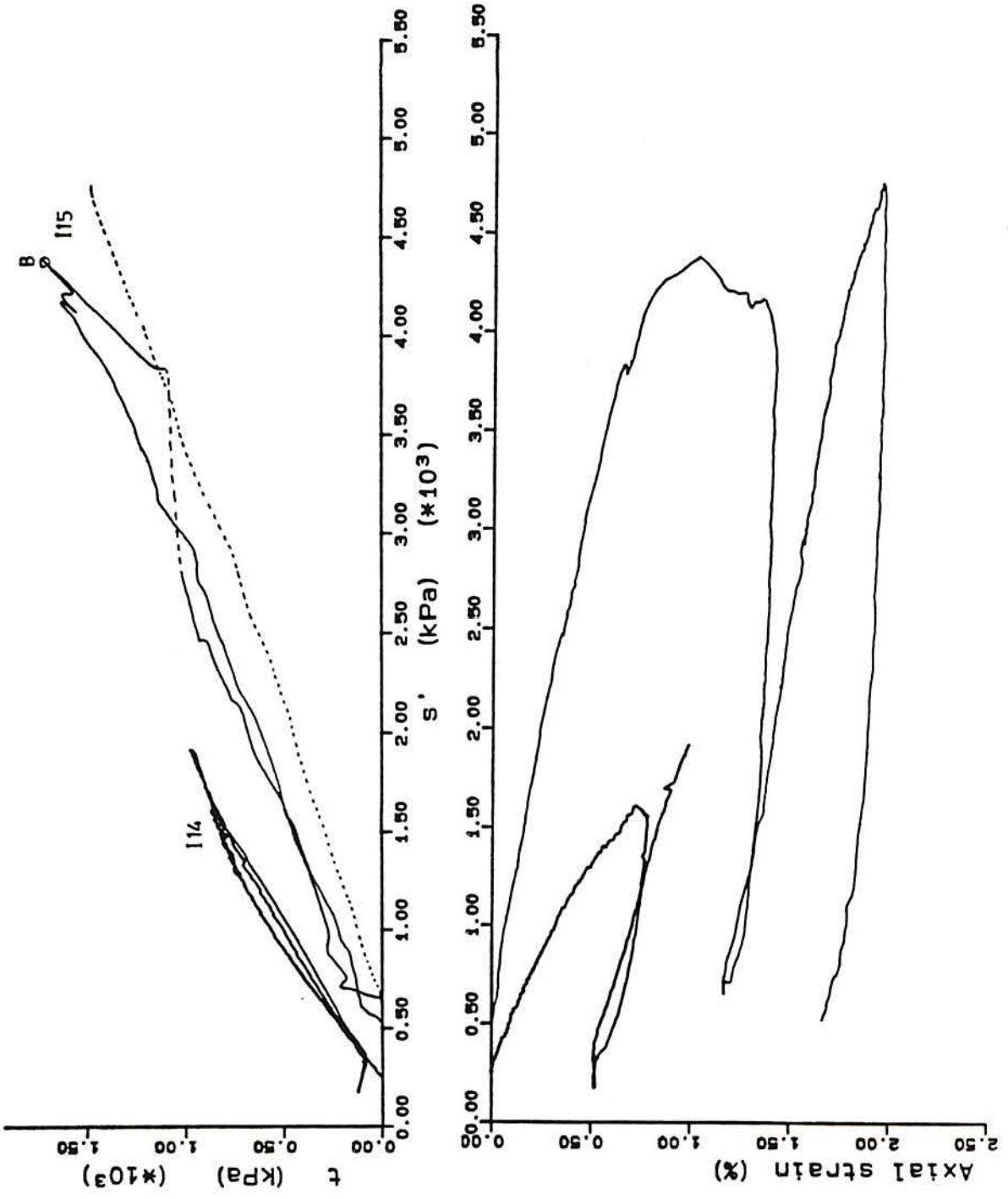

Figure 8.39 – The combined results of two one-dimensional compression tests; stress-path and axial deformation

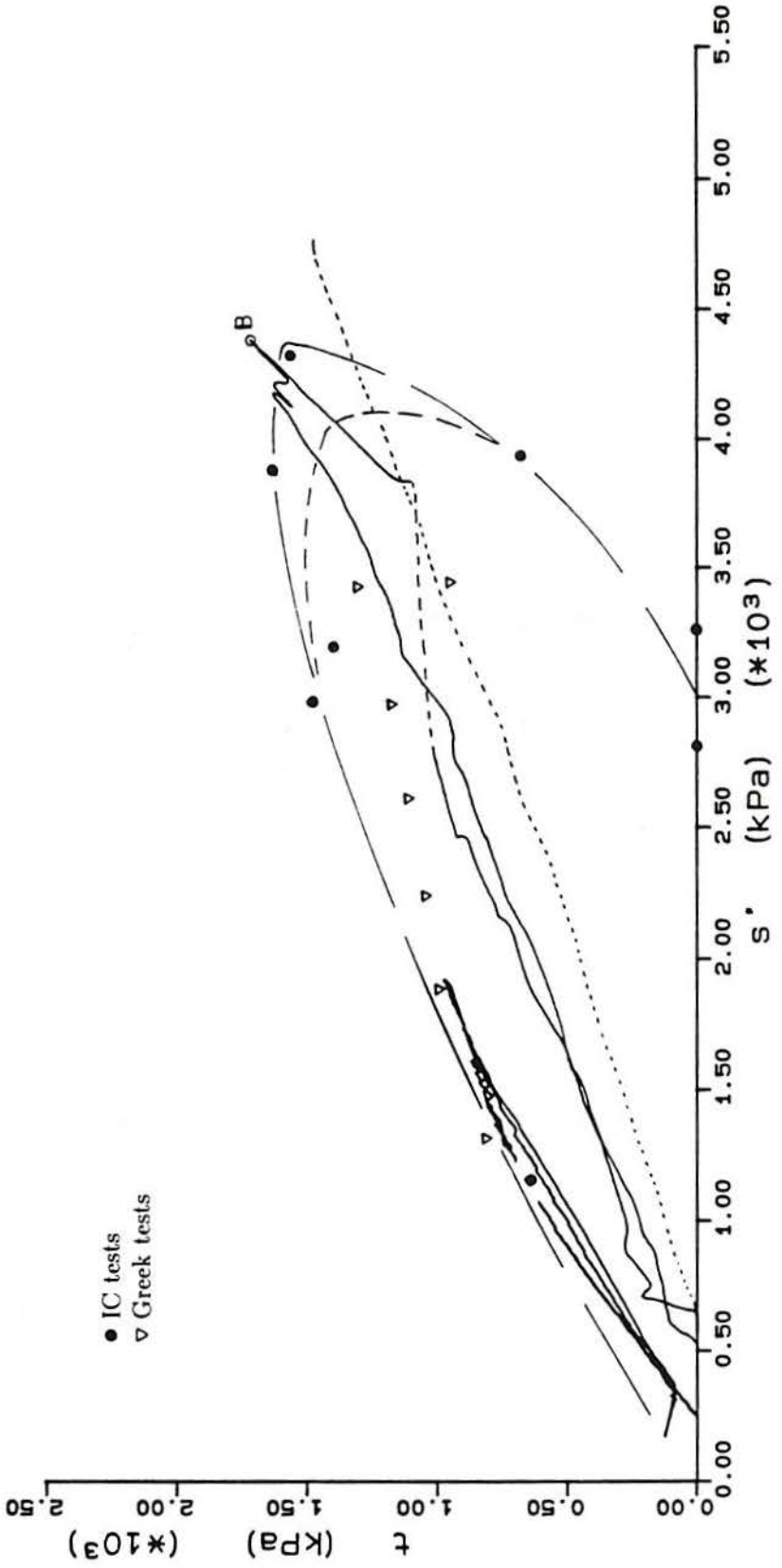

Figure 8.40 – Comparison between the stress-path of one-dimensional tests and the yield points

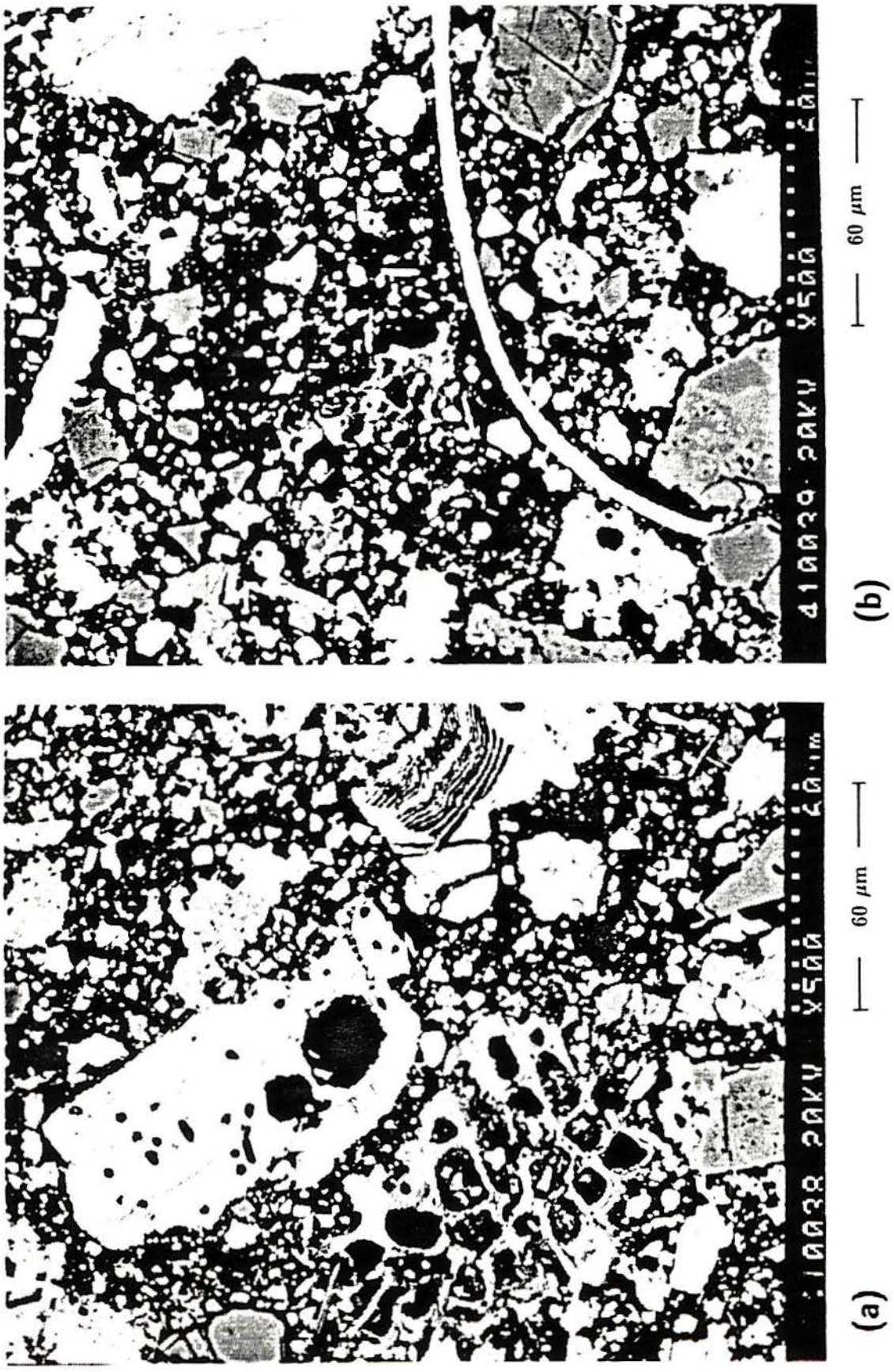

Figure 8.41 – Microphotograph of undisturbed sample of Corinth Marl, e=0.620

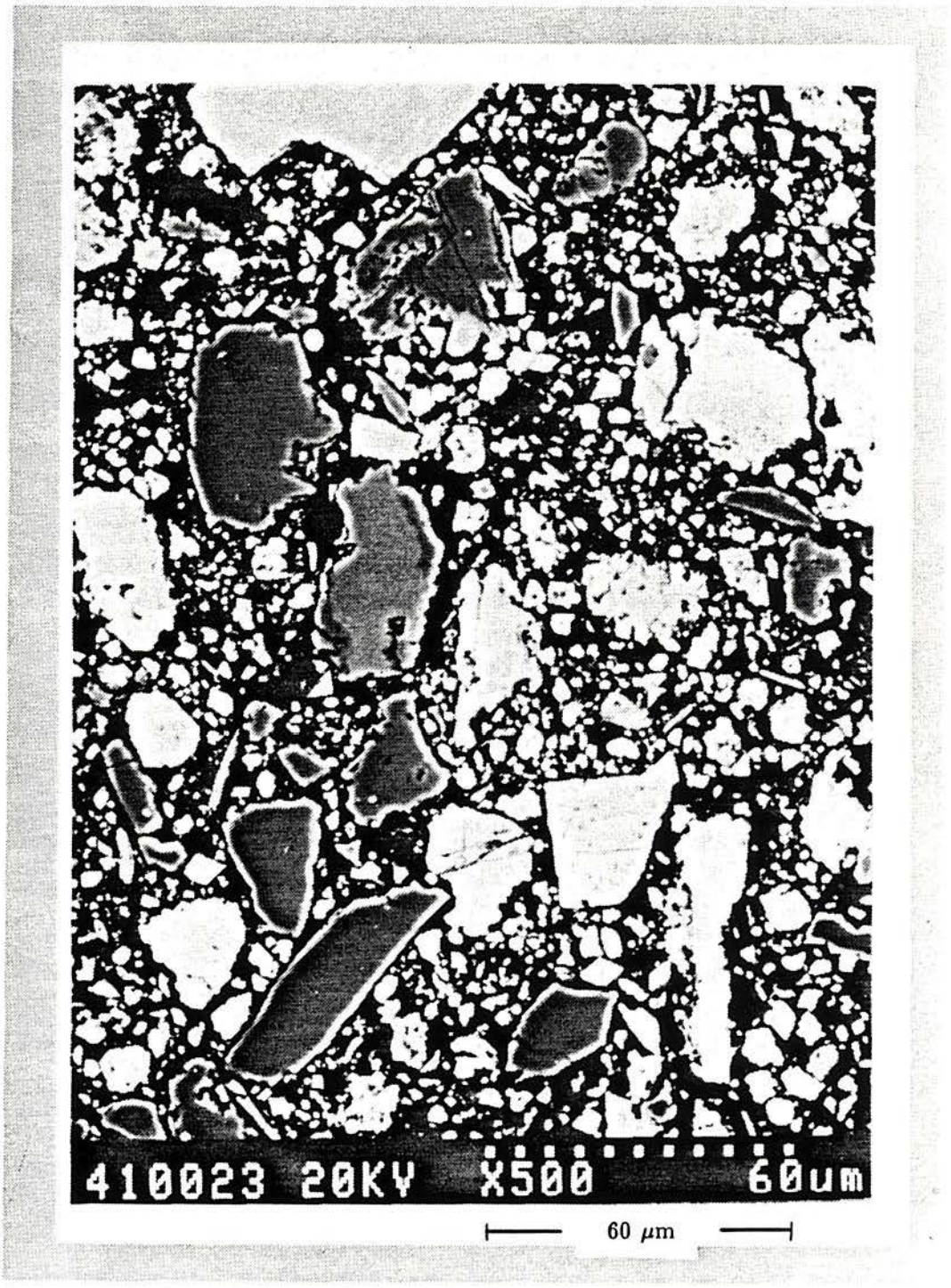

Figure 8.42 – Microphotograph of Corinth Marl sample tested as IC 2 (undrained, σ'_3=525 kPa, e_f=0.618)

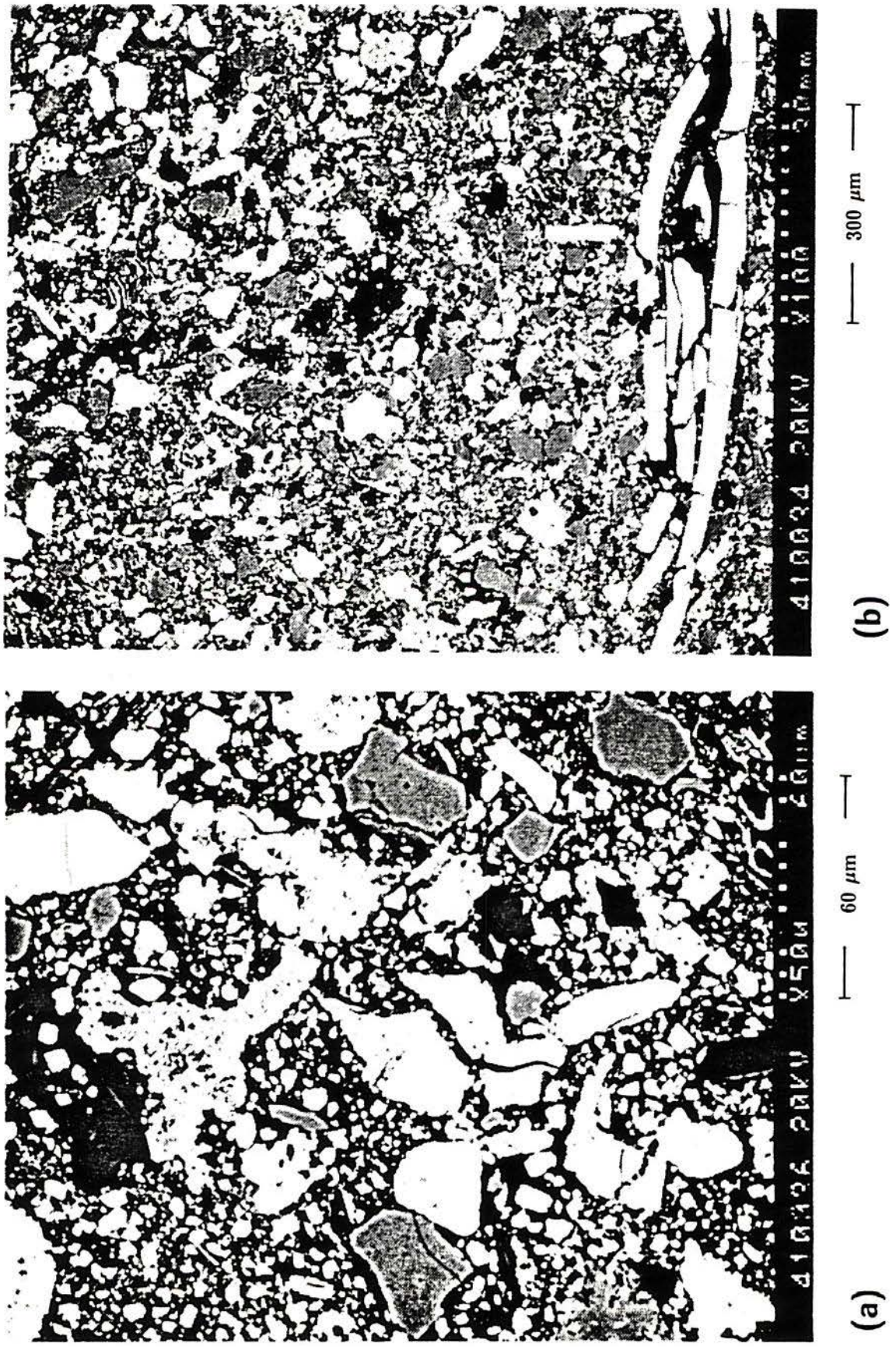

Figure 8.43 – Microphotograph of Corinth Marl sample tested as I11 (drained, σ'_3=3250 kPa, e_f=0.425)

9. CHEMUSUSU DAM SOIL

9.1 INTRODUCTION

The use of natural soil samples is of great importance in verifying the results obtained from the artificial soil. Contacts made by Prof. P.R. Vaughan with the Transport and Road Research Laboratory (TRRL) and British Geological Survey (BGS) enabled tests to be performed on undisturbed and disturbed samples of a red soil from Kenya. At the time of writing some characterization, mineralogical and consolidation tests are being carried out at BGS as part of a larger testing programme.

9.2 GEOLOGY AND CLASSIFICATION TESTS

9.2.1 Geology

The information on the geology of the area was provided by the BGS (Northmore, 1990). The site of the proposed Chemususu Dam is located in a forested area adjacent to the western margin of the Rift Valley, Baringo District in Kenya, 60 km south east of Eldoret and 13 km north west of Eldama Ravine. The climate is cool and humid with average annual rainfall of between 1100 and 2700 mm (March-November). The mean annual temperature is 12-14°C with an occasional night frost. The site elevation is 2330 m above mean sea level.

The bedrock geology is composed of tertiary volcanics comprising lavas (generally non-porphyritic), basic tuffs and sediments.

The general landscape includes a series of closely-spaced, low, round crested ridges separated by narrow V-shaped or slightly wider flat-bottomed valleys. The narrow valley bottoms are 2-10 m wide, concave or V-shaped and contain the stream channel only. Wider

flat-bottomed valley floors are level, up to 200 m wide and 1.5 km long, with very narrow (2-3 m wide) stream channels.

The ridge crests and ridge slopes are well drained and above the influence of groundwater. The flat valley floors, with brown-grey loams and mottled grey-brown clays, are poorly drained and subject to seasonal flooding. The stream channels have perennial flow.

9.2.2 Sample description

Samples from different trenches and depths were sent to Imperial College. The undisturbed samples had been collected using a technique described by Culshaw et al. (1989), which consists of cutting a cylindrical sample using a plastic tube as a guide and container of the soil sample. Samples with 150 mm diameter and 200 mm height were obtained.

The samples used in the triaxial testing described later came from trench 15 at the dam borrow area (3.80 to 4.00 m depth). The soil has been described as red and dark red (Munsell colour code 2.5 YR 4/6-3/6), containing small pale-coloured weathered fragments of parent rock (Northmore, 1990).

The undisturbed sample received by Imperial College had an average water content of 33%, an overall dry density of 10.95 kN/m^3 (e=1.47) and a degree of saturation of 62%. The sampling was carried out in September and hence the sample was probably at its wettest because the rainy season was drawing to a close.

Filter paper was used to measure the suction present in the sample due to the partial saturation, following the technique currently in use at Imperial College. The calibration curve for low suctions (Fig. 9.4, Crilly, 1989) was used. Two filter paper discs left in contact with the sample in a sealed chamber for seven days each had a water content of 72% indicating a suction of 35 kPa.

The author tried to trim undisturbed samples taken from shallower depths (1.20-1.40 m) at the same site without success. The soil had pronounced localized non-uniformities, with parts denser than the surrounding weak matrix and when trimming the sample with a sharp

knife these parts tended to be dislodged. The size of the intended sample (38 mm diameter) was such that excessively large stresses were induced by the knife. It would probably be much more feasible to trim larger samples and this should be considered in future work.

The deeper sample used in the testing programme had the same kind of macroscopic structure as the shallower sample but the matrix was stronger. When trimming, it was sometimes possible to cut the denser areas to a smooth finish using a sharp knife, whereas in other cases it was better to gently scarify to minimize the damage. The final dimensions of the trimmed samples were occasionally well above the standard size because further cutting would have been very difficult without destroying the sample. Two samples were lost during the final trimming.

It is recommended that in future the samples should be trimmed in the field to their final testing dimensions. If this were to prove difficult, it would almost certainly be impossible to do so in the laboratory, in which case larger diameters should be used for testing and sampling. The field trimming of the samples seemed successful in maintaining the friable structure of the soil and the same technique should be tried for smaller sizes.

9.2.3 Grading

Tests to determine the soil grading were carried out on four of the disturbed samples using different techniques. The results for the soil used in the triaxial testing are shown in Fig. 9.1 and the results from the other samples are presented in Fig. 9.2. Three test procedures were used: (*a*) sedimentation using sodium hexametaphosphate as a deflocculant, (*b*) sedimentation using only distilled water, and (*c*) dry sieving. In the first two methods the procedure described by Head (1980) was followed, except that in the latter no chemical agent was used. The soil samples were agitated for 24 hours prior to the sedimentation test and had not been previously dried. In the third alternative the samples were first dried under lamps and then worked in a pestle and mortar until the soil appeared to have broken down into its individual particles prior to sieving.

Different results were obtained for each procedure. The drying had a marked effect in increasing the apparent particle sizes into the sand/gravel region. Similar results have been reported for other residual soils. Wesley (1973a) showed a clay fraction reduction from 67% to 5% by pre-drying. This effect would probably be reduced if sieving were done wet. The other two methods were carried out with no pre-drying of the soil. The only difference between the two procedures was the use or non use of the chemical deflocculant. The difference in grading obtained is large, the soil in each case appears to pass from a silty sand or sandy silt to a silty clay. The chemical seems to be very effective in separating the individual particles. The results show how strong the inter-particle forces can be because silt size groups are maintained even after 24 hours continuous agitation in water.

9.2.4 Atterberg limits and compaction tests

The results presented here are for soil from trench 15, 3.80-4.00 m depth. The Atterberg limits were determined using the cone penetrometer apparatus because it gives more consistent results than the Casagrande equipment. However, it has been shown to give liquid limit values that are 10% larger than those obtained with the Casagrande apparatus for some tropical residual soils (Carvalho, 1986).

The influence of mixing time prior to the determination of the Atterberg limits of tropical residual soils is well documented. They are also affected by pre-drying (Hobbs, 1990 among others). In order to obtain consistent results, a thorough mixing is necessary. Hobbs (1990) suggested that a "greaseworker" apparatus should be used to completely destroy any structure of the soil prior to testing. He presents some results of tests carried out in tropical soils from Indonesia and Kenya using this technique. The values of liquid limit obtained were considerably larger when using this apparatus compared to the method of hand mixing suggested by the British Standard Institution (1975), even when the latter was performed for one hour. Hobbs' data suggests increases as large as 50% in the liquid limit value (average of 35% approximately). Similar results were found for lateritic soils from Brazil by Cozzolino &

Nogami (1988), with increases in liquid limit between 18% and 45% when intense manual remoulding was used. The effect was not evident in saprolitic soils. Hobbs (1990) also points out that the new values cause the soils to plot further to the right of the A-line on the Casagrande plasticity chart. Data for soils derived from similar rocks were found to group much closer together on this chart than when using results of hand mixed tests. This indicates that a great deal of mechanical distortion is necessary to obtain the separation of the particles such that their true mineralogical chemistry will control the Atterberg limits.

The author experienced difficulties in obtaining consistent results when attempting hand mixing. As the greaseworker was not available, an ultrasound bath was used to separate the soil particles. The soil was put inside a beaker with enough distilled water to cover it. The beaker was then subject to the ultrasound action for a total of 2 hours. Although visually it did not change much, the following hand mixing was very successful in obtaining a homogeneous mixture which gave consistent results. The liquid limit was measured using the cone penetrometer procedure recommended by the British Standard Institution (1975), giving a result of LL=89%.

The plastic limit was estimated to be 33% using the procedure described by Harison (1988) which uses an extrapolation of the cone results to a penetration of 2 mm. It is worthwhile mentioning that the tests were done on the whole soil grading. All particles were reduced by the mixing, to a size which did not interfere with the test. The sensitivity of the soil to the mixing procedure is due to the aggregation of particles, with sizes varying according to the preparation which the sample has been subjected to, as was clearly illustrated by the grading tests. Tests on a completely mixed soil will define the extreme limit or the intrinsic properties of the soil and these results must be pursued.

It has been suggested by Vaughan et al. (1988) that the in-situ density of residual soil could be indexed according to its relative void ratio, i.e.:

$$e_R = \frac{(e - e_{OPT})}{e_L - e_{OPT}}$$

where e is the in-situ void ratio of the soil, e_{OPT} is the void ratio at the maximum density obtained in a compaction test with standard Proctor energy and e_L is the void ratio at the liquid limit.

As the amount of soil available was not enough to perform a standard compaction test an alternative test was investigated. There is a smaller version of the compaction test called Harvard miniature (Wilson, 1970). Head (1980) discussing the use of the same apparatus, suggests that a three layer compaction with 25 tamps/layer of the spring loaded ram gives a density roughly equivalent to that obtained from the standard Proctor test.

A modified apparatus was built at Imperial College workshop for the compaction (Appendix 2). The sample volume was increased from the 62.4 cc of the described apparatus (Head, 1980) to 87 cc with the sample dimensions being 38.1 mm diameter and 76.2 mm height. The spring loaded ram was maintained as described by Wilson (1970), the applied load being set-up to the same level of 178 N. To keep the same ratio of energy/soil volume, the number of tamps had to be increased from 75 to 105. A compaction procedure was adopted with 20 tamps to each of five layers of soil which provided very uniform samples.

The apparatus and compaction energy were tested on a soil available in the laboratory at the time (a mixture of 30% fine sand, 50% silt, 8% kaolin and 12% bentonite). The soil was compacted using the standard Proctor procedure and with the modified procedure and equipment described above. The dry densities and optimum water contents obtained with the conventional Proctor test were 16.65 kN/m^3 and 20.8% and with the small equipment were 16.95 kN/m^3 and 19.4%. These values indicate that the new apparatus gives results which are close to the standard Proctor test with the advantage of using a much smaller soil quantity (around 200 g for each sample). The extruded sample is of a convenient size for triaxial testing and there is no need for further trimming.

A compaction test using the new equipment was carried out in the soil from trench 15, 3.80-4.00 m depth. The soil was hand mixed at its natural water content (approximately 35%) and separated into eight portions of 200 g each. Some were then allowed to dry whilst exposed

to the air, until the water content had reduced to the desired value, whereas others had a small quantity of water added. The soil portions were thoroughly mixed, placed in plastic bags and left sealed overnight. The compaction test results are shown in Fig. 9.3 together with the saturation curve for the soil. The results all lie on the dry side of the optimum water content and this side seems well defined. An attempt was made to compact a sample wetter than optimum but it proved impossible, the soil being too wet and showing large movement around the ram. The sample compacted at the defined optimum represents the wettest condition attainable because, even then, the compaction was difficult due to this movement. This behaviour was probably caused by the unusual proximity of the experimental points to the saturation line. The maximum dry density obtained was 13.2 kN/m^3 which corresponds to a void ratio of 1.05 (e_{OPT}).

Using the values quoted before, the relative void ratio can be calculated for the whole sample as:

$$e_R = \frac{1.47 - 1.05}{2.46 - 1.05} = 0.3$$

9.3 TEST RESULTS

9.3.1 Introduction

Five triaxial soil samples were tested during the work, all from trench 15, 3.80-4.00 m depth. The size of the sample received from field did not allow a larger number of tests to be carried out. Three oedometer tests on disturbed samples were also carried out to compare their results with those of tests on undisturbed samples. The shallower samples proved to be very difficult to trim down to size and were not used (see item 9.2.2).

The physical characteristics of the triaxial samples tested are presented in Table 9.1. The samples were cut to non-standard sizes due to the described difficulties in trimming. Their initial void ratios vary considerably as a consequence of the sample macro-structure.

The samples surfaces were very irregular for the same reasons and therefore the external volume measurement was susceptible to large errors. All the triaxial samples had their axial strain measured with local transducers.

9.3.2 Saturation

A back-pressure was employed for saturation of all the samples. This was necessary so that the volumetric strain during shear could be accurately measured (as the effective confining pressure is constant and no membrane error arises) and the effective stress known with certainty.

Although the saturation with back-pressure can cause considerable disturbance of the soil structure as discussed in Chapter 4, the main factor causing the disturbance seems to be the oscillation of the effective cell pressure. This oscillation can arise due to a stepwise increase in either the cell pressure or the pore-pressure or due to measurements of the parameter B when the sample is still not fully saturated. These two causes were eliminated by using the following procedure. After assembly, the cell pressure and back-pressure were applied simultaneously (their values being in general 20 kPa and 15 kPa). After the volume intake of the sample had stabilized (a matter of a few minutes) the cell pressure and back-pressure were increased simultaneously with the use of manostats driven by a stepper motor. Rates of increase of 1.0 kPa/min were typically employed following the experience with the artificial soil which has similar permeability. Once the desired value of back-pressure had been reached, the pressures were kept constant and the volume of water intake monitored with time. The stabilization of the water intake with time provided a good indication that the sample fluid was in equilibrium, i.e., that for such back-pressure no more dissolution of air would occur. The saturation was then verified by increasing simultaneously in equal amounts the cell pressure and the back-pressure while still monitoring the volume intake of water. If no more water entered the sample it was assumed to be fully saturated. Measurements of parameter B confirmed the saturation ($B \geq 0.98$).

However, no standard value of back-pressure seemed to work for every sample. This was highlighted by the results of samples C3 and C4. Initially a back-pressure of 200 kPa was applied to the samples and the volume intake monitored for a period of 30 days. Then, an increase of both pressures showed that sample C4 was saturated (this was confirmed with the measurement of B=1.00) but under similar conditions sample C3 was not saturated. The back-pressure had to be increased to 520 kPa and maintained for another nine days to fully saturate this sample. The B value was also measured before shearing giving B=1.00. The first sample tested (test C1) was not fully saturated, even with a back-pressure of 420 kPa for a period of five days.

9.3.3 Consolidation results

Four of the triaxial samples were isotropically consolidated before shearing. Sample C2 was loaded at a nearly constant stress ratio up to its final anisotropic consolidation stresses. The consolidation pressures of all samples are indicated in Table 9.1.

The axial compressibility of three samples are presented in Fig. 9.5. The stress-path of test C2 is also presented. The axial measurements had been measured locally. There is a considerable difference in compressibility between the two isotropically compressed samples (C1 and C5) but this difference is consistent with their initial void ratios (e=1.55 and e=1.23, respectively). Sample C2 presented a high initial compressibility up to $s' \simeq 125$ kPa, a transition zone and an approximately linear compressibility for $160 \leq s' \leq 360$ kPa.

The axial strain is plotted in Fig. 9.6 versus the logarithm of vertical stress on the samples. On this scale, sample C2 shows a pronounced discontinuity at around 240 kPa.

In order to compare the results of the volumetric compressibility for the undisturbed soil, three oedometer tests were carried out on disturbed samples. Two of the samples were remoulded at their natural water content. The soil was thoroughly hand mixed and even though considerable effort was applied, small aggregations of particles of around 0.3-1.0 mm diameter were still present. Two oedometer rings were filled with the homogeneous soil at a

high initial void ratio (e_i=3.40 and e_i=2.88). Both samples were flooded at the end of consolidation at 10 kPa, showing significant deformation (Fig. 9.7). They were then loaded to 800 kPa and unloaded. The compression curves obtained are closely parallel and the samples maintained their initial difference in void ratio throughout the test.

The other oedometer test was carried out on the sample used for liquid limit determination. The sample had been remoulded under quite extreme conditions of vibration (see item 9.2.4) and its initial void ratio was 2.43. The compressibility of this sample was larger than the other two. The average compression index (C_c) of each test was 0.48 and 0.49 for the remoulded samples, and 0.56 for the slurry.

The comparison between the compressibilities of the two classes of samples is shown in Fig. 9.8. The undisturbed samples had considerably smaller compressibilities and this appears to be related to the initial void ratio. The plot illustrates well the large variation in the initial conditions of the samples, which presented difficulties in the interpretation of the data. Note that the test results from the undisturbed samples were affected by the membrane penetration error. The data was not corrected in any way because no correction can reliably be applied. This error gives results which show the samples to have a larger compressibility than the true one.

It seems evident that there is a pattern of reduction in stiffness from the undisturbed state, to the remoulded and slurry states. This is well demonstrated by the disturbed test results and test C1. Tests C2 and C5 showed greater stiffness, but their initial void ratio was lower than the other undisturbed samples. Sample C1 seems to have reached a "virgin consolidation line" after about 45 kPa. Using that line, the compression index calculated gives a value of 0.20 which is well below the values from the disturbed samples. Sample C5 showed a compressibility similar to the unloading compressibility of the disturbed samples (C_c=0.051 compared with C_s of 0.059, 0.040 and 0.044 obtained from the disturbed samples).

9.3.4 Strength results

Following the consolidation the five undisturbed samples were sheared in triaxial compression. The rate of straining used was 1%/h in all of the tests. Three tests were carried out drained throughout (samples C3, C4 and C5) and two had the drainage closed near the end of the test (samples C1 and C2). The test results are presented in Fig. 9.9 (stress and strain curves) and Fig. 9.10 (stress path and failure envelope).

The results of triaxial tests showed a consistent trend. Test C4, carried out at the lowest effective confining pressure (σ'_3=25 kPa), was the only test to show expansion. Test C1, performed at σ'_3=360 kPa, showed the highest compression during the test and the other two isotropically consolidated tests (C3 and C5) have volumetric compressions more or less proportional to their initial effective confining pressures.

The stress-paths of these tests seem to define two distinct failure envelopes, similarly to the general behaviour of the artificial soil. One curved failure envelope for $s' \leq 600$ kPa (Fig. 9.10) and a straight line passing through the origin with a corresponding value of ϕ'=28.2°, which may define the de-structured strength of the soil. The reasons which caused sample C5 to show such smaller strength are not clear. The sample had the lowest initial void ratio and was the stiffest one during the consolidation. The laboratory notes were re-examined to see if any different procedure had been used. Following the previous experience with sample saturation, this sample had the cell pressure and back-pressure increased simultaneously as had the other samples. However, to reduce the time to accomplish full saturation, the cell pressure and the back-pressure were increased directly to a higher value (σ_3=510 kPa, u=500 kPa) at a rate of 1.0 kPa/min. Although the initial permeability of the sample was quite high ($k \simeq 3.5 \times 10^{-6}$ m/s) it seems that the behaviour of the sample in shearing was affected by this slightly different procedure and this deserves further study.

9.3.5 Stiffness measurements and yield points

The measurement of axial strain in the triaxial tests using local instrumentation

provided reliable information to calculate the secant stiffness. The values calculated at 0.1% axial strain, $E_{SEC\ 0.1}$, are plotted in Fig. 9.11 versus confining pressure. In the same figure are also plotted the normalized stiffness, $E_{SEC\ 0.1}/\sigma'_3$ (continuous line). Both lines show some similarity with the same plots produced for the 200 series artificial soil mixture. The stiffness of the soil is quite high at a low confining stress, there is a small increase with increasing pressure up to σ'_3=150 kPa and then a considerable variation. Note that the normalized value stays constant for pressures larger than σ'_3=150 kPa.

The test results were also analysed to see if yield points could be determined. Log-log plots were produced from the stress-strain results (Fig. 9.12). The resulting lines show that tests C3, C4 and C5 have clear bi-linear plots. Test C1 had a very steep initial line, followed by a smooth concave curve. The points of intersection of the two lines were used to define the value of t at yield and they are plotted in Fig. 9.13 together with the stress-paths. The yield point of test C2 was selected from Fig. 9.5 and 9.6 instead, because its stress-path was not a conventional compression one. Using Fig. 9.5 a value of s' equal to 168 kPa was chosen as the yield pressure and using Fig. 9.6 (logarithmic scale for vertical pressure) a value of σ'_v=240 kPa was adopted. This latter value corresponds to s'=172 kPa for the stress-path followed.

The yield curve at small stresses is much lower than the failure envelope defined in the region. Although the yield locus seems to follow the same pattern as the locus of other materials, i.e. it is centered around the isotropic axis, a greater number of tests are needed to define the soil behaviour with more clarity.

9.3.6 Permeability measurements

The samples had their permeability measured during the triaxial test programme. The test is simple to perform and gives reliable values; the pressures at the top and bottom of the sample can be continuously monitored whilst the volume change is measured. The values referred to here are the average of five or more measurements, except for the result at the end of test C1 when, due to its very low permeability, only the average value was calculated for a

seepage period of 2.5 hours.

The measured values of permeability varied considerably. The natural soil samples had quite high permeabilities ($2x10^{-6}$ m/s). The results of the measurements are plotted in Fig. 9.14 and 9.15. In the first figure, the permeability of three undisturbed samples, measured at different levels of stress, is plotted versus the void ratio. The permeability calculated from the oedometer test results performed on the slurry is also shown. It is clear that the void ratio has a minor effect on the permeability. The undisturbed soil had a large variation in permeability (4.5 orders of magnitude) and no correlation with the void ratio while the slurry had a relatively small variation of permeability associated with a considerable change in void ratio (from 1.94 to 1.23). However, the permeability of the slurry may not represent the true value as it was indirectly obtained from the coeficient of consolidation (C_v).

The permeability results plotted versus s' in Fig. 9.15 suggest a more obvious pattern. The experimental points are marked with the identification test number and a letter (i) for initial permeability, (e) for permeability measured at the end of the test and (ac) for anisotropic consolidation. Although the influence of s' on the undisturbed samples seems clear, it should be noted that probably the most important component in this reduction is the shear stress applied during the tests. Sample C5 showed this influence most clearly. Its initial permeability reduced only slightly from $3.5x10^{-6}$ m/s to $2.6x10^{-6}$ m/s when the isotropic effective stress was increased from 10 kPa to 150 kPa. However, after the sample was sheared the permeability dropped to $1.7x10^{-9}$ m/s, a reduction of 1500 times.

These reductions can be explained by the closing down of structural spaces between the aggregations due to the shearing distortion imposed by the testing. Most of the samples which were tested showed shear planes at the end of the test (C1, C3, C4, C5) which can also have a large influence on the vertical permeability of the sample.

Test	Dimensions Height (mm)	Diameter (mm)	wc_0 (%)	e_0	Degree of saturation (%)	Consolidation (kPa) s'	t	e_i
C1	66.6	41.97	32.0	1.55	57	360	0	1.44
C2	70.7	37.40	31.4	1.37	63	350	152	1.25
C3	99.7	41.80	32.8	1.44	63	55	0	1.41
C4	92.0	40.35	37.2	1.32	78	25	0	1.32
C5	78.0	44.12	33.9	1.23	76	150	0	1.21

$G_s = 2.76$

Table 9.1 — Initial state of samples of Chemususu dam soil, trench 15, 3.80-4.00 m depth

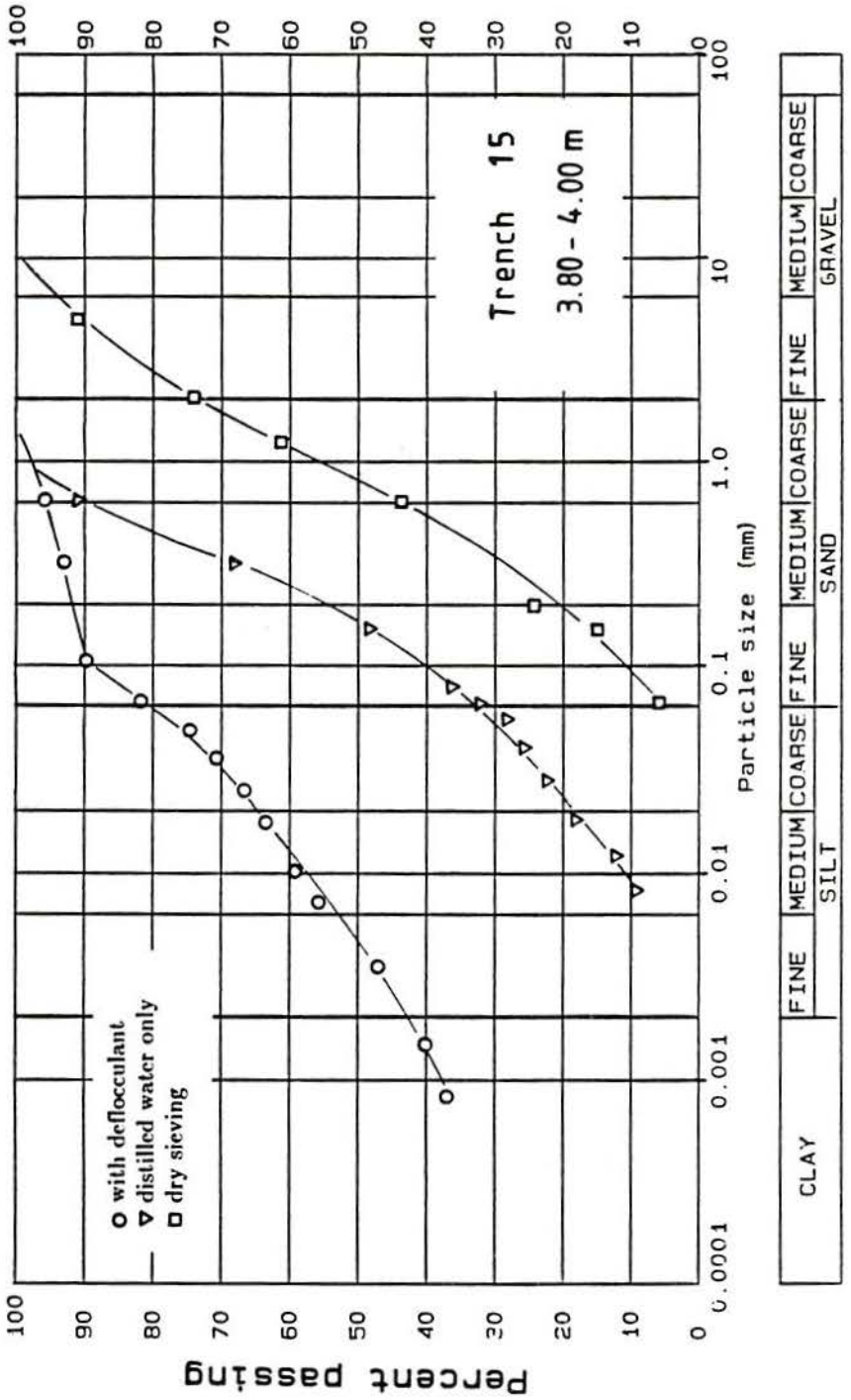

Figure 9.1 – Grading curves obtained for the soil used in the main testing programme with three different methods

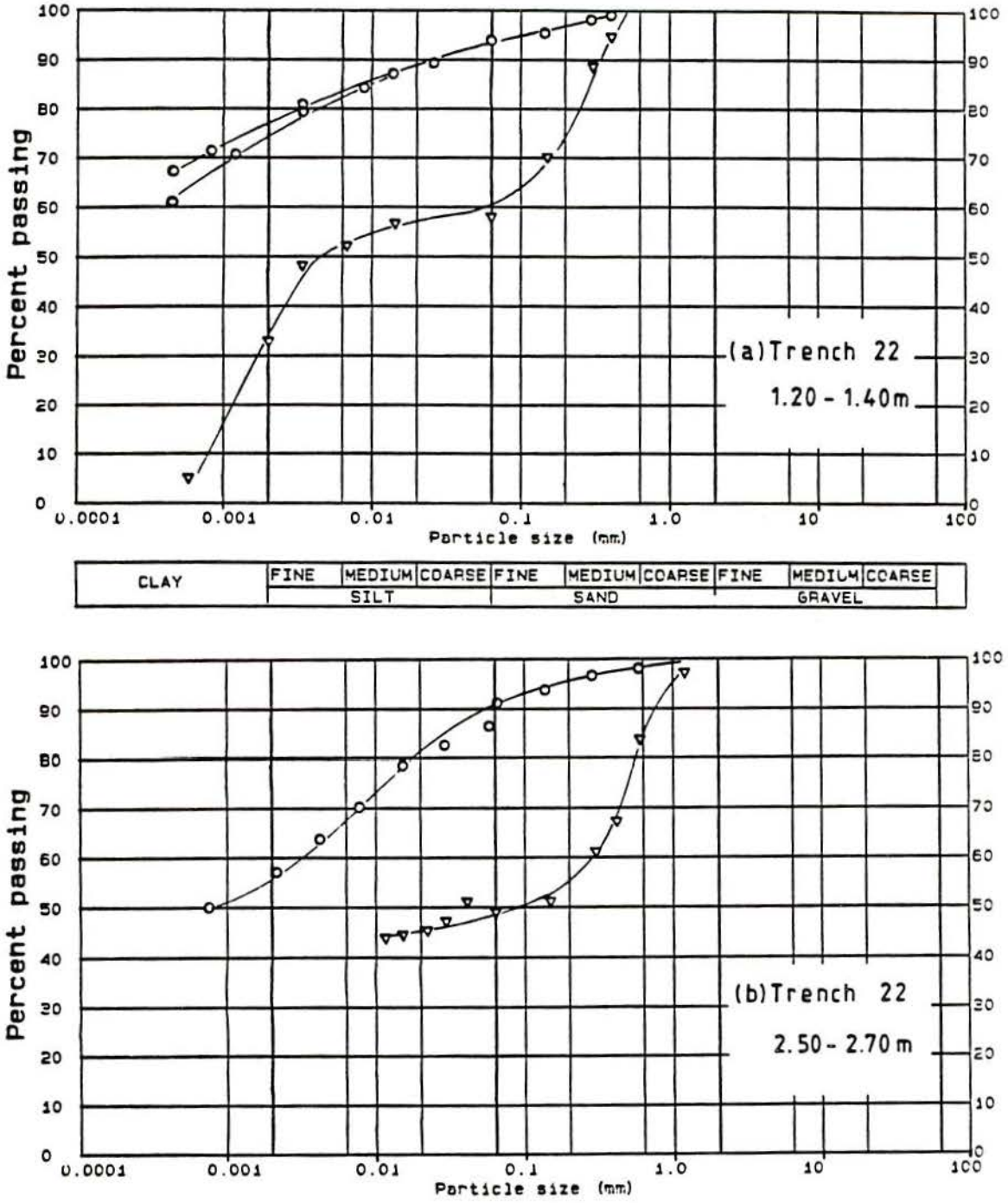

Figure 9.2 – Grading curves of three samples using different methods. (*a*) trench 22, 1.20-1.40 m; (*b*) trench 22, 2.50-2.70 m; (cont.)

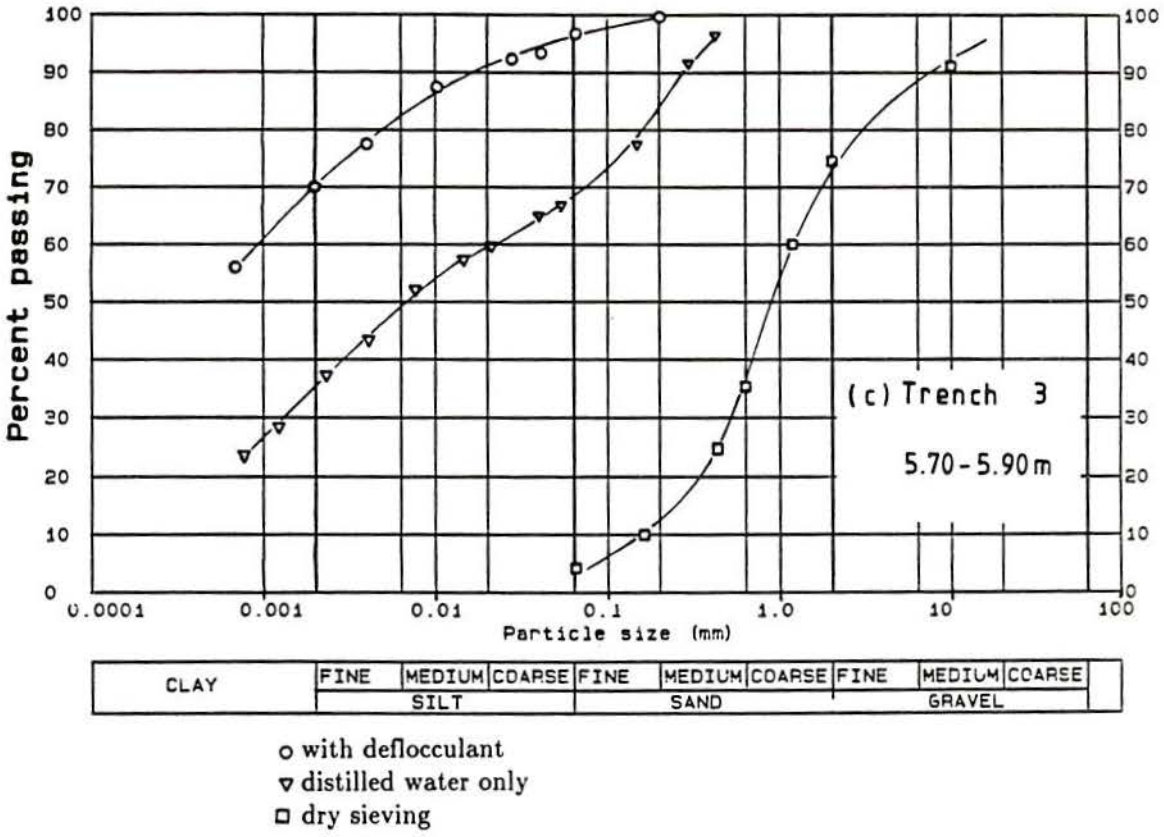

Figure 9.2 – (cont.) (*c*) trench 3, 5.70-5.90 m

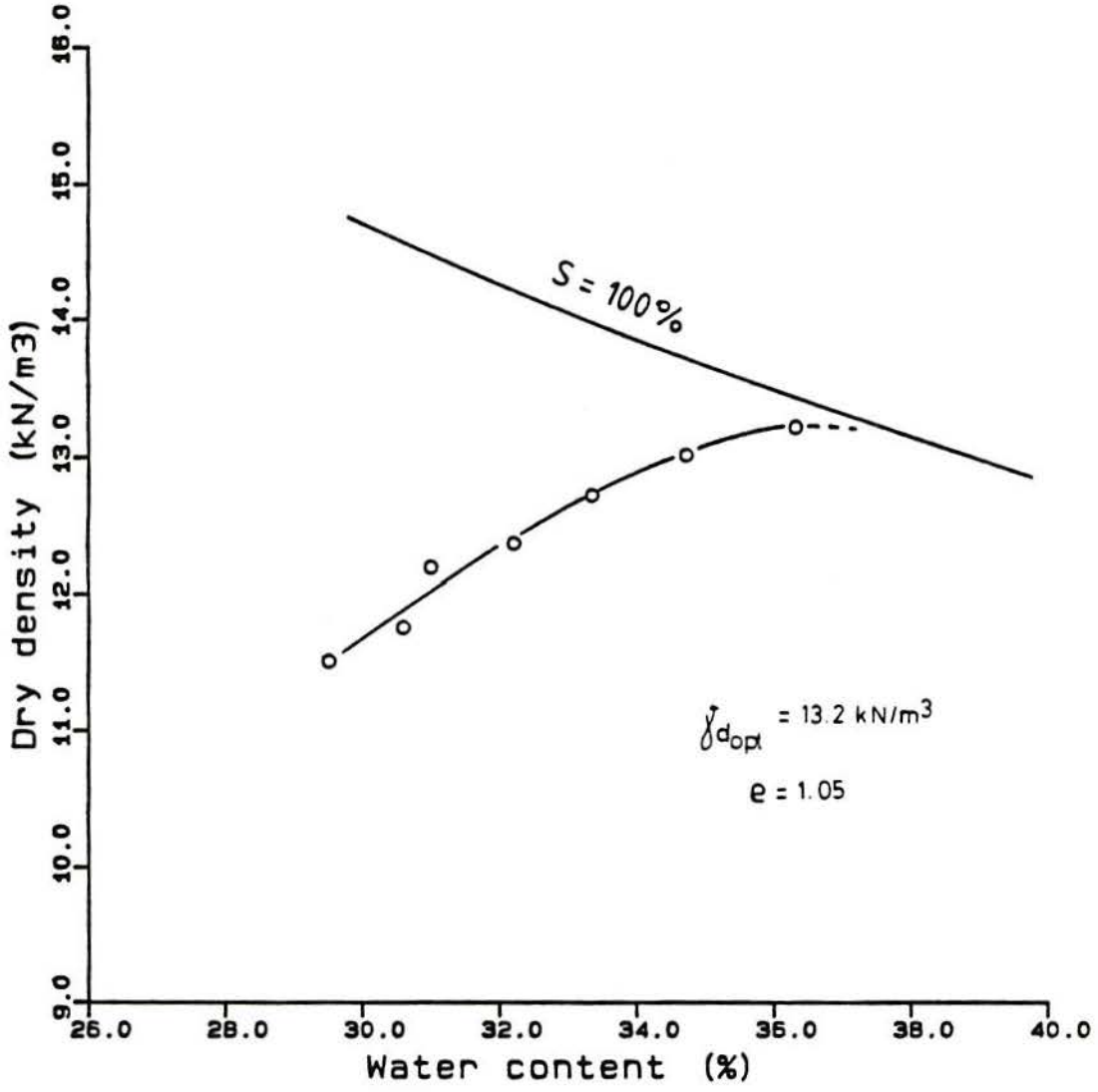

Figure 9.3 – Compaction curve of soil from trench 15, 3.80-4.00 m depth obtained with the modified Harvard equipment

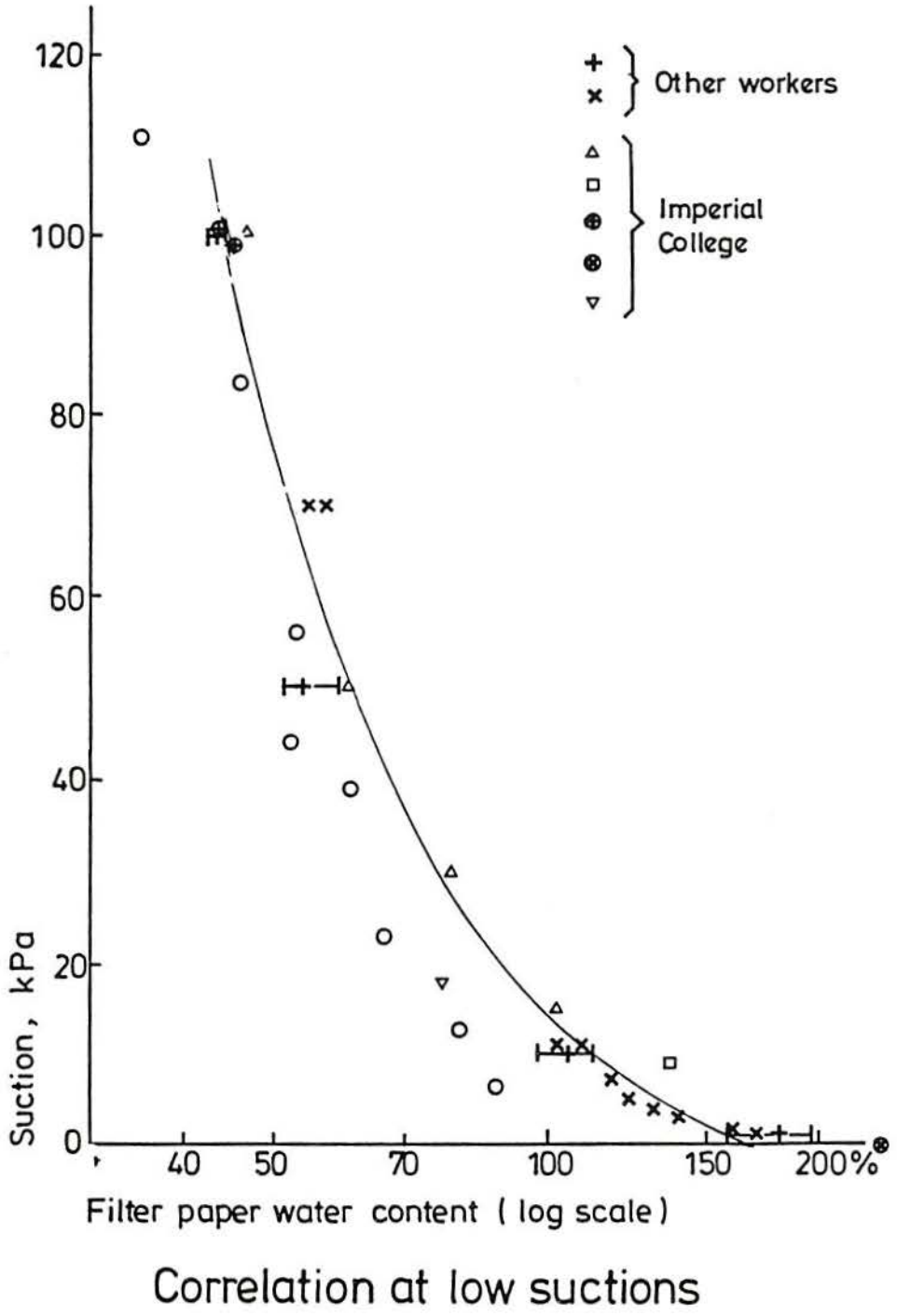

Figure 9.4 – Calibration curve of filter paper for soil suction measurement (after Crilly, 1989)

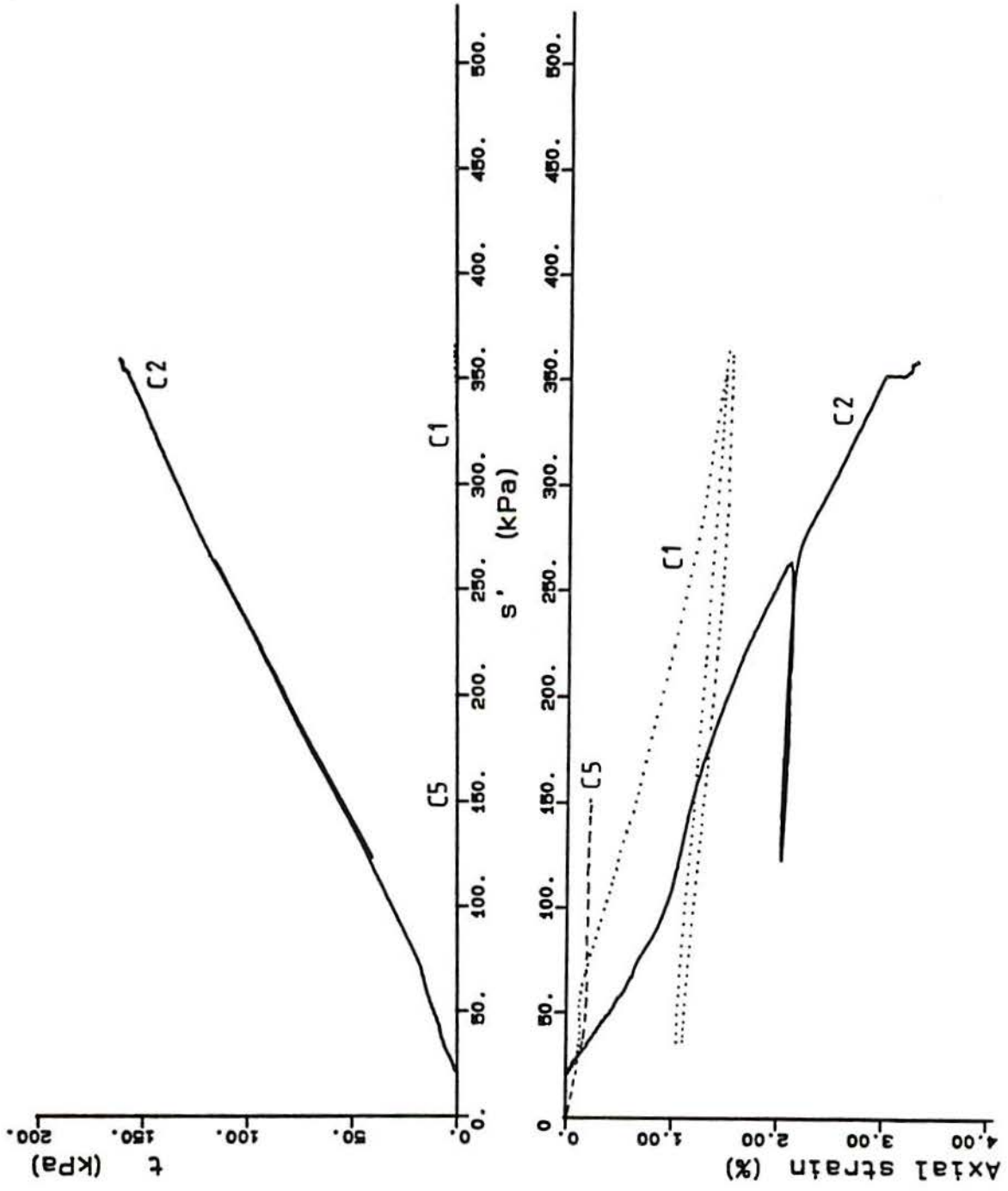

Figure 9.5 – Axial compressibility of Chemususu Dam soil. C1 and C5 are isotropic tests, C2 is an anisotropic test

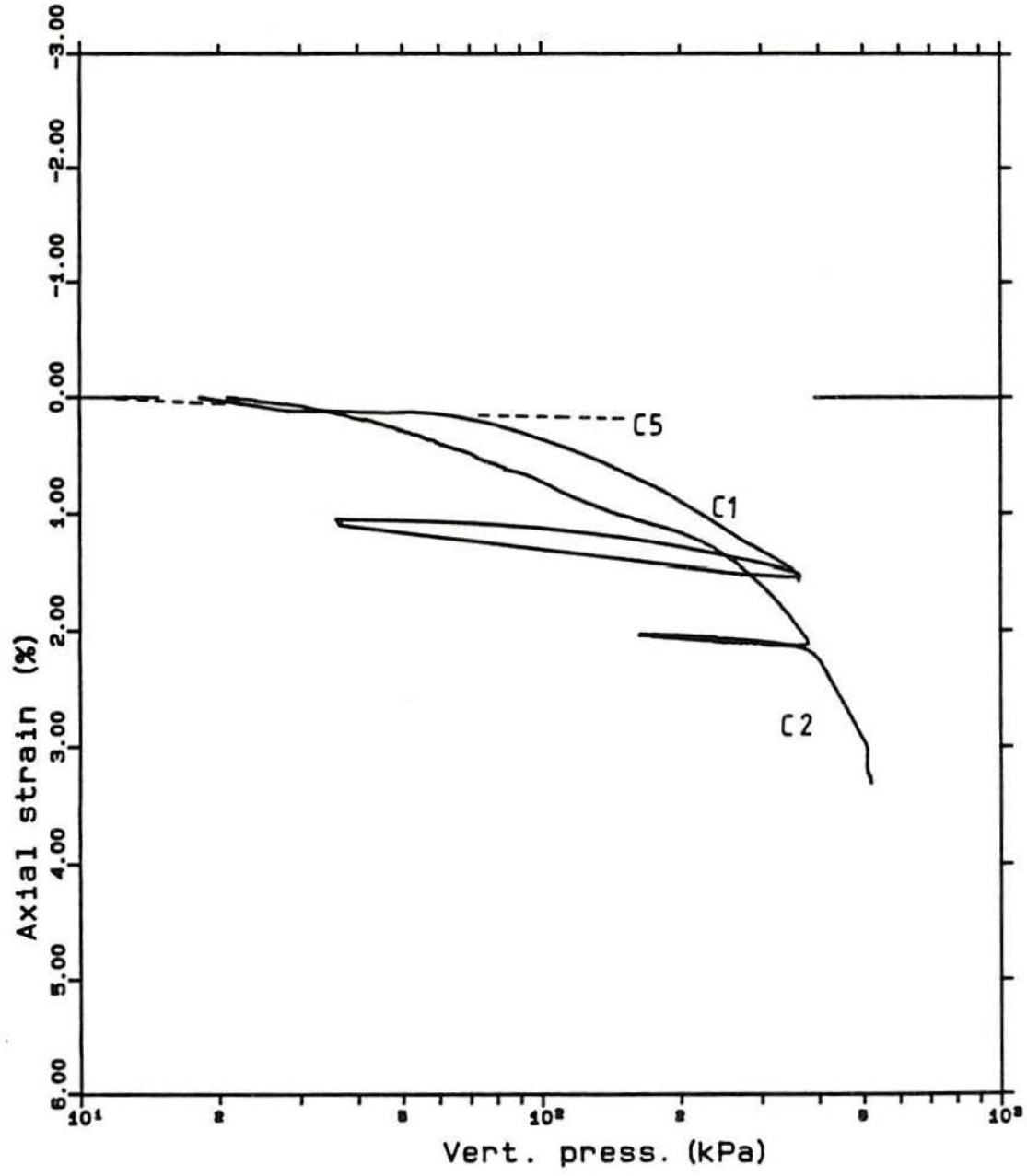

Figure 9.6 – Axial compressibility of Chemususu Dam soil versus vertical stress in logarithmic scale

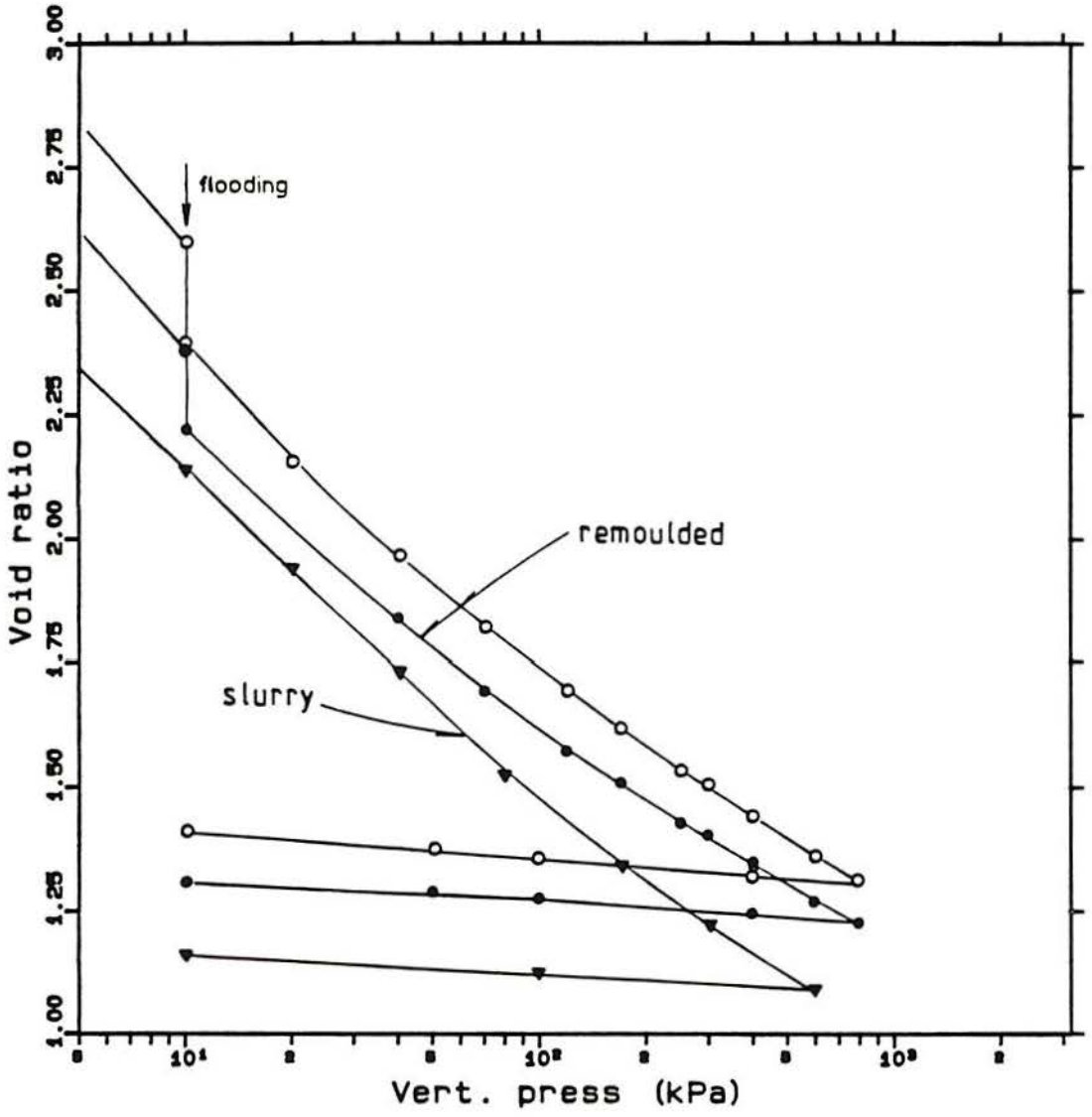

Figure 9.7 – Void ratio versus vertical pressure of disturbed samples of Chemususu Dam soil

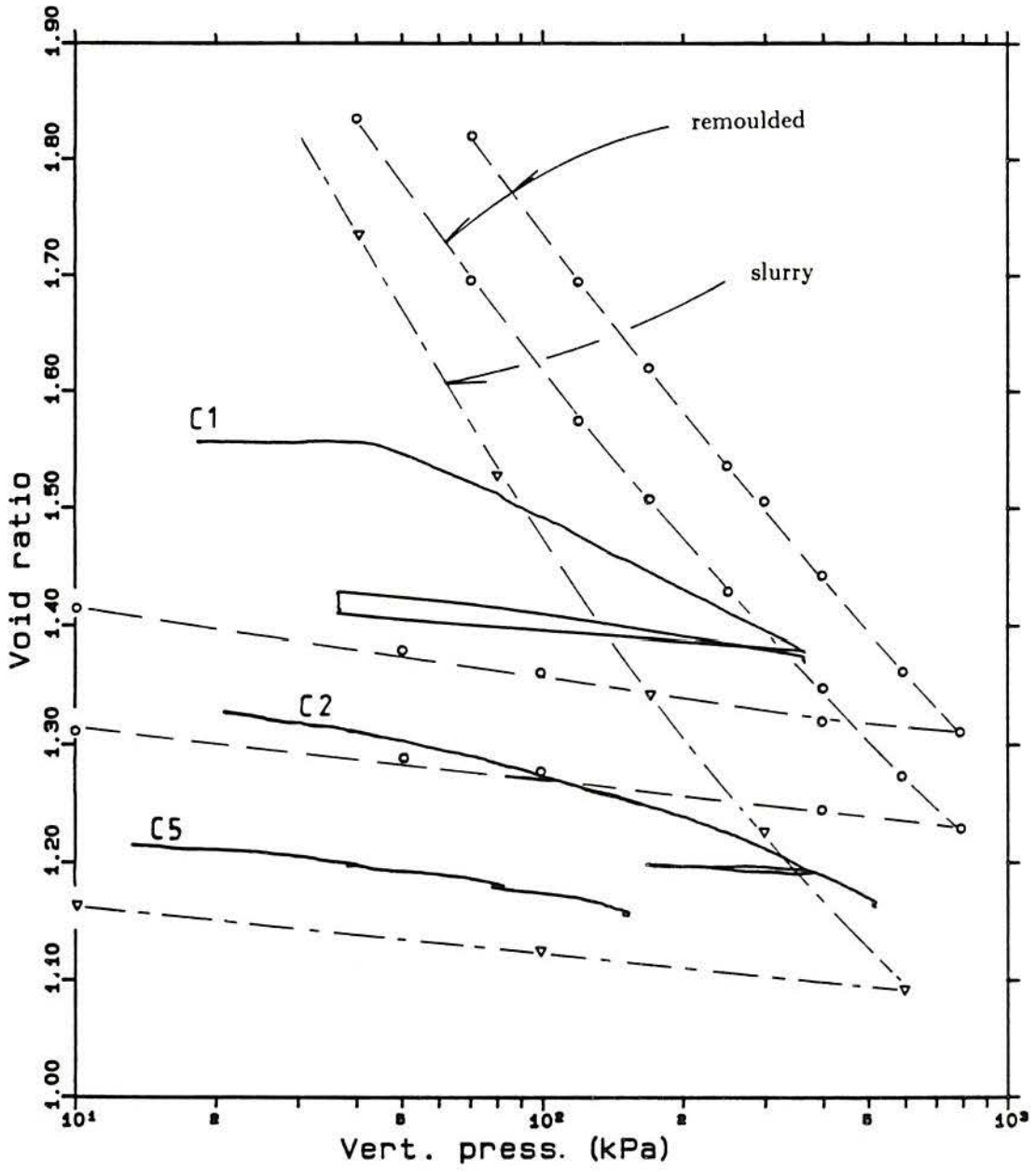

Figure 9.8 – Comparison between the compressibility of oedometer tests on disturbed samples and isotropic compression on undisturbed samples (continuous lines)

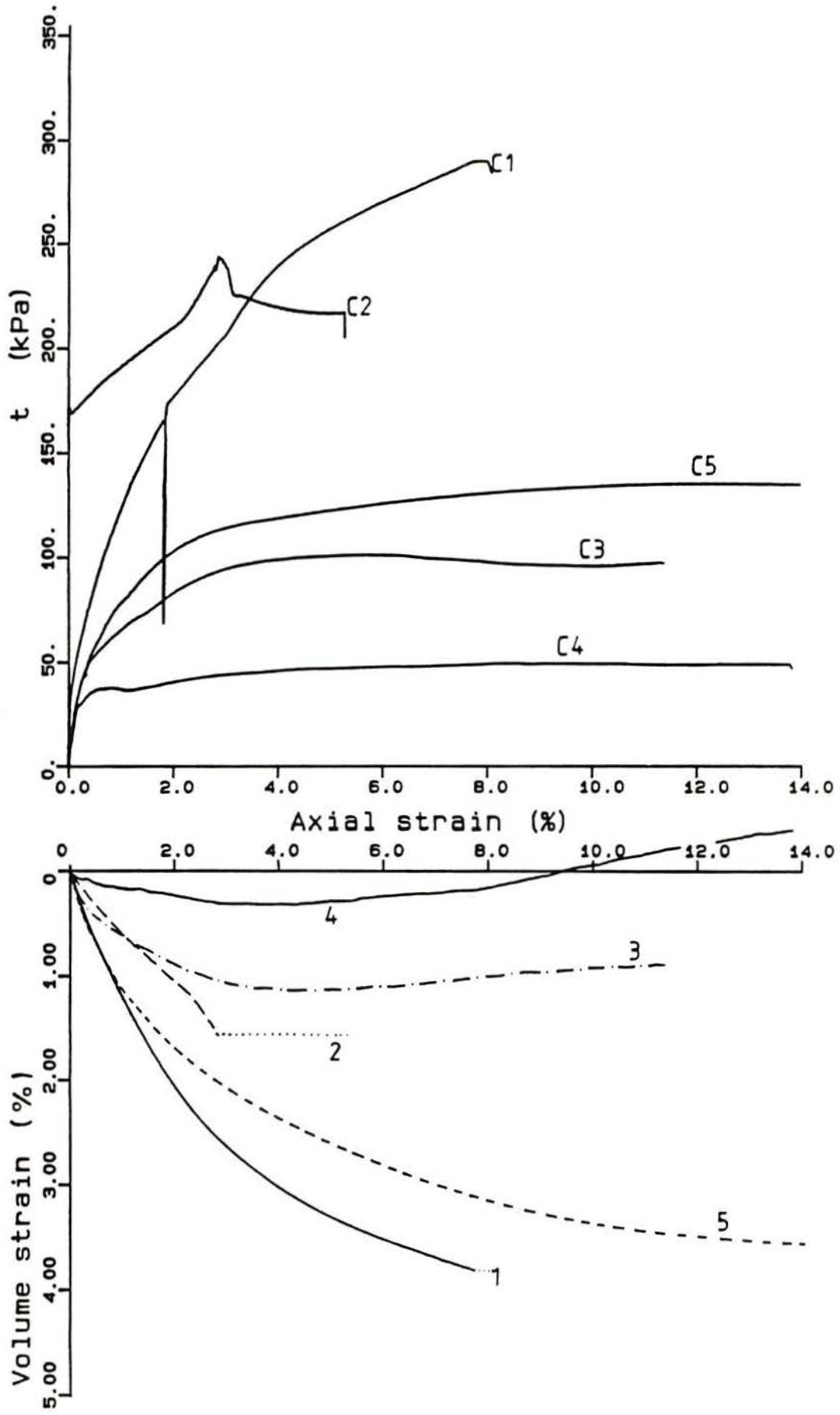

Figure 9.9 – Triaxial test results of Chemususu Dam soil. Stress and strain curves

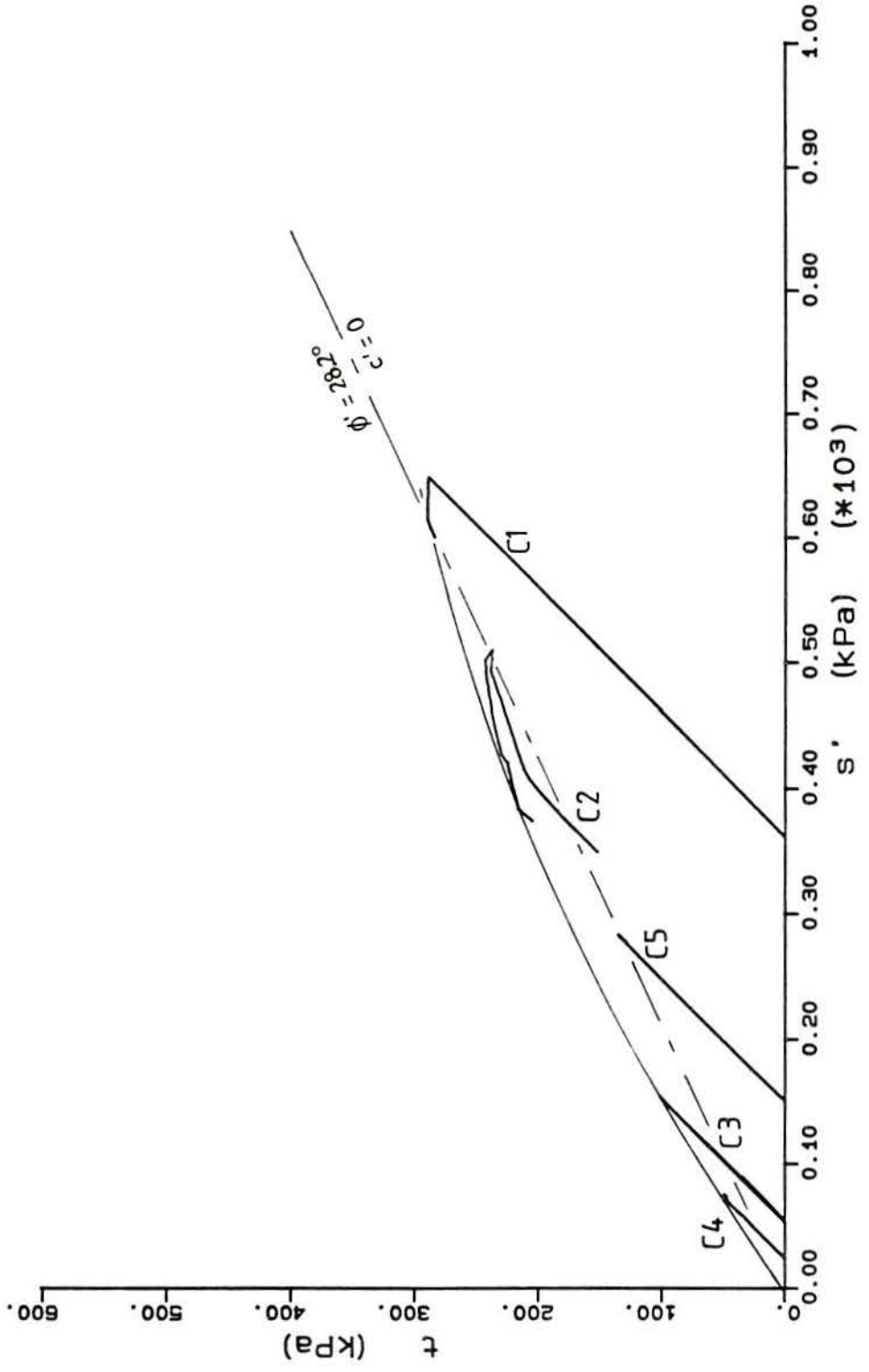

Figure 9.10 – Stress-paths and failure lines for Chemususu Dam soil triaxial tests

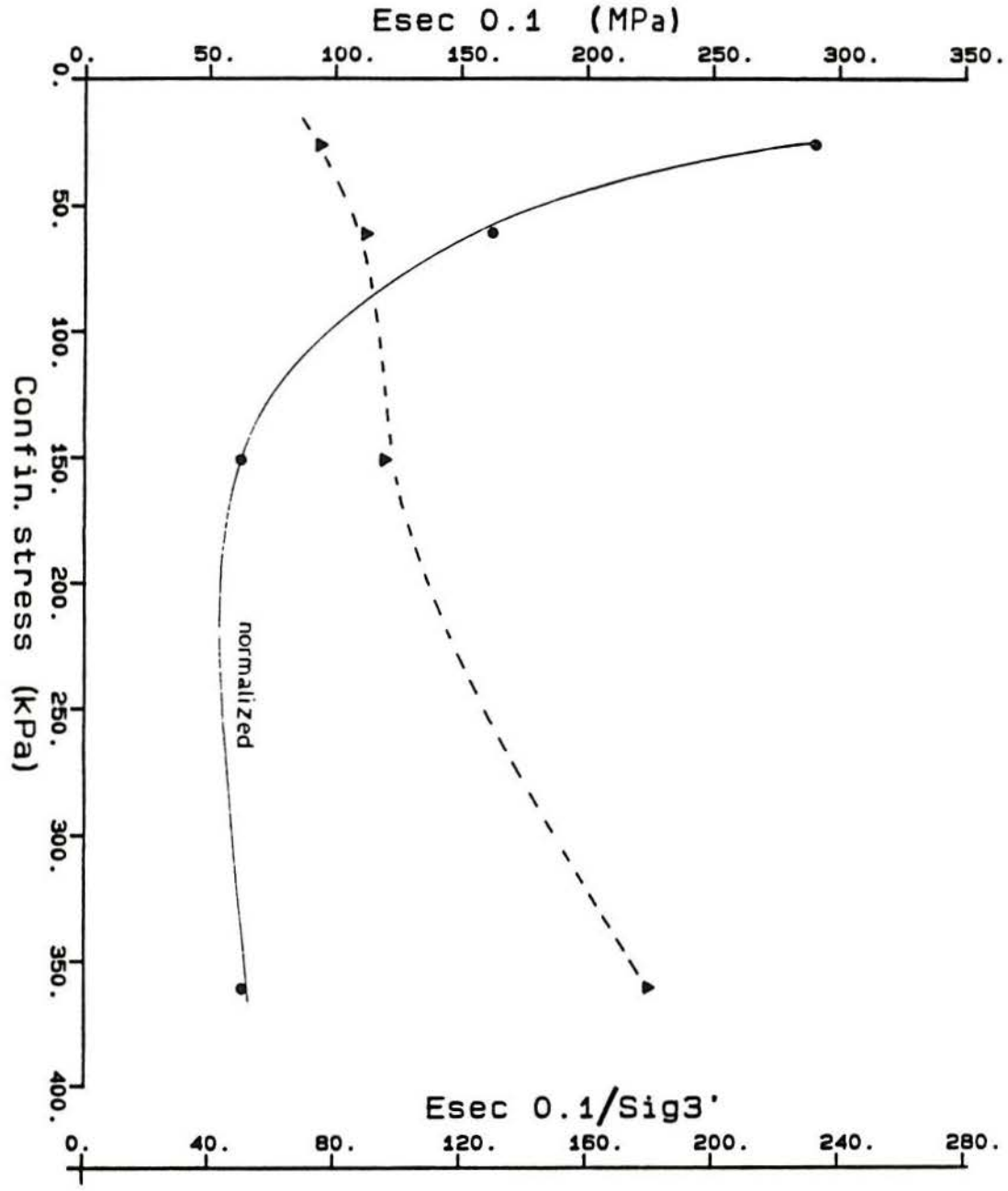

Figure 9.11 - Results of secant stiffness measurements on the Chemususu Dam soil

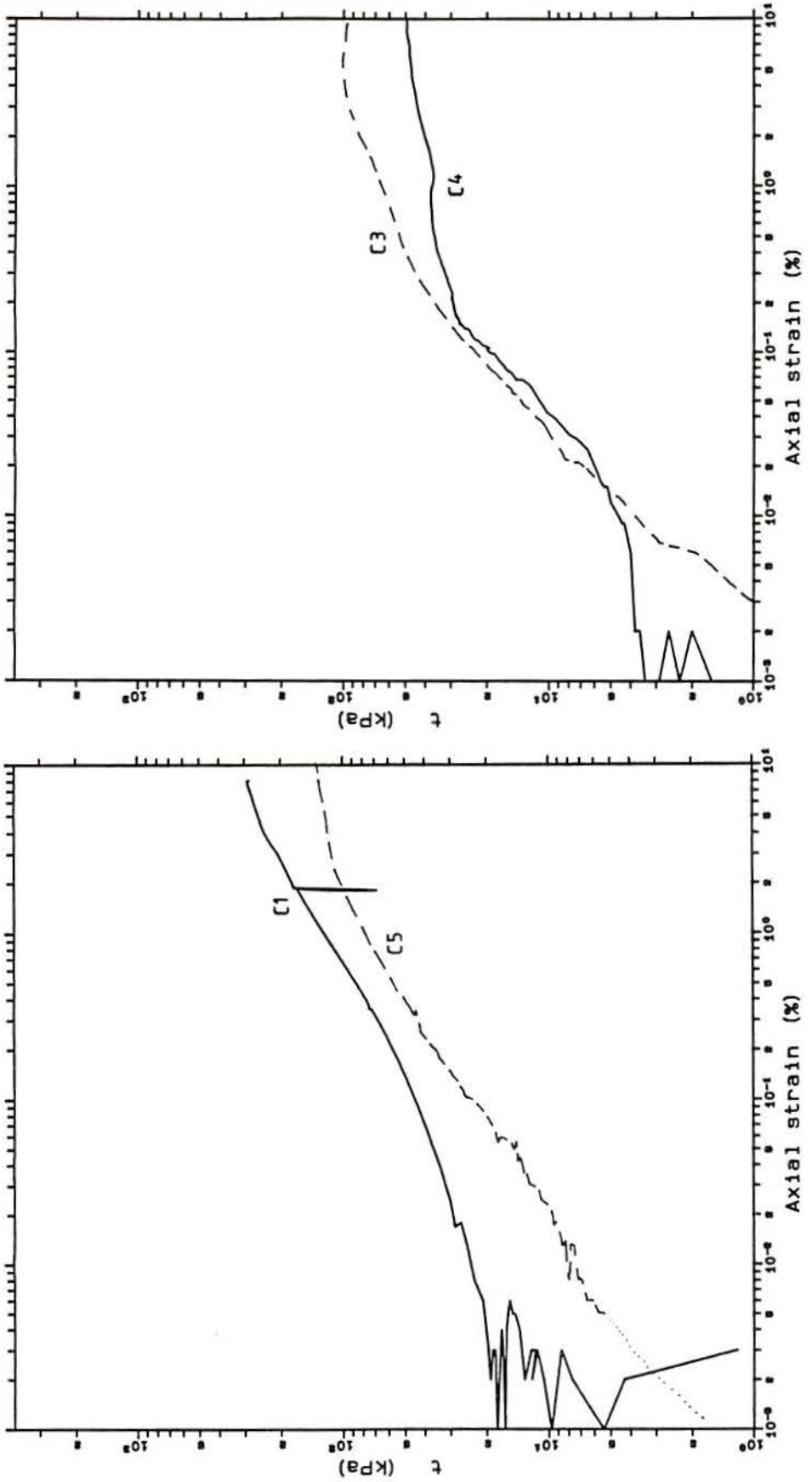

Figure 9.12 – Stress versus strain plots in logarithmic scales of Chemususu Dam soil tests

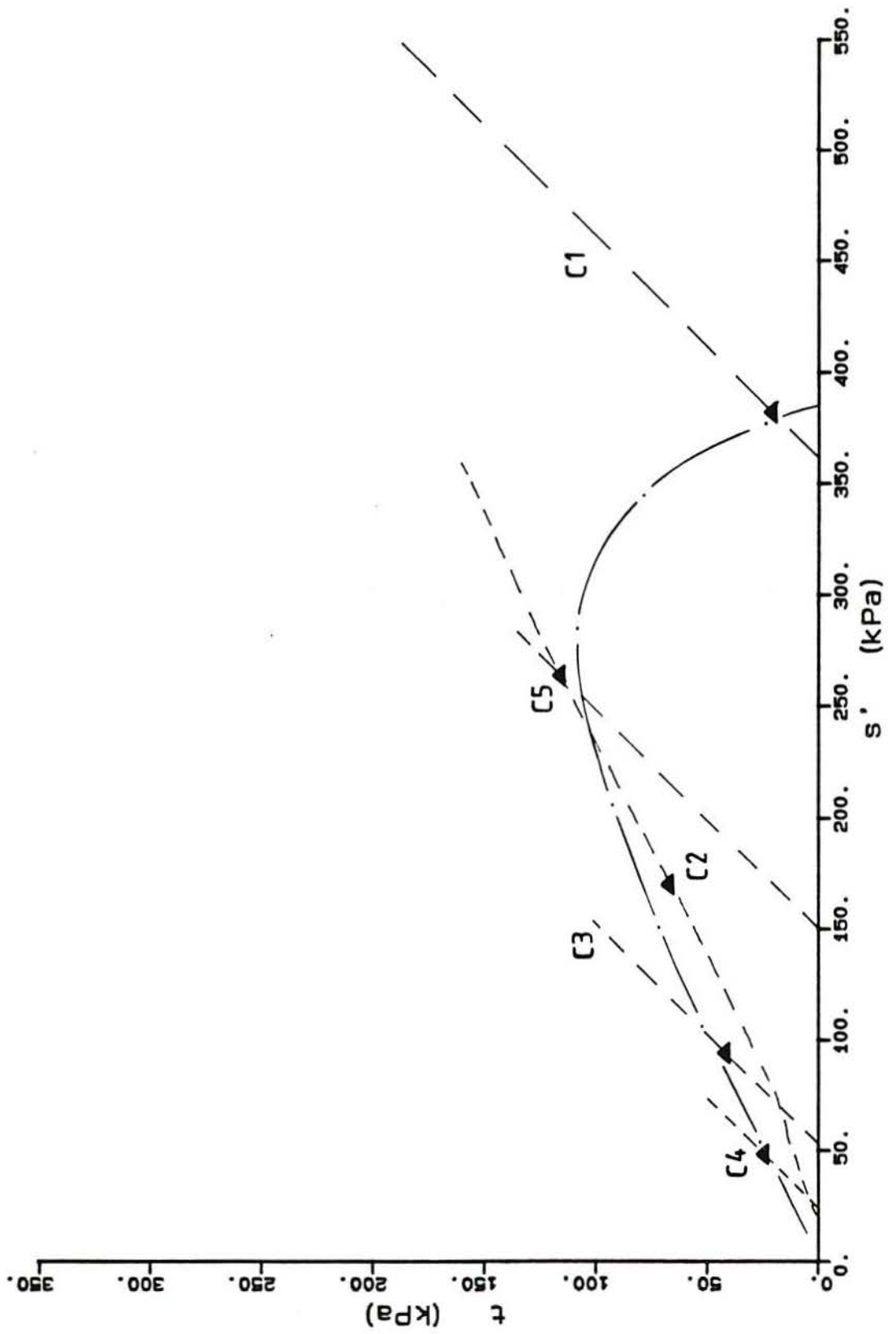

Figure 9.13 – Yield points determined from Fig. 9.12, Fig. 9.5 and 9.6 (test C2)

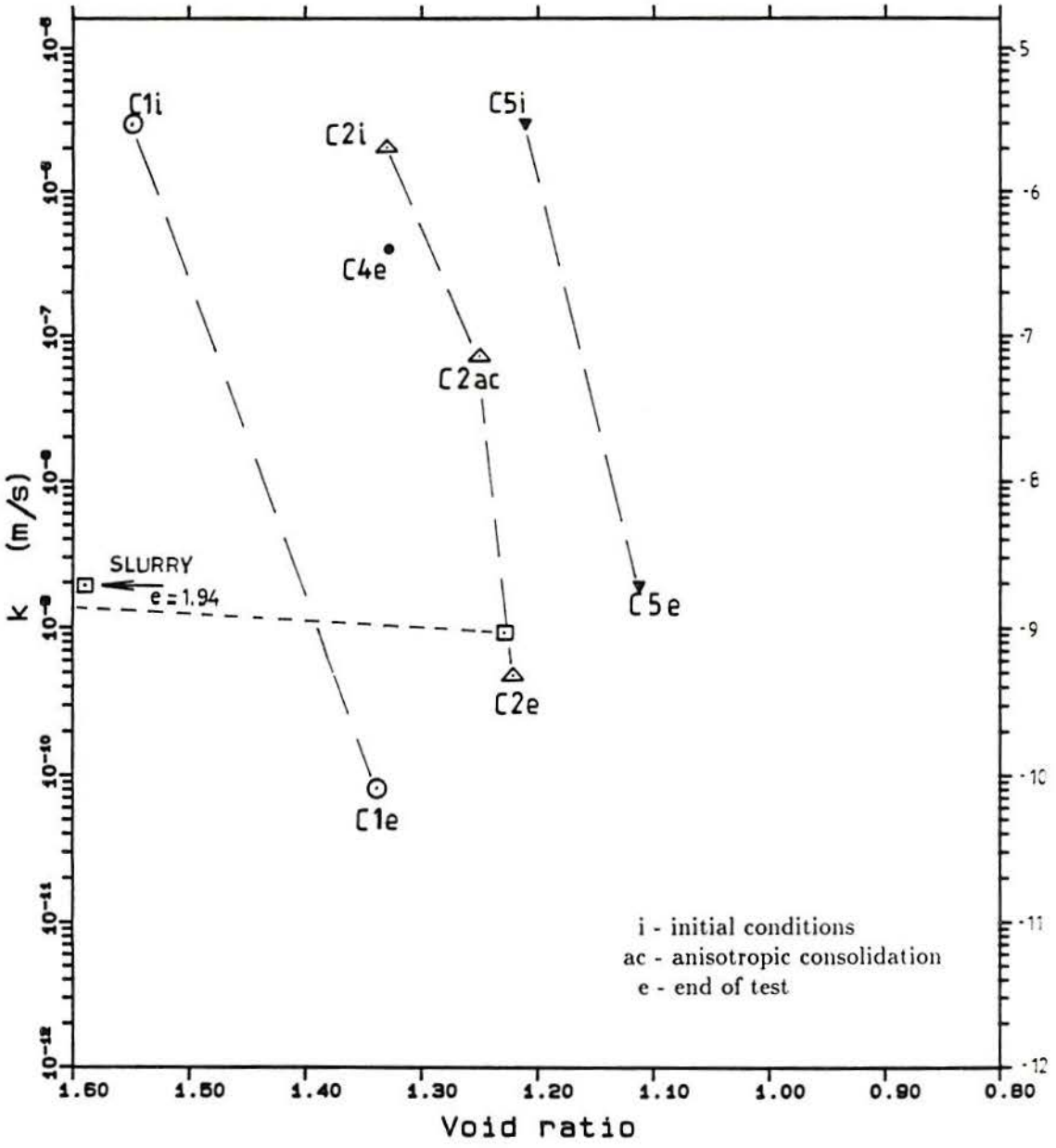

Figure 9.14 – Permeability test results versus void ratio of Chemususu Dam soil samples

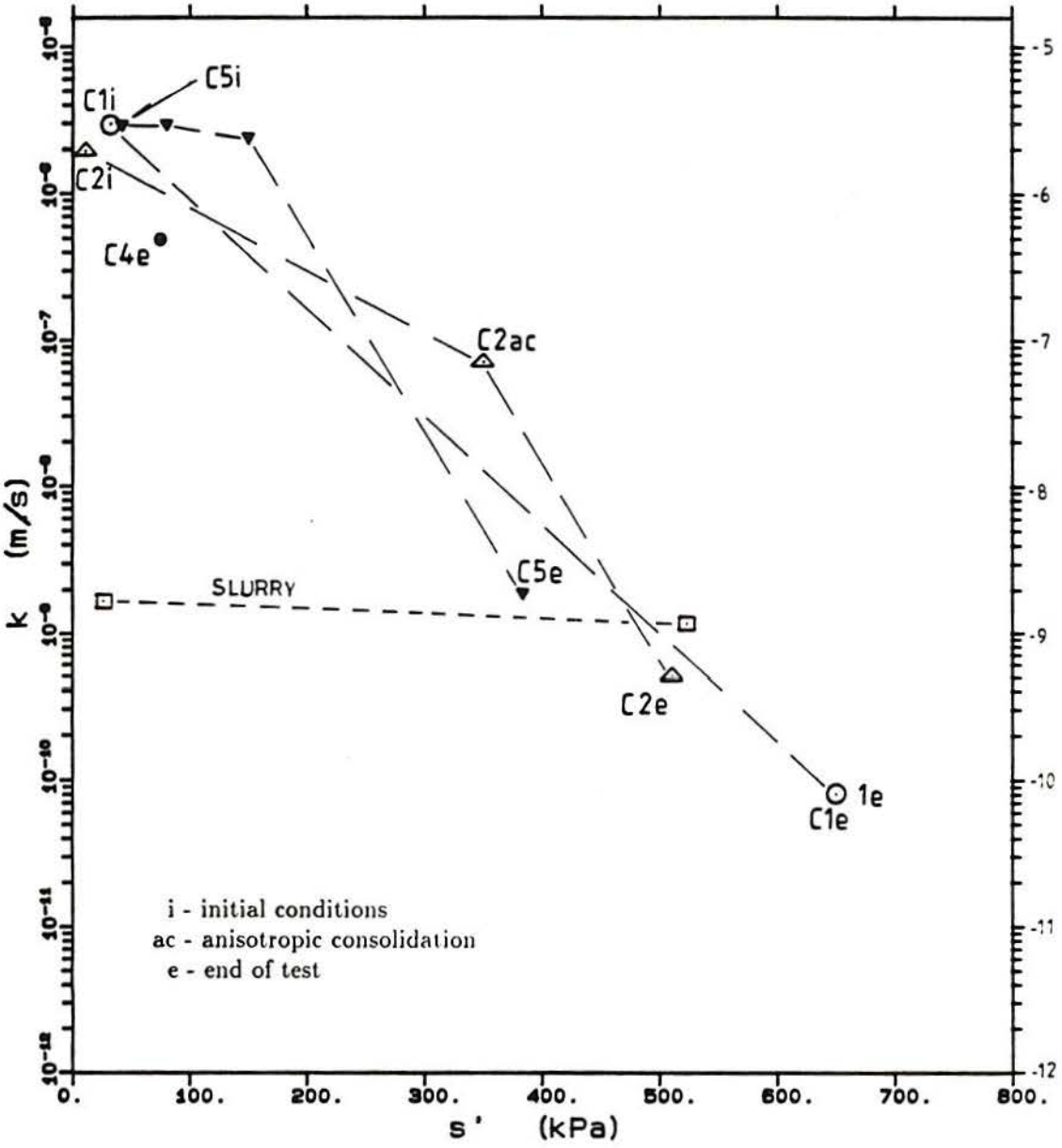

Figure 9.15 – Permeability test results versus s' of Chemususu Dam soil samples (the results for slurry were calculated from oedometer tests)

10. DISCUSSION AND CONCLUSIONS

This chapter compares and discusses the main results of the triaxial tests described in the thesis. Comparisons with results given in the literature are made where possible.

10.1 DISCUSSION

Testing techniques

The discovery of the importance of saturation technique and stress uniformity on the test results (Chapter 4) eliminated two experimental factors which could mask the effects of structure in the artificial soil. The use of back-pressure to obtain full saturation in the testing of natural soils should be reconsidered in the light of the structural damage that it seems to have caused in the artificial soil.

There are also some indications that the back-pressure, even when applied relatively slowly, affects the behaviour of natural residual soils reducing their strength (Dias, 1987; Allam & Sridharan, 1980; test C5, Chapter 9).

The influence of the stress concentration due to the conventional loading arrangement (Chapter 4) and the influence of the saturation technique are present in some of the results given by Maccarini (1987) and this should be taken into consideration when analysing the data.

Artificial soil yield

For the artificial soil with a high void ratio, it was not possible to identify the presence of a first yield, although some of the strain measurements in isotropic compression at stresses below 30-50 kPa were not considered. The major yield was very clear and coincident with the one reported by Maccarini(1987).

For the artificial soil of higher density (e=1.1) there were two different levels of yield in isotropic compression, one at 300 kPa and another at 1500 kPa. The major yield in shearing was clear and the yield curve is well defined for pressures below s'=1400 kPa (Fig. 6.33). However, there is a discontinuity on the stress-strain curves of some tests (Fig. 6.28) which seems to imply that there is another yield surface above s'=1400 kPa (Fig. 6.33). This behaviour is unusual and requires further investigation.

The study of the denser artificial soil concentrated on tests at higher confining pressures, and so the first yield locus was not verified. It is interesting though to compare the results obtained from the two different densities of artificial soil. The two different sets of yield points are plotted together in Fig. 10.1. They represent the main yield points of the high void ratio soil and the first yield points of the lower void ratio soil. Results obtained by Maccarini (1987) are also plotted on the figure. Although there is some scatter in the values, they seem to lie in the same stress region. The reason for this coincidence may not be a simple one, but examination of the results of the 300 series tests (without quartz) provides some useful information. Axial strain from local measurements has been plotted against confining effective stress for the isotropic compression stage of test 305 in Fig. 10.2. There are two linear portions, and their intersection indicates a yield stress of 280 kPa. Note that this sample had a void ratio of 1.4 but a denser grain packing than the others (intergranular void ratio=0.32: Appendix 1, case 2). This yield is likely to have been caused by the start of collapse of the fired kaolin grains (500° C/5 h). A similar collapse of the same material is likely to have occurred at the same stress in the other artificial soils, where the kaolin provides the bonding between the quartz and CFK grains. For the lower void ratio artificial soil this caused a small increase in the volumetric compressibility (Fig. 6.16) but for the higher void ratio artificial soil this caused a significant change in the volumetric compressibility (Fig. 5.7 and 5.9).

The presence of a second yield on the 200 series soil (e=1.1) may be related to the crushing of the stronger CFK grains which were fired at 1000°C for 5 hours. Further tests are required to find out the pressure at which the CFK grains start to crush and whether or not

this pressure coincides with the isotropic yield shown by the artificial soil at 1500 kPa (Fig. 6.19).

Influence of the bonding material strength

The influence of bonding strength on the yield during a drained compression test is clearly demonstrated by the results of tests 208 and 301 (Fig. 7.18). Both tests were carried out under drained conditions, and the yield stress shown by test 208 corresponds very closely to the maximum strength of sample 301, which is composed only of the bonding material of the former.

In the same figure the increase in bonding strength is shown by tests 208 and 601 which had different yield stresses as a result of different bonding strengths.

Results of one-dimensional compression tests

During a one-dimensional compression triaxial test the stresses are increased in such way that the sample does not show any radial deformation. This implies that the individual grains have to accommodate the vertical deformation by sliding or rotating to new positions. Shearing of contacts is involved.

In the artificial soil, the grains are surrounded by the bonding material and so its strength will define the stresses involved. At low stresses the bonding is intact and considerable vertical loads can be sustained with negligible lateral movement. This gives rise to a steep stress path which initially climbs towards the failure line. At this point the bonding cannot sustain the stresses and large increases in lateral stress are needed in order to prevent lateral strain. For high void ratio materials large axial deformations are likely to occur. Examples are given in Fig. 2.8, 2.9, 8.35 and 8.36.

Due to this behaviour, the test stress-path turns to the right on a t-s' stress space plot. It is likely that the strength of the contacts remains the factor controlling the soil behaviour. Examination of Fig. 10.3 seems to confirm such a hypothesis. The stress path of the one-

dimensional test 212 climbed rapidly in stress space until it reached the failure line defined for the de-structured bonding (Fig. 7.13). It showed some instability close to that point and, thereafter, the coincidence between the stress path and the failure line was striking.

In natural samples the internal structure may not be as simple as the one shown to exist in the artificial soil, and shearing of the grains may also be involved. This would lead to a stress path which is not purely a function of the bonding material strength but will also be influenced by the other grains.

Variation of void ratio during testing

The determination of the void ratio-pressure relationship can provide useful information and has been suggested as a means of classifying residual soils (Vaughan, 1988) in relation to their potential compressibility. Tests carried out at high pressures provided further information on this relationship. The results obtained from the high void ratio artificial soil (100 series) are plotted in Fig. 10.4. The results from two remoulded samples are also shown for comparison. All samples were isotropically consolidated and then sheared under drained conditions. The crosses mark the beginning of shearing. The shear stage caused large variations in the void ratio of the bonded samples which did not show any tendency to stabilize, even after considerable straining (Fig. 5.24 and 5.25).

The results from the denser artificial soil (200 series) are shown in Fig. 10.5(a) and (b). The first plot gives the results of the isotropic compression tests together with results from the two remoulded samples; the second shows the void ratio variation during shearing of the 200 series and remoulded samples. It can be seen that the variation in the void ratio is quite large during the shearing stages of the tests. In addition, the bonded samples can sustain much higher stresses during isotropic compression than the remoulded ones at similar void ratios [Fig. 10.5(a)].

The results from the two artificial soil test series during shear are plotted together in Fig. 10.6. They show a similar trend of void ratio variation with the mean effective pressure

p'. A summary of these data is shown to a larger scale in Fig. 10.7 (the dotted lines indicating the shear stages of the tests). Test 212 (K_0) shows a more compressible behaviour than the isotropically consolidated tests but far less than any of the conventional drained compression tests. The variation of the void ratio seem to be very dependent on the shear stress applied to the samples.

The variation of void ratio of the Corinth Marl was also examined. The data obtained from the two one-dimensional compression tests ($I14K_0$ and $I15K_0$) is shown in Fig. 10.8.

The results of two oedometer tests on slurry (Kavvadas, 1990 - see also Fig. 8.4) and another on the intact material (Anagnostopoulos, 1989) are also plotted. The curves are not directly comparable as the oedometer tests were plotted in terms of vertical stress. However, it is clear that the slurry has a much higher compressibility than the other samples.

These results are interesting when compared with the variation of void ratio during the shear stages of the tests (Fig. 10.9). During shear the variation in the void ratios is large, but seem to lie inside the limits defined roughly by the oedometer tests on the intact material and on the slurry. It seems that the potential variation in void ratio is at least equal to the difference in void ratio between the slurry and the intact sample at a similar stress level. As with the artificial soil, isotropic compression seems to reduce the void ratio much less than the shearing does. The samples can sustain quite high void ratios at considerable pressures during isotropic or one-dimensional compression.

Stiffness variation with pressure in bonded materials

The results obtained in this thesis show a consistent pattern of variation of secant stiffness with confining effective stress. It seems that there is a threshold of confining pressure above which the stiffness drops or, at least, stabilizes. This was shown by the artificial soil mixtures (Fig. 7.21), the Corinth Marl (Fig. 8.34) and the Chemususu Dam soil (Fig. 9.11). It appears to be a common feature in other bonded materials as well, although not specifically noted in the literature. A typical example is shown in Fig. 2.2 for a mudstone, where the

stress-strain curves at higher confining pressures are clearly much less stiff than the ones obtained at lower pressures. The same pattern can also be seen in the results given by Sandroni (1981) for a residual soil from gneiss, by Elliot and Brown (1985) for a porous rock, by Dias (1988) for a lateritic soil and by Conlon (1966) for a soft clay.

Poisson's ratio

The results obtained from the artificial soil show that the samples have very low values of Poisson's ratio when initially loaded. A good example is given by the results of test 208 (Fig. 6.30). Direct measurements of radial strain show no radial deformation (ν=0) up to an axial strain of approximately 1.0% and a deviator stress level close to 80% of the yield stress. Small values of Poisson's ratio (zero or even negative) have been reported for an Australian calcarenite by Semple (1988) from a large testing programme carried out to study the unusual behaviour of that material.

Small values of Poisson's ratio can also be derived[1] from the steep stress-path shown during one-dimensional tests carried out on chalk by Ledra(1990) [Fig. 2.9(a)], on sandstone by Goldsmith(1989) (Fig. 2.11), on the artificial soil by Maccarini (1987) (Fig. 6.39), and on Corinth Marl, test I14K_0 (Fig. 8.35).

This steep stress-path is characteristic of the behaviour of one-dimensional tests on bonded materials (Fig. 2.8 and Leroueil & Vaughan, 1990), indicating that an initial low Poisson's ratio is also a general characteristic of these materials.

10.2 CONCLUSIONS

The stiffness of clay samples in triaxial tests can be effectively measured down to 0.01% axial strain with minor modifications to conventional testing equipment measuring platten to

[1] $\nu = K_0/(1+K_0)$

platten.

Errors generally referred to as due to bedding were shown mainly to comprise avoidable errors, especially the error due to non-parallelism of top cap and load cell, and the deformation of filter paper discs if these are used.

The influence of the last two testing techniques on the behaviour of artificial soil samples was shown to be important. The concentration of stress due to non-parallel loading surfaces during a compression test can cause an overall early yield (or failure at low confining stresses). The cyclic application of effective stress appears to be a major factor in causing a similar effect. This is likely to occur when saturation by back-pressure is used. There is evidence in the literature that this happens during the testing of natural soils.

The yield stress of the artificial soil is dependent on the size of the fired sample. There are indications that longer heating and cooling periods can reduce this effect.

The method of stress increase during an isotropic compression test (constant rate of stress increase or incremental) is not an important factor in defining the isotropic yield of the high void ratio artificial soil. However, fast application of isotropic stress (7.5 kPa/min) caused a 30% increase in this stress over that obtained at 1.5 kPa/min (Fig. 5.13).

There is a large reduction in bulk stiffness (of approximately ten times) after the isotropic yield with the high void ratio soil. The 200 series of tests (e=1.1) has a much less marked decrease.

The yield locus for both artificial soils is centered around the isotropic line. However, the Corinth Marl yield locus shows some effect of anisotropy.

The stress path has considerable influence on the yield locus (and failure envelope) at low stresses for the high void ratio artificial soil. This influence was also found for the Corinth Marl (Fig. 8.24). Evidence of the same phenomenom for a residual soil from Hong Kong is also given by Bressani & Vaughan (1989).

The use of log-log plots of deviator stress versus axial strain to examine the existence of yield has been used successfully. These yield points were also shown to coincide in most cases

with the onset of radial dilation of the sample.

The secant stiffness determined at 0.1% axial strain was shown to vary in a characteristic way for the bonded samples tested. There is usually a large increase in the stiffness with the confining pressure. However, this increase ceases at a certain confining pressure, dependent on the material. In some cases this is followed by a drop in stiffness but, at larger pressures, the stiffness tends to increase again (Fig. 7.21).

The permeability measurements on the artificial soil indicated a small reduction with the strains imposed during the tests. However, for the Chemususu Dam soil there was a very considerable reduction due to the application of shear stress [a drop of approximately 10^4 (Fig. 9.15)].

The influence of over-consolidation on the behaviour of the artificial soil samples is very clear both in drained and undrained tests. The overconsolidated samples show a higher value of yield stress in drained tests (Fig. 6.33) and there is a clear difference in the stress paths of undrained tests due to previously applied stresses (Fig. 6.51).

For the 200-300 series tests the yield stress and failure envelope at low confining pressures are functions of bonding strength alone since they are coincident. At higher stresses they differ considerably especially in strength which is then controlled by their mineralogy.

The microphotographs of the artificial samples sheared at σ'_3=100 kPa showed very little visible structural damage (Fig. 7.28). However, there was widespread crushing of the CFK grains in the sample consolidated to 3250 kPa (Fig. 7.29).

The apparent tensile strength of the Corinth Marl increased by a factor of six due to negative pore pressure (suction) relative to the drained tensile strength (approximately 14 kPa).

The stress path of the one-dimensional compression test on artificial soil appears to be very influenced by the strength of the bonding material (Fig. 10.3).

10.3 SUGGESTIONS FOR FURTHER RESEARCH

There are a number of points which deserve closer examination and many questions either raised by this work or not completely answered by it.

The artificial soil has proven to be a very versatile material. However, its use for model studies would necessitate larger size samples, requiring careful control of firing and cooling, as these affect its mechanical properties.

The results given here were all obtained for positive values of t ($=\sigma'_V-\sigma'_H$). It was assumed that the yield locus was symetric in relation to the isotropic axis but this hypothesis needs to be verified by, for instance, extension tests.

Additional tests on the 300 series would be desirable to better define its strength envelope over a larger stress range.

The microphotographs were a useful tool in examining the artificial soil structure before and after shearing. It would be of interest to verify if the isotropic yield of the 200 series, at around 1500 kPa, coincides with the onset of CFK crushing.

The few results obtained on the residual soil from Kenya (Chemususu Dam) provided an indication of its similarities with the other bonded materials. However, more tests should be performed to examine its behaviour. The trimming of triaxial samples to final dimensions should be carried out on site.

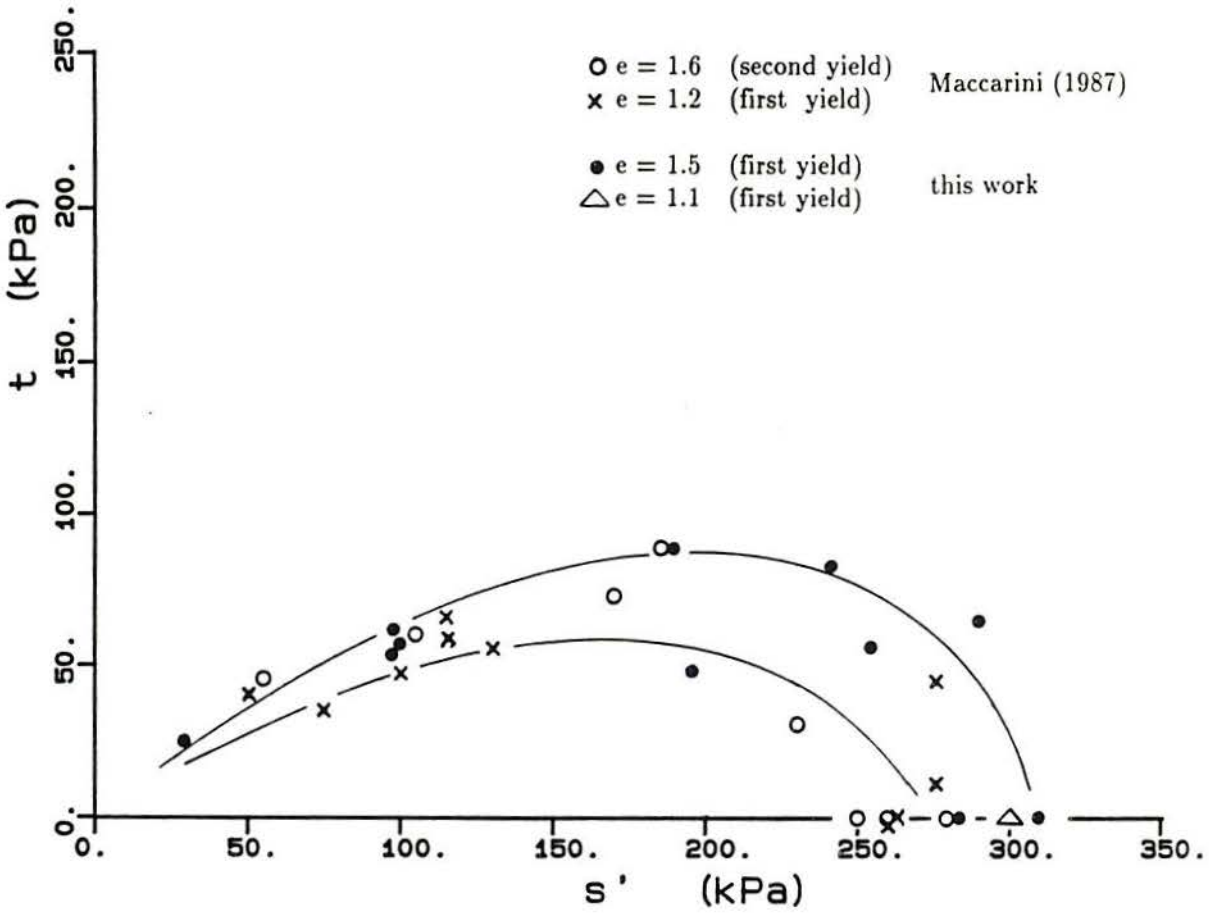

Figure 10.1 – Comparison of yield points obtained from two densities of the artificial soil

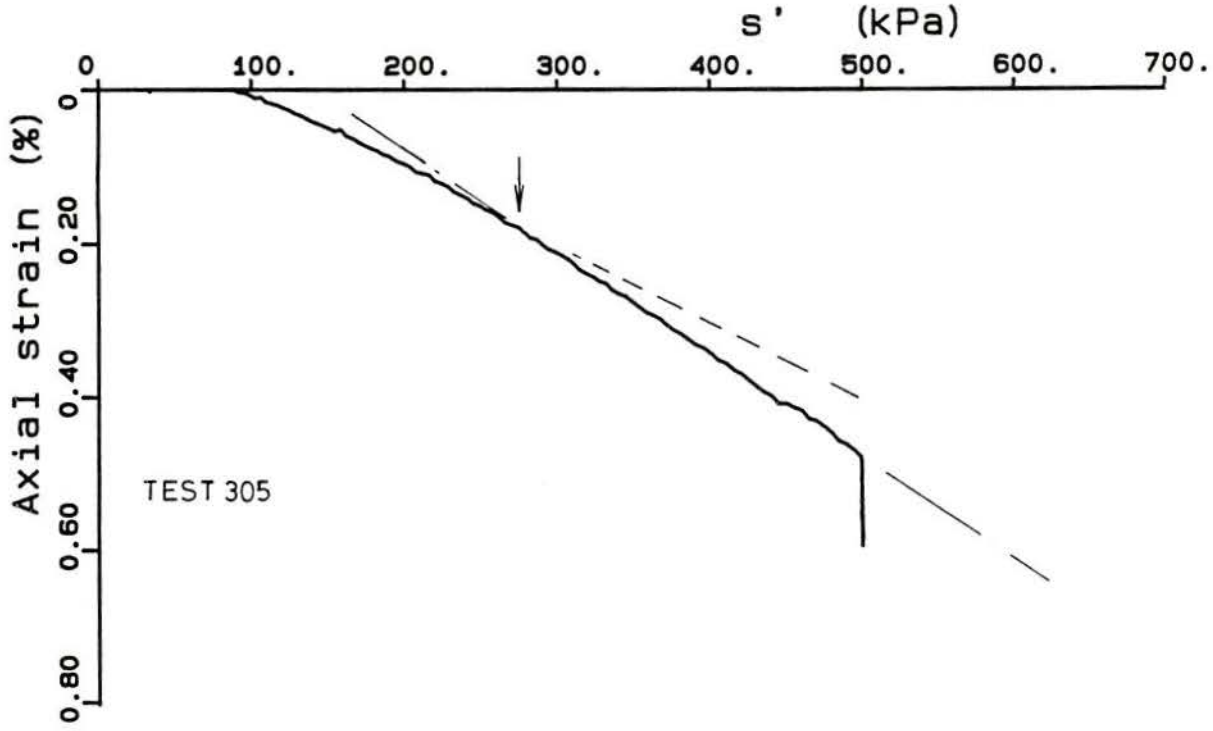

Figure 10.2 – Isotropic compression test on 300 series and associated yield

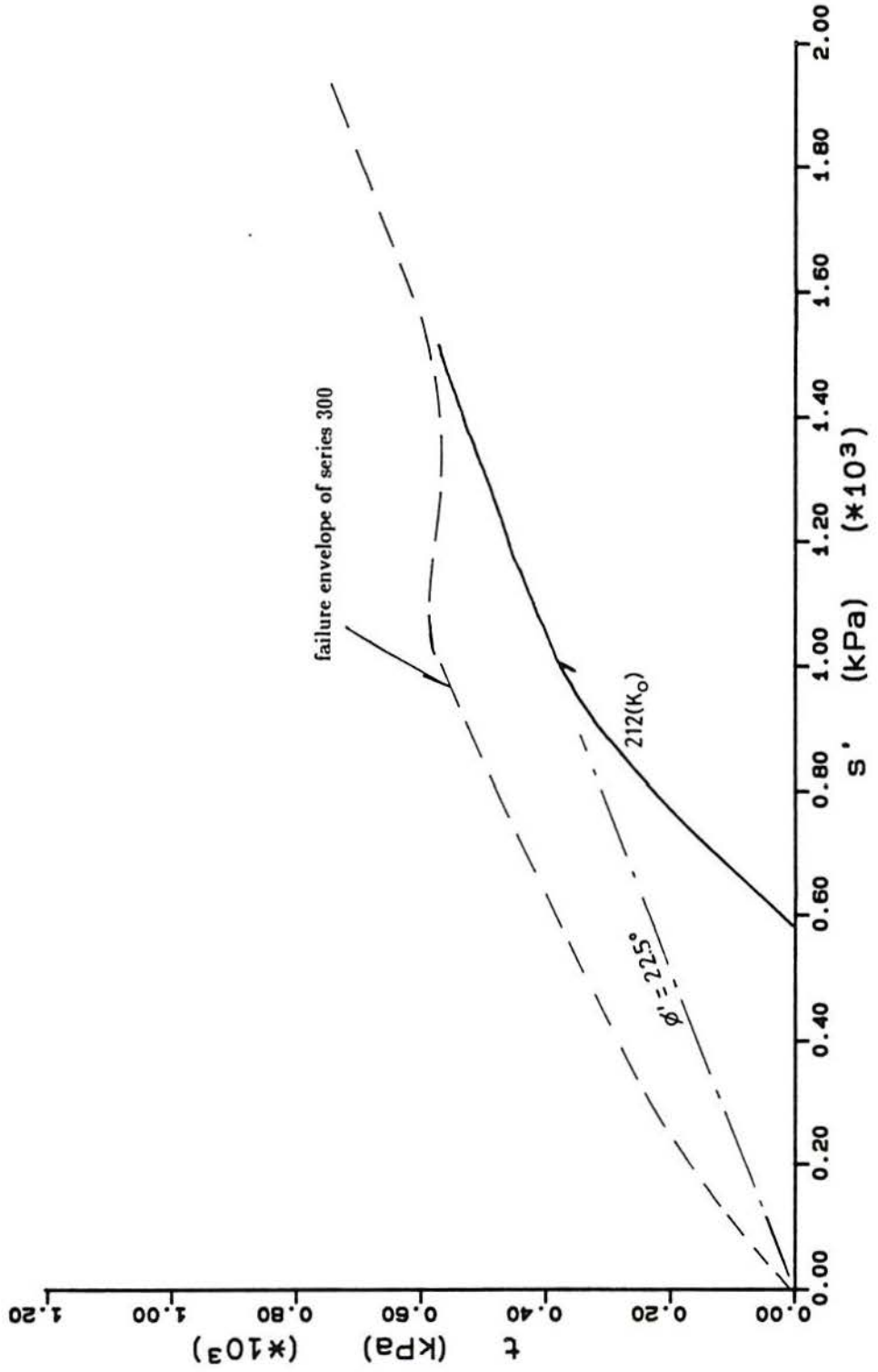

Figure 10.3 – Comparison of failure envelope of 300 series (kaolin only, fired at 500°C) and one-dimensional stress path of 200 series (quartz sand, CFK and bonding kaolin)

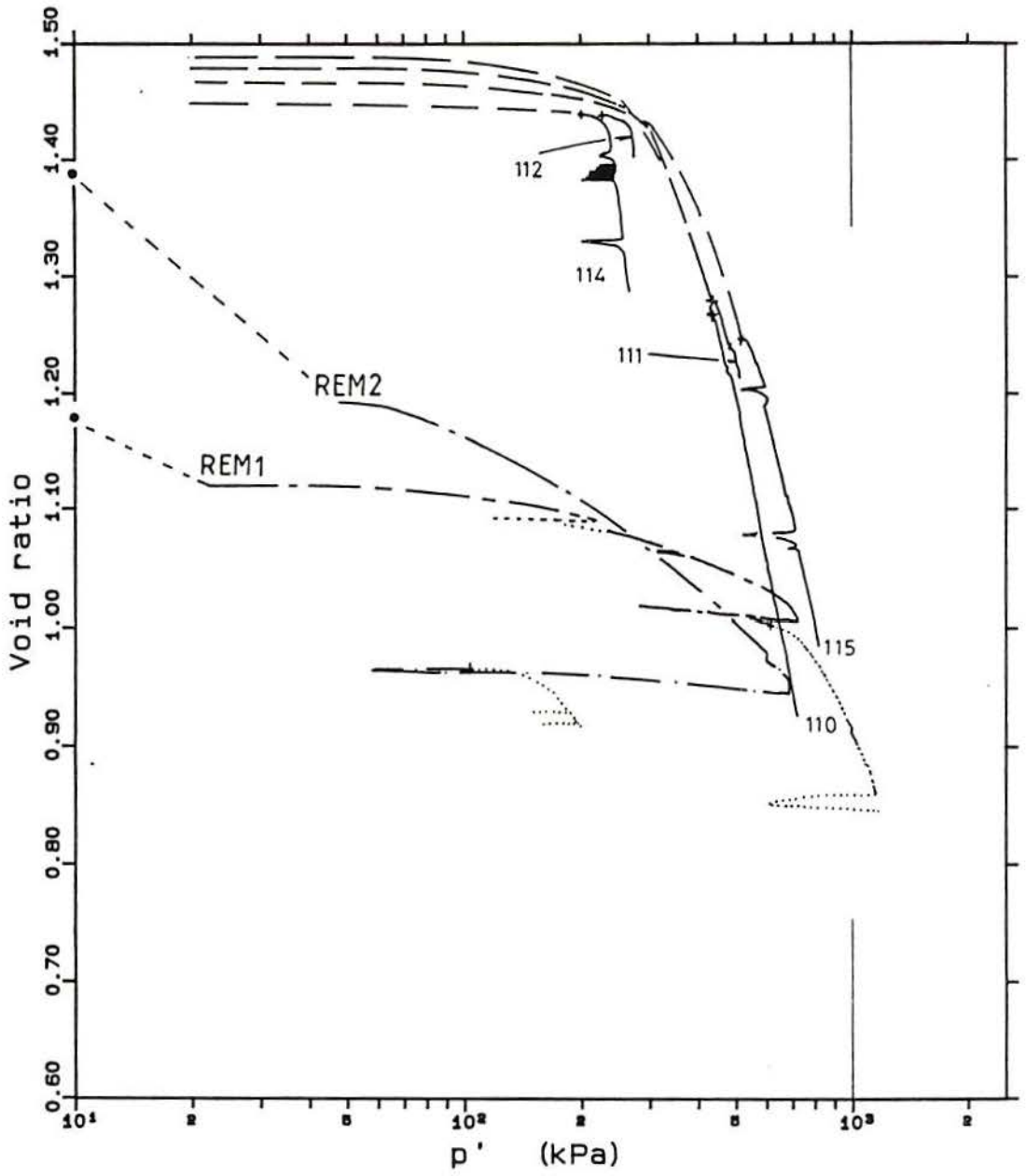

Figure 10.4 – Variation of void ratio with p′ for the 100 series artificial soil and remoulded samples. Isotropic compression and shear stages

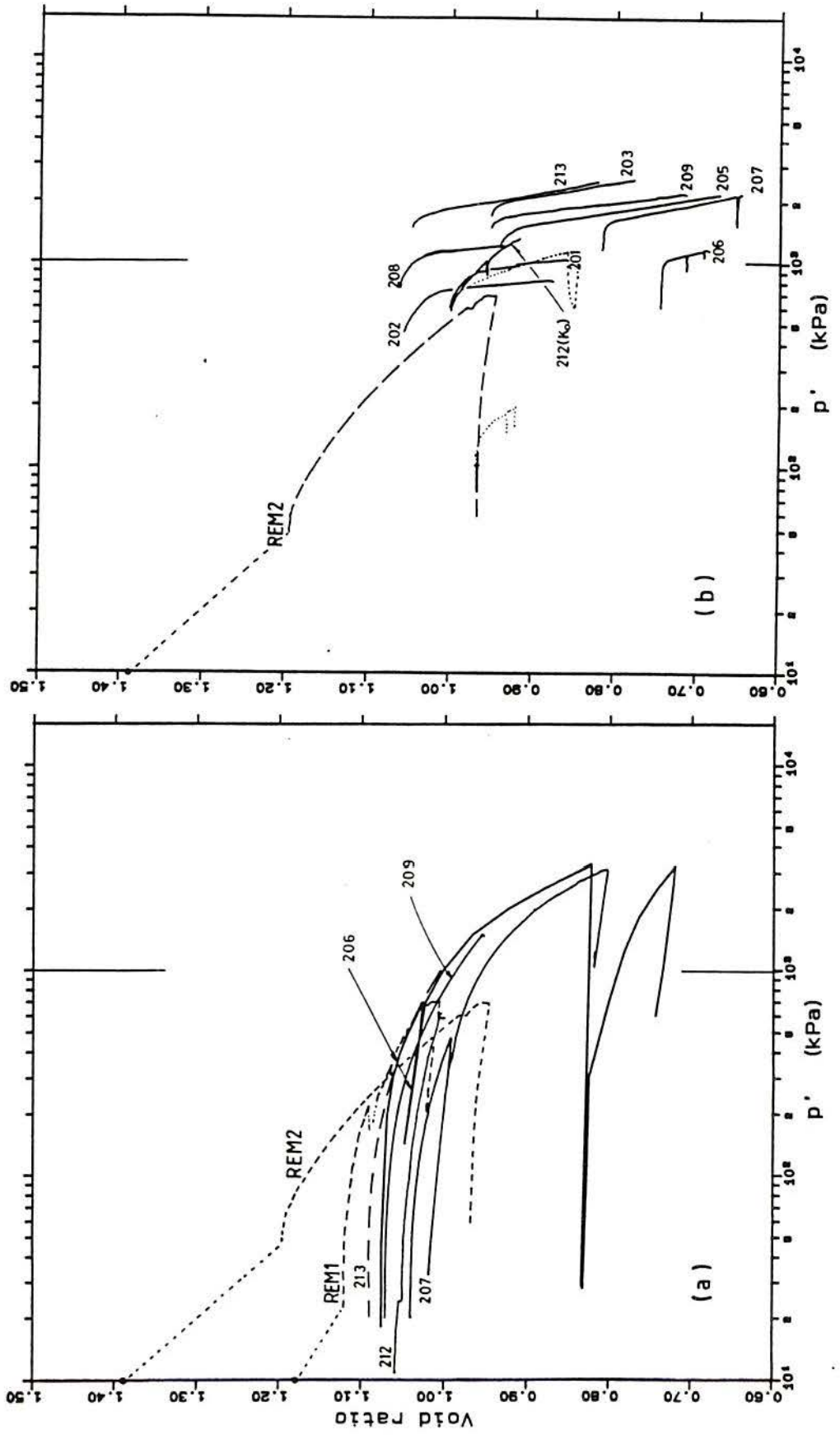

Figure 10.5 – Variation of void ratio with p′ for the 200 series artificial soil and remoulded samples. (*a*) isotropic compression; (*b*) shear stages of 200 series

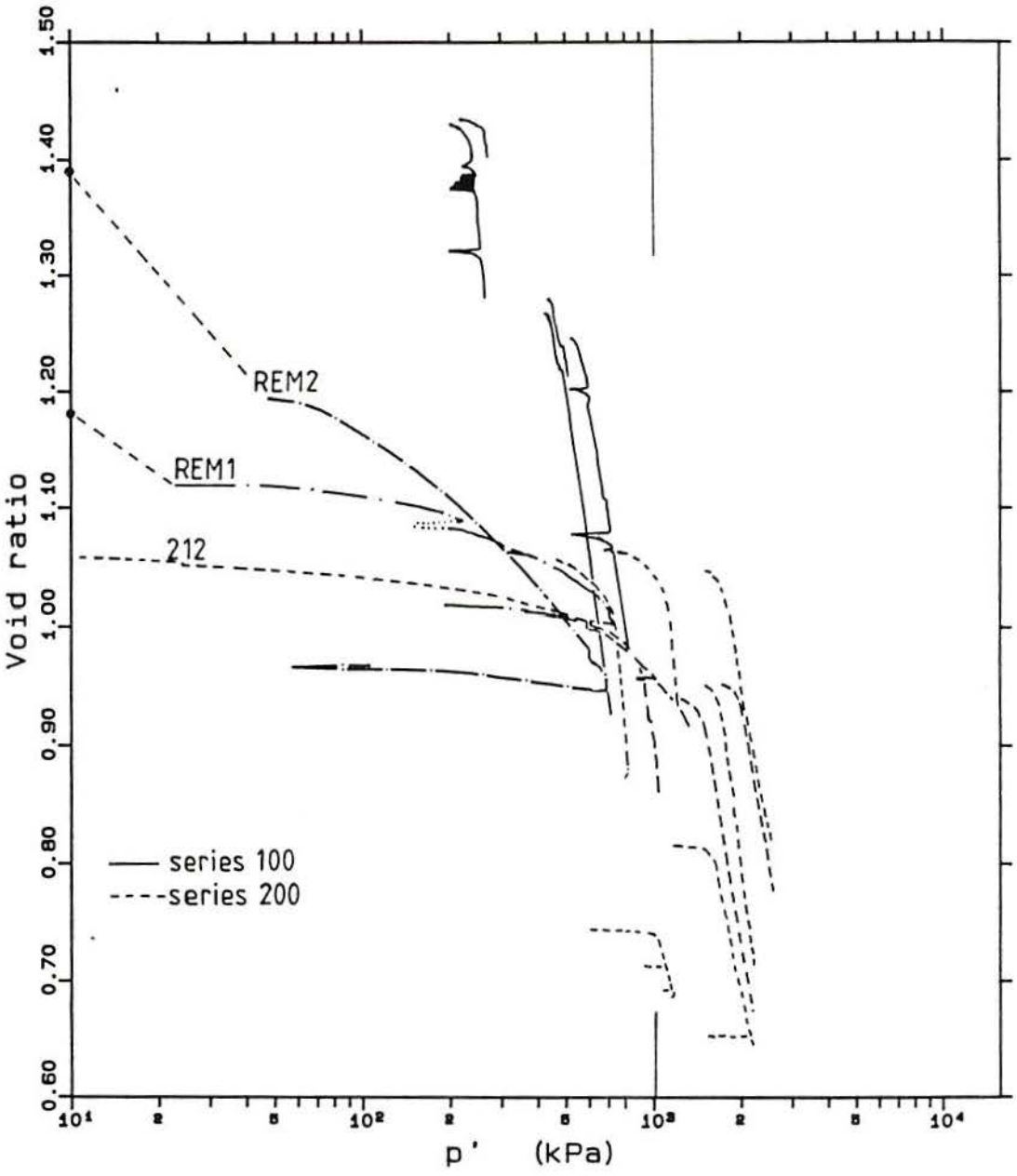

Figure 10.6 – Variation of void ratio with p' for artificial soil of two initial densities

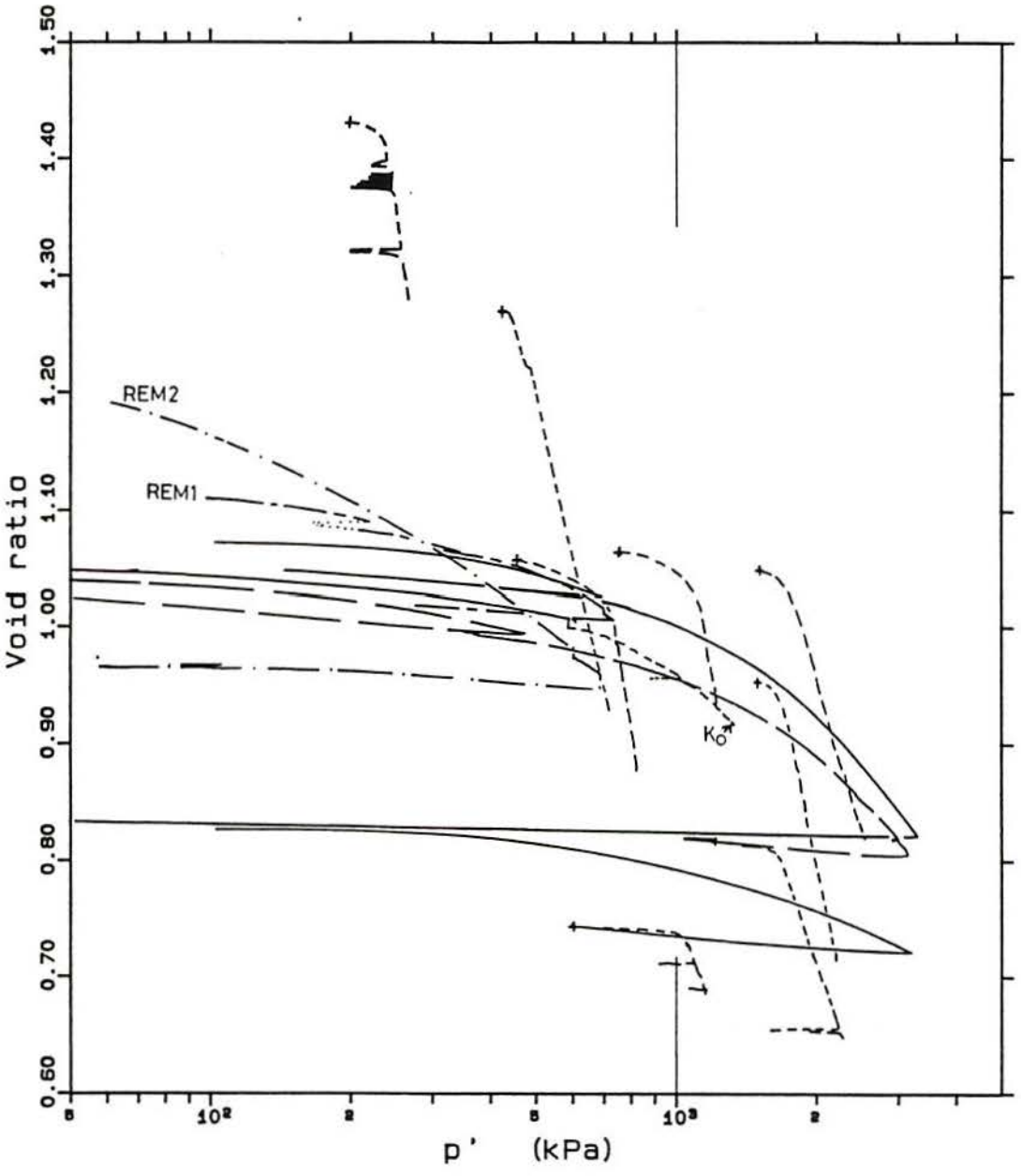

Figure 10.7 – Summary of data of void ratio variation for tests on the artificial soil (the crosses indicate the start of shear tests)

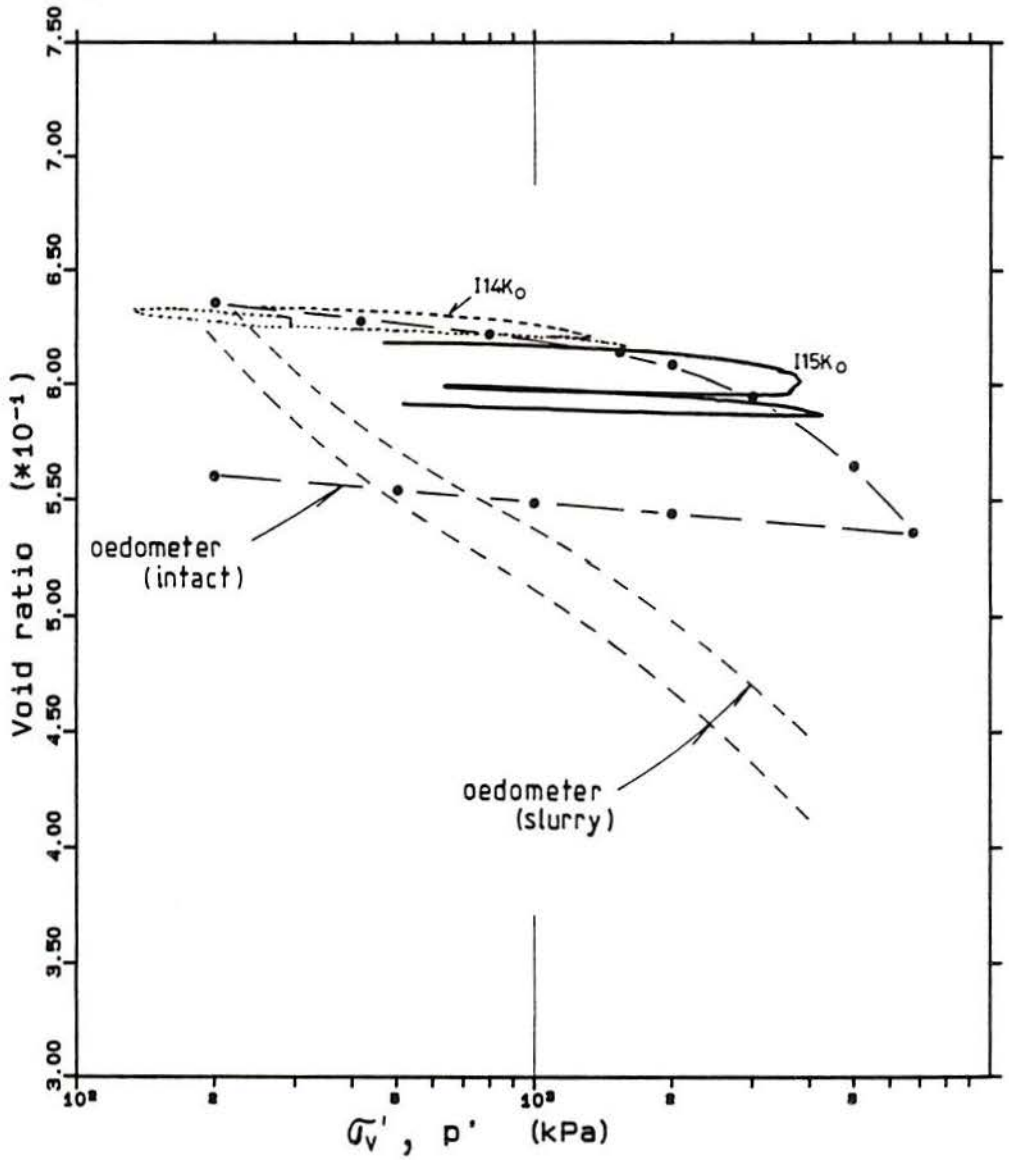

Figure 10.8 – Variation of void ratio of Corinth Marl during one-dimensional compression (note oedometer tests plotted versus σ'_v)

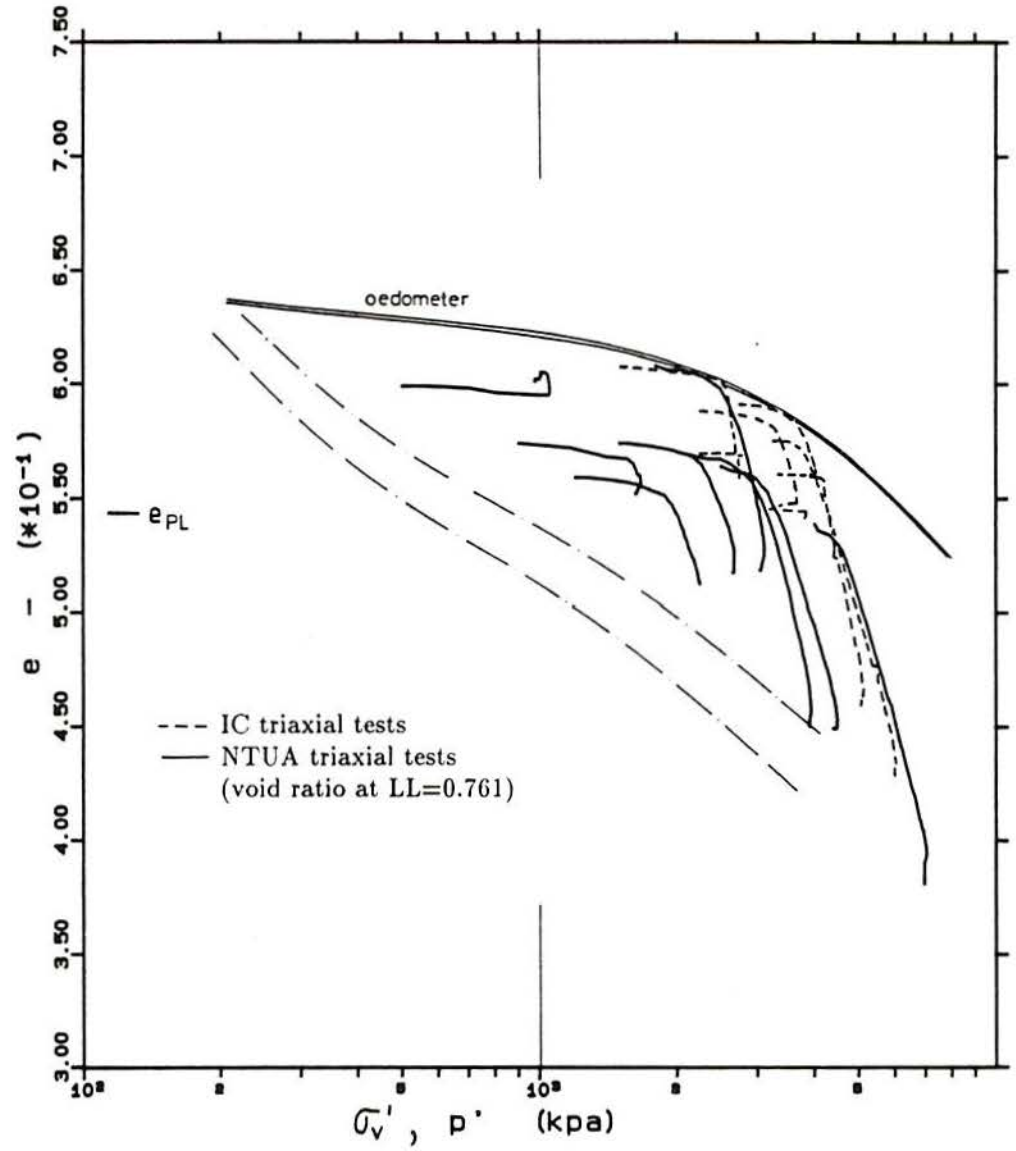

Figure 10.9 – Variation of void ratio of Corinth Marl samples during shear stages (note oedometer tests plotted against σ'_v)

LIST OF SYMBOLS

C_c	Coefficient of compression
C_v	Coefficient of consolidation
e_0, e_i	Natural and initial void ratios
e_f	Final void ratio
e_{int}	Intergranular void ratio
e_L	Void ratio equivalent to liquid limit
e_{OPT}	Void ratio equivalent to the maximum density from a compaction test
e_R	Relative void ratio (see Chapters 2 and 9)
E, E_{sec}	Secant stiffness
G_s	Specific gravity of the soil grains
k	Permeability
K_0	σ'_3/σ'_1 ratio for one-dimensional compression
K	Bulk compressibility
p'	Mean effective stress [$=((\sigma'_1 + 2\sigma'_3)/3)$]
q	Deviator stress [$=(\sigma_1 - \sigma_3)$]
s'	Average effective stress [$=((\sigma'_1 + \sigma'_3)/2)$]
t	Half deviator stress [$=((\sigma_1 - \sigma_3)/2)$]
wc_0	Initial water content
ϵ_a	Axial strain
ϵ_r	Radial strain
ϵ_v	Volumetric strain
σ'_1	Maximum principal effective stress
σ'_3	Minimum principal effective stress
σ_t	Tensile strength
γ_d	Dry unit weight

LIST OF FIGURES

LIST OF TABLES

APPENDIX 1

THE INTERGRANULAR VOID RATIO AND THE SPECIFIC GRAVITY OF ARTIFICIAL SOIL MIXTURES

The artificial soil used in this work was intended primarily as a convenient material to simulate the behaviour of natural soils. It incorporates three basic constituents: the quartz sand, the crushed fired kaolin and the bonding (fired kaolin). The kaolin constituents are porous themselves so that when the traditional definition of void ratio is used one finds that the void ratio value is rather low compared with a similar structure composed of non-porous grains. To account for this Maccarini (1987) proposed the inter-granular void ratio so that two soils with the same structural arrangement would have the same e_{int} value. In this thesis the traditional definition was used instead, mainly because the natural soil may also have porous particles and the calculation of e_{int} requires a knowledge of the specific gravity of individual grains.

Nevertheless, the concept is an useful one, especially in cases where the structure similarity needs to be shown.

The author carried out a series of measurements of the specific gravity of different minerals, the results of which were as follows:

(*a*) quartz sand: 2.65,

(*b*) kaolin fired at 1000°C (CFK): 2.71,

(*c*) kaolin fired at 500°C (bonding): 2.51,

(*d*) artificial soil mixture 133057: 2.65.

The dry density of kaolin fired at 500°C was also measured using five small cylinders and the average value was 12.54 kN/m^3. The dry density of kaolin fired at 1000°C is very close to this value – 12.45 kN/m^3 (Maccarini, 1987).

These specific gravity values are similar to those reported in literature. For kaolin Grim

(1953) quoted values of 2.74 and 2.47 for temperatures of 1000°C and 500°C respectively and he noted that these values vary with the specific clay chemistry. The quartz has a well established value of G_s=2.65.

Using the definition of the intergranular void ratio (Maccarini, 1987)

$$e_{int} = \frac{V_T}{V_S^*} - 1 \tag{A1}$$

where

V_T = total volume of the soil

V_S^* = total volume of the grains (including internal voids)

$$V_S^* = \sum \frac{P_i}{\gamma d_i} \tag{A2}$$

where

P_i = weight of the grains

γd_i = dry density of the grains

Some calculations are presented below, in order to clarify the various assumptions used.

CASE 1

Calculation of the intergranular void ratio for soil 133057 (100 and 200 series). Two calculations of W_s can be made using (A2):

(*a*)
$$V_S^* = W_s \left[\frac{0.13}{1.28} + \frac{0.30}{1.28} + \frac{0.57}{2.65}\right] \tag{A3}$$

or

(*b*)
$$V_S^* = W_s \left[\frac{0.13}{2.51} + \frac{0.30}{1.28} + \frac{0.57}{2.65}\right] \tag{A4}$$

where W_s is the dry weight of the soil.

In the first case (A3) the porous nature of the bonding has being taken into account as well as the crushed kaolin (CFK). In the second case (A4) only the porosity of the CFK grains is accounted for. The respective intergranular void ratios will therefore be:

(*a*)
$$e_{int} = \frac{1.815}{\gamma d} - 1$$

or

(*b*)
$$e_{int} = \frac{1.994}{\gamma d} - 1 \qquad \text{(A7)}$$

depending on which calculation method is adopted.

CASE 2

Calculation of the intergranular void ratio of artificial soil of 300 series (168400, only sand and kaolin fired at 500°C).

(*a*)
$$V_S^* = W_s \left[\frac{0.16}{1.28} + \frac{0.84}{1.28}\right]$$

$$e_{int} = \frac{1.28}{\gamma d} - 1$$

or

(*b*)
$$V_S^* = W_s \left[\frac{0.16}{2.51} + \frac{0.84}{1.28}\right]$$

$$e_{int} = \frac{1.39}{\gamma d} - 1$$

CASE 3

Calculation of the intergranular void ratio of artificial soil 00 series (130087).

(*a*)
$$V_S^* = W_s \left[\frac{0.13}{1.28} + \frac{0.87}{2.65}\right]$$

$$e_{int} = \frac{2.326}{\gamma d} - 1$$

(*b*)
$$V_S^* = W_s \left[\frac{0.13}{2.51} + \frac{0.87}{2.65}\right]$$

$$e_{int} = \frac{2.631}{\gamma d} - 1$$

CASE 4

The same formulation can be used to calculate the true specific gravity of any mixture.

(*a*) This can be done for soil 133057 (100 and 200 series) for example.

$$\frac{1}{G_s} = \left[\frac{0.13}{2.51} + \frac{0.30}{2.71} + \frac{0.57}{2.65}\right]$$

giving $G_s = 2.648$. This value agrees very well with the value measured in the laboratory (G_s=2.65).

(*b*) For, for soil 130087 (00 series):

$$\frac{1}{G_s} = \left[\frac{0.13}{2.51} + \frac{0.87}{2.65}\right]$$

giving $G_s = 2.631$.

CASE 5

In order to compare the results presented here with those of Maccarini (1987) it is necessary to convert the void ratio appropriately. The value used by that author (Maccarini, 1988) was G_s^*=2.061 for soil 133057. Therefore, to calculate the real void ratio of his samples, the following formulas should be used:

(*a*) For soil 133057

$$e = \frac{2.65\ (1 + e_{int})}{2.061} - 1 = 1.286\ (1 + e_{int}) - 1$$

(*b*) For soil 130087

$$e = \frac{2.63\ (1 + e_{int})}{2.47} - 1 = 1.065\ (1 + e_{int}) - 1$$

APPENDIX 2

MODIFIED HARVARD MINIATURE COMPACTION EQUIPMENT

There is a volume increase in the amount of soil in relation to that proposed by Wilson (1970) (see figure).

The compaction effort on each sample was modified to achieve the same results as the conventional Proctor test. The same ram and ram force (178 N) were maintained. The compaction comprises:

five layers of soil/sample

20 tamps/layer

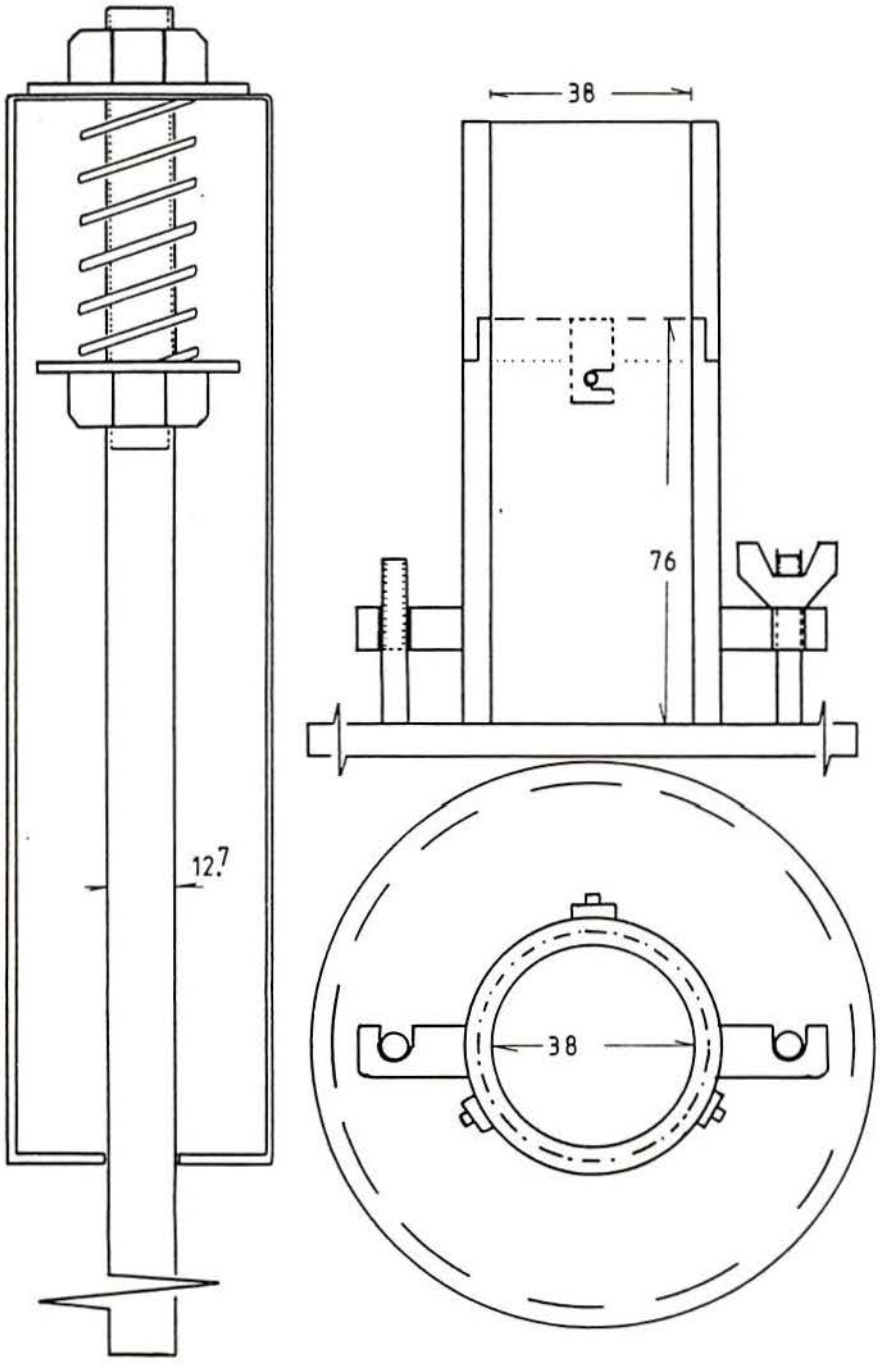
38
76
12.7
38

REFERENCES

Ackerley, S.K., Hellings, J.E. & Jardine, R.J. (1987). Discussion. *Géotechnique* 37, 3:414-415.

Akai, K. (1963). The effect of back pressure on the consolidation and shear of an undisturbed saturated clay. *Proc. 2nd Asian Reg. Conf. Soil Mechs. Fdn Engng*, Tokyo, 1:105-107.

Allam, M.M. & Sridharan, A. (1980). Influence of the back pressure technique on the shear strength of soils. *Geotech. Testing J.*, 3, 1:35-40.

Anagnostopoulos, A. (1989). Personal communication. Internal reports and test results. National Technical University, Athens, Greece.

Bishop, A.W. & Garga, V.K. (1969). Drained tension tests on London Clay. *Géotechnique* 19, 2:309-313.

Bishop, A.W. & Henkel, D.J. (1962). *The measurement of soil properties in the triaxial test.* 2nd Edition. London: Edward Arnold.

Bishop, A.W. & Wesley, L.D. (1975). A hydraulic triaxial apparatus for controlled stress path testing. *Géotechnique* 25, 4:657-670.

Brady, B.H.G. & Brown, E.T. (1985). *Rock mechanics for underground mining.* London: George Allen & Unwin.

Brand, E.W. (1975). Back pressure effects on the undrained strength characteristics of soft clay. *Soils and Fdns*, 15, 2:1-16.

Bressani, L.A. & Vaughan, P.R. (1989). Damage to soil structure during triaxial testing. *Proc. 12th Int. Conf. Soil Mechs Fdn Engng.* Rio de Janeiro, 1, 17-20.

British Standards Institution (1975). *Methods of test for soils for civil engineering purposes*, BS 1377. London: BSI.

Bromhead, E.N. (1979). A simple ring shear apparatus. *Ground Engng*, 12:40-44.

Brown, S.F., Austin, G. & Overy, R.F. (1980). An intrumented triaxial cell for cyclic loading of clays. *Geotech. Testing J.*, 3, 4:145-152.

Brown, S.F. & Snaith, M.S. (1974). The measurement of recoverable and irrecoverable deformations in the repeated loading triaxial tests. *Géotechnique* 24, 2:255-259.

Burland, J.B. & Baylis, F.V.S. (1989). Settlement and yielding of upper chalk supporting the foundations for a silo complex. *Proc. Int. Chalk Symp., Brighton*, 149-158.

Burland J.B. & Symes, M. (1982). A simple axial displacement gauge for use in the triaxial apparatus. *Géotechnique* 32, 1:62-65.

Carter et al. (1988). Triaxial testing of North Rankin calcarenite. *Proc. Int. Conf. Calcareous Sediments*, Perth, 2:515-530.

Carvalho, J.B.Q. (1986). The applicability of the cone penetration to determine the liquid limit of laterite soils. *Géotechnique*, 36, 1:109-113.

Chandler, R.J. (1967). *Shear strength properties of Keuper Marl.* PhD thesis, University of Birmingham.

Chandler, R.J. (1969). The effect of weathering on the shear strength properties of Keuper Marl. *Géotechnique*, 19, 3:321-334.

Chaney, R.C., Stevens, E. & Sheth, N. (1979). Suggested test method for determination of degree of saturation of soil samples by B value measurement. *Geotech. Testing J.*, 2, 3:158-162.

Christoulas, S.G., Kalteziotis, N.A. & Tsiambaos, G.K. (1984). Geotechnical problems in a bridge over Corinth Canal. *Proc. Int. Conf. Case Histories in Geotech. Engng*, St Louis. Missuri, 3:849-854.

Clayton, C.R.I. & Khatrush, S.A. (1986). A new device for measuring local axial strain on triaxial specimens. *Géotechnique* 36, 4:593-597.

Clayton, C.R.I., Khatrush, S.A., Bica, A.V.D. & Sidique, A. (1989). The use of Hall effect semiconductors in geotechnical instrumentation. *Geotech. Testing J.*, 12, 1:69-76.

Clough, G.W., Sitar N., Bachus, R.C. & Rad, N.S. (1981). Cemented sands under static loading. *J. Geotech. Engng Div., Am. Soc. Civ. Engrs.* 107, 6:799-817.

Collins, K. (1985). Towards characterization of tropical soil microstructure. *Proc. 1st Int.*

Conf. Geomech. Trop. Lateritic and Saprolitic Soils, ABMS, 1, 85-96.

Conlon, R.J. (1966). Landslide on the Toulnustouc River, Quebec, Canada. *Can. Geotech. J.*, 13, 3:113-144.

Costa Filho, L.M. (1980). *A laboratory investigation of the small strain behaviour of London Clay.* PhD thesis, University of London.

Costa Filho, L.M. (1985). Measurement of axial strains in triaxial tests on London Clay. *Geotech. Testing J.*, 8, 1:3-13.

Costa Filho, L.M. & Vaughan, P.R. (1980). Discussion. *Géotechnique* 30, 3:336-339.

Cozzolino, V.M.N. & Nogami, J.S. (1988). Use of cone penetrometer for tropical soils characterization. *Simp. Novos Conceitos em Ensaios de Campo e Laboratório em Geotecnia.* 210, 1:201-212. (in Portuguese).

Crawford, C.B. (1963). Cohesion in an undisturbed sensitive clay. *Géotechnique* 13, 2:132-146.

Crilly, M.S. (1989). Personal communication. Civil Engng Dept, Imperial College, London.

Culshaw, M.G., Northmore, K.J. & Hobbs, P.R.N. (1989). Undisturbed pit sampling of tropical red clay soils. *Proc. 25th Conf. Engng Group of Geological Society.* Geological Society, London, 383-392.

Daramola, O. (1978). *The influence of stress history on the deformations of sand.* PhD thesis, University of London.

Daramola, O. & Vaughan, P.R. (1982). Discussion. *Géotechnique* 32, 1:71-73.

Deere, D.V. & Patton, F.D. (1971). Slope stability in residual soils. *Proc. 4th Panam. Conf. Soil Mechs Fdn Engng.* San Juan, 1, 87-170.

Dias, R. (1987). *Application of pedology and geotechnics to power lines foundation design.* PhD thesis, UFRJ, COPPE, Rio de Janeiro. (in Portuguese).

Dias, R. (1988). Influence of the moisture content in the shear strength of undisturbed lateritic soil. *Proc. 2nd Int. Conf. on Geomech. in Trop. Soils, Singapore*, 1:135-142.

Dobereiner, L. (1984). *Engineering geology of weak sandstones.* PhD thesis, University of

London.

Dobereiner, L. & Freitas, M.H. de (1986). Geotechnical properties of weak sandstones. *Géotechnique* 36, 1:79-94.

Elliott, G.M. (1983). *An investigation of a yield criterion for rock.* PhD thesis, University of London.

Elliott, G.M. & Brown, E.T. (1985). Yield of a soft, high porosity rock. *Géotechnique* 35, 4:413-423.

Farmer, I. (1983). *Engineering behaviour of rocks.* New York: Chapman and Hall.

Geotechnical Control Office (1982). *Mid-levels study — Report on Geology, Hydrology and Soil Properties.* Hong Kong: Government Printer, 264 p.

Goldsmith, A.S. (1989). Permeability decline and compressibility in sandstone reservoir rocks. *Proc. Int. Symp. Rock at Great Depth*, Pau, 1:923-928.

Goodman, R.E. (1989). *Introduction to rock mechanics.* 2nd Edition. New York: John Wiley & Sons, 562 p.

Grim, R.E. (1962). *Applied clay mineralogy.* New York: McGraw Hill, 422 p.

Harison, J.A. (1988). Using the BS cone penetrometer for the determination of the plastic limit of soils. *Géotechnique*, 38, 3:433-438.

Head, K.H. (1980). *Manual of soil laboratory testing.* London: Pentech Press, 1.

High, D.W. (1983). *Laboratory investigations of sea-bed clays.* PhD thesis, University of London.

Hobbs, P.R.N. (1990). Bonded red clays. Notes on the course: Tropical and Residual soils, Civil Engng Dept, Imperial College, London.

Jardine, R.J., Brooks, N.J. & Smith, P.R. (1985). The use of electrolevel transducers for strain measurements in triaxial tests in weak rock. *Proc. Int. J. Rock Mechs Min. Sci. & Geomech. Abstr.*, 22, 51:331-337.

Jardine, R.J., Potts, D.M., Fourie, A.B. & Burland, J.B. (1986). Studies of the influence of non-linear stress-strain characteristics in soil-structure interaction. *Géotechnique* 36,

3:377-396.

Jardine, R.J. & Potts, D.M. (1988). Hutton tension leg platform foundations: prediction of driven pile behaviour. *Géotechnique* 38, 2:231-252.

Jardine, R.J., Symes, N.J. & Burland, J.B. (1984). The measurement of soil stiffness in the triaxial apparatus. *Géotechnique* 34, 3:323-340.

Jones, M.F. & Preston, R.M.I. (1987). *Introduction in: Deformation of sediments and sedimentary rocks.* Geological Society Special Publication, London, 29:1-8.

Kavvadas, M. (1990). Some considerations on the stability of the Corinth Canal slopes. Paper presented on the *4th Young Geotech. Engng Conf.*, Delft.

Kimmance, G.P. (1988). *Computer aided risk analysis of open peat mine slopes in kaolin mineral deposits.* PhD thesis. University of London.

Lacerda, W.A. (1985). Compressibility properties of lateritic and saprolitic soils. In: *Peculiarities of Geotechnical Behaviour of Tropical Lateritic and Saprolitic Soils, Progress Report.* ABMS, São Paulo, 85-113.

Ledra, M.J. (1990). *Deformation of chalk through compaction and flow.* PhD thesis, University of London.

Leroueil, S. & Vaughan, P.R. (1990). The general and congruent effects of structure in natural soils and weak rocks. *Géotechnique*, 40, 3:467-488.

Lowe, J. & Johnson, T.C. (1960). Use of back-pressure to increase degree of saturation of test specimens. *Proc. Research Conf. Shear Strength of Cohesive Soils*, Boulder, ASCE, 819-836.

Lumb, P. (1962). The properties of decomposed granite. *Géotechnique* 12, 3:226-243.

Maccarini, M. (1987). *Laboratory studies of a weakly bonded artificial soil.* PhD thesis, University of London.

Maccarini, M. (1988). Personal communication. Letter of May 1988. Universidade Federal Santa Catarina, SC, Brazil.

Mitchell, J.K. & Sitar, N. (1981). Engineering properties of tropical residual soils. *Proc.*

Engng and Constr. in Tropical and Residual Soils, ASCE. Honolulu, Hawaii, 30-57.

Ninis, N.L. (1988). Personal Communication. Civil Engng Dept, Imperial College.

Northmore, K.J. (1990). Personal communication. Letter of February 1990. British Geological Survey.

Ohtsuki, H., Nishi, K., Okamoto, T. & Tanakas, S. (1981). Time-dependent characteristics of strength and deformation of a mudstone. *Proc. Int. Symp. Weak Rock.* Tokyo, 1:119-125.

Price, G.P. (1988). Fabric of calcareous sediments at North Rankin "A", North West Shelf. *Proc. Int. Conf. Calcareous Sediments*, Perth, 2:367-376.

Rad, N.S. & Tumay, M.T. (1986). Effect of cementation on the cone penetration resistance of sand: a model study. *Geotech. Testing J.*, **9**, 3:117-125.

Sandroni, S.S. (1981). Gnaissic residual soils - research carried out at PUC/RJ. *Proc. Simp. Brasileiro Solos Tropicais em Engenharia*, Rio de Janeiro, 2:30-65. (in Portuguese).

Sandroni, S.S. (1985). Stress relief effects in Gneissic saprolitic soils. *Proc. 1st Int. Conf. Geomech. Trop. Lateritic and Saprolitic Soils.* Brasília, 3, 290-296.

Sangrey, D.A. (1972). Naturally cemented sensitive soils. *Géotechnique* 22, 1:139-152.

Schofield, A.N. & Wroth, C.P. (1968). *Critical state soil mechanics.* London: McGraw-Hill.

Semple, R.M. (1988). The mechanical properties of carbonate soils. *Proc. Int. Conf. Calcareous Sediments*, Perth, 2:807-836.

Symes, M.I. & Burland, J.B. (1984). Determination of local displacements on soil samples. *Geotech. Testing J.*, 17, 2:49-59.

Tanimoto, K. & Tanaka, Y. (1986). Yielding of soil as determined by acoustic emission. *Soils and Fdns*, 26, 3:69-80.

Taylor, D.W. (1948). *Fundamentals of soil mechanics.* New York: John Wiley.

Terzaghi, K. (1958). Design and performance of the Sasamua dam. *Proc. Instn Civil Engrs*, **9**, 369-394.

Uriel, R.S. & Serrano, A.A. (1973). Geotechnical properties of two collapsible soils of low bulk density at the site of two dams in Canary Islands, Spain. *Proc. 8th Int. Conf. Soil Mechs*

Fdn Engng. (Moscow), v. 2.2:257-264.

Vaid, Y.P. & Negussey, D. (1984). A critical assessment of membrane penetration in triaxial test. *Geotech. Testing J.*, 7, 2:70-76.

Vargas, M. (1953). Some engineering properties of residual clay soils occurring in Southern Brasil. *Proc. 3rd Int. Conf. Soil Mechs Fdn Engng.* Zurich, 1, 67-71.

Vaughan, P.R. (1985). Mechanical and hydraulic properties of tropical lateritic and saprolitic soils, particularly as related to their structure and mineral components. *Proc. 1st Int. Conf. Geomech. Trop. Lateritic and Saprolitic Soils.* Brasília, 3:231-263.

Vaughan, P.R. (1988). Characterising the mechanical properties of in-situ residual soil. *Proc. 2nd Int. Conf. on Geomech. in Trop. Soils.* Singapore, 2, 469-487.

Vaughan, P.R., Maccarini, M. & Mokhtar, S.M. (1988). Indexing the engineering properties of residual soil. *Quart. J. Engng Geo.* 21, 69-84.

Wallace, K.B. (1973). Structural behaviour of residual soils of the continuously wet highlands of Papua, New Guinea. *Géotechnique*, 23, 2:203-218.

Webb, D.L. (1966). *The mechanical properties of undisturbed samples of London Clay and Pierre Shale.* PhD thesis, University of London.

Wesley, L.D. (1973a). Cluster hypothesis and shear strength of a tropical red clay. *Géotechnique*, 23, 1:109-113.

Wesley, L.D. (1973b). Some basic engineering properties of Halloysite and Allophane Clays in Java, Indonesia. *Géotechnique* 23, 471-494.

Wesley, L.D. (1974). Discussion on "Structural behaviour of residual soils of the continually wet highlands of Papua New Guinea". *Géotechnique* 24, 1:101-105.

Wilson, S.D. (1970). Suggested method of test for moisture-density relations of soils using Harward compaction apparatus. In: *ASTM Special Tech. Publ.* 479 - *Special Proc. for Testing Soil and Rock for Engng Purposes.* 5th Edition, 101-103.

Worral, W.E. (1982). *Ceramic raw materials.* London: Pergamon Press.